

THE MOVEMENT AND BASAL SLIDING OF THE
NISQUALLY GLACIER, MOUNT RAINIER

by

STEVEN McNIVEN HODGE

A dissertation submitted in partial fulfillment
of the requirements for the degree of

DOCTOR OF PHILOSOPHY

UNIVERSITY OF WASHINGTON

1972

Approved by Norbert Untersteiner
(Chairman of Supervisory Committee)

Department GEOPHYSICS PROGRAM
(Departmental Faculty sponsoring candidate)

Date 14 AUGUST, 1972



UNIVERSITY OF WASHINGTON

Date: July 24, 1972

We have carefully read the dissertation entitled The Movement and Basal Sliding of the Nisqually Glacier, Mount Rainier

submitted by
Steven McNiven Hodge in partial fulfillment of
the requirements of the degree of Doctor of Philosophy

and recommend its acceptance. In support of this recommendation we present the following joint statement of evaluation to be filed with the dissertation.

The exact mechanism of the sliding of a glacier on its bed is perhaps the central problem in the study of glaciers, as it is critical to relating glacier variations quantitatively to changes in climate and to an explanation of glacier surges. The considerable theoretical work on this subject has not been adequately tested, as direct observations are exceedingly difficult.

Hodge's study is a detailed examination of seasonal and shorter-period variations in the flow of Nisqually Glacier. These variations are then studied in relation to the possible changes in those variables such as ice thickness, surface slope, and water discharge which are thought to determine the rate of sliding or internal deformation. Stakes set in the glacier surface with a steam drill developed for the purpose were located by precise triangulation surveys at intervals of one week or more over a 2-year period. A meticulous numerical analysis of the data included correction for tilts or bends in the stakes and an unusually complete error analysis. Ice thickness was measured with a gravimeter aided by two borings through the glacier. The results show that the flow is predominantly by sliding on the bed, the seasonal speed variations are not in phase with the seasonal variations in shear stress, nor are they in phase with the meltwater discharge, and the seasonal wave of ice flow moves down the glacier at a speed too high for propagation by the internal deformation or pressure melting/creep enhancement mechanisms but too low for propagation by a kinematic wave in a thin water film. One is then led to the conclusion that the rate of sliding of this glacier on its bed is determined primarily by the amount of water in temporary storage in the glacier. This important result has widespread implications, and clearly points the way for future work on this difficult problem.

DISSERTATION READING COMMITTEE:

Mark Fournier

Charles F. Raymond

Norbert Untersteiner

Doctoral Dissertation

In presenting this dissertation in partial fulfillment of the requirements for the doctoral degree at the University of Washington, I agree that the Library shall make its copies freely available for inspection. I further agree that extensive copying of this dissertation is allowable only for scholarly purposes. Requests for copying or reproduction of this dissertation may be referred to University Microfilms, 300 N. Zeeb Road, Ann Arbor, Michigan 48106, to whom the author has granted "the right to reproduce and sell (a) copies of the manuscript in microform and/or (b) printed copies of the manuscript made from microform."

Signature Steven M. Kufel

Date 14 August, 1972

University of Washington

Abstract

THE MOVEMENT AND BASAL SLIDING OF THE
NISQUALLY GLACIER, MOUNT RAINIER

by Steven McNiven Hodge

Chairman of Supervisory Committee: Professor Norbert Untersteiner
Geophysics Program

Accurate and detailed measurements of the positions of stakes along the centerline of the lower Nisqually Glacier were made on the average every twelve days for a period of two years. Changes in surface velocity, surface slope and thickness were calculated, with corrections made for tilting and bending of the stakes. Run-off from the glacier over the same period was measured continuously at a stream gage below the terminus.

Bedrock topography was determined by measurements of the gravity field over the glacier. Accurate terrain corrections and three dimensional modelling were done using a modification of the technique of Talwani and Ewing (1960). The regional gravity field was determined by requiring the calculated bedrock to agree with areas of known bedrock and with two depths determined by drilling. The glacier was found to be thinner than expected, with an average centerline depth of only 71 m.

The glacier flow model of Nye (1952) was used to reduce surface velocities to sliding velocities on the bed. Variables were smoothed over distances of several times the ice thickness to minimize the effect of longitudinal stress

gradients and shape factors were used to allow for the friction of the valley walls. Existing data on the flow law of ice were examined and an average flow law and a least viscous flow law chosen. The effect of uncertainties in the flow model was investigated by using these two flow laws and by simultaneously perturbing the thickness, surface slope and shape factor by acceptable amounts.

Internal deformation of the glacier is found to account for much less than 50 % of the observed surface motion. Sliding of the glacier is negligible only if the ice obeys the least viscous flow law, the depths are everywhere too shallow by at least 10 m and the shape factors are close to unity. Furthermore, internal deformation contributes progressively less to the surface motion with distance up-glacier; in the area near the equilibrium line sliding probably accounts for 80-90 % of the total motion.

The surface velocity of the glacier has a pronounced seasonal fluctuation superimposed on a long period trend. At the equilibrium line the maximum velocity occurs in late May or June and the minimum in November. The existence of a "seasonal wave" is verified, the maximum and minimum velocity occurring progressively later with distance down-glacier. The wave travels from the equilibrium line to the terminus with a speed of about 20 km a^{-1} . This is one to two orders of magnitude greater than a normal kinematic wave, assuming that ice motion is due to internal deformation and/or the pressure melting/enhanced plastic flow mechanism of basal sliding. It is also two orders of magnitude smaller than that of a kinematic wave in a water film 0.5 mm thick.

The maximum deviation of the surface velocity from the long period trend is approximately $\pm 25 \%$ and does not vary significantly with distance along the glacier. The maximum velocity occurs 2-3 months after the maximum loading of the glacier and about one month before the peak in the run-off. The minimum velocity occurs 1-2 months after the minimum loading and four months before the minimum run-off. The acceleration of the glacier throughout the winter,

while the run-off is still decreasing, is clearly demonstrated.

It is concluded that the seasonal variations in the motion of a glacier are due to variations in the amount of basal sliding and are controlled not by the run-off, the surface melting or the loading but by the amount of liquid water *stored* within the glacier. The peak in the liquid water storage curve of the South Cascade Glacier correlates well, on the average, with the peak in surface velocity of the Nisqually Glacier. The seasonal wave can be explained with this hypothesis also.

The velocity variations of the Nisqually Glacier are considered to be independent verification that glaciers store water in the fall, winter and spring and then release it in the summer, after the hydrostatic head of water becomes great enough to open the drainage channels. The data suggest that relatively more water is stored higher up the glacier and that possibly most of the storage occurs at the equilibrium line.

The results support the idea that the dominant controlling parameter in the basal sliding mechanism is the hydrostatic pressure of water having access to the bed. Any dependence of sliding on the basal shear stress is probably masked by the varying water pressure.

Finally, it is suggested that the volume of liquid water stored in a glacier may vary annually and that jökulhlaups represent the catastrophic release of any accumulated water, and glacier surges may be caused by a more gradual release. It might be possible to predict jökulhlaups by detecting abnormal accelerations in the surface motion of glaciers.

TABLE OF CONTENTS

	Page
LIST OF FIGURES	v
LIST OF TABLES	xii
LIST OF PLATES	xiii
LIST OF ABBREVIATIONS	xiii
LIST OF CONVERSION FACTORS AND CONSTANTS	xiv
LIST OF SYMBOLS	xv
ACKNOWLEDGMENTS	xx
CHAPTER:	
1 INTRODUCTION	1
2 HISTORICAL REVIEW	4
2.1 Before 1880	4
2.2 1880 to 1914	15
2.3 1914 to 1954	20
2.4 After 1954	28
2.5 Summary	41
2.6 Comments	43
3 THE NISQUALLY GLACIER	48
3.1 Location	48
3.2 Characteristics	49
3.3 Meteorological conditions	54
3.4 Advance and retreat of the terminus	59
3.5 The kinematic wave	62
3.6 Outburst floods	64
3.7 Other measurements	65
4 THE TRIANGULATION NET AND THE GRID SYSTEM	67
4.1 Description of the triangulation points	67
4.2 The basic net	73
4.3 The extended net	75
4.4 The final triangulation net and its accuracy	78
5 THE THICKNESS OF THE NISQUALLY GLACIER	85
5.1 The field measurements	87
5.2 Reduction of the gravity observations	93

5.2.1	The regional correction	94
5.2.2	The latitude correction	94
5.2.3	The elevation correction	95
5.2.4	The terrain correction	96
5.2.5	The Talwani and Ewing method	98
5.2.6	Digitizing of the terrain	100
5.2.7	The reduction program	105
5.2.8	The rock density	106
5.2.9	Numerical evaluation of the line integral	108
5.2.10	Numerical integration of $V(z)$	110
5.2.11	Results of the gravity reductions: the Bouguer anomalies	122
5.3	Interpretation of the Bouguer anomalies	131
5.3.1	Two dimensional modelling	134
5.3.2	Three dimensional modelling	140
5.4	Accuracy of the gravity results	152
6	THE SURFACE VELOCITY VARIATIONS	157
6.1	The movement stakes and the surveys	157
6.2	Reduction of the survey measurements	162
6.2.1	Calculation of the mean horizontal and vertical angles	162
6.2.2	Calculation of the coordinates of a point	164
6.2.3	Corrections for tilt of the stake	168
6.2.4	Corrections for bend of the stake	174
6.3	Error analysis	179
6.3.1	Errors in the angle measurements	179
6.3.2	Errors in the coordinates	189
6.3.3	Errors in the tilt	192
6.3.4	Errors in the bend	194
6.4	The reduction program and the results	196
6.5	The velocity calculations	201
6.5.1	Correcting the coordinates to the bottom of the stake	202
6.5.2	The flex method	204
6.5.3	Filtering and smoothing of the data	207
6.5.4	Error analysis	208
6.5.5	The spatial variations in the velocity field	212
6.5.6	Corrections for transverse velocity gradients	219
6.5.7	Corrections for longitudinal velocity gradients	223
6.5.8	Elimination of faulty data points	224
6.5.9	The final velocity field: $s(x,t)$	226
7	THE THICKNESS VARIATIONS	229
8	THE SURFACE SLOPE VARIATIONS	234
8.1	Calculation of slopes between adjacent pairs of stakes	234
8.2	Calculation of slopes by differentiation of $\Delta h(x',t)$	239
9	THE MASS BALANCE	243
9.1	The surface slope	243
9.2	The snow density	246
9.3	The reference surface	246

122	The long period trend of surface velocities over the two years of measurements	305
123	The deviation of the maximum and minimum velocities from the long period trend	307
124	The mean surface speed, the mean speed due to internal deformation, the monthly discharge of the Nisqually River and the cumulative liquid water storage, as a function of time	310
125	The small jökulhlaup released from the Nisqually Glacier on July 4, 1970	316
126	Longitudinal velocity profiles for the four years 1968-71	317

LIST OF TABLES

Table:	Page:
1 Summary of the previous measurements of the seasonal variations in the motion of a glacier	45
2 Climatological summary for Paradise, Mt. Rainier National Park	58
3 The coordinates of the triangulation points	76
4 Results of the calculations for the additional triangulation points added in 1969	79
5 The distances between the triangulation points	80
6 The angular bearings between the triangulation points	81
7 The standard deviations in the coordinates of 36 stakes which were observed from more than two triangulation points	83
8 Analysis of the gravity readings made at the sub-base stations	90
9 The drift of the gravity meter on all loops made between fixed base stations	91
10 Details of the terrain zones and the calculations of the terrain corrections for the 195 glacier stations	102
11 The standard deviations in the angles turned to the cross on August 5, 1970	180
12 The mean error in the coordinates and tilt of the centerline stakes	200
13 The scatter of the velocity data points for various reduction methods and corrections, the number of survey combinations, and the corrections for transverse velocity gradients	209
14 The mean error in the velocity components of the centerline stakes	211
15 The change in snow depth between Nov. 29, 1969, and Feb. 10, 1970	251
16 The parameters for the flow law of ice which have been determined to date	270
17 Values of the classical shape factor and the Nye shape factor for various channel cross sections and various half-width to depth ratios	274

LIST OF PLATES

Plate:		Page:
I	Composite 180° panorama of the Nisqually Glacier, March 1970	340
II	The Nisqually Glacier and the south side of Mount Rainier from Pinnacle Peak, January 1972	341
III	The region around the equilibrium line of the Nisqually Glacier from TP-1, September 1968	341

LIST OF ABBREVIATIONS

a	year
d	day
s	second (of time)
m	meter
km	kilometer
mm	millimeter
cm	centimeter
g	gram
Mg	megagram
kg	kilogram
h	hour
N	Newton
mgal	milligal
°C	degrees Celsius
° or deg	degrees of arc
' or min	minutes of arc
" or sec	seconds of arc
TP	triangulation point
MB	main base (gravity measurements)
SB	sub-base (gravity measurements)
U.S.G.S.	United States Geological Survey

LIST OF CONVERSION FACTORS

1 m	=	3.280833 feet
1 km	=	0.62137 miles
1 mm	=	0.0393701 inch
1 bar	=	10^5 N m^{-2}
1 radian	=	57.295779 deg
1 mgal	=	10^{-5} m s^{-2}
1 mm d ⁻¹	=	1.198 feet a ⁻¹
	=	0.3652 m a ⁻¹
1 a	=	8766.144 h
	=	$3.1558 \times 10^7 \text{ s}$
1 N m ⁻³	=	$10^{-5} \text{ bar m}^{-1}$

LIST OF CONSTANTS

γ	=	$6.670 \times 10^{-11} \text{ m}^3 \text{ kg}^{-1} \text{ s}^{-2}$
π	=	3.1415926536
ρ	=	0.9 Mg m ⁻³
g	=	9.80 m s ⁻²
e	=	2.7182818284

LIST OF SYMBOLS

Only the more important symbols are given. Ones used briefly in the text are defined when they are introduced and are omitted from this list. Some symbols (both listed and unlisted) have more than one meaning; however, their location in the text will resolve any ambiguity. Many of the symbols listed here can be subscripted, primed or barred.

Equations are numbered starting at one at the beginning of each chapter. The rare occasions when reference is made to an equation in another chapter is indicated by placing the chapter number at the beginning of the equation number, for example, equation 10 of chapter 5 becomes equation 5.10.

Roman symbols are listed first, then Greek symbols, both in alphabetical order. The units used are indicated in brackets.

(A, A')	temperature dependent coefficient in the flow law of ice (A when stress and strain rate are in "effective" form and A' when they are in "uniaxial compression" form) [$\text{bar}^{-n} \text{a}^{-1}$]
b	base line in a triangle (i.e., the horizontal distance between two triangulation points) [m]
b_i	mass balance, ice equivalent [m]
c	wave speed [km a^{-1}]
d	horizontal distance between a TP and a stake [m]
D	distance used in smoothing (or calculating) surface slopes, ice thicknesses or shape factors [m]
$\dot{\epsilon}$	strain rate in uniaxial compression [a^{-1}]
f	arbitrary mathematical function
f	classical shape factor [dimensionless]
f'	Nye shape factor [dimensionless]
F_i	body force per unit volume [N m^{-3}]

- g acceleration of gravity at the earth's surface; the "value of gravity" at a point; the gravitational attraction of a body (always understood to be just the vertical component of the total attraction) [mgal or m s^{-2}]
- g_i the measured gravity anomaly at station i (used in the two dimensional modelling) [mgal]
- G_i the calculated gravity anomaly at station i (used in the two dimensional modelling) [mgal]
- g_m the measured value of gravity (corrected for drift of the meter, arbitrary but fixed origin) [mgal]
- Δg_b the measured Bouguer anomaly [mgal]
- g_o the value of gravity on the reference spheroid (i.e., as given by the International Gravity Formula) [mgal]
- g_∞ the gravitational attraction of a parallel-sided infinite horizontal sheet [mgal]
- g_r the value of the regional gravity [mgal]
- h the thickness of the glacier (any snow layer present is assumed to be converted to an "ice equivalent" depth) [m]
- Δh the change in thickness, i.e., the change in surface elevation [m]
- H the horizontal angle from the reference mark to a point (if possible, the mean of the direct and inverted positions of the telescope), measured clockwise, looking down [deg]
- (I_1, I_2) the two line integrals in Talwani and Ewing's method [dimensionless]
- K the number of terms in the flow law of ice [dimensionless]
- (l, m, n)
 (L, M, N) the direction cosines of a line in space (cosines of the angles between the line and each of the X, Y, Z axes respectively) [dimensionless]
- m the number of depth variables across a profile (used in the two dimensional gravity modelling) [dimensionless]
- m the exponent in the basal sliding law (pressure melting/enhanced plastic flow mechanisms only) [dimensionless]
- n the number of gravity stations across a profile (used in the two dimensional gravity modelling) [dimensionless]
- n the exponent in the flow law of ice (possibly stress dependent) [dimensionless]
- r the horizontal distance from the origin to a point in space [m]

- r_o the distance from the bottom of a stake to the reference surface (summer surface), measured along the direction of the lowermost segment of the stake, positive upward [m]
- R the surface level on a stake (the distance up along the stake from its bottom to the glacier surface) [m]
- R' the distance down along a stake from its top to a specified point [m]
- R the total length of a stake [m]
- s the measured surface speed [mm d⁻¹]
- s' the measured surface speed corrected for transverse velocity gradients [mm d⁻¹]
- s'_o the measured surface speed corrected for transverse and longitudinal velocity gradients (in chapter 11 the primes and subscripts are dropped) [mm d⁻¹]
- s_b the basal sliding speed [mm d⁻¹]
- s_d the speed due to internal deformation (i.e., the contribution to the surface speed from internal deformation) [mm d⁻¹]
- t time, measured from 0000 hours, Pacific Standard Time, January 1, 1968 [d]
- t_o the "standard" times, i.e., the mid-points of each month [d]
- T temperature [°C]
- (u, v, w) the rectangular components of the velocity vector [mm d⁻¹]
- w the weight of an observation [dimensionless]
- V the vertical angle from the nadir to a point (if possible, the mean of the direct and inverted positions of the telescope) [deg]
- V the gravitational attraction per unit thickness of a thin horizontal sheet (or "lamina") of infinitesimal thickness [mgal m⁻¹]
- (x, y, z) the rectangular Cartesian coordinates of a point in the "standard" system: x true south from the summit of Mount Rainier, y true east from the summit of Mount Rainier, and z vertically upwards from sea level [m]

The following special meanings apply when referring to a point on a stake:

- Subscript "o": the top
- Subscript "b": the bottom
- Subscript "s": the surface mark (the mark closest to the surface)

Subscript "m":	the measured point (either the top of the stake or the surface mark, if it was measured from more than one TP)
No subscript:	the surface point (the point where the stake enters the glacier surface)
Δz	the difference in the z coordinate determined from two TP's (the first TP minus the second TP) [cm]
(X, Y, Z)	the coordinates of a TP [m]
(x', y')	the curvilinear horizontal coordinates of a point (x' down the centerline from a point near the equilibrium line; y' everywhere perpendicular to x') [m]
x'_0	the "standard" position of a stake (the average curvilinear x' coordinate of a stake over the two years of measurements) [m]
Z	the elevation of a point on the August 1966 glacier surface [m]
α	the surface slope (measured from the horizontal plane, positive down) [deg or radians]
β	the azimuth* of one TP with respect to another [deg or radians]
γ	the gravitational constant [$\text{m}^3 \text{kg}^{-1} \text{s}^{-2}$ or $\text{mgal m}^2 \text{kg}^{-1}$]
γ	the azimuth of the velocity vector [deg or radians]
δ	the dip of the velocity vector (angle from the horizontal plane, positive up) [deg or radians]
$\dot{\epsilon}_{ij}$	the strain rate tensor [a^{-1}]
$\dot{\epsilon}$	the effective shear strain rate [a^{-1}]
$\dot{\epsilon}_0$	the octahedral strain rate [a^{-1}]
ζ	the effective body force in the down-slope direction [N m^{-3}]
θ	the amount of tilt of a stake (measured from the zenith) [deg or radians]
κ	the stake angle (the horizontal angle subtended by the two TP's at the stake) [deg or radians]
λ	the geocentric latitude [deg or radians]
ν	the viscosity of ice [$\text{kg m}^{-1} \text{s}^{-1}$ or bar a]

* All "azimuths" in this report are angles measured from the +X direction (true south), positive to the east and negative to the west.

ξ	the depth unknowns in the two dimensional gravity modelling [m]
ρ	the density of ice [Mg m^{-3}]
ρ_s	the density of snow [Mg m^{-3}]
ρ_r	the density of rock [Mg m^{-3}]
$\Delta\rho$	the density contrast (rock density minus ice density) [Mg m^{-3}]
σ	the (best estimate of the) standard deviation of a single observation (subscripts used to denote the variable; units accordingly)
σ_m	the standard deviation of the mean of a set of observations (units according to the variable)
τ_{ij}	the stress tensor [bar]
τ'_{ij}	the stress deviator tensor [bar]
τ	the effective shear stress [bar]
σ	the stress in uniaxial compression [bar]
τ_o	the octahedral shear stress [bar]
τ_b	the basal shear stress [bar]
ϕ	the azimuth of the tilt of a stake [deg or radians]
χ	the interior angle of a triangle at a TP [deg or radians]
ω	the azimuth of a sighting to a stake [deg or radians]
$\langle \rangle$	average over time
$\langle\langle \rangle\rangle$	average over time and distance

ACKNOWLEDGMENTS

I am deeply indebted to Professor Mark Meier for suggesting the research topic and for guiding me throughout the field work, the data analysis and the preparation of the dissertation. I am equally grateful to Professor Norbert Untersteiner for providing a congenial research atmosphere and the essential financial support, field expenses and computer funds.

Sincere thanks go to Professor Charles Raymond for his many helpful suggestions during the data reduction and for his criticisms of the dissertation. Professor Robert Crosson is to be thanked for commenting on chapter 5. Professors William Budd, John Glen and Edward LaChapelle also helped at various points in the research.

The assistance of all the staff members of the Glaciology Project Office, U.S. Geological Survey, Tacoma, Washington is gratefully acknowledged. The installation, maintenance and continual calibration of the stream gage at the Nisqually River bridge was handled entirely by this office. In particular, I wish to thank Mr Donald Richardson for performing the crucial discharge reductions and for providing me with some of the data presented in chapters 3 and 9. Mr Robert Krimmel gave me needed instruction on the operation of a gravity meter.

Permission to work on the Nisqually Glacier was generously granted by the National Park Service and the assistance of the staff members of Mount Rainier National Park is deeply appreciated. I especially wish to thank Mr Norm Bishop and Mr Dale Thompson for the many hours of work they put in on my behalf.

The gravity measurements were made possible by the loan of a gravity meter from Professor Frank Danes of the University of Puget Sound, Tacoma, Washington. I also wish to thank Professor Danes for his helpful suggestions concerning the gravity measurements and interpretation.

Mr Jerry Hautamaki of the University of Washington Computer Center willingly performed the adjustments of the basic triangulation net, without which the remaining measurements would not have been as accurate.

Manuscripts of several papers in press were provided by Professor Mark Meier and unpublished data on the flow law of ice was furnished by Professor Charles Raymond.

This research was supported by the National Science Foundation through Contract GU-2655 and by the Office of Naval Research through Contract N00014-67-A-0103-0007.

* * * *

The measurement of the motion of a glacier throughout the year is not an easy project and would have been completely impossible for me to make by myself. Although much of the field work was done under very pleasant, sunny conditions, there were many encounters with fog, rain, deep snow, high winds, crevasses, avalanches, cold temperatures, mosquitoes, and even falling logs, not to mention the difficulties of getting out of bed at two or three in the morning.

To each individual who assisted in the execution of the field work, whether in recording theodolite readings or in carrying generators, I wish to express my very sincere thanks. It is hoped that the reader will keep in mind that the measurements reported here were obtained only with the help of many people, all of it without remuneration.

My wife, Susan, assisted on approximately half of all the field work and offered help and encouragement at all stages. To her is reserved a very special "thank-you".

Personal friends and employees of the National Park Service, the U.S.

Geological Survey and the University of Washington provided most of the remaining field assistance, many on more than one occasion: Egels Virsniecks, Imants Virsniecks, Don Richardson, Jeff Corkill, Leslie Rhoades, John Quin, Phil Hill, Ron Roulet, Bob Sprenger, Shirley Sprenger, Alan Thorndike, Sam Colbeck, Ed LaChapelle, Dolores LaChapelle, Bill Mathers, Colin Anderson, Mark Meier, Bob Krimmel, Stan McAbee, Wendell Tangborn, Dick Gadsby, Fraser Just, John Joyce, Mike Nolan, Larry Guilbert, Christy Lea, Norm Bishop, Dale Thompson, Jim Garnett, Robert Hentges, Paul Haertel, Pete Hart, Barbara Lea, Don Immerwahr, Ruth Kilpatrick, Jan Anthony, Mike McGuire, Tim Keliher, Bill Budd, John Reid, Roley Hill, Bob Brown, Viv Viera, John Ungar, Carolyn Ungar, George Hodge, Kathleen Hodge, Paul Wehrenberg, Phil Taylor, Dick Armstrong, Dave McClung, Dave Bell, the Highlander Tavern and my old but faithful car.

In addition, I wish to thank those whose name I have misplaced but whose help is not forgotten.



Chapter 1

INTRODUCTION

Glacier ice is a crystalline solid whose temperature is close to the melting point. Such a solid will deform when stresses are applied to it. The force of gravity applies stresses to the ice of a glacier throughout its mass and as a result the glacier flows. This is termed movement by "internal deformation". This deformation has been investigated experimentally, both in the laboratory and in the field, and the relation between the applied stress and the resulting strain rate, known as the "flow law", has been used to construct models of the flow of glaciers and ice sheets. These models are far from complete but they do predict the general features of the internal deformation of a glacier.

If the temperature at the base of a glacier or ice sheet is at the pressure melting point, the ice can also slide over its bed. This mechanism is termed "basal sliding". It has been observed directly at isolated points under several glaciers (in tunnels or boreholes) and at the margins of others. It is also strongly suggested by the well-known erosive features left behind by glaciers: bedrock polished smooth and marked with long parallel grooves and striations, presumably caused by boulders being dragged over the bedrock by the ice. Indirect evidence comes from vertical velocity profiles determined from many boreholes; extrapolation usually indicates a non-zero velocity at the bed. In very steep temperate glaciers, such as icefalls, sliding could account for almost all of the total motion.

If sliding is significant for a given glacier then clearly the above models of glacier flow are incomplete. Models of the sliding mechanism are also needed. Considerable theoretical work has already been done but direct experimental verification is extremely difficult. Furthermore, the theories

do not agree on which parameters are important and which are not. The problem of basal sliding is perhaps the most crucial aspect of the flow of glaciers which is yet to be solved.

Further insight into the sliding mechanism will possibly have to come through an experimental rather than a theoretical approach. One would attempt to correlate the sliding velocity with some other parameter such as mass balance, temperature, precipitation or run-off. Admittedly, this technique would not prove a direct causal relationship between the two, but it nevertheless might shed some light on the theoretical models of sliding and point out the significant parameters.

In a sense this approach has already been used. The fluctuations in the flow of a glacier on a time scale of hours, days or weeks are invariably attributed to variations in the amount of basal sliding, since significant variations in the applied stress or the flow law, and hence in the internal deformation mechanism, are unlikely to occur on this short time scale. Variations in sliding are usually assumed to be due to "changes in the amount of meltwater at the bed" but there has never been any conclusive verification of this statement, nor is there a satisfactory explanation of how such changes could affect the sliding mechanism.

Changes in the amount of meltwater at the bed are also used to explain the well-known seasonal variations in the motion of a glacier. On this time scale significant variations in the applied stress could take place, due to the raising and lowering of the surface between summer and winter. However, this "loading effect", as we shall call it, would be insignificant except in the case of very thin glaciers.

Seasonal velocity variations of glaciers have been recorded for over a century, but few observations are very detailed. Furthermore, we shall see that the existing data are not entirely consistent with the meltwater

hypothesis.

The objective of this investigation is to study the seasonal variation in the motion of a glacier, to deduce its causes, and, if possible, to make inferences about the basal sliding mechanism. The changes in surface elevation, the changes in surface slope, the accumulation and ablation, the precipitation, the temperature and the run-off will be measured in addition to the surface velocity. A glacier flow model will be used to reduce the surface velocities to sliding velocities at the bed. For this, the thickness of the glacier will have to be determined.

Chapter 2

HISTORICAL REVIEW

2.1. BEFORE 1880

The first time it was realized that glaciers move is undoubtedly buried in antiquity, since it was probably a well-known fact to those who lived near them. For example, Kuhn (1787) talks of a nameless shepherd from Grindelwald, in Switzerland, who apparently had systematically demonstrated this fact. However, it is only in the last twenty years that we are finally starting to understand the flow of glaciers in detail.

Various explanations of this motion have been proposed over the years, but one of the original ideas is none other than the one being investigated here, namely that a glacier slides over its bed. This idea was first suggested by Altmann (1751) and Gruner (1760). Gruner also thought that water thawed from the glacier by the earth's heat might have a lubricating action and thus aid the sliding. These ideas were later expanded by de Saussure (1803) and defended by Escher von der Linth (1821), but were rejected by Hugi (1830) who considered that glaciers move as a result of "internal work" and left it at that. It is interesting to note that de Saussure conceived the idea that the hydrostatic pressure of water imprisoned between the ice and the rock might be able to "float" the glacier and thus enable it to overcome obstacles on the bed.

In the first half of the nineteenth century people such as Venetz (1821) and de Charpentier (1835) were beginning to realize that glaciers in the Alps had had a much greater extent in the past. This led to a renewed interest in glaciers and to the presentation of the "Ice Age Theory" by Agassiz (1837). Agassiz thought that sliding could occur in the lower "parts" of glaciers where the basal temperature was 0°C , but he maintained that the general move-

ment of glaciers could not be due to sliding (Agassiz, 1967). Instead he subscribed to the "dilatation theory", originally proposed by Scheuchzer (1723), in which motion results from the freezing and expanding of water which infiltrates down into a system of capillary cracks and other interstices which are presumed to occur throughout the glacier.

Agassiz was a prolific worker and he recorded many valuable measurements (Agassiz, 1847). The most important of these was the first demonstration that glaciers move fastest in the middle and progressively slower towards the margins. Moreover, it was at his prompting that Ziegler made the first measurements of the seasonal variations in the movement of a glacier. These were done at a single point near the terminus of the Lower Grindelwald Glacier over a period of half a year from November 1842 to May 1843. Despite the fact that only four velocity measurements were made they do reveal a definite minimum in January (Figure 1). This observation interested Agassiz and so in 1845-46 he made a more extensive set of measurements of both the seasonal and the daily variations in velocity on the lower part of the Glacier de l'Aar (Unteraargletscher) in the hope that he could use the results to verify the dilatation theory.

The seasonal observations were made at three points, or "stations", along the glacier: at the station de Brandlamm (at 2.5 km from the 1845 terminus), at the station de Trift (at 4.5 km), and at the station de l'Hôtel des Neuchâtelais (at 7.2 km, just below the confluence of the Unteraargletscher and the Finsteraargletscher). Initially, during the summer of 1845, Agassiz made measurements on transverse profiles of 20 points at the upper station and 11 points at the lower station, but for the rest of the time only one point at each station was measured. The results are shown in Figures 2 and 3. The upper two points were measured approximately every month but the lower one was measured only four times.

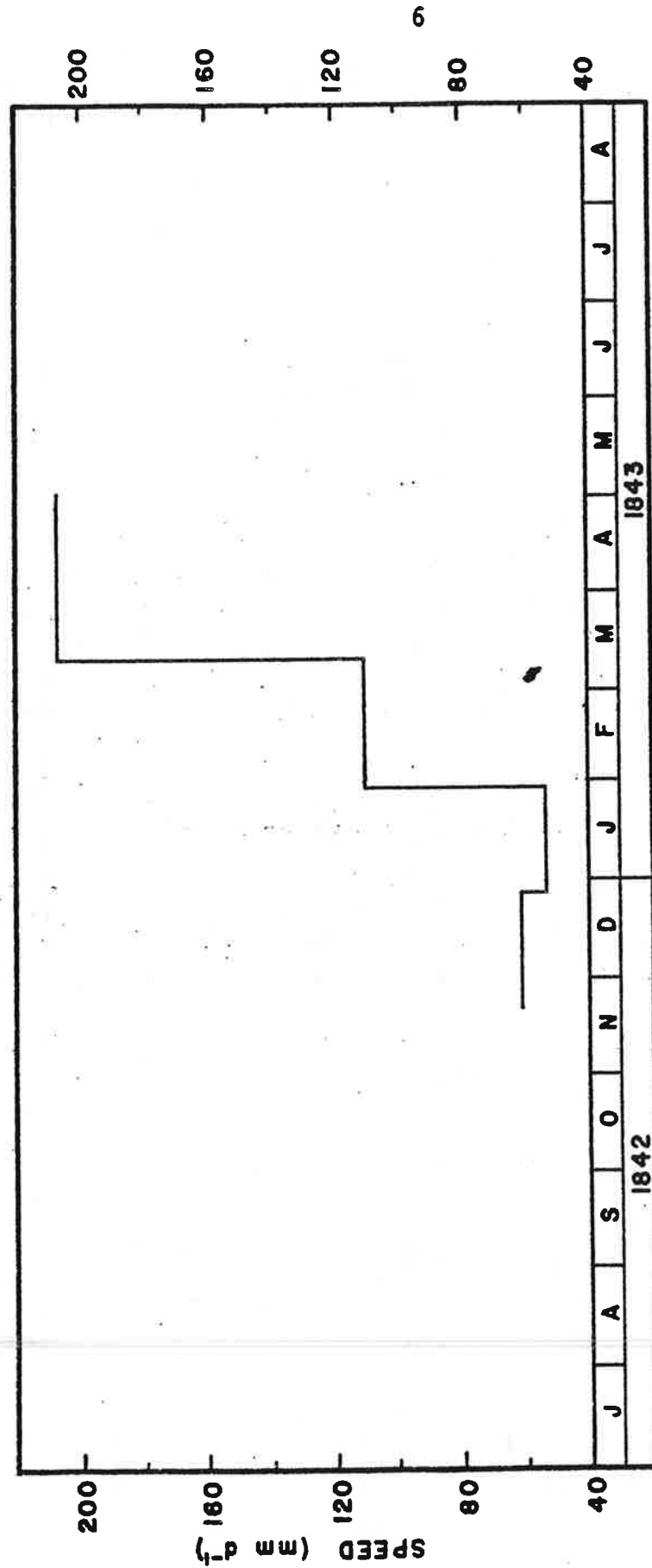


Figure 1. The first measurements of seasonal variations in the movement of a glacier. These were made by Ziegler from November 1842 to May 1843 at a single point near the terminus of the Lower Grindelwald Glacier, Switzerland. (from Agassiz, 1847)

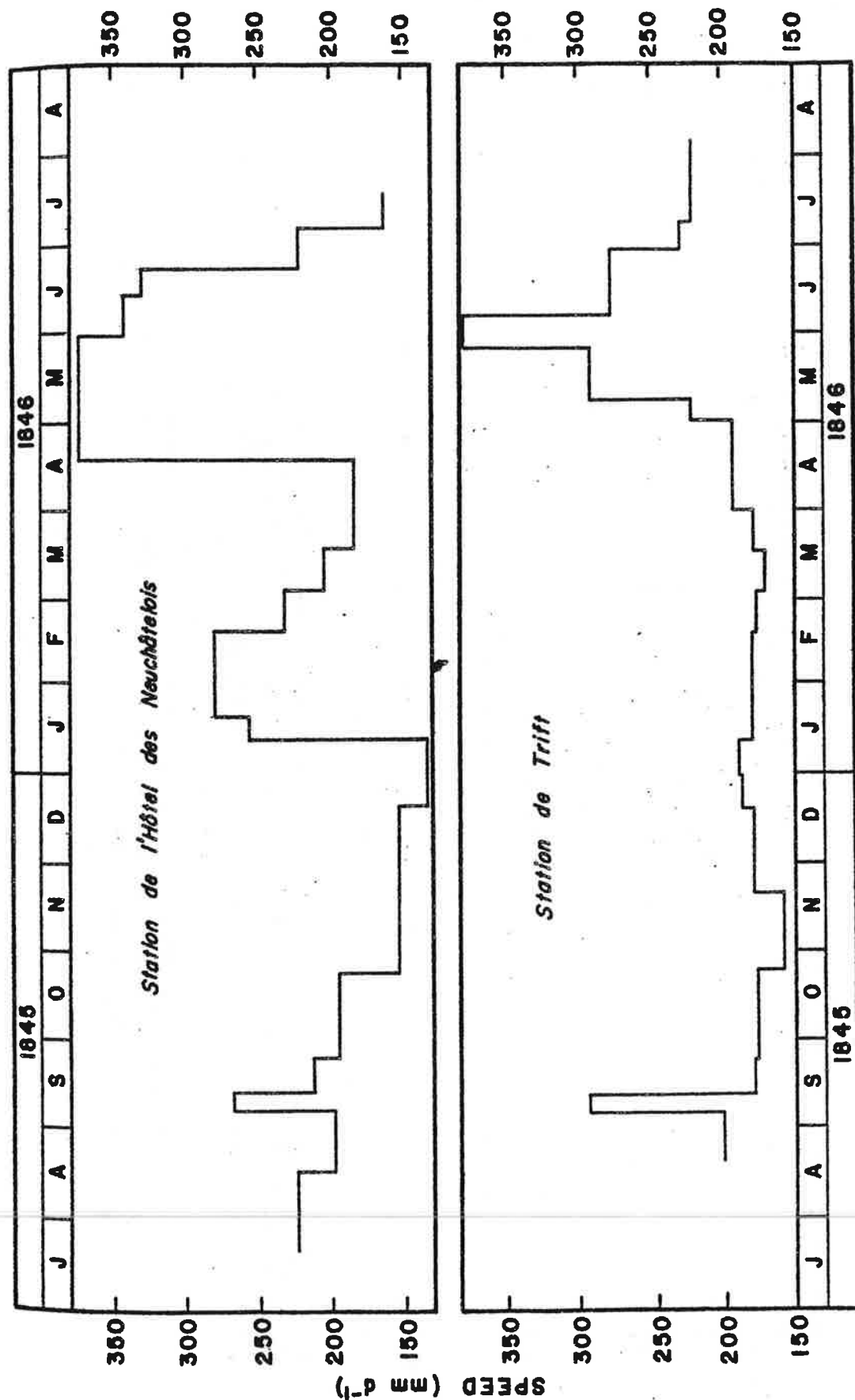


Figure 2. Agassiz's measurements of seasonal variations in the movement of the Unteraargletscher, Switzerland. The station de l'Hôtel des Neuchâtelais was 7.2 km from the 1845 terminus and the station de Trift 4.5 km. (from Agassiz, 1847)

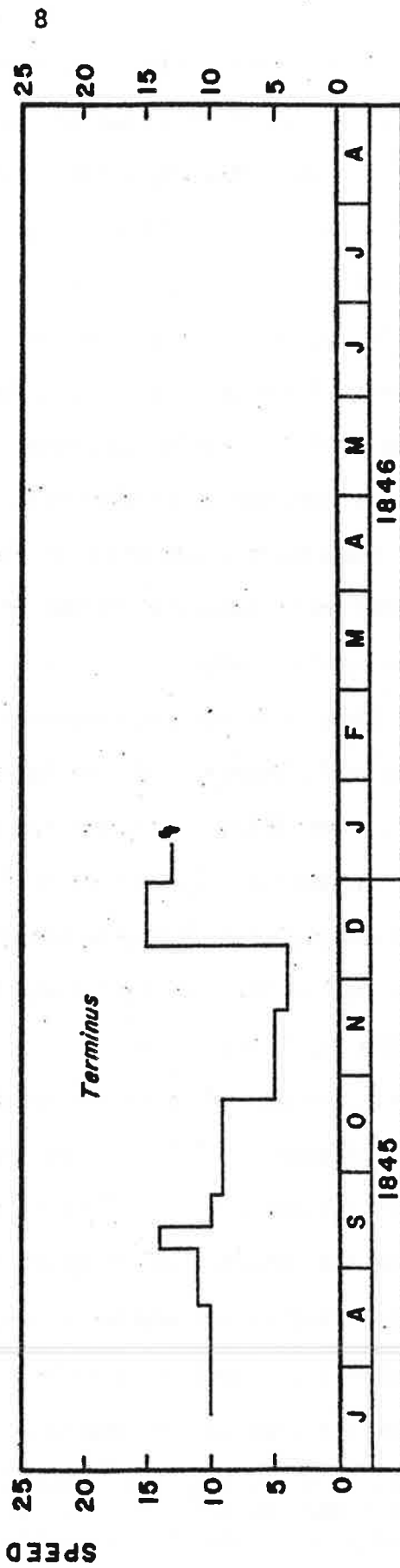
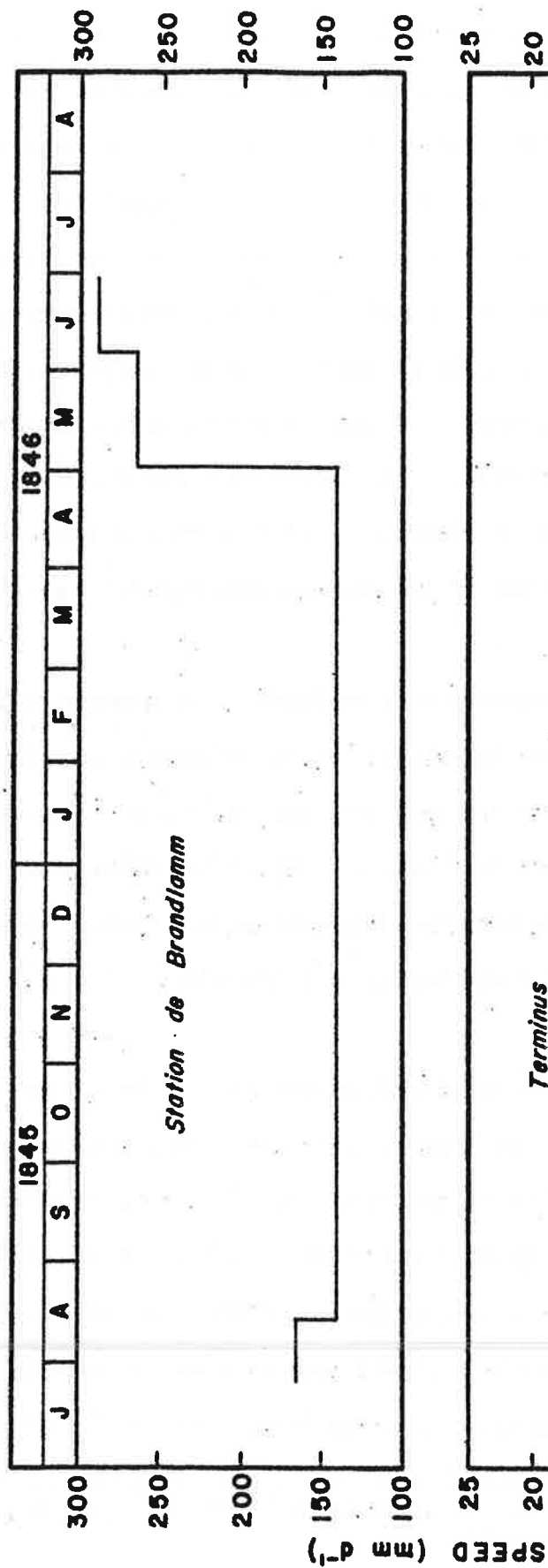


Figure 3. (Upper half) Agassiz's measurements of seasonal variations in the movement of the station de Brandlamm, 2.5 km from the terminus of the Unteraargletscher. (from Agassiz, 1847)

Figure 4. (Lower half) Desor's measurements of seasonal variations in the rate of advance of the terminus of the Unteraargletscher. (from Agassiz, 1847)

Agassiz also notes (Agassiz, 1847) some measurements made by Desor on the rate of advance of the terminus of the Glacier de l'Aar from July 1845 to January 1846, at approximately monthly intervals (Figure 4). The observations were terminated because of heavy snowfall. Desor also measured the advance of the terminus on a daily, and sometimes an hourly, basis in the summers of 1844 and 1845 (Figure 5), and in 1845 Agassiz made measurements roughly every twelve hours of the position of a stake at the station du Pavillon (near the station de Trift). At the same time, and also at the Pavillon, he measured the motion at the margin of the glacier; these results, along with the measured air temperature, are shown in Figure 6. It is not clear whether the marginal motion is actually sliding of the ice past the rock or just motion of a stake near the edge.

From these data Agassiz concludes that the speed is a maximum in the spring and early summer. He attributes this to the abundance of meltwater at this time, which fills the "capillary cracks", freezes, expands, and then causes an increase in movement of the glacier. As winter approaches the glacier gradually slows down, to less than the mean annual speed; this he attributes to the "stiffening" of the ice as it gets colder and there is less water in the capillary cracks*.

Agassiz was not the only person at work on glaciers at this time. The Scottish professor, J.D. Forbes, was busy on the Glacier des Bois and the Glacier des Bossons (in the Chamonix region of France) gathering evidence to demonstrate the "plasticity" of glacier ice (Forbes, 1843a, 1843b, 1846). Forbes subscribed to the viscous theory of glacier motion, originally suspected by Bordier (1773) and later by Hall (1841) and which we now know to be more or less correct (ice can be thought of as a non-linear viscous fluid). Forbes

* According to Tyndall (1896), Agassiz later proved the dilatation theory to be incorrect when he found that the interior temperatures of glaciers were not significantly below the freezing point.

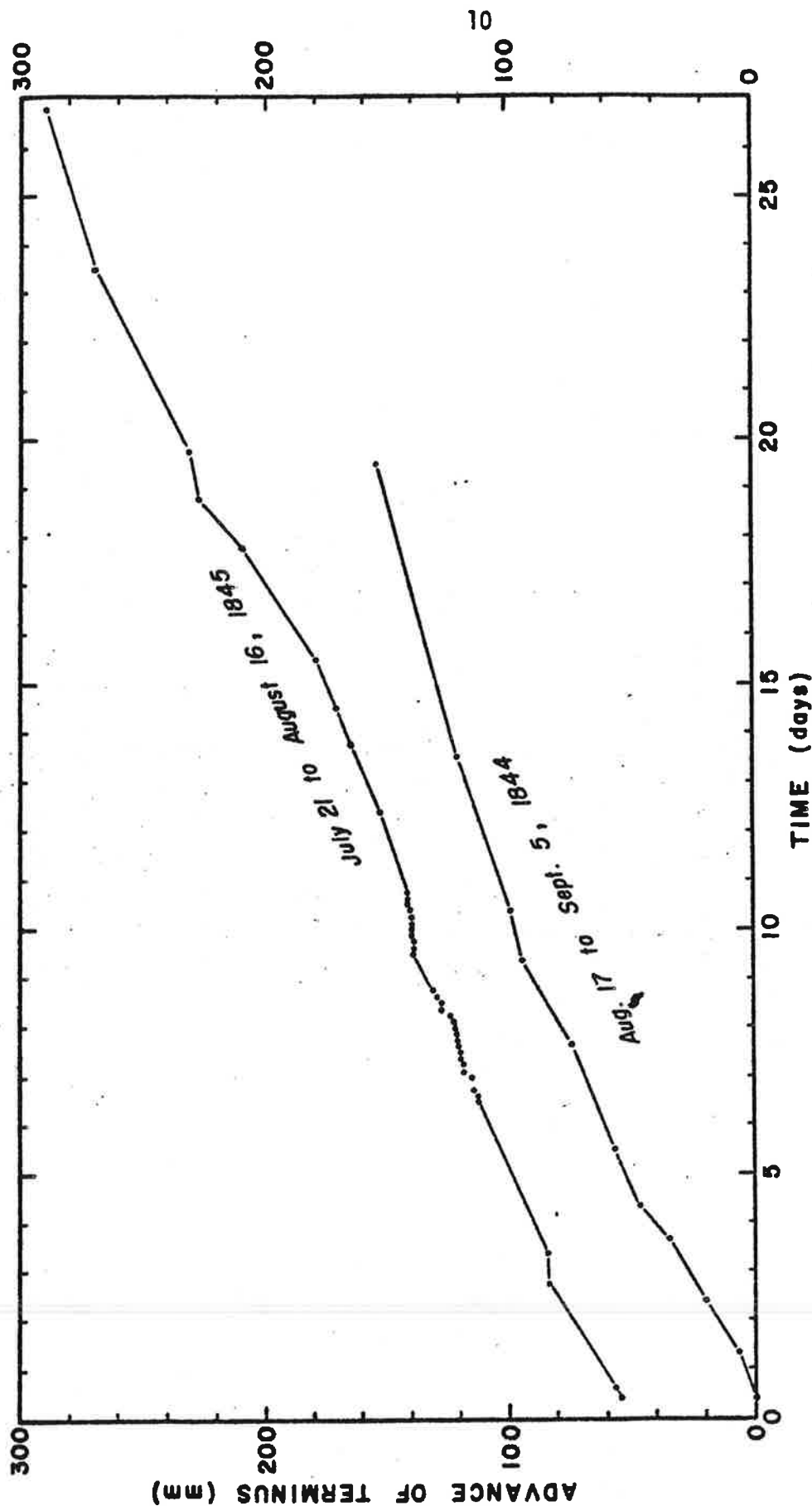


Figure 5. Desor's measurements of the advance of the terminus of the Unteraargletscher during the summers of 1844 and 1845. (from Agassiz, 1847)

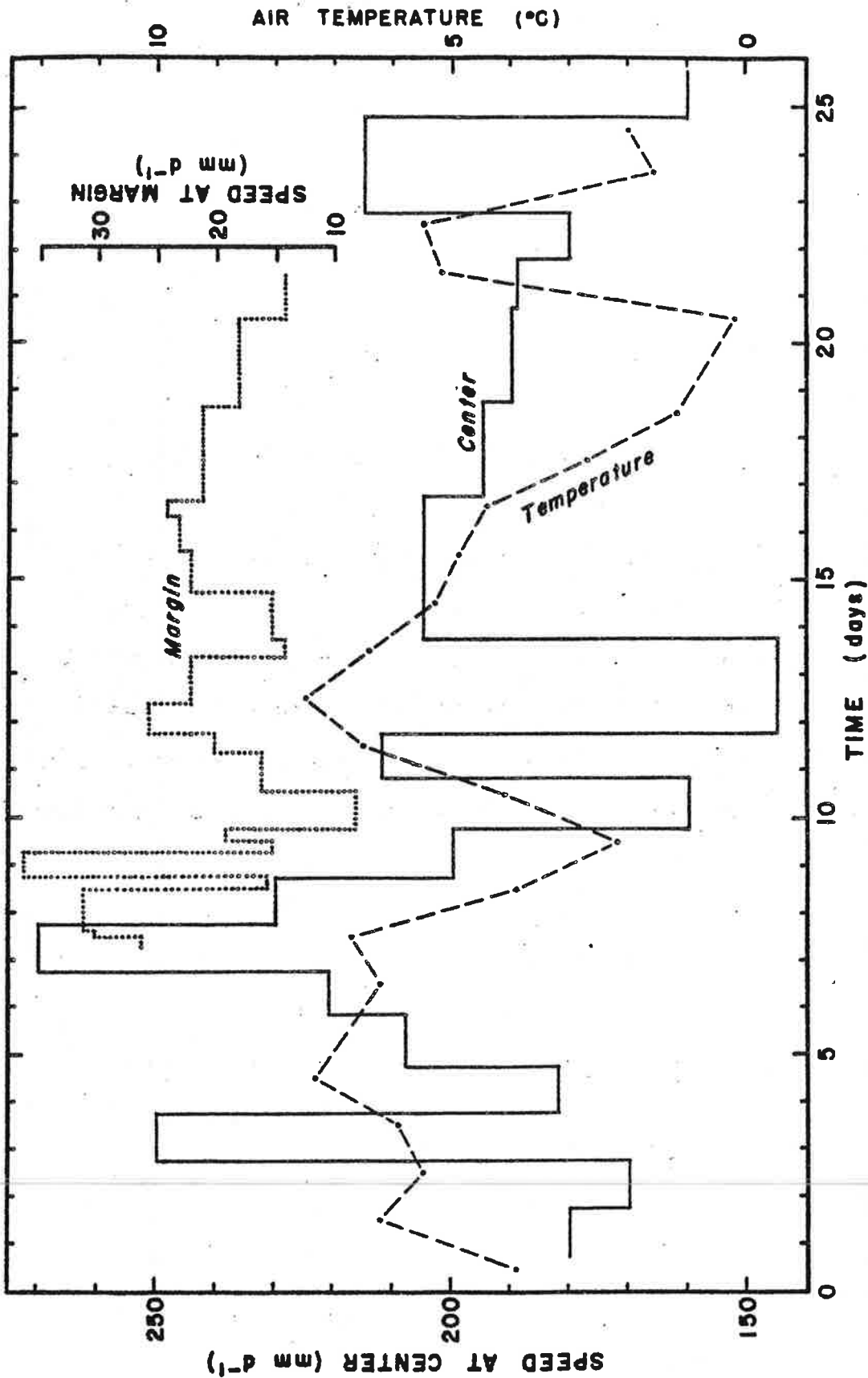


Figure 6. Agassiz's measurements of daily and hourly fluctuations in the movement of the station du Pavillon, Untervargletscher. Two points were measured, one at the center and one at the margin of the glacier. The measured air temperature is also shown. (from Agassiz, 1847)

was probably led to believe in the viscous theory when he realized that if glaciers slid as a solid body they would be stopped at the first constriction in the valley walls; in other words, Forbes made the rather obvious observation that glaciers "mold" themselves to the shape of the valley.

During the year 1844-45, a year *before* Agassiz's measurements, Forbes had his trusted guide, A. Balmat, measure the movement of four points on these glaciers roughly every month. The results are shown in Figures 7 and 8, along with the average air temperature from nearby towns. The variation is similar to that found by Agassiz. Forbes noted that the magnitude of the variation increased with decreasing elevation and he asserted that the data provide a proof of a principle, made by him in 1842, that "the motion of the ice is more rapid in summer than in winter, in hot than in cold weather, and especially more rapid after rain, and less rapid in sudden frost" (Forbes, 1846, p. 187). This statement was made before Ziegler's measurements and so it was probably just a proposition and not an experimental fact at the time. Forbes considered the seasonal variations in velocity to be a result of both temperature and the amount of water available at the surface. The more "saturated" the ice became with water, the lower its viscosity and the faster it moved. He claimed to find a correlation between velocity variations and the amount of water discharging from the terminus; this was based, however, on subjective estimates of the stream level.

In 1862 Hopkins published his theory of the motion of glaciers (Hopkins, 1862). He allowed both sliding and internal deformation, terming the latter the "pressure theory". According to Hopkins, the motion of a glacier is a result of "internal pressures and tensions" becoming so great as to result in "dislocations": tensions give rise to "open fissures", compressions to a "crushing" or breakdown of the crystal structure and tangential forces to a sliding of one element past another. This is a primitive form of modern

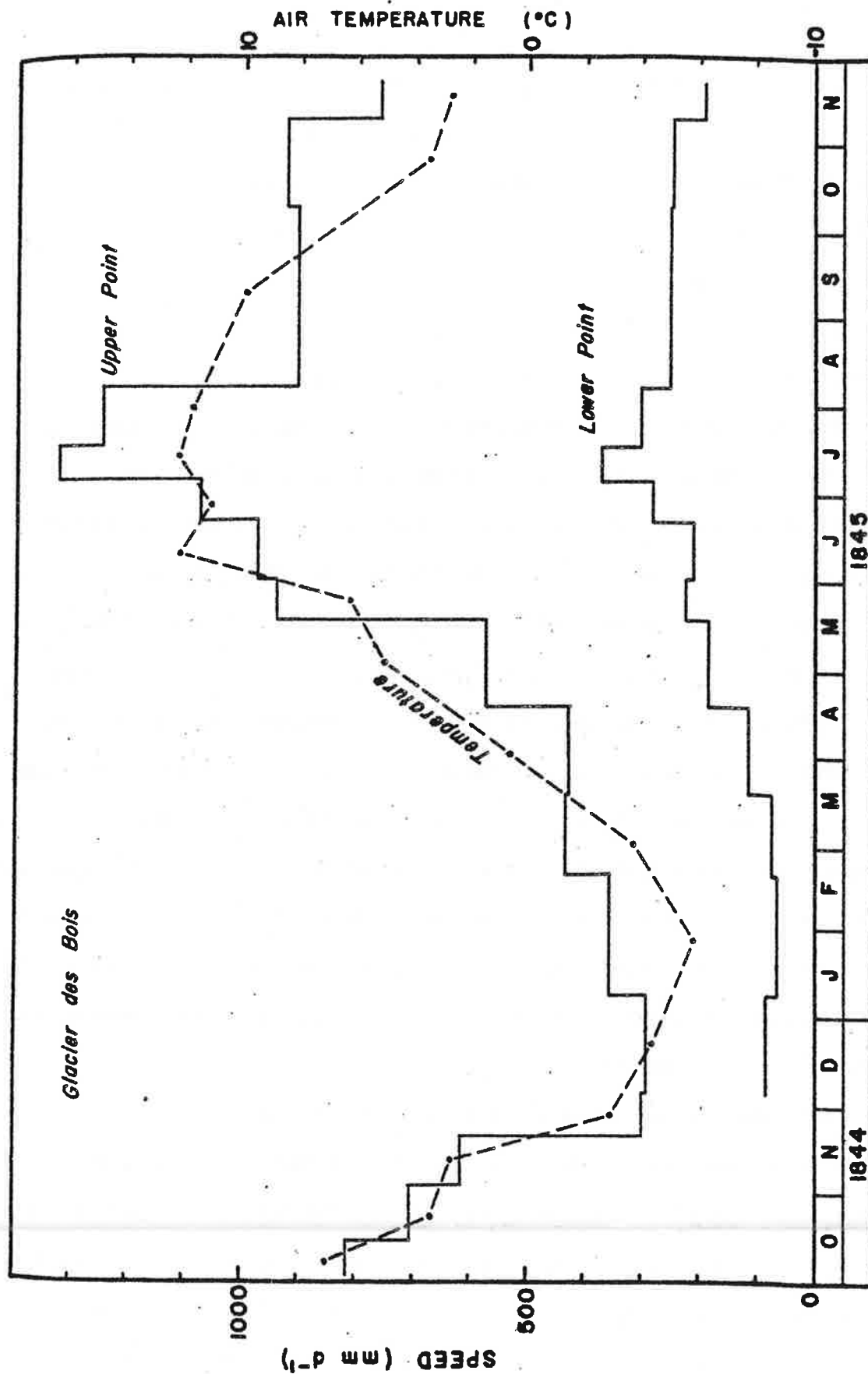


Figure 7. Forbes' measurements of seasonal variations in the movement of the Glacier des Bois, France. The average air temperature from nearby towns is also shown. (from Forbes, 1846)

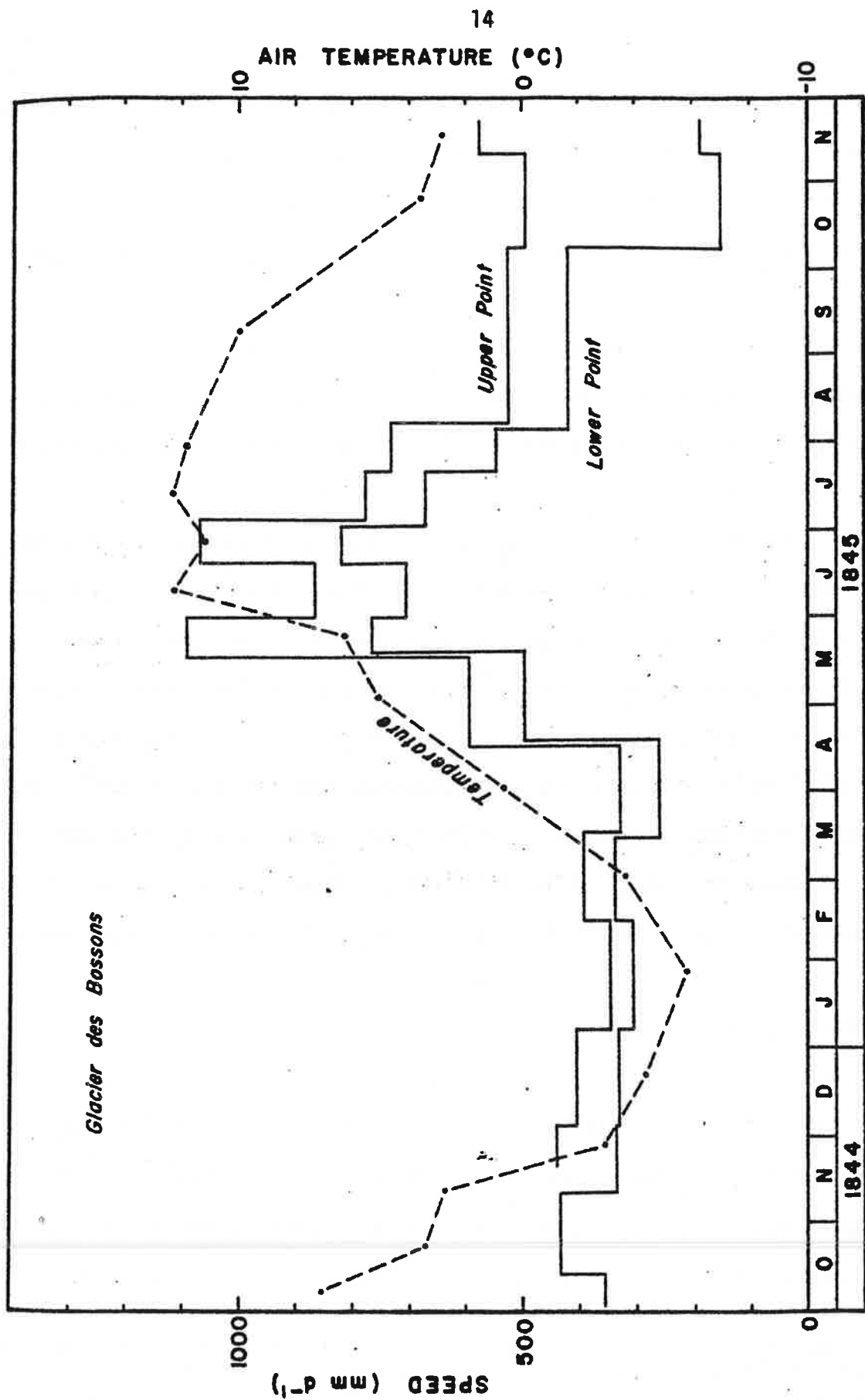


Figure 8. Forbes' measurements of seasonal variations in the movement of the Glacier des Bossons, France. The average air temperature from nearby towns is also shown. (from Forbes, 1846)

glacier mechanics. Hopkins was also the first to suggest that the process of regelation was "essential to the uniform sliding of glaciers".

Tyndall (1876, 1896) also made some velocity observations on the Mer de Glace in December of 1859. With twenty-one stakes distributed in two profiles he found the winter velocity to be roughly 50% of the summer velocity (determined at the same profile two years earlier). Tyndall unfortunately made his velocity measurements over a twenty-four hour period, despite the fact that Agassiz (1847) had already shown that velocities could change by 50% over such a short time interval*.

The measuring technique used by Tyndall and Agassiz was to use a theodolite to establish a vertical plane between two fixed points, one on each side of the glacier. An assistant taped the distance from the stake to this plane. No errors are given but the accuracy was probably a few centimeters. Forbes' method was similar, except no theodolite was used.

Tyndall and Forbes also made the first measurements of the rate of flow as a function of depth (Shumskii, 1964, p. 310), Tyndall on the side wall of the Mer de Glace and Forbes on the front wall. When extrapolated to bedrock both measurements gave a sliding velocity of about 25% of the surface velocity.

2.2 1880 TO 1914

Tyndall did not subscribe to the viscous theory of glacier motion. Instead he had his own "regelation theory", in which ice would fracture under tension, the cracks being healed by pressure melting and refreezing. This idea was disposed of, however, by a series of experiments done in the late nineteenth century (for example, Main, 1888), in which it was shown that ice

* The danger of equating long period velocities to short period ones was substantiated by de Seue (1876) on Østerdalsisen, Norway. He found that the movement over a period of hours was jerky and irregular, so much so, in fact, that he recorded a backwards movement on one occasion.

could yield, rather than fracture, under a tensile stress. The viscous theory of glacier motion was accepted and elaborate, long term studies of the velocity field of a glacier were done around the turn of the century to test this theory: Blümcke and Hess (1899) on the Hintereisferner, Mercanton (1916) on the Rhonegletscher, and Finsterwalder (1897) on the Vernagtferner.

Seasonal variations were measured as part of these studies, the best known observations being those of Blümcke and Finsterwalder (1905). These were done at 18 stakes on the tongue of the Hintereisferner, Austria, between 1900 and 1904 (Schimpp, 1958, p. 302). Apparently the winter speed was not actually measured (Deeley and Parr, 1913, p. 95); instead they measured the summer speed relative to the mean annual speed, as a function of distance along the glacier (Figure 9).

It was only along the lower third of the tongue that the summer speed exceeded the (implied) winter speed; in the upper two-thirds the winter speed was greater. The point where the two speeds are equal is at an altitude of 2530 m, well below the present equilibrium line*. Blümcke and Finsterwalder's reason for this is worth quoting:

"The driving force of glacier movement is manifestly gravity, and the pressure of the névé layers produced through it. One resistance to glacier movement proceeds from the interior friction of the ice-mass and from friction on the glacier bed. The velocity-condition of the glacier originates from the cooperation of driving force and resistance; the winter acceleration of movement in the upper parts is in the first place attributable to the increased névé pressure in the winter; while the summer acceleration of movement in the lower parts must be traced to lessened friction-resistance, in consequence of penetration of the ice and glacier-bed by melting water."
(Deeley and Parr, 1914, p. 163)

Probably these measurements led Hess (1933, p. 73) to conclude that a wave of

* Lliboutry (1965, p. 624) places the "névé line" at an altitude of 3100 m, about 5.5 km from the terminus (year not specified). In 1952-54, Schimpp (1958, p. 308) found the equilibrium line to be at 2950 m, about 5 km from the terminus. The Hintereisferner, however, has retreated considerably since 1900 and so the equilibrium line could have been lower at the time of Blümcke and Finsterwalder's work.

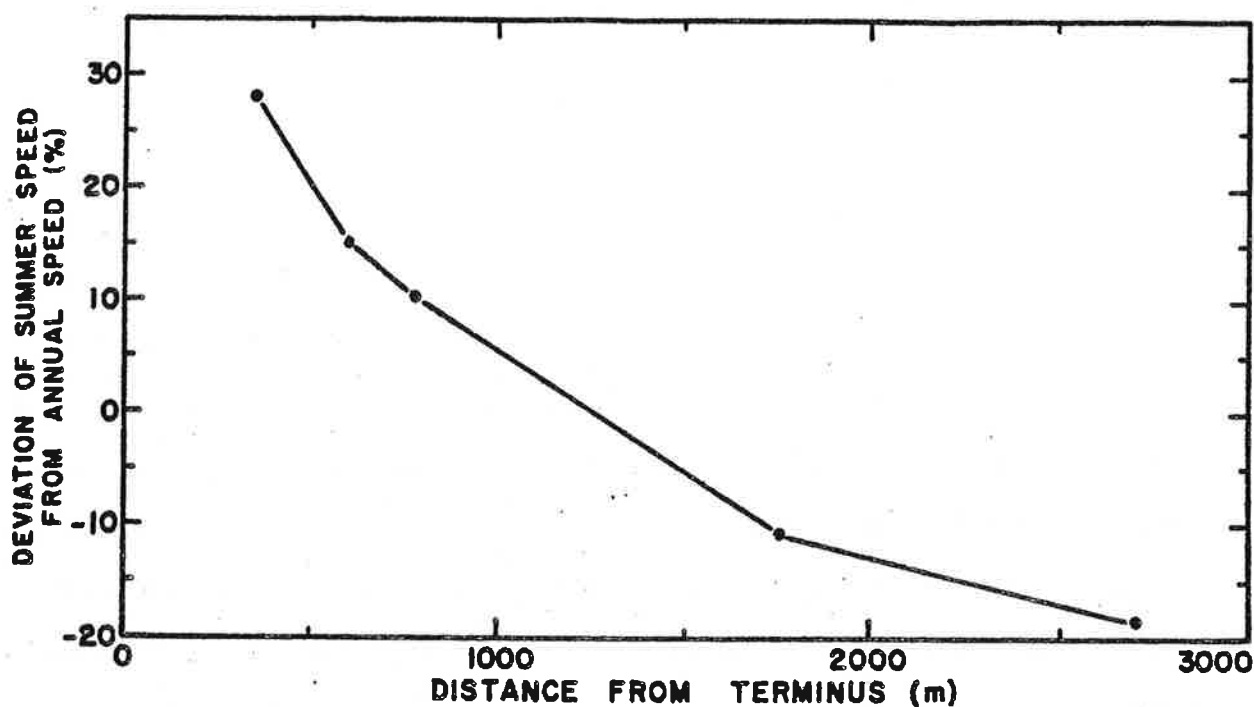


Figure 9. Blümcke and Finsterwalder's measurements of seasonal variations in the movement of the Hintereisferner, Austria, from 1900 to 1904. (from Deeley and Parr, 1913)

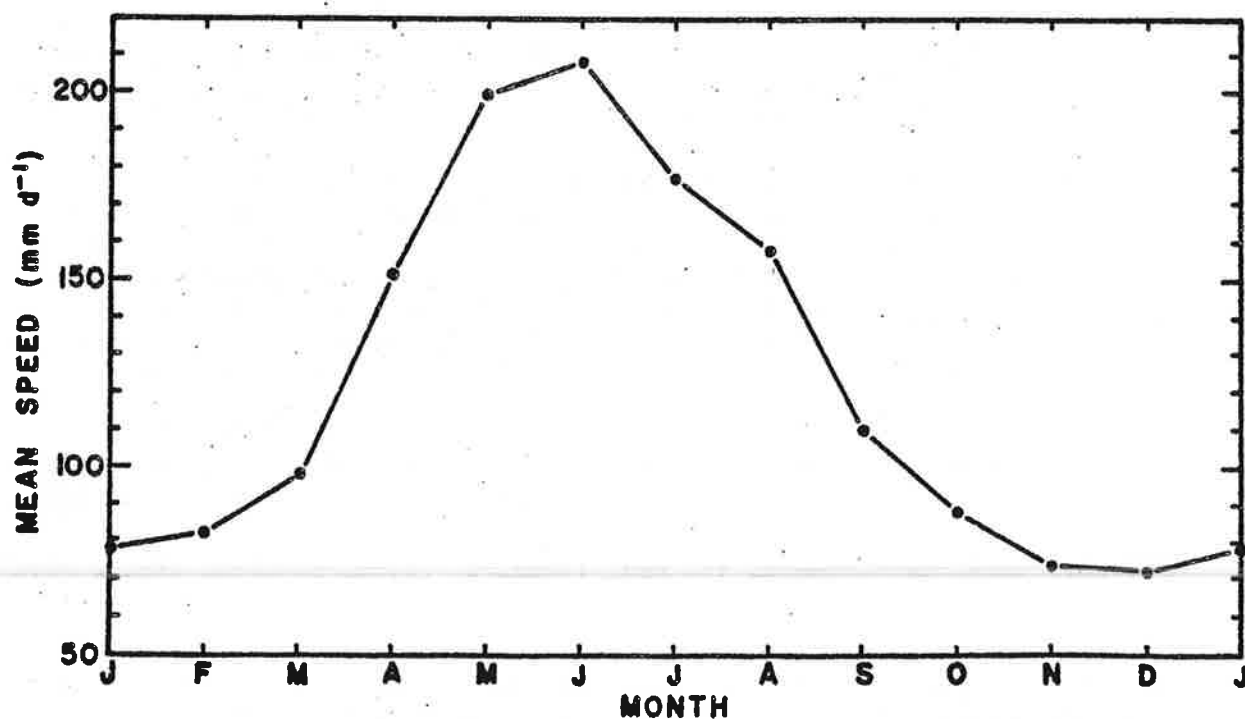


Figure 10. Lütischg-Lotscher's measurements of seasonal variations in the movement of a point near the terminus of the Upper Grindelwald Glacier (average of all seven years). (from Hess, 1933)

velocity maximum travelled down the glacier starting in the accumulation area in the winter and ending at the terminus in the summer.

As part of their investigation, Blümcke and Hess made a number of thermal borings through the glacier. On one profile, seven holes were considered to have reached bottom, and Deeley and Parr (1913) used data from them to estimate the rate of slipping along the bed. They obtained values between 16% and 69% of the surface velocity, depending on the reduction method. The slip at the side of the glacier was found to be about 25% of the center velocity. Some boring rods left in these holes were rediscovered in 1931 and Hess (1939) found that in the intervening 30 years the bottom of the glacier had moved 90.2% as far as the surface (Shumskii, 1964, p. 315).

By the early 1900's it was becoming generally accepted that glaciers moved by two mechanisms, sliding on their bed and differential motion within the ice, and that the thickness and surface slope were the primary controlling parameters. Ice was considered to be a Newtonian fluid of high viscosity and much of the laboratory and field experiments performed at this time were directed at finding the coefficient of viscosity of ice.

Mathematical models of glacier flow were also developed. Assuming a constant viscosity ν and an infinitely wide plane bed, Weinberg (1906) showed that the Navier-Stokes equation could be integrated to give

$$h = \sqrt{\frac{2\nu s}{\rho g \sin \alpha}} \quad (1)$$

where s is the surface speed, ρ is the density of the ice, g is the acceleration of gravity, α is the surface slope, and h is the thickness of the glacier. This formula has often been used to calculate h or ν given the other parameters (Deeley and Parr, 1913; Somigliana, 1925; Lagally, 1929; Hofmann, 1958). However, it was originally derived by Deeley (1895)

by considering the steady flow of a viscous fluid through a capillary tube, which is mathematically equivalent to Weinberg's model.

On the other hand, Deeley and Parr (1914) recognized the importance of sliding and that very little was known about it, a fact which plagues glaciology to the present day. They postulated two mechanisms for sliding: pressure melting for small obstacles and viscous deformation for large obstacles. Ice pressing on the upstream side of an obstacle would be melted and the water would flow around the obstacle and refreeze on the downstream side, where the pressure is lower. In this way ice could move past obstacles on the bed. They also realized that the thermal conductivity of the obstacle would influence the motion, as heat would have to be conducted back through the obstacle from the downstream side, otherwise the process could not be maintained. The pressure melting mechanism would therefore not work for large obstacles since the time for heat to flow through the obstacle would be prohibitively long. The resistance to flow of a large obstacle is thus "a purely viscous one", the glacier having "to change its form to accomodate itself to the bends and larger irregularities of its channel".

Deeley and Parr made measurements in the laboratory of the movement of a glass bar, under load, through a block of ice and of the slip of a piece of ice across a flat stone surface. They found, in the second experiment, that slip would occur only when the temperature was within 0.1°C of the freezing point. Using the results of these experiments, some intuitive reasoning, and conical projections as the model of a glacier bed, Deeley and Parr conclude the velocity of slip should be proportional to the shear stress on the bed and to the thickness of the glacier.

2.3 1914 TO 1954

These principles of dynamic glaciology developed in the early 1900's have since been refined considerably, largely due to the realization that ice has a non-linear rather than a linear viscosity (Glen, 1953, 1955), and mathematical models of glacier flow have been developed (Nye, 1951, 1952, 1953, 1957, 1965). Measurements on glaciers have also been refined.

From 1921 to 1928 the seasonal and shorter term variations in the movement of a single point near the terminus of the Upper Grindelwald Glacier, Switzerland, were continuously recorded with a "gletscheruhr", or "glacier clock"^{*} (Lütschg-Lotscher, 1944). Rapid acceleration occurred in the spring, followed by a more gradual decrease through the summer, autumn, and winter (Figures 10 and 11). Large fluctuations on a time scale of days or weeks were also apparent, particularly in the spring and summer^{**}. Lliboutry (1965) attributed these to changes in the amount of water at the glacier bed.

The winter velocity in the accumulation area was found to exceed the summer velocity on the Claridenfirn (Streiff-Becker, 1938) and on the Great Aletsch Glacier (Haefeli, 1944)^{**}. Fluctuations at approximately twenty minute intervals were recorded by Washburn and Goldthwait (1937) on the South Crillon Glacier, Alaska. They also found that the day-time speed was greater than the night-time^{**}.

From 1938 to 1939 Pillewizer measured the seasonal variations in the flow of the Mittelbergferner, Austria (Pillewizer, 1949). The results for his upper two profiles are shown in Figure 12. A third profile, at the top of the

* Usually a wire running from a point on the glacier over a pulley to a weight. Movement of the glacier rotates the pulley; this can be recorded on a chart drive.

** It was pointed out to the author by M.F. Meier that many glaciologists consider experimental artifacts to have caused part of these velocity fluctuations. Lütschg-Lotscher's results, however, will be retained and mentioned later since their omission does not change the conclusions reached.

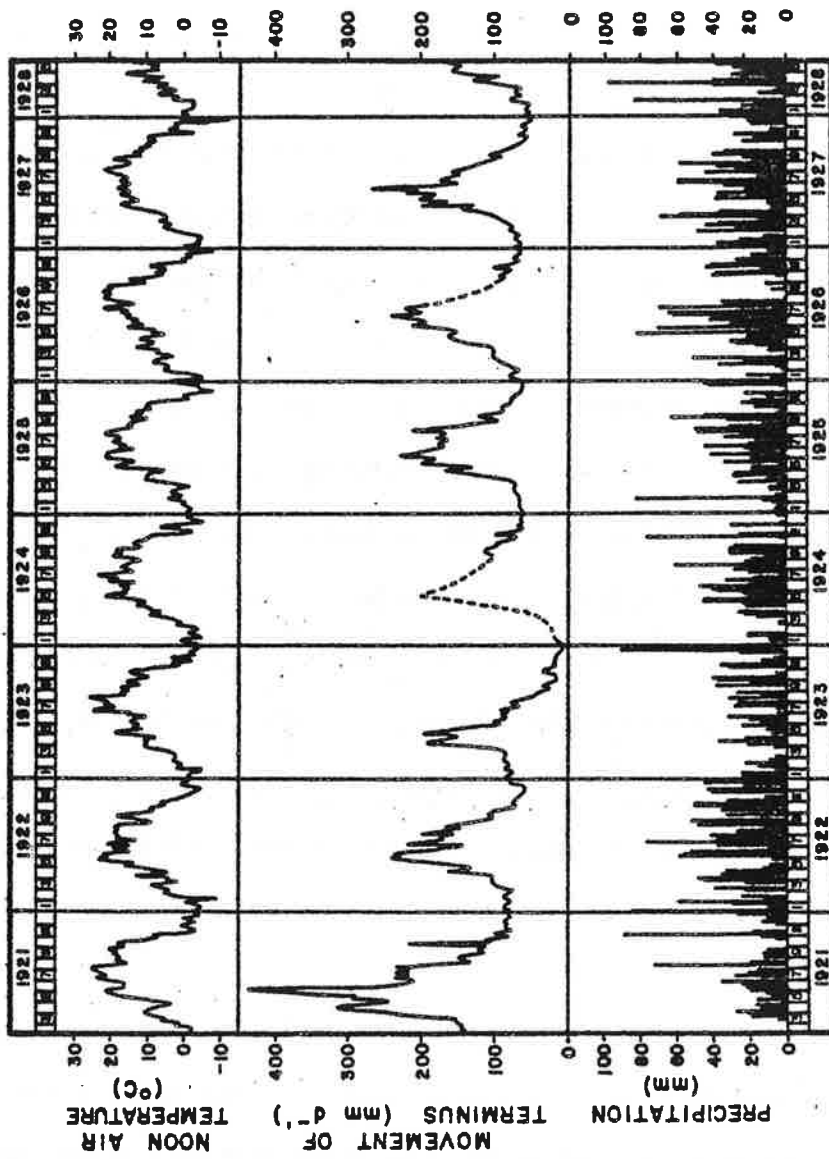


Figure 11. The continuous record obtained by Lüttschg-Lotacher of the movement of the terminus of the Upper Grindelwald Glacier from 1921 to 1928. The noon air temperature and daily precipitation at Grindelwald are also shown. (from Lliboutry, 1965)

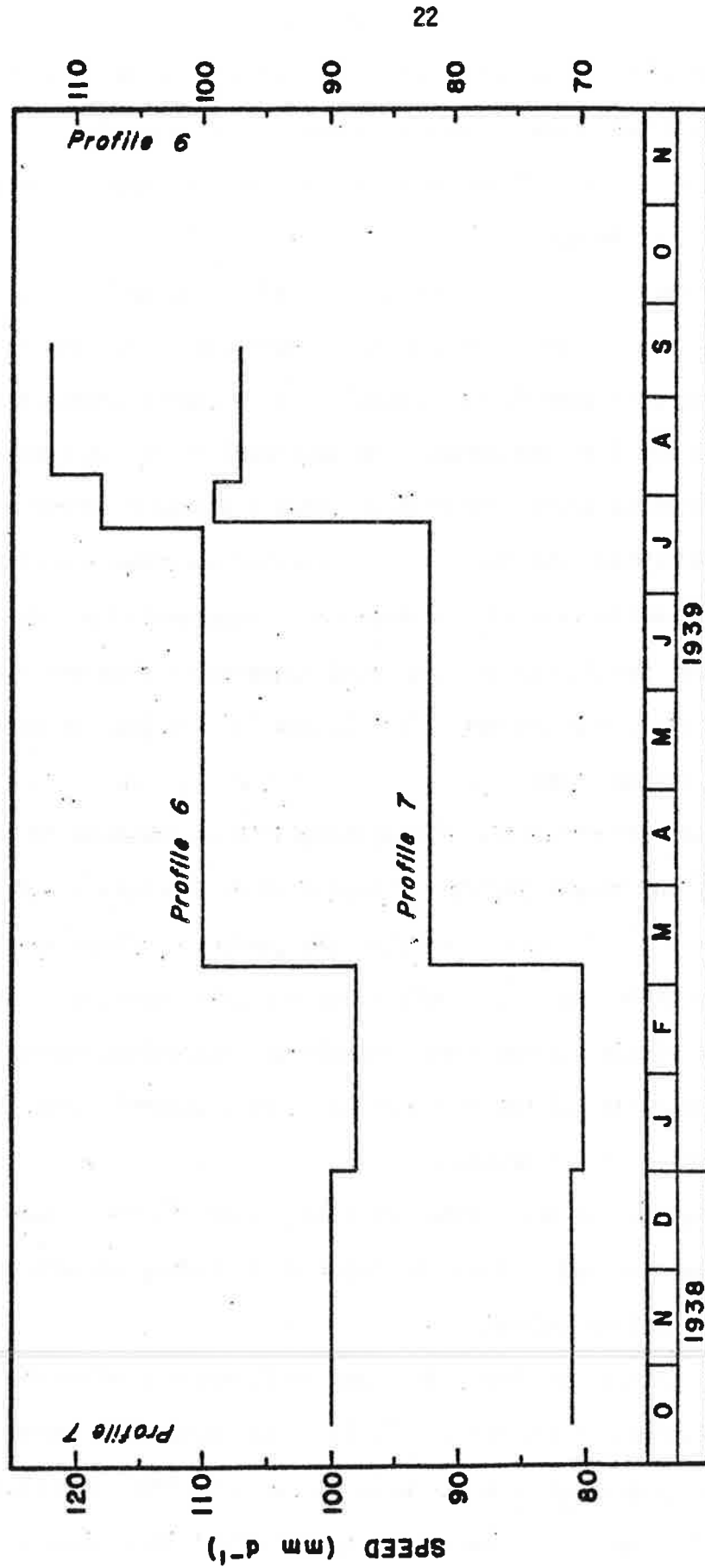


Figure 12. Pillewizer's photogrammetric measurements of seasonal variations in the movement of Mittelbergferner, Austria. Profile 6 was further down-glacier than Profile 7 (note change of origin between curves). The point on each profile with the greatest speed was used for the plot as this should be the most accurate. (from Pillewizer, 1949)

icefall, is not shown because no significant variations through the year were observed. These measurements were made photogrammetrically. It is questionable whether or not differences of millimeters per day can be obtained reliably with this technique (Mercanton, 1950).

For three weeks in August 1949, Battle made daily and weekly measurements of the surface velocity of Frøya Gletscher, northeast Greenland (Battle, 1951). The observations were made with a theodolite on 8 stakes arranged in two profiles, 6 on one and 2 on the other. He concluded: (a) an overall decrease in speed seemed to be correlated with an overall decrease in air temperature during the same period, (b) the decrease in speed occurred sooner in the upper profile, (c) the motion during a 24-hour period was distinctly discontinuous and in many cases the discontinuities were synchronous from one stake to the next (the area was crevassed very little), and (d) the glacier appeared to move faster in the day-time.

Direct observations of the sliding of glaciers were made in this period by Carol (1947) and McCall (1952). Carol used deep marginal crevasses to work his way to a point about 50 m below the surface. There he observed a sliding velocity of 370 mm d^{-1} . McCall, on the other hand, drilled a tunnel through a small cirque glacier (Vesl-Skautbreen, Jotunheim, Norway). At the head of the tunnel the ice was found to be sliding smoothly over the bedrock, with no detectable daily fluctuations.

Gerrard, Perutz and Roch (1952) drilled a borehole 137 m deep in the Jungfraufirn, Switzerland. They concluded that sliding accounted for about one half of the surface motion.

During the summers of 1952, 1953, and 1954, Meier studied the flow of the Saskatchewan Glacier, Canada (Meier, 1960). He found that summer velocities were significantly greater than the mean annual velocities and that the percentage deviation depended on position, varying from about zero near the firn

limit to about 20% 3 km further down-glacier. The short interval variations were also studied. In 1952, three stakes were measured once a day for 22 days and very pronounced fluctuations were found. In 1953 five stakes were measured every 12 hours for 18 days and this time the theodolite was placed inside a tent to protect it from wind and sun. The results, shown in Figure 13, are probably the most accurate short interval velocities obtained until very recently (see Harrison and Lee, 1971).

Meteorological observations were made concurrently with the 1953 velocity observations. The velocities showed large and sudden variations and did not exhibit any obvious correlation with the meteorological data. Meier found that a linear relationship between air temperature and velocity was statistically not significant. The precipitation possibly might have had some effect, as the large velocity fluctuation shown by all stakes on 30 and 31 August occurred at the time of the heaviest rainfall. He concluded "that the total flow is built up from many minor jumps or jerks along shearing planes", and that the jerky motion was probably not due "to the erratic opening or closing of crevasses".

Meier also showed that the amplitude of the velocity fluctuations decreased with increasing period of observation; this velocity "dispersion spectrum" is reproduced in Figure 14. For periods of one day or greater the deviation was inversely proportional to the logarithm of the time interval. Meier's velocity values are all accompanied by an estimate of the error in their measurement.

In the same years that Meier was doing his research, Schimpp was recording the seasonal variations in velocity of the Hintereisferner, Austria (Schimpp, 1958, 1960). Measurements were done with a theodolite every other month, on the average, from autumn 1952 to autumn 1954 at 54 points on 11 transverse profiles. The published results (5 profiles only) are shown in Figure 15. The

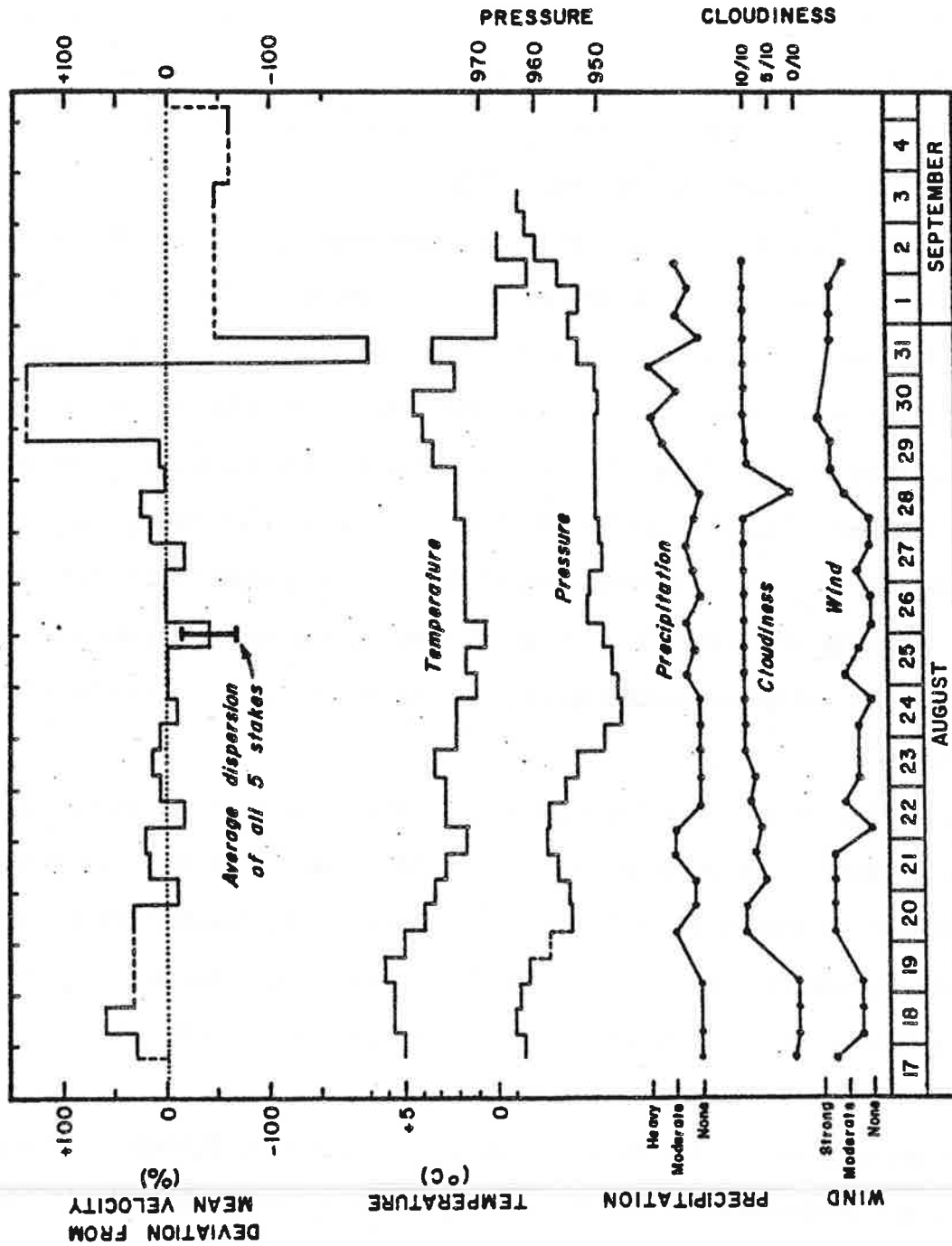


Figure 13. Meier's measurements of hourly fluctuations in the movement of Saskatchewan Glacier, Canada. Meteorological parameters measured concurrently with the velocity observations are also shown. (from Meier, 1960)

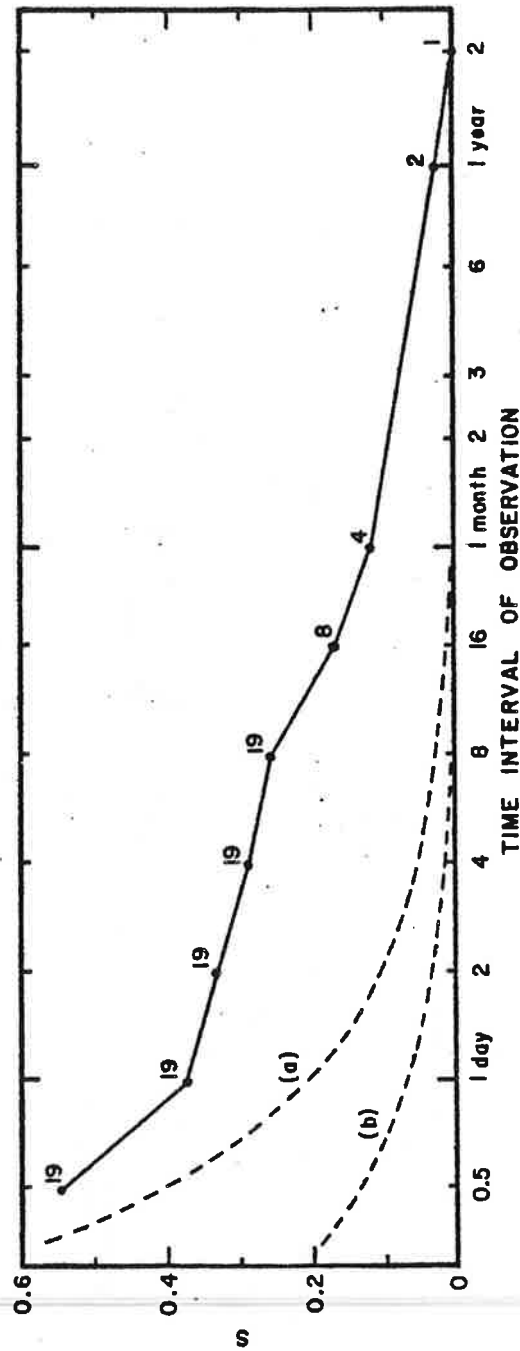


Figure 14. The velocity dispersion spectrum obtained by Meier (1980). s is the standard deviation of any one measurement from the 2-year average, divided by the 2-year average velocity. (a) Standard deviation, crudest procedure. (b) Standard deviation, refined procedure.

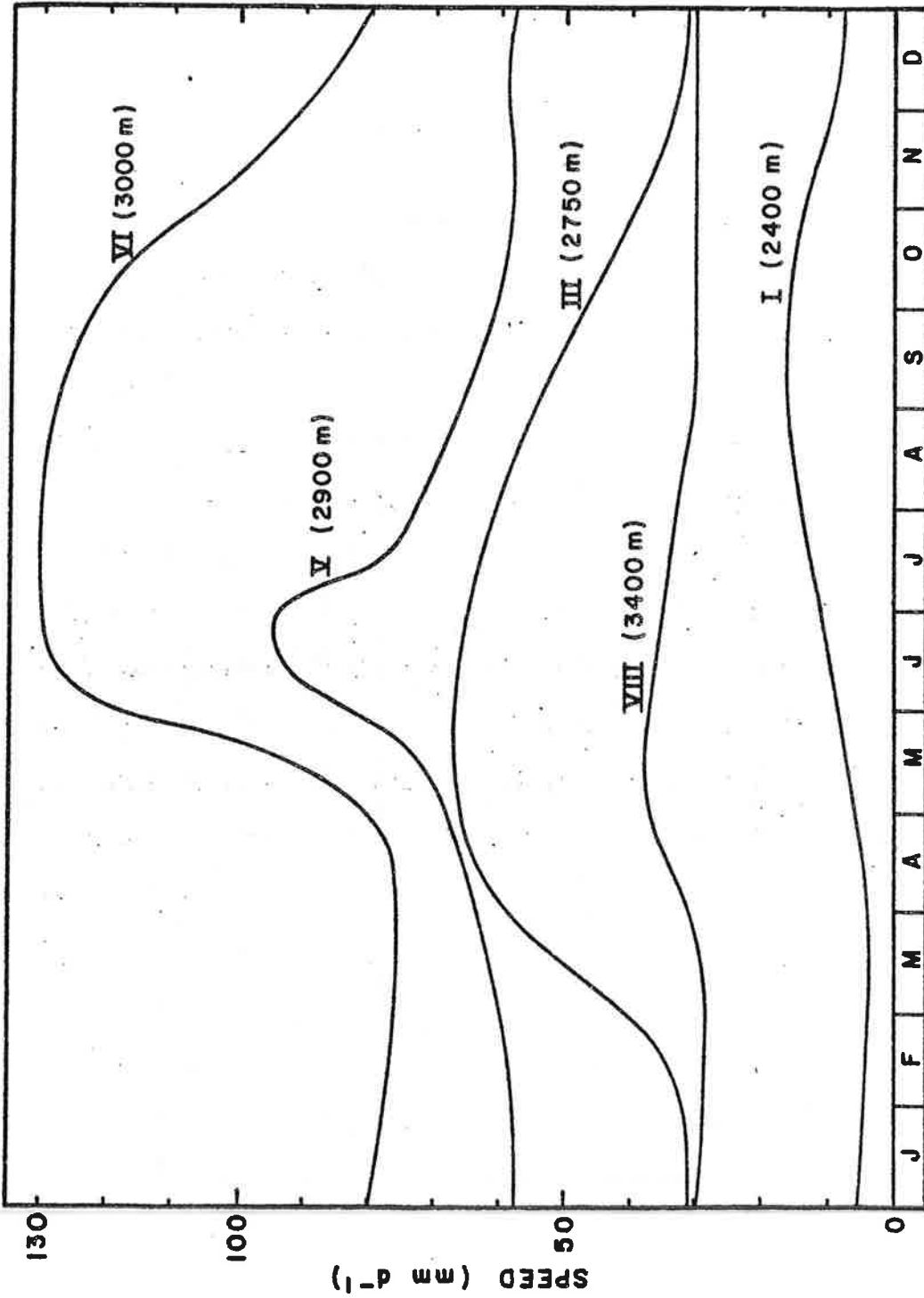


Figure 15. Schimpp's measurements of seasonal variations in the movement of the Hintereisferner, Austria, from 1952 to 1954. The numbers in parentheses are the approximate elevations of the profiles. (from Schimpp, 1958)

changes in velocity were about 40 to 50 %. According to Finsterwalder (1961) these changes were "caused by a kinetic wave coming down the glacier from the highest firn region to the end of the tongue within a year. The wave starts when melting in the highest firn region starts in May or June". Whether or not this statement was a consequence of Schimpp's work is not clear, but if the time of maximum velocity is plotted against distance along the glacier (Figure 16), the possibility of such a wave is suggested.

Schimpp did not give his experimental error, nor did he indicate the actual data points, so the error bars have been estimated assuming a very conservative error of $\pm 3 \text{ mm d}^{-1}$. This implies* a wave speed somewhere between 20 and 100 km a^{-1} . Schimpp estimated the wave speed to be $18\text{--}25 \text{ km a}^{-1}$.

It must be emphasized, however, that if these error bars are doubled they are greater than the separation between maximum and minimum on the uppermost and lowermost profiles (Figure 15). This makes the upper and lower points in Figure 16 meaningless and the remaining points imply a wave moving up-glacier. Unless Schimpp's unpublished data are more definitive, the existence of the seasonal wave is thus questionable. Also, a speed of 18 km a^{-1} or higher is much greater than that of a normal kinematic wave described by Nye (1960) or Weertman (1958).

2.4 AFTER 1954

By the late 1940's and early 1950's it was realized that, since naturally-occurring ice was a crystalline solid near its melting point, it should deform like rocks and metals near their melting points (Orowan, 1949; Judd, 1964). This led Glen (1955) to make his important laboratory experiments on the

* Note that the higher the wave speed the more difficult it would be to measure, since no variation of peak velocity with distance (a vertical line in Figure 16) implies an infinite wave speed.

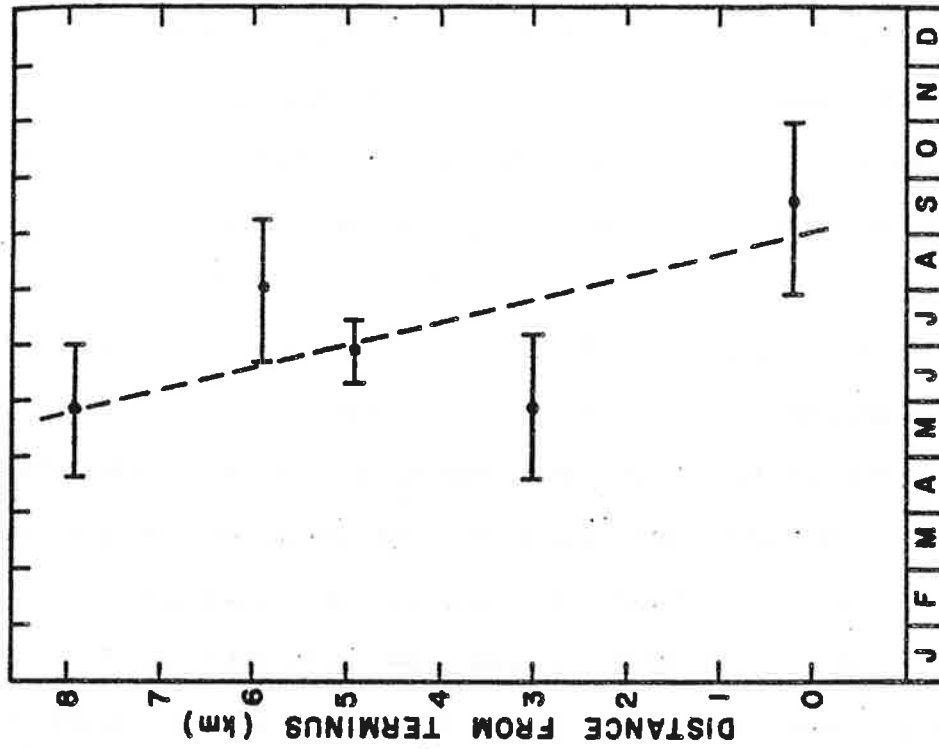


Figure 16. The time of maximum velocity on the Hintereisferner as a function of distance along the glacier (Schimpp, 1958). Provided the upper and lower points are valid, the data suggest a seasonal wave moving down the glacier with a speed between 20 and 100 km a^{-1} .

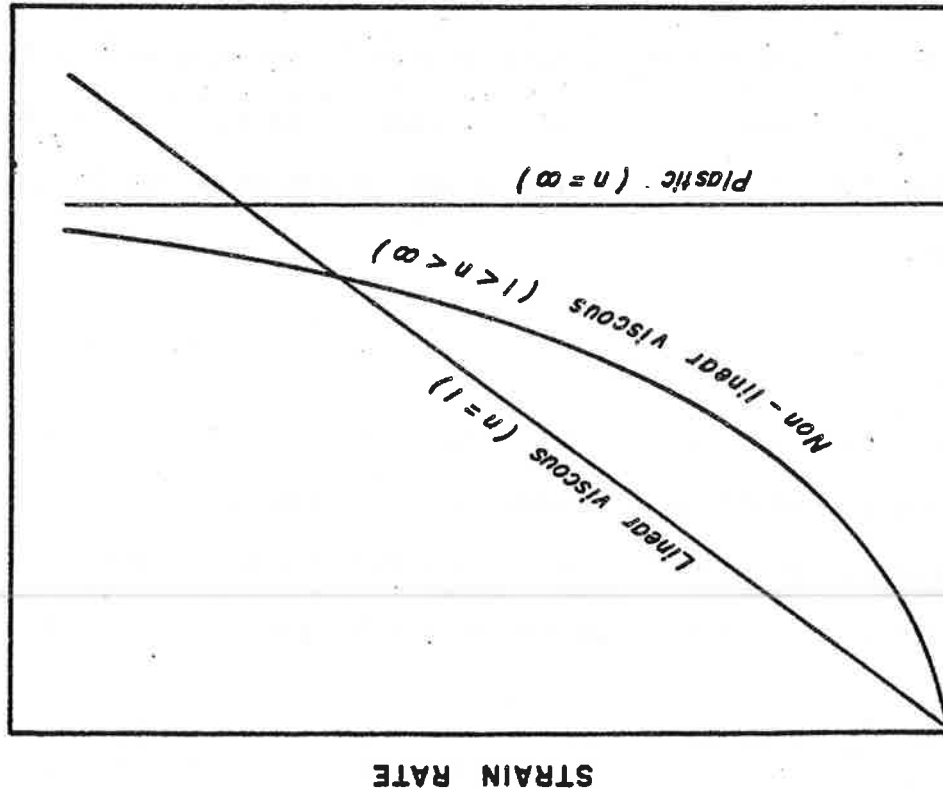


Figure 17. Flow laws for plastic, linear viscous and non-linear viscous materials. Glacier ice has a non-linear viscosity, with n typically around 3.

steady-state creep of polycrystalline ice. This ice, grown in the laboratory, was subjected to uniaxial compression and the resulting strain, after the initial transient creep had occurred, was measured as a function of time, stress and temperature. The relation between strain rate $\dot{\epsilon}$ and stress σ found by Glen,

$$\dot{\epsilon} = A' \sigma^n \quad (2)$$

is known as Glen's flow law. Ice is thus intermediate between a linear-viscous (or Newtonian) material and a perfectly plastic material (Figure 17). For a given temperature A' and n are constants.

The recent work on glacier sliding and glacier fluctuations is now summarized, with the more important works being given in greater detail:

Ives and King (1955), Morsárjökull, Iceland: flow irregular and appeared to be faster after periods of heavy rainfall. The velocity observations were made for 17 days during the summer at approximately 2-day intervals. They concluded precipitation was the controlling factor, not temperature.

Bauer (1955), Ege Glacier, Greenland: daily movement irregular, both in magnitude and direction.

Millecamps (1956a, 1956b), Mer de Glace, France: movement very erratic, with many of the larger fluctuations occurring simultaneously at all stakes (see Lliboutry, 1965, p. 627). The observations of velocity were made twice a day for one month during the summer on a group of 7 stakes, all within an area roughly 200 m by 300 m.

Galloway (1956), Lyngsdalsbreen, Norway: movement irregular, jerky and even backwards at times. The highest velocity was in the evening. The measurements were made with an improved "gletscheruhr" at one point near

the margin over a period of 18 hours.

In 1957 Weertman published the first detailed mathematical treatment of the theory of glacier sliding (Weertman, 1957). The two mechanisms used, pressure melting and enhanced plastic flow, had been suggested previously but Weertman applied them to a "tombstone model" of the glacier bed: equal sized cubes, equally spaced, on a plane. He found that pressure melting permits a faster sliding velocity the smaller the obstacle, whereas plastic flow permits a faster sliding velocity the larger the obstacle. Thus he assumed the flow is controlled by obstacles of an intermediate size, referred to as the "controlling obstacle size", for which there are equal contributions from the two mechanisms. He found the basal sliding speed to be

$$s_b = (\text{constant}) R^{n+1} \tau_b^m \quad (3)$$

where R is a roughness parameter (ratio of obstacle spacing to obstacle size), τ_b is the basal shear stress, n is the exponent in Glen's flow law, and $m = \frac{1}{2}(n+1)$. The constant does not involve any unknown quantities.

Lindig (1958), Gepatschferner, Hintereisferner, Gurglerferner: flow regular on the first glacier but jerky on the other two. The observations were made at intervals of 30-60 minutes.

Glen (1958), Austerdalsbreen, Norway: marginal sliding velocity of the same order of magnitude as the central velocity, with no significant time variation.

Mathews (1959), Salmon Glacier, British Columbia, Canada: sliding velocity 45 % of the surface velocity (depth 495 m).

Paterson (1961), Sefstrøms Gletscher, N.E. Greenland: made weekly observations with a theodolite of the surface velocity over a small portion of the glacier. Even though the observations lasted only one month (August) he found a significant and consistent "decrease in velocity as the season advanced", but he was unable to explain the decrease since he did not think that surface meltwater could penetrate to the bed of a polar-type glacier.

Vilesov (1961), Tuyuksu Glacier, Soviet Union: sliding velocity 65 % of the surface velocity (depth 52 m).

Knizhnikov (1961), Irik Glacier, Soviet Union: no significant changes in the flow on a time scale of hours.

Glen and Lewis (1961), Austerdalsbreen, Norway: sliding at the margin varied from one point to the next and was only one-sixth of the central velocity. Some of the more rapid movements could be correlated with periods of high temperature or heavy rainfall, but others showed no such correlation.

- Moores (unpublished; see Ostenso, Sellmann, and Péwé, 1965), Gulkana Glacier, Alaska, U.S.A: the two ice streams of the ablation area appeared to flow similarly during the winter, with a velocity of only 6 % less than the yearly value. In summer, however, the eastern stream reached a maximum velocity in July, 170 % above the yearly value, whereas the western stream reached its maximum in August, 140 % above the yearly value.

Savage and Paterson (1963), Athabasca Glacier, Alberta, Canada: sliding velocity 75 % of the surface velocity in one borehole (depth 322 m) but only 10 % of the surface velocity in another borehole (depth 209 m).

From August 1959 to September 1960 Elliston made measurements of the surface velocity of 25 stakes in a longitudinal line down the length of the Gornergletscher, Switzerland ([Union Géodésique et Géophysique Internationale], 1963, p. 65-66). The seasonal velocities of five of the stakes are shown in Figures 18 and 19. In the accumulation zone, and down to 1 km below the "accumulation limit" (3000 m), there was no significant change of the surface velocity with time. However, from this point down to the terminus Elliston did find a seasonal fluctuation, apparently increasing in magnitude as the terminus was approached. The glacier was 20 to 70 % slower in winter and 20 to 100 % faster in summer. No evidence of a wave progressing from the firn to the terminus, as suggested by Schimpp and Blümcke and Finsterwalder, could be found. The increase of speed occurred in mid-April, the same time that the ablation started, and the surface speed variations could apparently be correlated with stream discharge variations recorded at Zermatt, the latter lagging behind the surface speed by approximately one to two weeks. Elliston's investigation suggests that surface meltwater might cause the seasonal fluctuations in the velocity of glaciers.

Kamb and LaChapelle (1964), Blue Glacier, Washington, U.S.A: observed basal sliding 26 m below the surface at the head of a tunnel near the top of an icefall. They found about 90 % of the surface motion was due to sliding and also noted that the sliding velocity "was not steady with time but showed marked irregularities over time intervals of the order of seconds". It also varied about 10 % from day to day. A regelation layer (relatively bubble free ice containing chains of bubbles) up to 3 cm thick was also seen on the downstream side of the obstacles. This layer was deformed over horizontal distances of 50 cm and greater and they took this figure to be the "controlling obstacle size". This is an

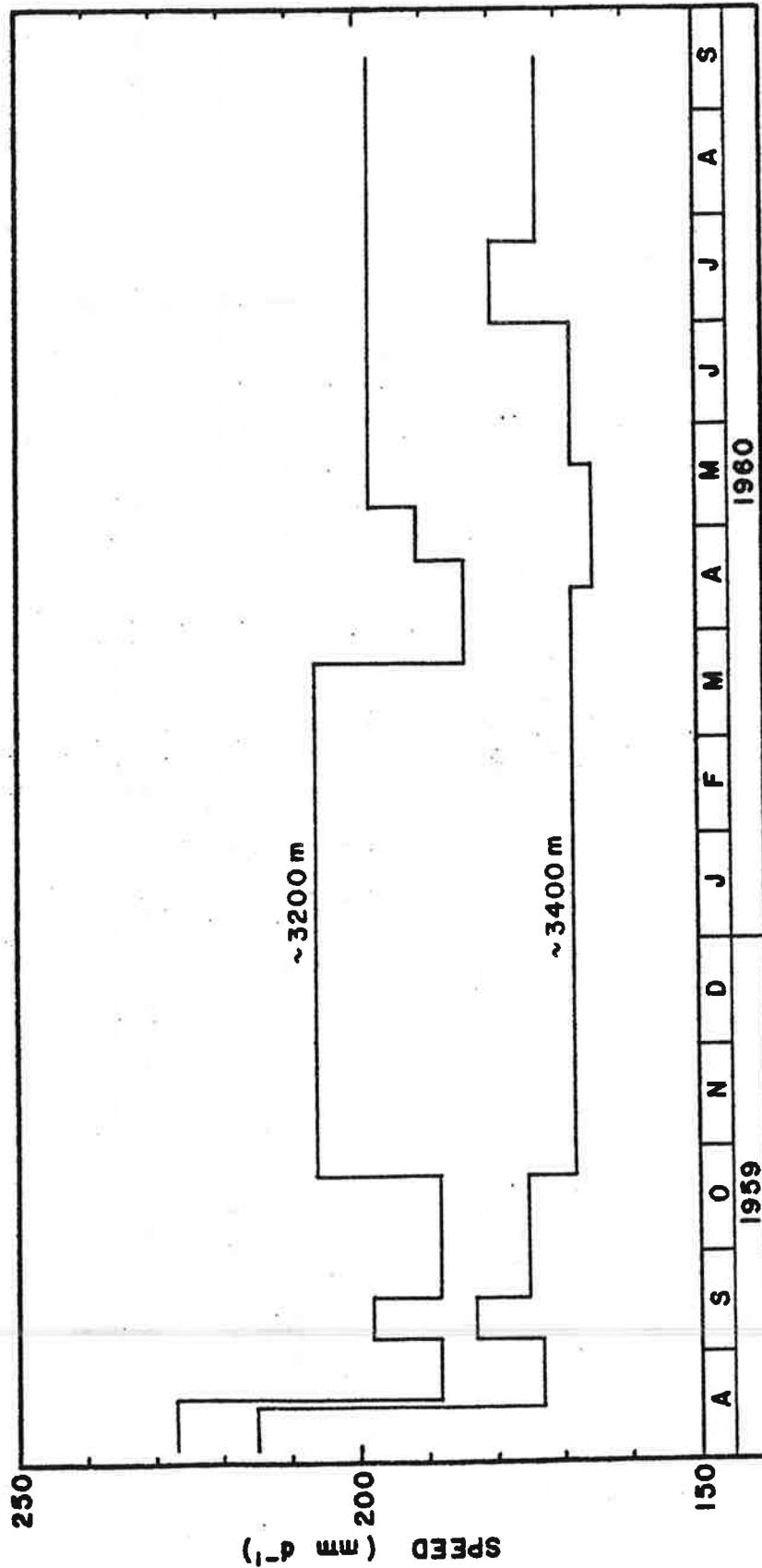


Figure 18. Elliston's measurements of seasonal variations in the movement of the Gornegletscher, Switzerland, above the equilibrium line. The numbers above each curve indicate the approximate elevation of the measurement.
(from Lliboutry, 1965, p. 624)

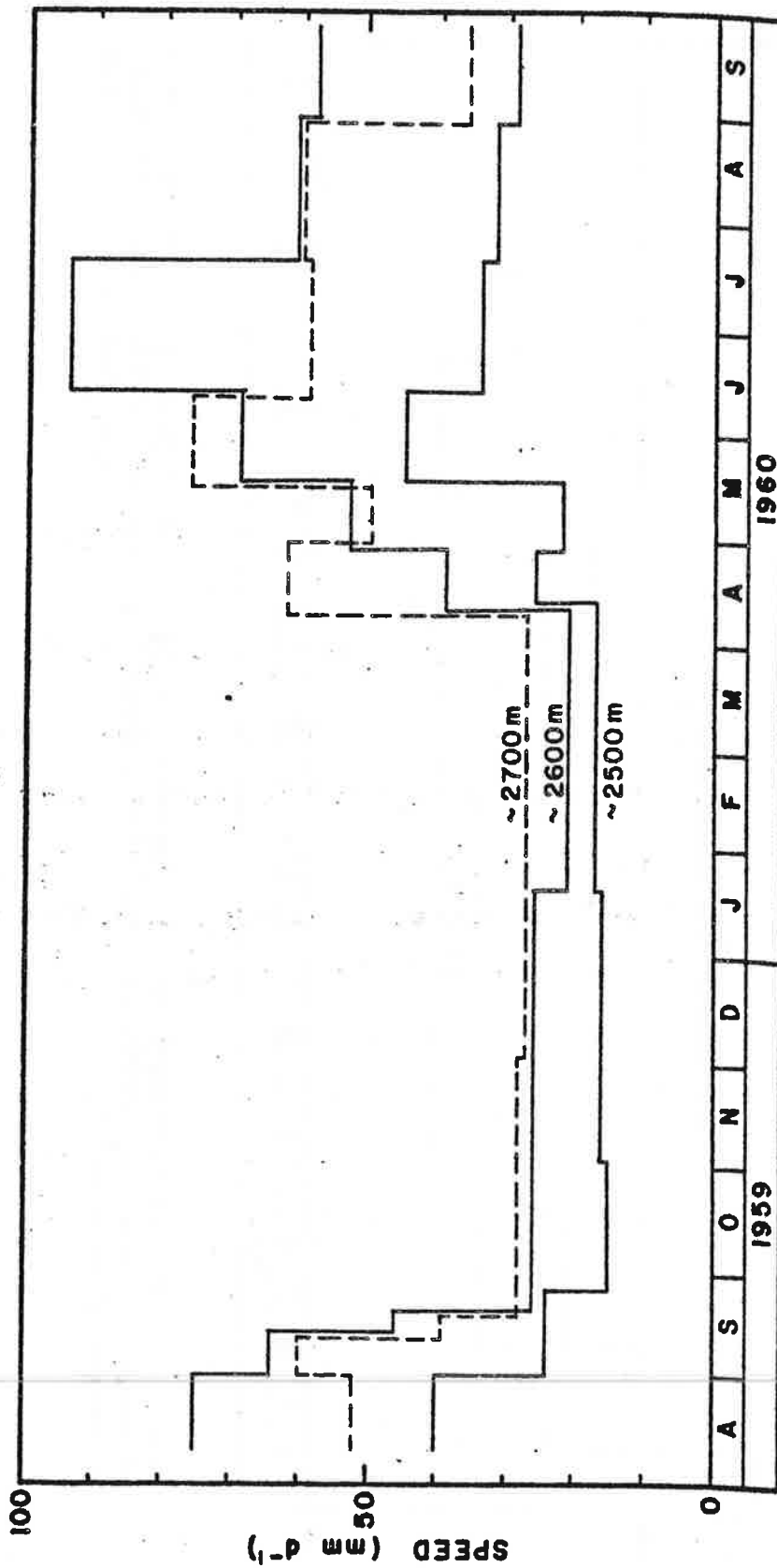


Figure 19. Elliston's measurements of seasonal variations in the movement of the Gornegletscher, Switzerland, below the equilibrium line. The numbers above each curve indicate the approximate elevation of the measurement.
(from Lliboutry, 1965, p. 624)

order of magnitude larger than Weertman predicted (1957). The ice bridged hollows in the bedrock anywhere from 4 cm to 10 m in length.

Weertman (1964): expanded his earlier theory of sliding to include a range of roughness element sizes and to allow for separation in the lee of obstacles, thus making it somewhat more realistic. The only thing to change was the value of the constant in equation 3. He also considered the effect of a water layer at the glacier bed. This layer is assumed to be continuous and to be at the overburden pressure of the ice. Thus it can flow freely along the interface. Weertman calculated that a layer 0.35 mm to 0.60 mm in thickness could submerge enough of the smaller obstacles to account for the changes in the velocity observed by Elliston ([Union Géodésique et Géophysique Internationale], 1963, p. 65-66).

Paterson (1964), Athabasca Glacier, Alberta, Canada: measured velocities over intervals of 3 or 4 months on 12 markers in a more or less longitudinal line 3 km long and found summer velocities to be about 15 % greater, and winter velocities from 4 to 13 % less, than the annual velocities. He attributed these variations to changes in the amount of water at the glacier bed. This hypothesis was given further support by weekly observations of velocity made in July and August, 1960. These showed an overall decrease during the period and, according to Paterson, were positively correlated with measurements of the stream flow at the terminus, with a delay time of 3 or 4 days.

Friese-Greene and Pert (1965), Bersaekerbrae, East Greenland: surface flow and ablation were correlated on two out of three profiles. Like Elliston they could find no suggestion of a wave in maximum velocity moving down-glacier.

Lliboutry (1958, 1959, 1965): developed a theory of sliding which, in addition to the pressure melting and enhanced plastic flow mechanisms, considered the effects of water-filled cavities. He assumed the bed to be sinusoidal (a "washboard model"), rough in the direction of flow but smooth in the transverse direction. The water pressure in the cavities is regarded as an independent variable.

Brecher (1966), Kaskawulsh Glacier, Yukon, Canada: no significant departures of the surface velocities measured over intervals of several days from the average velocity during the entire period.

Flotron (unpublished; see Haefeli, 1970), Unteraargletscher, Switzerland: made several velocity measurements at the Pavillon Dollfuss profile from 1965 to 1966. However, the interval between observations ranged from several days to 4 and 6 months and so all that can be said of the results is that the glacier moved faster between January and August than between August and January.

Theakstone (1967), Østerdalsisen, Norway: sliding made up 50 % of the surface motion and it varied from month to month and from year to year. The motion of the ice was jerky close to the rock but became smoother away from the rock. The measurements were made in natural caves at the margin of the glacier.

Müller and Iken (in press), Axel Heiberg glaciers, Canada: hourly velocities appeared to be correlated to the frequency and amplitude of the run-off. They also correlated the velocities measured over a few days with the rate of melting.

Müller (1968), Khumbu Glacier, Nepal: the maximum velocity preceded the

maximum ablation rate by more than a month. Müller attributed this to changes in the subglacial drainage system which allowed the "ground water level" in the glacier to increase and thus inject water into the ice-rock interface. The measurements were made at 2-week intervals over a period of 8 months.

Meier (1968), Nisqually Glacier, Washington, U.S.A: over a period of 22 years the surface velocity, surface slope and ice thickness changed by large amounts. Using these data Meier calculated the corresponding changes in shear stress and sliding velocity at the bed and was unable to find any simple relationship. This implied to him that either (a) the internal deformation model of glacier flow which he used was invalid, or at least was very incomplete, or (b) the theories of glacier sliding which relate shear stress to sliding velocity are invalid.

Kamb and LaChapelle (1968), Blue Glacier, Washington, U.S.A: investigated the sliding at the head of a tunnel drilled through the middle of an icefall. The surface velocity was 400 mm d^{-1} and the surface slope was 45° . The tunnel, 65 m below the surface at bedrock, had two branches: one, with extensive separation between ice and rock, had a sliding velocity of 350 mm d^{-1} , and the other, with no separation, had a sliding velocity of only 10 mm d^{-1} .

Kamalov (1969), Davydov Glacier, Soviet Union: the average autumn velocity (September to November) was higher than the average spring velocity (March to May) and the average autumn velocity was close to the average annual velocity. The measurements were made monthly along a transverse profile near the terminus.

Paterson (1970), Athabasca Glacier, Alberta, Canada: devised a method of

estimating the sliding velocity at various points along the bed by extrapolating from at least one measured value. The method has few assumptions and does not use a flow law. Like Meier, however, Paterson was unable to find a significant relation between basal shear stress and sliding velocity. On the other hand, he did find a significant relationship between sliding velocity and ice thickness, but he did not offer any explanation for this.

Harrison and Kamb (1970), Blue Glacier, Washington, U.S.A: used borehole photography to measure the sliding velocity directly during the summer of 1969. They found that it was 15 mm d^{-1} initially, but that it increased to 30 mm d^{-1} when the water pressure in the borehole changed suddenly (over a period of about 30 minutes). A separation of a few centimeters was observed between the ice and the rock. The sliding velocity as calculated from the deformation of the borehole and the surface velocity was considerably higher than that actually observed. On the other hand, a nearby hole drilled a year later yielded a photographed sliding velocity of 20 mm d^{-1} , in good agreement with that calculated from borehole inclinometry, 24 mm d^{-1} (Harrison, written communication, 1972). Harrison also noted that the surface velocity of the lower Blue Glacier decreased steadily through the summer (within the experimental error) and did not exhibit any noticeable daily or weekly fluctuations; this fact has been verified by Raymond (personal communication, 1972), at other points on the glacier.

Nye (1969, 1970): developed a theory of glacier sliding in which linear viscosity and no separation of the ice from the bedrock are assumed. The bedrock is taken as a plane with sinusoidal perturbations of small slope superimposed. He calculates a regelation layer thickness in good agreement with the observations of Kamb and LaChapelle (1964). He compares

the root-mean-square fluctuation in normal pressure to the overburden pressure to decide when cavities can form; however, he does not calculate the effect on the sliding velocity should this take place.

Kamb (1970): developed the most elaborate theory of glacier sliding to date. The bedrock topography is Fourier-analyzed and is characterized by a "roughness spectral function". This is a much more realistic approach than that used by either Weertman or Lliboutry, but is similar to that used by Nye. Initially, linear viscosity is assumed, but this is later extended to the non-linear case. The separation of the ice from bedrock is treated from a point of view similar to that of Nye, but between that of Weertman and Lliboutry; he finds significant separation requires water "under a head of pressure comparable to half the glacier thickness".

Raymond (1971), Athabasca Glacier, Alberta, Canada: measured the sliding velocity in a transverse profile of boreholes, using small extrapolations (over less than 2 % of the depth of the glacier). Sliding contributed between 81 and 87 % of the surface motion on the centerline. About half-way from the center to the margin it was still 70 % of the surface velocity but near the margins the sliding velocity was very small. The glacier was thus held back mostly by the friction near its margins. Raymond suggested this lateral variation in sliding velocity could be due to a lateral variation in the difference between the pressure of water at the bed and the overburden pressure of the ice. Sliding would be enhanced in regions of high water pressure. Raymond did observe high water pressure in the one borehole which he monitored.

Harrison and Lee (1971), Coleman Glacier, U.S.A: very large velocity

fluctuations over approximately two-hour time intervals, with values ranging from near zero to about 700 mm d^{-1} . The fluctuations were not synchronous from one point to the next, nor was there any correlation with temperature. The measurements were made accurately with an electronic distance measuring instrument.

2.5 SUMMARY

Glacier sliding: observations

- (a) Glaciers do slide, at least when their basal temperature is at the pressure melting point.
- (b) The ratio of sliding velocity to surface velocity is highly variable, usually accounting for $50 \pm 40 \%$ of the total surface motion.
- (c) The sliding velocity varies from glacier to glacier and from point to point on the same glacier. In at least one case, it is greater at the middle than at the margins.
- (d) The sliding velocity has been observed to vary both in a smooth and an irregular fashion on time scales of seconds, minutes, hours or days.
- (e) The sliding velocity does not have any obvious empirical correlation with other parameters, except perhaps for the ice thickness (Paterson, 1970).

Glacier sliding: theory

- (a) Currently four mathematical theories of glacier sliding exist, but none has been verified experimentally.
- (b) All theories use the pressure melting and enhanced plastic flow mechanisms, both of which have been observed at the beds of glaciers.
- (c) The effect of cavities and meltwater at the bed is treated inadequately in these theories. However, even without this complication positive experimental verification in the field is very difficult.

Glacier fluctuations: hourly

- (a) The surface motion of glaciers is almost invariably found to have large and erratic fluctuations on a time scale of hours. Occasionally, however, a smooth motion is observed.
- (b) These fluctuations do not have any definite correlation with other parameters. They occur with or without crevasses in the vicinity.
- (c) Some workers have found the day-time speed to be faster than the night-time, the maximum usually being in the afternoon or evening. However, most observations are inconclusive.

Glacier fluctuations: daily and weekly

- (a) Irregular fluctuations also occur on a time scale of days or weeks but the deviations from the mean velocity are generally less than those for hourly fluctuations..
- (b) Often, but not always, large increases in velocity measured on this time scale appear to be related to periods of high temperature, heavy rainfall, high run-off, or large rates of melting.

Glacier fluctuations: monthly

- (a) Glaciers undergo a definite seasonal variation in velocity in the ablation area. The spring-summer velocities are greater than the fall-winter ones, and the magnitude of the variation, relative to the mean annual velocity, increases from the equilibrium line to the terminus.
- (b) In the accumulation area there is either no significant variation or a variation opposite in phase to that of the ablation area.
- (c) One glacier, the Hintereisferner, seems to have a seasonal wave, the velocity maximum occurring progressively later with distance down-glacier.
- (d) According to Elliston, the seasonal changes in velocity are in phase with the ablation and precede changes in the run-off by 1-2 weeks. However, according to Müller the movement precedes the ablation by more than a month.

2.6 COMMENTS

Velocity fluctuations are one of the oldest and most documented features of glaciers, and changes in the amount of sliding at the bed have long been suggested as their cause. This intuitive suggestion seems to be the most likely but a detailed experimental verification is still lacking. The evidence we do have points towards variations in the amount of water at the bed as being the controlling factor, but unfortunately this is also the least known part of any of the theories of sliding.

Of the three frequencies of fluctuations outlined above, the daily-weekly ones give the strongest support to this idea, as it is very difficult to envision what else could vary so markedly on such a time scale.

The often-quoted work of Paterson (1964) involves an eyeball comparison between 2 or 3 measurements of ice velocity and stream discharge. The velocity points were distributed over 3 km of the glacier surface and the stream discharge was from a lake at the terminus. Meier (1965) has pointed out that the delay time of 3 to 4 days found by Paterson is in conflict with the delay time of a few hours found from other measurements. These comments are not meant to refute Paterson's work; they are merely meant to show the need for further study.

The relations between seasonal variations in velocity, the sliding of glaciers, and the amount of water at the bed are also far from conclusive, despite many statements in the literature, for example, Paterson (1969, p. 196):

"...fluctuations in the amount of water at the glacier bed are *known* to produce seasonal velocity variations..."; or Weertman (1964, p. 300): "The field observations of Elliston ... on the Gornergletscher show *convincingly* that water at the bottom of a glacier *can* change markedly the velocity of glacier movement". [italics added] Elliston himself said the evidence was only "very suggestive". It is unfortunate that Elliston's work has never been properly

published, particularly as his is the only one in which the stream discharge was measured as well as the velocity. There is no indication of how representative the run-off measurements were of the actual discharge from the glacier.

Most of the measurements of seasonal variations in velocity are only a comparison between a winter value and a summer value or between a summer value and a mean annual value. The measurements which lasted at least one year and which were reasonably equispaced in time are considered of greatest interest: Forbes (1846), Agassiz (1847), Lütshg-Lotscher (1944), Pillewizer (1949), Schimpp (1958), and Elliston ([Union Géodésique et Géophysique Internationale], 1963, p. 65-66). Those of Kamalov (1969) are probably in this category also but not enough information is available to warrant including them. Similarly, the measurements of Röthlisberger and Aellen (unpublished) on monthly velocity variations of the Aletschgletscher, Switzerland, have been omitted.

Table 1 summarizes the main features of these observations and demonstrates that: (a) The time that the speed starts increasing after the minimum can be anywhere from January to April. April is generally the start of the melt season at the latitude of these measurements but January or February are definitely not (Hoinkes and Untersteiner, 1952). (b) The time that the speed starts decreasing after the maximum is usually around June or July. However, glacier run-off reaches a peak in July or August due to the higher albedo in the spring and early summer (Meier, 1969).

The correlation with meltwater is thus not as trivial as one is led to believe from the literature. Only point (b) has been noted before (Müller, 1968; Stenborg, 1970). It appears that the run-off lags *behind* the speed of the glacier.

Additional comments on these observations are:

(a) The experimental procedure is usually not explained very well. With the exception of Elliston, there is no discussion of the errors of measurement.

Worker	Location of Measurements	Range in Δt (d)	Dates of Measurements	Time of Maximum	Time of Minimum
Forbes	Glacier des Bois:	11 - 63	Oct. 1844 - Nov. 1845	July	Dec.
	Upper point	11 - 63	Dec. 1844 - Nov. 1845	July	Jan. - Feb.
	Glacier des Bossons:	11 - 63	Nov. 1844 - Nov. 1845	June	Jan. - Mar.
	Upper point	11 - 63	Oct. 1844 - Nov. 1845	June	Jan. - Mar.
Agassiz	Unteraargletscher:	6 - 57	July 1845 - July 1846	May	Dec.
	Station de l'Hôtel	6 - 36	Aug. 1845 - Aug. 1846	May - June	Sep. - Mar.
Lütschg-Lotscher	Grindelwald Glacier: Terminus	continuous	Feb. 1921 - May 1928	May - June	Nov. - Jan. **
Pillewizer	Mittelbergferner: Upper two profiles	12 - 138	Oct. 1938 - Sep. 1939	Aug.	Jan. - Feb.
Schimpp	Hintereisferner:	about 60	Sep. 1952 - Sep. 1954	May	Sep. - Mar.
	Profile at 3400 m	about 60	Sep. 1952 - Sep. 1954	June - Aug.	Jan. - Apr.
	Profile at 3000 m	about 60	Sep. 1952 - Sep. 1954	June	Nov. - Feb.
	Profile at 2900 m	about 60	Sep. 1952 - Sep. 1954	Apr. - June	Dec. - Jan.
	Profile at 2750 m	about 60	Sep. 1952 - Sep. 1954	Sep.	Mar.
Elliston	Gornergletscher:	12 - 171	Aug. 1959 - Sep. 1960	*	*
	Profile at 3400 m	12 - 149	Aug. 1959 - Sep. 1960	*	*
	Profile at 3200 m	6 - 126	Aug. 1959 - Sep. 1960	May - June	Oct. - Mar.
	Profile at 2700 m	6 - 121	Aug. 1959 - Sep. 1960	June - July	Oct. - Mar.
	Profile at 2600 m	15 - 83	Aug. 1959 - Sep. 1960	May - June	Oct. - Mar.
*no significant variations		**average of 7 years, with little variation			

Table 1. Summary of the previous measurements of the seasonal variations in the motion of a glacier. Only those data which are reasonably equispaced in time and cover at least one year are considered. Δt is the time interval between successive observations of the position of a stake.

- (b) No corrections were made for longitudinal velocity gradients or for changes in tilt of the stakes. These may not be necessary but at least they should be recognized.
- (c) Most of the absolute values of velocity are relatively small (of the order of 100 mm d^{-1}). Errors in measurement will have a greater effect on a slow glacier than on a faster one.
- (d) The data are not filtered properly. Short time intervals (several days) are mixed up with longer ones (several months). This means that the larger daily and weekly fluctuations can significantly distort the seasonal trend.
- (e) None of the results discuss the effect of the ice thickness and surface slope changes. Again, the effect may be negligible but it should be considered.
- (f) There are a number of contradictions in the literature, so that it is difficult to analyze some of the results. For example:
 - (i) In a review of Schimpp (1960), Finsterwalder (1961) states that "the measurements were repeated monthly throughout the year". Hoinkes and Rudolph (1962) claim that Schimpp surveyed the stakes "several times between February 1953 and September 1954". Schimpp himself, however, states that the stakes were measured on the average every other month from autumn 1952 to autumn 1954 (Schimpp, 1958). This discrepancy in the stated time intervals is essential to a discussion of the reliability of Schimpp's results.
 - (ii) In a synopsis of a paper presented by Elliston to a symposium on mass balance studies in Cambridge, England ([Glaciological Society], 1962, p. 289) it is claimed that Elliston's "top stake ... moved twenty-three per cent faster than average during August, fell off to about two per cent less

than average by February, accelerated to thirty-five per cent above average by May and then slowed down to five per cent below average". This directly conflicts with Elliston's later remark that there were no significant (greater than 5 %) variations in the accumulation zone ([Union Géodésique et Géophysique Internationale], 1963, p. 65-66). Hopefully the remarks at Cambridge were only based on preliminary results.

These comments should show that the problem of the seasonal variations of velocity of a glacier is by no means solved. The published measurements only *suggest* that these variations reflect seasonal variations in the sliding velocity and that this is caused by changes in the amount of water at the bed. The measurements are not adequate enough to indicate any details of the mechanisms involved. This investigation is an attempt to fill this gap.

Chapter 3

THE NISQUALLY GLACIER

3.1 LOCATION

A glacier suitable for a detailed study of seasonal velocity variations must be easily accessible at all times of the year. The most year-round accessible glacier in the United States, and also one of the most in the rest of the world, is the Nisqually Glacier, Mount Rainier National Park, Washington. From the University of Washington in Seattle, the Nisqually Glacier is a direct distance of 110 km, a road distance of 188 km and a driving time of approximately 135 minutes. The Park Service keeps the road open to the ranger station and visitor center at Paradise, only 1.3 km away from, and 200 m above, the terminus. It is for this reason alone that the Nisqually Glacier was chosen.

Mount Rainier, also known by the Indian name of Ta-co-man (or Takoma), is the highest of several late Tertiary and Pleistocene volcanoes rising above the Cascade Range of western North America. Its last eruption took place between 1820 and 1854 (Mullineaux, Sigafos and Hendricks, 1969) and there is still an active system of steam vents in the summit crater. It is not known if glaciers on the side of volcanoes exhibit any different characteristics from those in non-volcanic areas.

Mt. Rainier, latitude $46^{\circ} 51.2' N$ and longitude $121^{\circ} 45.6' W$, rises to an elevation of 4392 m (14410 feet)*. Two-thirds of this height is above the general level of the surrounding foothills. The mountain lies west of the crest of the Cascades and south of the Olympic Mountains and so is exposed to the full force of the prevailing westerlies from the Pacific Ocean, less than

* Elevations will be given in feet as well as meters because all available maps still have contours in feet.

160 km away. Extremely heavy orographic precipitation results, roughly 2 to 3 times that received in the Puget Sound lowlands, and about 86 % of it occurs between October and May, mostly in the form of snow (Meier, 1963a).

Despite heavy ablation at lower elevations in the summer, Mount Rainier, by virtue of this heavy winter accumulation and its high altitude, is able to support the most extensive system of glaciers in the conterminous United States. Forty-one glaciers can be counted, but 18 are smaller than 0.5 km^2 and only eight are larger than 4 km^2 (Meier, 1961). One of these large glaciers, and the largest on the south side of the mountain, is the Nisqually Glacier (Figure 20 and Plates I and II). Starting from the crater rim at an altitude of 4328 m (14200 feet) it descends southward a horizontal distance* of 6.53 km to an altitude of 1414 m (4640 feet), a total drop of 2914 m (9560 feet) and an overall slope of 24° .

3.2 CHARACTERISTICS

A map of the Nisqually Glacier, with contours in meters, is given in Figure 21.

At an altitude of 3960 m (13000 feet) the glacier is split by the Nisqually Cleaver. Most of the ice flows to the west of this through the Nisqually Icefall, but a substantial part of it passes to the east over the Nisqually Ice Cliffs. Below the cleaver the two streams reunite and descend to 2620 m (8600 feet) where the Nisqually Glacier is joined on the west by its major tributary, the Wilson Glacier. The Wilson continues to flow into the Nisqually down to 2160 m (7100 feet). At this point, 4.0 km from the crater rim, the Nisqually Glacier flattens out considerably and becomes a fairly valley glacier. Below 1830 m (6000 feet) it steepens slightly and is forced

* All figures in this report refer to the 1966 surface, the date of the most recent published map, unless otherwise stated.

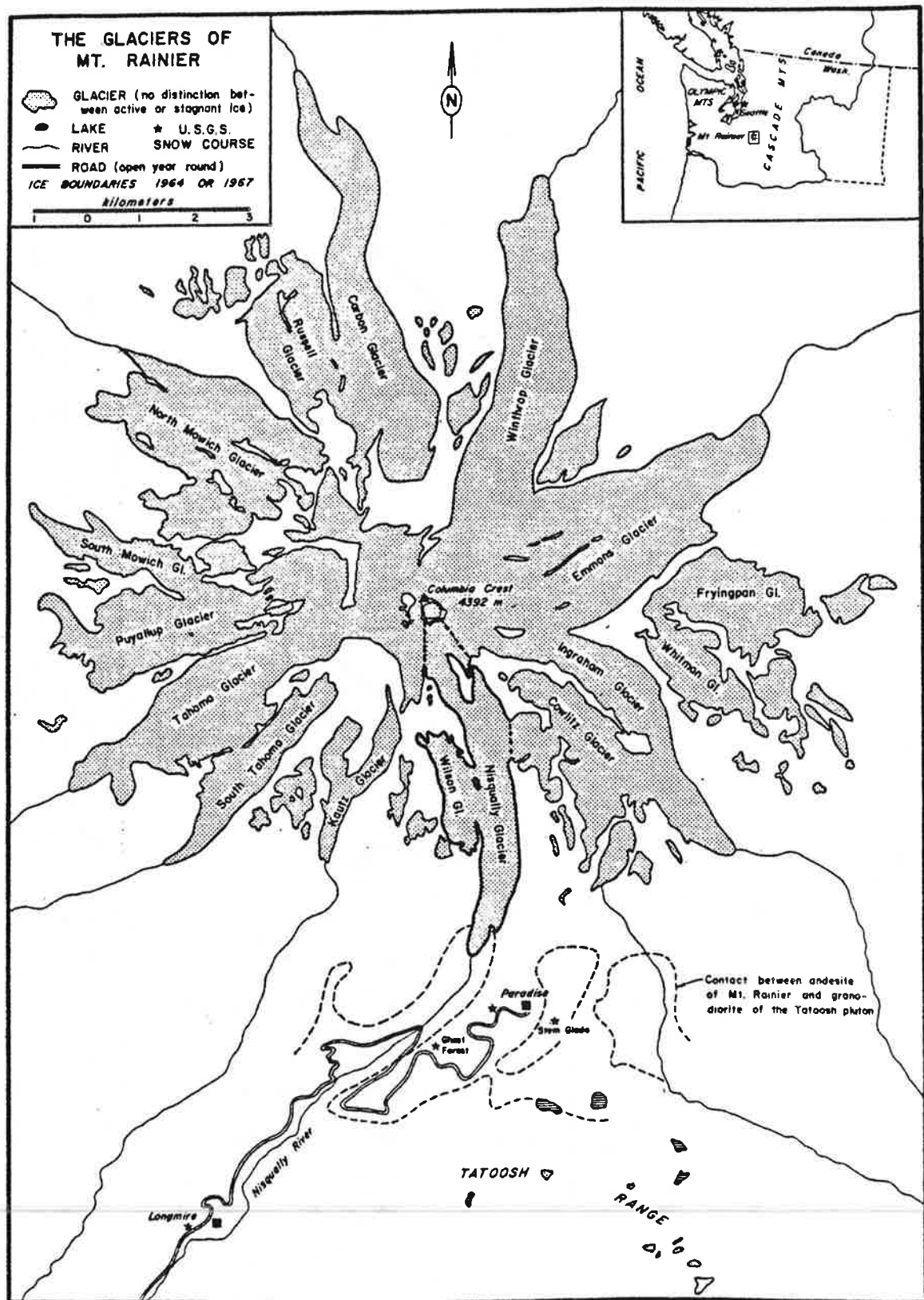


Figure 20. Schematic map of the glaciers of Mount Rainier, Washington.

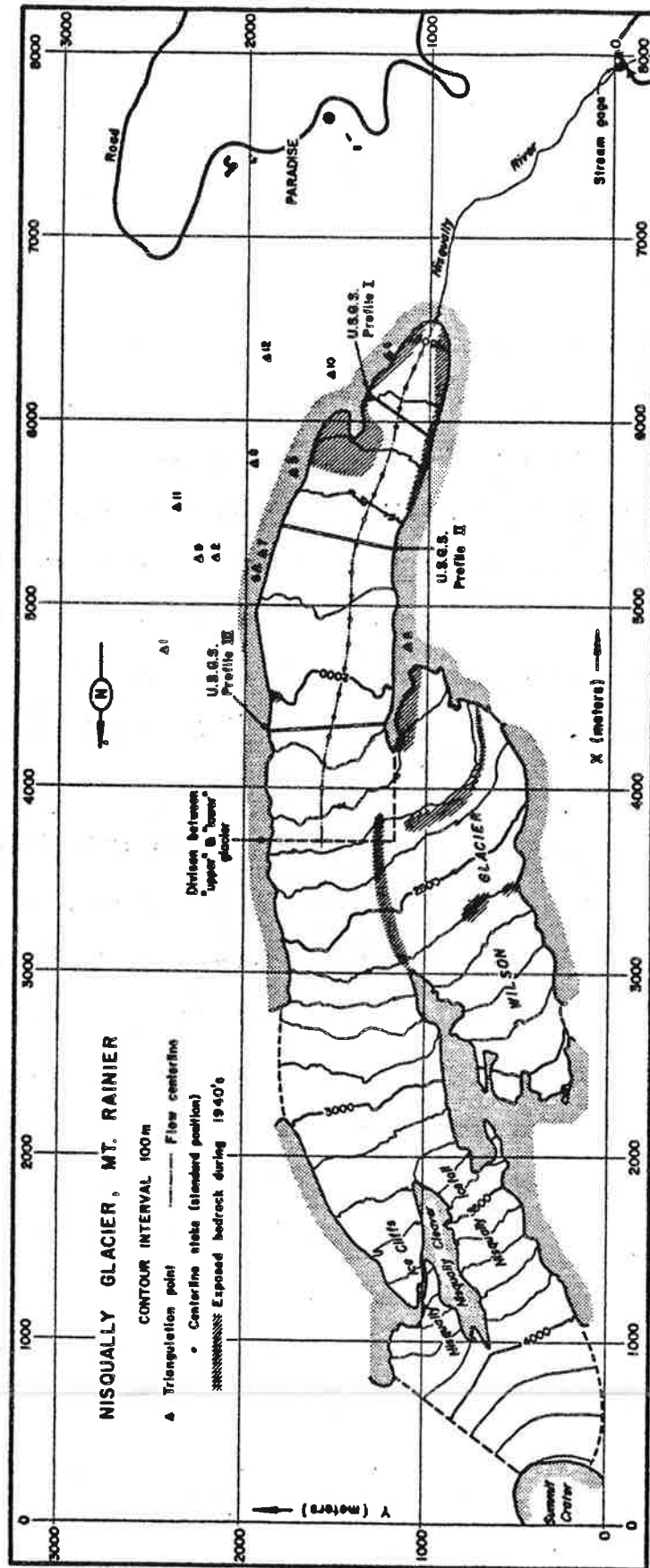


Figure 21. Map of the Nisqually-Wilson glacier system, adapted from the 1966 "Nisqually Glacier" map published by the Geological Survey. The grid system, the triangulation points and the centerline stakes are indicated. The bedrock under the Wilson Glacier was estimated from the photographs of Veatch (1969) and the bedrock under the terminus of the Nisqually Glacier was obtained from old maps. Contours on this map have been changed to meters but they have been left in feet on all subsequent maps.

against the west side of the canyon by two nunataks^{*}. The ice presently terminates at the south end of the lower nunatak.

The total area of the Nisqually-Wilson system is 5.92 km^2 . The Nisqually Glacier itself has an area of 4.43 km^2 and an average width of about 600 m.

The Wilson Glacier is a small cirque glacier which is fed by avalanches as well as snowfall. The contribution to the flux of ice in the lower Nisqually Glacier from the Wilson Glacier is small, probably less than 25 % of the total discharge at the 1900 m level (Meier, personal communication, 1972). In the 1940's a substantial amount of bedrock was exposed along the line separating the two glaciers and also over some of the present area of the Wilson Glacier itself. This is well documented by the photographs of Veatch (1969, p. 10, 11 and 19) and these photographs have been used to estimate the bedrock areas shown in Figure 21. For this study the effect of the Wilson Glacier will be neglected since all it does is complicate the spatial flow variations and presumably does not affect the time variations.

Around 3.7 km from the crater rim, at an elevation of 2225 m (7300 feet), the Nisqually Glacier undergoes an overall change of slope. Above this point the mean slope is 30° and the area is badly crevassed in the summer and frequently swept by avalanches in the winter; below this point the mean slope is only 14° and, except for isolated areas, this part does not have severe avalanche or crevasses problems. Confining the investigation to the lower part was not a difficult decision.

A boundary to this region was arbitrarily drawn slightly above this point, 3.6 km from the crater rim (Figure 21). The region will be referred to as the "lower Nisqually Glacier". It has an area of 1.73 km^2 , a length of 2.95 km, a maximum width of 750 m, and descends in altitude from 2280 m (7500 feet) to

* Not technically true "nunataks" because the ice does not completely surround them. However, it has in the recent past, and they are known locally by this term.

1414 m (4640 feet). Unless specifically stated otherwise all statements and all data will pertain to this area only.

This division of the Nisqually Glacier has further significance. Although very little mass balance information is known on the glaciers of Mount Rainier, aerial photography and general observation indicate that the firm line is currently between 2100 m and 2600 m (Meier, 1963b). Bender and Haines (1955) placed it at 2300 m in 1952 and Meier and Post (1962) placed it at 2100 m in 1961. Thus the lower Nisqually Glacier approximately corresponds to the ablation zone and the upper Nisqually Glacier to the accumulation zone. The boundary between the two (the equilibrium line) is difficult to specify exactly because of the heavily crevassed and complex surface (Plate III).

The lower Nisqually Glacier has a strip of rock-free ice about 100 m wide down its west half. On either side of this are thick morainal deposits. The valley walls on the west are steep, loose and dangerous and are accessible from the glacier at only one point with some degree of safety (at approximately 1925 m elevation). The entire west margin is buried under debris from rock and snow avalanches and the east margin is obscured by morainal material. Fortunately the east side can be reached safely and easily at a number of places. A prominent moraine (dated at about 1840) runs along most of the east side.

Because of its steep surface slope, the Nisqually Glacier is relatively fast-moving. Speeds of up to 1000 mm d^{-1} have been measured at the top of the lower Nisqually Glacier. The steepness also implies that the glacier should be relatively thin, for if we assume that ice is a perfectly plastic material with a yield stress of 1 bar then the thickness is given by (Nye, 1951):

$$h = (\rho g \sin \alpha)^{-1} \quad (1)$$

The lower part would have a mean thickness of 46 m, and the upper part 23 m. The irregular and badly crevassed surface topography suggests, however, that the bedrock topography is also complex, and so we would expect these values to be only very crude estimates of the depth.

3.3 METEOROLOGICAL CONDITIONS

Weather data has been recorded since 1916, with some interruptions, at Paradise, elevation 1652 m (5420 feet). Monthly values of the average daily temperature extremes, the total precipitation and the total snowfall, averaged over the period 1920-71 and over the twelve years 1960-71, are given in Figure 22. Figures 23 and 24 show the average annual temperature T , the annual precipitation P , the annual snowfall S , and the maximum depth of snow D , as a function of time. Other climatological highlights are listed in Table 2.

The trends in these quantities are more apparent if one plots the cumulative departure from the mean for the entire period. This is defined as

$$\Delta f(t) = \int_0^t (f(t') - \bar{f}) dt' \quad (2)$$

where

$$\bar{f} = \frac{1}{\Delta t} \int_0^{\Delta t} f(t') dt' \quad (3)$$

is the mean value of the function $f(t)$ over the time interval Δt . Values of ΔT , ΔP , ΔS and ΔD for Paradise are included in Figures 23 and 24. These curves clearly show the trend to a colder, wetter climate during the late 1940's and early 1950's*.

Snow usually begins to accumulate on the ground at Paradise in late Octo-

* Missing data has to be supplied by interpolation in order to evaluate equation 2. This introduces some error. However, the same trend is shown by continuous records from weather stations in the Puget Sound lowlands (Richardson, written communication, 1972).

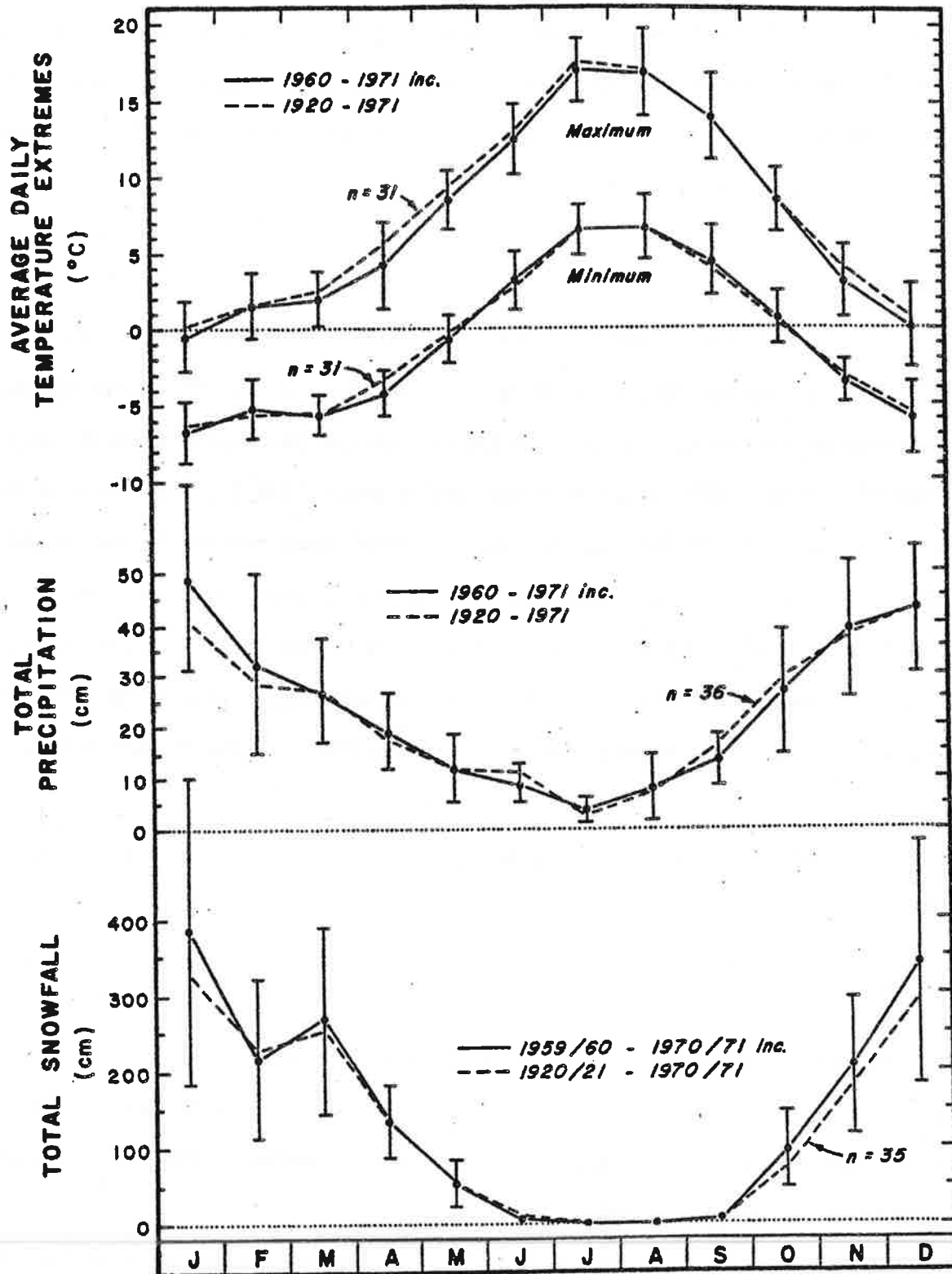


Figure 22. Monthly meteorological parameters for Paradise, Mt. Rainier National Park. The values are averaged over two periods, 1920-71 (n years of records) and 1960-71 (12 years of records). The error bars give the standard deviation (of a single observation) and are approximately the same for both averaging periods.

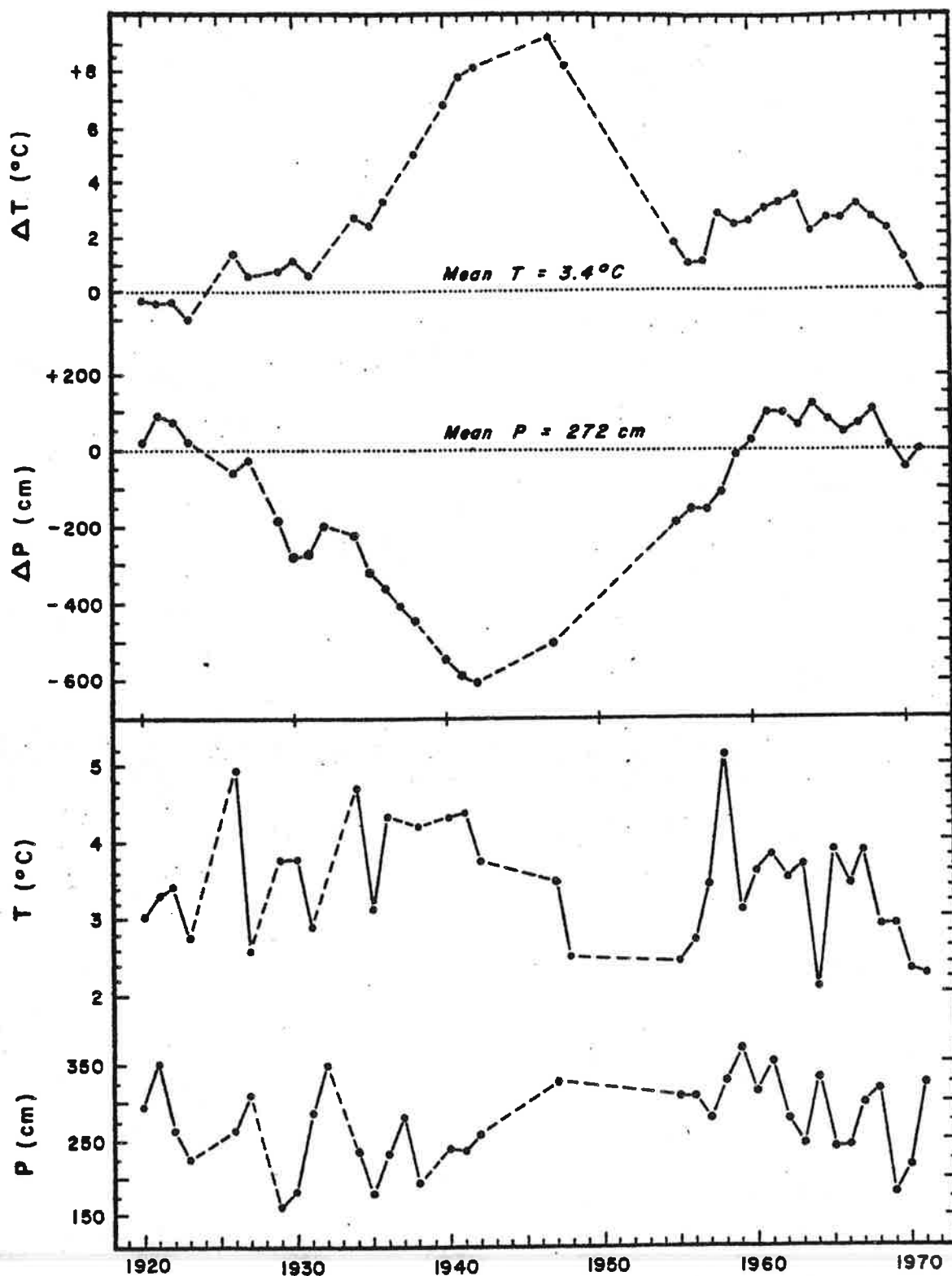


Figure 23. The average annual temperature T , the annual precipitation P and the cumulative departures of these quantities, ΔT and ΔP respectively, from the mean for the entire period 1920-71. Data for Paradise, Mt. Rainier National Park.

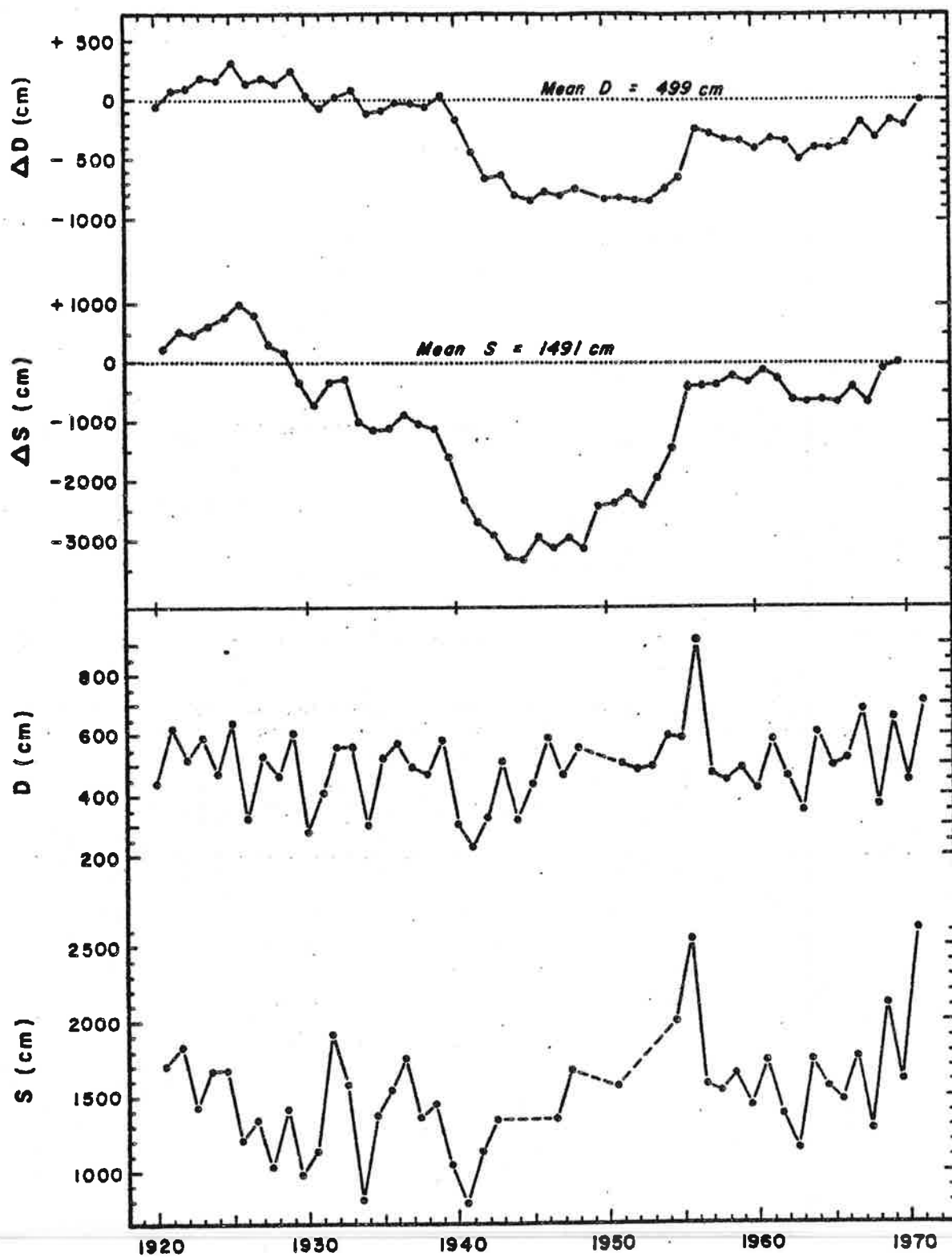


Figure 24. The annual snowfall S , the maximum depth of snow D , and the cumulative departures of these quantities, ΔS and ΔD respectively, from the mean for the entire period 1920-71. Data for Paradise, Mt. Rainier National Park.

	Period	n	Mean	σ	σ_m
Average annual temperature (°C)	1920 - 71	35	3.4	0.7	0.1
	1962 - 71	10	3.1	0.7	0.2
Annual precipitation (cm)	1920 - 71	36	272	55	9
	1962 - 71	10	267	51	16
Annual snowfall (cm)	1920 - 71	43	1491	378	58
	1962 - 71	10	1665	427	135
Maximum depth of snow (cm)	1920 - 71	50	499	126	18
	1962 - 71	10	526	128	41
Lowest temperature = -28.9 °C (Dec., 1932) Highest temperature = 33.3 °C (Aug., 1920) Greatest annual snowfall = 2841 cm (1971 - 72) Greatest depth of snow = 907 cm (March, 1956) Greatest 24-hour snowfall = 94 cm (Jan. 11, 1972) Greatest monthly snowfall = 704 cm (January, 1972)					

Table 2. Climatological summary for Paradise, Mt. Rainier National Park. Compiled by the author from data supplied by Phillips (1960), Richardson (written communication, 1972) and Bishop (written communication, 1969, 1970). n is the number of years of records, σ is the standard deviation of a single observation (one year) and σ_m is the standard deviation of the mean.

ber and continues to accumulate almost without interruption until March or April, when there is usually 5-6 m of snow on the ground. By late June or early July most of the snow at Paradise has melted away.

Snowfalls of 250 cm in one storm lasting several days are not uncommon. For example, in 10 days in January 1972, a total of 401 cm of snow fell, an average of 40 cm d^{-1} . The snowfall of 1971-72 (2841 cm) was the heaviest ever recorded in North America, surpassing the previous Paradise records of 2608 cm (1970-71) and 2541 cm (1955-56). Furthermore, the snowfall at Paradise agrees closely with that 2.5 km away on the Nisqually Glacier (section 9.3). Thus one of the world's heaviest snowfalls occurs on this glacier*.

The meteorological data given here were compiled by the author from information supplied by Phillips (1960), Bishop (written communication, 1969, 1970), and Richardson (written communication, 1972).

3.4 ADVANCE AND RETREAT OF THE TERMINUS

In the late Wisconsin, the Nisqually Glacier was about 33 km long, extending just past the town of Ashford (Crandell, 1963). It reached its maximum extent in recent times around 1840, at a point about 300 m downstream from the new Nisqually River Bridge. This position, approximately 2 km below the present terminus, is marked by a noticeable demarcation between a young and old forest. It was accurately dated by Sigafos and Hendricks (1961) by determining the ages of 253 tree samples. On the moraine the oldest trees date from 1842-48 whereas down-valley from the moraine there is volcanic ash about 3200 years old. The Nisqually thus reached its maximum recent length about 100 years later than most other glaciers in the world. A 1750 moraine exists for

* When drilling boreholes through the Nisqually Glacier in March 1972, the author measured snow depths of 13.5 m in three different locations. It is interesting to compare this to the maximum snow depth of 0.8 m recorded by Balpat during the winter of 1844-45 on the Glacier des Bois and the Glacier des Bossons (Forbes, 1846, p. 182).

the Emmons Glacier on the other side of the mountain (Sigafos and Hendricks, 1963) but there appears to be no evidence for a 1750 maximum at the terminus of the Nisqually Glacier, as suggested by Harrison (1956).

The Nisqually Glacier was discovered by Kautz in 1857 (Meany, 1916). It was visited again in 1870 by Emmons and Wilson and the terminus was first photographed in 1884 by Mason. In 1896 Russell, Smith and Willis noted that a general recession of all the glaciers on Mount Rainier was taking place (Russell, 1898).

The first measurement of the position of the terminus of the Nisqually, and of the rate of movement*, was done by LeConte in July 1905 (LeConte, 1906, 1907). There is fairly good evidence, however, that around this time the glacier was undergoing a minor advance. A photograph taken in 1903 shows a steep, bulging terminus with vertical crevassing, typical of one that is advancing (Meier and Post, 1962). Other photographs, two more measurements in 1908 and 1910, and some small moraines left behind all point to an advance of about 100 m just after the turn of the century (see Harrison, 1951, p. 8, and Veatch, 1969, p. 24-25, for photographs). In 1918 the National Park Service accurately measured the position of the terminus and has continued this measurement annually ever since.

Figure 25 shows the recession from 1840 to the present; the data before 1918 have been taken from Harrison (1956) but the incorrect (1750, 1825) and the doubtful (1855, 1870, 1893) points have been eliminated. From 1908 to 1953 the terminus receded 940 m, at a fairly steady rate of about 21 m a^{-1} . For the next ten years the terminus was stagnant and the measurements indicate merely the haphazard melting of the residual ice. In 1963, however, the terminus started to advance and by 1968 it had covered approximately 130 m of bare ground

* Found to vary from 155 mm d^{-1} to 412 mm d^{-1} at a point about 1355 m from the present bridge (about 915 m above the terminus at that time, but about 400 m below the present terminus).

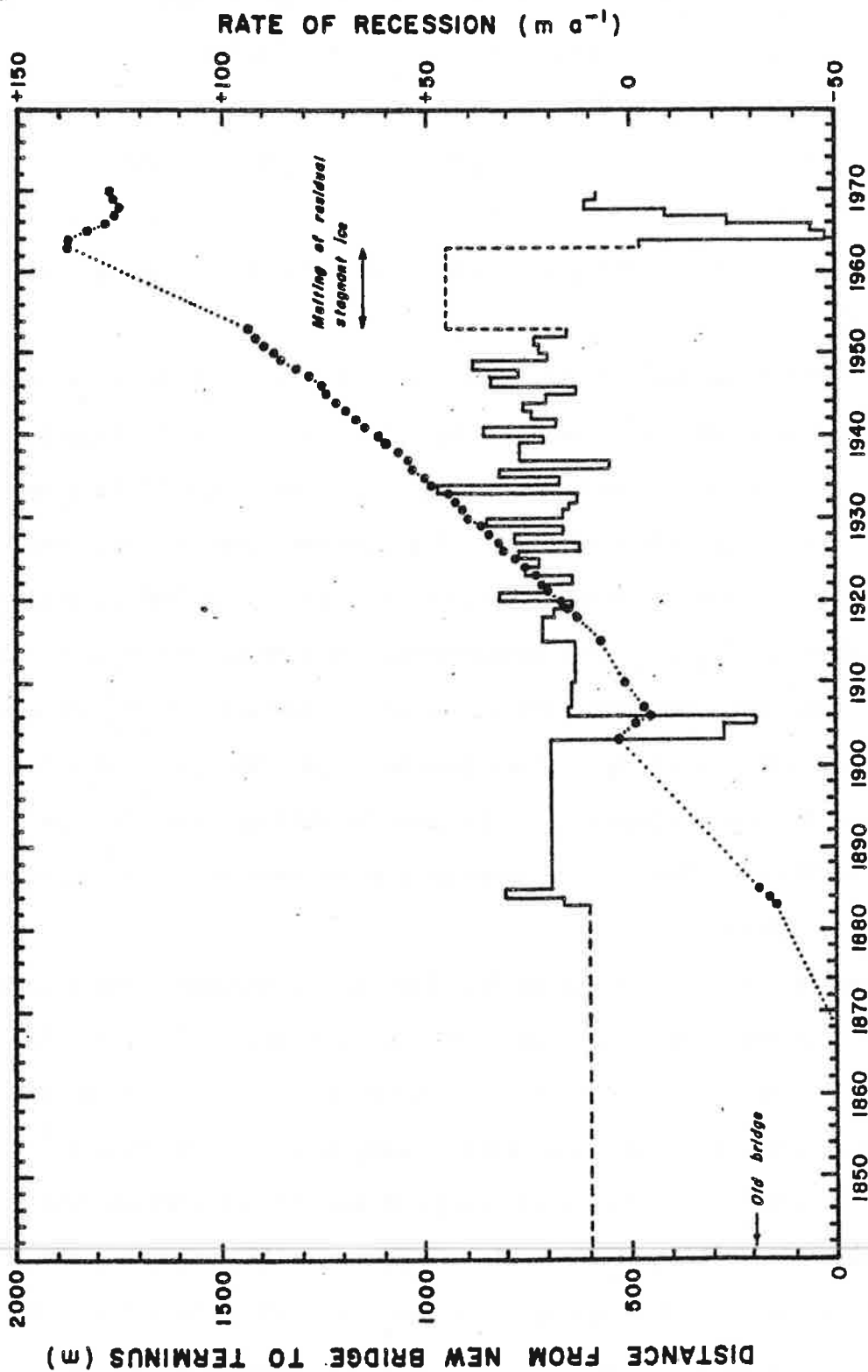


Figure 25. The recession of the Nisqually Glacier during the past century. In 1840, the terminus reached its maximum recent position, about 300 m below the new bridge. Note the two small advances which took place during 1903-08 and 1964-68. The rate of recession is shown by the solid line (scale at right).

with 70 % of the advance occurring in the two years 1964-66. Since 1968 the terminus has been retreating again, about $5-10 \text{ m a}^{-1}$. It is interesting to note the period of 4 years (1963-67) is almost identical to that of the advance 60 years earlier.

3.5 THE KINEMATIC WAVE

The last advance of the Nisqually Glacier was part of an overall increase in activity of glaciers in the Cascade and Olympic Mountains of Washington State which took place in the 1950's and 1960's. This is attributed to a general increase in precipitation since the late 1940's in this area (Hubley, 1956; see also Figure 23). However, the Nisqually Glacier is unique in that the advance had been anticipated and has been well documented by A. Johnson (1949, 1954, 1960), Giles (1960) and Richardson (written communication, 1972).

In 1931 the U.S. Geological Survey established two profiles across the glacier at distances of 530 m and 1260 m from the (1966) terminus (known as "Profile I" and "Profile II" respectively). Surface elevation and velocity were measured on each profile. This was repeated in 1932, 1933, and 1936, and then was discontinued. It was resumed in 1941 by A. Johnson, who added a third profile (III) 2280 m from the (1966) terminus (Figure 21). The measurements have been repeated annually ever since.

In 1946 A. Johnson noticed a definite thickening in the uppermost profile. In 1949 the middle profile started to thicken and in 1955 the lowermost one did also. Thus, while the terminus was continually thinning out and receding, the glacier was increasing in volume at higher elevations and a "wave" of thickening was travelling down the glacier. In 1955 this wave reached the stagnant ice at the terminus. In 1962 it reached bare ground and caused the advance recorded in Figure 25.

This wave can be clearly seen in Figure 26, which shows the change in mean

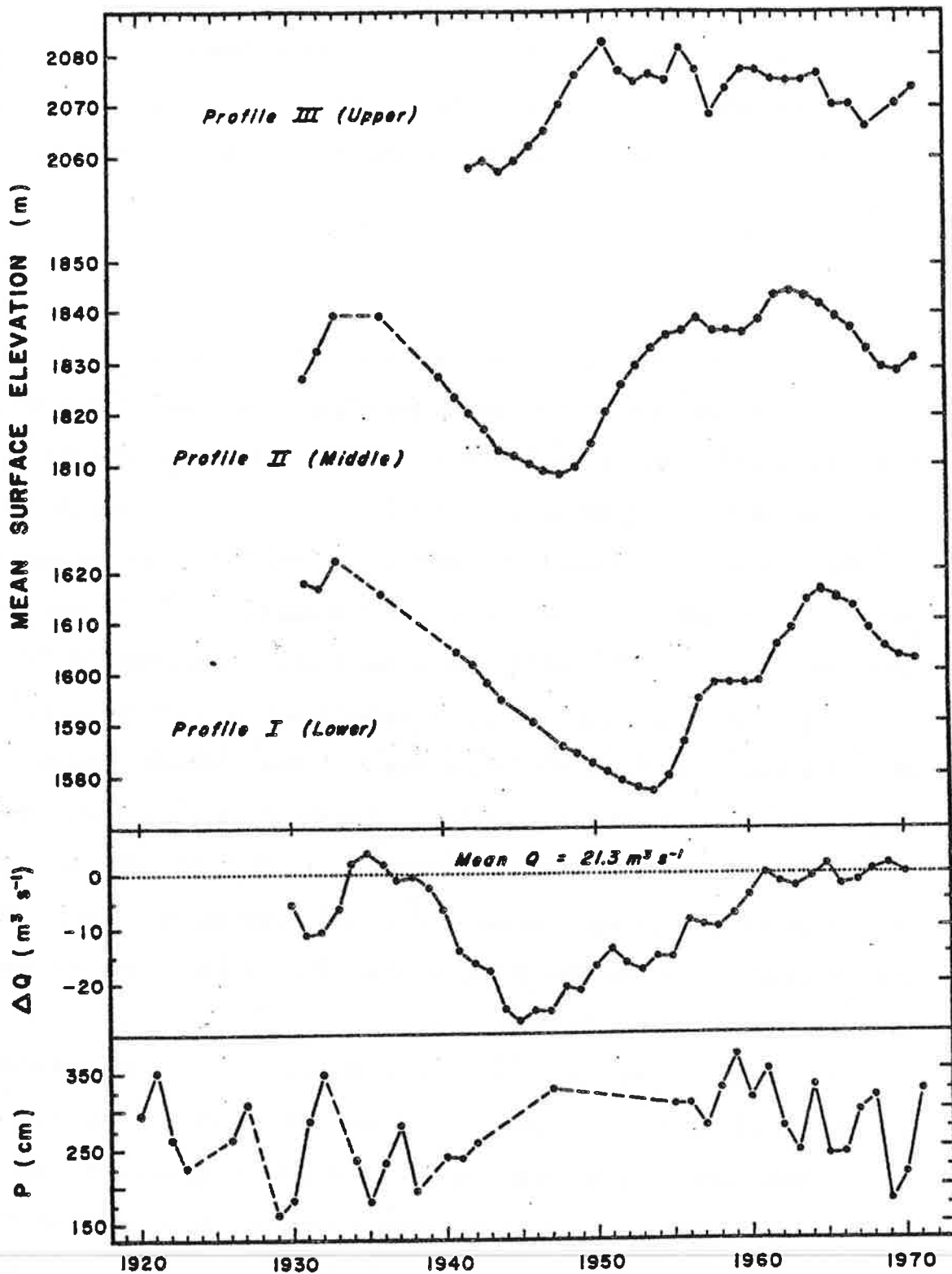


Figure 26. The kinematic wave on the Nisqually Glacier. Upper section: variation of ice surface elevation. Middle section: cumulative departure of the annual discharge of the Nisqually River from the mean discharge during the period 1929-70. Lower section: annual precipitation at Paradise. The wave crest moved down-glacier with a speed of about 0.4 km a^{-1} . (from Richardson, written communication, 1972)

surface elevation at the three profiles as a function of time, and it is excellently portrayed in the photographs of Veatch (1969, p. 28-33 and 36-40). The crest of the bulge reached an amplitude of over 30 m and the ice velocity increased by a factor of 20 (Meier, 1963c). Moreover, the wave form changed shape as it progressed down-glacier, with the crest travelling faster than the trough. In fact, when it reached the lowermost profile the change in ice velocity due to the approaching wave had become discontinuous and the wave had developed the characteristics of a "shock wave". Physically, this simply corresponded to the fast active ice overriding the almost stagnant ice at the terminus.

The Nisqually wave is one of the best examples of the "kinematic waves" predicted mathematically by Nye (1958, 1960, 1963) and Weertman (1958). It has been partially analyzed by Meier and J. Johnson (1962) and by J. Johnson (1968). The crest of the wave travelled down-glacier with a speed of 0.4 km a^{-1} , much less than the speed of the seasonal wave noted by Schimpp on the Hintereisferner but in agreement with that predicted for kinematic waves, about 2-6 times the ice velocity. According to J. Johnson the diffusive effect of the surface slope should be sufficient to prevent the wave front from steepening and forming a shock wave. This difficulty is probably caused by the fact that the Nisqually wave is not a "small" perturbation, as assumed in the theories, since the ice thickness is probably no greater than 100 m and the amplitude of the wave was 30 m.

3.6 OUTBURST FLOODS

Apart from this kinematic wave the Nisqually Glacier is also known for its infamous glacier outburst floods, or "jökulhlaups" (Richardson, 1968). Huge quantities of water appear to be released from within or beneath the glacier. Four major floods are known to have occurred from the Nisqually Glacier, all in

the month of October. The floods of 1926 and 1934 only damaged the bridge below the terminus but the floods of 1932 and 1955 completely destroyed it. The cause of these is not known. Some occur during or after a heavy rain, but others occur in dry periods.

3.7 OTHER MEASUREMENTS

A topographic map of Mt. Rainier National Park was made by Mathes of the U.S. Geological Survey between 1910 and 1913, using planetable techniques. It has a scale of 1:62500 and a contour interval of 30.480 m (100 feet). Unfortunately it is still the only map available for most of the mountain *. In 1913 the glaciers covered an area of 104 km², down from the estimated maximum of 140 km² in the middle of the nineteenth century. By 1950 this area had shrunk to 88 km², but does not appear to have changed much since (Post, 1963).

Topographic maps of the Nisqually Glacier have been made every five years since 1931. These were initiated by Evans and Parker because they wanted to know the effect of the recession of the Nisqually Glacier on the hydroelectric power developments on the Nisqually River. In 1931, 1936, 1941 and 1946 the maps were made at a scale of 1:9600 with planetable methods and cover only the lower part of the glacier, with a contour interval of 15.240 m (50 feet). The 1951, 1956, 1961 and 1966 maps were done with aerial photogrammetry and they extend almost to the top of the mountain, with a scale of 1:12000 and a contour interval of 6.096 m (20 feet). The 1956 map extends over some of the surrounding terrain with a contour interval of 12.192 m (40 feet). This map, and the 1966 one for the glacier surface, together comprise the most up-to-date map available of the Nisqually Glacier and its nearby terrain.

Yearly photographs of the Nisqually Glacier from a number of fixed points

* Aerial photographs for a new map of the park were taken in 1970 and the ground control was done in 1971. However, it is not due for publication until 1974 (Bishop, personal communication, 1972).

have been taken by Veatch (1969). This started in 1942 and has continued to the present.

In 1952 and 1956 the Nisqually Glacier was mapped using terrestrial photogrammetry by Hofmann (1955, 1958). Hofmann concluded there had been a net increase in volume in the four year period, and that most of this appeared to come from the Wilson Glacier. He also measured short term velocity profiles by photogrammetry.

Time lapse photography of the lower Nisqually Glacier was done by Miller in 1959.

In 1961 Meier made some ablation measurements on the lower Nisqually Glacier (Meier and Post, 1962). He estimated the average net mass balance to be -8.7 m of water equivalent at the 1600 m level, with an activity index (vertical gradient of net mass balance at the equilibrium line) of 15 mm m^{-1} .

In conjunction with the surface elevation measurements made annually at each of the cross profiles, the U.S. Geological Survey has also made many measurements of mean annual velocity and surface slope.

Chapter 4

THE TRIANGULATION NET AND THE GRID SYSTEM

Basic to all measurements is the establishment of a set of fixed reference points in a three dimensional coordinate system. From these known points (referred to as "triangulation points", or simply "TP's) horizontal and vertical angles to an object can be measured and its coordinates calculated by simple trigonometry.

4.1 DESCRIPTION OF THE TRIANGULATION POINTS

So that measurements can be made all through the year the triangulation points have to be at prominent, windy locations so that little or no snow accumulates on them. Fortunately, practically all storms on the Nisqually Glacier are windy ones. A number of U.S. Geological Survey bench marks already existed on the east side of the glacier but only one of them (BM 5298) was suitable for winter surveying. Moreover, none of their coordinates were known reliably enough for precise surveying (Meier, personal communication, 1968). It was decided to start from scratch and establish an accurate triangulation net suitable for winter as well as summer use.

In February, 1968, a reconnaissance of the area was made and suitable sites chosen. They not only had to be in windy locations, but they also had to be safely accessible within a reasonable time from Paradise. Ideally, two points from which the entire glacier was visible would be sufficient; unfortunately not one such point exists, even in the summer. Instead four points (TP-1, TP-2, TP-3, and TP-4) had to be used so that the entire lower glacier could be covered (Figure 27). Sites closer than TP-1 to the upper part do exist but they require too much time to reach and they are exposed to avalanches in the winter.

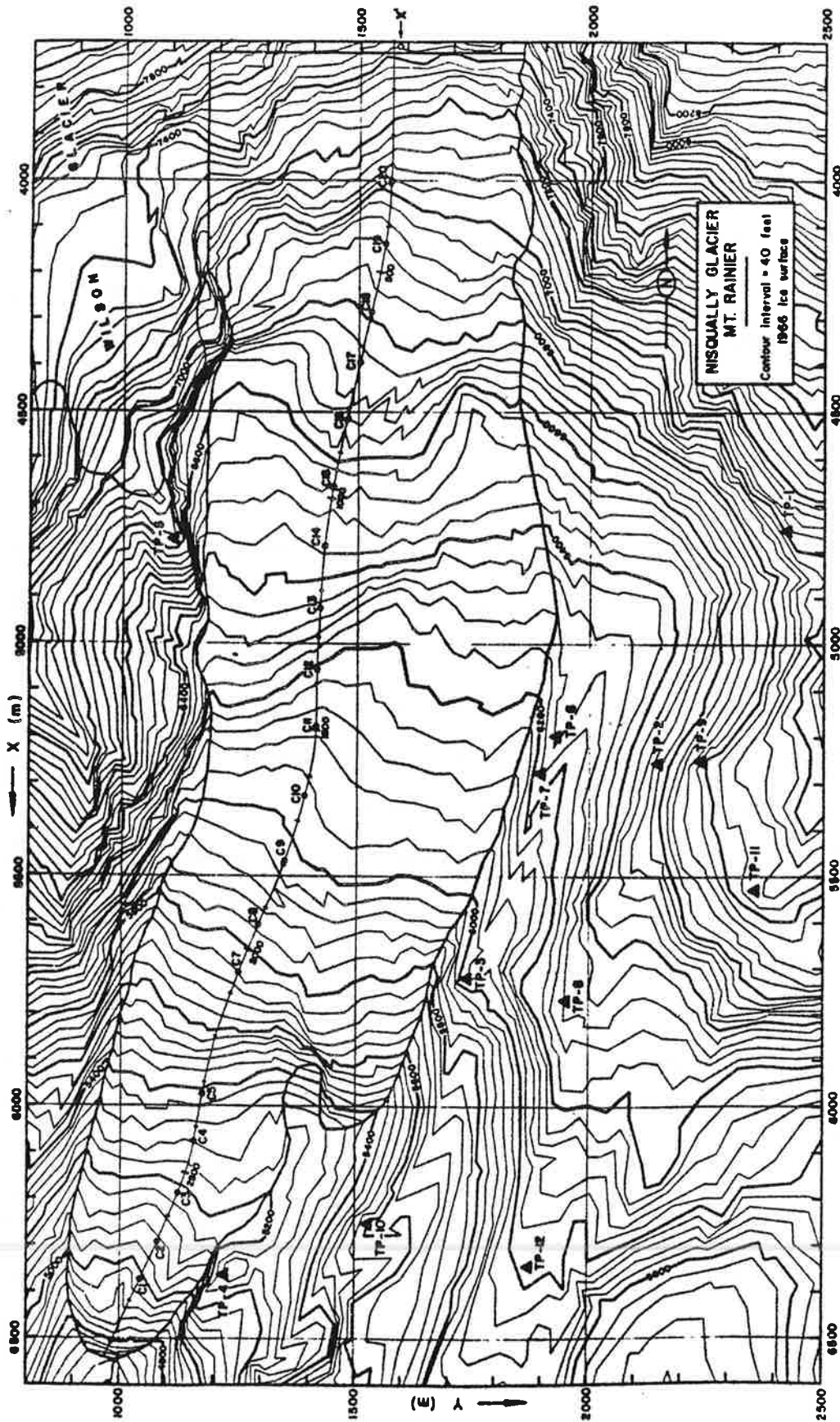


Figure 27. The Lower Nisqually Glacier, the surrounding terrain, the grid system and the triangulation points. The contour interval is 12.192 m (40 feet). The curvilinear X' axis along the flow centerline and the standard position of the centerline stakes are also shown. This figure is reproduced as a transparent overlay (in rear pocket) for use with most maps in this report.

These four points are almost collinear and by themselves define a very "weak" net. To correct this a fifth point, TP-5, was established on a bluff about 130 m above the west side of the glacier*. Finally, two points, TP-6 and TP-7, were placed on the moraine below TP-2 to form a base line. The seven points TP-1 through TP-7 comprise the "basic" net of triangulation points (Figure 28).

The four points, TP-1 through TP-4, were used for the first year of measurements. However, TP-1 and TP-4 were far enough away that two days were necessary to complete a survey of the entire glacier. This became a considerable disadvantage in the winter, when days of good weather are few and far between. During the course of the first winter three more points, TP-8, TP-9 and TP-10, were located which, together with TP-3, enabled the entire glacier to be surveyed in one day. Two more points, TP-11 and TP-12, were added so that more of the terrain on the east side could be covered. These five additional points and the original seven points make up the "extended" net (Figure 29).

Only the points 1, 2, 3, 4, 8, 9, and 10 were intended for winter use. Of these 1, 2, 3, 4 and 9 proved to be excellent for this purpose, with never more than a few centimeters of snow accumulating at each one. TP-8 and TP-10, although they remained free of snow the first winter (when they were not in use), both got buried under some snow in succeeding winters. They were never lost but the snow level in May 1971 did come within 5 cm of the top of the marker at TP-8. This point, however, has the advantages of being one of the closest triangulation points to Paradise and of having more coverage of the glacier than any other point.

* No points on the west side of the glacier could be used for normal surveying because (a) the avalanche danger is high, (b) they would take too long to reach, and (c) they would involve the usual hazards of glacier travel each time they were used.

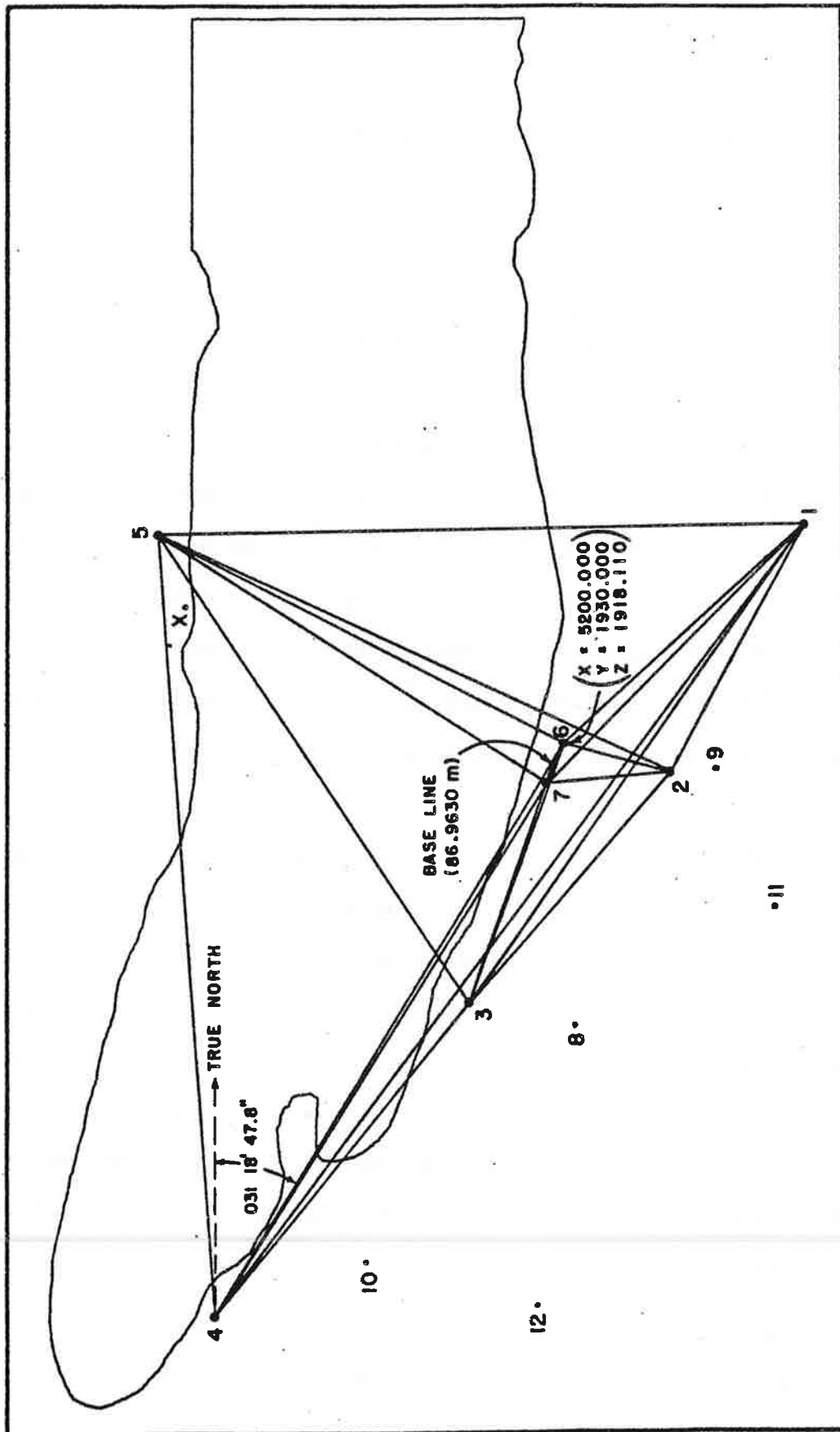


Figure 28. The basic net of triangulation points. TP's 1 through 4 were used for surveying stakes on the glacier; TP's 5 through 7 were necessary for strengthening the net and establishing a base line. All lines were observed in both directions.

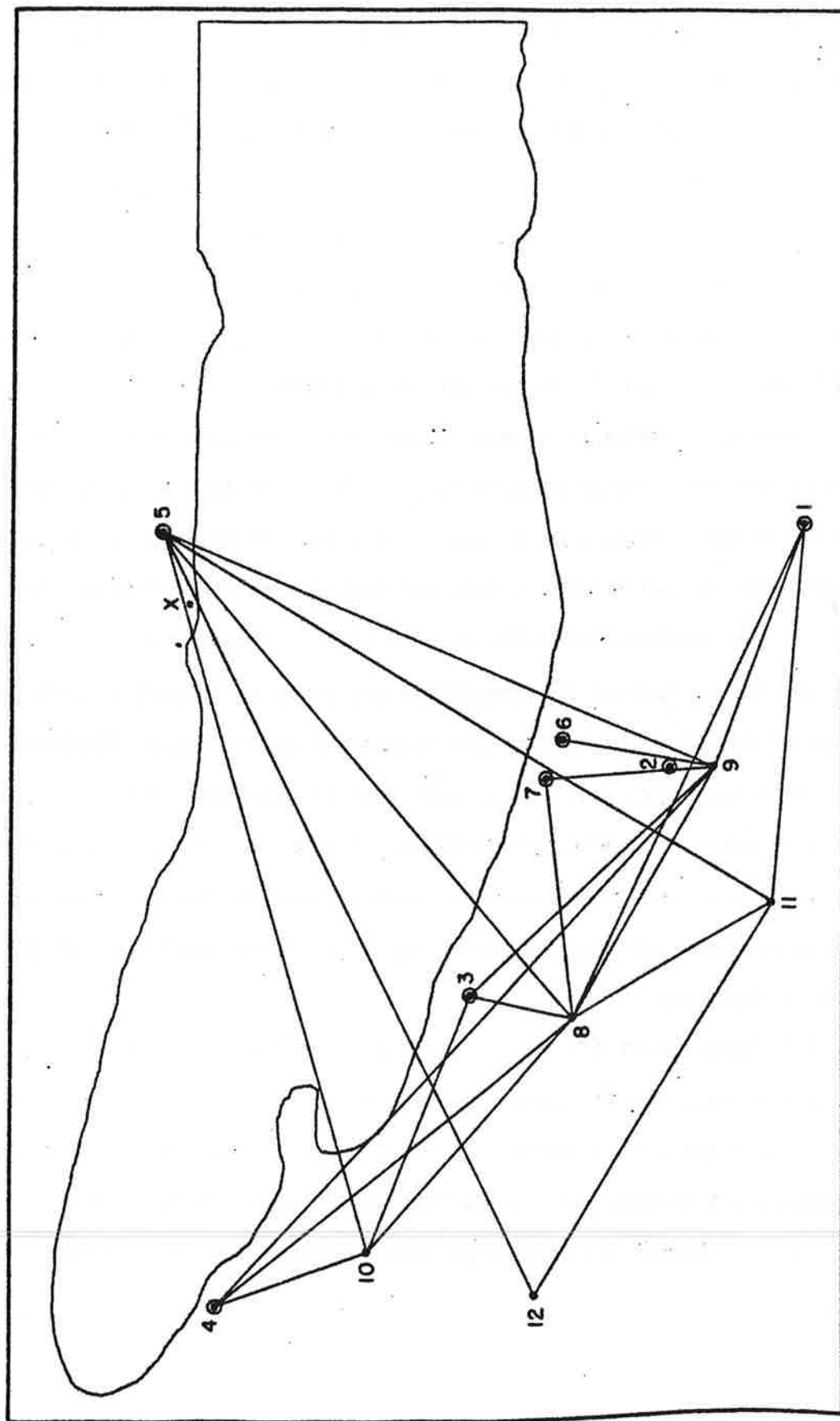


Figure 29. The extended net of triangulation points. TP's 8 through 10 were used for surveying stakes on the glacier (along with TP-3) and TP-11 and TP-12 were necessary for surveying gravity stations on the terrain on the east side of the glacier. Only the new sightings which were not part of the basic net (circled points) are shown here. All lines were observed in both directions.

The exact position of each triangulation point was marked by a 25 mm (1 inch) diameter hole drilled 20-30 mm into the rock. A length of steel tubing, 1.7 m long and painted bright orange, was placed in this hole. The hole could be neither tight nor deep as otherwise this marker pole might freeze in place. The pole was therefore held upright with three light cables running to pitons or bolts in the surrounding rock. Turnbuckles were placed in each cable so that the marker pole could be positioned vertically with a small carpenter's level and removed easily when occupying the point.

Three small holes were made in the rock to hold the tripod legs securely and the legs were marked clearly for each TP. In this way, the instrument height for each TP was always constant and the set-up time was greatly reduced. The position of the telescope axis was marked with black tape on the marker pole and all observations refer to this mark. Errors caused by the marker pole not being plumb or the theodolite not being positioned exactly over the center of the hole in the rock are never more than a few millimeters.

The theodolite was always shaded from direct solar radiation. An umbrella was mounted on the end of a pole and this pole was braced in a suitable position with guy lines running to the anchors used for the main marker pole. The sun was never allowed to strike any part of the theodolite except the wood of the tripod legs.

All theodolite measurements in this study were made with a Kern DKM-2 theodolite, read to the nearest second of arc. Instrument #35133 was used for over 90 % of the observations. A newer model, #65779, was used only when necessary, either when two theodolites were needed simultaneously or when the other one was being repaired (after being knocked over by a sudden gust of wind).

4.2 THE BASIC NET

At various times during July 1968 each triangulation point in the basic net was occupied and horizontal and vertical angles were measured to all the remaining points, with the sole exception of TP-2 to TP-4, which is not inter-visible (Figure 28).

A total of 40 directions were measured, with either 4 or 8 observations being made of each direction. By "direction" we mean a sighting along one side of one triangle in one direction. By "observation" we mean an average of *two* readings of the theodolite, one in the "direct" and one in the "inverted" position. In many surveying analyses, these are considered as separate observations. However, the "standard deviation of a single observation" then becomes meaningless for the vertical angles when there is a significant collimation angle, which is almost always the case. Averaging the direct and inverted angles eliminates this effect and makes the standard deviation meaningful. Thus this convention will be used and, in a sense, the number of observations can be considered to be twice that which is quoted.

The standard deviation of the mean of the horizontal angles varied from 0.3" to 2.3", with an average of 0.96", whereas that for the vertical angles varied from 0.4" to 4.5", with an average of 1.64". [It is always understood that "standard deviation" refers to the *best estimate* of the standard deviation.] Many more angles were observed than the minimum required to calculate the coordinates of the triangulation points. This redundancy can be used to make slight adjustments to the angles by making the net satisfy certain physical and geometric requirements.

The horizontal part of the net was adjusted using the condition equation method (Rainsford, 1958). A total of 25 condition equations were written, relating 35 observed horizontal angles. These consisted of 2 station conditions (the sum of all angles around a point must be equal to 360°), 14 triangle con-

ditions (the sum of all interior angles in a triangle must be equal to 180° plus the spherical excess of the triangle), and 9 side conditions (the value of a side must be the same by whatever route it is computed). The spherical excess of a triangle in seconds of arc is approximately $A/197$ where A is the area of the triangle in square kilometers. Thus, since the largest triangle only covers about 1 km^2 , the spherical excess is completely negligible and a rectangular Cartesian coordinate system can be used.

Each condition equation represents one redundancy and so the horizontal net is "over-observed" to order 25. A least-squares solution to this set of equations was done using a general purpose matrix solution program (SMIS) available from the University of Washington Computer Center. The standard deviation of unit weight of the corrections to the observed angles was $5.30''$.

The scale of the net was determined by measuring the distance from TP-6 to TP-7 with a steel surveyor's tape. The tape was supported at three intermediate points and a spring balance was used to determine the applied tension. Ten observations were made of the distance and corrections for sag were made. No corrections for tension, temperature or standardization were made as the tape constants were unknown. The mean slope distance, adjusted for sag, was $88.3976 \pm 0.00082 \text{ m}$. The mean slope of the base line, determined from the vertical angles measured at each end, was $010^\circ 20' 11.4'' \pm 1.1''$. The horizontal component of the base line is thus $86.9630 \pm 0.00082 \text{ m}$.

The axes of the grid system are, of course, arbitrary, but they have been chosen so that, as close as possible, the X axis is in the true south direction, the Y axis is in the true east direction, and the origin is at sea level directly under the highest summit of Mt. Rainier (Columbia Crest). The transformation was facilitated by the fact that one of the triangulation points, TP-6, was placed exactly over the U.S. Geological Survey bench mark 6293 and another, TP-4, was placed 23 cm north of bench mark 5298. On the map these two bench

marks make an angle of $031^{\circ} 21.5'$ with the north-south direction; after the net adjustment this angle became $031^{\circ} 18' 47.8''$. This fixed the orientation of the grid system. The origin was fixed by requiring TP-6 to have coordinates $x = 5200.000$ m, $y = 1930.000$ m, $z = 1918.110$ m (6293 feet). The resulting system not only satisfies the above requirements but also has the properties that the entire Nisqually-Wilson glacier system is in the first quadrant and the dominant motion of the Nisqually Glacier is in the $+x$ direction (Figure 21).

The vertical net was also adjusted using the condition equation method, but the differences in elevation were adjusted instead of the observed angles. These differences in elevation were calculated from the observed reciprocal vertical angles by using the method described by Hosmer (1919). A total of 14 condition equations, relating 20 elevation differences, were used in the adjustment. The standard deviation of unit weight of the elevation differences after adjustment was 14 mm.

The adjustment of both the horizontal and vertical nets was done by Mr. Jerry Hautamaki of the University of Washington Computer Center. The setting up of the condition equations was done by hand but they were solved numerically with an IBM 7090/7094 digital computer. The final coordinates of the seven basic triangulation points are given in Table 3.

4.3 THE EXTENDED NET

The adjustment of a triangulation net containing 7 points is a very tedious chore. Consequently when the 5 additional points (TP-8 through TP-12) were added to the net a year later, after the basic net had been adjusted, it was decided not to attempt to adjust the entire set of 12 points but rather to consider the basic net as forming a set of accurate base lines from which the new points could be calculated by simple trigonometry. As will be shown later

TP	x	y	z	h_i	z_r
1	4755.354	2422.966	2151.090	1.258	2149.832
2	5257.778	2149.169	2003.161	1.545	2001.616
3	5723.550	1737.804	1843.592	1.580	1842.012
4	6363.052	1222.481	1616.375	1.497	1614.878
5	4775.584	1108.275	2083.488	1.478	2082.010
6	5200.000	1930.000	1919.279	1.169	1918.110
7	5280.011	1895.929	1903.424	1.257	1902.167
8	5771.353	1952.190	1932.611	1.551	1931.060
9	5251.688	2241.189	2069.633	1.066	2068.567
10	6254.592	1529.125	1707.939	1.514	1706.425
11	5531.699	2357.483	2096.587	1.381	2095.206
12	6345.384	1872.986	1836.755	1.480	1835.275
X	4923.541	1164.143	--	--	1945.014

Table 3. The coordinates of the triangulation points. All values are in meters. "X" refers to a painted cross on the rock cliffs under TP-5. (x, y, z) are the coordinates of the telescope axis of the theodolite, z_r is the elevation of the rock surface, and h_i is the height of the instrument, $z = z_r + h_i$.

this procedure does not cause any significant error.

All triangulation points, except TP-2, were occupied at various times during the summer of 1969, and all new sightings which were possible were measured. TP-2 was not occupied since none of the new points could be seen from it. The terrain intervened on a number of sightings this time; the successful ones are shown in Figure 29. Six observations were made along each direction. The standard deviation of the mean of the horizontal angles ranged from 0.4" to 2.1", with an average of 1.02", whereas that for the vertical angles ranged from 0.4" to 2.9", with an average of 1.26".

The calculations were done in the following fashion:

(a) All possible triangles were formed which involved two TP's from the basic net and one unknown TP, and in which all three interior angles were observed. The misclosure (the difference between the sum of the interior angles and 180°) was distributed equally among the three horizontal angles and the (x,y) coordinates of the unknown TP were calculated*. The z coordinate was calculated from the mean of the two reciprocal vertical angles measured at the ends of each leg of the triangle. Each triangle was weighted directly as the sine of the interior angle at the unknown TP and inversely as the mean distance to the two known TP's. Weighted mean coordinates, known as "primary" coordinates, for the unknown TP were then found by averaging over all such triangles involving that TP.

(b) All other possible triangles were formed, thus ensuring that all observed angles were eventually used in the calculations. At least one of the TP's at the ends of each "base line" was now a new TP. Such TP's were assumed known and their coordinates from the primary calculations used. A secondary set of coordinates for the "unknown" TP was then calculated, using the same procedure as described above; these were then combined with the primary ones to give

* A complete discussion of the equations used is given in section 6.2.2.

the final values. The secondary coordinates were only weighted half as much as the primary ones.

The mean coordinates of the new points, their standard deviations and the number of triangles used are given in Table 4 for the primary, secondary and combined calculations. TP-12 could only be calculated by the secondary procedure.

4.4 THE FINAL TRIANGULATION NET AND ITS ACCURACY

Table 3 gives the final coordinates of all 12 triangulation points and Tables 5 and 6 give characteristics of the net which are needed for calculating the coordinates of a point observed from the net. Since all observations, both with the theodolite and the surveyor's tape, were made at the position of the telescope axis of the theodolite, which remained constant, the instrument height h_i and the elevation z_r of the rock surface are irrelevant to this study; they are included in Table 3 only for the sake of completeness. The z value of a triangulation point is always understood to refer to the telescope axis, not the rock surface, and the (x,y) values to the center of the hole drilled in the rock.

A thirteenth point, labelled "X", has been added to the tables. This refers to a white cross painted on the rocks below TP-5. It was placed there for other reasons but unexpectedly had to be used as a theodolite reference mark in May 1971 when the record snowfall of that winter blocked off all other triangulation points from TP-8. Its coordinates are not nearly as accurate as the other points; however, this does not affect velocity calculations provided it is also used as the reference mark on succeeding surveys.

Errors in the coordinates are due to three sources: (a) errors in the location of the origin and the orientation of the axes, (b) errors in the base line measurement, and (c) errors in the angle measurements. Since the grid

		TP-8	TP-9	TP-10	TP-11	TP-12
Primary Calculations	n	10	15	3	1	0
	x	5771.353	5251.687	6254.595	5531.704	--
	y	1952.192	2241.189	1529.122	2357.479	--
	z	1932.612	2069.630	1707.933	2096.597	--
	σ_x	0.010	0.007	0.007	--	--
	σ_y	0.007	0.007	0.015	--	--
	σ_z	0.010	0.006	0.014	--	--
Secondary Calculations	n	19	13	11	10	1
	x	5771.353	5251.691	6254.587	5531.698	6345.384
	y	1952.188	2241.189	1529.128	2357.484	1872.986
	z	1932.610	2069.638	1707.947	2096.586	1836.755
	σ_x	0.006	0.009	0.009	0.007	--
	σ_y	0.006	0.005	0.007	0.007	--
	σ_z	0.005	0.003	0.006	0.005	--
Difference	x	0	-0.004	+0.008	+0.006	--
	y	+0.004	0	-0.006	-0.005	--
	z	+0.002	-0.008	-0.014	+0.011	--
Combined Calculations	x	5771.353	5251.688	6254.592	5531.699	6345.384
	y	1952.190	2241.189	1529.125	2357.483	1872.986
	z	1932.611	2069.633	1707.939	2096.587	1836.755
	σ_x	0.006	0.006	0.006	0.007	--
	σ_y	0.005	0.006	0.009	0.007	--
	σ_z	0.006	0.004	0.008	0.005	--

Table 4. Results of the calculations for the additional triangulation points added in 1969. All values are in meters. The primary calculations are weighted twice as heavily as the secondary ones. (x, y, z) are the coordinates averaged over the n triangles and $(\sigma_x, \sigma_y, \sigma_z)$ are the corresponding standard deviations in the mean.

		From					
		TP-1	TP-2	TP-3	TP-4	TP-5	TP-6
TP-1			572.184	1186.107	2006.454	1314.847	663.872
TP-2		-147.929		621.422	1442.353	1147.158	226.657
TP-3		-307.498	-159.569		821.292	1137.957	557.713
TP-4		-534.715	-386.786	-227.217		1591.571	1361.350
TP-5		-67.602	80.327	239.896	467.113		924.857
TP-6		-231.811	-83.882	75.687	302.904	-164.209	
TP-7		-247.666	-99.737	59.832	287.049	-180.064	-15.855
TP-8		-218.479	-70.550	89.019	316.236	-150.877	13.332
TP-9		-81.457	66.472	226.041	453.258	-13.855	150.354
TP-10		-443.151	-295.222	-135.653	91.564	-375.549	-211.340
TP-11		-54.503	93.426	252.995	480.212	13.099	177.308
TP-12		-314.335	-166.406	-6.837	220.380	-246.733	-82.524
To							
		From					
		TP-7	TP-8	TP-9	TP-10	TP-11	TP-12
TP-1		743.662	1119.770	528.574	1745.470	779.102	1682.461
TP-2		254.214	550.055	92.221	1173.922	344.133	1122.125
TP-3		470.883	219.651	689.964	570.572	648.698	636.358
TP-4		1275.347	939.459	1507.613	325.260	1406.903	650.745
TP-5		935.332	1305.277	1228.889	1537.719	1460.216	1746.154
TP-6		86.963	571.784	315.452	1128.213	541.078	1146.802
TP-7			494.553	346.420	1041.323	525.718	1065.620
TP-8		29.187		594.619	642.265	470.847	579.469
TP-9		166.209	137.022		1229.980	303.200	1154.012
TP-10		-195.485	-224.672	-361.694		1099.432	355.645
TP-11		193.163	163.976	26.954	388.648		947.006
TP-12		-66.669	-95.856	-232.878	128.816	-259.832	
To							

Table 5. The distances between the triangulation points. All values are in meters. The horizontal component is above the dashed line and the vertical component is below. These are used in the computation of the coordinates of a point observed with a theodolite from two of the triangulation points.

		From					
		TP-1	TP-2	TP-3	TP-4	TP-5	TP-6
To	TP-1	-028 35 17.8	151 24 42.2	144 42 50.9	143 15 03.3	090 52 53.7	132 02 59.5
	TP-2	-035 17 09.0	-041 27 02.2	138 32 57.8	140 01 21.8	065 08 38.7	075 13 53.5
	TP-3	-036 44 56.7	-039 58 38.2	-038 51 45.1	141 08 14.9	033 35 15.0	-020 09 29.7
	TP-4	-089 07 06.3	-114 51 21.3	-146 24 45.0	-175 53 06.4	004 06 53.6	-031 18 48.2
	TP-5	-047 57 00.5	-104 46 06.5	159 50 30.2	148 41 11.8	062 41 02.1	-117 18 57.9
	TP-6	-045 07 46.8	-084 58 57.5	160 22 42.5	148 07 34.1	057 21 49.7	-023 03 56.6
	TP-7	-024 51 40.5	-020 59 02.6	077 25 48.1	129 02 15.2	040 16 52.7	002 13 26.8
	TP-8	-020 06 53.0	093 47 11.0	133 08 55.2	137 29 26.7	067 12 20.0	080 34 09.7
	TP-9	-030 48 11.8	-031 52 57.6	-021 27 10.5	109 28 43.3	015 53 01.1	-020 48 46.7
	TP-10	-004 49 16.9	037 15 09.4	107 12 08.6	126 13 17.7	058 48 52.2	052 11 27.1
	TP-11	-019 04 48.5	-014 14 54.0	012 15 53.4	091 33 20.9	025 58 21.1	-002 50 58.8
	TP-12	-082 23 23.9	-108 44 34.8	-144 21 24.8	-177 40 45.4	020 41 10.8	-109 50 54.8
X							
		From					
		TP-7	TP-8	TP-9	TP-10	TP-11	TP-12
To	TP-1	134 52 13.2	155 08 19.5	159 53 07.0	149 11 48.2	175 10 43.1	160 55 11.5
	TP-2	095 01 02.5	159 00 57.4	-086 12 49.0	148 07 02.4	-142 44 50.6	165 45 06.0
	TP-3	-019 37 17.5	-102 34 11.9	-046 51 04.8	158 32 49.5	-072 47 51.4	-167 44 06.6
	TP-4	-031 52 25.9	-050 57 44.8	-042 30 33.3	-070 31 16.7	-053 46 42.3	-088 26 39.1
	TP-5	-122 38 10.3	-139 43 07.3	-112 47 40.0	-164 06 58.9	-121 11 07.8	-154 01 38.9
	TP-6	156 56 03.4	-177 46 33.2	-099 25 50.3	159 11 13.3	-127 48 32.9	177 09 01.2
	TP-7		-173 28 04.1	-085 18 37.1	159 22 30.4	-118 36 14.0	178 45 58.7
	TP-8	006 31 55.9	150 55 13.6	-029 04 46.4	138 47 54.9	-059 24 13.4	172 08 38.4
	TP-9	094 41 22.9	-041 12 05.1	-035 22 29.4	144 37 30.6	-157 26 45.4	161 23 37.4
	TP-10	-020 37 29.6	120 35 46.6	022 33 14.6	131 06 38.2	-048 53 21.8	-104 47 26.4
	TP-11	061 23 46.0	-007 51 21.6	-018 36 22.6	075 12 33.6	-030 46 15.9	149 13 44.1
	TP-12	-001 14 01.3	-137 05 32.4	-106 56 40.5	-164 39 57.8	-117 00 16.6	-153 30 07.2
	X	-115 58 18.4					

Table 6. The angular bearings between the triangulation points. All values are in degrees, minutes, and seconds. These are used in the computation of the coordinates of a point observed with a theodolite from two of the triangulation points.

system is a relative one and all measurements are confined to it, the choice of origin and axes is an arbitrary one. Thus the first type of errors are of no consequence to this study.

Errors in the base line result in a constant scale error over the entire net. The base line was measured to a precision of 1 part in 10^5 ; however, it was not corrected for tension, temperature or standardization of the tape. These corrections are generally less than the correction for sag, which was approximately 10 mm, and so the measured length of the base line is undoubtedly well within 100 mm of the true length. This is an error of 1 part in 10^3 , or 0.1 %. Velocity values will be in error by this amount also; for example, a velocity of 500 mm d^{-1} will have an error of only 0.5 mm d^{-1} . This is negligible compared to other errors, particularly when one considers it is only the *scale* of the velocity values which is affected. Furthermore the effect is independent of both position and time.

Errors in the angle measurements are the only ones which affect the "internal" accuracy of the net, that is, the relative orientation of one TP with respect to the others. The error in the horizontal angles is of the order of 1" and for the vertical angles, 1.5". This corresponds to less than 10 mm at a distance of 1 km, a typical distance in the net. The effect of all the net adjustments is difficult to estimate but it undoubtedly decreases this error. Hence it is probably safe to say that the triangulation points are located to within 10 mm of their true position.

A final check on the internal accuracy of the net is obtained by observing a fixed object from more than two triangulation points. The coordinates calculated from the different triangles which can be formed should be in good agreement with one another. Two circumstances allow this test to be made:

- (a) The coordinates of TP's 8 through 12 were calculated by multiple observations from the basic net. From Table 4 it can be seen that the standard devi-

ations of their coordinates average about 6 mm and none are greater than 10 mm. This is in excellent agreement with the estimate made above and also justifies the procedure used in the calculations.

(b) During the second year of surveying several movement stakes were sometimes measured from three, and occasionally four, triangulation points. A total of 53 such situations were analyzed but 17 were eliminated because they contained too many "weak" triangles, that is, the angle subtended by the triangulation points at the stake (referred to as the "stake angle") was small. All stake angles less than 20° were rejected. For the remaining 36 situations, each involving about 4 or 5 triangles, the standard deviation of the coordinates from their mean position was calculated. The results are summarized in Table 7.

	σ_x	σ_y	σ_z
Average	12	14	10
Minimum	1	2	1
Maximum	53	58	25

Table 7. The standard deviations in the coordinates of 36 stakes which were observed from more than two triangulation points. All values are in millimeters. This gives an estimate of the internal consistency of the triangulation net.

The average error is again close to 10 mm but a somewhat larger error than the previous estimates is to be expected since only one observation was made at each triangulation point, rather than the 6 observations made when determining the extended net. Furthermore, the error is of the same magnitude as that to be expected from the movement of the stakes during the time of observation.*

In summary, the internal error of the triangulation net is no more than

* A minimum speed would be about 120 mm d^{-1} and a minimum time interval between two successive triangles would be about 2 h. Thus the stake would move about 10 mm between triangles.

several millimeters. Like the base line, the effect of this error on velocities is completely negligible, since velocities are *differences* of position. The error will be approximately the same both in magnitude and direction for two successive measurements of the position of a stake, provided the stake is observed from the same triangulation points, and so it will more or less cancel out when the velocity is calculated. Since this was the usual situation the coordinates of the triangulation points are assumed to be error-free.

The grid lines, the triangulation points and the 1966 glacier surface have been given in Figure 27. This figure is reproduced as a transparent overlay in the rear pocket, and can be used with most maps in this study.

Chapter 5

THE THICKNESS OF THE NISQUALLY GLACIER

The determination of the ice thickness is necessary for an adequate interpretation of the velocity data. Using simple models of glacier flow the surface velocity can be shown to vary strongly with the ice thickness (Nye, 1951), and a velocity proportional to the fourth or fifth power of the ice thickness is commonly quoted in the literature (for example, Paterson, 1964). A 10 % variation in thickness would then produce up to a 60 % variation in surface velocity. The high accumulation and ablation on the Nisqually could provide a thickness change of 10 m in a depth of 100 m. To examine this loading effect the bedrock topography is crucial.

There are currently four methods for determining the thickness of glaciers:

Drilling. Boreholes are drilled through the ice by thermal means. This has the advantages of being simple, direct and relatively inexpensive. It requires no complex data reduction but does require some heavy equipment and a considerable amount of work in the field. Only a limited number of spot measurements are practical and each one is only an upper limit to the bedrock elevation, since the drill can just as easily stop at a debris layer as at the bottom (Harrison, personal communication, 1972). Drilling in regions covered by morainal deposits on the surface would, for this reason, be almost impossible because the debris usually extends below the surface as well. Finally, although simple and easy in theory, the technique is fraught with unforeseen practical problems (Meier, 1960).

Radio Echo Sounding. This technique has only been completely successful on "cold" glaciers since radio waves are attenuated by meltwater layers (Smith and Evans, 1972). Since the lower Nisqually Glacier is a very temperate glacier, with large amounts of liquid water present, this method was not consider-

ed feasible.

Seismic sounding. Like radio echo sounding, this requires some expensive and elaborate equipment and considerable field work to yield relatively few measurements. The technique is quite accurate when a well defined signal is returned, but such returns are difficult on shallow glaciers. Crossley and Clarke (1970) failed to obtain either seismic or radio echoes on the "Fox Glacier", Yukon, Canada. They attributed this to its thinness, about 50-90 m. The Nisqually Glacier turns out to have a similar thickness and so it is doubtful seismic sounding would work. The heavily crevassed areas of the Nisqually Glacier would also present problems, as seismic reflections are usually impossible in such areas (Meier, Kamb, Allen and Sharp, in press).

Gravity measurements. This also requires an expensive instrument; however, it is small, light and quickly read. Thus many more measurements can be made than with the other techniques. Readings can be made in more inaccessible places and a greater area of the glacier can be covered in a much shorter time. The *form* of the bedrock topography can be determined quite reliably, but the *scale* often presents a problem, particularly if there are no independent depth measurements. The biggest disadvantage of this method, however, is the elaborate and time-consuming reductions and interpretations required to transform values of gravity into values of thickness. Moreover, the technique is not very accurate and confidence limits of 5-10 m are typical.

Thermal drilling equipment and a gravity meter were available to the author but seismic equipment was not. Therefore it was decided to do an extensive gravity survey of the glacier and to tie the results to a few depths determined by drilling. The gravity measurements are the bulk of this work and will be described in detail. Drilling techniques, on the other hand, are simple and the results will be mentioned only when necessary to aid the interpretation of the gravity field.

5.1 THE FIELD MEASUREMENTS

A Worden gravity meter (No. 358) was used for all measurements. It has a calibration constant of 0.0922 mgal^* per small dial scale division and can range over approximately 100 mgal before resetting. The meter measures only *relative* values of gravity and consequently all readings must be referred to a single base station (called the "main base"). The relative values can be read to a precision of 0.1 small dial divisions, or about 0.01 mgal.

Gravity values measured by the meter at a fixed point will vary with time, primarily because of three effects: (a) inherent instrument drift, (b) temperature changes (despite elaborate thermal barriers in the instrument), and (c) tidal variations. The tidal effect is predictable and has a maximum of about 0.05 mgal h^{-1} (Nettleton, 1940). The other two effects are much less predictable and usually all three are combined into a single "drift correction" determined by occupying the same fixed station before and after a series of measurements and assuming that the drift was linear during the elapsed time. To help ensure this linearity one tries to complete each loop within one quarter of the tidal period, or about 3 hours; this requires establishing several "sub-bases", each accurately tied to the main base.

The gravity measurements were done in May 1969. At this time of the year practically all of the glacier surface is accessible, quickly and in straight-line traverses. The thick cover of snow (about 3-5 m in May 1969) raises the point of observation above large boulders or crevasses and thus lessens their effect.

On May 9 the main base was established at TP-8. Four sub-bases were placed on rock outcroppings above this point and three below, either on or near the 1840 moraine which runs along the east side of the glacier (Figure 30). These

* The conventional unit of gravitational attraction is the milligal (mgal).
 $1 \text{ mgal} = 10^{-5} \text{ m s}^{-2} = 10^{-5} \text{ N kg}^{-1}$.

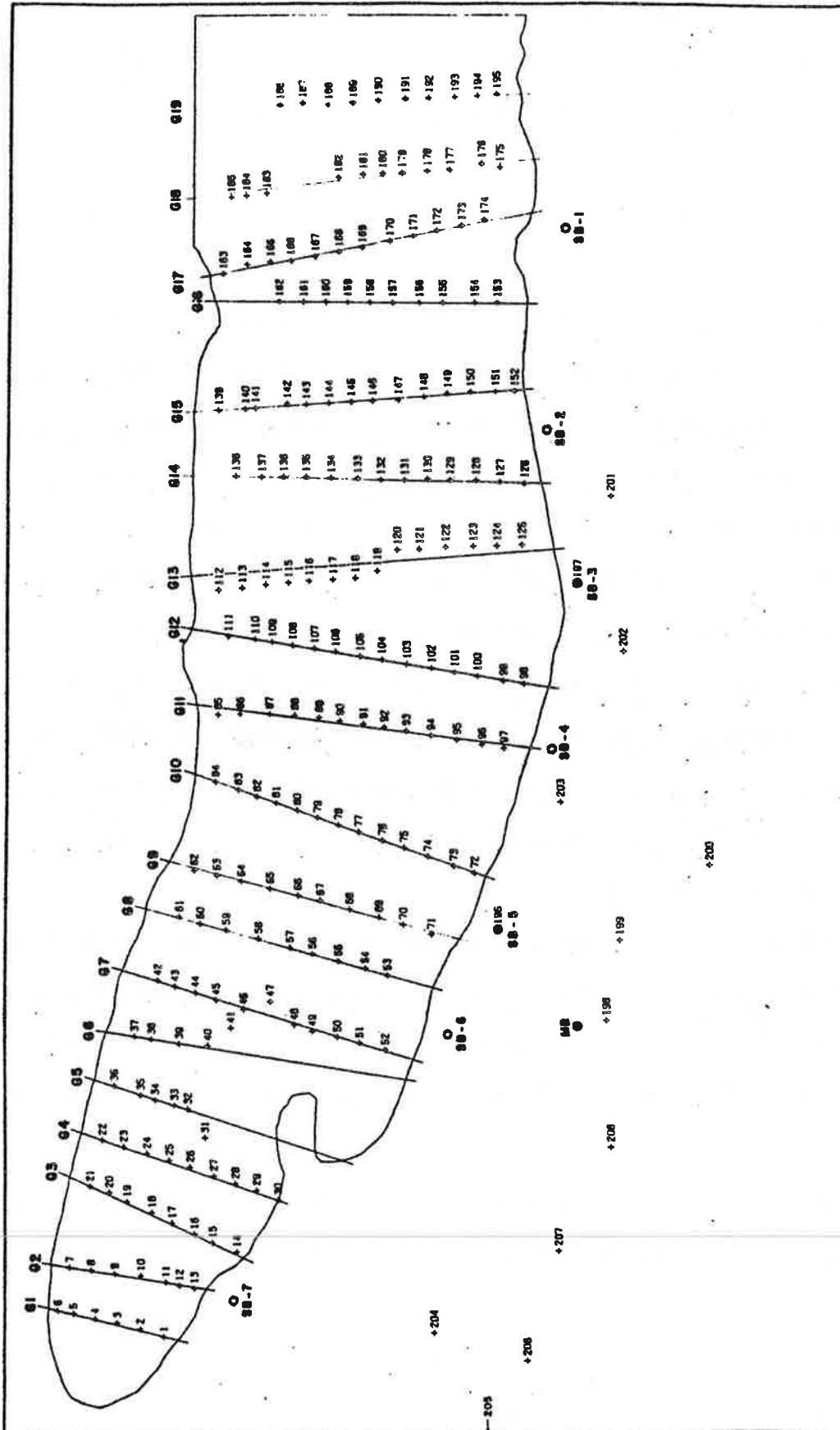


Figure 30. The location of the gravity stations (+ symbols), the main base (MB), the sub-bases (SB), and the profile lines. Station 205 is approximately 100 m south of the left border; it is not shown on any subsequent maps.

were tied in with two loops to the main base station, the measurements being repeated four times. The results are normalized so the main base reads 100.0 mgal and are summarized in Table 8. The elapsed time and drift on each loop can be found in Table 9.

Despite the fact that the gravity meter was always read until at least 3 readings were within 0.3 scale divisions of one another (about 0.03 mgal), the data in Table 8 show that the reproducibility of the gravity values is only about ± 0.06 mgal (estimated by taking the mean of one half the absolute value of the May 13 - June 3 differences). This is of the same magnitude as the often-quoted accuracy of 0.05 mgal for a Worden gravity meter (Krimmel, 1970; Heiskanen and Vening-Meinesz, 1960).

Only readings taken on May 13 and June 3 were used to determine the gravity at the sub-bases. On the initial two sets (May 9 and 10) the gravity meter was read only once, when the author was becoming familiar with the operation of the meter. The left portion of Table 8 shows that the residuals on May 9 were all positive and those on May 10 were all negative, whereas those on May 13 and June 3 were about equally positive and negative. This is confirmed in the right portion of the table; the May 9 - May 10 difference averages +0.15 mgal but that for May 13 - June 3 averages -0.01 mgal. Thus the May 9 and May 10 readings are probably faulty and they have been discarded.

A total of 195 gravity stations on the glacier surface were laid out in nineteen transverse profiles (Figure 30). The profiles averaged 140 m apart and the stations are spaced approximately 50 m apart on each profile. The complex surface topography made it difficult to keep the profiles equally spaced, straight and reasonably parallel. One profile (G13) has a pronounced jog in it near the middle and three stations (numbers 31, 41 and 47) do not lie on any profile. The profiles could not be continued onto the rock at the margins because the west side is too steep, and is exposed to rockfall and

Base Station	Mean of all four days	Residuals				σ	σ_m	May 9 - May 10		May 13 - June 3	
		May 9	May 10	May 13	June 3			Mean	Δ	Mean	Δ
MB	100.00	-	-	-	-	-	-	-	-	-	-
SB-1	58.93	+0.11	-0.02	-0.15	+0.06	0.11	0.06	58.98	+0.13	58.88	-0.21
SB-2	87.03	+0.07	-0.02	-0.09	+0.04	0.07	0.04	87.06	+0.09	87.01	-0.14
SB-3	96.93	+0.08	-0.13	+0.05	-0.01	0.09	0.05	96.91	+0.21	96.95	+0.03
SB-4	102.30	+0.11	-0.06	-0.01	-0.04	0.08	0.04	102.33	+0.17	102.28	+0.03
MB	100.00	-	-	-	-	-	-	-	-	-	-
MB	100.00	-	-	-	-	-	-	-	-	-	-
SB-5	115.89	+0.09	-0.13	+0.03	+0.01	0.09	0.05	115.86	+0.22	115.91	-0.07
SB-6	133.12	+0.10	-0.07	+0.05	-0.07	0.09	0.04	133.13	+0.17	133.10	+0.12
SB-7	164.45	+0.03	-0.02	+0.06	-0.06	0.05	0.03	164.45	+0.04	164.44	+0.13
MB	100.00	-	-	-	-	-	-	-	-	-	-
Means:		+0.08	-0.06	-0.01	-0.01	0.08	0.04	-	+0.15	-	-0.01

Table 8. Analysis of the gravity readings made at the sub-base stations. All values are in milligals. σ is the standard deviation of a single observation, σ_m is the standard deviation of the mean, and Δ is the difference between the two days indicated. Only the May 13 - June 3 readings were retained.

Loop No.	Date (1969)	Ends of loop Start Finish	Observations made on loop	Elapsed time (min)	Drift (mgal)	Drift rate (mgal h ⁻¹)
1	May 9	MB	SB-1 to SB-4	181	-0.28	-0.09
2	May 9	MB	SB-5 to SB-7	151	+0.11	+0.04
3	May 10	MB	SB-1 to SB-4	132	+0.18	+0.08
4	May 10	MB	SB-5 to SB-7	151	+0.24	+0.10
5	May 13	MB	SB-1 to SB-4	182	+0.07	+0.02
6	May 13	MB	SB-5 to SB-7	163	+0.12	+0.05
7	May 15	SB-7	Glacier stations 1 - 13	150	-0.51	-0.20
8	May 15	SB-7	Glacier stations 14 - 30	139	-0.18	-0.08
9	May 15	SB-6	Glacier stations 31 - 52	231	+0.01	0.00
10	May 20	SB-5	Glacier stations 53 - 71	208	-0.26	-0.07
11	May 20	SB-4	Glacier stations 72 - 97	196	+0.03	+0.01
12	May 23	SB-3	Glacier stations 98 - 125	202	-0.22	-0.07
13	May 23	SB-3	Glacier stations 126 - 152	237	+0.03	+0.01
14	June 1	SB-2	Glacier stations 153 - 174	238	-0.31	-0.08
15	June 1	SB-1	Glacier stations 175 - 195	204	+0.15	+0.05
16	June 3	MB	SB-1 to SB-4	161	+0.02	+0.01
17	June 3	MB	SB-5 to SB-7	162	+0.14	+0.05
18	Sept. 26	MB	Terrain stations 198 - 203	221	-0.26	-0.07
19	Sept. 26	SB-6	Terrain stations 204 - 208	154	-0.01	0.00
Average absolute value of drift rate = 0.06 mgal h ⁻¹						
Maximum absolute value of drift rate = 0.20 mgal h ⁻¹						

Table 9. The drift of the gravity meter on all loops made between fixed base stations. The drift is assumed to be linear with time. MB stands for the main base and SB for the sub-bases.

avalanches, and the east side can usually not be seen from two triangulation points.

Each station must have its elevation determined accurately, since changes in elevation completely dominate the readings of a gravity meter^{*}. To avoid placing a marker at each gravity station, surveying it at a later date, and then making corrections for ablation and movement, all stations were surveyed *simultaneously* with the reading of the gravity meter. This required two theodolites, portable radios and four to six people, but it enabled the field measurements to be completed in only four days and it simplified the reductions later on. It took approximately 5 minutes to complete the measurements at a station and at least two profiles could be completed before it was necessary to return to a sub-base. The procedure worked well and is highly recommended.

At the end of the summer, when most of the snow was gone from the ridges, 11 gravity readings were made on the terrain along the east side of the glacier. These values (referred to as "terrain stations") are useful for determining the regional field. They could only be made in relatively flat areas, where the terrain correction should be more reliable, and so this drastically limited the number of possible points^{**}. Furthermore, no points on the west side were made since the relatively high drift of a Worden gravity meter would make this a difficult and time-consuming project.

Table 9 gives the elapsed time and drift corrections for all loops made with the gravity meter. The drift rates are compatible with those obtained by Krimmel (personal communication, 1972), who used the same instrument as the author, and with those reported by Corbató (1965b), who used another Worden

* Raising a gravity meter by 3 m changes the reading by about 1 mgal.

** This statement is based on the experience of previous workers who used the "Hammer zones" for calculating terrain corrections. It is felt, however, that the method developed here for evaluating these corrections is considerably more accurate and that, in retrospect, it would have been feasible to make gravity readings in areas of severe terrain (for example, along the margins).

gravity meter.

The coordinates of the gravity stations were calculated from the theodolite measurements using the same procedure developed for the movement stakes (section 6.2.2). The z values refer to the glacier surface. All gravity values were placed on a rough absolute basis by fixing the main base at 980.592588 gal^{*}, and they were corrected for drift by assuming it to be linear with time. Errors will be discussed later (section 5.4).

5.2 REDUCTION OF THE GRAVITY OBSERVATIONS

Before gravity observations can be interpreted one must first remove all effects other than the one of interest, which in this case is the anomaly caused by the presence of the glacier. This anomaly is unfortunately very small compared to the magnitude of the other effects and so the reduction of the gravity observations must be done with great care. The following corrections are made:

- (a) Latitude correction (C_ℓ). This allows for the oblateness and rotation of the earth.
- (b) Elevation correction (C_e). This allows for the variation of gravity with distance from the earth's center.
- (c) Terrain correction (C_t). This allows for the departure of the surrounding topography from a plane.
- (d) Regional correction (C_r). This allows for horizontal trends in the gravity field, on a scale larger than that of the disturbing body.

When these corrections are added to the measured gravity g_m the values have been effectively reduced to sea level at the equator. If the "theoretical

* Computed from the International Gravity Formula using the altitude (1931 m) and latitude (046° 48' 05" N) of the main base and applying a plane Bouguer correction with standard rock density (2.67 Mg m⁻³). It ignores the effects of the terrain and the regional field.

gravity" G_o at this point is subtracted from g_m we get the "residual anomaly" Δg of the disturbing body:

$$\Delta g = g_m + C_l + C_e + C_t + C_r - G_o \quad (1)$$

5.2.1 *The Regional Correction*

The values of g_m are only relative and we consider the unknown origin to be part of the regional correction. In addition to this C_r contains the effects of isostatic compensation and of mass anomalies larger than the glacier. It cannot be calculated independently and must be inferred from the measurements. For this reason consideration of the regional field is usually left to the interpretation of the results, and the reduction of the observations deals only with the first three corrections:

$$\Delta g_b = g_m + C_l + C_e + C_t - G_o \quad (2)$$

The result, Δg_b , is called the "Bouguer anomaly"; it contains both the effect of the glacier and the regional field and it has an arbitrary origin.

5.2.2 *The Latitude Correction*

The latitude correction C_l is usually never evaluated explicitly. Instead one refers all measurements to the "reference spheroid". This is the mathematical equipotential surface that a transversely-isotropic, rigid rotating spheroid would have; such a surface has the form

$$g(\lambda) = \sum_{m=0}^{\infty} \alpha_m \sin^2 m\lambda \quad (3)$$

where λ is the geocentric latitude (Grant and West, 1965, p. 236). By fitting this with least-squares to world-wide pendulum measurements of gravity, reduced to sea level, we get* the "International Gravity Formula" for the reference spheroid (Heiskanen and Vening-Meinesz, 1960):

$$g_o(\lambda) = G_o - C_\lambda = 978049.0[1 + 5.2884 \sin^2\lambda - 0.0059 \sin^2 2\lambda] \quad (4)$$

Higher order terms are insignificant. Equation 2 then becomes

$$\Delta g_b = g_m + C_e + C_t - g_o(\lambda) \quad (5)$$

At middle latitudes this correction is about $0.812 \text{ mgal km}^{-1}$ in a north-south direction.

5.2.3 The Elevation Correction

The elevation correction traditionally has been separated into two parts, the "free-air" correction and the "Bouguer" correction. The free-air correction expresses the effect of moving the gravity meter toward or away from the earth's center. The vertical gradient of the earth's gravity field is given by (Grant and West, 1965; Garland, 1965):

$$\frac{\partial g}{\partial z} = -0.3086 - 0.00295 \cos 2\lambda + 0.73 \times 10^{-7} z \quad (6)$$

[Grant and West have a typographical error in the first term (equation 9-5, p. 239) and Garland has a mistake in the third term (equation 4.3, p. 46). The two sources do not agree on the second term either but Grant and West's value

* Based on data available in 1930. More recent satellite information has revised this somewhat but it is convention to take this as the reference spheroid. The error is completely negligible for small scale gravity surveys.

has been used since any error has negligible effect at the latitude of the Nisqually Glacier ($\cos 2\lambda \approx 0$).

The Bouguer correction allows for the fact that the space between the observation point and sea level is rock and not air. The terrain is assumed to be flat and the density of the rock ρ_r to be constant; the correction is then the attraction of a parallel-sided infinite sheet of thickness z ,

$$g_\infty = 2\pi\gamma\rho_r z \quad (7)$$

where γ is the gravitational constant. This opposes the free-air correction and so the total elevation correction is

$$C_e = -z \frac{\partial g}{\partial z} - 2\pi\gamma\rho_r z \quad (8)$$

Substituting numerical values we get

$$C_e = (0.3086 + 0.00295 \cos 2\lambda - 0.73 \times 10^{-7} z - 0.04186 \rho_r) z \quad (9)$$

For a standard rock density (2.67 Mg m^{-3}) this is approximately 0.2 mgal m^{-1} .

Hence the need for accurate elevations*.

5.2.4 The Terrain Correction

So far the corrections have been simple and can be accurately calculated to well within the experimental error. However, the fact that the terrain

* Ideally the elevation should be measured from the reference spheroid. However, all maps and surveyed elevations are with respect to the geoid, the equipotential surface that coincides with mean sea level (undisturbed by winds or tides). This deviates from the reference spheroid because of the mass anomalies of the earth's crust. The maximum departure is about 50 m but the effect is negligible on small scale gravity measurements (Grant and West, 1965, p. 266).

surrounding the station is not a plane means that the Bouguer correction is not rigorous and an additional correction has to be applied to account for the departure from this plane. The gravitational attraction of the material above the plane and of the *missing* material below the plane makes up the "terrain correction". Its value is always positive for local surveys (that is, it is added to the measured gravity) because the hills represent the addition of an upward component of attraction whereas the valleys represent the removal of a downward component of attraction. Evaluation of this effect is difficult and very tedious but it is essential in areas where the relief is greater than 1 in 20 (about 3°).

Terrain corrections have usually been estimated by graticule methods, such as those of Hammer (1939). The terrain is divided into a series of concentric rings about the station and each ring is divided radially into a number of compartments. The mean elevation of each compartment must be estimated manually. The number of compartments is kept small in order to reduce the time required; consequently the model of the terrain (portions of cylinder walls with flat tops) is rather crude. It is adequate in areas of moderate relief but in areas of high relief the zones are often subdivided in an attempt to make them more realistic (Corbató, 1963).

The Nisqually Glacier is located on the side of a very prominent volcano. Above it rises a huge mass of rock and ice and below it stretches much empty space. The valley walls are often very close and very steep. The terrain corrections are thus likely to vary over one of the widest ranges ever encountered in a gravity survey. Furthermore, the shallow depth of the glacier will produce relatively small anomalies and so the terrain corrections become all that more crucial. An accurate representation of the terrain would be very desirable. Talwani and Ewing (1960) suggested a suitable method, but to the author's knowledge it has not yet been applied to terrain corrections.

In view of the high accuracy required it was decided to develop the method for such a use. It has the additional benefit that, in future, gravity terrain corrections can be done more accurately, more quickly and far less painfully than has been possible in the past. A description of the method and the results is now given.

5.2.5 The Talwani and Ewing Method

Talwani and Ewing's method (1960) computes the gravitational attraction of a three dimensional body of arbitrary shape. Basically it is an extension of Hubbert's (1948) line-integral method to modern digital computers. The body is divided up into a number of "laminae", the attraction of each lamina is computed, and the results then integrated over all laminae. The laminae are made horizontal so that their boundaries can be represented by ordinary elevation contours.

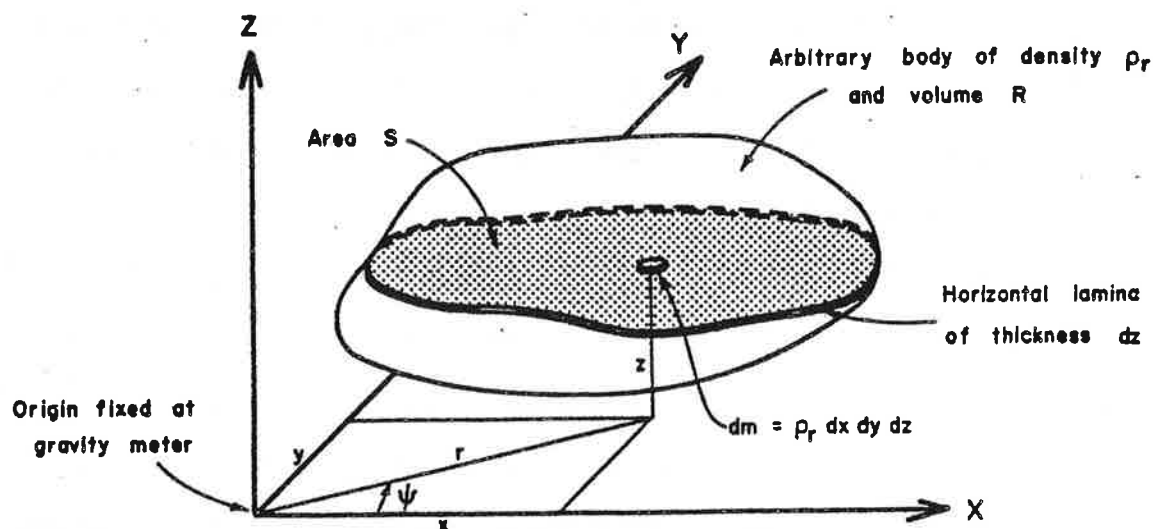


Figure 31. The calculation of the gravitational attraction of an arbitrary three dimensional body by the method of Talwani and Ewing (1960).

The gravitational attraction, at the origin, of the body R (Figure 31) is given by

$$g = \frac{\partial U}{\partial z} = -\gamma \frac{\partial}{\partial z} \int_R (r^2 + z^2)^{-1/2} dm \quad (10)$$

where U is the gravitational potential of the body. The coordinate system is assumed fixed at the gravity meter for this discussion. The "gravitational attraction" is *always* understood to be just the vertical component of the total gravitational attraction, since this is all that can be measured with a gravity meter. Differentiating (10),

$$g = \gamma \rho_r \int_R z r (r^2 + z^2)^{-3/2} dr d\psi dz \quad (11)$$

or

$$g = \int V(z) dz \quad (12)$$

where

$$V(z) = \gamma \rho_r \iint_S z r (r^2 + z^2)^{-3/2} dr d\psi \quad (13)$$

is the gravitational attraction per unit thickness of the lamina of area S and infinitesimal thickness dz . By writing Green's theorem in cylindrical coordinates, this surface integral can be converted to a line integral around the boundary of the lamina:

$$V(z) = \gamma \rho_r \oint [1 - z(r^2 + z^2)^{-1/2}] d\psi \quad (14)$$

Evaluation of equations 12 and 14 are the basis of this method.

To calculate this line integral the boundary of the lamina is replaced with an n -sided polygon. Talwani and Ewing show how the line integral can be written as the sum of a series of terms involving the coordinates of the

vertices of the polygon. The calculations require the use of a high-speed digital computer.

5.2.6 *Digitizing of the Terrain*

From a practical point of view the only significant preparation required is the "digitizing" of the topographic contour lines. Each contour line must be expressed as an array of (x,y) points, each point being a place where the contour changes direction significantly. Machines are now available to facilitate this process. In this case the University of Washington Computer Center's Benson-Lehner Digitizer was used. A cursor is moved manually along a contour line and the (x,y) coordinates are recorded digitally on magnetic tape either automatically at a fixed grid spacing or manually whenever a footpedal is pressed. The latter mode was used in order to keep the number of points to a minimum and still get an accurate representation of the contour. The resolution of the digitizer is 0.0254 mm (0.001 inch).

The terrain around the Nisqually Glacier was divided into five zones, with either rectangular or irregular boundaries (Figure 32). Unlike the Hammer zones these remain fixed and do not change from one gravity station to the next. Consequently the digitized terrain is slightly less accurate for stations near the boundaries of a zone; however, the size of the zones and the contour interval used were chosen so that this effect is completely negligible. Zone 1 consists of the entire lower Nisqually Glacier and thus contains all the glacier stations. The outer boundary of zone 2 was drawn about 1 km away from the nearest glacier stations*, and the remaining zones were drawn successively larger. All available contours were digitized in zones 1 and 2 but only certain contour levels were digitized in zones 3, 4 and 5. The outermost zone extends

* The figure of 1 km was determined mainly by the fact that this was the greatest distance which could be contained entirely on the 1956 map (1:12000). Any greater distance would have meant using the much poorer 1910-13 map (1:62500).

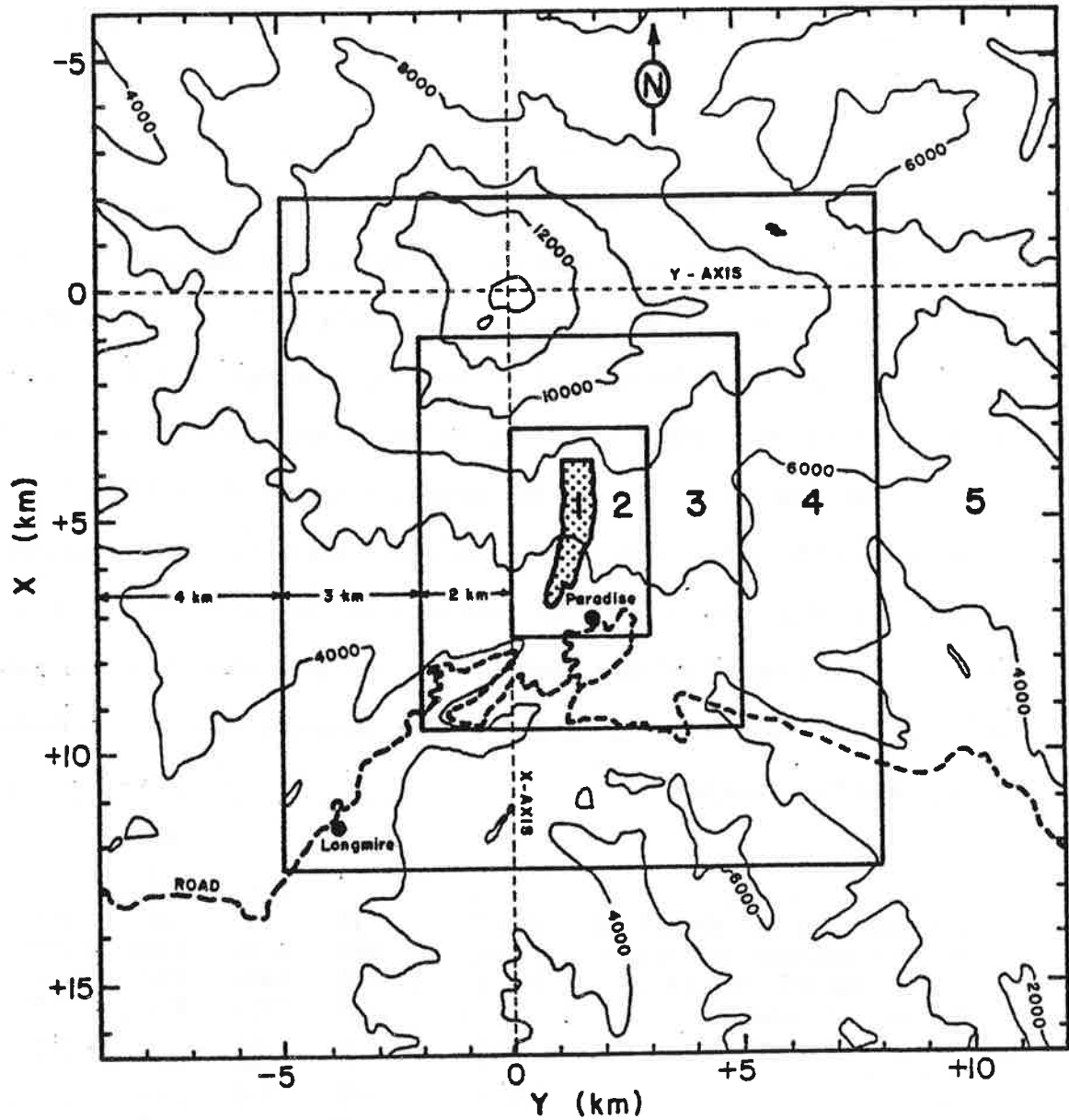


Figure 32. The location and dimensions of the five zones used in calculating the terrain corrections. The contour interval is 2000 feet (609.601 m). Zone 1 is the lower Nisqually Glacier.

at least 10 km from the glacier, the same distance used for gravity surveys on other glaciers (Danes, personal communication, 1969; Corbató, 1965b). Adding more zones is not justified as the contribution is indistinguishable from the regional field.

The terrain in the immediate vicinity of a station dominates the correction. To minimize errors the density of points was increased when digitizing in the area around a gravity station, so that within approximately 200 m of any station the terrain is represented as accurately as the original map permits. In addition the elevation of each station was adjusted so that it lies as close as possible to the surface formed by the digitized contours (see p. 121).

Various characteristics of the zones are tabulated in Table 10. The digitized terrain is shown in Figures 33 and 34; these have been computer-drawn on a Calcomp plotter with the actual data used in the reductions. This illustrates a side benefit of this technique: one ends up with a digitized map of the topography, which can be used for other purposes (such as producing a map to any desired scale).

	Zone				
	1	2	3	4	5
Contour interval digitized...(feet)	20	40	200	500	1000
Highest contour digitized....(feet)	7600	9200	13200	14000	12000
Lowest contour digitized.....(feet)	4800	4400	3600	3000	2000
Maximum elevation.....(m)	2365	2925	4142	4392	3749
Minimum elevation.....(m)	1416	1229	969	780	530
Width of zone.....(m)	--	~1000	2000	3000	4000
Δz_0(feet)	200	400	600	0	0
Δz_1(feet)	20	80	200	0	0
δ(feet)	100	640	2000	0	0
Execution time.....(s)	1350	1460	450	480	240
Approx. time for digitizing....(h)	2	4	3	2	1
Average terrain correction...(mgal)	1.47	5.04	5.31	3.81	0.98
Standard deviation of above..(mgal)	0.47	0.82	1.06	0.54	0.24
Minimum terrain correction...(mgal)	0.67	3.77	4.02	3.13	0.61
Maximum terrain correction...(mgal)	2.88	7.20	7.75	4.97	1.52

Table 10. Details of the terrain zones and the calculations of the terrain corrections for the 195 glacier stations. Δz_0 , Δz_1 , and δ are explained on p. 120.

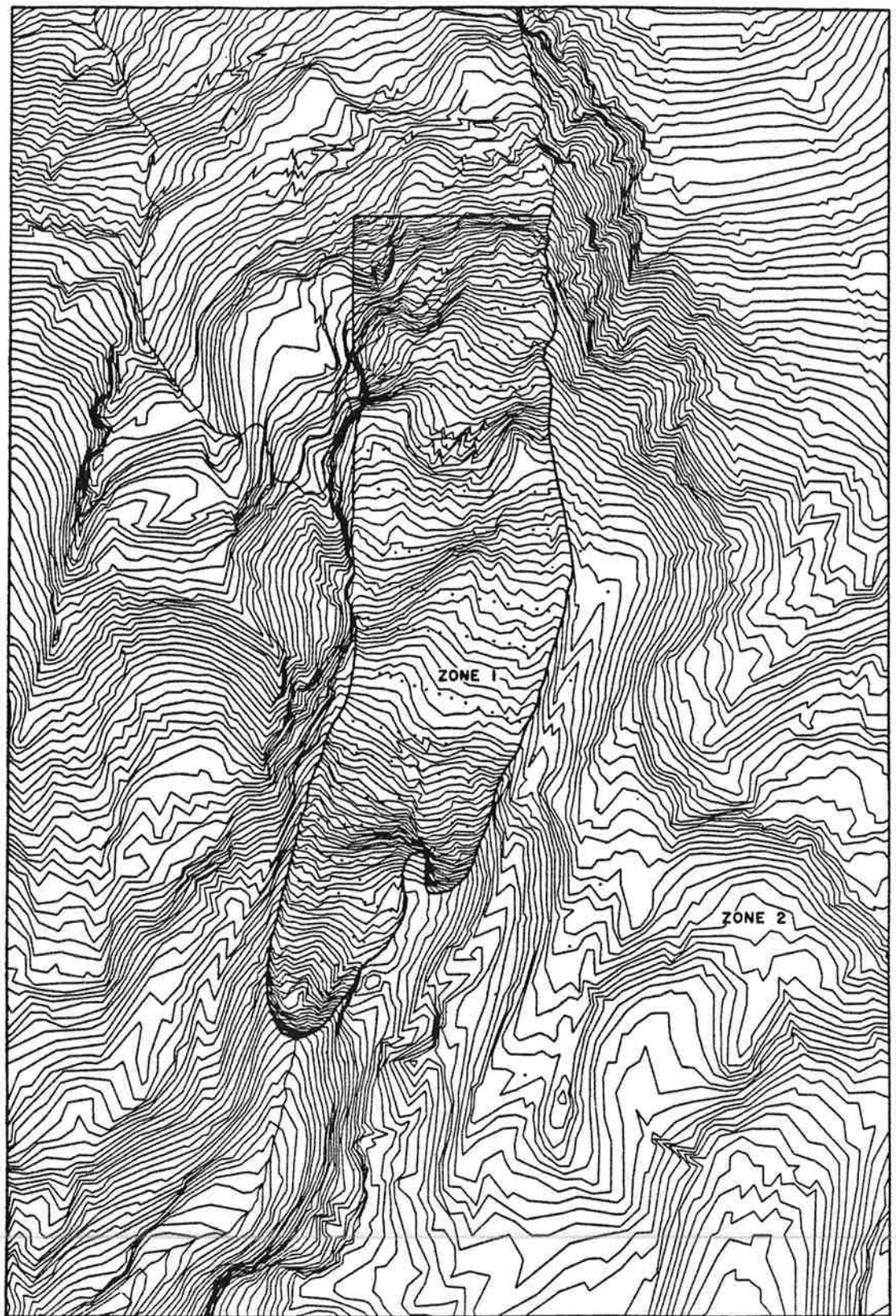


Figure 33. The digitized contours of zones 1 and 2. The contour intervals are 20 feet (6.096 m) and 40 feet (12.192 m) respectively.

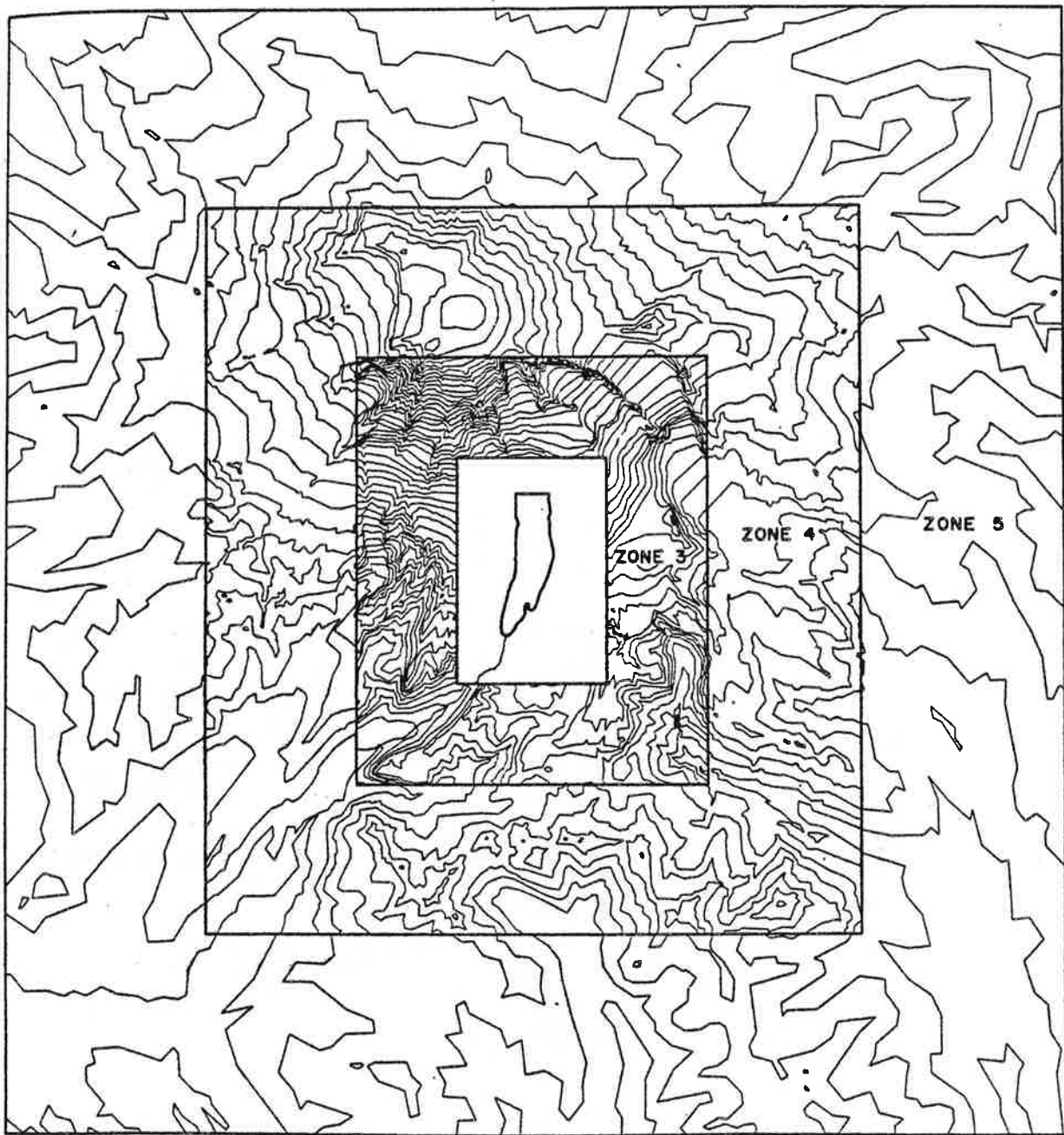


Figure 34. The digitized contours of zones 3, 4 and 5. The contour intervals are 200 feet (60.960 m), 500 feet (152.400 m) and 1000 feet (304.800 m) respectively. Zone 1 (the lower Nisqually Glacier) and the Nisqually River are also shown for reference.

5.2.7 *The Reduction Program*

An elaborate computer program was written to perform all gravity reductions, from the measured gravity to Bouguer anomalies. Besides the measured gravity values, input to the program consists of the station coordinates, the digitized terrain data, the rock density ρ_r , and various quantities necessary to define the glacier coordinate system and the digitized map coordinate system relative to one another and to the surface of the earth. A number of parameters control the execution of the program and the units and contour intervals used. The program has been written in a general, "black-box" manner so that it can be used by other people.

Only a few simple rules must be followed when digitizing the terrain; the program combines contour segments with the appropriate zone boundaries to form the necessary closed laminae, enclosing terrain above the station and empty space below. The line integral of equation 14 is calculated for each loop on each contour level and then the results are integrated over z (equation 12) to give the terrain correction for that zone. The total terrain correction is obtained by summing the results for each zone. The elevation correction is evaluated using equation 9, the latitude correction using equation 4 and the Bouguer anomaly using equation 5. All calculations are repeated for each gravity station.

All programming in this study (other than the basic net adjustments) was done by the author in FORTRAN IV (CDC version 2.3) and all executions were done on the University of Washington's CDC 6400 computer. This is a high speed scientific digital computer with remote terminal facilities. The word size is 60 bits, approximately 14 significant figures for real numbers, and so round-off error was never encountered.

5.2.8 *The Rock Density*

The density of the bedrock and its variations are usually the big unknowns in any gravity survey of a glacier. The lava flows which make up the bulk of Mount Rainier are composed of pyroxene andesite of uniform composition (Fiske, Hopson and Waters, 1963). Two bulk density samples, three cores each, were made by Christensen (personal communication, 1971) of representative andesite rock near Paradise. The average density found was $2.604 \pm 0.007 \text{ Mg m}^{-3}$. Christensen does not expect this value to vary more than $\pm 0.1 \text{ Mg m}^{-3}$, and so the value $2.6 \pm 0.1 \text{ Mg m}^{-3}$ will be assumed for this investigation. No rock samples were collected from around the glacier because it is very doubtful they would be any more characteristic of the underlying bedrock.

The range of densities found around glaciers not on the flanks of volcanoes could well be greater. For example, Corbató (1965b) reports a range of 0.1 Mg m^{-3} for the Blue Glacier (low grade metamorphic rocks) and Crossley and Clarke (1970) report a range of 0.3 Mg m^{-3} for the "Fox Glacier" (predominantly basalt and andesite).

The extent of the andesite is shown in Figure 20. It covers all of the terrain surrounding the Nisqually Glacier, except in the valley below the terminus. Here the underlying Tatoosh pluton is exposed. This was formed between the early Miocene and late Pliocene, before the volcanic eruptions of the Pleistocene which built the volcano of Mount Rainier. It is composed of granodiorite and quartz monzonite. Although these have densities close to that of andesite (Coombs, personal communication, 1972), the more complex geology near the terminus of the glacier does suggest that the regional field may have more pronounced variations here than over the remainder of the glacier.

There is some confusion in the literature as to the correct method of calculating terrain corrections in a region containing both ice and rock. Since we desire the residual anomalies to be due *only* to the effect of the

disturbing body (the glacier), we should correct for everything else *except the disturbing body* as realistically as possible. Terrain which is not part of the disturbing body would, in general, have two possible densities, that of rock and that of ice (where other glaciers exist). Terrain which is part of the disturbing body, on the other hand, should be treated as though it were rock. The resulting anomalies would then be a manifestation of the fact that the disturbing body is actually ice and not rock.

Kanasewich (1963) used a different density depending on whether the sector was ice or rock, *including* those sectors within the disturbing body. When later modelling the glacier only the ice *below* a station was considered, the rest presumably having "been accounted for by the terrain correction" (p. 622). This procedure would be reasonably valid provided (a) the glacier has a large enough thickness and a small enough slope that the part of it above the station is ice throughout and remains essentially unchanged during the modelling, and (b) any ice-covered terrain outside the glacier is treated as ice only down to a certain depth (which must be assumed somehow). If the terrain is treated as ice all the way from the surface to the horizontal plane through the station then the error might be appreciable when the surface is high enough above the station.

For the terrain below the station this procedure is not valid, however, since here the terrain correction applies to the empty spaces. These *must* be treated as rock because they were originally assumed to be such in the Bouguer part of the elevation correction.

Kanasewich (1963, p. 618) states only that "care had to be taken to distinguish between the sectors containing ice ... and sectors containing rock..." Thus it is not clear if the above restrictions were followed.

On the other hand, Crossley and Clarke (1970), who follow a similar procedure, do treat the terrain below the station correctly. The terrain above

the station, including that within the glacier, is considered to be either rock or ice of 50 m thickness. If this figure is valid this procedure gives the proper terrain correction *provided* the modelling is restricted to the region below the station. They do not appear to have done this and so the ice above the station is effectively accounted for twice.

In this study terrain corrections are done using the density of the rock (2.60 Mg m^{-3}) everywhere. Thus a small error is introduced because some of the terrain outside the disturbing body is actually ice and not rock. However, because the glaciers on Mount Rainier are steep and thin the effect is probably insignificant and, at any rate, is undoubtedly indistinguishable from the regional trends. Furthermore, to allow for it one would have to guess at the ice thickness and the computer program would become unjustifiably complicated. This is the same technique used by Corbató (1965b) on the Blue Glacier.

5.2.9 Numerical Evaluation of the Line Integral

For the numerical evaluation of equation 14, Talwani and Ewing's expressions were replaced with those of Corbató (1965b):

$$V(z) = -(\text{sign } z)\gamma\rho_r \sum_{i=1}^n \tan^{-1}\left(\frac{P_i}{Q_i}\right) \quad (15)$$

where, using Corbató's notation,

$$\left. \begin{aligned} P_i &= T_i A_i + S_i B_i & A_i &= |z| S_i (D_i C_{ij} + D_j C_{ii}) \\ Q_i &= T_i B_i - S_i A_i & B_i &= S_i^2 D_i D_j - z^2 C_{ii} C_{ij} \\ R_i &= x_i^2 + y_i^2 & C_{ij} &= T_i - R_j \\ S_i &= x_j y_i - x_i y_j & D_i &= (R_i + z^2)^{1/2} \\ T_i &= x_i x_j + y_i y_j & j &= i + 1 \end{aligned} \right\} \quad (16)$$

Rather than evaluating n arctangents, the summation in equation 15 is computed by repeated use of the trigonometric formula:

$$\tan^{-1}\left(\frac{P_a}{Q_a}\right) + \tan^{-1}\left(\frac{P_b}{Q_b}\right) = \tan^{-1}\left(\frac{P_a Q_b + P_b Q_a}{Q_a Q_b - P_a P_b}\right) \quad (17)$$

The principal values of arctangent (which are calculated by the computer) are between $-\pi$ and $+\pi$. However, the summation

$$\sum_{i=1}^n \tan^{-1}\left(\frac{P_i}{Q_i}\right) \quad (18)$$

must lie between 0 and $\pm 2\pi$, since $\pm 2\pi \gamma_P$ would be the anomaly per unit thickness of an infinite sheet*. Thus the summation represented by (18), as calculated by repeated use of (17), must either have (a) 2π subtracted from it if it is positive and the integration is in the mathematically negative sense (the vertices numbered clockwise when viewed from above), or (b) 2π added to it if it is negative and the integration is in the negative sense.

Because only *one* arctangent is calculated per loop when equation 17 is used the machine time required is cut in half (to about 0.7 milliseconds per vertex). The procedure was tested by calculating the attraction of a sphere of radius 100 m at a point 300 m above and 300 m to the side. When the sphere was represented with a contour interval of 2 m, with points spaced every 3° , the error was 0.00013 mgal, and when it was represented with 10 m contours, with 15 points each, the error was 0.0032 mgal. The error decreased as the observation point was moved further away. For this test case, the error is cumulative since *all* polygons were inscribed in the sphere. For actual terrain the polygons are both inside and outside the real contours and so the error should be less.

* We are indicating signs in this discussion because we are dealing with the general case of the attraction of a lamina which is either above or below the station. For terrain corrections, however, we *always* take the absolute value.

5.2.10 Numerical Integration of $V(z)$

The numerical evaluation of equation 12 is not always a simple matter as a discontinuity in $V(z)$ can occur when $z = 0$, the elevation of the station. Many problems were encountered until it was realized that treatment of this discontinuity is not correct in the literature. For this reason a more detailed discussion is given.

Ignoring the factor of $\gamma\rho_r$ we can write $V(z)$ as the sum of two dimensionless line integrals:

$$I_1 = \oint d\psi \quad (19)$$

$$I_2 = - \oint z(r^2 + z^2)^{-1/2} d\psi \quad (20)$$

The first integral is simply the net cylindrical angle ψ swept out in one circuit around the lamina, and therefore it can have the following values:

(a) $I_1 = 0$ if the Z axis lies outside the lamina, or (b) $I_1 = 2\pi$ if the Z axis lies inside the lamina, or (c) $I_1 =$ the angle subtended by the lamina if the Z axis lies on the boundary [for a smooth boundary (no discontinuities in its curvature) this angle would be π , but for a polygonal boundary (as used in the calculations) it could also have some other value, between 0 and 2π , if the Z axis coincided with a vertex of the polygon].

If a station is not enclosed by any lamina*, then I_1 is always identically zero. Furthermore, the coordinate r will always be non-zero and so I_2 is always defined, and, in particular, $I_2 = 0$ at $z = 0$. The curve $V(z)$ is thus continuous everywhere, as shown in Figure 35. It does not approach the Z -axis asymptotically, but instead becomes zero at the highest and lowest

* It is assumed that the zone boundaries are always drawn so that the stations are either inside or outside the zone, that is, stations never lie on a zone boundary.

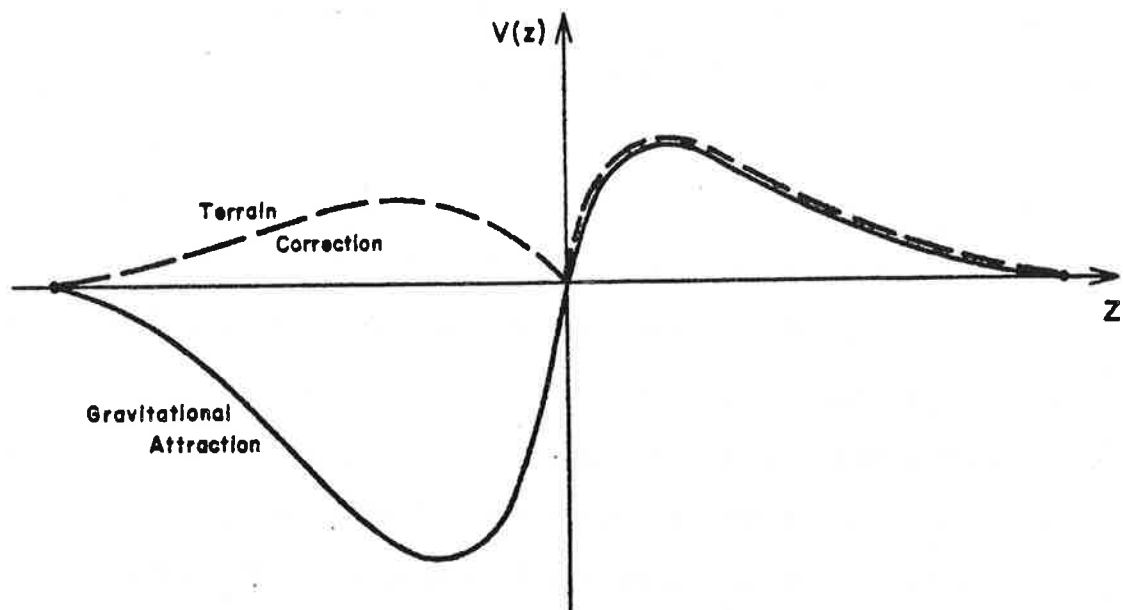


Figure 35. The form of $V(z)$ for (a) the gravitational attraction of a body and (b) the terrain correction of a body.

points of the body.

If instead of calculating the gravitational attraction of the body, we are calculating the terrain correction, two changes occur when $z < 0$. First, the sign of V is changed since the terrain correction must always be positive. Second, the integration is performed around the empty spaces instead of the body. We then get a curve such as the dashed line in Figure 35. As before, it passes through the origin, but there is now a discontinuity in slope at this point.

The real difficulties arise, however, when the station is enclosed by some of the laminae, for example, when doing the terrain corrections for zone 1. Now (a) the integral I_1 can undergo a jump of 2π when the station changes from outside to inside a lamina, and (b) both r and z can become zero if the boundary of a lamina passes through the station.

To illustrate what happens in this situation consider moving a lamina at

constant z past a station at the origin (line (a) of Figure 36). This is equivalent, apart from a possible sign change, to moving the gravity meter parallel to a fixed lamina (Figure 37). The results of actual computations for the lamina shown are given in Figures 38 and 39, where (x, z) are the coordinates of the gravity meter along line (a). I_2 undergoes a discontinuity of 2π at $x = 0$ (Figure 38). This is offset by an equal but opposite discontinuity in I_1 at the same place (Figure 39). Thus, as long as $z \neq 0$, $V(z)$ is continuous everywhere.

However, when $z = x = 0$, the integral I_2 is undefined. From Figure 39 we see that $V(z)$ becomes a discontinuous function as $z \rightarrow 0$. Since the discontinuity is 2π it must arise solely from the 2π discontinuity in I_1 , and thus I_2 can be taken as zero at this point.

Now consider the situation shown by line (b) in Figure 36. Here the leading edge of the lamina follows a path of slope α , passing through the point $x = z = 0$. Since gravity stations are by necessity located on the glacier surface, there will always, at least in principle, be some lamina whose boundary passes exactly through the station. Hence this is the situation encountered in practice.

By the above reasoning, at $z = 0$, $I_2 = 0$ and $V(z) = \gamma \rho_F I_1 = \pm \gamma \rho_F \pi$ for a smooth boundary. However, nothing in the above reasoning implies that $V(z)$ approaches this value at $z = 0$. This is clearly shown in the actual computations shown in Figure 40 for line (b) of Figure 36. Because z now changes sign as the leading edge passes the station, the discontinuities in I_1 and I_2 add together instead of cancelling. However, since $I_2 = 0$ at this point, we end up simply with a 2π discontinuity from I_1 .

The calculations were done for various slope angles α . The discontinuity of 2π is always present but there is absolutely no indication of $I_1 + I_2$ approaching $\pm\pi$, even with the expanded scale shown in Figure 41. A different

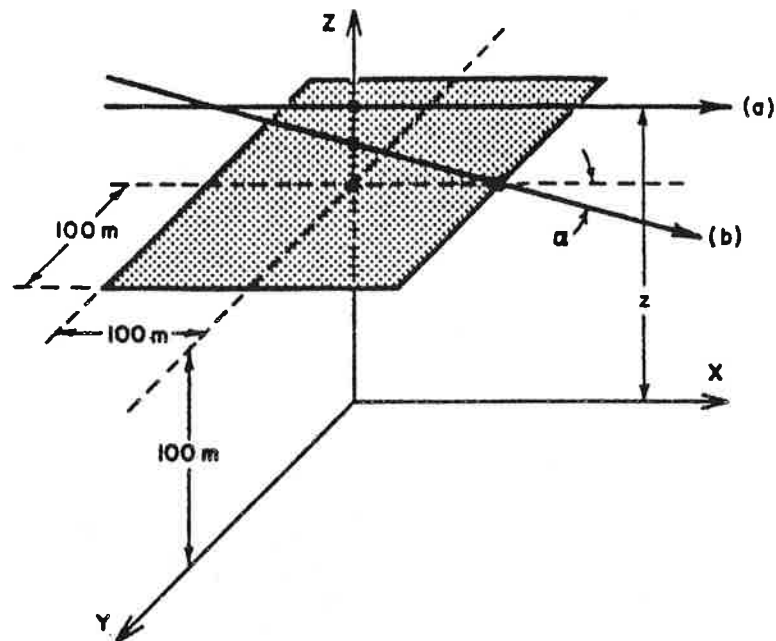


Figure 37. The hypothetical situation used for illustrating the discontinuity in $V(z)$: the gravity meter moved past a fixed lamina. (a) in the horizontal plane. (b) at an angle α to the horizontal, passing through the edge of the lamina.

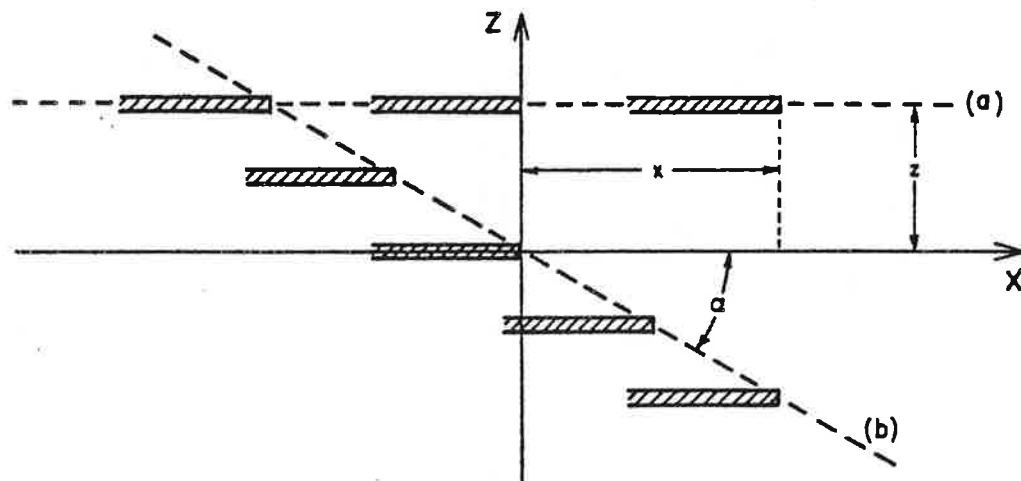


Figure 36. The hypothetical situation used for illustrating the discontinuity in $V(z)$: a lamina moved past the gravity meter fixed at the origin. (a) in the horizontal plane. (b) at an angle α to the horizontal, passing through the edge of the lamina.

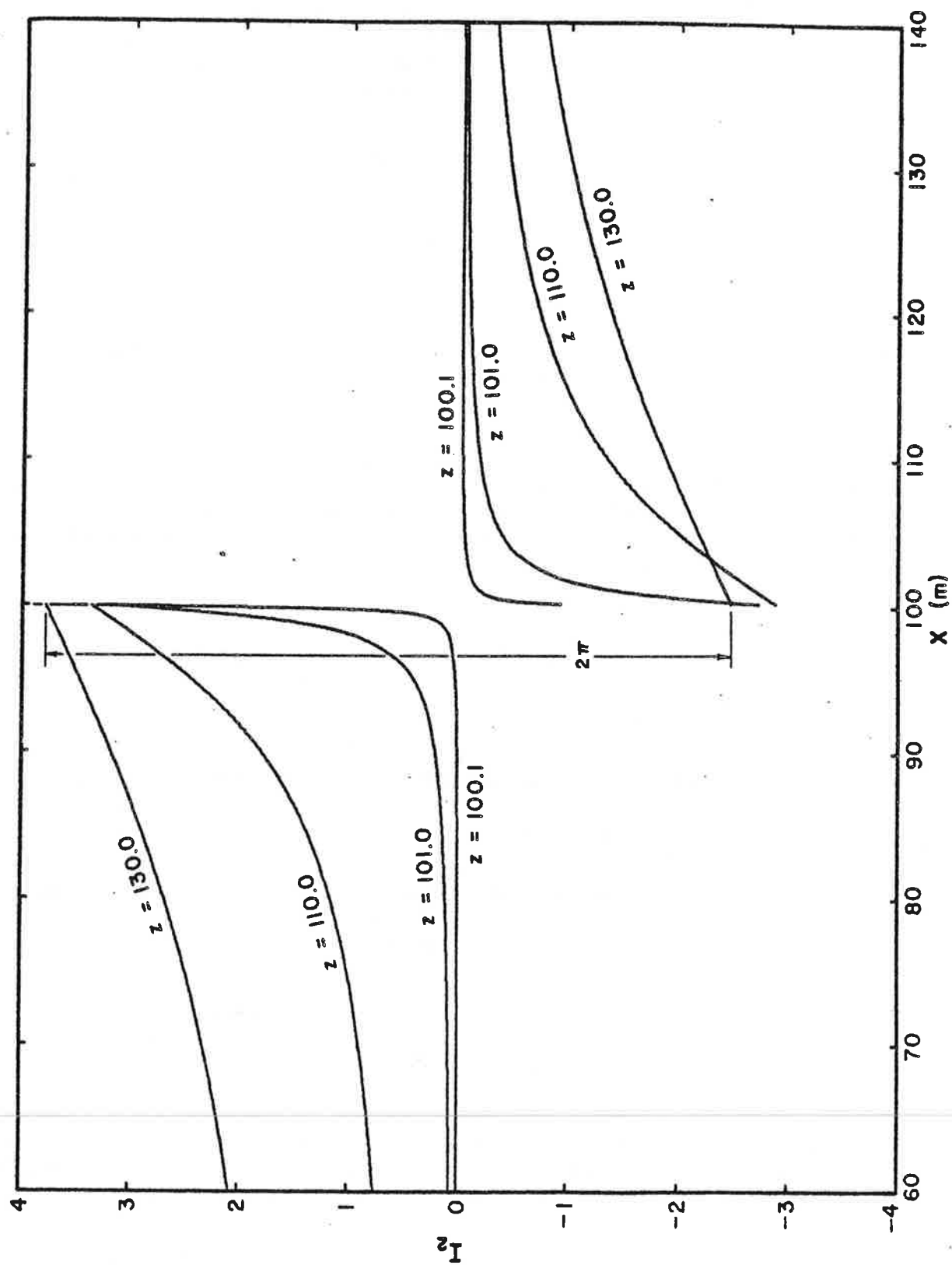


Figure 38. The integral I_2 for case (a) of Figures 36 and 37. The discontinuity is always 2π .

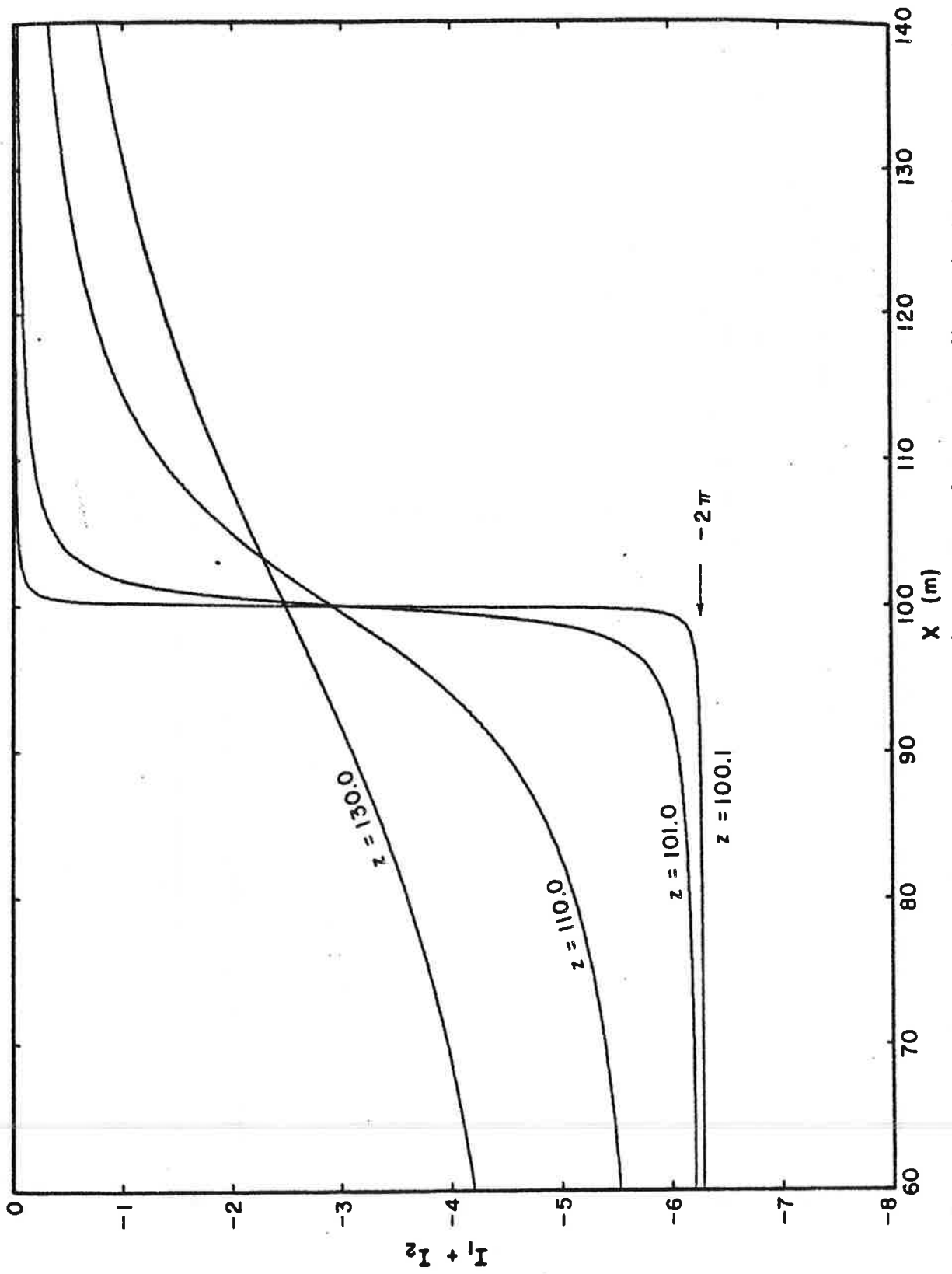


Figure 39.. The sum $I_1 + I_2$ for case (a) of Figures 36 and 37. The discontinuities now cancel.

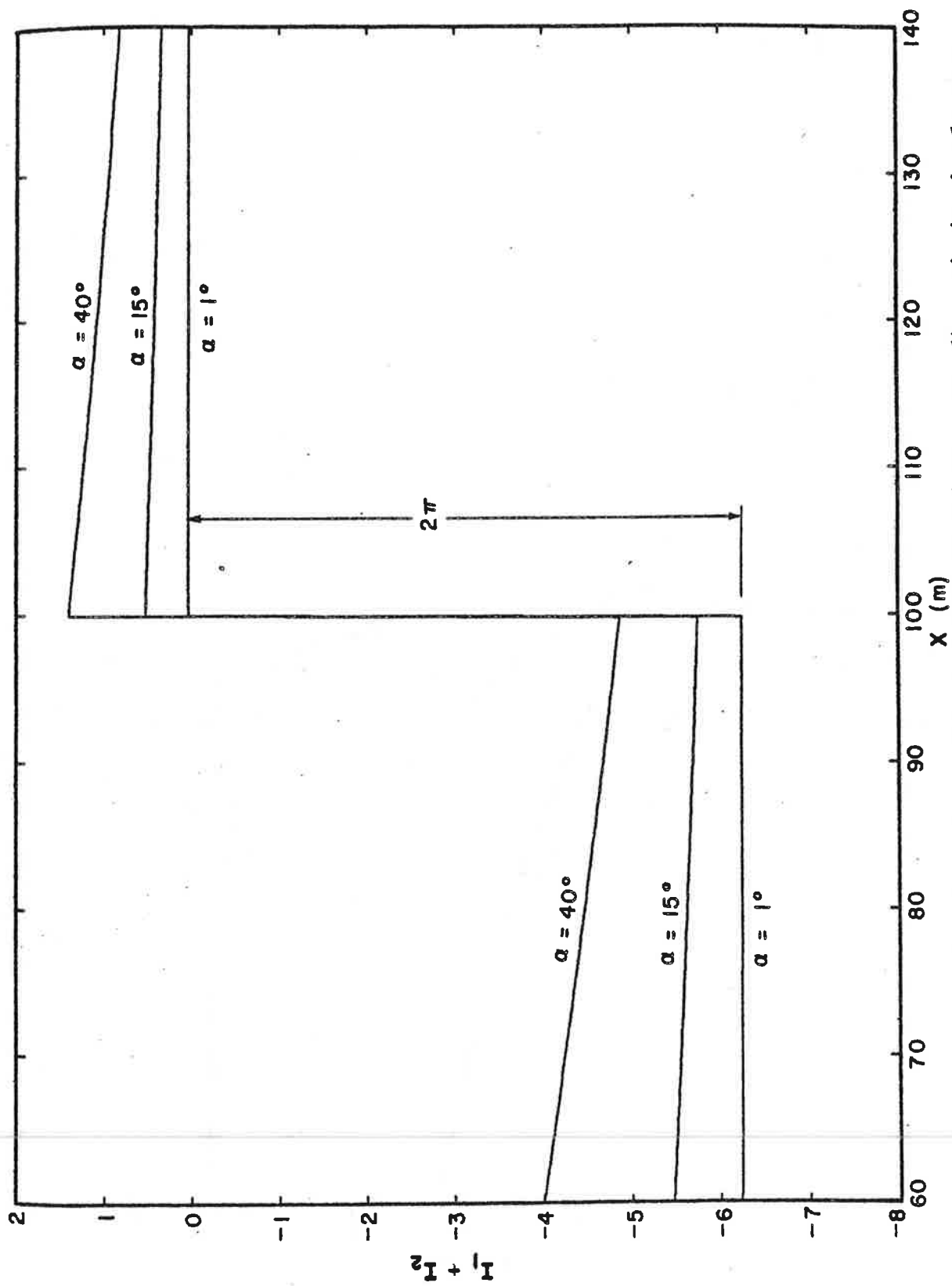


Figure 40. The sum $I_1 + I_2$ for case (b) of Figures 36 and 37. The discontinuity is always 2π .

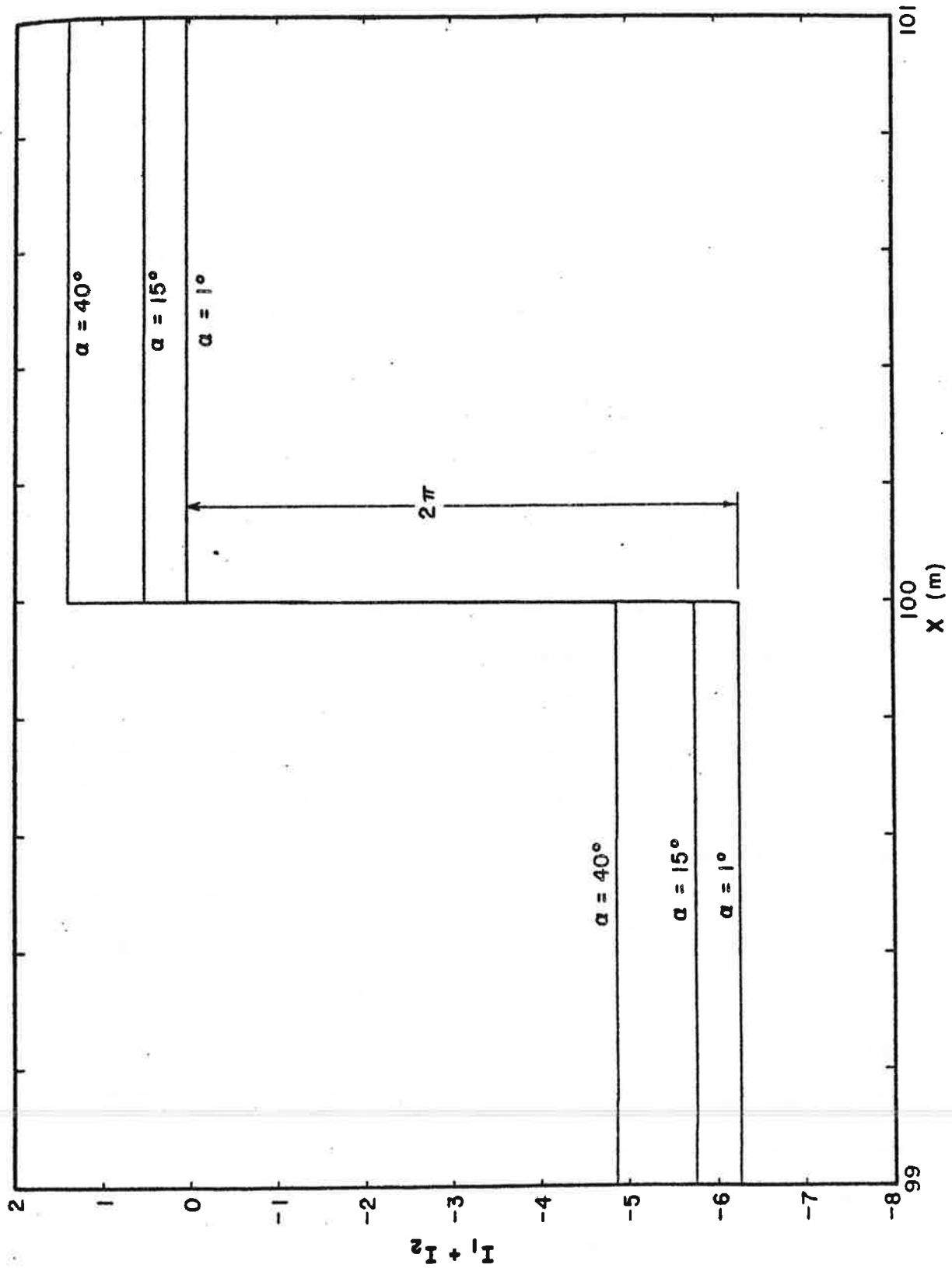


Figure 41. The sum $I_1 + I_2$ for case (b) of Figures 36 and 37, expanded scale.

value is approached depending on the slope angle α .

Another verification of this is seen by taking the limiting case of $\alpha \rightarrow 0$. This is identical with the limiting case of $z \rightarrow 0$ shown in Figure 39. The value of zero is approached by laminae not enclosing the station and 2π by laminae enclosing the station.

The true $V(z)$ curve would therefore show a $\pm\gamma\rho_x\pi$ spike exactly at the point $z = 0$. However, since it is of finite height but zero width, its contribution to the total integral is zero. Consequently we neglect it on any of the curves.

Corbató (1965b, p. 646) claims the integral approaches $\pm\gamma\rho_x\pi$ and Kanasevich (1963, p. 618, p. 622) has it approaching $\pm 2\gamma\rho_x\pi$. Both of these are incorrect. The values at the station elevation should be obtained by evaluating the line integral for laminae infinitesimally close to the station, but not at the station. In practice we do not have such laminae, as they would have to be drawn and digitized for each station. Instead it is easier to extrapolate the two halves of the curve up to the station elevation. The only limitation is that *the two values must differ by 2π* . This is shown in Figure 42, along with the error caused by Corbató's assumption. This error is usually significant, at times being as high as 1 mgal.

This figure also illustrates another problem. As the laminae approach the station elevation, variations in $V(z)$ become more pronounced and the points in this region can show considerable "scatter" or "noise". This is real and is simply due to the peculiarities of the individual laminae. The problem arises when one attempts to extrapolate these points to the station elevation. In order not to introduce misleading values of V^+ and V^- (Figure 42), the values of V at the adjacent laminae are used, with an adjustment so that $V^+ - V^- = 2\pi$. If z^+ and z^- are the elevations of the laminae immediately above and below the station respectively, then the adjustment is

$$I_1 = V(z^+) - V(z^-) - 2\pi \quad (21)$$

This is weighted according to the distance from the lamina to the station and applied as follows:

$$V^+ = V(z^+) - \epsilon \left(\frac{z^+}{z^+ - z^-} \right) \quad (22)$$

$$V^- = V(z^-) - \epsilon \left(\frac{z^-}{z^+ - z^-} \right) \quad (23)$$

These equations apply only when calculating the gravitational attraction of the body. They do not apply to terrain corrections since below the station the laminae enclose the empty space and hence, like the laminae above the station, they never enclose the station. Thus for terrain corrections, I_1 is *always* identically zero. A discontinuity still occurs at the station elevation; however, we can not put any restrictions on it. In practice, the discontinuity is seldom very large and no significant error is introduced by setting $V(z=0)$ to a single value found by interpolating between $V(z^+)$ and $V(z^-)$.

These discontinuities which occur at $z = 0$ limit the numerical integration scheme which can be used. Immediately above and below the station only the trapezoid rule should be used, as fitting of a polynomial of degree greater than one in this region could easily have disastrous results. Similarly, if there is significant "noise" in the points the trapezoid rule is the safest. On the other hand, if the points lie on a reasonably smooth curve the Lagrangian rule can be used for a more accurate integration. The reduction program has the option of using the trapezoid rule throughout, the Lagrangian rule throughout, or a combination of the two. The worst "noise" occurs with the

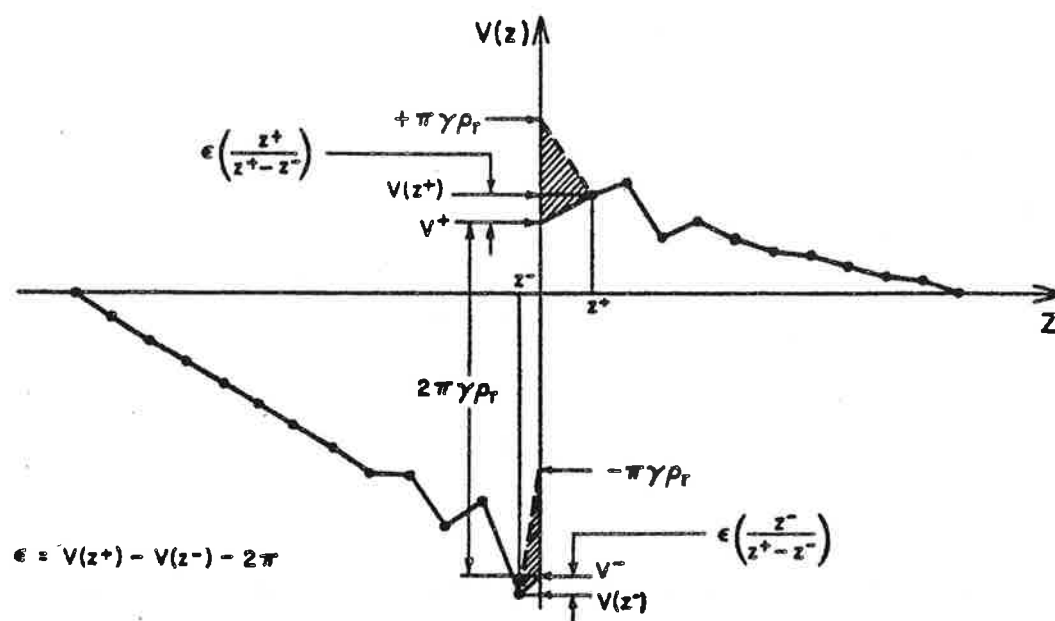


Figure 42. The method for handling the discontinuity in $V(z)$ at the station elevation. The shaded area represents the error caused by assuming the two halves of the curve approach $\pm\pi\gamma\rho_f$. This is used when calculating the gravitational attraction of a body with Talwani and Ewing's method; for terrain corrections a simple interpolation between $V(z^+)$ and $V(z^-)$ is used instead.

terrain in the immediate vicinity of the station (Figure 42). Thus the trapezoid rule only was used for the glacier stations, zone 1, and for the terrain stations, zone 2. Otherwise, the Lagrangian rule was used up to the contours immediately above and below the station, and the trapezoid rule in between.

Since values of $V(z)$ change most markedly when z approaches the station elevation, the program was written so that $V(z)$ could be calculated for two different increments in z : a close spacing Δz_0 near the station and a wider spacing Δz_1 away from the station. The half width δ of the closely spaced region was also made a variable and was chosen so that it always encompassed the maxima in $V(z)$ on either side of the station elevation. In this way computation time was kept to a minimum without sacrificing accuracy in the

integration. Values of Δz_0 , Δz_1 and δ for each zone were included in Table 10.

One final problem must be mentioned. The coordinates of the gravity stations are obtained from survey measurements, whereas the coordinates of the vertices of the polygons representing the contour lines are obtained by digitizing a map. The two systems can never be aligned perfectly and consequently it occasionally happens that a contour line lies on the wrong side of the gravity station. For example, a contour lying just above a station could actually enclose the station by accident. This would add $2\pi\gamma\rho_T$ to V and thus produce a point which lies far from the proper curve. This problem was very frequent for the Nisqually Glacier since the elevations of the glacier stations as determined from the map were up to 12 m different from those determined by surveying (Figure 43). The differences are real and represent (a) dynamic changes in the glacier surface in the three years between the map survey and the gravity survey, and (b) variations in the winter snow depth (the gravity survey was done near the beginning of the ablation season, whereas the map was made near the end). To correct for this new elevations for each station were estimated from a plot of the digitized terrain. These were used only for the terrain corrections, the surveyed elevations being used for the elevation corrections. A small, but probably insignificant error is thus introduced.

Even this procedure, however, is not perfect and occasionally the above situation would occur. Consequently it was necessary to reject contours within a certain (vertical) distance of the gravity station. This distance turned out to be about 0.6 m (2 feet) in practice.

Figure 44 shows the $V(z)$ curves for all five zones for a gravity station near the center of the glacier. The total terrain correction for the station is the total area under all five curves. The discontinuity which occurs at the station elevation on the zone 1 curve is apparent, but the error caused by

interpolating between $v(z^+)$ and $v(z^-)$ is clearly negligible*.

5.2.11 Results of the Gravity Reductions: the Bouguer Anomalies

Figures 45 through 48 show the distribution of the terrain correction for each of the five zones. These were computer-contoured using a procedure developed for analysis of the thickness variations (chapter 7). The agreement with hand-contouring is less than 0.1 mgal. As expected, the distribution becomes smoother as the zones get larger and further away. The corrections for the final zone (number 5) are almost linear with x and reflect the predominantly north-south trend of the topography. Other features of the terrain correction calculations were given in Table 10.

Figure 49 gives the total terrain corrections and Figure 50 the resulting Bouguer anomalies. The total terrain correction ranges from 10.1 to 22.1 mgal, the highest values and greatest range of values yet obtained on a glacier. The Bouguer anomalies, on the other hand, have a *maximum* range of only 7.27 mgal, which corresponds to an infinite slab thickness of about 100 m (for a density contrast of 1.7 Mg m^{-3}). This is one of the thinnest glaciers that gravity measurements have been done on. Thus we have ample justification for doing detailed and accurate terrain corrections.

* Since the trapezoid rule was always used in the region around the station elevation it is not actually necessary to interpolate a value, since the trapezoid rule automatically does this. However, we have indicated the interpolation to emphasize the fact that the curve is *not* continuous at this point.

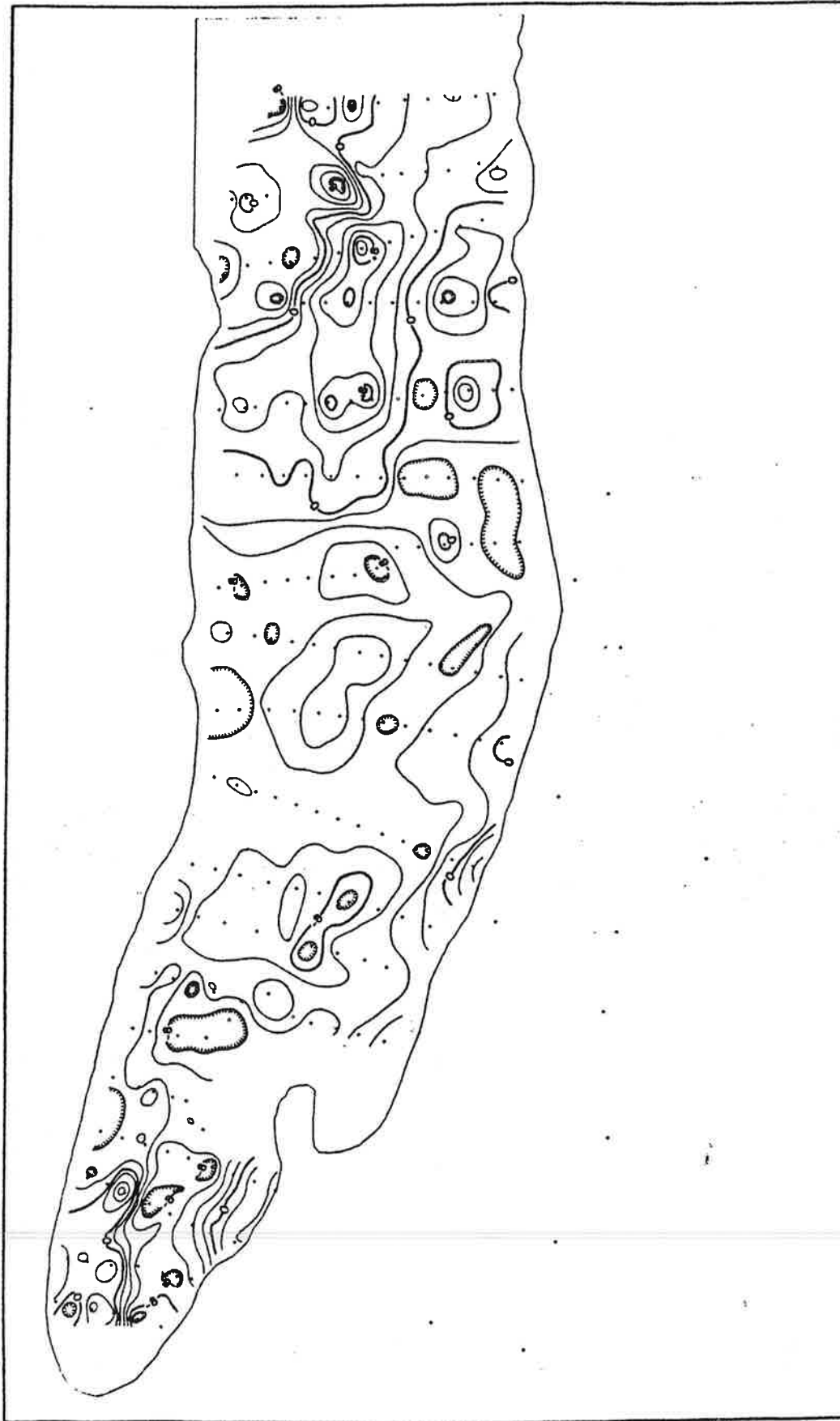


Figure 43. The difference in elevation between the 1966 map surface and the surveyed elevations of the gravity stations. The contour interval is 2 m. Positive values indicate an increase in thickness since 1966.

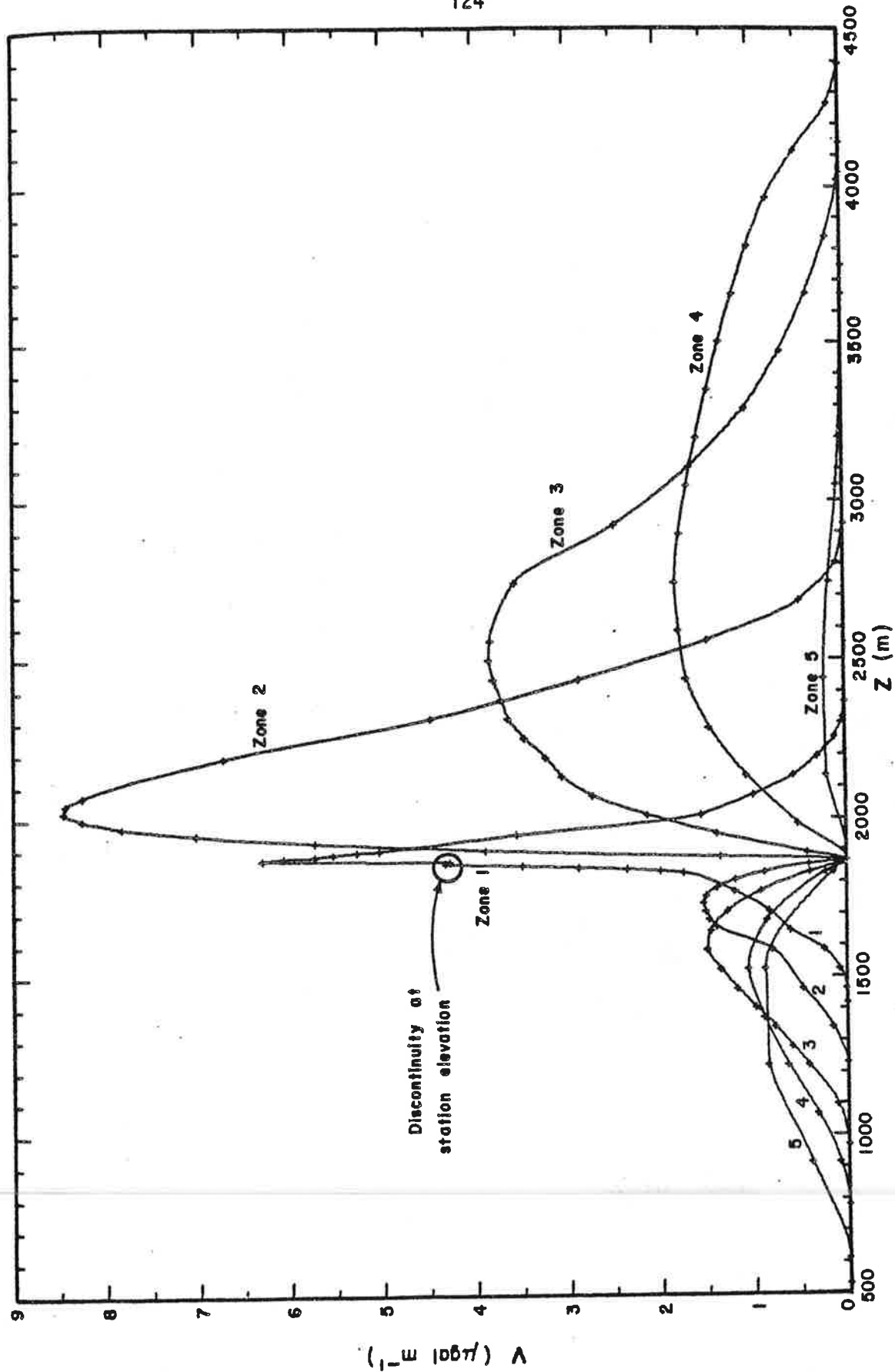


Figure 44. Typical $V(z)$ curves for the five zones used in the terrain correction calculations (for station 90, near the center of the glacier). Note the discontinuity at the station elevation for zone 1.

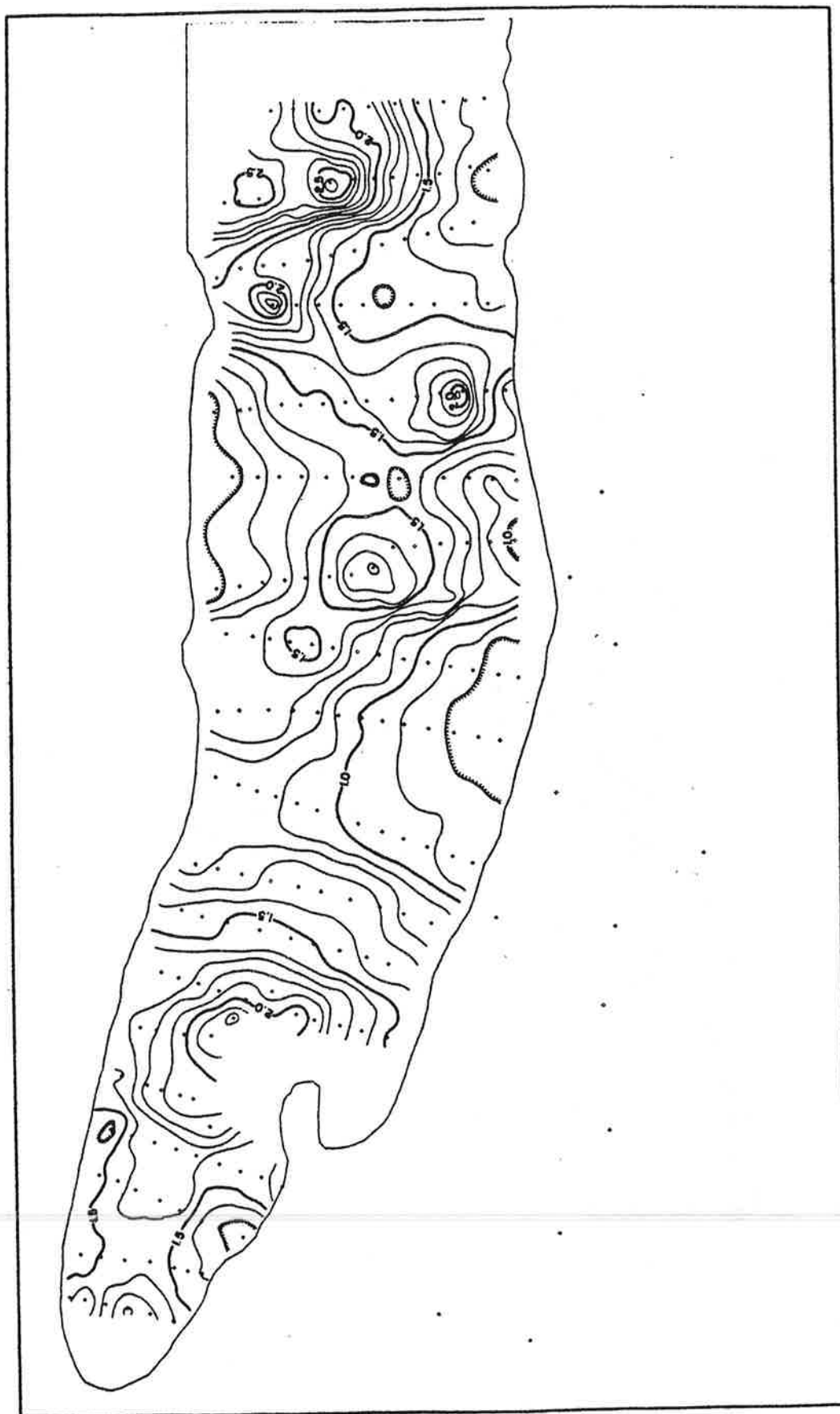


Figure 45. The terrain corrections for zone 1. The contour interval is 0.1 mgal.

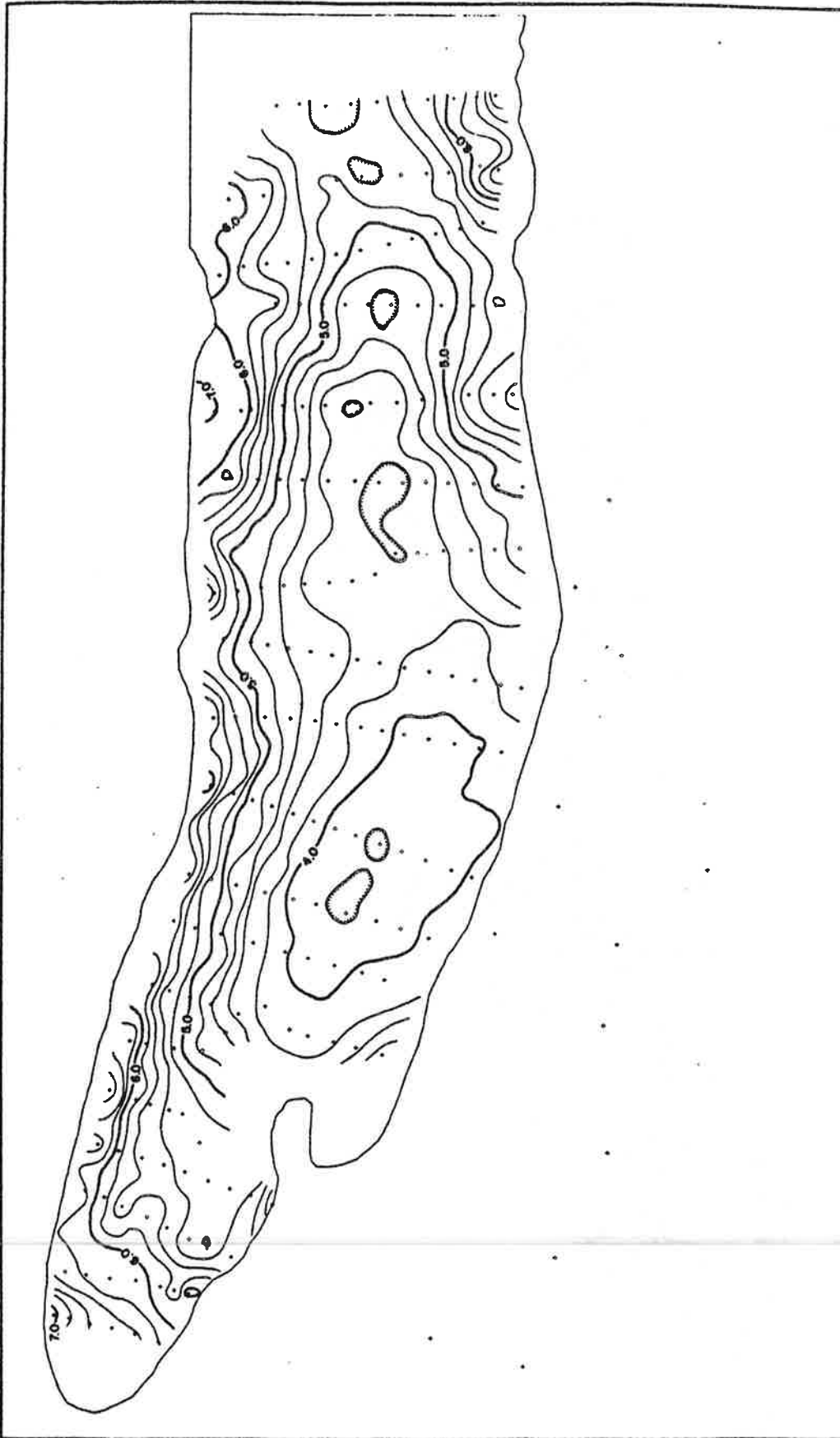


Figure 46. The terrain corrections for zone 2. The contour interval is 0.2 mgal.

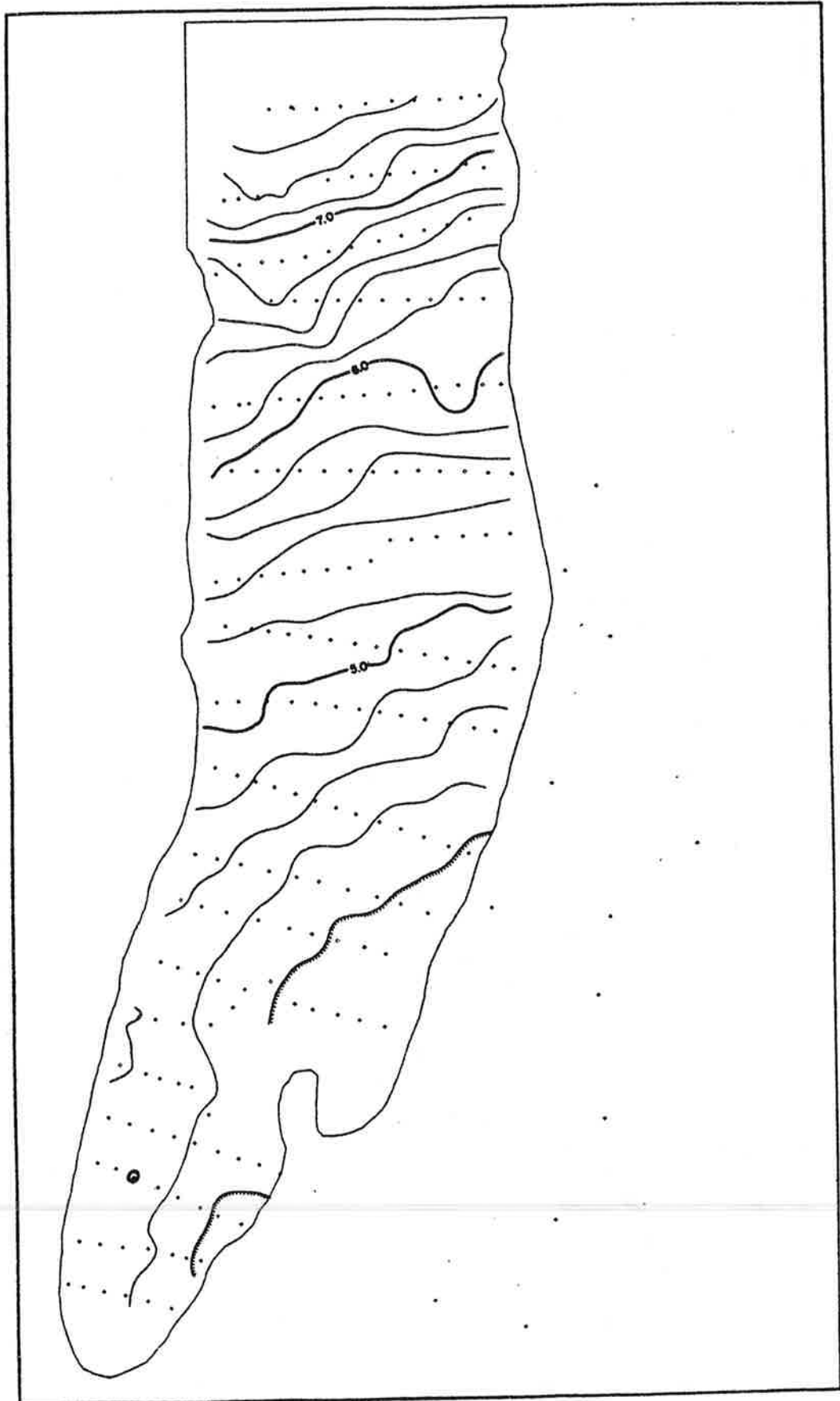


Figure 47. The terrain corrections for zone 3. The contour interval is 0.2 mgal.

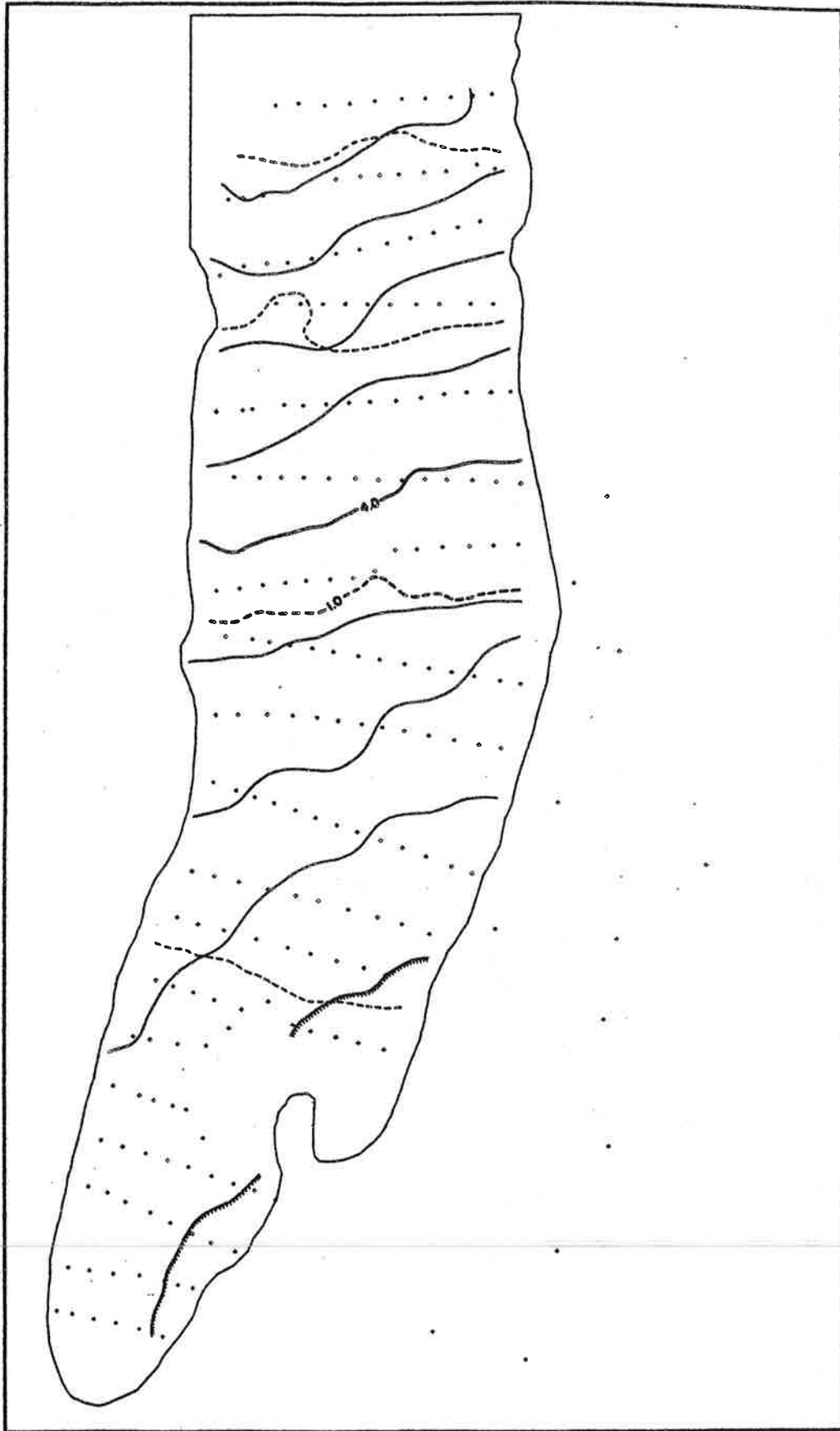


Figure 48. The terrain corrections for zone 4 (solid lines) and zone 5 (dashed lines). The contour interval is 0.2 mgal.

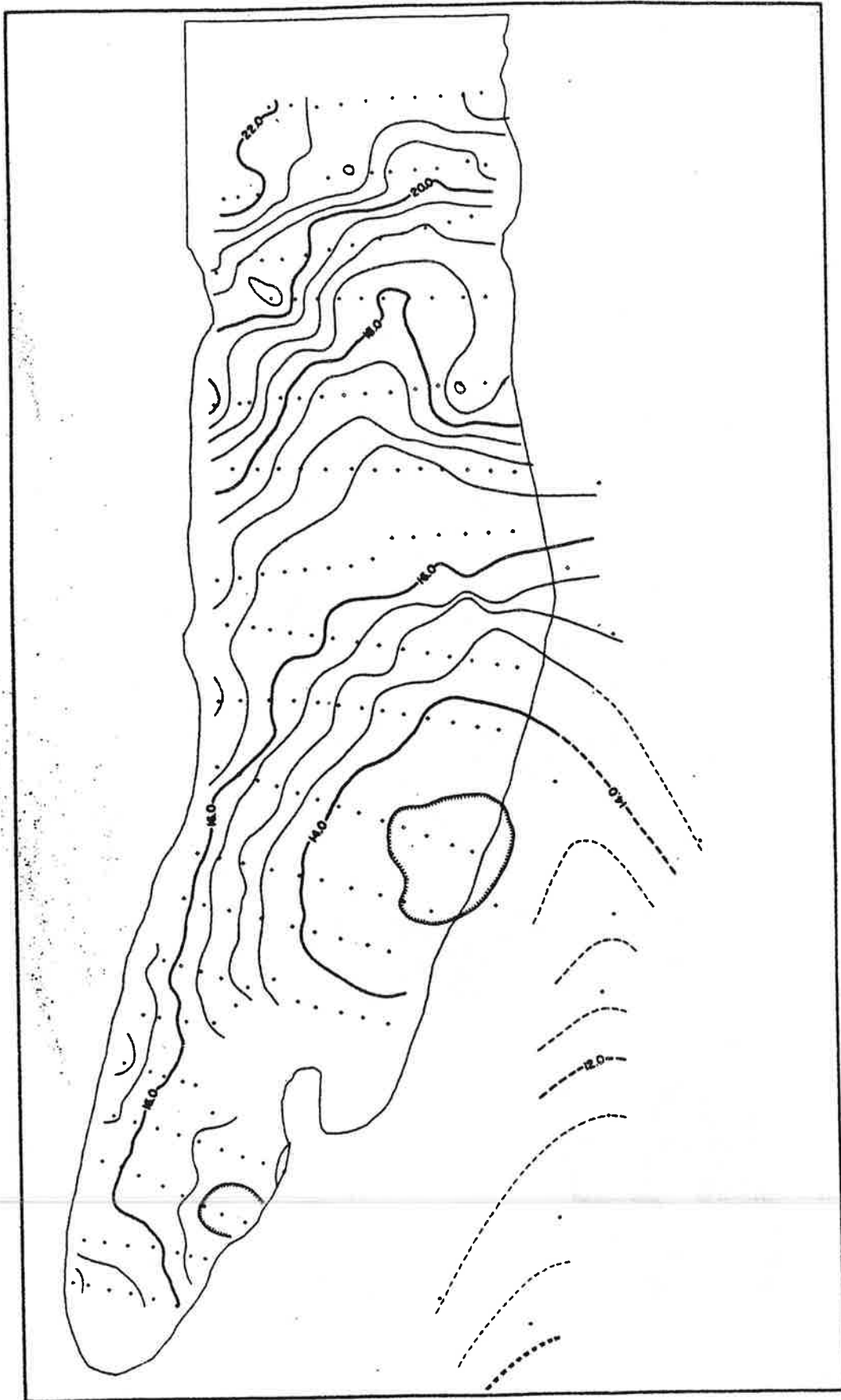


Figure 49. The total terrain corrections. The contour interval is 0.5 mgal.

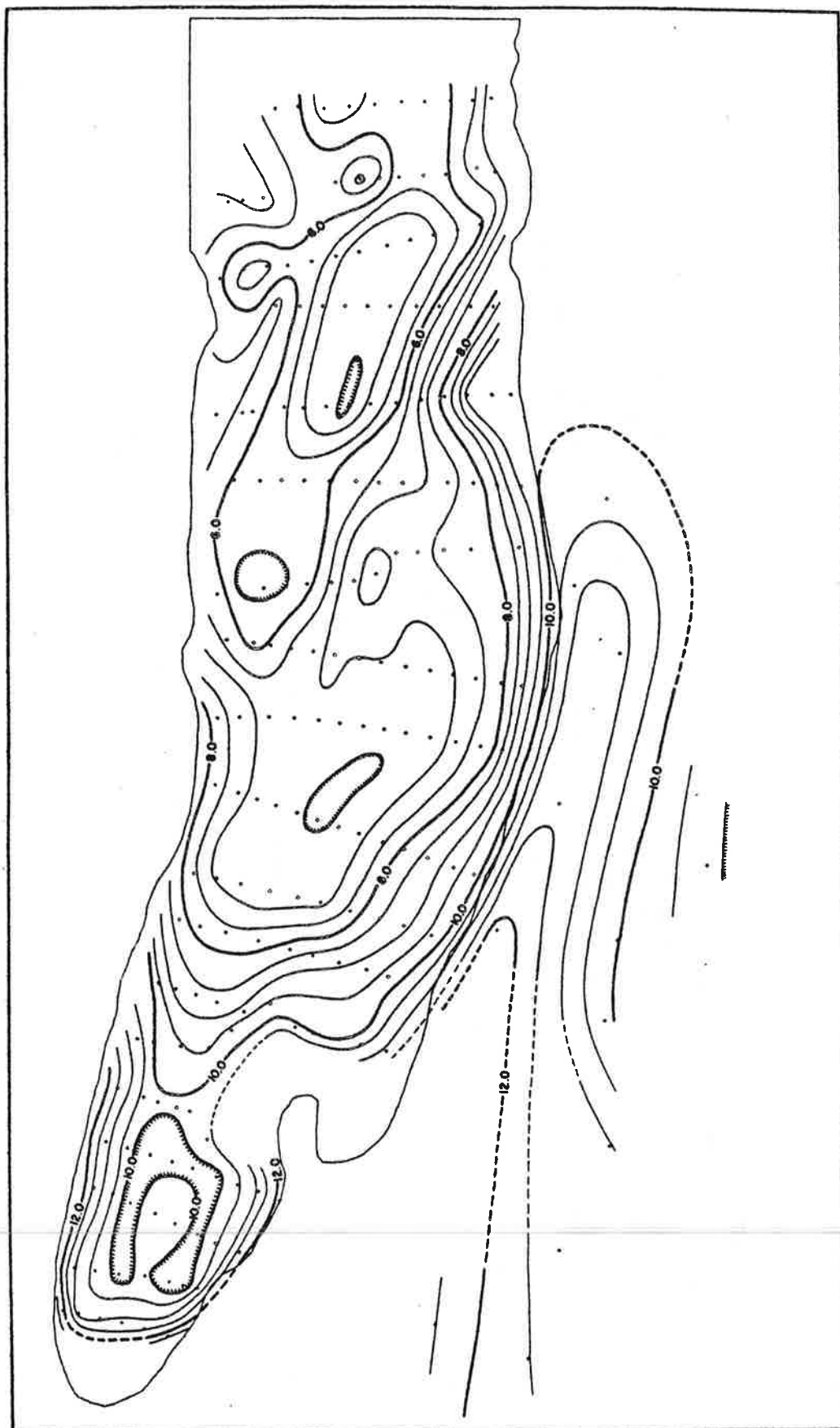


Figure 50. The Bouguer anomalies. The contour interval is 0.5 mgal. These are the anomalies caused by the presence of the glacier, with a regional field superimposed. Interpretation procedures are applied to these anomalies to obtain ice thicknesses.

5.3 INTERPRETATION OF THE BOUGUER ANOMALIES

The interpretation of the gravity anomalies, that is, finding the dimensions of the disturbing body, is a problem in potential theory and in general no unique solution exists. However, in the special case where the disturbing mass has a uniform density and at least one point on the boundary of the body is known, it can be shown that a unique solution does exist (Roy, 1962). A glacier is such a case but unfortunately analytic expressions for the solution do not exist. Instead an iterative procedure is usually used (Corbató, 1965b). An initial approximation for the shape of the disturbing body is assumed and the resulting gravity anomalies and the residuals are used to adjust the initial model. The procedure is then repeated until the residuals are within the experimental error.

The first part of this procedure, calculating the gravity anomalies of the body, is basically similar to calculating terrain corrections. As a result many different methods have been used: graticules, dot-charts, tables, mechanical integrators and digital computers. Ideally the body is allowed to be three dimensional but very often it is assumed to be two dimensional for simplicity.

The second part of the procedure, adjusting the model, is usually made on a trial and error basis, with the residual being converted into a depth change by using the expression for an infinite slab (equation 7). This usually underestimates the correction needed. Convergence is thus probable, but slow. To speed up the convergence Corbató (1965a) has devised a least squares procedure as follows.

Consider n gravity stations and m depth unknowns. If g_i and G_i are the measured and calculated gravity anomalies respectively, at station i , then the sum of the squares of the residuals is

$$s = \sum_{i=1}^n (G_i - g_i)^2 \quad (24)$$

Let ξ_j be the depth unknowns and $\Delta\xi_j$ be the desired adjustments to the depths. To a first approximation we can write

$$G_i = G_i(1) + \sum_{j=1}^m \Delta\xi_j \left(\frac{\partial G_i}{\partial \xi_j} \right) + \dots \quad (25)$$

where $G_i(1)$ is the first approximation to G_i , and the partial derivatives are understood to be evaluated at the first approximation. We desire to reduce s to a minimum; hence we set

$$\frac{\partial s}{\partial \Delta\xi_k} = 0 \quad (26)$$

Substituting (25) and (24) into (26) and rearranging terms we get m equations in the m unknowns $\Delta\xi_j$:

$$\sum_{j=1}^m \left\{ \Delta\xi_j \sum_{i=1}^n \left(\frac{\partial G_i}{\partial \xi_k} \frac{\partial G_i}{\partial \xi_j} \right) \right\} = \sum_{i=1}^n \left(\frac{\partial G_i}{\partial \xi_k} \right) (g_i - G_i(1)) \quad (27)$$

These equations are solved for $\Delta\xi_j$, the model is adjusted, and the process is repeated. Usually only one or two iterations are necessary to give satisfactory results. The $G_i(1)$ come from the first part of the interpretation procedure, and the partial derivatives can be obtained approximately by changing the initial approximation by a small amount and then recalculating $G_i(1)$.

Regardless of whether or not this least-squares method is used, the crux of the procedure is being able to calculate the gravity anomalies $G_i(1)$ of the body, given only a limited number of depth unknowns ξ_j . The surface of the disturbing body has to be interpolated between these points. For a three-dimensional body, with arbitrarily spaced points, this is a very difficult

procedure. One must either settle for a very crude model, such as triangular prisms, rectangular prisms or vertical plates, or else the points have to be hand-contoured and then the method of Talwani and Ewing (1960) used.

A two dimensional body, on the other hand, is much easier, since it can be approximated by an n-sided polygon, for which the gravity anomalies G_1 and the partial derivatives $\partial G_1 / \partial x_j$ can be evaluated (Talwani, Worzel and Landisman, 1959). The above least-squares procedure of Corbató (1965a) can then be applied.

The complex surface topography of the Nisqually Glacier suggests that three dimensional modelling of the gravity field will be necessary. Furthermore, if the glacier is relatively thin this modelling will have to be as realistic as possible. Talwani and Ewing's method is the best available and so it was decided to use it, despite the necessity of hand-drawing the bedrock contours at each iteration. For a first approximation to the bedrock the two dimensional least-squares technique mentioned above will be used. This is the procedure used by Corbató (1965b) on the Blue Glacier*.

As input to the modelling the residual anomalies should be used. This requires that the regional field be removed from the Bouguer anomalies. The best way of determining the regional field is to measure gravity at distances far enough away from the glacier that the effect of the glacier is insignificant. However, the limited number of stations on the surrounding terrain made the determination of the regional field over the Nisqually Glacier a difficult task. How this problem was treated will be discussed as the modelling progresses.

* Again, it is emphasized that ideally the contours would be calculated by the computer from the set of depth values. However, when the points are arbitrarily and sparsely spaced, as on a glacier survey, it is extremely difficult, if not impossible, to develop a procedure which is both realistic and foolproof. Hand-contouring has the distinct advantage of allowing one to add intuitive or supplementary information about the bedrock contours.

One additional piece of data is required: the density of the glacier ice. This was not measured but will be assumed to be 0.9 Mg m^{-3} (Seligman, 1950). This is the same value used on practically all other gravity surveys of glaciers and is also the value commonly used for glacier flow studies. The density contrast $\Delta\rho$ is thus 1.7 Mg m^{-3} , which corresponds to an infinite slab of ice 14 m thick.

5.3.1 *Two dimensional Modelling*

Nineteen transverse gravity profiles were made on the Nisqually Glacier. Each one can be considered independently and the glacier modelled two dimensionally at 19 separate locations. The glacier is considered to extend horizontally to infinity and to have a polygonal cross section. This polygon is defined by the following points (Figure 51): (a) the n gravity stations along the surface, (b) the m depth unknowns along the bedrock, and (c) two end points at the margins of the glacier.

The positions of the gravity stations are taken from the surveying measurements*, the end points are taken from the 1966 map and the depth unknowns are specified initially by assuming a parabolic shape and guessing at the central depth. An attempt was made to estimate the central depth by comparing the mean relative difference between the Bouguer anomaly at the center and at the margins with that caused by a two-dimensional parabolic glacier with a vertical symmetry axis and horizontal upper surface (Corbató, 1964), but the Nisqually Glacier is so non-parabolic that the results were meaningless. When the values obtained were used for initial approximations to the least-squares procedure, the solution was immediately unstable in many cases. Experience showed that simply guessing at the central depth was a far more "accurate"

* The actual surveyed elevations were used rather than the elevations determined from the 1966 map.

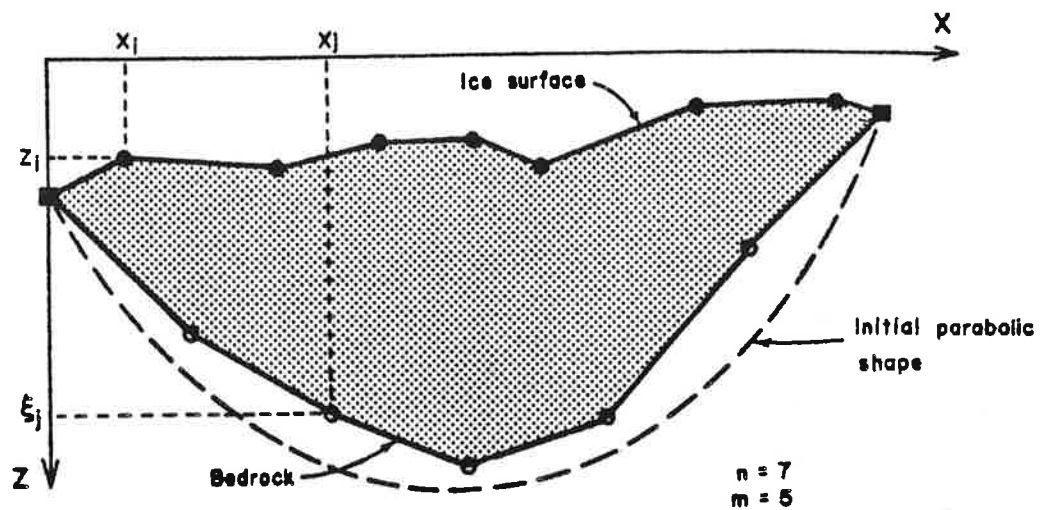


Figure 51. The two dimensional model of the glacier used with the least-squares procedure of Corbató (1965a). The polygonal cross section is made up of the n gravity stations (solid circles), the m depth unknowns (half open circles) and the two end points (solid squares).

(and less tedious) technique.

We wish to apply Corbató's least-squares procedure (equations 27) to this model. One convenient feature about the method is that the regional field may be treated as an unknown and can be solved for along with the depths. The regional field is assumed to be of the form $a + bx$ where a and b are treated as the $(m+1)^{\text{th}}$ and $(m+2)^{\text{th}}$ unknowns: $\xi_{m+1} = a$ and $\xi_{m+2} = b$. It is very important to realize, however, that the solution for a and b is only a mathematical one and, like the depth solution, it results solely from the criterion that the sum of the squares of the residuals be a minimum. It does not necessarily have any resemblance to reality.

Expressions for $G_1(1)$ and $\partial G_1 / \partial \xi_j$ for a polygonal cross section are given by Corbató (1965a):

$$G_i(1) = 2\gamma \Delta\rho \sum_{k=1}^{m+n+2} Z_k + a + bx_i \quad (i=1,2,\dots,n) \quad (28)$$

$$\frac{\partial G_i}{\partial \xi_j} = 2\gamma \Delta\rho (P_j - Q_j) \quad (j=1,2,\dots,m) \quad (29)$$

$$\frac{\partial G_i}{\partial \xi_{m+1}} = 1 \quad (30)$$

$$\frac{\partial G_i}{\partial \xi_{m+2}} = x_i \quad (31)$$

Letting ξ be replaced, for convenience, with z , and following the notation of Corbató, Z , P and Q are given by:

$$Z_k = \frac{S_k}{U_k} (B_k V_k - A_k W_k) \quad (32)$$

$$P_k = \frac{S_k}{U_k} \left(\frac{x_k A_k - z_k B_k}{R_k} - V_k \right) - (B_k V_k - A_k W_k) \left(\frac{x_{k+1} U_k - 2B_k S_k}{U_k^2} \right) \quad (33)$$

$$Q_k = \frac{S_{k-1}}{U_{k-1}} \left(\frac{x_k A_{k-1} - z_k B_{k-1}}{R_k} - V_{k-1} \right) - (B_{k-1} V_{k-1} - A_{k-1} W_{k-1}) \left(\frac{x_{k-1} U_{k-1} - 2B_{k-1} S_{k-1}}{U_{k-1}^2} \right) \quad (34)$$

where

$$\left. \begin{aligned} A_k &= x_{k+1} - x_k & B_k &= z_{k+1} - z_k \\ R_k &= x_k^2 + z_k^2 & U_k &= A_k^2 + B_k^2 \\ S_k &= x_k z_{k+1} - x_{k+1} z_k & T_k &= x_k x_{k+1} + z_k z_{k+1} \\ V_k &= \frac{1}{2} \ln \left(\frac{R_{k+1}}{R_k} \right) & W_k &= \tan^{-1} \left(\frac{S_k}{T_k} \right) \end{aligned} \right\} \quad (35)$$

It is understood that $-\pi < W_k < +\pi$. [Equation 33 as given by Corbató contains a mistake; instead of x_{k+1} in the second term on the right-hand side he has

x_k .] The index k proceeds around the $m+n+2$ vertices of the polygon in the clockwise direction.

The depth variables are distributed evenly across the profile. The number of variables m is allowed to vary from 1 to $n-2$ (the 2 allows for the two unknowns a and b). Since m can be thought of as the number of "degrees of freedom" that the least-squares solution has, an increase in m allows observational and round-off errors to impart more and more "instability" to the solution as it strives to minimize s . When m is small compared to n this "noise" inherent in the observations is smoothed by the least-squares technique and a physically reasonable solution can usually be obtained. As m increases, the solution starts to oscillate (shallow depths alternating with deep ones) since it has more freedom to adjust to the noise. For data on the Blue Glacier, Corbató found that stable solutions usually required $m \sim n/2$, or less.

The above equations were programmed for the CDC 6400 computer. Figure 52 shows the solutions obtained for profile G10 using various values of m . The break-down of the technique as m approaches $n-2$ is clearly evident and the most "reliable" solution is probably the one for $m = 8$.

Profile G10 was used for debugging the program. When the remaining profiles were run it was obvious that this had been a fortuitous choice, for none of the others showed the distinction between the stable and unstable solutions as well as profile G10 did. The solution for each profile which has the highest value of m and which appears to be both stable and physically reasonable is shown in Appendix A. The values for a and b are also indicated; in all cases an initial regional field of $a = 10$ mgal and $b = 0$ was used.

One profile, G16, was unstable regardless of the choice of m , the initial regional field or the initial central depth and no solution could be obtained. In some cases the maximum m that could be used was much less than $n/2$ and

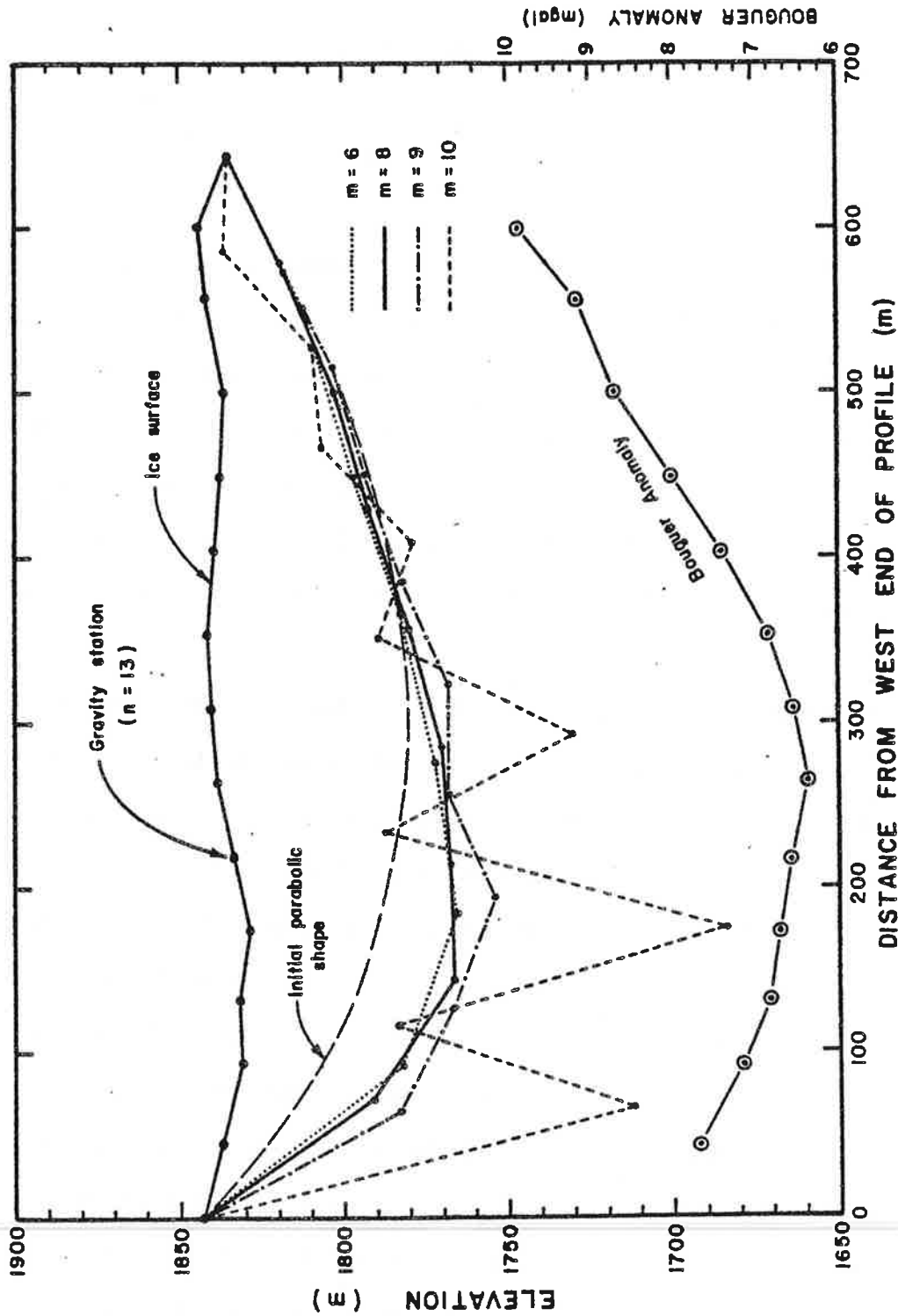


Figure 52. Corbató's two dimensional least-squares procedure applied to profile G10. As the number of depth unknowns m is increased the solution starts to oscillate, eventually breaking down completely for $m = 11$. The Bouguer anomalies across the profile are also indicated (scale at right). The solution for $m = 8$ is considered the most reliable.

in others (such as G13, G17 and G18) the resulting bedrock shape inspired little confidence.

This inability to obtain many reliable solutions was very perplexing at first. The program was checked out very carefully and has been subsequently verified by using it on gravity data obtained by Krimmel (1970; written communication, 1971) on the South Cascade Glacier and the lower Seward Glacier, Alaska. Both of these glaciers have much simpler topography than the Nisqually Glacier and the results appear to be very good. In particular, those for the South Cascade Glacier agree well with depths determined by Krimmel by other means.

The explanation of this problem is probably a combination of several factors: (a) The Bouguer anomalies vary over a relatively small range and so any observational error is relatively more important. Unstable solutions will therefore be more likely. (b) The Nisqually Glacier is thin and has a complex surface topography (and probably a complex bed topography also). The approximation that the glacier extends horizontally to infinity, with a constant cross-section, may not be realistic enough. This combination probably means that the higher order derivatives $\partial^2 G_1 / \partial \xi_j^2$, $\partial^3 G_1 / \partial \xi_j^3$, ... are not negligible. Thus the approximation made in equation 25 would be invalid and it is not surprising that the solution breaks down. (d) The stations are not always distributed uniformly across the profile. The polygon formed by joining the stations with straight lines may differ significantly from the real cross section. (e) Many stations do not lie exactly on the profile line, and so their measured anomalies will be different from the values they would have had if they had been positioned correctly. This contributes real "noise" to the observations which, like point (a) above, can impart instability to the solution. This is illustrated by the solution for profile G7, which was completely unstable until station 47, which lies about 30 m off the profile, was omitted.

The two dimensional results (excluding the most doubtful profiles G13, G16, G17 and G18) have been used to draw the bedrock contours in Figure 53. Part of this map is guesswork but it will be adequate for a first approximation to the three dimensional modelling.

In previous years, particularly the mid 1950's, some of the bedrock in the lower part of the glacier was exposed. This was mapped by the U.S. Geological Survey during their regular 5-year mapping program and the results are indicated where possible on the cross sections in Appendix A. The two dimensional gravity results for profile G7, where most of the bedrock was exposed, are within 10 m of the known bedrock. This is excellent agreement considering that the modelling is only two dimensional.

5.3.2 *Three dimensional Modelling*

It is obvious from the above discussion that three dimensional techniques are absolutely essential for a correct interpretation of the Nisqually Glacier gravity data. The procedure is as follows. Assume a regional gravity field g_r and a bedrock configuration. A theoretical anomaly Δg_c for each station can then be calculated:

$$\Delta g_c = G + g_r \quad (36)$$

where G is the attraction of the entire glacier at the station. This will be compared with the measured Bouguer anomaly Δg_b and the residual $\Delta g_b - \Delta g_c$ converted to a depth adjustment using the infinite slab factor. A new bedrock map will then be drawn and the process repeated until the residuals are within an acceptable range.

The regional field was initially assumed to be planar:

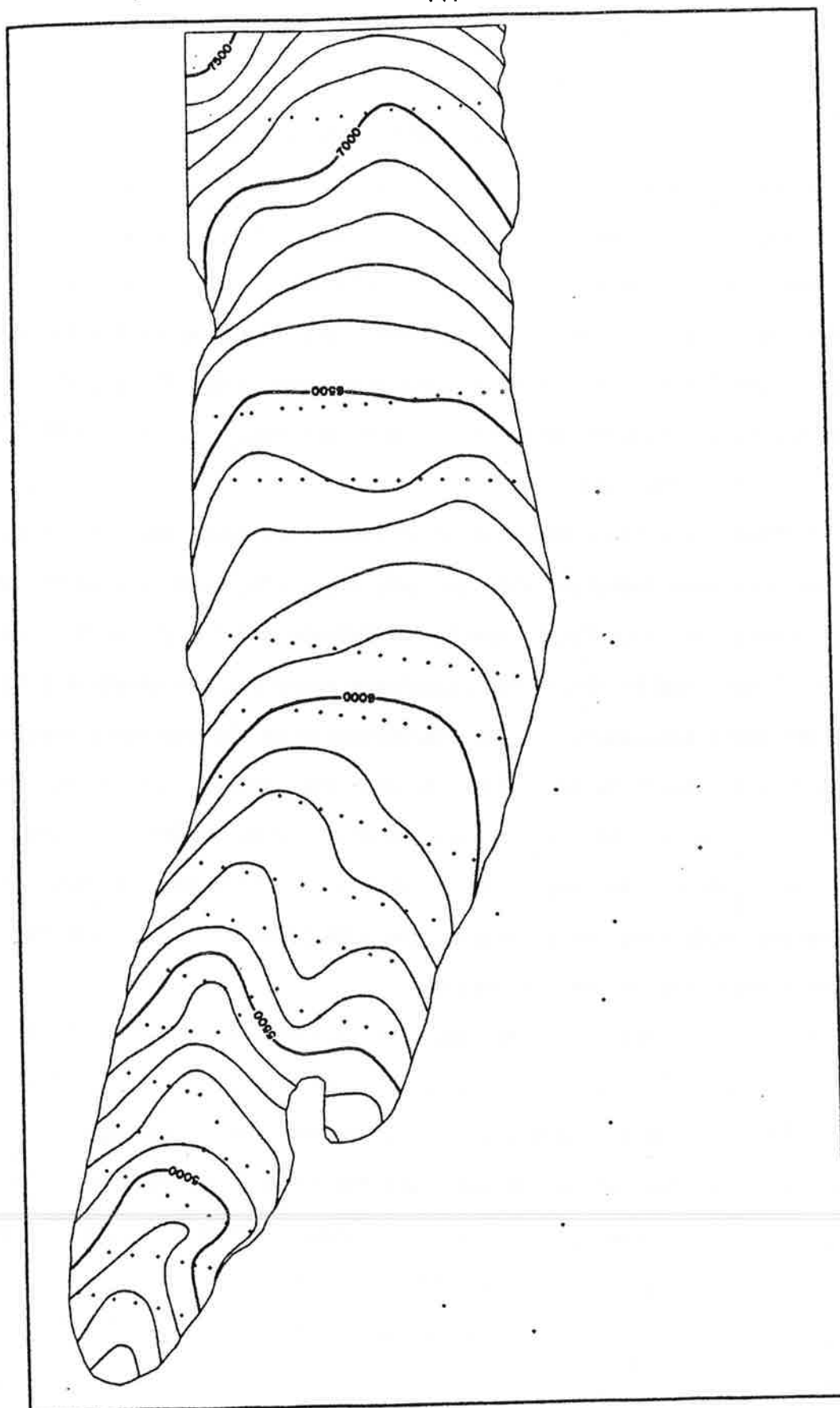


Figure 53. The estimated bedrock contours from the two dimensional modelling, used as initial input to the three dimensional modelling. The contour interval is 30.480 m (100 feet). Profiles G13, G16, G17 and G18 were not used in the construction of this map.

$$g_r = ax + by + c \quad (37)$$

The constants (a, b, c) were determined by fitting a plane by least-squares to (a) the Bouguer anomalies at the 13 terrain stations (which up to now have not been used), and (b) the values of the regional field determined by the two dimensional modelling at the ends of 6 profiles which were considered to be reasonably reliable. The latter 12 points are necessary to fix the east-west trend of the field. The profiles used were numbers G1, G6, G7, G10, G11 and G15; the resulting constants are $a = 0.001629 \text{ mgal m}^{-1}$, $b = -0.001031 \text{ mgal m}^{-1}$ and $c = -3.73979 \text{ mgal}$.

Initially a contour interval of 30.480 m (100 feet) was used (Figure 53). The contours were digitized with the same digitizing machine used for the terrain corrections. Corbató's version of Talwani and Ewing's method (equations 15 to 17) was used to obtain the calculated anomalies and equation 7 to estimate the depth adjustments. The discontinuity at the station elevation was handled using equations 21 to 23. As with the terrain corrections, the surveyed elevations of the gravity stations were replaced with the elevations read from the digitized 1966 map. It is important to keep in mind that all three dimensional modelling was done using the 1966 glacier surface, *not* the surface at the actual time of the observations.

After two iterations the contour interval was decreased to 12.192 m (40 feet). After four iterations the bedrock had the configuration shown in Figure 54. For this topography the mean residual was 0.038 mgal, the root-mean-square residual was 0.180 mgal, and the maximum residual was 0.596 mgal.

Unfortunately the agreement with the known bedrock is now very poor. Profile G7, for example, is only half as deep as it should be, despite the excellent agreement that the two dimensional modelling gave. Profile G1 is similar.

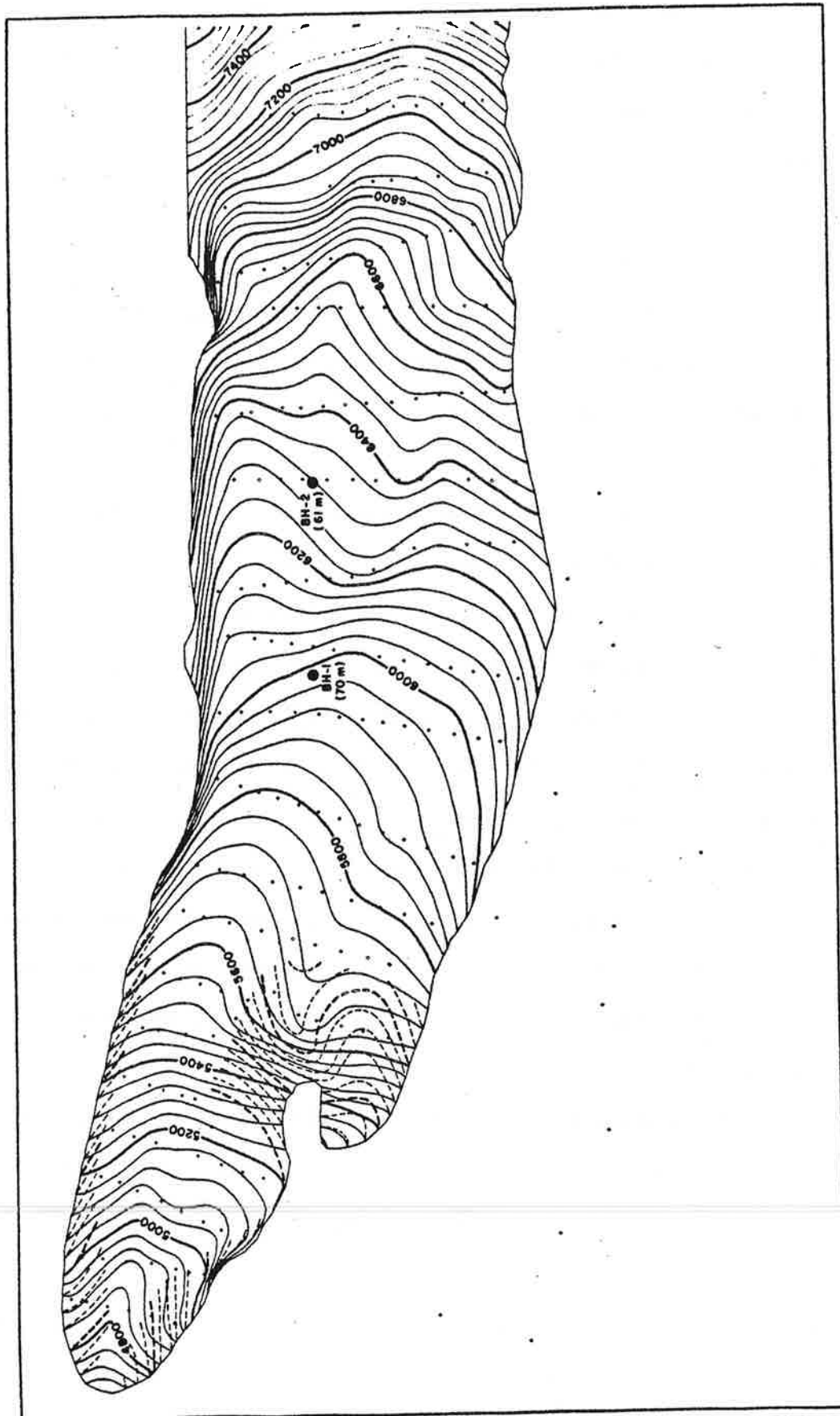


Figure 54. Initial results of the three dimensional modelling. This was obtained after four iterations from the bedrock of Figure 53, using a plane regional field. The contour interval is 12.192 m (40 feet). The dashed lines indicate the known bedrock contours from old maps. BH-1 and BH-2 are the approximate locations of the boreholes drilled in March 1972 (ice depths in parentheses).

It became apparent that the reason for this poor agreement was the regional field. This had been assumed to be a plane determined by a least-squares fit to a set of 25 points. The points lying near profiles G1 and G7 were found to lie away from this plane by approximately the right amount and direction to account for the discrepancy.

The assumption of a plane regional field is thus not valid. In fact, inspection of the Bouguer anomaly field (Figure 50) supports this idea. A ridge in the field appears to run along the east side of the glacier. This might be due to the morainal material in this area, which probably has a different bulk density than that of andesitic bedrock.

Longitudinal variations in the regional field are also likely in view of the radial nature of Mount Rainier. The huge mass of this volcano should be in isostatic adjustment and hence the anomaly contours should be approximately circular and centered on the summit. Such a regional field has indeed been measured by Danes (personal communication, 1972) but the scale of the measurements is too large to give detailed estimates in the region of the lower Nisqually Glacier. They do, however, show that the regional field in this area is predominantly north-south, with no east-west trend detectable.

It seems safe, therefore, to assume no east-west component to the regional field. If one does exist it is probably quite small and at any rate it would be of little consequence to this study, which is mainly concerned with longitudinal variations.

On the first attempt to determine the north-south component a straight line was fitted to the terrain stations only. No improvement to profiles G1 and G7 resulted. The terrain stations are thus too few and too far from the glacier to be useful.

The only way out of this dilemma, apart from making many more measurements of the regional field, is to turn the problem around and assume the known depths

to be given. The regional field is then treated as a variable and is adjusted, along with the ice depths, to give the known depths.

Profiles G1 and G7, however, are inadequate for this purpose and it was necessary to obtain some independent depth measurements by thermal drilling*. This was undertaken in the winter and early spring of 1972 using new hot-points developed at the University of Washington. Two boreholes were successfully completed in the upper part of the glacier (Figure 54). Admittedly there is no guarantee that they reached true bedrock. However, the drills did not advance more than 10 mm at either site under full power for one hour, and BH-2 reached "bottom" quite abruptly. Both holes agree remarkably well with the gravity results. Thus it is felt that even if they did not reach bedrock, they were very close to it.

There are now four areas along the length of the glacier (profiles G1-G2, G6-G7, G11-12, and G14) where at least the magnitude of the ice thickness is known independently of the gravity data, the first two from old maps and the second two from the boreholes. This can be used to determine the regional field. The topography shown in Figure 54 was adjusted to agree with the known bedrock contours. Most of the adjustment took place below profile G9, since the upper part of the glacier was already in good agreement with the borehole depths. When the theoretical attraction G of the resulting glacier shape is subtracted from the measured Bouguer anomaly we should get a good estimate of the regional field (Figure 55). The solid dots indicate gravity stations lying above or very close to known bedrock.

For $x < 6020$ m, a straight line can be fitted through the points (emphasizing the solid dots) with reasonable confidence, giving

* This had been attempted in June and July of 1969, with this purpose in mind, but was unsuccessful. One hot point burned out and a second one developed a leak. No other hot points were available and so the project had to be abandoned.

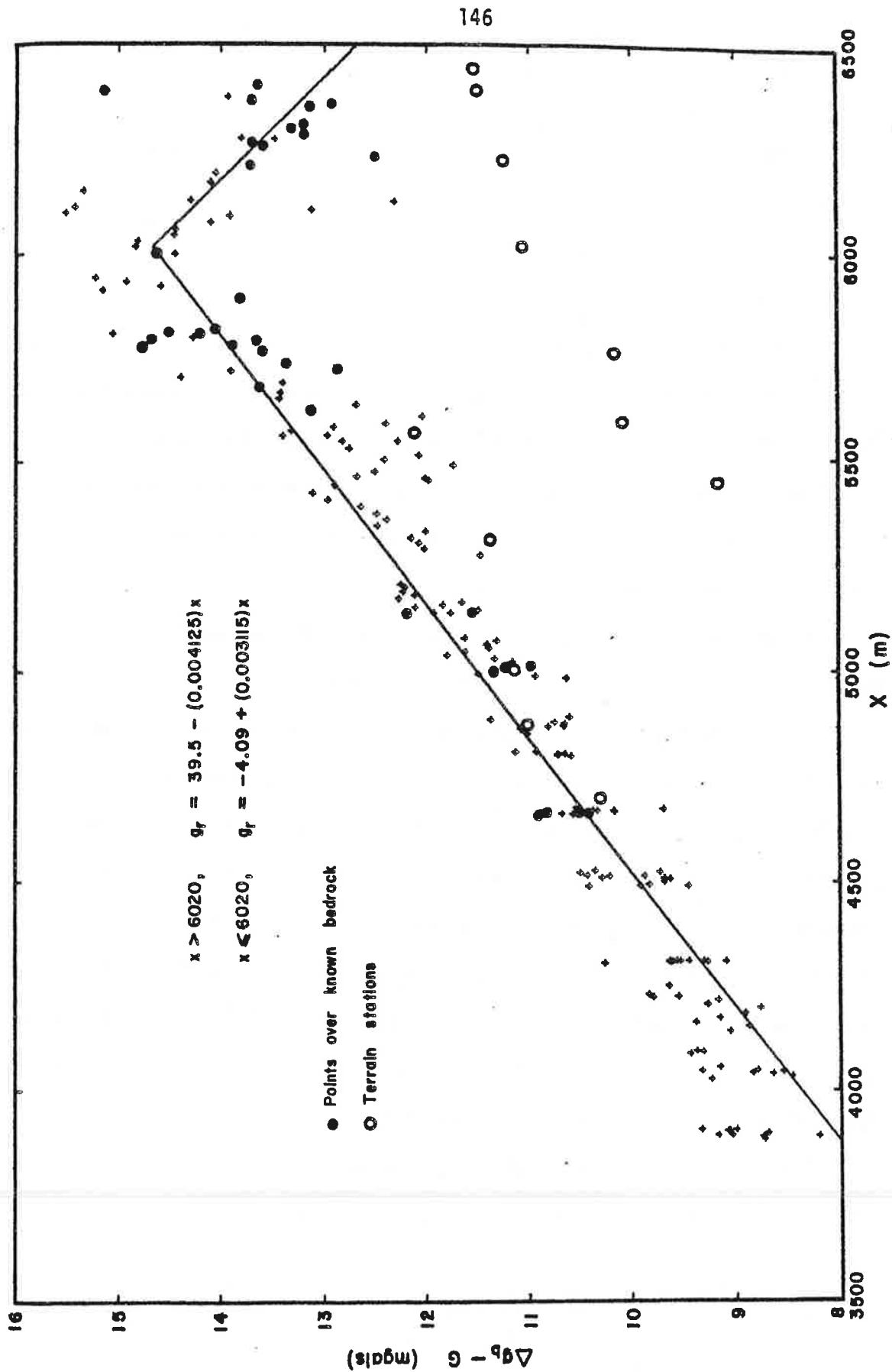


Figure 55. The regional gravity field assuming the bedrock of Figure 54, adjusted to agree with the known bedrock, is valid. G is the attraction of the glacier and is always negative.

$$g_r = -4.09 + 0.003115 x \quad (37)$$

This represents a regional field dipping towards the main mass of Mount Rainier, in agreement with the principle of isostasy (Garland, 1965, p. 51). For $x > 6020$ m, the regional field appears to have a reverse slope:

$$g_r = 39.5 - 0.004125 x \quad (38)$$

This point ($x = 6020$ m) coincides with the transition from the Mount Rainier andesite to the granodiorites and quartz monzonite of the Tatoosh pluton which extends up the Nisqually River valley to the upper nunatak (Figure 20). Thus it is not surprising that the regional field becomes more erratic as the terminus is approached. A higher degree of variation than the two straight lines indicated is not justified by the data, however.

Also shown in Figure 55 are the Bouguer anomalies of the terrain stations. The northernmost three stations lie closest to the glacier and show good agreement with the above regional field. This verifies that the east-west component of the regional field is small, at least in this area of the glacier. As the terminus is approached the terrain stations get further away from the glacier and probably give little indication of the regional field over the ice, particularly as we already suspect the regional field to have significant fluctuations in this area.

Assuming the two straight lines shown in Figure 55 are the true regional field, minor alterations can now be made to the bedrock in order to reduce the root-mean-square residual to a minimum, that is, to reduce the scatter of the "+" symbols from the straight lines of Figure 55. Two iterations were performed and the final bedrock configuration is shown in Figure 56. The calculated regional field $\Delta g_b - G$, using this final bedrock, is shown in Figure 57.

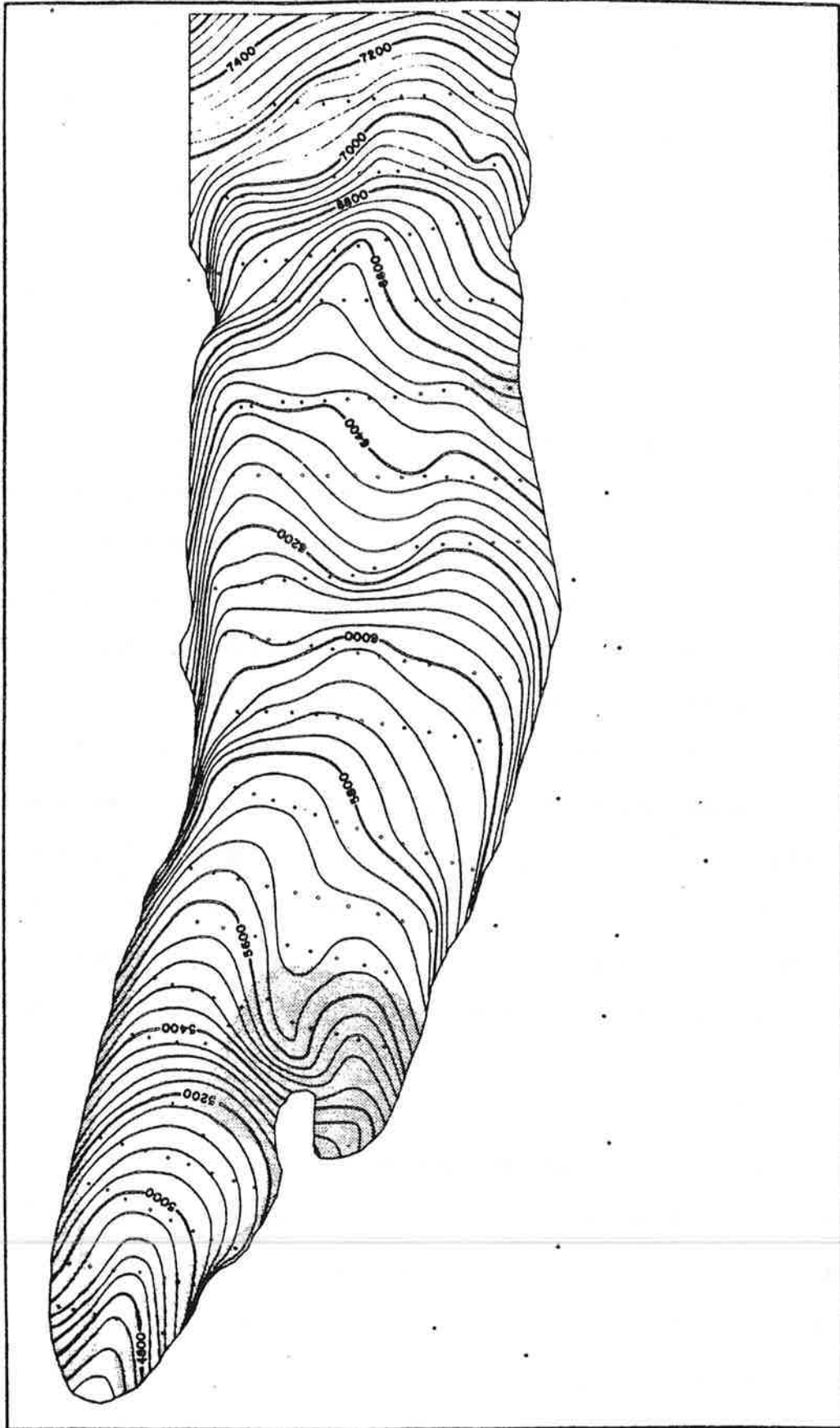


Figure 56. The final results of the three dimensional modelling. The contour interval is 12.192 m (40 feet). The contours are constrained to agree with the known bedrock (stippled region) and with the two borehole depths.

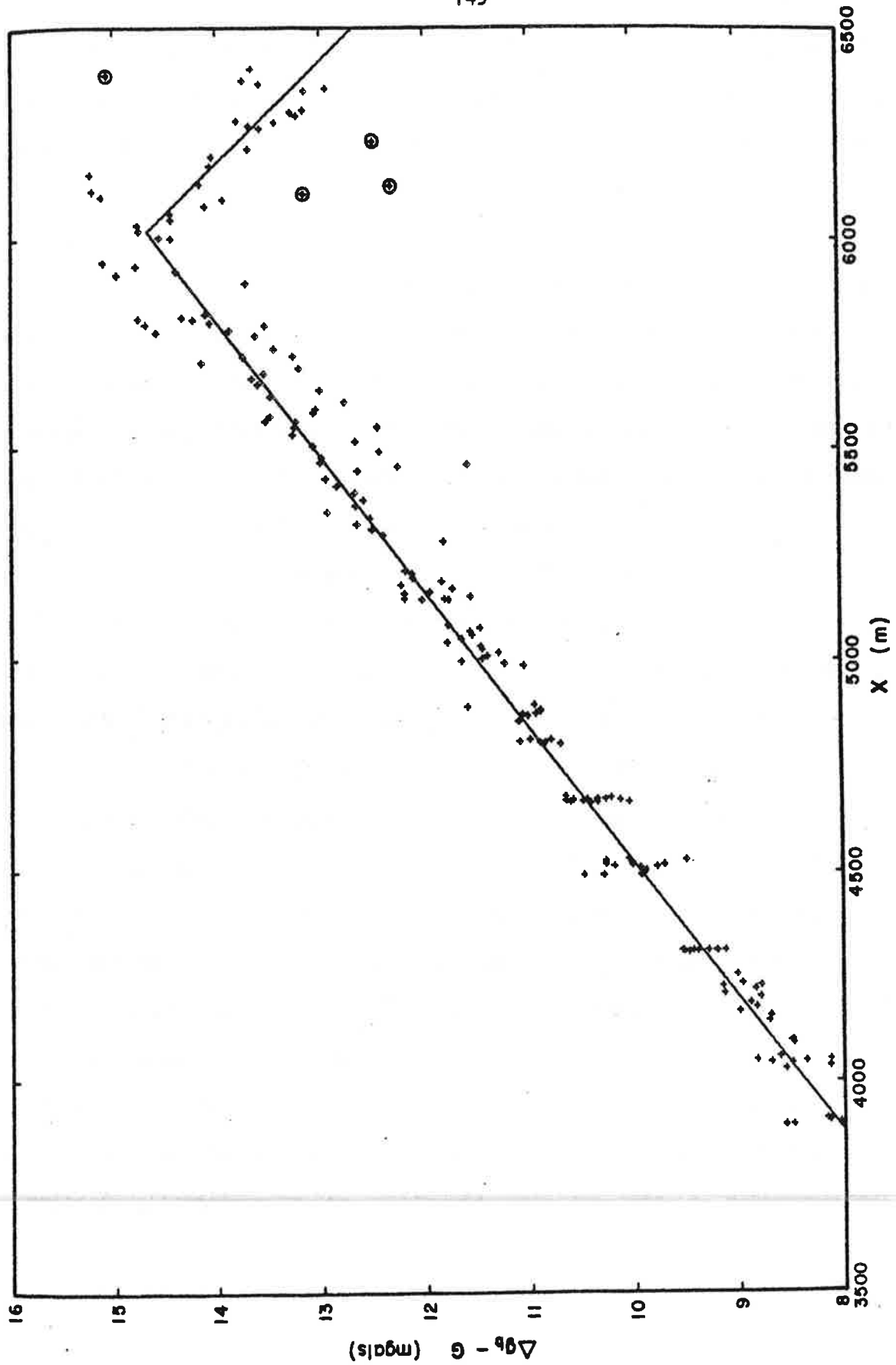


Figure 57. The regional gravity field assuming the bedrock of Figure 56 is valid. The circled points lie in dubious areas, such as near the margins.

As expected, the scatter is reduced, particularly in the upper portion of the glacier. The lower part has not changed much since we always constrain the bedrock to agree with the known contours. The mean residual was reduced to -0.030 mgal and the root-mean-square residual to 0.382 mgal. This omits the circled points in Figure 57, as these points lie in dubious areas, such as near the margins or where the ice is very thin.

The final glacier cross sections at each of the nineteen gravity profiles are shown in Appendix A and a three dimensional view of the glacier is given in Figure 58. It must be emphasized that the excellent agreement between the known and calculated bedrock apparent in Appendix A does *not* indicate the accuracy of the gravity measurements. It merely reflects the fact that the regional field was adjusted to give this agreement.

The maximum depth of the Nisqually Glacier is about 90 m and occurs at the position of the U.S.G.S. Profile II, where the surface slope is a minimum. Along the centerline the depth ranges from 60 to 90 m, except in the uppermost part where it decreases to 30 to 40 m (as expected, since this is part of the much steeper upper Nisqually Glacier). The average centerline depth is 71 m.

The "upper nunatak" is not a true nunatak but is rather the end of a long shoulder, or ridge, extending down from the flatter region around Profile II. West of this ridge there is a deep trough through which most of the ice flows. The various steps apparent on the glacier surface usually correspond to steps in the bedrock. An exception is the prominent centerline bulge on the surface at $x \sim 4500$ m; there is no indication in the gravity data of a corresponding bedrock bulge. Possibly it is due to dynamic effects of the steeper, faster ice converging in this area from the Wilson and upper Nisqually Glaciers.

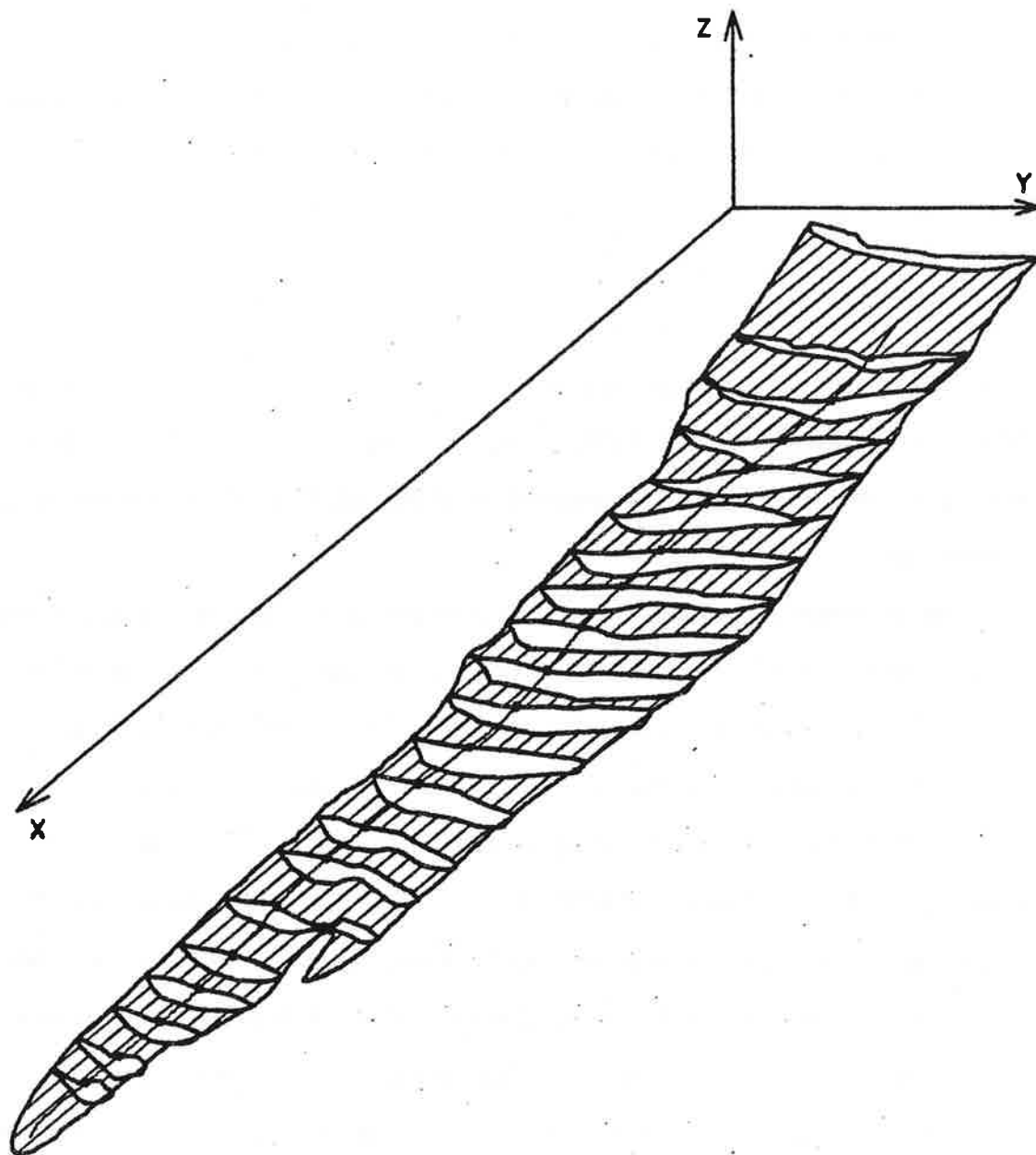


Figure 58. The bedrock of the lower Nisqually Glacier, isometric view. The profiles are perpendicular to the centerline at each of the standard stake positions (solid dots). There is no vertical exaggeration.

5.4 ACCURACY OF THE GRAVITY RESULTS

Errors fall into two categories: those whose effect can be calculated and those whose effect can not. In the former are the inherent precision of the gravity meter and the accuracy of the drift correction; the combined effect of this is ± 0.06 mgal (the reproducibility of the meter, mentioned on p.89). In addition there is a surveying error in the determination of the coordinates of the gravity stations. This is almost always within ± 30 mm, both horizontally and vertically (section 6.4). Horizontally, this error is negligible but vertically it amounts to about ± 0.01 mgal in the elevation correction.

These errors, however, are insignificant when compared to the errors in the second category. Here we have the unknown errors in the terrain corrections, the regional field and the modelling. These have a number of causes:

(a) The density of the glacier ice was assumed to be a constant 0.9 Mg m^{-3} and the density of the rock to be a constant 2.6 Mg m^{-3} . The former could have local fluctuations, particularly near the glacier surface, due to the snow cover, morainal debris, large boulders, crevasses, and cavities and debris within the ice. The latter is bound to have local fluctuations due to moraines, lava flows, pumice layers and other variations in the local geology. Furthermore, the density of the surrounding terrain is definitely in error where there are other glaciers covering the terrain. As mentioned earlier, this effect was ignored when doing the terrain corrections.

A feeling for the magnitude of the effect of local density variations can be obtained by considering the attraction per unit mass of a point source at (x, z) :

$$g/m = \gamma z(x^2 + z^2)^{-3/2} \quad (39)$$

Figure 59 shows a contour plot of $\log(g/m)$ versus $\log(x)$ and $\log(z)$, where

x and z are in meters and g/m is in mgal kg^{-1} . A large boulder 3 m in radius and 10 m to the side and 3 m below the gravity meter would have an attraction of less than 0.001 mgal. Figure 60 is an alternate presentation of this; it gives the logarithm of the radius (in meters) of a sphere of uniform density 2.6 Mg m^{-3} necessary to give a 1 mgal attraction at the origin. Out to a distance of about 30 m the sphere would have to be so large that it would enclose the origin. Despite the fact that equation 39 is no longer valid in this case, it does show that local density variations would probably have to be unrealistically large to produce a detectable effect on a gravity meter.

(b) The topographic surface of the glacier which was used in both the terrain corrections and the three dimensional modelling is known to differ by several meters from the actual surface at the time of the gravity measurements (Figure 43). Ideally a map should have been made for the May 1969 surface. This was not done as it would have been impossible to draw a map as detailed as the 1966 map from only 195 spot measurements of the surface elevation.

A very approximate estimate of the effect of this error can be obtained by examining Figure 45, which shows the terrain corrections for the 1966 glacier surface. If we assume that the "roughness" of the surface remains about the same between 1966 and 1969, then the maximum difference in the terrain correction between any two adjacent stations, about $\pm 0.2 \text{ mgal}$, gives the required estimate.

(c) Errors in the digitizing of the terrain and the calculation of the gravitational attraction by Talwani and Ewing's method could be present, but it is felt that these are much less than the other errors mentioned (see p. 109).

(d) The regional field could depart appreciably from the straight lines used in the final modelling (Figure 55). In fact the data suggest that this is indeed the case near the terminus.

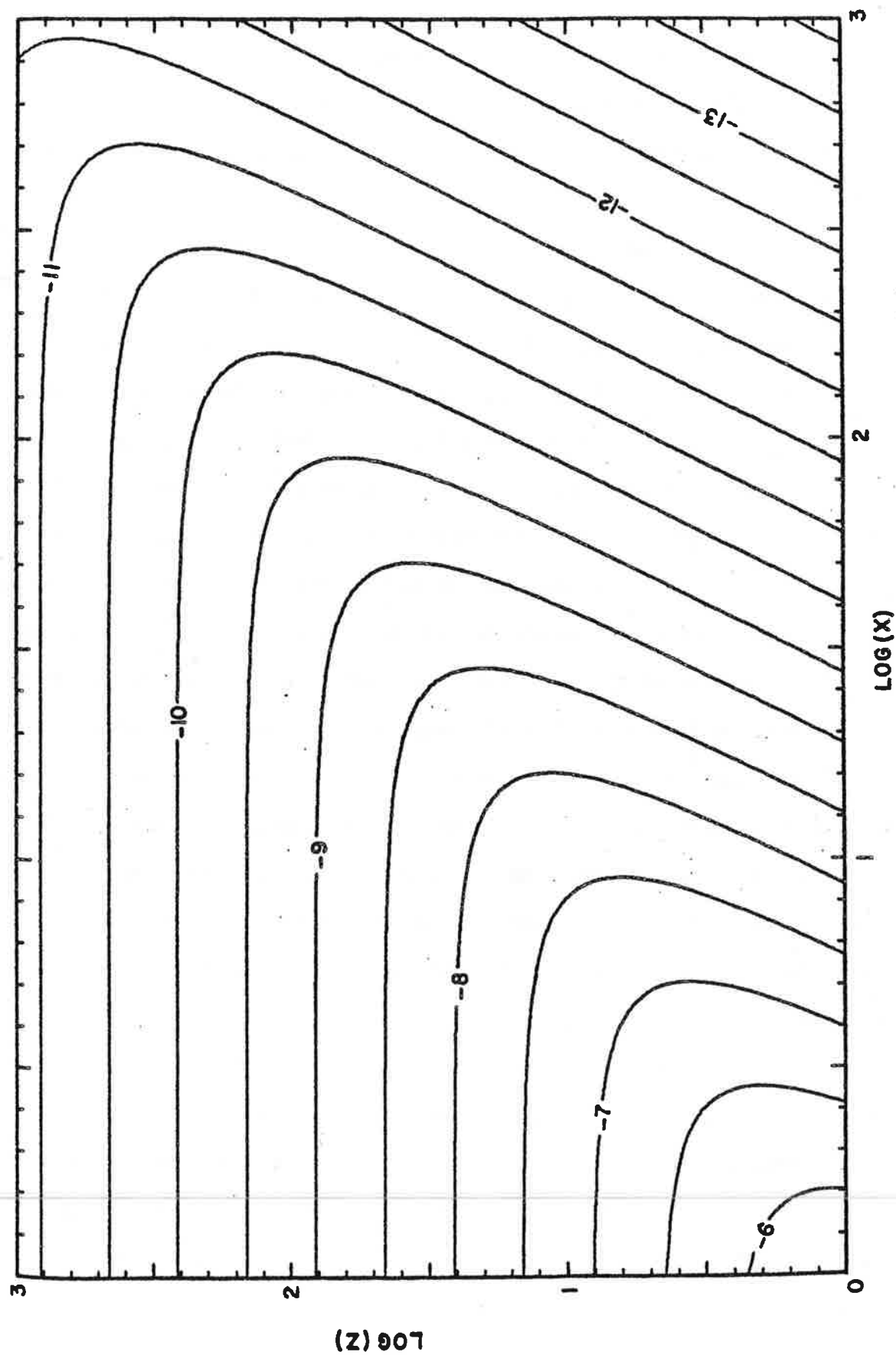


Figure 59. The gravitational attraction per unit mass at (x, z) . The contours are in units of $\log(g/m)$ where g is in mgal and m is in kg . x and z are in meters.

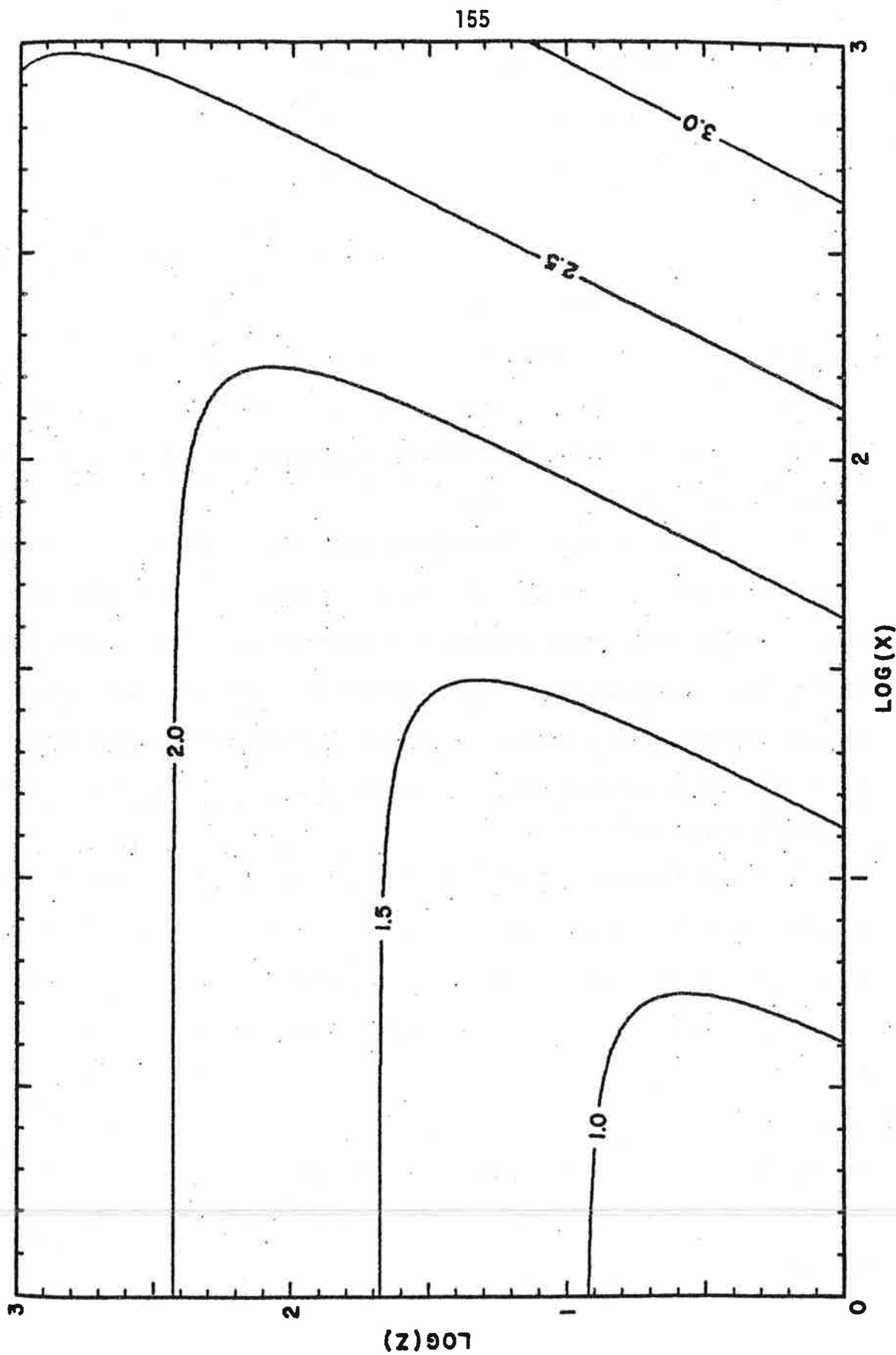


Figure 60. The logarithm of the radius of a sphere of uniform density 2.8 Mg m^{-3} necessary to give a 1 mgal attraction at the origin. All quantities are in meters.

These errors influence the terrain corrections, the regional field and the modelling and thus their effect on the final depths is inter-related and complicated, even if definite figures could be ascribed to them. However, if we assume the infinite sheet factor $2\pi\gamma\Delta\rho\Delta z$ to apply, then we can make some guesses as to the overall effect. For a mean depth of 60-70 m and a mean density contrast of 1.7 Mg m^{-3} , an error in the density contrast of $\pm 0.1 \text{ Mg m}^{-3}$ implies an error in the depth of $\pm 7 \text{ m}$. The same uncertainty in z results from an error in Δg of $\pm 0.5 \text{ mgal}$. Figure 57 shows that the regional field is probably known to within this amount, except towards the terminus, where the error may be as much as $\pm 1 \text{ mgal}$.

Based on these figures, the bedrock topography is considered accurate to $\pm 10 \text{ m}$, increasing to $\pm 15 \text{ m}$ as the terminus is approached (below the upper nunatak). These limits agree with those of other workers (for example, Corbató, 1965b; Crossley and Clarke, 1970). Without the areas of known bedrock and the two boreholes, the regional field could not have been defined nearly as accurately and the bedrock uncertainties could well have been too great for an adequate analysis of the flow.

The terrain correction and modelling procedure used here are considered to be quite accurate. The integration of $V(z)$ effectively smooths the topography between the contour lines and so the model of the attracting mass is considerably more realistic than if discrete compartments, such as Hammer zones, are used. Gravity stations near the margins of the glacier or near areas of severe terrain can be handled, provided an accurate map is available. Taking gravity measurements in such areas should not be avoided in future, especially readings adjacent to the margin, as these are very valuable in fixing the regional field.

Chapter 6

THE SURFACE VELOCITY VARIATIONS

6.1 THE MOVEMENT STAKES AND THE SURVEYS

The surface motion of the Nisqually Glacier was measured with a theodolite using standard surveying techniques. This is the only feasible method for measuring the movement accurately at a number of points, independently of accumulation and ablation effects. Electronic instruments are now available which can measure distances very accurately but to obtain the three dimensional coordinates of a point *three* stations have to be occupied instead of two. Furthermore, such devices are limited to more or less the same weather conditions that theodolites are, the accuracy of the vertical coordinate is no greater than that obtained with theodolites, and the corner reflectors required on the glacier are expensive.

The triangulation points are discussed elsewhere (section 4.1). For measuring vertical ice motion, the markers on the glacier have to be stakes placed in holes drilled in the ice. Normally wooden stakes are used so that melting of the surrounding ice by absorbed radiation is reduced. However, wood stakes could not be used in the winter as they would break easily during storms, especially with the heavy riming conditions common on the Nisqually Glacier. Moreover, the stakes would have to be extendable and protrude high enough above the surface so that heavy snowfalls would not bury them.

Therefore metal stakes were used. They were made from high strength aluminum alloy tubing (6061-T6), 31.75 mm (1.250 inch) outside diameter, 1.59 mm (1/16 inch) wall thickness, and 2 m long. At one end a short piece of thicker tubing, 28.60 mm (1.125 inch) outside diameter and 3.18 mm (1/8 inch) wall thickness, was inserted. It protruded 120 mm so that it could be matched with the open end of a similar length of tubing. In this way "sections" could be

added or subtracted to each "stake". A roll pin was mounted in the coupling to lock with an L-shaped slot in the open end of the other section. To help offset the higher thermal conductivity of metal the stakes were painted white and a wood plug placed in the bottom of each stake. Black marks, 80 mm long, were painted at 1 m intervals and 25 mm black marks at 0.5 m intervals. These were used to sight on and to read the surface level on the stake. All sightings were made to the middle of the marks.

To avoid resetting the stakes frequently during the heavy ablation season they were initially placed in the ice to a depth of 4-8 m. Mechanical drilling to this depth is difficult and time-consuming, so a steam drill was used. During the first summer (1968) a Norwegian steam drill was used but it fell apart by the end of the summer. The author designed and had built an improved steam drill (Hodge, 1971) and this was used successfully for the remaining time. The use of a steam drill allowed stakes to be placed in ice containing morainal debris.

Under the circumstances the sectioned metal stakes worked very well. Radiation absorption by the metal did not appear to cause appreciably more enlargement of the hole than normally occurs with wood stakes. There was some indirect evidence* that the stakes did slowly melt down into the ice, despite the wood plug, but the effect on the vertical motion is insignificant (less than 1 mm d^{-1}). The stakes were not flagged since it was found easier to locate them by using the readings from previous surveys.

The greatest problems, as expected, occurred in the winter. Ideally sections would be added to the stakes to keep ahead of the snowfall but too many could not be added otherwise the combination of wind and rime would easily bend the stake over horizontally and then bury it. As days of good weather were

* Plastic tape wrapped around the tubing to replace painted black marks which had been scraped off was pushed up the stake about 300 mm over a 1 year period. This occurred on several stakes.

few it was difficult to meet these criteria. During the first winter 10 stakes were demolished by an avalanche which came all the way from the icefall to just opposite TP-2, and during the second winter 18 stakes were bent over and buried in a very severe riming storm. In both winters many stakes were simply buried by heavy snowfalls before sections could be added. Temporary, or "alternate", stakes were added as soon as possible to replace lost ones. Many sections were recovered later in the ablation season, but many were bent, mangled or even severed in two. Only a third of the original 260 sections survived two seasons.

The primary set of stakes was a longitudinal line down the band of bare ice which lies approximately two-thirds of the way toward the west side. This band was presumed to mark the line of maximum velocity. The surface velocity field measured in May 1970 confirms this. The longitudinal, or "centerline", stakes are denoted by the letter "C" and are numbered consecutively up-glacier, from C1 to C20. They were spaced approximately 130 m apart. A transverse profile (M) of seven stakes, about 80 m apart, was placed in the same area as the U.S.G.S. Profile II. These two lines of stakes were maintained as well as possible throughout the entire study*. Two other transverse profiles (L and U) were also established, corresponding roughly to the U.S.G.S. Profile I and Profile III respectively, and a short longitudinal line (X) was run between the upper and the middle transverse profiles on the east half of the glacier. Part of the U profile and all of the X line were discontinued after the first year of measurements. The centerline, the transverse lines and the positions of the 19 centerline stakes are indicated on the panorama taken from TP-8 (Plate I).

The stakes were surveyed from June 4, 1968, to June 4, 1970. During this

* Except stake C6. This was in the middle of a small icefall and proved to be more trouble than it was worth. It was abandoned after the first summer. Only the remaining 19 centerline stakes will be considered from now on.

two year period 59 successful surveys were made, an average of one every twelve days (Figure 61). The time between two successive measurements of the position of any stake varied from 6 days to 73 days.

A stake is said to be "redrilled" when it has been reset (by either extending the old hole or by making a new hole) and the amount of shift is known (by measuring it with a tape measure and Brunton compass). It is said to be "shifted" when it has been reset and the amount of shift is unknown. A gap in the line connecting the measurements of a stake's position in Figure 61 indicates that no velocities can be calculated by bridging the gap (for example, when a stake was shifted).

In the first year two days were required to survey all the stakes, the division between the "upper" and "lower" surveys usually being between C5 and C9. In the second year, new triangulation points were established so that all stakes could be measured in one day. Some surveys were only partially completed due to bad weather. All measurements consist of both horizontal and vertical angles, and almost all are the mean of the direct and inverted positions of the telescope (bad weather occasionally prevented the use of both positions). Finally, in the second year several stakes were sometimes measured from more than two triangulation points on the same survey.

During the first summer, 40 stakes were placed and measured. This was reduced to 29 the following summer. The number dropped to a low of 14 the first winter and 10 the second winter (excluding the alternate stakes). Surveys were attempted in the winter months whenever the weather looked favorable but nevertheless large gaps during December and January still occurred.

High winds prevented or prematurely terminated more surveys than did unexpected fog or clouds. Most surveys were done under clear, sunny skies, with a light breeze. Air temperatures ranged from -21°C to $+22^{\circ}\text{C}$. Completely calm air occasionally caused slight problems, such as heat shimmering or

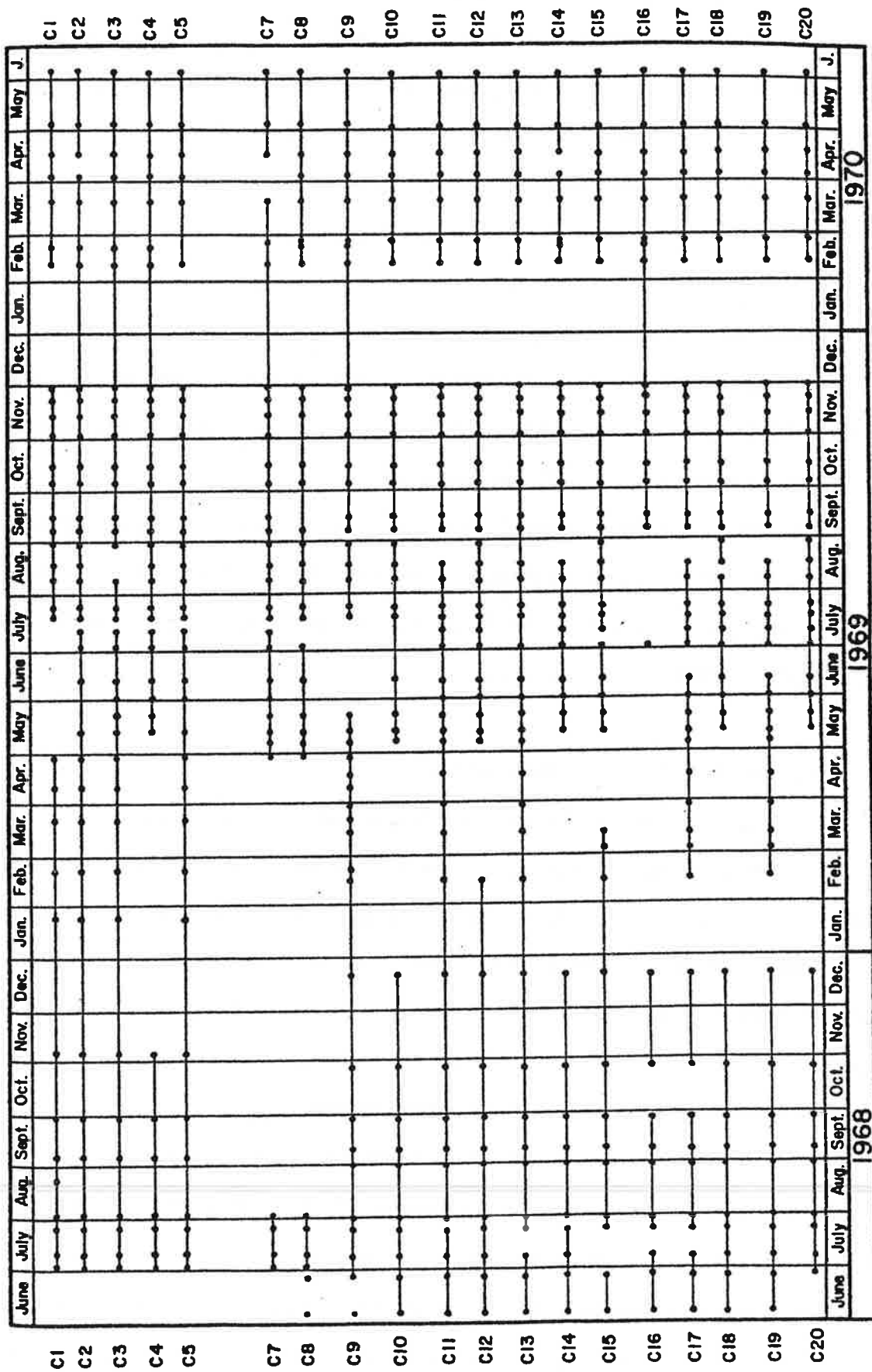


Figure 61. The dates of the surveys of the centerline stakes. Measurements later found to be faulty have been omitted. Velocities can only be calculated along the lines connecting the dots (section 6.5.9).

drifting of the theodolite level, and ice in the holes for the tripod legs was disastrous if it was not thoroughly removed beforehand. Image shaking generally became too great when the wind exceeded approximately 10 m s^{-1} , although it was accidentally found that this limit could be exceeded when the TP was buried under snow and a hole had to be dug for the theodolite.

The times that the measurements were started and ended at each TP were recorded and then averaged to give a mean time for that particular survey. The time is specified in days, and decimal parts of a day, from an arbitrary origin at 0000 hours, Pacific Standard Time, January 1, 1968. On this scale, the surveys started at $t = 155$ and ended at $t = 885$.

As mentioned earlier, three transverse profiles and one secondary longitudinal line were measured in addition to the main longitudinal line. This study, however, will be concerned only with the analysis of the data from the 19 longitudinal (centerline) stakes.

6.2 REDUCTION OF THE SURVEY MEASUREMENTS

6.2.1 *Calculation of the Mean Horizontal and Vertical Angles*

With a theodolite horizontal angles are measured with respect to some fixed reference point, usually another triangulation point, and vertical angles are measured with respect to a level bubble on the instrument. Both angles should be read in the direct and inverted positions. This is particularly important for the vertical angles, since this eliminates any collimation error between the telescope axis and the reference bubble.

For speed and convenience all direct positions were measured first and then all the inverted, the horizontal setting to the reference mark being measured before and after inverting the telescope. It is best to invert the telescope at each stake, but this is more time-consuming. Errors caused by the faster technique are probably negligible (section 6.3.1). The more rigorous

method, however, was used for the gravity stations because of the accuracy required in the vertical angles.

The following angles, in degrees, were read with the theodolite:

$H(D)$ = horizontal direct reading on the stake

$V(D)$ = vertical direct reading on the stake

$H(I)$ = horizontal inverted reading on the stake

$V(I)$ = vertical inverted reading on the stake

$H^0(D)$ = mean horizontal direct reading on the reference mark^{*}

$H^0(I)$ = mean horizontal inverted reading on the reference mark^{*}

Ideally the direct and inverted readings are related by

$$\left. \begin{aligned} H(I) &= 180 + H(D) & [H(D) < 180] \\ H(I) &= H(D) - 180 & [H(D) \geq 180] \\ V(I) &= 360 - V(D) \end{aligned} \right\} (1)$$

In practice we allow level adjustments to be made, if needed, between the direct and inverted sets of readings. If this is done the above expressions for $H(I)$ are not necessarily true since we may have effectively shifted the horizontal circle. To allow for this, the reference mark is first subtracted from the readings:

$$\left. \begin{aligned} H'(D) &= H(D) - H^0(D) \\ H'(I) &= H(I) - H^0(I) \end{aligned} \right\} (2)$$

Since the horizontal angle is the angle measured clockwise (looking down) from the reference mark to the stake, then 360° must be added to $H'(D)$ or $H'(I)$

* Usually the mean of two settings on the reference mark, one before a set of stake readings and one after. Occasionally only one setting was obtained.

if they turn out to be negative. The mean horizontal and vertical angles are then

$$\left. \begin{aligned} H_{ik} &= \frac{H'(D) + H'(I)}{2} \\ V_i &= \frac{V(D) + 360 - V(I)}{2} \end{aligned} \right\} (3)$$

where i is an index indicating the TP occupied and k is an index indicating the TP used as a reference mark.

For finding mistakes in the data it is useful to calculate the discrepancies between the direct and the inverted readings:

$$\left. \begin{aligned} \Delta H &= H'(D) - H'(I) \\ \Delta V &= V(D) - 360 + V(I) \end{aligned} \right\} (4)$$

If weather prevented either the direct or the inverted readings from being obtained then mean values of ΔH or ΔV from the same survey or from previous surveys were used to calculate H_{ik} or V_i .

6.2.2 Calculation of the Coordinates of a Point

Let (x, y, z) be the coordinates of a point in space which is observed from two triangulation points. These coordinates can be calculated by simple trigonometry, given the measured mean horizontal and vertical angles to the stake and the known coordinates of the occupied TP's and the reference TP's. The horizontal coordinates (x, y) are first calculated from the horizontal angles and then the z coordinate is found by using the horizontal distances to the point and the measured vertical angles. For clarity, we will refer to this "point" as a "stake" for the remainder of this discussion.

First, we convert the horizontal angles H_{ik} to azimuth angles ω_i .

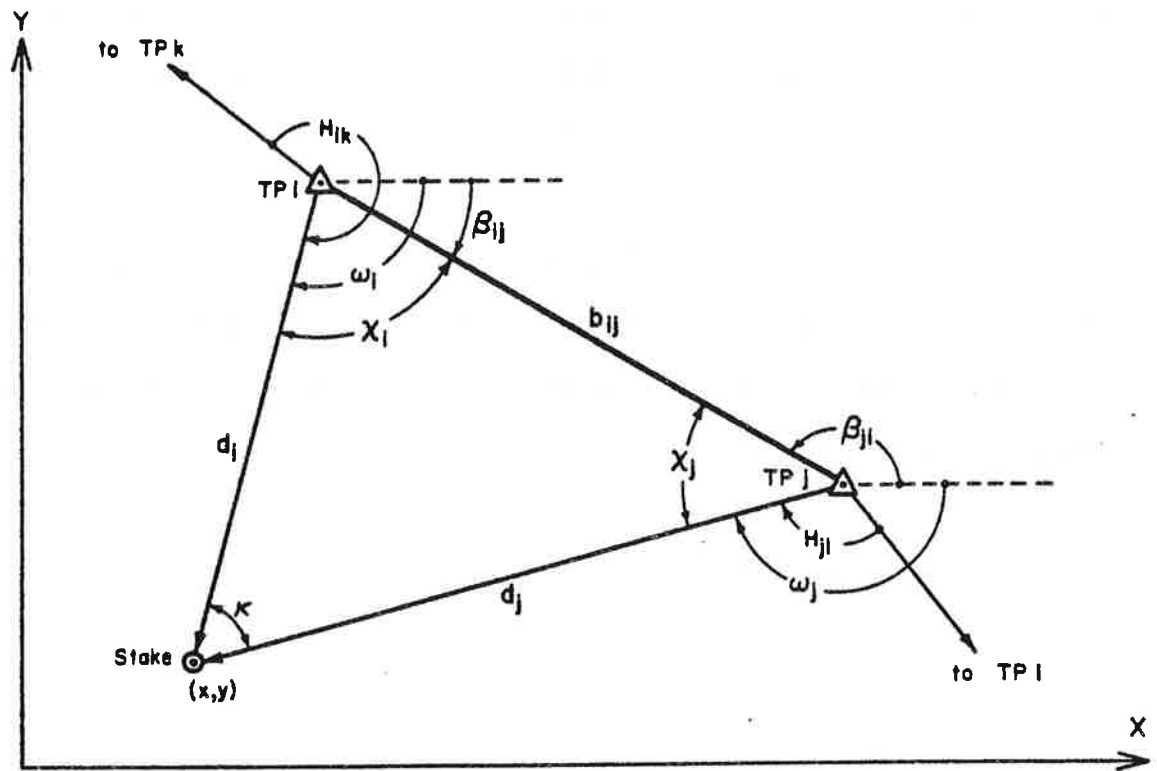


Figure 62. The calculation of the horizontal coordinates (x, y) of a point which is observed with a theodolite from two triangulation points. In the situation shown, $\beta_{ij} < 0$, $\beta_{ji} > 0$, $\omega_i < 0$ and $\omega_j < 0$.

All "azimuths" in this study are understood to be angles measured from true south (+X axis) to the stake, positive to the east (+Y direction) and negative to the west (-Y direction). Hence they vary from $-\pi$ to $+\pi$. All angles are assumed to be converted to radians at this point.

The algorithm for ω_i is (Figure 62):

$$\begin{aligned}
 \beta_{ij} &= \tan^{-1} \left(\frac{Y_j - Y_i}{X_j - X_i} \right) \\
 \text{if } \beta_{ij} < 0, &\text{ add } 2\pi \\
 \omega_i &= \beta_{ij} - H_{ik} \\
 \text{if } \omega_i > \pi, &\text{ subtract } 2\pi
 \end{aligned}
 \quad \left. \vphantom{\begin{aligned} \beta_{ij} &= \tan^{-1} \left(\frac{Y_j - Y_i}{X_j - X_i} \right) \\ \text{if } \beta_{ij} < 0, &\text{ add } 2\pi \\ \omega_i &= \beta_{ij} - H_{ik} \\ \text{if } \omega_i > \pi, &\text{ subtract } 2\pi \end{aligned}} \right\} (5)$$

where β_{ij} is the azimuth of TP_j from TP_i (Table 6) and (x_i, y_i, z_i) are the coordinates of TP_i. Throughout this study arctangent is written " $\tan^{-1}(\frac{Y}{X})$ " to denote the use of the FORTRAN function ATAN2(Y,X). This function returns a value between $-\pi$ and $+\pi$ and will handle all values of X and Y except $X = Y = 0$.

Let x_i and x_j be the interior angles of the triangle at TP_i and TP_j respectively, and let κ be the angle subtended by the two TP's at the stake (called the "stake angle"). The horizontal distances from the TP's to the stake are then

$$\left. \begin{aligned} d_i &= b_{ij} \left(\frac{\sin x_j}{\sin \kappa} \right) \\ \text{and} \\ d_j &= b_{ij} \left(\frac{\sin x_i}{\sin \kappa} \right) \end{aligned} \right\} (6)$$

where

$$b_{ij} = \sqrt{(x_i - x_j)^2 + (y_i - y_j)^2} \quad (7)$$

is the known horizontal distance between the two TP's (Table 5). The interior angles (x_i, x_j) are calculated by the algorithm:

$$\left. \begin{aligned} x_i &= |\beta_{ij} - \omega_i| \\ x_j &= |\beta_{ji} - \omega_j| \\ \text{if either } x_i \text{ or } x_j > \pi, &\text{ subtract from } 2\pi \end{aligned} \right\} (8)$$

The stake angle is given by

$$\kappa = \pi - x_i - x_j \quad (9)$$

The horizontal coordinates of the stake are then

$$\left. \begin{aligned} x &= X_1 + d_1 \cos \omega_1 \\ y &= Y_1 + d_1 \sin \omega_1 \end{aligned} \right\} (10)$$

Vertical angles in a theodolite are measured from the nadir point (Figure 63). The z coordinate can be fixed by measuring the vertical angle to the stake from only *one* triangulation point:

$$z_1 = Z_1 - d_1 \cot V_1 \quad (11)$$

Thus when vertical angles are measured from both TP's the results can be weighted according to their respective standard deviations (section 6.3.2) and averaged:

$$z = \frac{w_i z_i + w_j z_j}{w_i + w_j} \quad (12)$$

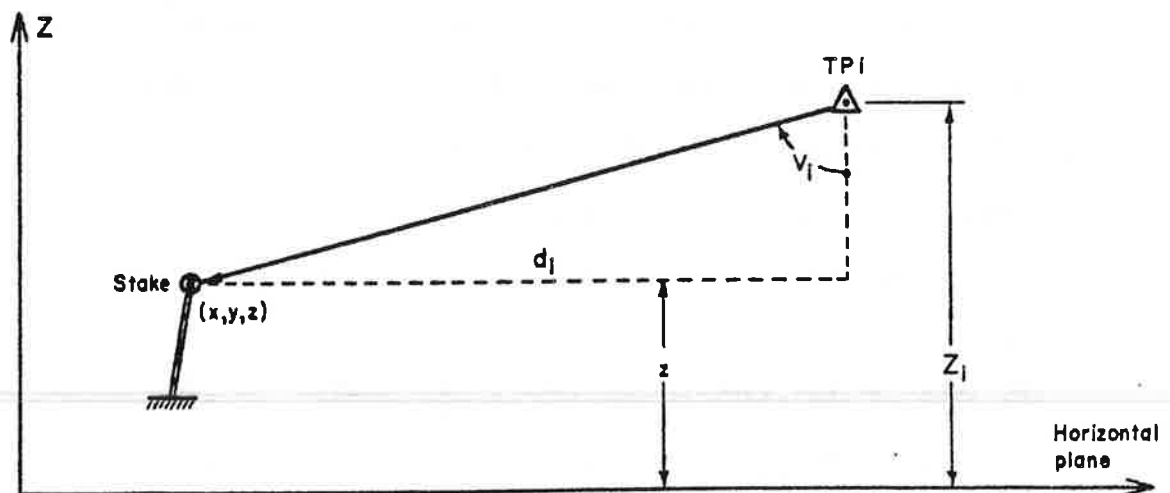


Figure 63. The calculation of the vertical coordinate z of a point which is observed with a theodolite from one triangulation point. The horizontal distance d_1 is assumed known.

where the weight w of a measurement is related to its standard deviation by

$$w = \frac{1}{\sigma^2} \quad (13)$$

The difference

$$\Delta z = z_i - z_j \quad (14)$$

is a useful quantity for picking out errors in the data.

6.2.3 *Corrections for Tilt of the Stake*

It was obvious from the beginning that corrections would have to be made for the tilt of the stake, as this was likely to change from one survey to the next. To calculate the tilt two points on the stake were measured with the theodolite, the mark at the top of the stake (which was always measured) and then the mark closest to the glacier surface, known as the "surface mark" (Figure 64). Alternately, if the stake appeared to deviate from the vertical by not much more than the width of the cross-hair in the theodolite, it was assumed to be vertical from that TP and no surface mark was measured. Since the marks on the stake were at half-meter intervals a surface mark could only be measured if at least 0.5 m of the stake was visible from both TP's. Situations where less than 0.5 m of the stake was visible *and* the stake had appreciable tilt were fortunately very rare and the tilt of the stake was obtained in almost all cases.

The tilt of the stake is denoted by two angles, θ , the amount of tilt from the vertical (+Z), and ϕ , the azimuth of the tilt from true south (+X). Let (x_o, y_o, z_o) be the coordinates of the top of the stake and let (x_s, y_s, z_s) be the coordinates of the surface mark. Then (θ, ϕ) are given by

$$\left. \begin{aligned} \theta &= \tan^{-1} \left\{ \frac{[(x_o - x_s)^2 + (y_o - y_s)^2]^{1/2}}{z_o - z_s} \right\} & (0 \leq \theta \leq +\pi) \\ \phi &= \tan^{-1} \left\{ \frac{y_o - y_s}{x_o - x_s} \right\} & (-\pi \leq \phi \leq +\pi) \end{aligned} \right\} (15)$$

This is known as method A. The singularity point ($x_o = x_s$, $y_o = y_s$) has to be treated appropriately.

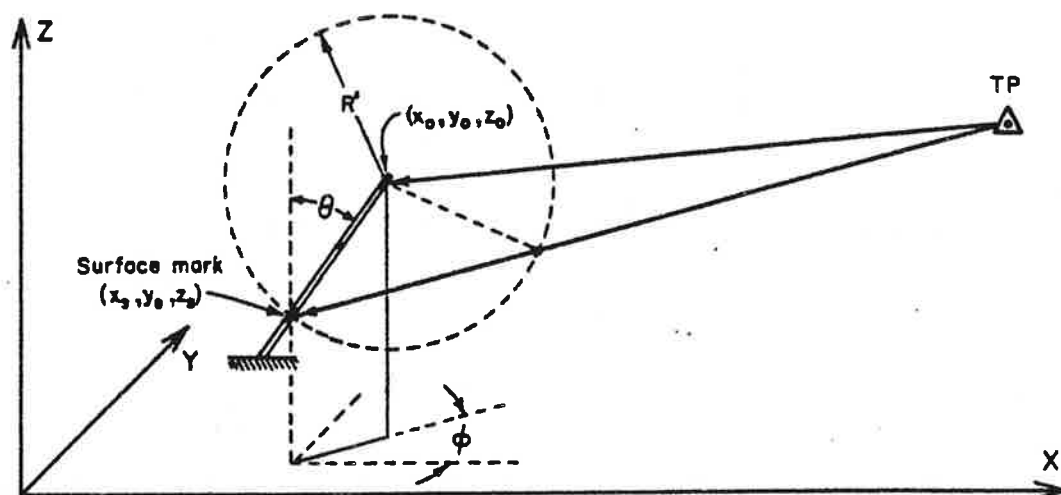


Figure 64. The calculation of the tilt (θ, ϕ) of a stake.

We have tacitly assumed here that the surface mark is the same for both TP's, so that it is possible to calculate the coordinates (x_s, y_s, z_s). A substantial number of situations arose, however, where the surface mark was different for the two TP's, due to blocking by intervening parts of the glacier surface. It is still possible to calculate the tilt though, because the distance R' between the surface mark and the top of the stake is known. This method, known as method B, is now described.

The desired point (x, y, z) must lie on a sphere of radius R' about the

point (x_0, y_0, z_0) :

$$R^2 = (x - x_0)^2 + (y - y_0)^2 + (z - z_0)^2 \quad (16)$$

The line of sight from the TP to the surface mark can (a) intersect the sphere in two distinct points (x_1, y_1, z_1) and (x_2, y_2, z_2) , (b) be tangent to the sphere at a single point, or (c) miss the sphere completely. The direction cosines (l, m, n) of the line of sight are determined by the measured azimuth ω and the vertical angle V :

$$\left. \begin{aligned} l &= \cos \left[\tan^{-1} \left\{ \frac{[\sin^2 \omega + \tan^2(V - \pi/2)]^{1/2}}{\cos \omega} \right\} \right] \\ m &= \cos \left[\tan^{-1} \left\{ \frac{[\cos^2 \omega + \tan^2(V - \pi/2)]^{1/2}}{\sin \omega} \right\} \right] \\ n &= \cos(\pi - V) \end{aligned} \right\} \quad (17)$$

ω is calculated from the measured horizontal angle using equations 5. The line of sight has the form

$$\frac{x - X}{l} = \frac{y - Y}{m} = \frac{z - Z}{n} \quad (18)$$

where (X, Y, Z) are the coordinates of the TP. Solving (16) and (18) we get a quadratic equation $Ax^2 + Bx + C = 0$ with the solution

$$x = \frac{-B \pm [B^2 - 4AC]^{1/2}}{2A} \quad (19)$$

where

$$\begin{aligned}
 A &= 1 + (m/l)^2 + (n/l)^2 \\
 B &= 2(-x_0 + D + E) \\
 C &= x_0^2 + D^2 + E^2 - R^2 \\
 D &= (Y - y_0 - mX/l)m/l \\
 E &= (Z - z_0 - nX/l)n/l
 \end{aligned}
 \tag{20}$$

The three cases for the roots of (19), two distinct real roots, one real root, or two imaginary roots, correspond respectively to the three physical situations mentioned above. Rather than discard the imaginary case as unsolvable, the point on the line of sight closest to the top of the stake was solved for and used to replace the imaginary roots. If the direction cosines of the line from this point to the top of the stake are (L, M, N) then

$$\frac{x - x_0}{L} = \frac{y - y_0}{M} = \frac{z - z_0}{N} \tag{21}$$

and

$$L^2 + M^2 + N^2 = 1 \tag{22}$$

Solving (18), (21), and (22), and using the condition that the distance

$$r' = [(x - x_0)^2 + (y - y_0)^2 + (z - z_0)^2]^{1/2} \tag{23}$$

be a minimum, we get

$$x = -\frac{B}{2A} \tag{24}$$

Once x is known (from equation 19 or 24), y and z are calculated from the relations:

$$\left. \begin{aligned} y &= Y + (x - X)m/L \\ z &= Z + (x - X)n/L \end{aligned} \right\} (25)$$

and the tilt angles (θ, ϕ) from equations 15.

The distance $(r' - R')$ that the point lies outside the sphere was also calculated. Values of this greater than 100-200 mm were usually considered to be due to factors other than random errors in the measurement of the angles and the tilt was considered unknown in this case. Fortunately the majority of values were only a few centimeters and only very rarely were tilts discarded.

This method thus gives either one or two solutions for (θ, ϕ) using the data from only one TP. The other TP also gives one or two solutions. Ideally one solution from the first TP and one from the second would be identical.

In practice we compute the angle between each of the solutions for the two TP's and choose the pair which gives the smallest such angle. The mean of this pair is taken as the correct solution. This is found as follows:

The angle τ between two line segments is given by

$$\cos \tau = l_1 l_2 + m_1 m_2 + n_1 n_2 \quad (26)$$

where (l_1, m_1, n_1) and (l_2, m_2, n_2) are the respective direction cosines. These are calculated from (θ, ϕ) with the relations

$$\left. \begin{aligned} l &= \cos \left[\tan^{-1} \left\{ \frac{[1 - \sin^2 \theta \cos^2 \phi]^{1/2}}{\sin \theta \cos \phi} \right\} \right] \\ m &= \cos \left[\tan^{-1} \left\{ \frac{[1 - \sin^2 \theta \sin^2 \phi]^{1/2}}{\sin \theta \sin \phi} \right\} \right] \\ n &= \cos \theta \end{aligned} \right\} (27)$$

The mean $(\bar{\theta}, \bar{\phi})$ of the two tilts (θ_1, ϕ_1) and (θ_2, ϕ_2) is then given by

$$\left. \begin{aligned} \bar{\theta} &= \tan^{-1} \left(\frac{[F^2 + G^2]^{1/2}}{\cos \theta_1 + \cos \theta_2} \right) \\ \bar{\phi} &= \tan^{-1} \left(\frac{G}{F} \right) \end{aligned} \right\} \quad (28)$$

where

$$F = \sin \theta_1 \cos \phi_1 + \sin \theta_2 \cos \phi_2$$

$$G = \sin \theta_1 \sin \phi_1 + \sin \theta_2 \sin \phi_2$$

Method B can also be used in the original situation where the two surface marks are the same (Method A). The two methods do not necessarily give the same answer since method B uses additional information that is not used in method A, namely the known distance R' . Consequently values of (θ, ϕ) were always calculated with method B and, if possible, with method A also. When both methods are used the mean of the two is used for the final tilt angles. The difference between the two methods gives a measure of the accuracy of the tilt calculations; such differences were usually only a few degrees and seldom exceeded 10° .

The special situation where the stake appeared to be vertical from one TP (a subset of method B) is easily handled since the stake lies in a vertical plane whose normal has direction cosines $l_1 = \cos(\omega + \pi/2)$, $m_1 = \cos \omega$, $n_1 = 0$ where ω is the stake azimuth observed from that TP. Method B can be used for the other TP and, in general, it gives two possible values for the tilt. The correct value is the one which lies closest to the above plane, that is, has the smallest value of the distance

$$\delta = |l_1(x - X) + m_1(y - Y)| \quad (29)$$

where (x, y, z) represents the two solutions from method B (equations 19, 24 and 25) and (X, Y, Z) are the coordinates of the TP from which the stake appears to be vertical.

6.2.4 Corrections for Bend of the Stake

During the winter the long metal stakes were frequently bent over by wind, riming and snowfall. As will be shown later, the effect of this on the velocities was often drastic, even producing backward motions at times. Although it is impossible to tell exactly how the stake was bent it was necessary to make some attempt to estimate a correction factor.

Suppose a stake has a tilt (θ_1, ϕ_1) and that the distance along the stake from its bottom to the glacier surface, known as the "surface level", is R_1 (Figure 65). The next time the stake is surveyed, snowfall has increased the the surface level to R_2 and the portion of the stake still exposed is found to have a new tilt (θ_2, ϕ_2) . If we assume that the segment between R_1 and R_2 has been bent in a circular arc tangent to the adjacent segments, then it is possible to obtain a unique solution for the coordinates $(\Delta x, \Delta y, \Delta z)$ of the point at R_1 relative to the point at R_2 . This assumption also implies that all three segments lie in the same plane (the plane of the paper in Figure 65).

From now on, the "bend" of a stake is always assumed to be like this. It is one of the simplest models that can be used and experience in the field has shown that only occasionally were stakes more severely contorted.

Each time another survey is done, new values of (R, θ, ϕ) are found. The above process is repeated and a picture of the stake's shape is built up as the winter progresses. When ablation commences the surface level drops and the stake becomes more and more upright. The equations to be developed will handle this situation equally well.

When the lowermost of the three segments is itself bent, its tilt values

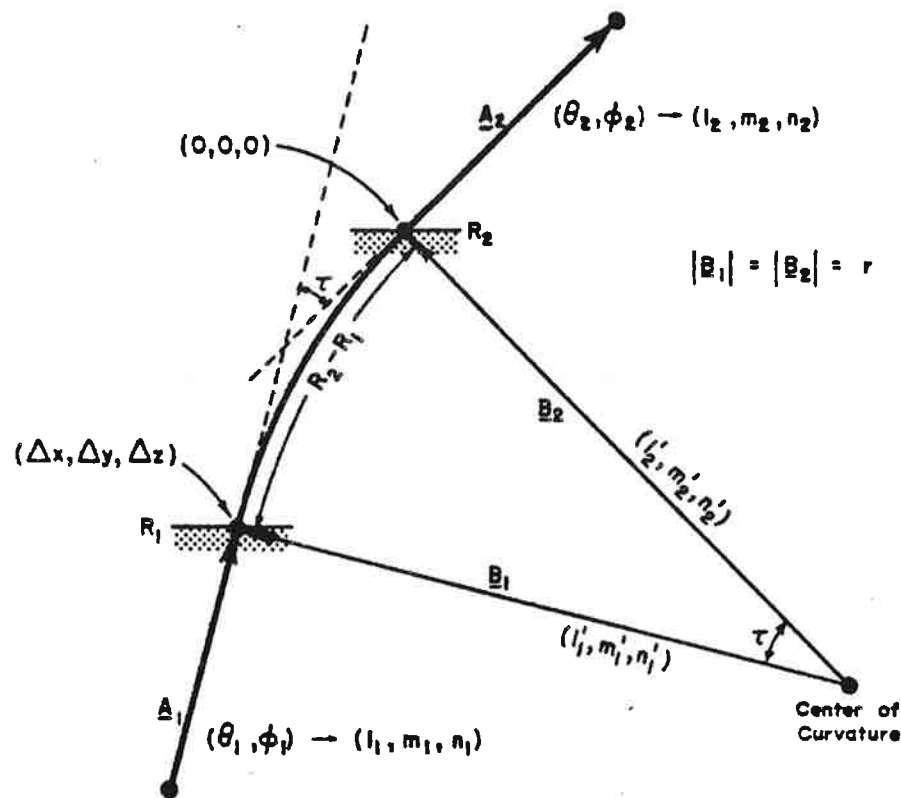


Figure 65. The calculation of the bend of a stake. The bent segment is assumed to be a circular arc tangent to the adjacent segments.

apply to its uppermost point. One bent segment can run smoothly into another bent segment, but the planes containing the two bent segments do *not* have to be identical. Hence, although each segment must be two dimensional, the shape of the entire stake can be three dimensional. No generality is lost, however, in the following derivation by assuming the upper and lower segments are straight.

Let the lower and upper segments be vectors \underline{A}_1 and \underline{A}_2 (Figure 65). Their direction cosines, (l_1, m_1, n_1) and (l_2, m_2, n_2) respectively, can be determined from their tilt angles, (θ_1, ϕ_1) and (θ_2, ϕ_2) , by use of equations 27. Let \underline{B}_1 and \underline{B}_2 be radius vectors of the circular middle segment, with direction cosines (l'_1, m'_1, n'_1) and (l'_2, m'_2, n'_2) respectively. Let the normal of the plane

containing all these vectors have direction cosines (L, M, N) .

The angle of bend τ can be found from equation 26, using the known values of (l_1, m_1, n_1) and (l_2, m_2, n_2) . This is also the angle subtended by the bent segment and hence the length of \underline{B}_1 or \underline{B}_2 is

$$r = \left| \frac{R_2 - R_1}{\tau} \right| \quad (30)$$

Our basic assumptions can now be used to set up six equations in six unknowns, (l'_1, m'_1, n'_1) and (l'_2, m'_2, n'_2) :

$$\left. \begin{aligned} \underline{A}_1 \cdot \underline{B}_1 &= 0 \\ \underline{A}_2 \cdot \underline{B}_2 &= 0 \\ \underline{B}_1 \cdot (\underline{A}_1 \times \underline{A}_2) &= 0 \\ \underline{B}_2 \cdot (\underline{A}_1 \times \underline{A}_2) &= 0 \\ |\underline{B}_1| &= r \\ |\underline{B}_2| &= r \end{aligned} \right\} \quad (31)$$

or, in terms of the direction cosines,

$$\left. \begin{aligned} l_1 l'_1 + m_1 m'_1 + n_1 n'_1 &= 0 \\ l_2 l'_2 + m_2 m'_2 + n_2 n'_2 &= 0 \\ l'_1(m_1 n_2 - n_1 m_2) + m'_1(n_1 l_2 - l_1 n_2) + n'_1(l_1 m_2 - m_1 l_2) &= 0 \\ l'_2(m_1 n_2 - n_1 m_2) + m'_2(n_1 l_2 - l_1 n_2) + n'_2(l_1 m_2 - m_1 l_2) &= 0 \\ l_1'^2 + m_1'^2 + n_1'^2 &= 0 \\ l_2'^2 + m_2'^2 + n_2'^2 &= 0 \end{aligned} \right\} \quad (32)$$

The solution for (l'_1, m'_1, n'_1) is

$$\left. \begin{aligned} l'_1 &= \pm [1 + \gamma_1^2 + \{(\lambda - \gamma_1 \mu)/v\}^2]^{-1/2} \\ m'_1 &= -\gamma_1 l'_1 \\ n'_1 &= -(\gamma_1 \lambda + m'_1 \mu)/v \end{aligned} \right\} (33)$$

where

$$\left. \begin{aligned} \lambda &= m_1 n_2 - n_1 m_2 \\ \mu &= n_1 l_2 - l_1 n_2 \\ v &= l_1 m_2 - m_1 l_2 \end{aligned} \right\} (34)$$

$$\gamma_1 = (\lambda n_1 - v l_1)/(\mu n_1 - v m_1) \quad (35)$$

A similar solution for (l'_2, m'_2, n'_2) results, provided we replace γ_1 with

$$\gamma_2 = (\lambda n_2 - v l_2)/(\mu n_2 - v m_2) \quad (36)$$

We thus get four possible solutions, $\pm(l'_1, m'_1, n'_1)$, $\pm(l'_2, m'_2, n'_2)$, corresponding to the four combinations of the vectors \underline{B}_1 and \underline{B}_2 shown in Figure 66.

The correct solution, case (a), is determined by defining a temporary coordinate system fixed on the point R_2 as shown. The possible coordinates of the point R_1 with respect to R_2 are, in the old system,

$$\left. \begin{aligned} \Delta x &= \pm (l'_1 \pm l'_2) r \\ \Delta y &= \pm (m'_1 \pm m'_2) r \\ \Delta z &= \pm (n'_1 \pm n'_2) r \end{aligned} \right\} (37)$$

and in the new system:

$$\left. \begin{aligned} x' &= l'_2 \Delta x + m'_2 \Delta y + n'_2 \Delta z \\ y' &= l_2 \Delta x + m_2 \Delta y + n_2 \Delta z \end{aligned} \right\} (38)$$

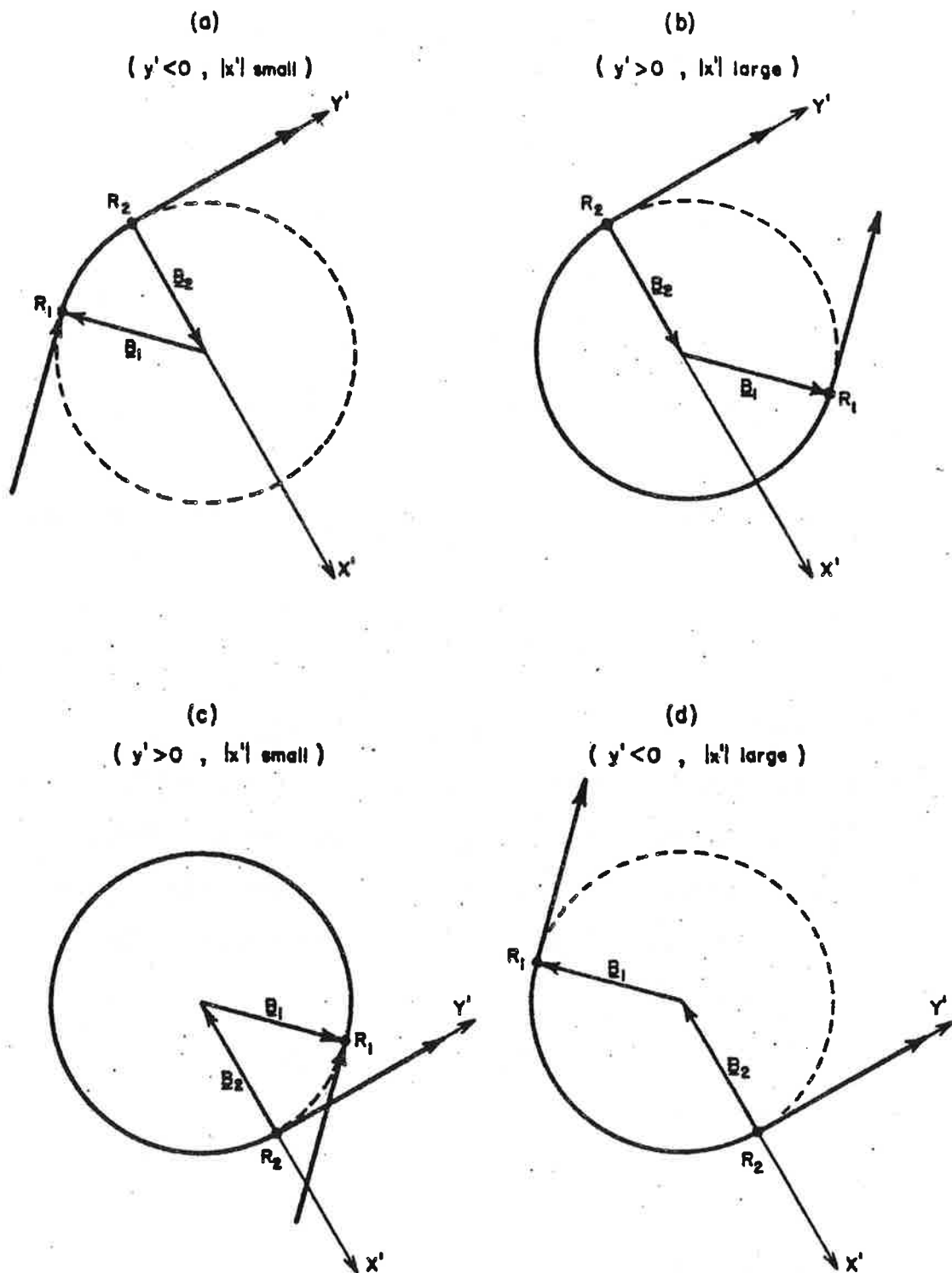


Figure 66. The four possible solutions for the bend of a stake. The physically correct one is case (a).

The correct solution is the one for which $y' \leq 0$ and $|x'|$ is a minimum. This tells us which sign to use in (37).

Knowing $(\Delta x, \Delta y, \Delta z)$ the "bend corrections" are easily calculated. These are defined as the adjustments needed to the coordinates of the bottom of the stake after they have been corrected for tilt. If R_0 is the total length of the stake, from its bottom (x_b, y_b, z_b) to its top (x_o, y_o, z_o) , then

$$\left. \begin{aligned} x_b &= x_o - R_0 \sin \theta_o \cos \phi_o + b_x \\ y_b &= y_o - R_0 \sin \theta_o \sin \phi_o + b_y \\ z_b &= z_o - R_0 \cos \theta_o + b_z \end{aligned} \right\} (39)$$

where (θ_o, ϕ_o) is the tilt of the uppermost (straight) segment. The required bend corrections (b_x, b_y, b_z) are

$$\left. \begin{aligned} b_x &= R_2 \sin \theta_o \cos \phi_o - R_1 \sin \theta_b \cos \phi_b + \sum \Delta x \\ b_y &= R_2 \sin \theta_o \sin \phi_o - R_1 \sin \theta_b \sin \phi_b + \sum \Delta y \\ b_z &= R_2 \cos \theta_o - R_1 \cos \theta_b + \sum \Delta z \end{aligned} \right\} (40)$$

where (θ_b, ϕ_b) is the tilt of the lowermost (straight) segment. The summation is over all bent segments between R_1 and R_2 . $(\Delta x, \Delta y, \Delta z)$ are given by equations 37.

6.3 ERROR ANALYSIS

6.3.1 Errors in the Angle Measurements

Errors, σ_h and σ_v , in the measurement of the horizontal and vertical angles result in errors, $\sigma_x, \sigma_y, \sigma_z, \sigma_\theta$, and σ_ϕ , in the coordinates and tilt of a stake. Ideally σ_h and σ_v would be measured on each survey by taking a number of readings of each angle. This would also give a more accurate mean

value for the angle. However, this would have made each survey prohibitively long and so it was decided to make only one observation of each angle and use "standard values" for σ_h and σ_v . These were determined on August 5, 1970, by making 75 observations from TP-8 of the horizontal and vertical angles to the painted cross on the rock cliffs below TP-5. TP-4 was used as a reference mark. The cross is close to the glacier surface and the sighting paths are representative of those usually made. The weather was sunny with a light breeze, typical of most surveys. The observations lasted 6 hours, covering that part of the day when most surveying was done.

The first 50 observations were made in two groups of 25 each. In each of these two groups the direct readings were done first and then the inverted ones (as was the technique on regular surveys). The remaining 25 observations were done in the more rigorous manner, inverting the telescope at each sighting. The observations were reduced using equations 1 to 4 and the results are shown in Table 11.

	n	σ_h	σ_v
First group	25	2.6	4.3
Second group	25	2.1	3.0
Third group	25	2.6	3.4
All together	75	3.1	5.3

Table 11. The standard deviations in the angles turned to the cross on August 5, 1970. All values are in seconds of arc. In the first and second group all direct angles were measured before the inverted angles. In the third group the telescope was inverted each time (the correct practice to use with a theodolite). n is the number of observations.

This table shows that there is no significant difference between the two techniques, justifying the use of the faster but less rigorous one. Taking

all the observations together we get the "standard values" $\sigma_h = 3.1''$ and $\sigma_v = 5.3''$.

The frequency distribution of the residuals for all the cross observations is shown in Figure 67. The distribution is not very Gaussian, particularly for the vertical angles, and so an independent estimate of σ_h and σ_v would be desirable.

The angle measurements made for the triangulation net provide such a check. They have the disadvantage that they are only 4, 6 or 8 measurements of many separate angles and so the residuals are deviations from many means rather than a single mean, but, taken together, they have the advantage of being a much larger sample (436 and 387 versus 75) distributed over a much wider range of conditions. The frequency distribution of the residuals is very clearly Gaussian (Figures 68 and 69). The standard deviations are $\sigma_h = 2.13''$ and $\sigma_v = 3.28''$, both noticeably smaller than those of the cross measurements.

A possible explanation of this is shown in Figure 70, which shows the residuals of the cross measurements as a function of the time of observation. There appears to be a significant variation, particularly with the vertical angles. This is very suggestive of changing atmospheric refraction. Since the 4-8 measurements of the net angles were usually made over a period of only one to three hours, compared with the six hours for the cross measurements, refraction effects are likely to be smaller in the former case. In fact if we take an average of the three groups in Table 11, rather than considering all observations together, we get values in much better agreement with the results from the net angles.

Thus the values $\sigma_h = 3.1''$ and $\sigma_v = 5.3''$ are likely to be conservative estimates of the angle errors. Using these values will also allow for refraction effects, which are very difficult, if not impossible, to calculate over a glacier surface (Brecher, 1966; Meier, personal communication, 1968). Since the

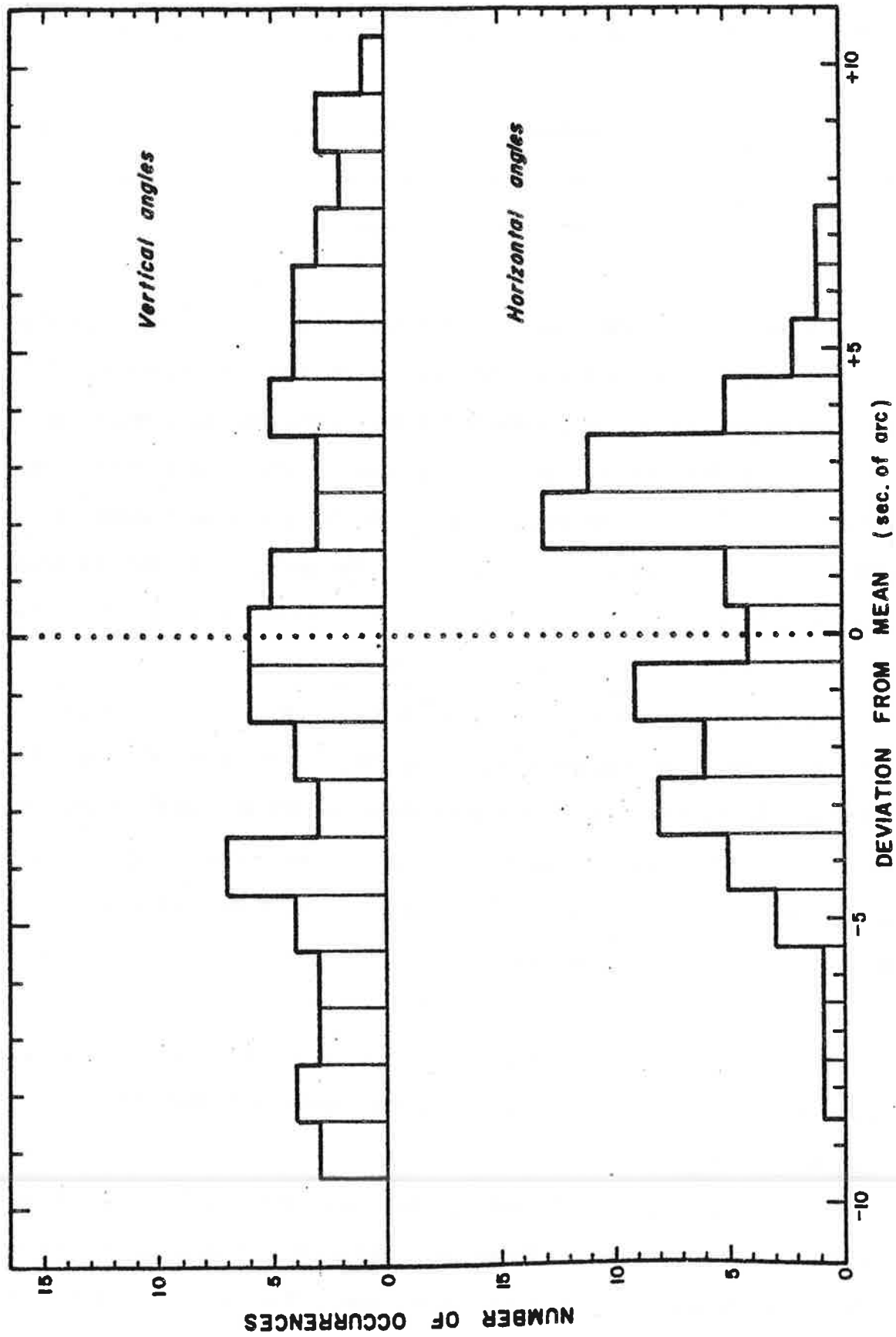


Figure 67. The frequency distribution of the residuals of the horizontal and vertical angles measured to a fixed point (the cross on the rock cliffs below TP-5J).

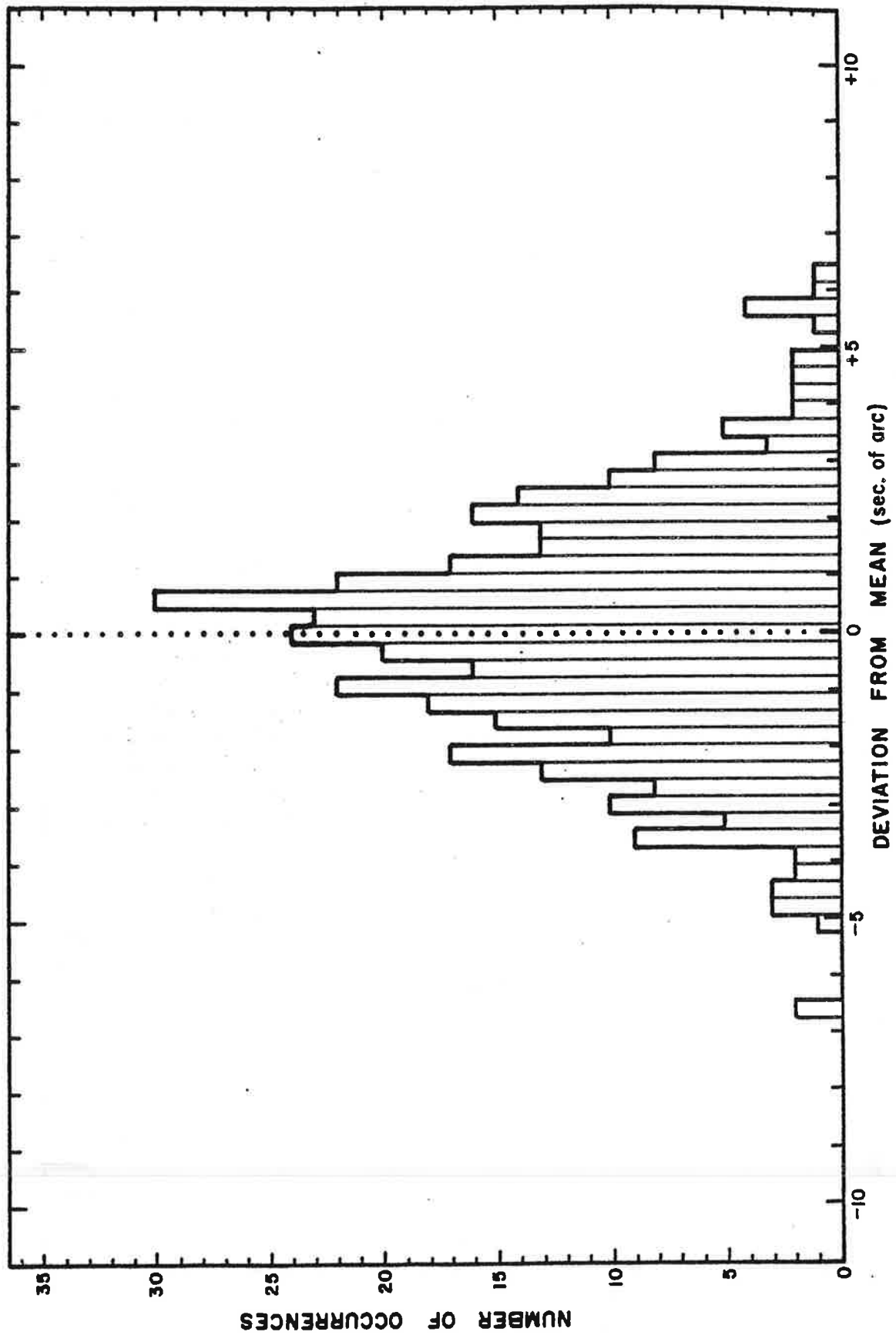


Figure 68. The frequency distribution of the residuals of the horizontal angles measured for the triangulation net. The total number of observations is 387. Each angle was observed 4, 6 or 8 times.

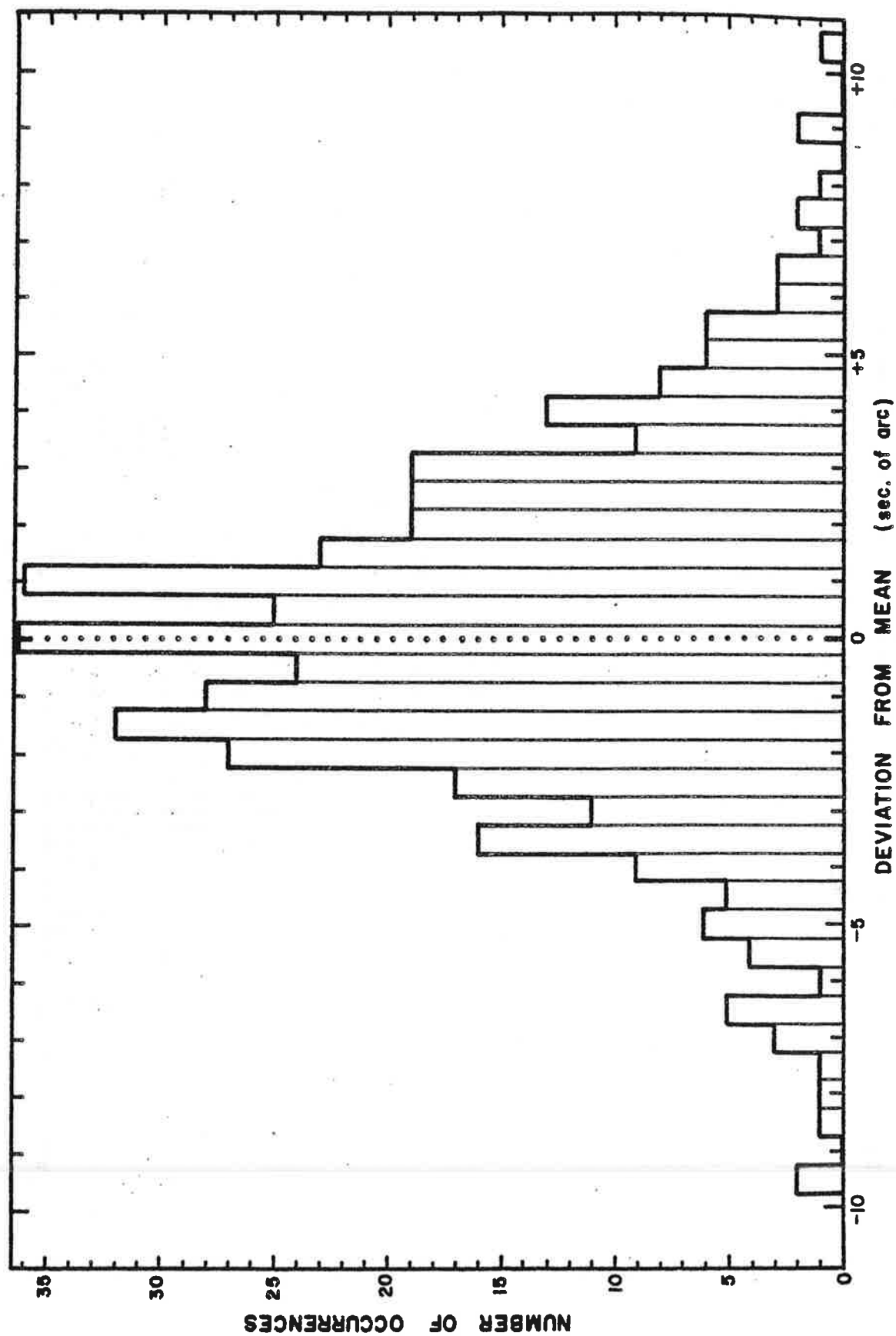


Figure 69. The frequency distribution of the residuals of the vertical angles measured for the triangulation net. The total number of observations is 436. Each angle was observed 4, 6 or 8 times.

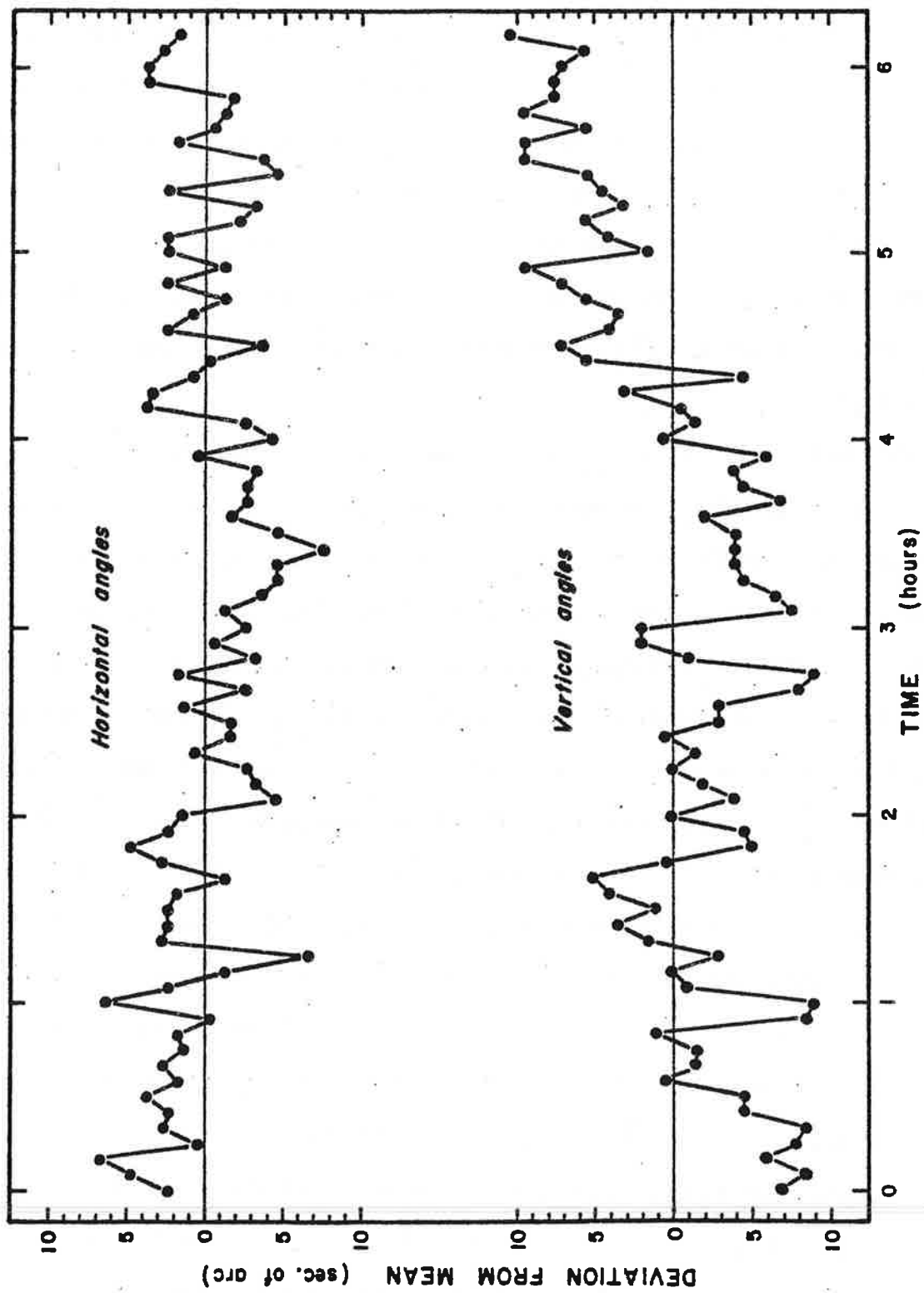


Figure 70. The residuals of the horizontal and vertical angles to the cross as a function of time. The long period trend is considered to be a result of changing atmospheric refraction.

cross measurements were made with the same instrument on the same glacier and under the same conditions as encountered on most surveys it seems safe to assume that these errors represent the combined effects, not only of short term changes in atmospheric refraction, but also of the inherent accuracy and stability of the instrument, the accuracy of setting up and levelling it properly, the accuracy of aligning the cross-hairs on a stake, and the accuracy of reading the scales. Finally, the value of σ_h agrees remarkably well with the value of 3.0" obtained by Meier (1960) on the Saskatchewan Glacier with a Wild T2 theodolite.

The difference, $\Delta z = z_1 - z_2$, between the z values determined from the two TP's has a possible bearing on the refraction effect. Figure 71 shows the frequency distribution of nearly all the Δz values calculated during the course of this study. The distribution is very close to Gaussian except for a curious displacement of the mean of about +1 to +3 cm. Because z_1 is from the first TP occupied and z_2 is from the second, z_2 is usually measured about three hours later in the day than z_1 . Since z_1 was usually measured around noon, when temperature gradients above the glacier surface are probably the strongest, it should be subjected to greater refraction. This would make it higher. Since this is indeed found to be the case, it seems reasonable to suppose the displacement of 1-3 cm is due to refraction and that this value is a crude estimate of its average effect. This corresponds to about 2 to 6 seconds of arc at typical sightings of 1 km. This verifies that $\sigma_h = 3.1''$ and $\sigma_v = 5.3''$ probably includes most refraction effects.

A fourth, and final, estimate of the accuracy of the horizontal angles comes from examining the "closure" on each loop made with the theodolite. This is the difference between readings on the reference mark before and after a series of stake readings. If we consider the initial setting as the "reference reading" and the final setting as the "stake reading", we can view the closure

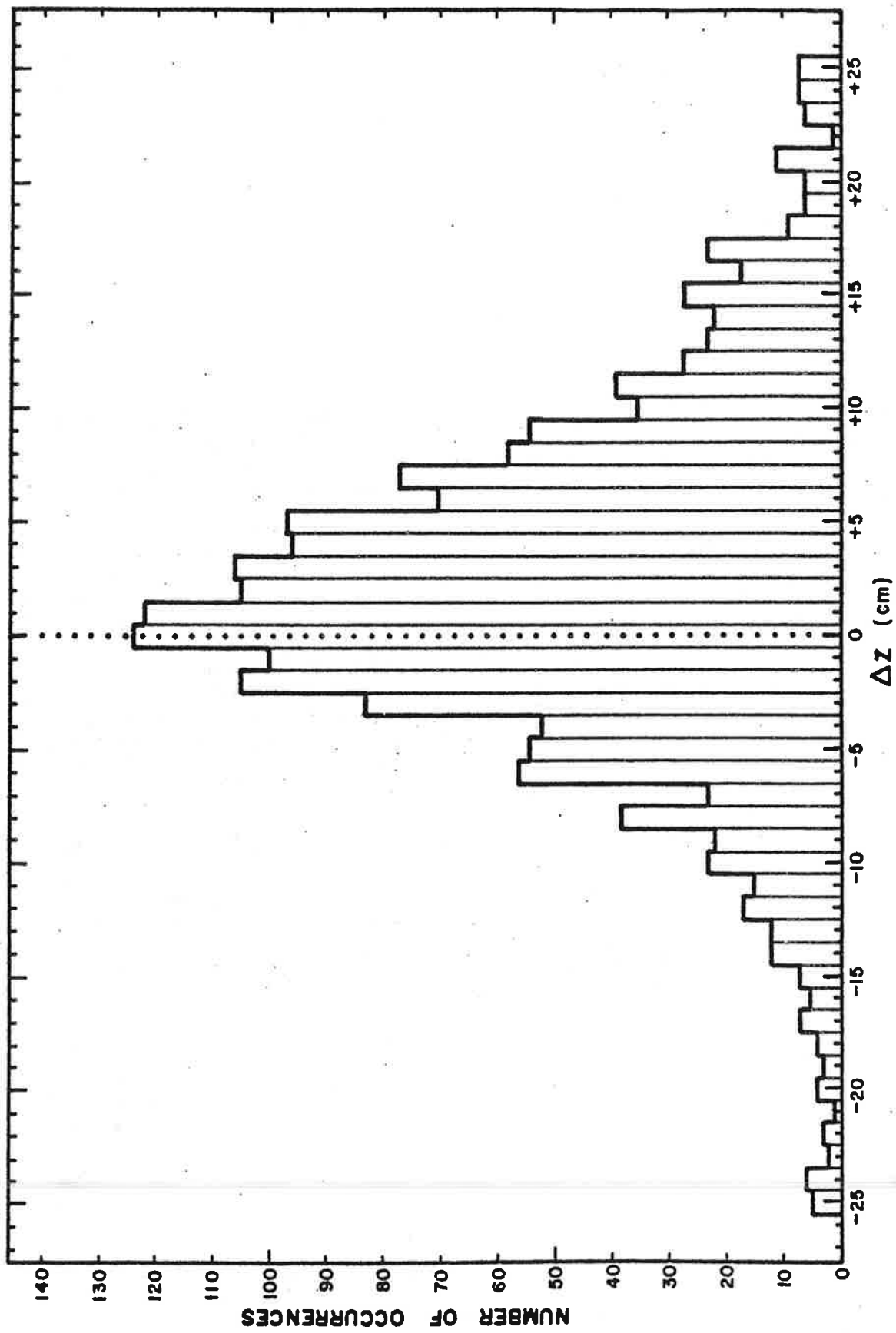


Figure 71. The frequency distribution of the difference Δz between the s values determined from two triangulation points. The total number of observations is 1832.

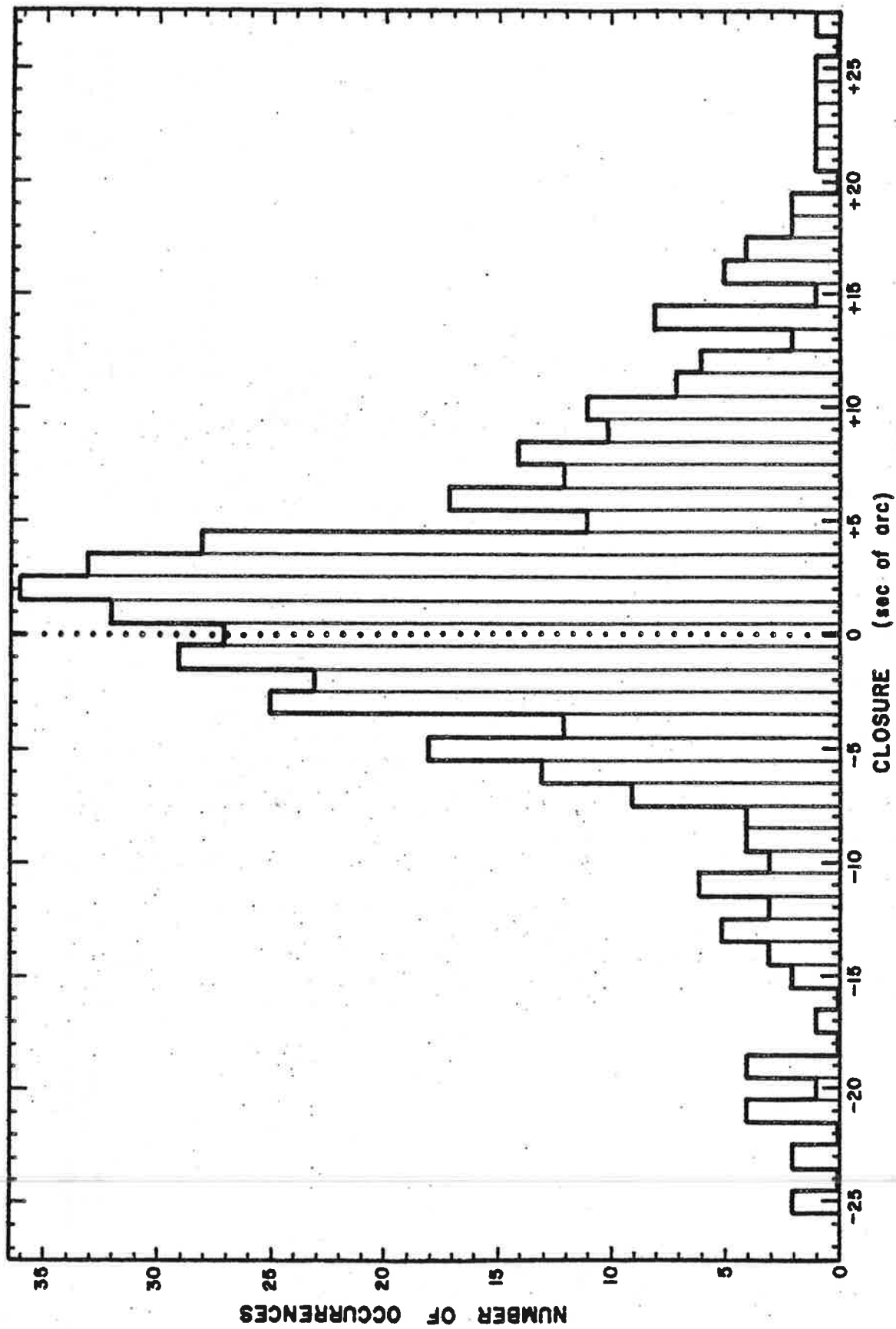


Figure 72. The frequency distribution of the closure angle (the difference between the readings on the reference mark before and after a series of stake readings). The total number of observations is 448.

as simply turning an angle to a stake which happens to be 360° away.

The frequency distribution of the closure is shown in Figure 72; the standard deviation is about 7". [This excludes 17 points which fall outside $\pm 30''$ (about 4σ) since these probably represent events other than atmospheric effects or random setting error.] This value is roughly twice the values quoted above. This is not unreasonable, however, since the closure spans a time interval about twice as great, on the average, as that involved in the normal measurement of horizontal angles, where a mean of the two reference settings is used. Thus, on an equivalent time scale, the closure would be of the same order as the standard values of σ_h and σ_v .

The distribution of Figure 72 also shows a mean closure of about 1.5". Since the closure was always calculated by subtracting the final reading from the initial one, this is suggestive of a drift of the reference mark with time. Changing atmospheric refraction could again be the cause of this.

6.3.2 *Errors in the Coordinates*

Since we assume the angle errors to be constant, the errors in the coordinates and tilt of a stake are due solely to geometric effects. The calculation of these errors is now described.

If $f(x,y)$ is a function of two independent variables x and y , each of which is subject to standard deviations σ_x and σ_y , then it can be shown (Baird, 1962, p. 63) that the standard deviation of f is, to a first approximation,

$$\sigma_f^2 = \left(\frac{\partial f}{\partial x}\right)^2 \sigma_x^2 + \left(\frac{\partial f}{\partial y}\right)^2 \sigma_y^2 \quad (41)$$

provided the variations in x are independent of the variations in y , that is,

$$\sum_{i=1}^n (x_i - \bar{x})(y_i - \bar{y}) = 0 \quad (42)$$

where (\bar{x}, \bar{y}) are the means of the n values (x_i, y_i) .

First consider the x coordinate of a stake. Combining (6) and (10) we get

$$x = X_i + b_{ij} \left(\frac{\sin \chi_j}{\sin \kappa} \right) \cos \omega_i \quad (43)$$

From (5) we see that ω_i is of the form

$$\omega_i = \beta_{ij} + k_i \chi_i - 2\pi z_i \quad (44)$$

where $k_i = +1$ if the stake azimuth is to the anticlockwise side of the base line (looking down) and $k_i = -1$ if it is on the clockwise side, and where $z_i = +1, 0$ or -1 . The term $2\pi z_i$ has no effect on $\sin \omega_i$ or $\cos \omega_i$ and can be omitted. Hence, substituting (9) and (44) into (43), we get

$$x = X_i + b_{ij} \left\{ \frac{\sin \chi_j \cos(k_i \chi_i + \beta_{ij})}{\sin(\pi - \chi_i - \chi_j)} \right\} \quad (45)$$

We assume there are no errors in X_i , b_{ij} and β_{ij} (section 4.4) and that each of χ_i and χ_j is subjected, independently, to an error of σ_h . If we evaluate the partial derivatives $\partial x / \partial \chi_i$ and $\partial x / \partial \chi_j$ and substitute the results into (41) we get

$$\sigma_x^2 = \frac{\sigma_h^2 b_{ij}^2}{\sin^4 \kappa} \left\{ \sin^2 \chi_j (\cos \kappa \cos \omega_i - k_i \sin \kappa \sin \omega_i)^2 \right. \\ \left. + \cos^2 \omega_i (\cos \kappa \sin \chi_j + \sin \kappa \cos \chi_j)^2 \right\} \quad (46)$$

Using standard trigonometric formulae and the relation (Selby, 1962, p. 467)

$$d_j = b_{ij} \cos \chi_j + d_i \cos \kappa \quad (47)$$

we can condense (46) into

$$\sigma_x^2 = \frac{\sigma_h^2}{\sin^2 \kappa} \left\{ d_i^2 \cos^2(\kappa + k_1 \omega_1) + d_j^2 \cos^2 \omega_1 \right\} \quad (48)$$

An analysis of all possible geometric configurations will show that

$$\omega_j = \omega_1 + k_1 \kappa \quad (49)$$

Using this, plus the relation

$$\cos(\kappa + k_1 \omega_1) = \cos(\omega_1 + k_1 \kappa) \quad (50)$$

equation 48 simplifies to

$$\sigma_x^2 = \frac{\sigma_h^2}{\sin^2 \kappa} \left\{ d_i^2 \cos^2 \omega_j + d_j^2 \cos^2 \omega_1 \right\} \quad (51)$$

By a similar analysis, the standard deviation in y is

$$\sigma_y^2 = \frac{\sigma_h^2}{\sin^2 \kappa} \left\{ d_i^2 \sin^2 \omega_j + d_j^2 \sin^2 \omega_1 \right\} \quad (52)$$

The z coordinate has to be handled slightly differently since two independent values can be calculated from each triangle. From (6) and (11) these are given by

$$\left. \begin{aligned} z_i &= z_i - b_{ij} \left(\frac{\sin \chi_j \cot V_i}{\sin \kappa} \right) \\ z_j &= z_j - b_{ij} \left(\frac{\sin \chi_i \cot V_j}{\sin \kappa} \right) \end{aligned} \right\} (53)$$

This time, in addition to an error σ_h in χ_i and χ_j , we have an error σ_v in V_i and V_j . The analysis is similar to that for equations 45 to 48; the results are

$$\left. \begin{aligned} \sigma_{z_i}^2 &= \left(\frac{d_i^2 \cos^2 \kappa + d_j^2}{\tan^2 V_i \sin^2 \kappa} \right) \sigma_h^2 + \left(\frac{d_i^2}{\sin^4 V_i} \right) \sigma_v^2 \\ \sigma_{z_j}^2 &= \left(\frac{d_j^2 \cos^2 \kappa + d_i^2}{\tan^2 V_j \sin^2 \kappa} \right) \sigma_h^2 + \left(\frac{d_j^2}{\sin^4 V_j} \right) \sigma_v^2 \end{aligned} \right\} (54)$$

The two z values are combined using equations 12 and 13; the mean error in z is then

$$\sigma_z^2 = \frac{\sigma_{z_i}^2 \cdot \sigma_{z_j}^2}{\sigma_{z_i}^2 + \sigma_{z_j}^2} \quad (55)$$

Note that this reduces the standard deviation and thus tends to offset the inherently greater error in the measurement of the vertical angles.

6.3.3 Errors in the Tilt

To calculate the standard deviation in θ and ϕ we assume that only method A was used in their calculation. The standard deviation is assumed to be no different if only method B was used or if both methods were used.

If the coordinates of a surface mark (x_s, y_s, z_s) have not already been calculated we must therefore substitute some values so that we can estimate σ_θ and σ_ϕ . To do this we translate the coordinates (x_o, y_o, z_o) of the top of the stake a distance R' down the stake by the relations

$$\left. \begin{aligned} x_s &= x_o - R' \sin \theta \cos \phi \\ y_s &= y_o - R' \sin \theta \sin \phi \\ z_s &= z_o - R' \cos \theta \end{aligned} \right\} (56)$$

where R' is taken as positive down the stake.

If the stake appeared to be vertical at one TP, the surface mark at the other TP is used for R' . If the stake appeared to be vertical from both TP's then R' is set equal to the distance from the top of the stake to the glacier surface.

Using equations 15 to evaluate the partial derivatives of θ and ϕ with respect to each of x_o, y_o, z_o, x_s, y_s , and z_s and substituting into (47) we get

$$\left. \begin{aligned} \sigma_\theta^2 &= \frac{2}{v^2(1+v^2)^2(z_o-z_s)^4} \left[(x_o-x_s)^2 \sigma_x^2 + (y_o-y_s)^2 \sigma_y^2 + v^4(z_o-z_s)^2 \sigma_z^2 \right] \\ \sigma_\phi^2 &= \frac{2}{(1+\mu^2)^2(x_o-x_s)^2} \left[\mu^2 \sigma_x^2 + \sigma_y^2 \right] \end{aligned} \right\} (57)$$

where

$$\left. \begin{aligned} \mu &= \frac{y_o - y_s}{x_o - x_s} \\ v &= \frac{[(x_o - x_s)^2 + (y_o - y_s)^2]^{1/2}}{z_o - z_s} \end{aligned} \right\} (58)$$

The standard deviations of (x_s, y_s, z_s) have been assumed equal to those of (x_o, y_o, z_o) respectively. These equations have a number of singularity points, for which separate equations have to be developed. The results are:

$$x_o = x_s, y_o = y_s: \quad \sigma_\theta^2 = \frac{\sigma_x^2 + \sigma_y^2}{(z_o - z_s)^2} \quad ; \quad \sigma_\phi \text{ arbitrary} \quad (59a)$$

$$x_o = x_s : \quad \sigma_\phi^2 = \frac{2}{(y_o - y_s)^2} \sigma_x^2 \quad ; \quad \sigma_0 \text{ from (57)} \quad (59b)$$

$$z_o = z_s : \quad \sigma_\theta^2 = \frac{2\sigma_z^2}{(x_o - x_s)^2 + (y_o - y_s)^2} ; \quad \sigma_\phi \text{ from (57)} \quad (59c)$$

6.3.4 Errors in the Bend

The errors in the bend of a stake are much harder to calculate due to the cumbersome set of equations. Furthermore, they are probably meaningless since the assumption of a circular arc tangent to the adjacent segments is likely to introduce a greater error. It was felt that it would be more realistic to estimate limits to the bend by assuming first that all of it was concentrated at R_1 (that is, the stake had a "kink" at that point) and then, second, that it was all concentrated at R_2 (Figure 73).

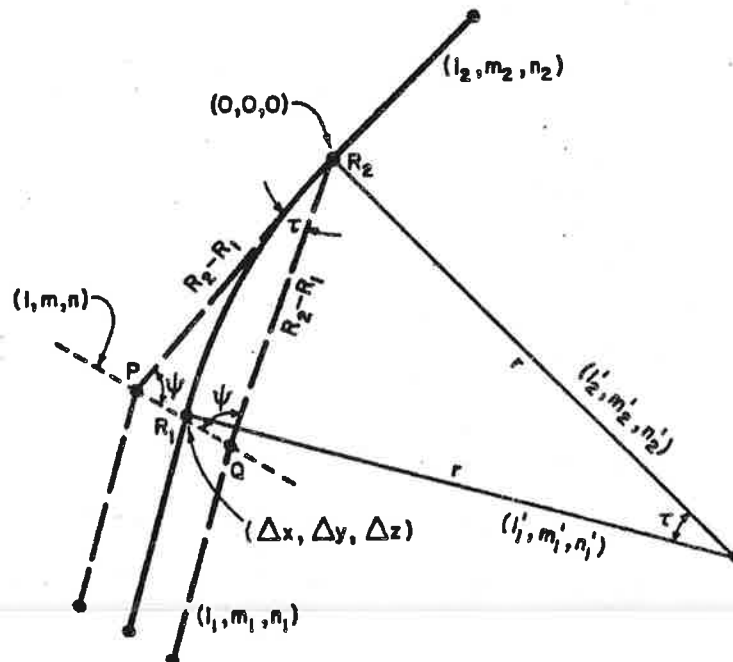


Figure 73. The calculation of the errors in the bend of a stake. The error is estimated by assuming that, instead of having a smooth circular bend (solid line), the stake has a sharp "kink" in it, first at R_1 and then at R_2 (dashed lines).

The notation is the same as used earlier to calculate the bend corrections (Figure 65). Since $|\underline{PR}_2| = |\underline{QR}_2| = |R_2 - R_1|$, triangle PQR_2 is isosceles, with a base angle

$$\psi = \frac{\pi - \tau}{2} \quad (60)$$

We define the errors (e_x, e_y, e_z) as one half the magnitude of the components of the vector \underline{PQ} :

$$\left. \begin{aligned} e_x &= |\underline{PQ}| \frac{l}{2} \\ e_y &= |\underline{PQ}| \frac{m}{2} \\ e_z &= |\underline{PQ}| \frac{n}{2} \end{aligned} \right\} \quad (61)$$

where (l, m, n) are the direction cosines of the vector \underline{PQ} , and

$$|\underline{PQ}| = |R_2 - R_1| \frac{\sin \tau}{\sin \psi} \quad (62)$$

If (L, M, N) are the direction cosines of the plane of the paper (in Figure 73) then

$$lL + mM + nN = 0 \quad (63)$$

We also require

$$\cos \psi = ll_1 + mm_1 + nn_1 \quad (64)$$

and

$$\cos \psi = ll_2 + mm_2 + nn_2 \quad (65)$$

The solution of (63), (64) and (65) is

$$\left. \begin{aligned}
 l &= \frac{(\cos \psi)[N(n_1 - n_2) + N(m_2 - m_1)]}{\lambda L + \mu M + \nu N} \\
 m &= \frac{(\cos \psi)(n_2 - n_1) + \mu l}{\lambda} \\
 n &= \frac{(\cos \psi)(m_1 - m_2) + \nu l}{\lambda}
 \end{aligned} \right\} (66)$$

where (λ, μ, ν) are given by equations 34. (L, M, N) are found by solving the equations

$$\left. \begin{aligned}
 l_1 L + m_1 M + n_1 N &= 0 \\
 l_2 L + m_2 M + n_2 N &= 0 \\
 L^2 + M^2 + N^2 &= 1
 \end{aligned} \right\} (67)$$

The solution is

$$\left. \begin{aligned}
 L &= \left[1 + \left(\frac{\mu}{\lambda} \right)^2 + \left(\frac{l_1}{n_1} + \frac{m_1 \mu}{n_1 \lambda} \right)^2 \right]^{-1/2} \\
 M &= \left(\frac{\mu}{\lambda} \right) L \\
 N &= - \left(\frac{l_1 L + m_1 M}{n_1} \right)
 \end{aligned} \right\} (68)$$

6.4 THE REDUCTION PROGRAM AND THE RESULTS

Approximately 25,000 angles were measured in the course of this study, each to the nearest second of arc. The sheer volume of data, plus the need for accurate and complex calculations, required the use of a high-speed digital computer. A FORTRAN program was written to perform all the computations outlined in the preceding sections, using as input the measurements directly

from the field note books.

On the normal movement surveys the direct and inverted readings were not checked for agreement in the field. Faulty reading of the theodolite scale, commonly a 10' error with a Kern theodolite, could easily be detected later and the reading corrected, because usually two points on the stake were measured, one of which was bound to be correct. In cases where only one point was measured, calculation of the coordinates and comparison with its position on adjacent surveys usually enabled the correct reading to be ascertained. The program printed out ΔH and ΔV (equations 4) as an aid to locating these errors. It is felt that virtually all faulty readings were properly corrected, provided ΔH or ΔV was greater than 1 or 2 minutes of arc. Errors less than this usually do not change the velocity values by much and, at any rate, they would probably not be detected in the field anyway.

The difference in x values (Δx , equation 14), the horizontal distances (d_1 and d_2 , equations 6), and the stake angle (κ , equation 9) were also printed out to help find survey errors and weak triangles (small κ). Details of the tilt calculations, such as the quantity $r' - R'$ (p. 172) and the individual tilt values from the two methods (A and B), enabled errors in the sightings to the surface mark to be spotted.

The need to allow for missing data complicated the coding considerably, as did three other circumstances:

(a) As the surface level increases, bend corrections can be calculated simply using the tilt and surface level on the previous survey. However, when the surface level is decreasing, the complete shape of the stake obtained *throughout* the winter must be specified, since the surface level could easily by-pass complete segments of the stake. This was a messy storage and coding problem.

(b) When some of the stakes melted out in the summer they were found to

have very sharp bends, or "kinks". The point of the kink was always surveyed so that the correct tilt and bend corrections could be calculated. This had to be allowed for in the programming. Sometimes three or four kinks were measured on a single stake.

(c) During the second year many stakes were often surveyed from three or occasionally four triangulation points. This means that three or six triangles, respectively, could be formed. All the calculations were done for each possible triangle. The coordinates are weighted according to their respective standard deviations (equations 13) and then averaged, for example,

$$\bar{x} = \frac{\sum_{k=1}^K w_{x_k} x_k}{\sum_{k=1}^K w_{x_k}} \quad (69)$$

$$\bar{\sigma}_x^2 = \frac{\sigma_{x_1}^2 \cdot \sigma_{x_2}^2 \cdots \sigma_{x_k}^2}{\sum_{k=1}^K \sigma_{x_k}^2} \quad (70)$$

where the summation is over the K possible triangles. This weighting procedure automatically eliminates "bad" triangles provided more than two TP's are occupied. The only time when the stake angle became small enough to cause appreciable error occurred when stake C8 passed the line between TP-3 and TP-8. Fortunately, the stake was also surveyed from TP-10 and TP-9 so no points had to be eliminated solely because of a "weak" triangle.

Figure 74 shows the trajectories of all stakes measured. The individual points are not marked as it would have made the plot incomprehensible. Gaps in the trajectories occur whenever a stake was redrilled or shifted. The point used in the plotting is the "surface point", defined as the point where

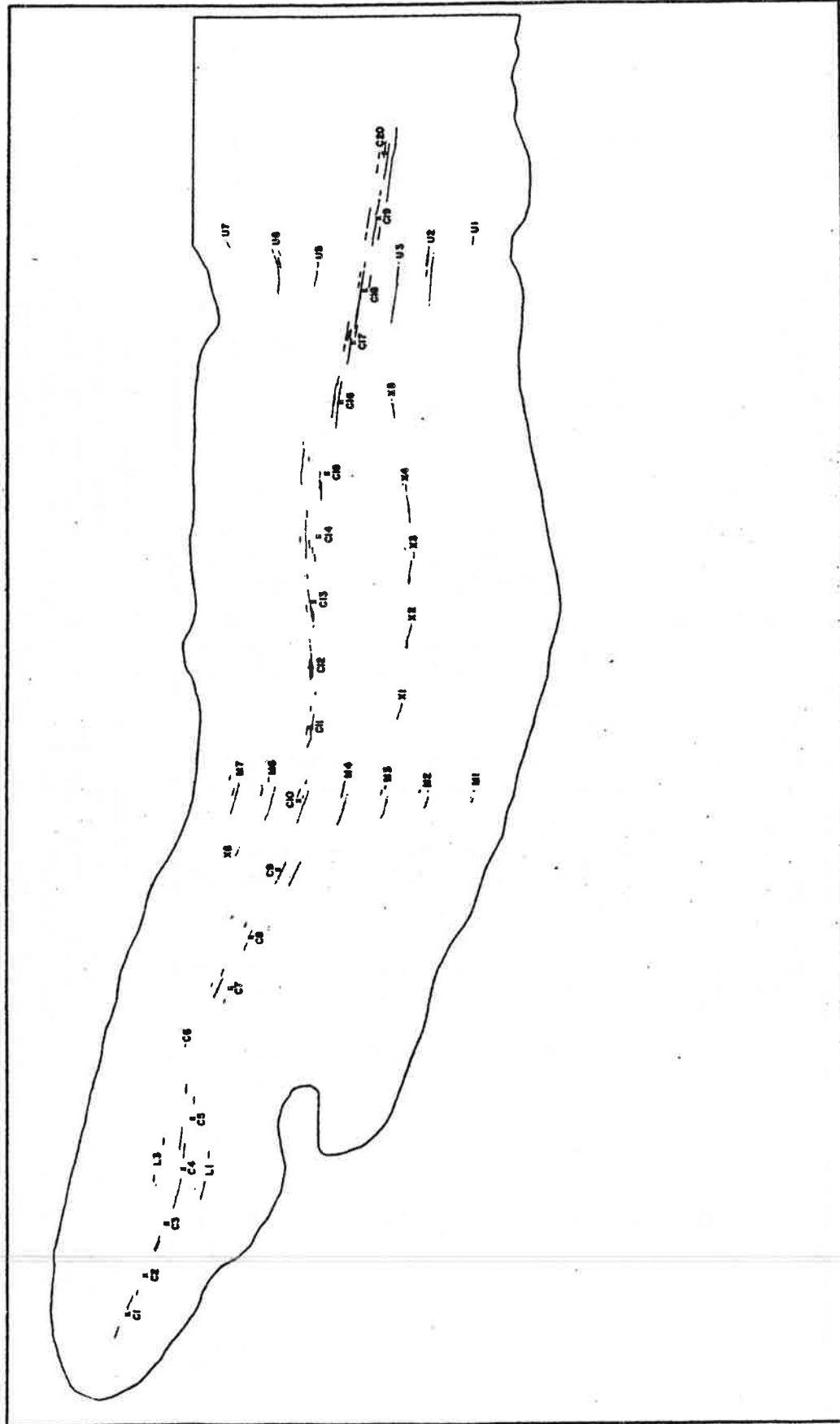


Figure 74. The trajectories of all stakes surveyed from June 4, 1968, to June 4, 1970. Gaps indicate times when the stake was shifted or redrilled. The small "x's" indicate the standard centerline stake positions. The trajectories refer to the point where the stake enters the surface; hence small irregularities occur when the stake is bent over by snowfall and wind.

Stake	n	Mean error in coordinates			Mean error in tilt	
		$\bar{\sigma}_x$	$\bar{\sigma}_y$	$\bar{\sigma}_z$	$\bar{\sigma}_\theta$	$\bar{\sigma}_\phi$
C1	32	1.0 ± 0.1	3.0 ± 0.4	1.8 ± 0.4	1.1 ± 0.8	7.0 ± 8.1
C2	37	1.8 ± 2.5	3.1 ± 2.8	1.4 ± 1.0	0.9 ± 0.6	8.0 ± 13.3
C3	37	3.4 ± 5.7	4.5 ± 7.0	1.9 ± 2.1	1.1 ± 1.4	4.1 ± 4.6
C4	36	2.6 ± 3.4	3.6 ± 4.9	1.6 ± 1.4	1.5 ± 2.5	11.7 ± 17.5
C5	36	1.4 ± 1.1	2.4 ± 2.8	1.3 ± 0.7	1.1 ± 1.1	3.8 ± 4.3
C7	32	1.0 ± 0.2	3.8 ± 4.2	1.6 ± 0.7	1.2 ± 1.2	19.7 ± 41.8
C8	33	12.4 ± 52.8	41.8 ± 173.9	8.4 ± 32.8	2.2 ± 3.4	15.8 ± 26.2
C9	43	1.7 ± 1.0	3.5 ± 2.3	1.6 ± 0.5	1.9 ± 2.9	11.0 ± 14.2
C10	35	1.0 ± 0.2	2.9 ± 1.4	2.0 ± 0.1	1.4 ± 0.9	12.7 ± 16.7
C11	40	1.2 ± 1.0	2.8 ± 1.0	2.0 ± 0.2	1.5 ± 1.7	6.9 ± 9.5
C12	39	1.8 ± 1.1	2.5 ± 0.9	2.0 ± 0.2	1.2 ± 1.0	8.5 ± 12.4
C13	39	1.8 ± 1.4	2.9 ± 0.6	1.9 ± 0.2	1.2 ± 0.8	5.5 ± 6.7
C14	38	2.9 ± 1.3	2.9 ± 0.4	1.9 ± 0.2	2.0 ± 2.0	14.5 ± 14.3
C15	41	3.4 ± 1.8	3.2 ± 0.7	2.0 ± 0.3	1.9 ± 1.7	12.9 ± 18.9
C16	26	3.6 ± 1.5	3.3 ± 0.8	2.0 ± 0.2	1.7 ± 1.5	8.9 ± 12.1
C17	41	4.7 ± 1.6	3.7 ± 0.5	2.0 ± 0.1	3.0 ± 6.2	19.3 ± 24.7
C18	36	5.8 ± 2.2	3.9 ± 0.2	2.4 ± 0.5	4.1 ± 5.9	20.9 ± 30.0
C19	41	6.9 ± 2.6	4.4 ± 0.6	2.6 ± 0.5	4.3 ± 8.7	19.5 ± 30.4
C20	36	9.3 ± 2.9	4.6 ± 0.6	2.7 ± 0.5	5.7 ± 11.8	22.7 ± 24.7
Means:	37	3.1 ± 1.8	3.4 ± 1.8	1.9 ± 0.1	2.1 ± 2.9	12.3 ± 17.4

Table 12. The mean error in the coordinates and tilt of the centerline stakes. Errors in the coordinates are in centimeters and those in the tilt are in degrees. n is the total number of measurements of the position of a stake over the two years of measurements, excluding points considered to be faulty. The number after the "+" sign gives the standard deviation (of a single observation) of the mean error. The means at the bottom of the table omit stake C8, which had abnormally large errors when it was in line with TP-3 and TP-8.

the stake enters the surface. Consequently the trajectories are not always smooth. The irregularities are caused by the tilting and bending of the stake and demonstrate the need for the elaborate reductions developed here.

Appendix B shows the tilt (θ, ϕ) of the centerline stakes as a function of time. The general increase of tilt in the fall and winter, followed by a decrease in the spring and summer, is apparent. From mid-summer to mid-fall no bend corrections are needed as the tilt changes very little.

Table 12 gives the mean errors in the coordinates and tilts of the centerline stakes. The errors are greatest with the uppermost stakes since these involve the longest sightings and relatively small stake angles ($20-30^\circ$).

σ_y is generally greater than σ_x , as expected.

In summary, the position of a stake is known to about ± 3 cm horizontally and ± 2 cm vertically. Its tilt is known to approximately $\pm 2^\circ$ in θ and $\pm 12^\circ$ in ϕ .

6.5 THE VELOCITY CALCULATIONS

The surface speed of the glacier is defined as the time rate of change of the position vector \underline{r} of a parcel of ice at the glacier surface:

$$s = \left| \frac{D\underline{r}}{Dt} \right| \quad (71)$$

If (x_1, y_1, z_1) and (x_2, y_2, z_2) are the coordinates of a given point on the stake on two different surveys, then

$$s = \frac{[(x_2 - x_1)^2 + (y_2 - y_1)^2 + (z_2 - z_1)^2]^{1/2}}{t_2 - t_1} \quad (72)$$

is the finite difference approximation to (71). $t_2 - t_1$ is the time interval between the two surveys. The speed s is assumed valid for a point $(\bar{x}, \bar{y}, \bar{z}, \bar{t})$

midway between the two data points (x_1, y_1, z_1, t_1) and (x_2, y_2, z_2, t_2) :

$$\left. \begin{aligned} \bar{x} &= \frac{x_1 + x_2}{2} & \bar{y} &= \frac{y_1 + y_2}{2} \\ \bar{z} &= \frac{z_1 + z_2}{2} & \bar{t} &= \frac{t_1 + t_2}{2} \end{aligned} \right\} (73)$$

The problem is ensuring that the two points (x_1, y_1, z_1) and (x_2, y_2, z_2) actually represent the *same* parcel of glacier ice. Since the stakes used in this study have sections added or removed, undergo changes in tilt, and become bent during the winter, this problem is not trivial. The bottom of the stake presumably moves with the ice and so the obvious approach is to reduce the measurements to this point before applying the above equations. We now discuss this procedure and show how it proved to be unsatisfactory.

6.5.1 *Correcting the Coordinates to the Bottom of the Stake*

In correcting the measured coordinates of a point on a stake to the bottom of the stake, four degrees of refinement can be used:

I. *No correction.* The stake is assumed to undergo no changes in length, tilt or shape. The measured point (x_m, y_m, z_m) can then be taken as the bottom point.

II. *Correction for change in length.* The stake is allowed to have sections added or subtracted, but it cannot change tilt or shape. The bottom point is then $(x_m, y_m, z_m - R_m)$.

III. *Correction for change in tilt.* The stake is allowed to undergo changes in length and tilt, but not shape. The bottom point is then given by equations 39, with $b_x = b_y = b_z = 0$.

IV. *Correction for change in shape.* The stake is allowed to undergo changes in length, tilt and shape. The bottom point is then given by (39)-(40).

Each of the above corrections contains the preceding correction as a subset, since the information necessary to calculate a particular correction can also be used to calculate the preceding one. Because correction II is obviously necessary, and simple to apply, we shall not discuss situation I further.

Reference has been made to a "measured point", (x_m, y_m, z_m) . In many cases a point closer to the surface than the top of the stake was surveyed from at least two TP's (corresponding to the times when method A of calculating the tilt could be used). Such a point is more suitable for calculating the velocity since the errors in the tilt do not amplify the errors in the coordinates as much when the above corrections are applied. These errors increase as they are "translated" along the stake, and thus they are kept to a minimum if we start from a point as close to the surface as possible. From now on we refer to this as the "measured point", (x_m, y_m, z_m) , defining it as the point closest to the surface which was observed from at least two triangulation points. Its distance from the bottom of the stake is denoted by R_m . If such a point exists, distinct from the top of the stake (x_o, y_o, z_o) , then we assume the equivalence $(x_o, y_o, z_o, R_o) \rightarrow (x_m, y_m, z_m, R_m)$ to be understood in any appropriate equations, for example, equations (39). The "measured point" is identical to the "surface mark" (x_s, y_s, z_s) only when the surface mark was observed from at least two TP's.

The above corrections were applied to each of the centerline stakes and velocities calculated. Appendix C shows, for selected stakes, the effect of corrections III and IV relative to correction II. The results are not very encouraging; in many cases the scatter is increased when the corrections are applied. Consequently a new method of reduction, called the "flex method", was developed.

6.5.2 The Flex Method

The reason that even the most refined of the above corrections does not seem to give very good results probably is that the bend corrections are cumulative quantities. The stakes at the end of the winter could be up to 12 m long and could consist of up to 7 bent segments, as well as two straight segments at the top and bottom. Each of these segments is subject to error, both the error of measurement and the unknown error in assuming the bends are smooth and circular. These errors could eventually produce a model of the stake which is completely unrealistic. It is entirely conceivable, in fact, that the results could be worse than if no correction for change in shape had been made.

It would be better, therefore, to choose the "fixed point" (the point fixed to a parcel of ice) as close as possible to the measured point so that the errors in calculating the position of the fixed point can be kept to a minimum. Any point on the stake can be used as a fixed point, provided it is at or below the surface on *both* surveys. The best point to use is the lower of the two surface points. A bend correction would then have to be calculated only for that part of the stake between the two surface points. In effect we are assuming that the change in tilt of the part of the stake exposed above the surface is real and due to a smooth circular bending of the stake between the two surveys (Figure 75).

This method is known as the "flex method"; it is simply an alternate way of doing the bend corrections. The measured points, R_{m1} and R_{m2} , are first reduced to their respective surface points, R_1 and R_2 , by using the measured tilt values (θ_1, ϕ_2) and (θ_1, ϕ_2) , and equations 56. The coordinates of the point P with respect to R_2 are found using equations 33-37 and the displacement of P from R_1 is then used to calculate the movement.

Appendix C shows the results of using this method for the same stakes used to illustrate the previous correction methods. The decrease in the scatter is

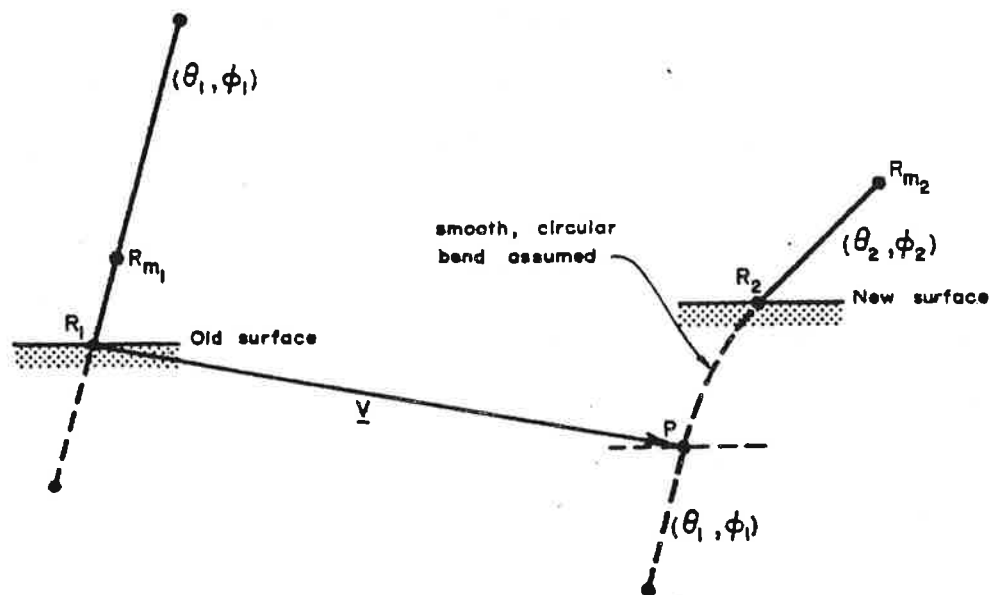


Figure 75. The calculation of the velocity of a stake using the flex method.

now quite noticeable.

Four important facts must be emphasized about this method: (a) It is not necessary, for velocity calculations, to compute bend corrections when doing the original coordinate calculations. Only the tilt values are needed. However, the bend corrections are required for a proper analysis of the accumulation and ablation (chapter 9). (b) The velocity vector usually refers to a *different* parcel of ice for each particular set of surveys, since the surface level generally varies from one survey to the next. Thus it would be difficult to interpret the slopes of (x,t) curves as velocities. (c) Any change of tilt, no matter how small, is always treated as real and the stake allowed to "flex". When the glacier surface is ice it is doubtful that changes in tilt are due to a bending of the stake in the ice, or even, for that matter, that the changes in tilt are real. However, the changes are very small under these

circumstances and any error introduced by applying this method is negligible.

(d) The method *optimizes* the available data. The coordinates are adjusted over the shortest possible distance and so errors are minimized. Furthermore, unlike correction method IV, the estimate of the bend error is much more realistic since we deal with only one segment rather than several.

Once the two points (x_1, y_1, z_1) and (x_2, y_2, z_2) are known the velocity vector can be calculated. The components of this vector can be either rectangular (u, v, w) :

$$\left. \begin{aligned} u &= \frac{x_2 - x_1}{t_2 - t_1} \\ v &= \frac{y_2 - y_1}{t_2 - t_1} \\ w &= \frac{z_2 - z_1}{t_2 - t_1} \end{aligned} \right\} (74)$$

or spherical (s, δ, γ) , where the speed s is given by (72), the dip δ by

$$\delta = \tan^{-1} \left[\frac{w}{(u^2 + v^2)^{1/2}} \right] \quad (75)$$

and the azimuth γ by

$$\gamma = \tan^{-1} \left(\frac{v}{u} \right) \quad (76)$$

This study will be concerned only with the distribution of the speed s in time and space. The units chosen for s are mm d^{-1} , simply for the convenience of not requiring a decimal place.

One final point should be mentioned. Speeds can only be calculated between two surveys if the stake has not been shifted during the intervening time.

If the stake was redrilled, however, a correction can be made to one of the points and the true movement found.

6.5.3 *Filtering and Smoothing of the Data*

It is well known that the velocity of a glacier depends upon the time interval of observation (p. 24). The data should be "filtered" to eliminate the inherent large noise in observations done with short time intervals. All survey pairs with time intervals less than 15 days were eliminated. Other low end cutoffs were tried (0, 10, 20 and 30 days) but 15 days gave a good balance between too large a scatter and too many gaps in the data. Those with intervals greater than 90 days were also eliminated because the interval was spanning more than one quarter of the seasonal cycle.

Rather than calculating n velocity values from $n+1$ successive measurements of the position, *all* possible survey combinations whose time interval was in the allowed range (15-90 days) were used*. This increases the number of points on the velocity curves and has the effect of "smoothing" the data. It also minimizes any erroneous effects which might be caused by a fortuitous choice of survey combinations. Since the largest possible number of different time intervals is used, the effect of any one particular interval is reduced. The velocity curves should thus be as unbiased as they can be. It should, however, be kept in mind that the number of points shown on the velocity curves does *not* represent the number of measurements. More rigorous filtering and smoothing techniques are not justified due to an insufficient number of data points distributed unevenly over an insufficient number of cycles.

The effect of this technique is shown in Appendix C. Many of the points which deviated considerably from the mean curve are eliminated and the scatter

* Each survey combination was also checked to make sure that the stake was not shifted in the intervening time.

is reduced still further. These curves also show two more adjustments to the data, to be discussed later: corrections for transverse velocity gradients (section 6.5.6) and elimination of faulty points (section 6.5.8).

Table 13 summarizes all reduction techniques which were applied to the coordinate data to give velocities. The "scatter" for a particular stake is defined as

$$\sigma^2 = \frac{\sum_{i=1}^n [s(t_i) - \bar{s}(t_i)]^2}{n - 1} \quad (77)$$

where $s(t_i)$ is the actual velocity at the time of the i^{th} survey combination and $\bar{s}(t_i)$ is the corresponding velocity value on the mean curve through the points (Appendix C). n is the total number of survey combinations.

The failure of correction methods III and IV and the success of the flex method to reduce the overall scatter is clear. Rejecting all time intervals less than 15 days also produces a pronounced decrease in the scatter.

6.5.4 Error Analysis

Given σ_x , σ_y , σ_z , σ_θ , and σ_ϕ we wish to calculate the standard deviation in the velocity components. First the error in each of the fixed points must be calculated. This consists of one or two parts: (a) the error in reducing the coordinates along a straight segment, and (b) the error in reducing the coordinates along any bent segments. The first is found by applying equation 41 to equations 56:

$$\left. \begin{aligned} \sigma_x^2 &= (R_m - R)^2 (\cos^2 \theta \cos^2 \phi \sigma_\theta^2 + \sin^2 \theta \sin^2 \phi \sigma_\phi^2) + \sigma_{x_m}^2 \\ \sigma_y^2 &= (R_m - R)^2 (\cos^2 \theta \sin^2 \phi \sigma_\theta^2 + \sin^2 \theta \cos^2 \phi \sigma_\phi^2) + \sigma_{y_m}^2 \\ \sigma_z^2 &= (R_m - R)^2 (\sin^2 \theta) \sigma_\theta^2 + \sigma_{z_m}^2 \end{aligned} \right\} (79)$$

Stake	Scatter as a function of Reduction method or correction							Number of survey combinations				$ \Delta s $	
	(a)	(b)	(c)	(d)	(e)	(f)	(g)	(h)	(i)	(j)	(k)	Mean	Max.
C1	9	18	15	7	7	6	5	117	16	6	95	0	2
C2	19	67	35	7	7	6	6	135	17	6	112	1	2
C3	29	21	48	8	8	6	6	127	18	6	103	1	2
C4	24	27	31	18	17	15	13	128	21	8	99	1	1
C5	27	24	42	23	22	21	22	135	17	6	112	3	5
C7	21	17	26	13	12	7	6	125	21	6	98	7	10
C8	57	49	46	37	37	26	4	140	25	35	80	1	6
C9	13	17	20	10	10	8	7	159	27	1	131	0	1
C10	15	15	20	10	10	7	5	121	21	22	78	0	1
C11	11	14	32	9	9	8	6	152	20	8	124	0	2
C12	27	25	33	23	22	18	17	123	23	6	94	1	2
C13	36	28	28	22	22	11	10	151	22	13	116	0	3
C14	32	17	31	14	13	11	10	95	20	5	70	5	9
C15	24	22	27	19	17	13	11	133	23	6	104	5	17
C16	46	116	115	35	35	16	11	80	14	13	53	1	3
C17	14	33	37	15	16	11	11	117	21	2	94	1	2
C18	14	17	17	14	14	12	12	115	19	1	95	1	1
C19	23	25	30	22	21	17	16	129	22	9	98	2	6
C20	31	42	43	28	29	25	25	118	20	2	96	2	6
Means:	24.8	31.3	35.6	17.6	17.3	12.8	10.7	126	20	8	98	1.7	4.2
d(%):	0	+26	+44	-29	-30	-48	-57	-	-	-	-	-	-

(a) Correction method II ("raw data"). (b) Correction method III. (c) Correction method IV. (d) Flex method. (e) Flex method plus corrections for transverse velocity gradients. (f) Same as (e) plus removal of time intervals less than 15 days. (g) Same as (f) plus removal of faulty points ("final data").

(h) Number in raw data (column (a)). (i) Number with time intervals less than 15 days. (j) Number removed as faulty. (k) Number in final data (column (g)).

Table 13. The scatter of the velocity data points for various reduction methods and corrections, the number of survey combinations, and the corrections for transverse velocity gradients. The scatter is relative to the final mean velocity field. Velocity values are in mm d^{-1} . Δs is the correction for transverse velocity gradients. d is the percent deviation of the mean scatter from that for the raw data (correction method II).

(x, y, z) is the surface point, (x_m, y_m, z_m) is the measured point and $(R_m - R)$ is the distance between the two. The second part is estimated as before (section 6.3.4). The quantities R_m and R are assumed to have no error.

The errors in the velocity components (u, v, w) or (δ, δ, γ) are then found by applying (41) to equations 72, 74, 75 and 76:

$$\left. \begin{aligned} \sigma_u^2 &= \frac{\sigma_{x_2}^2 + \sigma_{x_1}^2}{(t_2 - t_1)^2} \\ \sigma_v^2 &= \frac{\sigma_{y_2}^2 + \sigma_{y_1}^2}{(t_2 - t_1)^2} \\ \sigma_w^2 &= \frac{\sigma_{z_2}^2 + \sigma_{z_1}^2}{(t_2 - t_1)^2} \end{aligned} \right\} (79)$$

$$\left. \begin{aligned} \sigma_\delta^2 &= \frac{u^2 \sigma_u^2 + v^2 \sigma_v^2 + w^2 \sigma_w^2}{s^2} \\ \sigma_\delta^2 &= \frac{u^2 w^2 \sigma_u^2 + v^2 w^2 \sigma_v^2 + (u^2 + v^2)^2 \sigma_w^2}{s^4 (u^2 + v^2)} \\ \sigma_\gamma^2 &= \frac{v^2 \sigma_u^2 + u^2 \sigma_v^2}{(u^2 + v^2)^2} \end{aligned} \right\} (80)$$

The times t_1 and t_2 have negligible error. On almost all surveys, the stakes were observed in the same sequence and the TP's were occupied in the same order. Hence the mean time of a survey should apply to each stake as well, at least to first order. The maximum effect of the stakes being observed out of sequence would be about 2 hours in 15 days, or about 0.7 %.

Table 14 gives the mean errors in the velocity components of the centerline stakes. Because the coordinates are least reliable with the uppermost stakes, so is the speed s . The direction of the velocity vector (δ, γ), on the other hand, is known more accurately in this area since the ice is flowing much faster. The overall accuracy of the velocity measurements is approximately $\pm 3 \text{ mm d}^{-1}$ in the speed and $\pm 1^\circ$ in the direction.

Time intervals in the range of 30-60 days are considered to be the most representative of seasonal variations. Velocities measured over time intervals toward the ends of the allowed range (15-90 days) probably exhibit fluctuations different from those in the middle of the range. To allow for this, all error bars in Appendix C have been increased in length inversely with the weighting function shown in Figure 76.

Stake	n	Mean error in velocity components		
		$\bar{\sigma}_s$	$\bar{\sigma}_\delta$	$\bar{\sigma}_\gamma$
C1	95	1.3 \pm 0.8	1.0 \pm 0.2	1.3 \pm 0.8
C2	112	3.1 \pm 5.6	2.4 \pm 3.7	2.1 \pm 2.8
C3	103	3.8 \pm 5.4	2.6 \pm 3.3	2.5 \pm 3.0
C4	99	1.4 \pm 1.3	1.1 \pm 0.9	1.0 \pm 0.9
C5	112	1.7 \pm 1.8	1.0 \pm 1.2	0.8 \pm 0.6
C7	98	1.7 \pm 1.7	0.9 \pm 1.2	1.0 \pm 0.9
C8	80	7.6 \pm 21.5	2.8 \pm 8.6	2.7 \pm 4.5
C9	131	1.7 \pm 1.4	0.5 \pm 0.1	0.8 \pm 0.5
C10	78	1.6 \pm 1.0	0.5 \pm 0.1	0.8 \pm 0.4
C11	124	1.6 \pm 1.2	1.2 \pm 1.5	0.8 \pm 0.5
C12	94	1.6 \pm 1.0	0.7 \pm 0.5	0.7 \pm 0.3
C13	116	1.6 \pm 1.1	0.8 \pm 0.7	0.8 \pm 0.4
C14	70	2.4 \pm 1.7	0.8 \pm 0.6	0.7 \pm 0.2
C15	104	2.1 \pm 3.4	0.7 \pm 0.6	0.6 \pm 0.3
C16	53	2.0 \pm 1.3	0.6 \pm 0.2	0.6 \pm 0.2
C17	94	2.4 \pm 1.6	0.6 \pm 0.2	0.6 \pm 0.2
C18	95	2.9 \pm 1.8	0.6 \pm 0.2	0.6 \pm 0.2
C19	98	3.5 \pm 2.4	0.7 \pm 0.3	0.7 \pm 0.3
C20	96	4.7 \pm 3.2	0.7 \pm 0.5	0.7 \pm 0.5
Means:	97	2.3 \pm 3.1	1.1 \pm 1.3	1.1 \pm 0.9

Table 14. Summary of the mean errors in the velocity components of the centerline stakes. Errors in the speed s are in mm d^{-1} and errors in the direction (δ, γ) are in degrees. n is the total number of survey combinations for each stake which have time intervals in the allowed range and which were not found to be faulty. C8 was excluded from the final means (see p. 200).

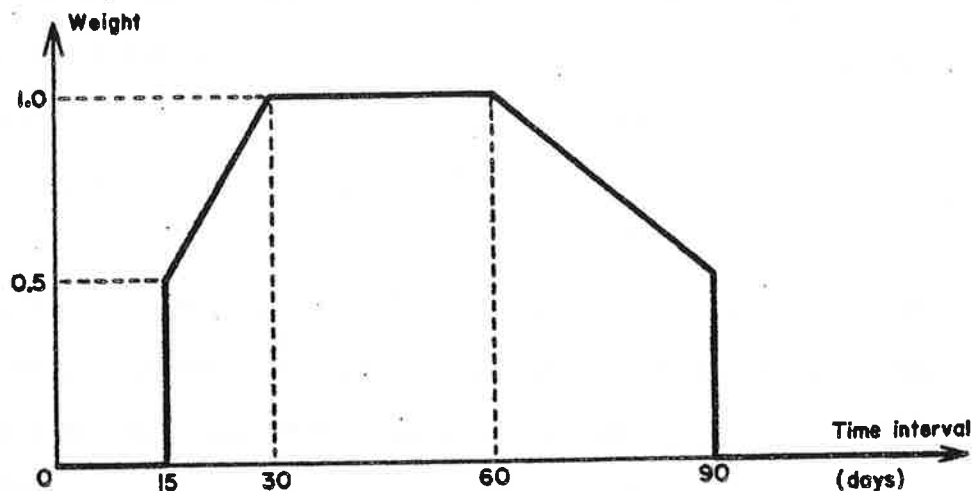


Figure 76. The function used to weight the velocity error bars (Appendix C).

6.5.5 The Spatial Variations in the Velocity Field

The surface speed of the glacier determined at a fixed point in time as a function of x and y is referred to as the "spatial velocity field". It was determined in May 1970 by supplementing the regular 25 metal stakes with 68 wooden ones. These were 3 m long, 25 mm square, and were driven into the spring snow by hand. They were arranged in 10 transverse profiles, with a spacing of about 80 m on each profile.

All stakes were surveyed over a 30 day time interval. No tilts were measured for the wood stakes and their velocities were calculated using method I. Several stakes on the lowermost profile had to be rejected because the large ablation here caused appreciable changes of tilt. The metal stakes were reduced using the flex method. The results are shown in Figure 77. The velocity field correlates well with the ice thickness and surface slope, as expected.

Unfortunately, the longitudinal resolution of this field is no greater than

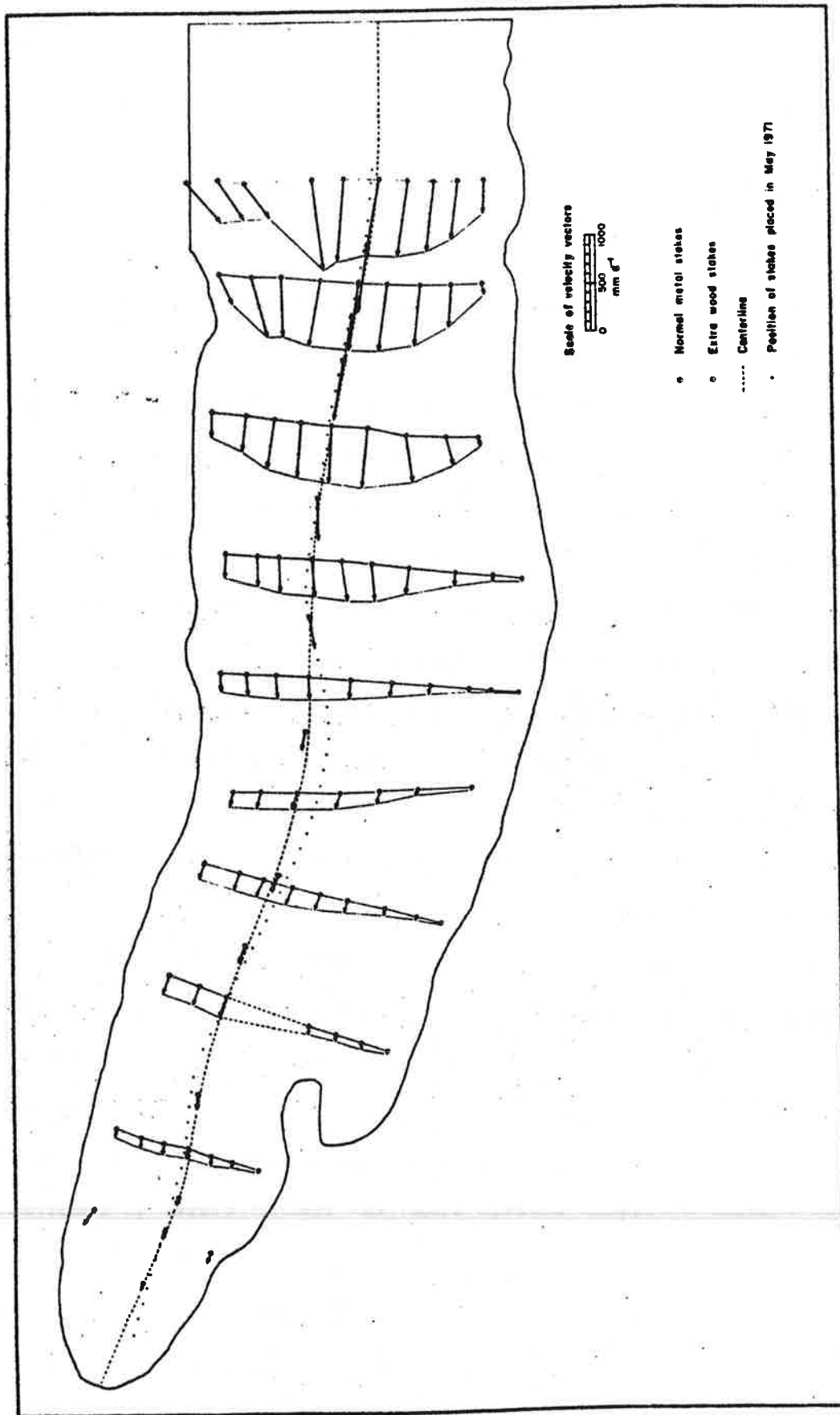


Figure 77. The spatial velocity field of May 1970. The velocities were measured over a 30-day interval. The small dots indicate the position of the stakes used to determine the longitudinal velocity profile in May 1971.

that of the regular movement stakes. Thus, one year later, in May 1971, a line of 75 wood stakes, spaced approximately 30 m apart, was placed down the middle of the glacier and surveyed and reduced as described above. Three surveys were made of each stake: May 7 and 9, June 6 and 9, and July 15 and 20. The third survey was possible because bad weather reduced melting of the snow and it was possible to reset the stakes on July 1 in the same holes without changing their tilt. Appropriate corrections were made to the coordinates obtained on the third survey.

Since these stakes were placed a year after all previous stakes had been removed it was difficult to keep them close to the centerline (Figure 77) and so corrections for transverse velocity gradients were applied (section 6.5.6). The longitudinal velocity profiles, reduced to the centerline, are shown in Figure 78. Very pronounced variations with distance along the glacier are evident. These variations remain fixed in space and are caused by topographic features of the bedrock. The crossing of the velocity profiles is very suggestive of a "seasonal wave" moving down the glacier, as found on the Hinter-eisferner (p. 16 and 28).

The surface slope, the relative elevation changes and the longitudinal strain rate were also calculated (Figures 79, 80 and 81 respectively). The surface slopes were calculated between each adjacent pair of stakes and so they are averages over approximately 30 m. Maxima and minima in the elevation changes correspond well with maxima and minima in the surface slope but the maxima and minima in the strain rate appear to occur approximately one ice thickness further down-glacier than the maxima and minima in the surface slope.

The surface elevation profile along the line of stakes is compared to the surface and bed profiles along the centerline in Figure 106 (p. 282). Even if the Nisqually Glacier were in equilibrium the surface profiles would not agree exactly because (a) the stakes deviate from the centerline by as much as

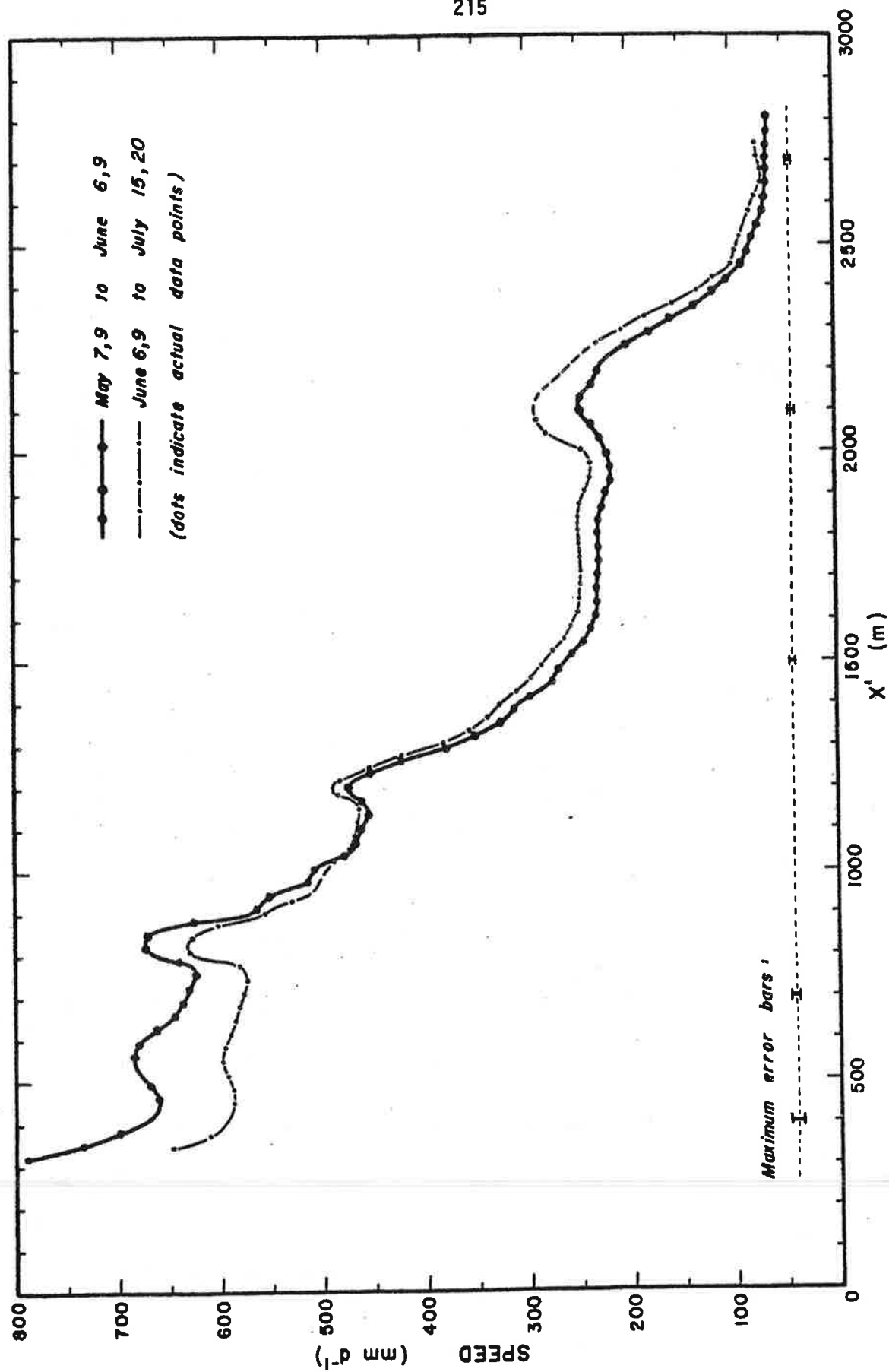


Figure 78. Longitudinal velocity profiles along the centerline of the Nisqually Glacier, May to July 1971. Values have been corrected for transverse velocity gradients.

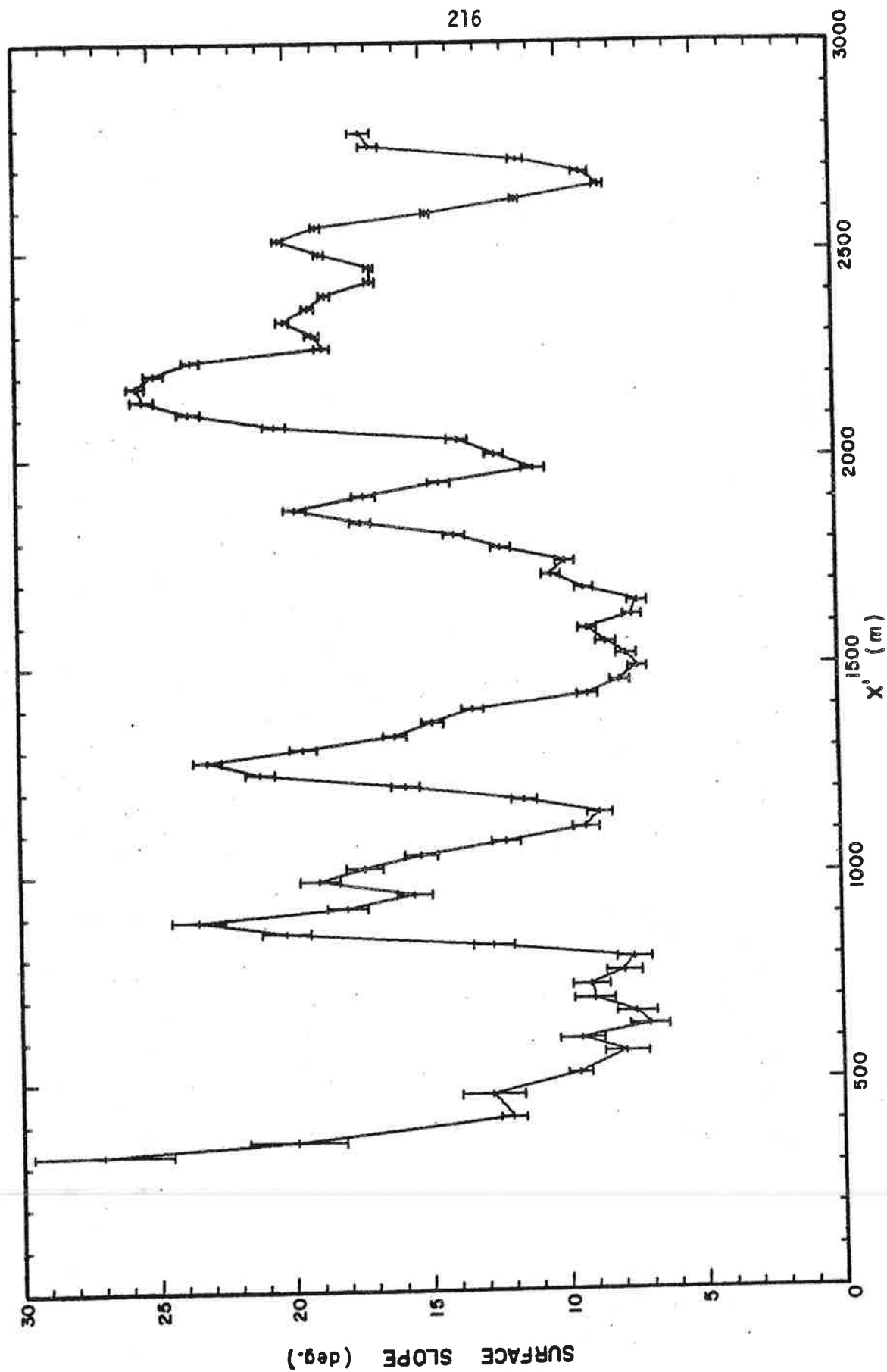


Figure 79. Surface slope profile, May 7 and 9, 1971. Values are averaged over approximately 30 m horizontally.

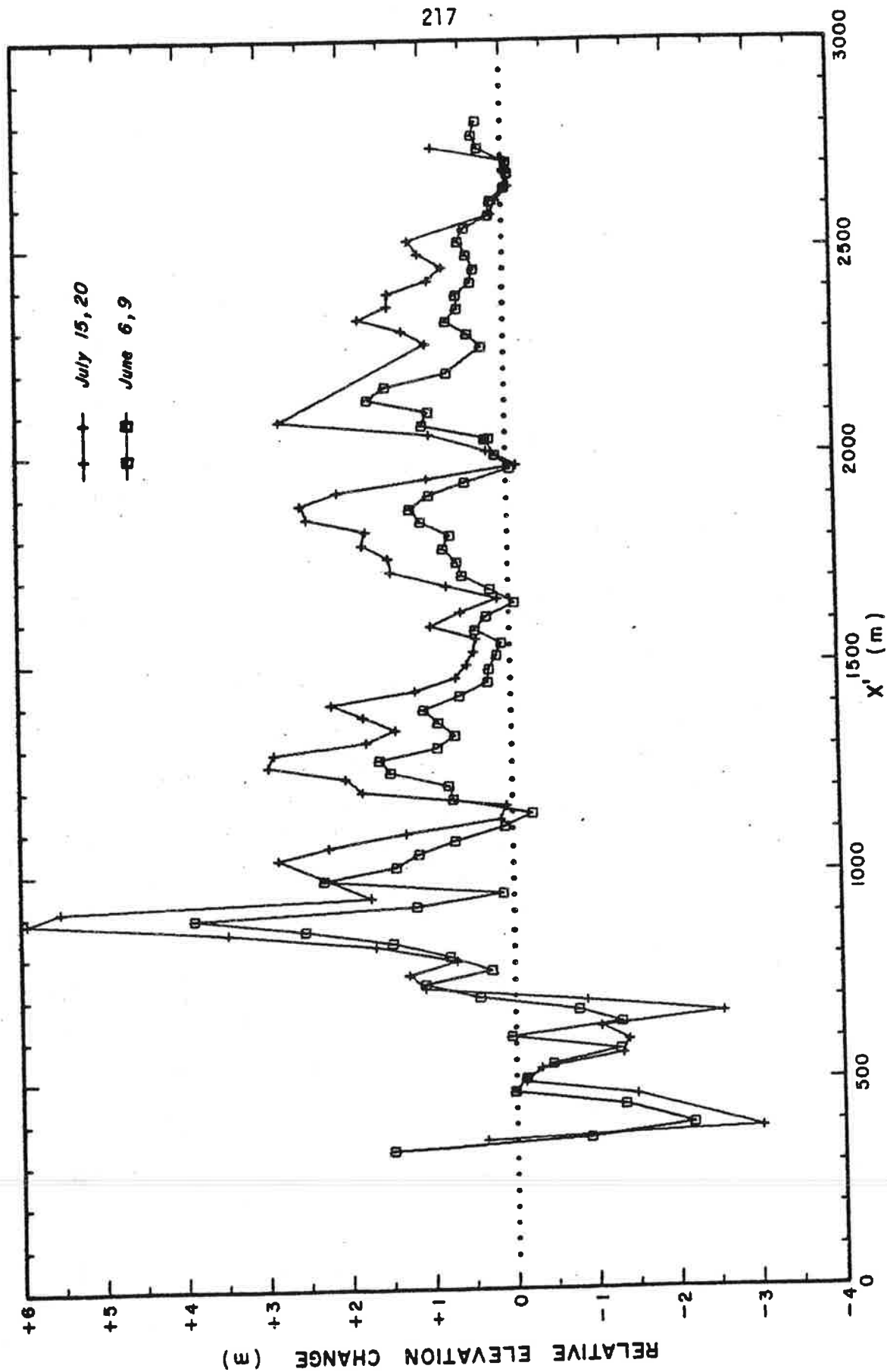


Figure 80. Surface elevation changes, May to July, 1971. The elevation refers to the top of the stakes and 80 is independent of ablation. The values are relative to the initial elevation profile (May 7 and 9).

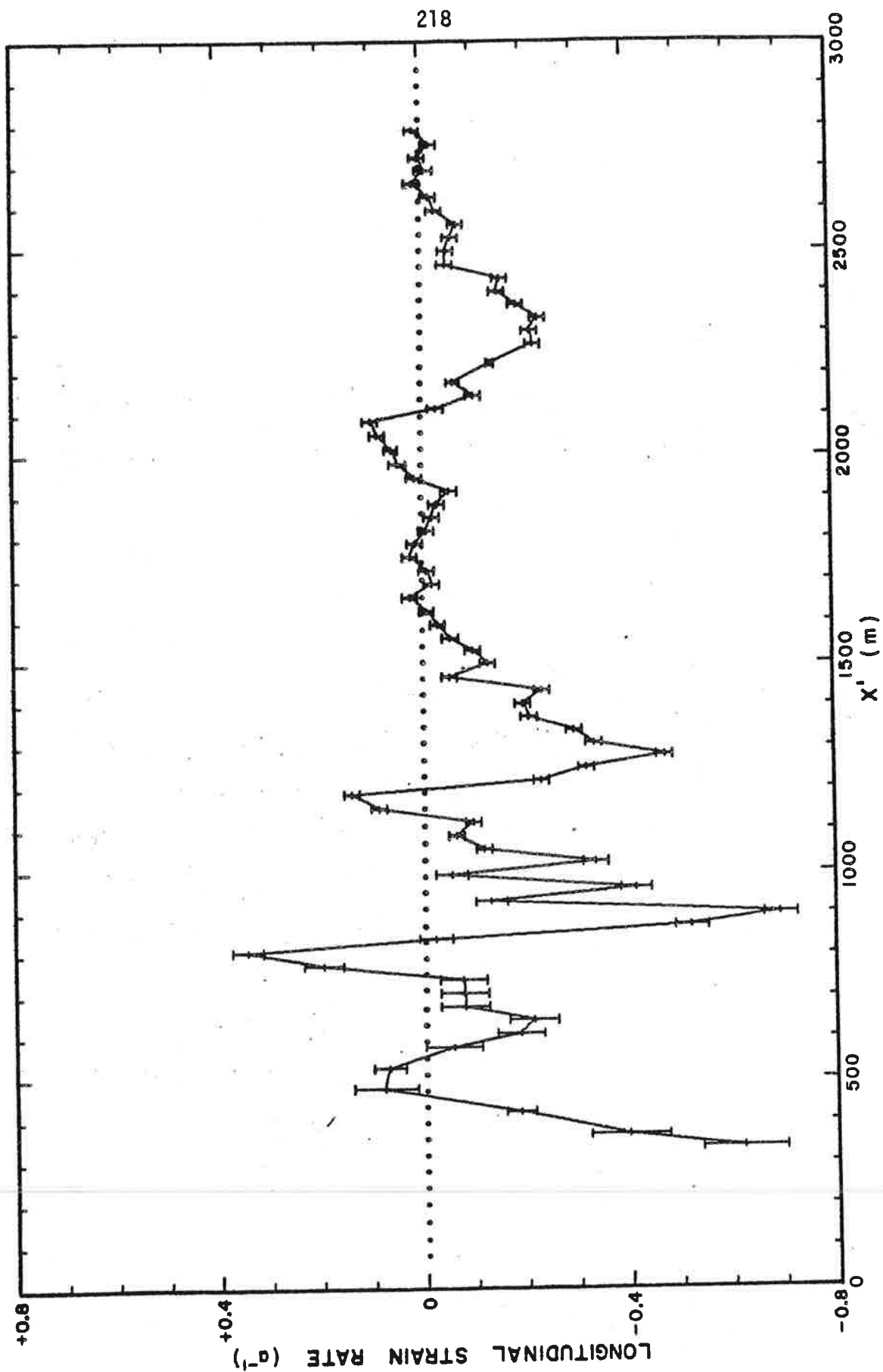


Figure 81. Longitudinal strain rate profile, May 1971. This curve is the gradient of the velocity profile determined between May 7, 9 and June 6, 9 (Figure 78).

50 m and (b) the stake profile is at the beginning of the melt season whereas the 1966 surface profile is near the end. However, these reasons probably cannot account for all the differences and there does appear to be an overall thickening in the upper part and an overall thinning in the lower part.

The presence of large variations in velocity in a relatively short distance has important consequences. The measurements of velocities on a glacier surface must be detailed enough to ensure that such variations are not affecting the correct interpretation of the data. Time variations, for example, could be simply spatial variations caused by the stake moving into a region of higher velocity.

6.5.6 *Corrections for Transverse Velocity Gradients*

We wish to examine the surface speed as a function of time and distance along the glacier. The dependence of s on y , evident in Figure 77, must therefore be eliminated. Two steps are necessary: (a) The coordinates of the point (x, y) must be transformed to a curvilinear system (x', y') , where x' runs down the centerline of the glacier and y' is everywhere perpendicular to x' . Both x' and y' are still horizontal, the z coordinate remaining unchanged. (b) A correction must be applied to the speed so that it approximates the value that would have been found if the stake had been located at $y' = 0$.

The first step can only be done uniquely if the X' axis has a sufficiently small curvature that the point (x, y) lies within its radius of curvature. The following algorithm was developed to perform the transformation under this condition:

(a) The X' axis was determined by drawing a smooth curve along the line of maximum velocity in Figure 77, keeping it as close as possible to the centerline stakes. The coordinates of 72 points (x_j, y_j) spaced about every 40 m

were read from this drawing. The X' axis is then defined as the line obtained by quadratic interpolation in this set of numbers. Y' is perpendicular to this curve, positive to the east.

(b) To determine (x', y') from a given (x, y) the point (x_j, y_j) which is closest to (x, y) is located (Figure 82) and a quadratic

$$y = C_3 x^2 + C_2 x + C_1 \quad (81)$$

is fitted between the points $j-1, j$ and $j+1$.

(c) The point (x_1, y_1) on this quadratic closest to (x, y) is found by solving the cubic equation*

$$2C_3^2 x_1^3 + 3C_3 C_2 x_1^2 + [2C_3(C_1 - y) + C_2^2 + 1]x_1 + [C_2(C_1 - y) - x] = 0 \quad (82)$$

for the real root. y is found by substitution in (81).

(d) x' is then defined as:

$$x' = x'_0 + [(X_k - x_1)^2 + (Y_k - y_1)^2]^{1/2} + \sum_{i=2}^k [(X_i - X_{i-1})^2 + (Y_i - Y_{i-1})^2]^{1/2} \quad (83)$$

where x'_0 is some arbitrary zero point (chosen in this case so that $x' = y' = 0$ at $x = 3700$ m, $y = 1570$ m), and where $k = j$ if (x_1, y_1) lies after (x_j, y_j) and $k = j-1$ if (x_1, y_1) lies before (x_j, y_j) .

(e) Finally, y' is defined as:

$$y' = \pm 2[(x - x_1)^2 + (y - y_1)^2]^{1/2} \quad (84)$$

* Obtained by minimizing the distance from (x_1, y_1) to (x, y) .

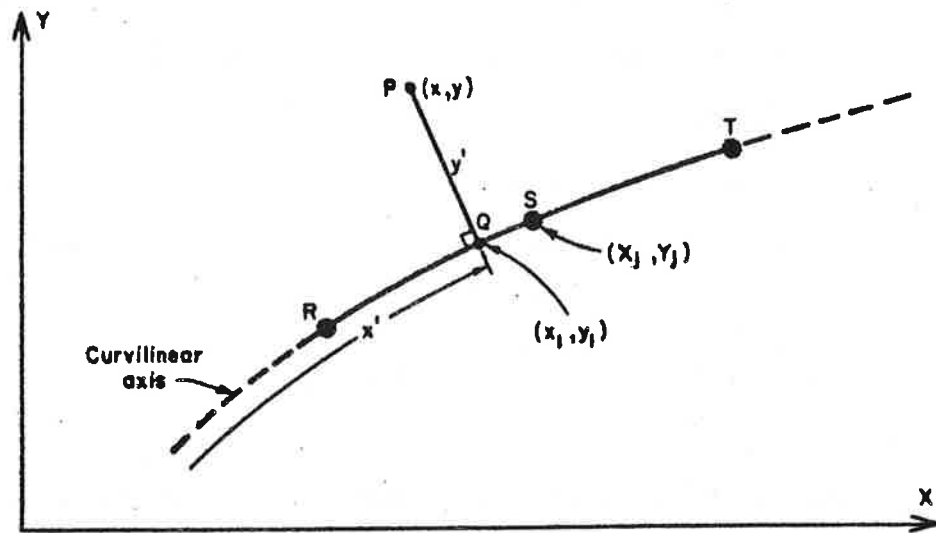


Figure 82. The calculation of the curvilinear coordinates (x', y') of a point P .

where $z = +1$ if $k = j-1$ and $z = -1$ if $k = j$. The sign is determined by rotating the vector \underline{QS} into the vector \underline{QP} (+ anticlockwise, - clockwise), and is given by

$$\text{sign}[(y - y_1)(x_j - x_1) - (y_j - y_1)(x - x_1)] \quad (85)$$

(f) Special cases have to be allowed for where (a) (x, y) coincides with one of the axis points (x_j, y_j) , (b) the three points $j-1, j$ and $j+1$ define a straight line, and (c) (x, y) is equidistant from two points on the axis (but not three, which is not allowed).

This coordinate transformation is only intended to give values of x' and y' to within the nearest 0.1 m. This is entirely adequate for analysis of the velocity field provided gradients are not calculated. These should be obtained using the original coordinates, otherwise artificial errors will be introduced.

This X' axis defines precisely the glacier "centerline" which has been referred to many times in the preceding pages. It was indicated in Figure 27 and on the overlay in the rear pocket.

Once the value of y' is known the speed may be corrected to $y' = 0$, provided the transverse velocity gradient $\partial s / \partial y'$ is also known:

$$s'(x', t) = s(x', y', t) - s(x', y', t) \quad (86)$$

where

$$\Delta s(x', y', t) = s(x', y', t) - s(x', 0, t) = \int_0^{y'} \frac{\partial s(x', y'', t)}{\partial y''} dy'' \quad (87)$$

Ideally $\partial s / \partial y'$ should be measured on each survey. However, this was not done. Instead the transverse velocity gradients are assumed to be independent of time and given by the spatial velocity field of May 1970. A table of corrections $\Delta s(x', y')$ was taken directly from the transverse velocity profiles in Figure 77, without having to perform the integration of equation 87. Values were tabulated at each x' corresponding to one of the profiles and at increments in y' of 20 m between -100 m and +100 m on each profile. Two dimensional quadratic interpolation in this table is used to obtain Δs for a particular (x', y') .

The curvilinear coordinate y' for the centerline stakes ranged from -58 m to +39 m with a mean absolute value of about 10 m. The corrections Δs ranged from -6 mm d^{-1} to $+17 \text{ mm d}^{-1}$ with a mean absolute value of 1.7 mm d^{-1} (Table 13). Since the stakes were maintained close to the centerline, where the transverse gradients are small*, the corrections only decrease the scatter of the velocity points by 1 %. The corrections are almost never greater than the experimental error and their effect on the shape of the velocity curves is

* Figure 77 shows that the Nisqually Glacier moves with the "plug-flow" typical of glaciers in their central portions.

not significant (Appendix C shows their effect for stake C7, which has the largest absolute value of $|\Delta s|$). Any variations with time are undoubtedly much smaller.

6.5.7 Corrections for Longitudinal Velocity Gradients

The longitudinal position of a stake varied as much as 150 m (Figure 74). It is clear from Figure 78 that this could, unlike the transverse gradients, have a very significant effect on the measured speed, particularly with the uppermost stakes. We must therefore correct the values of $s'(x', t)$ to fixed values x'_0 for each stake:

$$s'_0(x'_0, t) = s'(x', t) - \Delta s'(x', t) \quad (88)$$

where

$$\Delta s'(x', t) = s'(x', t) - s'_0(x'_0, t) = \int_{x'_0}^{x'} \frac{\partial s'(x'', t)}{\partial x''} dx'' \quad (89)$$

Following the same procedure as before, we would assume the longitudinal velocity gradients to be independent of time and then use the data from the longitudinal velocity profile measured in May 1971. However, initial examination of the velocity results showed that large relative changes in the velocities occurred over the two year period of measurements. The velocity profile of May 1971 differs considerably from that of November 1968 (see Appendix C and Figure 126, p. 317).

Ideally, therefore, one would use the actual data to establish a longitudinal velocity profile at each point in time. However, the stakes are usually much too sparsely spaced in x' for such a direct approach and so the following iterative scheme was used. The time variation of velocity $s'(t_i)$ was plotted for each stake and mean (smooth) curves $\bar{s}'(t)$ were drawn by eye through the points. Gaps in the data were interpolated by using information from nearby

stakes. Values of \bar{s}' were then read from the mean curves at fixed points in time t_0 . The mean position of each stake (over the two years) was used for x'_0 , and the mid-point of each month was used for t_0 . We thus have a table of \bar{s}' at fixed values of x' and t . This table was computer-contoured and minor adjustments were made in the interpolated regions by smoothing the contours by eye, simultaneously in both the time and distance coordinates.

Two-dimensional quadratic interpolation in this table was then used to calculate first approximations to $\Delta s'(x', t)$ for each of the original data points. The corrected points $s'_0(t_1)$ were then replotted as functions of time and mean curves again drawn. The process can then be repeated as often as desired. However, the initial corrections obtained were small enough that only one iteration was considered justified. The final result, mean curves $\bar{s}'_0(t)$ for each stake, gives the velocity variation at points x'_0 fixed in space.

6.5.8 Elimination of Faulty Data Points

The search for errors in the original coordinate calculations only caught the more obvious surveying mistakes. The velocity data itself can be used to eliminate additional points. Because all possible survey combinations were used, an error on one particular survey appears in a *group* of points. The $s'_0(t_1)$ plots for each stake were examined closely for groups of points which appeared to lie away from the main trend and which all had one survey in common. The original field notes, the survey reductions and the velocity calculations for this survey were then examined closely to see if there was a reason for the error.

Longitudinal velocity profiles $s'(x'_1)$ for each survey combination were also plotted and were used in a similar way to search for errors. There were far fewer points per survey combination, so all survey combinations within a three month period were plotted on one graph. When the points were connected

with straight lines this was a very effective means of detecting errors.

In many cases the mistake could be corrected. If there was a satisfactory explanation for the error, but it could not be corrected, then the points were eliminated. If no obvious mistake or explanation could be found the points were considered real and were retained.

Typical errors were as follows:

(a) Key punching errors. These could always be corrected.

(b) Errors in reading the surface level through the theodolite. These could usually be corrected by comparison with other measurements, especially since the error was usually a multiple of 0.5 m.

(c) Errors caused by observing the wrong stake. This occasionally happened with the upper stakes, when more than one was visible at the same time with the theodolite. Usually the correct stake could be inferred and the calculations corrected. Only on one or two occasions were points eliminated.

(d) Errors caused by faulty tilt values, manifest either as a large difference between the values calculated by the two methods (A or B) or as a value markedly different from those obtained on adjacent surveys. Sometimes a new value interpolated from other surveys would correct the error.

(e) Errors caused by large changes in the tilt when the stake was falling over as it melted out, generally when there was less than 0.5 m left below the surface. When the previous surface level was much higher on the stake, the flex method would yield a false value for the velocity. On the other hand, if the previous surface level was not much different then the stake would be flexed over too short a distance to have a significant effect. Usually a more realistic velocity could be calculated by using method III instead (corrections for changes in length and tilt only). The flex method is valid only when the change of tilt is actually due to bending of the stake.

(f) Errors caused by the tilt not being measured, for example, when less

than 0.5 m was exposed. When this happened the program would automatically use method II instead (corrections for changes in length only). If the tilt had not changed much since the previous survey the velocity value would usually be acceptable, but if it had changed considerably then a significant error could be introduced. Invariably such points had to be eliminated; only rarely was it possible to substitute a reliable value for the tilt.

(g) Errors caused by a very short time interval (approaching the lower limit of 15 days), coupled with a suspicion that one or more of the above errors might be present. The effect of the error would be amplified by the short time interval. Such points were eliminated if their presence made a marked change to the velocity curve; otherwise they were retained.

These errors have been described here because the elimination or correction of such points resulted in a further decrease in the scatter of the data points (Table 13 and Appendix C). The tracking down of the individual errors and attempting to correct them was a long and tedious process but the results were worth it. The average scatter of the final data points from the mean $\bar{s}'_0(t)$ curves was reduced by 57 % from the original uncorrected values.

6.5.9 The Final Velocity Field: $s(x, t)$

The measured surface speed $s'_0(t_1)$ for each centerline stake is given in Appendix C. The values are corrected for transverse and longitudinal velocity gradients to the point $(x' = x'_0, y' = 0)$ for each stake. The error bars are weighted according to the time interval (section 6.5.4). The mean curve $\bar{s}'_0(t)$ drawn through the data points represents the results of the iterative smoothing technique described in the previous section.

Figure 83 shows a contour plot of $\bar{s}'_0(x', t)$. This was computer-contoured from the final grid of corrected velocity values $\bar{s}'_0(x'_0, t_0)$, which, for convenience, will be denoted by s_{ij} from now on. The index i is understood to

range over 24 values of t (the mid-month times, t_0) and the index j over 19 values of x' (the average curvilinear x coordinate of each stake, x'_0). This 24 x 19 grid is referred to as the "standard grid".

For clarity the data points are not indicated on this plot. Instead the transparent overlay form of Figure 61 (in rear pocket) can be used. Velocity data points exist only along the solid lines; the gaps indicate (a) a time interval greater than 90 days, (b) a shift of the stake, or (c) rejected data points. This overlay also indicates the months of the year and the standard stake positions, x'_0 .

At the end of Appendix C are the longitudinal velocity profiles for each month of the two year period. These come directly from Figure 83 and thus represent mean, interpolated curves only. Data points are not indicated since they would make the diagram too confusing; only the grid points are shown.

These data will be the basis for later analysis and discussion. However, the surface slope and elevation changes must first be determined.

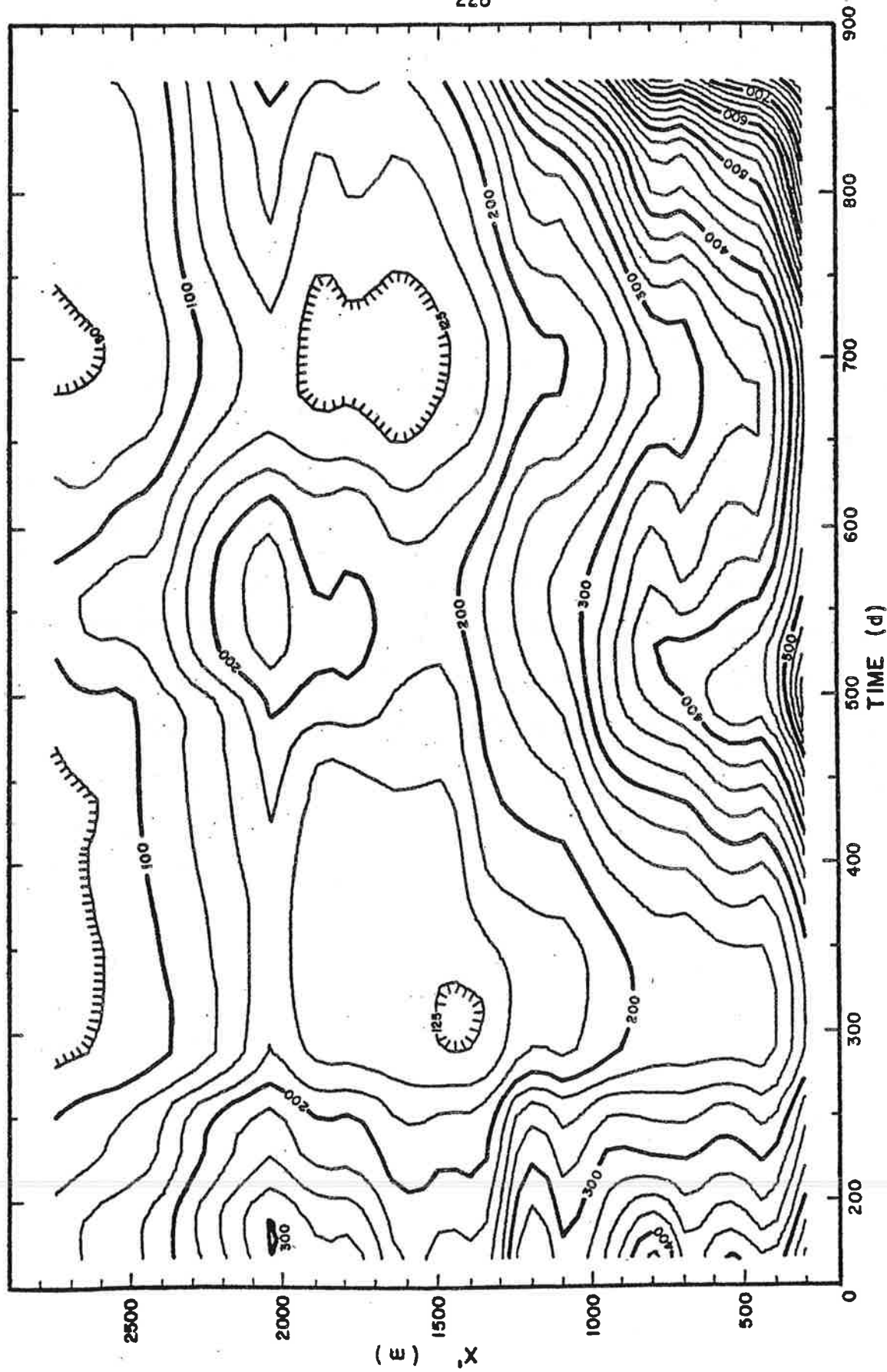


Figure 83. The measured surface speed of the Nisqually Glacier as a function of time and distance. The time axis runs from June 1968 to June 1970 and the x' axis from the equilibrium line to the terminus. The contour interval is 25 mm d⁻¹.

Chapter 7

THE THICKNESS VARIATIONS

Changes in thickness and surface slope will affect the surface speed of a glacier. It is necessary to see if this "loading effect" can account for all, or part, of the time variations in the motion. This chapter is concerned with a discussion of the thickness variations.

Every time a stake was surveyed, and the surface level measured, we have a spot measurement of the surface elevation. Such measurements will never, in general, be at the same fixed point in space, since the stakes are moving with the ice. The analysis of the thickness variations requires data fixed in space and so a correction for horizontal gradients in surface elevation, namely the surface slopes, must be made.

Ideally the surface slopes would be measured on every survey and these would be used to correct the surface elevations. Such slopes were in fact calculated from the coordinates of adjacent pairs of stakes (chapter 8) but the spatial resolution is poor longitudinally and almost non-existent transversely. The only way to obtain detailed enough surface slopes both longitudinally and transversely is to use the 1966 map. This assumes that *the surface slopes are independent of time* or, alternately, that *the rate of change of surface elevation is independent of position*.

Let (x'_0, y'_0) be the curvilinear coordinates of the fixed point in space at which the thickness variations are required and let z_0 be the surface elevation of this point on the 1966 map. Let (x', y') be the curvilinear coordinates of the surface point in question and let z be the measured surface elevation at this point. Let Z be the corresponding surface elevation on the 1966 map. The change in thickness at (x'_0, y'_0) is then



$$\Delta h = z - Z_0 - (Z - Z_0) \quad (1)$$

or simply

$$\Delta h = z(x',y') - Z(x',y') \quad (2)$$

Thus referring all surface elevations to the 1966 surface will correct for both longitudinal and transverse surface slopes, provided these remained constant from August 1966 to June 1970.

The reference elevation Z is calculated by interpolation in a grid $Z(x',y')$ which was calculated from the digitized 1966 glacier surface (zone 1 used in the gravity reductions) as follows. First, a grid $Z(x,y)$ in the standard rectangular coordinate system was calculated by locating the intersections of each contour line with each grid line. Two values of Z at each grid point were then found by interpolation along each coordinate direction and these were averaged to give the final value. Linear interpolation was used to avoid the usual curve-fitting problems encountered when using higher degrees of interpolation on arbitrarily spaced abscissa and abruptly varying ordinates. A grid spacing of 20 x 20 m was used, which corresponds approximately to the resolution of the 1966 map.

Second, the grid $Z(x',y')$ in the curvilinear system was created from the grid $Z(x,y)$ by interpolation, using the inverse of the transformation developed in section 6.5.6. The same grid spacing was used, but this time the grid only covered a region of ± 60 m either side of the centerline, as this adequately enclosed all stakes. From now on $Z(x',y')$ will be referred to as the "standard (1966) surface".

The surface elevation z is calculated by reducing the measured point to the surface point (x',y',z) using equations 6.56 and making a correction to convert any snow layer present to ice equivalent:

$$z_c = z - h_c \quad (3)$$

The correction h_c is evaluated in chapter 9 (equation 9.12).

Δh was calculated for each survey and for each centerline stake that was surveyed. Each stake was assigned to its standard curvilinear x coordinate x'_0 . The result is a grid of 24 values in x' and 59 values in t , corresponding to each of the 59 surveys. However, not all grid points possess values of Δh . An interpolation scheme was therefore developed to estimate values at the vacant grid points. The nearest data points in each of four sectors are located, weighted according to their distance away, and then averaged. When the entire grid is filled it can be computer-contoured.

The results are shown in Figure 84. The interpolation scheme was tested by independently hand-contouring the data points. Excellent agreement was obtained and in fact any discrepancies were usually found on closer examination to be due to faulty hand-contouring and not faulty interpolation.

Once this grid is obtained it is a simple matter to interpolate (linearly) to the standard times t_0 and obtain a standard grid of surface elevation changes $\Delta h_{ij} \equiv \Delta h(x'_0, t_0)$. The notation follows that used for the surface speed, s_{ij} (p. 226).

The surveying error in determining the surface elevation is a few centimeters. It will be shown in the next chapter that the assumption that slopes are constant in time is probably accurate to $\pm 0.75^\circ$. Assuming the stakes are typically 25 m from the centerline, this implies an error of about ± 0.4 m in the correction for elevation gradients. Thus we assume the values of Δh_{ij} to be accurate to within ± 0.5 m. The surveying error is much less than the inaccuracies in the slope correction.

Figure 84 shows that Δh is dominated by the accumulation and ablation, with maxima near April and minima near October. The annual thickness

variations range from 4 to 10 m, approximately 10 % of the ice depth. Over the two years, however, there was a net thickening of the glacier above stake C16 and a net thinning below this point. This was suggested earlier by the longitudinal velocity profile stakes (section 6.5.5).

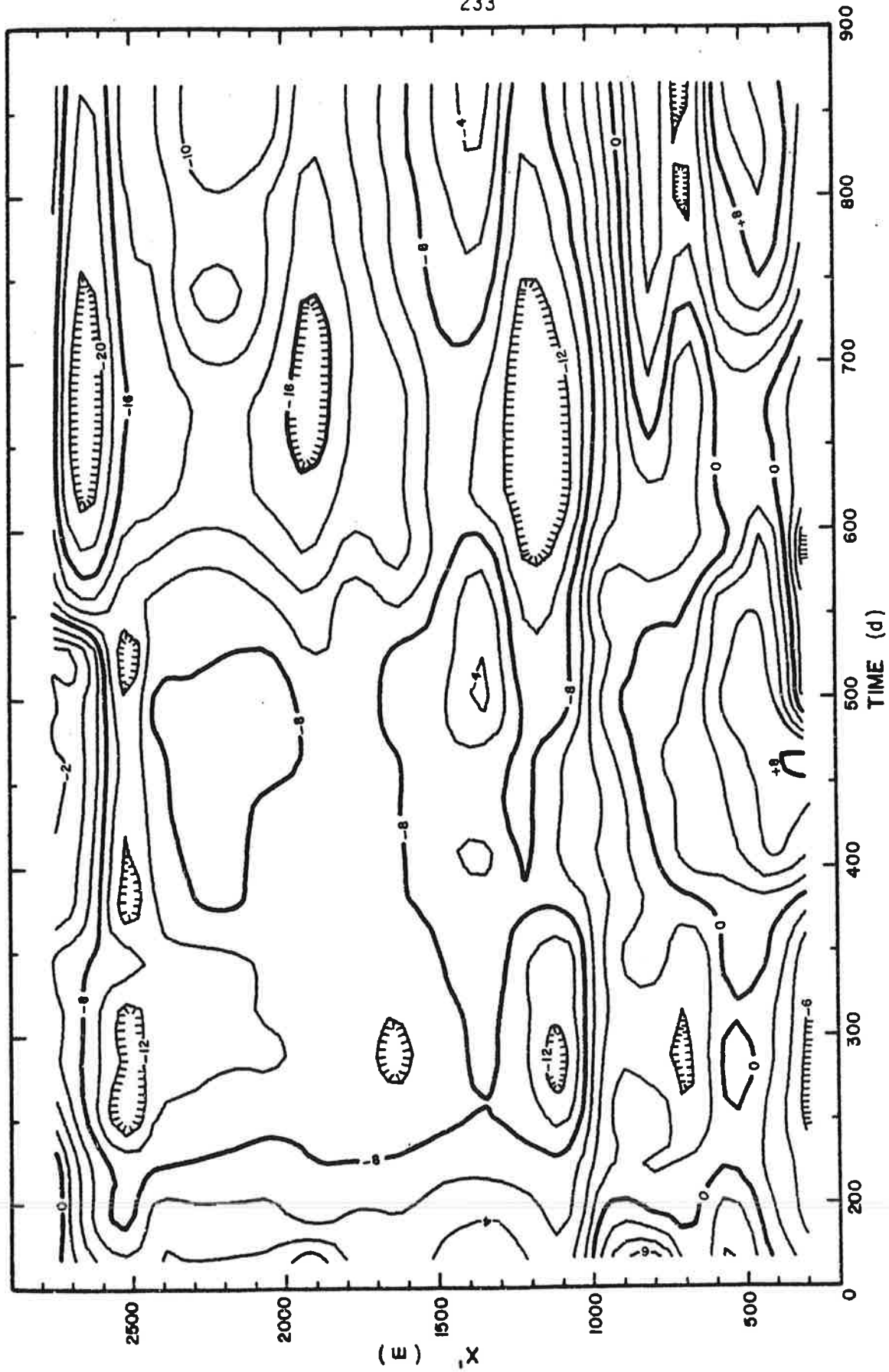


Figure 84. The measured changes in ice thickness as a function of time and distance. The contour interval is 2 m. All data values have been corrected to fixed points in space, assuming the surface slopes are constant in time. Any snow layer present has been converted into an equivalent depth of ice.

Chapter 8

THE SURFACE SLOPE VARIATIONS

Two techniques were used for calculating the surface slope variations, both involving the same original data. The scheme ultimately used was to simply differentiate Δh_{ij} with respect to x' . This will be discussed later.

The other technique, alluded to earlier, is to calculate the surface slope from the coordinates of adjacent pairs of stakes. The disadvantage of this is that the distance over which the slope is averaged cannot be kept fixed but instead is determined by the arbitrary, and somewhat haphazard, spacing of the stakes. On the other hand we shall see that this method can be used to give an idea of the error in the surface slope values.

8.1 CALCULATION OF SLOPES BETWEEN ADJACENT PAIRS OF STAKES

If (x_1, y_1, z_1) and (x_2, y_2, z_2) are the surface points of two stakes on the same survey then the average surface slope between them is

$$\alpha = \tan^{-1} \left| \frac{z_2 - z_1}{D} \right| \quad (1)$$

where

$$D = [(x_2 - x_1)^2 + (y_2 - y_1)^2]^{1/2} \quad (2)$$

is the horizontal distance between the stakes. [We take α to be everywhere positive; since the minimum surface slope of the Nisqually Glacier is several degrees, no ambiguity results.] This value of α is assigned to a point midway between the two stakes and the coordinates of this point are transformed to the curvilinear system. Note that no correction need be made for any snow present since the layer would be approximately the same thickness and density at each stake.

The calculations were repeated for each survey and for each stake pair whose separation D lay within a specified range. A range of 70-200 m was chosen. This restricts the stakes to adjacent pairs only and eliminates any overlapping or accidentally close pairs. The result is a set of points $\alpha(x', y', t)$.

Preliminary examination showed that the variation of α with x' was about two orders of magnitude greater than any other variation. Thus to conveniently present the results it is necessary to subtract a "standard" $\alpha(x')$ curve. Such a curve was obtained by plotting all the values of α as a function of x' , ignoring the variables y' and t (Figure 85). A mean curve was drawn through the points by eye and tabulated every 50 m. A point obtained by quadratic interpolation in this table is denoted by $\bar{\alpha}(x')$.

Figure 86 shows the deviation $\Delta\alpha^m = \alpha - \bar{\alpha}$ plotted as a function of x' and t , ignoring the effect of y' . This assumes that the transverse slope is constant, both in time and space. The rectangular grid necessary for computer-contouring was created from the data points using the interpolation scheme described on p. 231.

In Figure 87 α has been corrected for variations with y' . The transverse slope is now allowed to vary in space (but still not in time) and is obtained from the standard (1966) surface. All surface elevations are corrected back to the centerline using this surface and then the slope $\alpha_c(x', t)$ and the deviation $\Delta\alpha_c^m = \alpha_c - \bar{\alpha}$ from the mean are calculated.

Although practically all values of $\Delta\alpha^m$ and $\Delta\alpha_c^m$ were less than 1° , there were a few as high as 2 or 3° . These high values invariably turned out not to be real, but instead were caused by the fact that $\bar{\alpha}$ represents an average surface slope and does not resolve the small-wavelength fluctuations which are, in reality, present. Furthermore, the values of α are averaged over distances anywhere from 70 to 200 m; this by itself will impose some "noise" to the data.

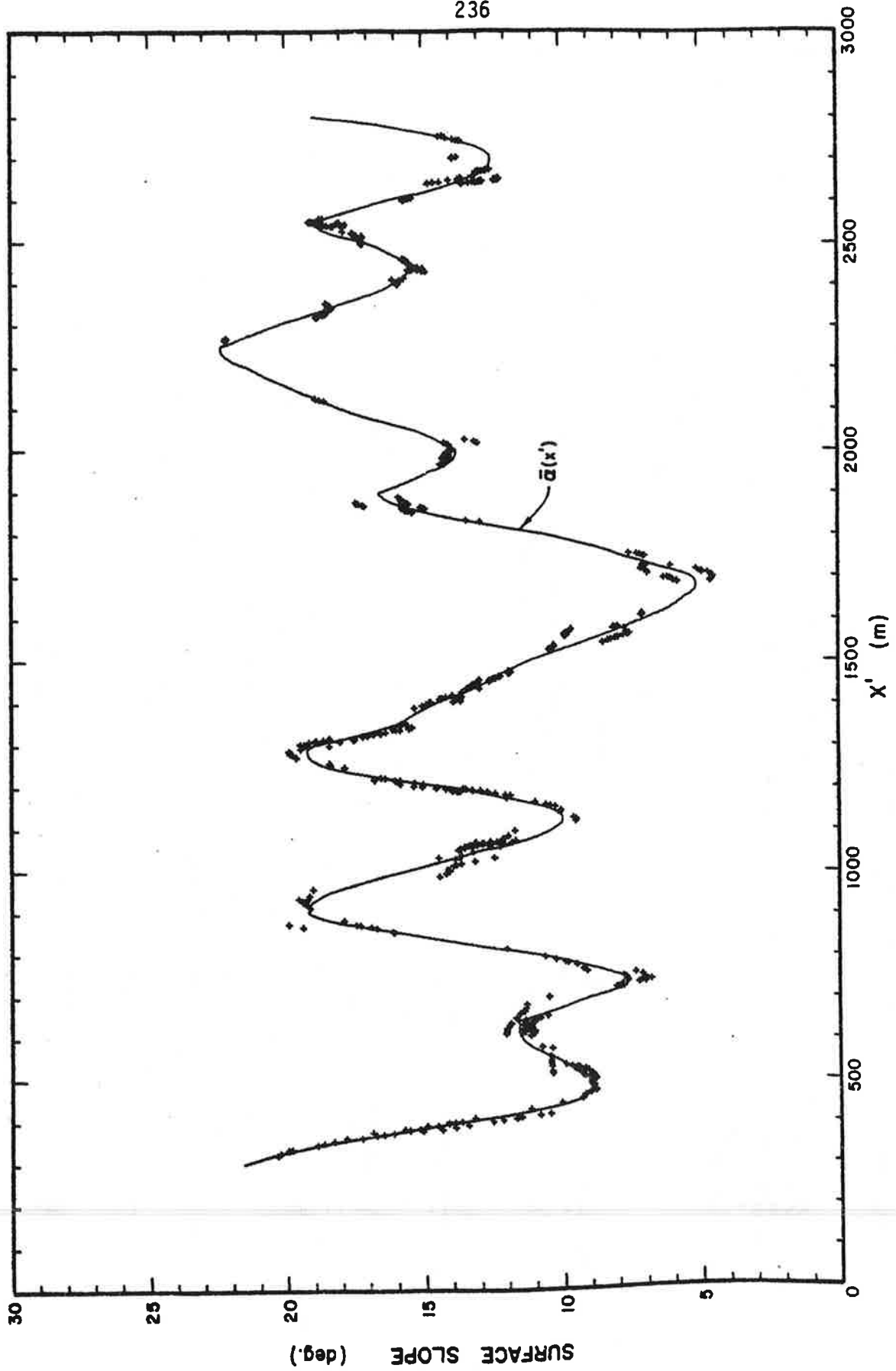


Figure 85. The measured surface slope as a function of distance, calculated between pairs of stakes 70-200 m apart. Any variation with y' or t is ignored. Measurement errors are insignificant on the scale used.

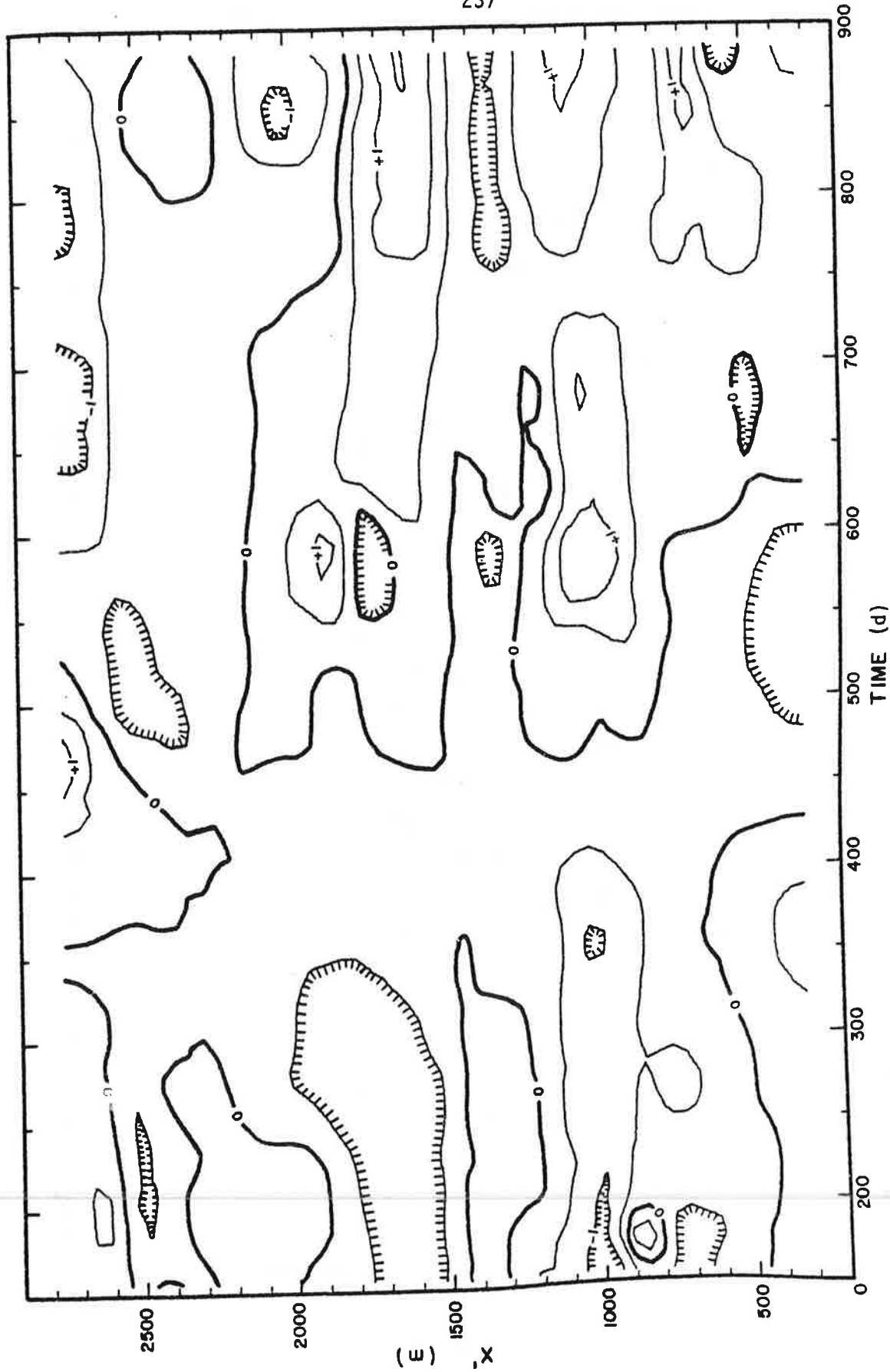


Figure 86. The smoothed deviation $\Delta\alpha^m$ of the measured surface slope from the mean slope $\bar{\alpha}(x')$ as a function of time and distance. This ignores any variation with y' . The contour interval is 0.5'.

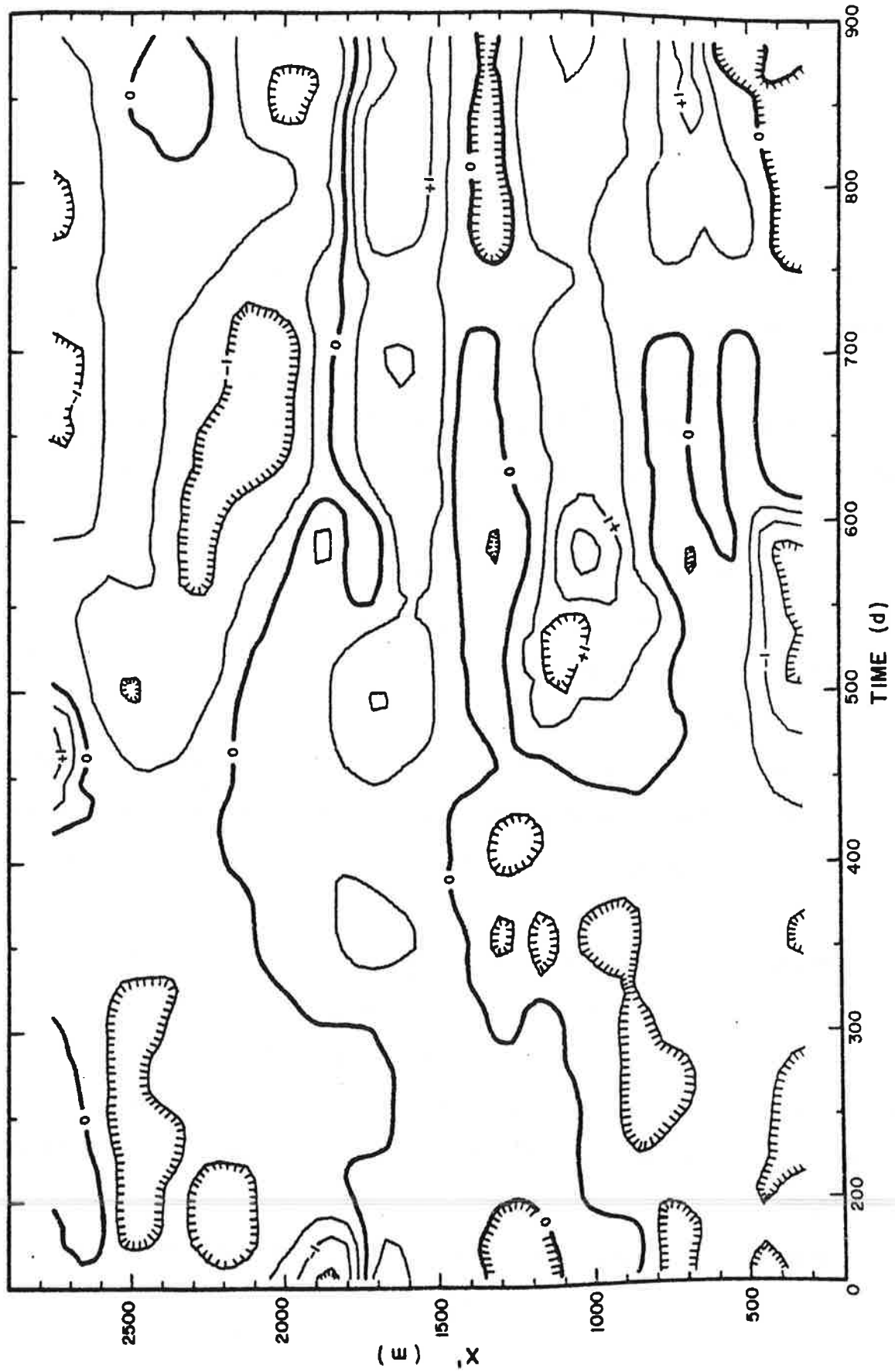


Figure 87. The smoothed deviation $\Delta\alpha_c^m$ of the measured surface slope from the mean slope $\alpha(x')$ as a function of time and distance. Values are corrected for transverse slopes. The contour interval is 0.5° .

Thus it was felt justified to treat $\Delta\alpha^m$ and $\Delta\alpha_c^m$ in a statistical sense and to apply a smoothing algorithm of the form

$$\bar{f}_{ij} = f_{ij} + \frac{1}{8}(f_{i+1,j} + f_{i-1,j} + f_{i,j+1} + f_{i,j-1}) \quad (3)$$

Figures 86 and 87 were smoothed twice with this function. Also, all values greater than 2° have been eliminated.

These diagrams demonstrate that: (a) Even with a mean $\bar{\alpha}(x')$ subtracted out, the dominant variation is still with x' . The time variation during the two years still appears to be essentially random. This probably results from the fact that stake pairs with different separations and different physical locations on the glacier are being used. (b) Making corrections for transverse slopes appears to *increase* the noise in the data rather than decrease it. This implies that the accuracy of the corrections is of the same order of magnitude as the deviations themselves, which are usually only fractions of a degree. Thus we shall assume the accuracy of the surface slopes to be of the order $\pm 0.75^\circ$. This is much greater than the surveying error (at most several centimeters over 100 m, or about 0.05°).

8.2 CALCULATION OF SLOPES BY DIFFERENTIATION OF $\Delta h(x', t)$

The main disadvantage of the previous method of calculating surface slopes is that there is little control over the averaging distance D . Differentiating the $\Delta h(x', t)$ values with respect to x' , however, allows us to specify D uniquely. Moreover, the results will be directly related to the thickness variations.

To do this we interpolate on the standard (1966) surface to obtain

$$z_2 = z(x' + \frac{D}{2}, 0) \quad \text{and} \quad z_1 = z(x' - \frac{D}{2}, 0) \quad (4)$$

and in the Δh_{ij} table to obtain

$$\Delta h_2 = \Delta h(x' + \frac{D}{2}, t) \quad \text{and} \quad \Delta h_1 = \Delta h(x' - \frac{D}{2}, t) \quad (5)$$

The surface slope is then

$$\alpha(x', t) = \tan^{-1} \left| \frac{Z_2 + \Delta h_2 - Z_1 - \Delta h_1}{D} \right| \quad (6)$$

Again, we subtract out a standard $\alpha_o(x')$ curve:

$$\Delta \alpha(x', t) = \alpha(x', t) - \alpha_o(x') \quad (7)$$

where

$$\alpha_o(x') = \tan^{-1} \left| \frac{Z_2 - Z_1}{D} \right| \quad (8)$$

is obtained from the standard (1966) surface. Linear interpolation is used throughout to avoid curve-fitting problems, and the distance D is reduced as necessary to keep the points $x' + \frac{D}{2}$ and $x' - \frac{D}{2}$ within the bounds of the table.

The results of these calculations are two tables, $\Delta \alpha_{ij}$ and α_{oj} , for each value of D . Figures 88 and 89 show $\Delta \alpha$ for $D = 75$ m and 600 m respectively (one and eight times the ice thickness). The corresponding α_{oj} curves are given later (Figure 108, p. 285). The variation in x' again dominates any time variation. As expected, the magnitude and the scatter of $\Delta \alpha$ decrease as D increases. Absolute values of $\Delta \alpha$ are greater than that obtained with the previous method since the reference surface is now three years old. Nevertheless, this procedure does give an overall smoother result, and these data will be used in the analysis of the flow. We assume the accuracy of the slopes to be the same as that estimated previously, namely $\pm 0.75^\circ$.

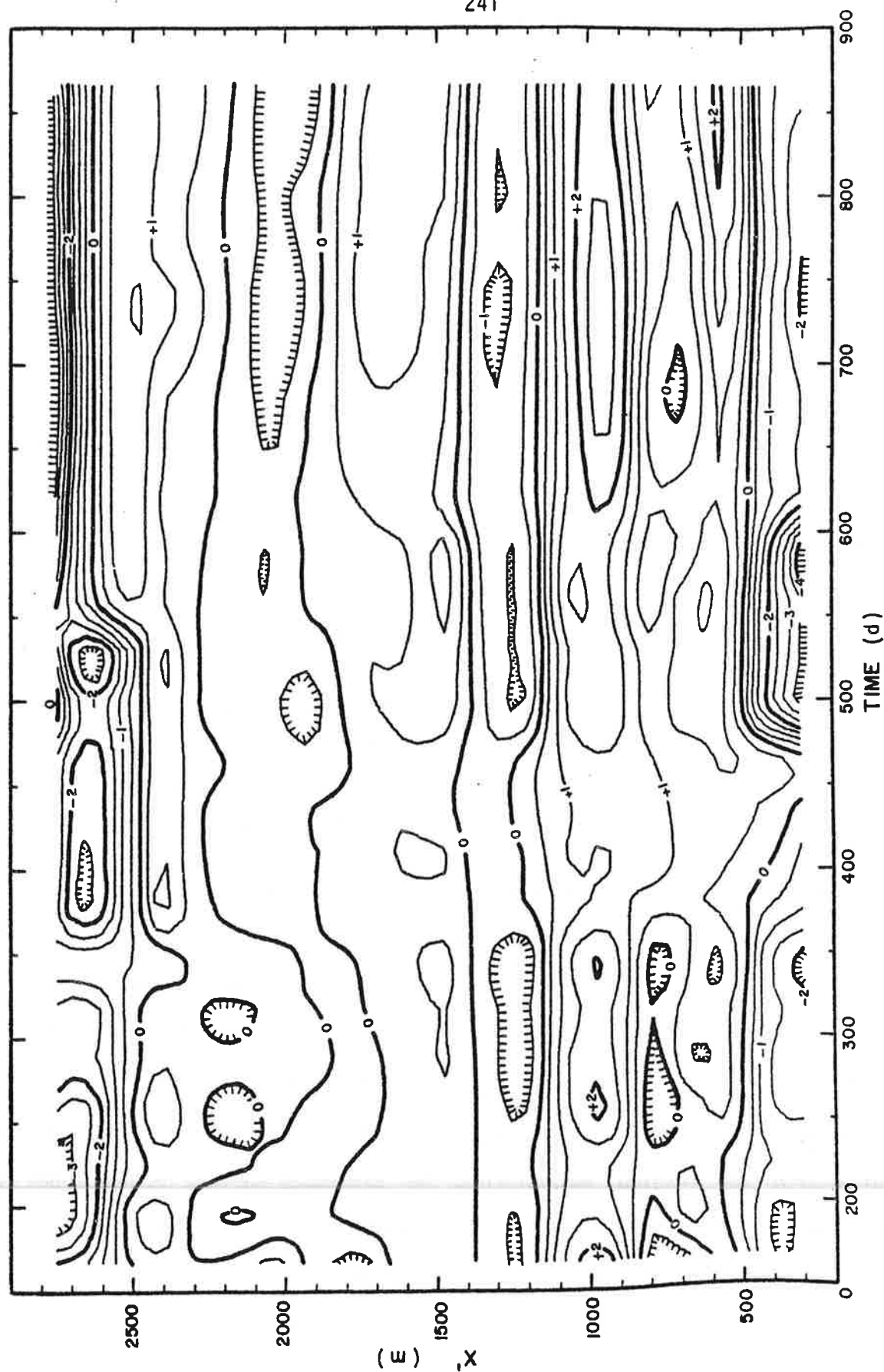


Figure 88. The deviation, $\Delta\alpha$, of the calculated surface slope from the standard slope $\alpha_0(x')$, as a function of time and distance, using an averaging distance of 75 m. The contour interval is 0.5°.

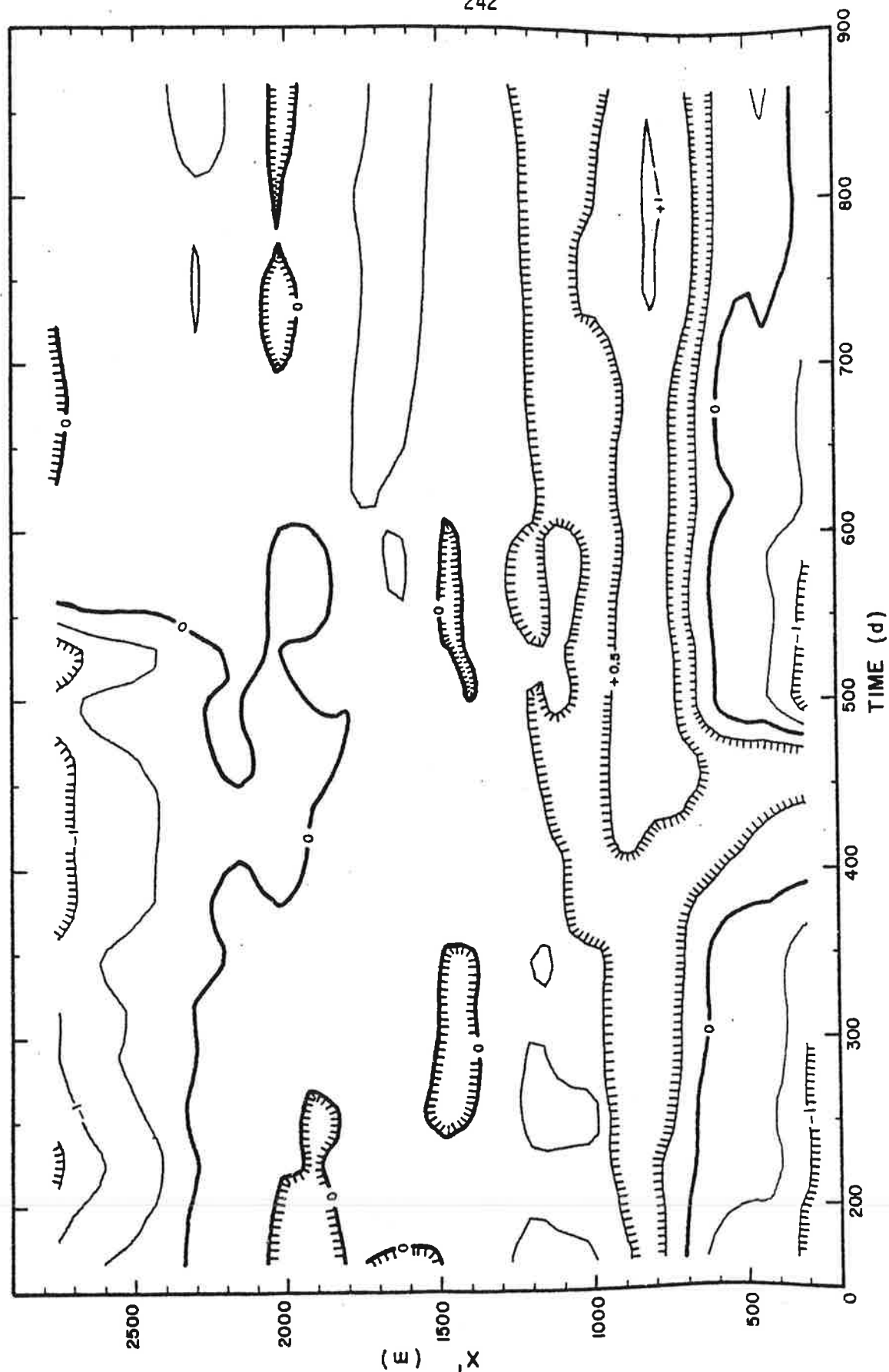


Figure 89. The deviation, $\Delta\alpha$, of the calculated surface slope from the standard slope $\alpha_0(x')$, as a function of time and distance, using an averaging distance of 600 m. The contour interval is 0.5° .

Chapter 9

THE MASS BALANCE

The mass balance of the Nisqually Glacier was not a specific object of this study. However, a knowledge of the snow depths was necessary for correcting the surface elevations to "ice-equivalent" depths. For this reason the mass balance curves of the centerline stakes were computed. The pattern of stakes used was intended for motion, not mass balance, studies and so no attempt will be made to determine the net balance of the glacier.

The curves to be obtained are the vertical distance from the glacier surface to some reference surface, as a function of time. The reference surface is taken as the glacier surface at the end of the previous ablation season (usually sometime in October)*; consequently it changes from one balance year to the next. All snow depths must be converted into an equivalent depth of ice.

Before proceeding, however, we require two additional pieces of information, the surface slopes and the snow densities.

9.1 THE SURFACE SLOPE

The surface slope is needed when the stake deviates from the vertical direction (primarily in the winter). It must be measured over distances of several meters (the typical length of a stake), which is a much smaller scale than that used for analysis of the motion (chapter 8). Thus it will have to be recalculated.

The standard (1966) surface $Z(x,y)$ tabulated in the standard rectangular coordinate system, was again used. Any errors between this surface and the actual one are assumed to be negligible compared to the errors in determining the tilt and bend of a stake.

* The reference surface is usually referred to as the "summer surface".

To determine the slope at a point (X, Y) all grid points within $(\pm\Delta x, \pm\Delta y)$ of (X, Y) are located, and each one is weighted according to its distance r_i from (X, Y) with a Gaussian weighting function:

$$w_i = e^{-\left(\frac{r_i}{\beta}\right)^2} \quad (1)$$

where β is a constant. A plane is then fitted by least-squares to the n grid points $z_i = Z(x_i, y_i)$ by minimizing the vertical distance from the plane to the points: if the plane is given by

$$z = Ax + By + C \quad (2)$$

then the quantity

$$S = \left[\sum_{i=1}^n w_i (z_i - Ax_i - By_i - C)^2 \right] / \left[\sum_{i=1}^n w_i \right] \quad (3)$$

is minimized by requiring that

$$\frac{\partial S}{\partial A} = \frac{\partial S}{\partial B} = \frac{\partial S}{\partial C} = 0 \quad (4)$$

This leads to three equations in three unknowns (A, B, C) :

$$\left. \begin{aligned} A \sum_{i=1}^n w_i x_i^2 + B \sum_{i=1}^n w_i x_i y_i + C \sum_{i=1}^n w_i x_i &= \sum_{i=1}^n w_i x_i z_i \\ A \sum_{i=1}^n w_i x_i y_i + B \sum_{i=1}^n w_i y_i^2 + C \sum_{i=1}^n w_i y_i &= \sum_{i=1}^n w_i y_i z_i \\ A \sum_{i=1}^n w_i x_i + B \sum_{i=1}^n w_i y_i + C \sum_{i=1}^n w_i &= \sum_{i=1}^n w_i z_i \end{aligned} \right\} \quad (5)$$

which can be solved by standard computer subroutines. The equation of the plane can be converted into the form

$$ax + by + cz + d = 0 \quad (6)$$

by the relations

$$\left. \begin{aligned} c &= (1 + A^2 + B^2)^{-1/2} \\ a &= -cA \\ b &= -cB \\ d &= -cC \end{aligned} \right\} (7)$$

(a, b, c) are the direction cosines of the upward normal to the plane and d is the perpendicular distance from the plane to the origin. The slope of this plane is defined as the dip α and the azimuth ω of the line in the plane which maximizes α . These are given by

$$\left. \begin{aligned} \alpha &= \cos^{-1} [-(a^2 + b^2)^{1/2}] - \pi/2 \\ \omega &= \tan^{-1} \left(\frac{b}{a} \right) \end{aligned} \right\} (8)$$

These angles were calculated for each stake on each survey, given its horizontal coordinates (x, y) .

The parameters $(\Delta x, \Delta y, \beta)$ are independent variables and were adjusted until the slopes calculated by this procedure agreed well with values estimated directly from the map. The values used were $\Delta x = \Delta y = \beta = 50$ m. This is a greater range than the "several meters" suggested above, the reason being the limitation imposed by the grid spacing, 20 m, of the standard (1966) surface.

9.2 THE SNOW DENSITY

Snow densities were never directly measured on the Nisqually Glacier. Instead values have been taken from the standard snow courses measured every winter in the Nisqually Valley by the U.S. Geological Survey, Tacoma, Washington (Richardson, written communication, 1972). These snow courses are sampled at the beginning of each month from January to April with a Federal sampler, and the mean water content of the snow pack evaluated. The snow courses are at Paradise (elevation 1652 m, or 5420 feet), Stem Glade (1539 m, 5050 feet), Ghost Forest (1387 m, 4550 feet), and Longmire (841 m, 2760 feet), and are indicated on Figure 20. The data are shown in Figure 90 for the period of this study.

The densities vary considerably, but Paradise almost always has the highest values. Since Paradise is the closest, both in distance and elevation, to the Nisqually Glacier its values have been used. The curves have been extrapolated to 0.50 Mg m^{-3} at the beginning of the summer (June 1), to 0.55 Mg m^{-3} at the end of the summer (September 30), and to 0.30 Mg m^{-3} at the beginning of the winter (October 1). This is based on information from snowpacks on other glaciers in the Pacific Northwest (Meier, personal communication, 1972).

It is apparent from Figure 90 that the densities used are an upper limit. This maximizes the loading effect of the snowpack, something which will be desirable later when analyzing the velocity data. In keeping with this, the low densities measured at Paradise in February and April 1968, and February 1970, have been eliminated and the curves interpolated as shown.

9.3 THE REFERENCE SURFACE

Before accumulation and ablation values can be calculated the location of the reference surface relative to the stake must be defined. When ice is exposed the reference surface is above the current surface, and either intersects

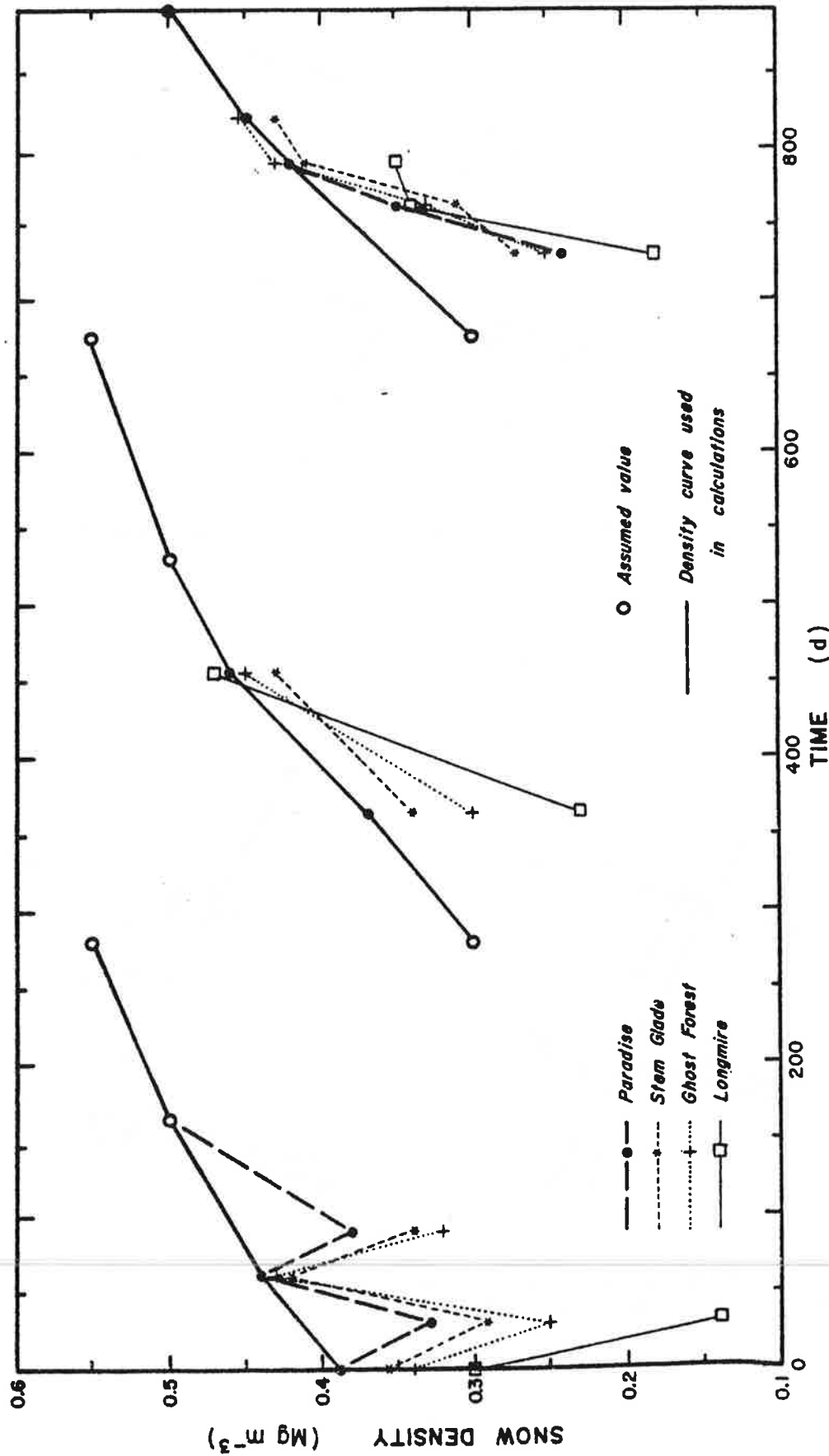


Figure 90. Snow densities measured by the U.S. Geological Survey at four snow courses in the Nisqually Valley of Mount Rainier National Park. The density curve used in the calculations is an upper limit to the data. (from Richardson, written communication, 1978.)

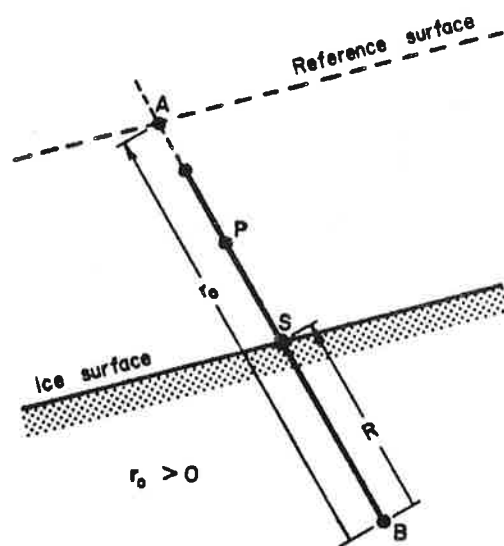


Figure 91. Location of the reference surface when the glacier surface is ice.

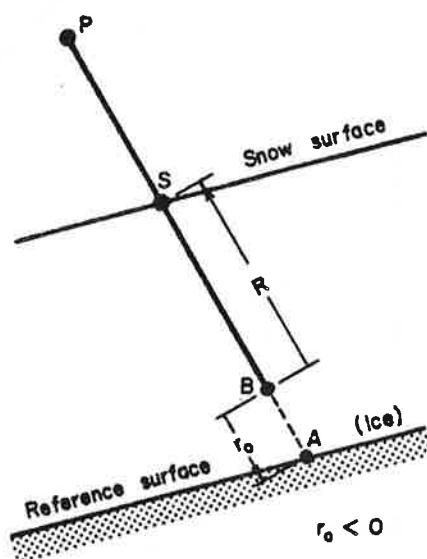
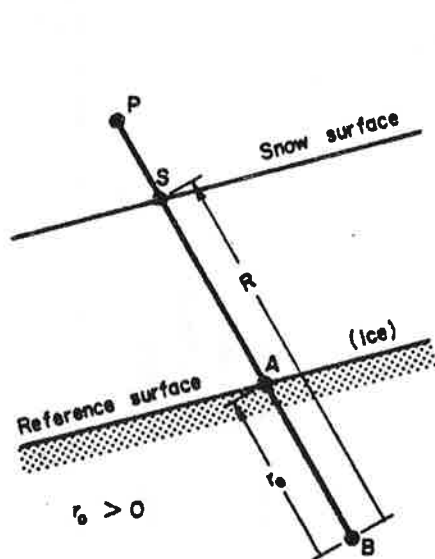


Figure 92. Location of the reference surface when the glacier surface is snow and the stake is straight.

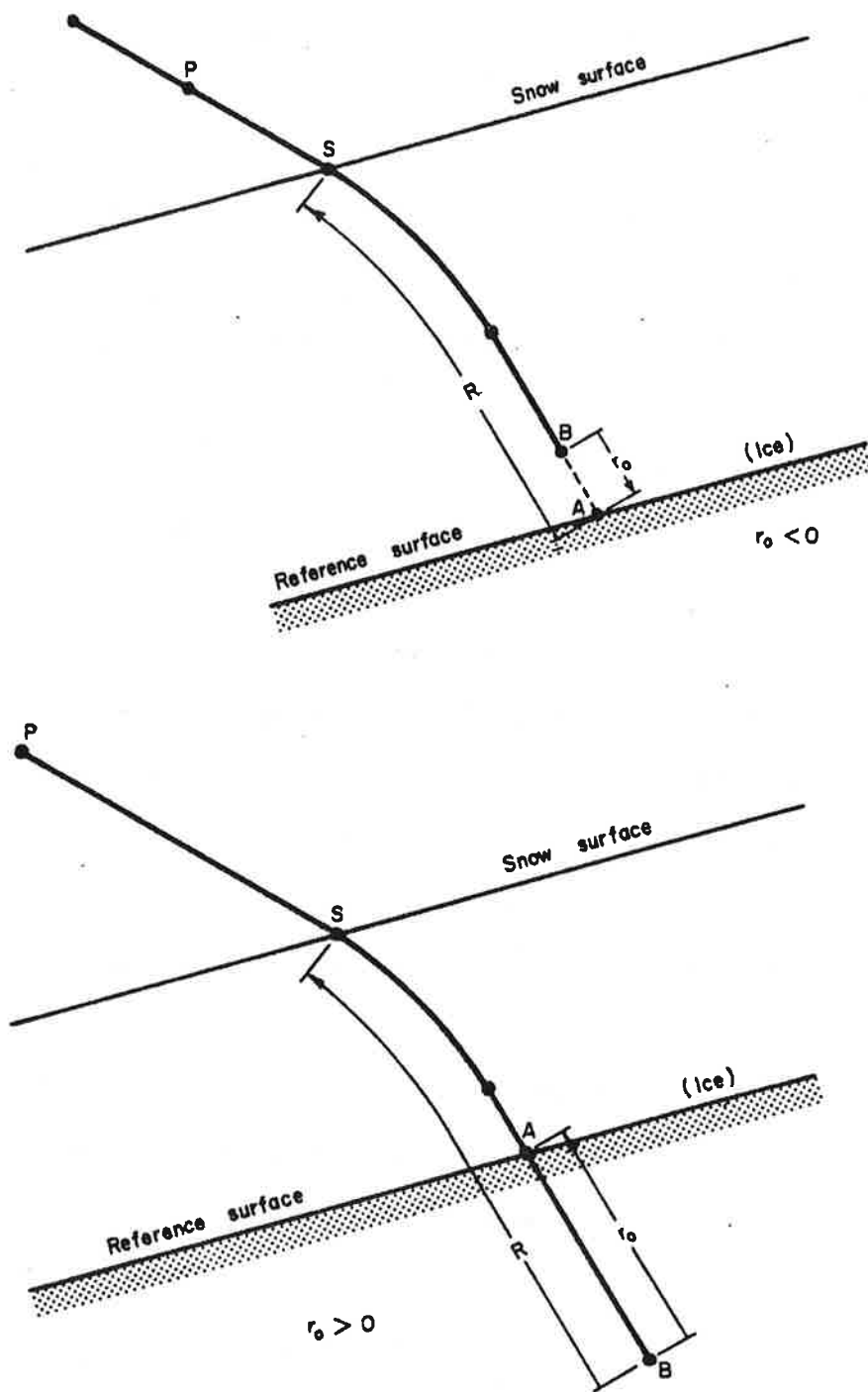


Figure 93. Location of the reference surface when the glacier surface is snow and the stake is bent.

or passes above the stake (Figure 91). On the other hand, when the surface is snow, the reference surface is below the current surface and either intersects or passes below the stake. In both of these cases the stake may be either straight (Figure 92) or bent (Figure 93).

The reference surface is defined by the distance r_o , measured along the direction of the bottommost segment of the stake from the bottom of the stake B to the reference surface A, positive if A is above B and negative if A is below B.

To determine r_o the surface level R was plotted as a function of time for each stake. Extrapolating or interpolating the curves to the end or beginning of the ice melt period gives the required values, since the stakes are then reasonably vertical. The time of the end or beginning of this period was inferred by using one or more of the following pieces of information: (a) the shape of the curves themselves (the maximum or minimum points), (b) the date of transition from a snow-covered to a snow-free surface, or vice-versa (the type of surface was always recorded), (c) the known date when snow started to accumulate at Paradise (section 10.2), or (d) the corresponding times used for nearby stakes.

Redrilling or resetting of the stakes did not present any problem during the ablation season, as then the stakes do not have appreciable changes of tilt and the curves can be extrapolated to a common point and the amount of shift determined. However, during the second winter, when vertical alternate stakes were used to replace stakes which had been bent over and buried in a heavy riming storm, the differences in tilt between the two were usually too large to allow such a matching of curves. No measurements were made after June 4, 1970, before ice had been exposed, and so the reference surface for the alternate stakes could not be determined by the above methods. In this case the snow depth was assumed to be uniform over the glacier and to be equal to an average

of the snow depth at Paradise and the snow depths at four stakes which managed to survive the storm. The agreement between these five values is quite good (Table 15).

Location	Change in snow depth
C3	3.01
C4	3.01
C8	2.85
M4	2.79
Paradise	2.95
Average:	2.90

Table 15. The change in snow depth, in the vertical direction, between Nov. 29, 1969, and Feb. 10, 1970. All values are in meters.

Finally, stakes C16 to C20, where ice was never exposed, are assumed to be at the equilibrium line. The reference surface is then taken to be the surface level observed at the end of the summer.

9.4 CALCULATION OF THE MASS BALANCE

Once x_0 is known, the coordinates of point A (the intersection of the stake with the reference surface) can be calculated with equations 6.56 using the coordinates of point B (the bottom of the stake) and the tilt of the lowermost segment. The coordinates of B are calculated from the measured point P using tilt and bend corrections where necessary. Similarly, the coordinates of the surface point S can be calculated, using the coordinates of P and the tilt of the uppermost segment.

A plane whose normal has direction cosines (l, m, n) is then fitted through S, and a parallel one through A. The distance between the two planes is

$$\Delta = l(x_S - x_A) + m(y_S - y_A) + n(z_S - z_A) \quad (9)$$

The direction cosines are calculated from the dip α and the azimuth ω of the surface using the relations

$$\left. \begin{aligned} l &= \sin \alpha \cos \omega \\ m &= \sin \alpha \sin \omega \\ n &= \cos \alpha \end{aligned} \right\} (10)$$

When converted to ice equivalent and the vertical direction, we get the mass balance:

$$b_i = \left\{ \begin{aligned} \Delta \sec \alpha & \quad \text{if } \Delta \leq 0 \\ \Delta \sec \alpha \left(\frac{\rho_s(t)}{\rho} \right) & \quad \text{if } \Delta > 0 \end{aligned} \right\} (11)$$

where ρ is the density of the glacier ice (assumed to be 0.9 Mg m^{-3}) and $\rho_s(t)$ is the density of the snow (Figure 90).

The correction to the surface elevation (used on p. 230), to allow for the snow layer, is

$$h_c = \left\{ \begin{aligned} 0 & \quad \text{if } b_i \leq 0 \\ \Delta (\sec \alpha) \left(1 - \frac{\rho_s(t)}{\rho} \right) & \quad \text{if } b_i > 0 \end{aligned} \right\} (12)$$

The mass balance curves for the centerline stakes are given in Appendix B. Error bars are not shown because they are either negligible or not known. The error in reading the surface level with a theodolite is about $\pm 0.05 \text{ m}$. On the scale of the diagrams this is less than the size of the plotting symbols. In the summer errors in the tilt contribute little error since the stakes are nearly vertical. In the winter, however, uncertainty in the bend corrections might cause errors in b_i by as much as $\pm 0.5 \text{ m}$ ice equivalent.

Chapter 10

THE RUN-OFF AND METEOROLOGICAL DATA

10.1 THE STREAM DISCHARGE MEASUREMENTS

In connection with this investigation a gaging station was established in the spring of 1968 on the Nisqually River at the highway bridge about 1.8 km below the glacier terminus (Figure 21). The drainage area is approximately 16.1 km^2 , four times the size of the Nisqually Glacier itself. Most of the discharge, however, comes from the glacier.

A 3.35 m length of pipe, 28 cm in diameter, is used as a stilling well. It is encased in reinforced concrete and is bolted to a granodiorite bedrock outcrop, against which most of the river flows at this point. A Stevens continuous recorder is mounted over the stilling well and produces an analog record of the water level in the well. The water in the well connects with the river water via intakes only 1 cm in diameter in order to dampen the rapid fluctuations of the turbulent water in the river.

The water level is converted to mean daily discharges ($\text{m}^3 \text{ s}^{-1}$) by calibrating the flow with discharge measurements, usually made by wading the river and sampling depths and velocities with a Price current meter. Unfortunately this can only be done at low flows. The channel bed changes almost continuously during the high flow in the late spring and summer. Some calibrations were made at such times using the salt-dilution technique, but nevertheless the "stage-discharge" relation is only very approximate.

Calibrations were made as often as possible to help alleviate this problem. Although the magnitude of the discharge may be in considerable error, the general shape of the curve, on a monthly basis, should be reasonably correct. For our purposes only the phase relationships with the velocity data, such as the time of maximum and minimum discharge, are really required.

The gaging station was built, maintained and calibrated by the Glaciology Project Office, U.S. Geological Survey, Tacoma, Washington. The data were kindly reduced by Richardson (written communication, 1970, 1972). Daily values of the discharge are shown in Figure 94 for the same time period that the glacier flow observations cover.

10.2 THE METEOROLOGICAL DATA

Figures 95 through 99 show daily meteorological parameters measured near the Paradise Ranger Station (elevation 1676 m) by the National Park Service. The parameters are the daily maximum and minimum temperature, the daily total precipitation, the daily snowfall and the snow depth.

The data are based on information supplied by Bishop (written communication, 1969, 1970).

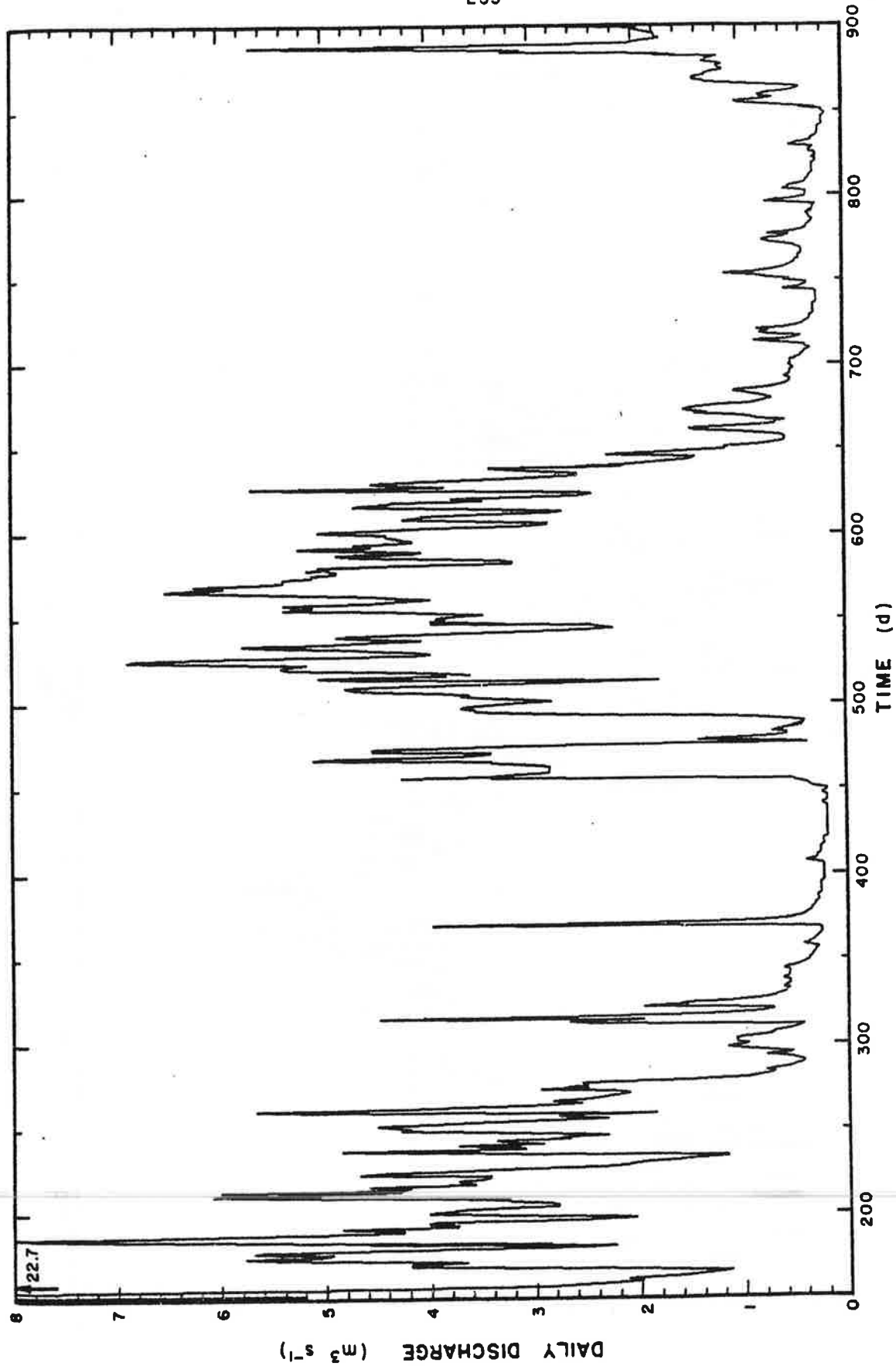


Figure 94. The daily discharge of the Nisqually River at the gaging station 1.8 km below the terminus of the Nisqually Glacier. A small outburst flood may have caused the high flow on June 2, 1968 (t = 153).

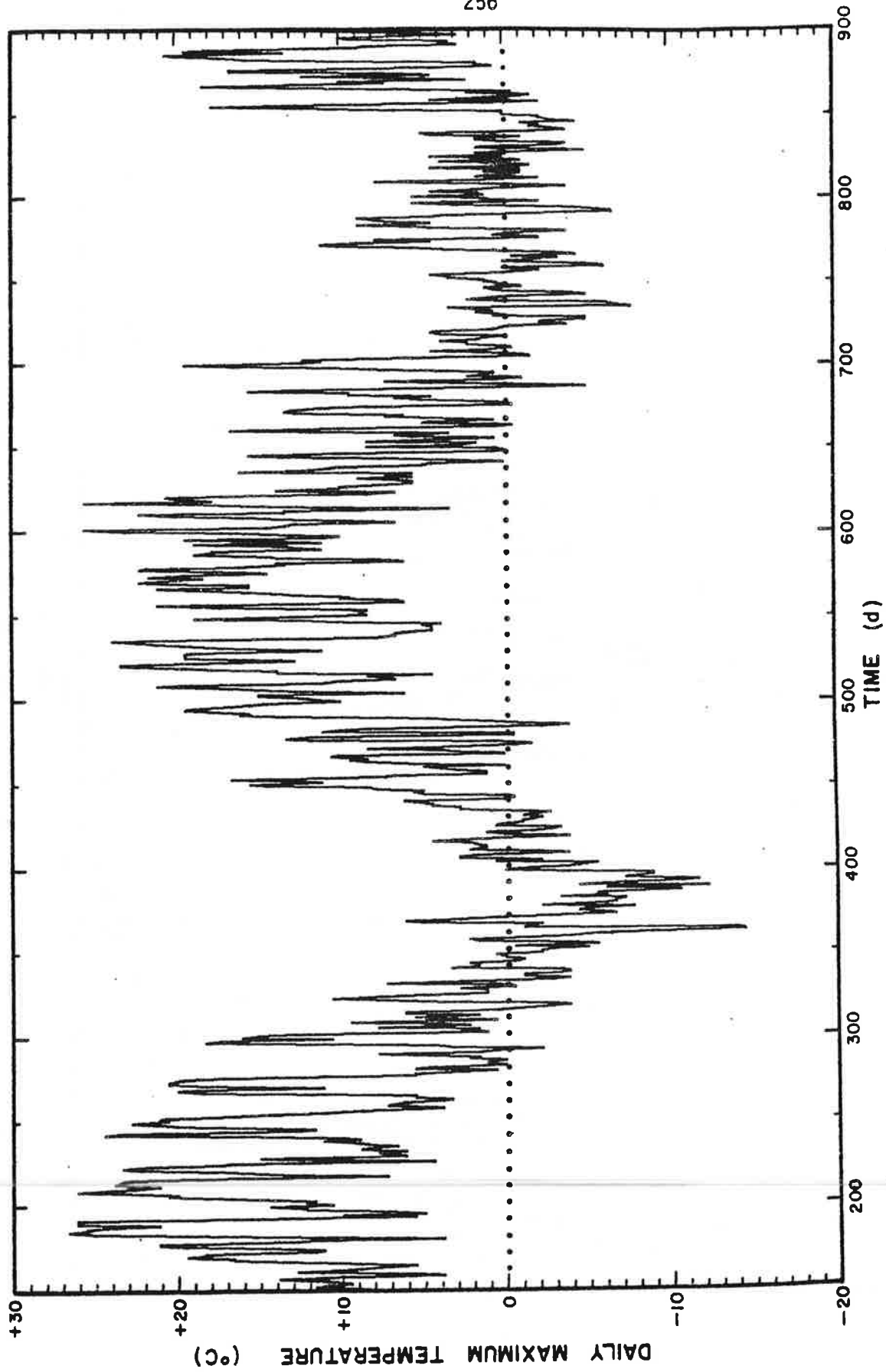


Figure 95. The daily maximum temperature at Paradise, Mount Rainier National Park, as a function of time.

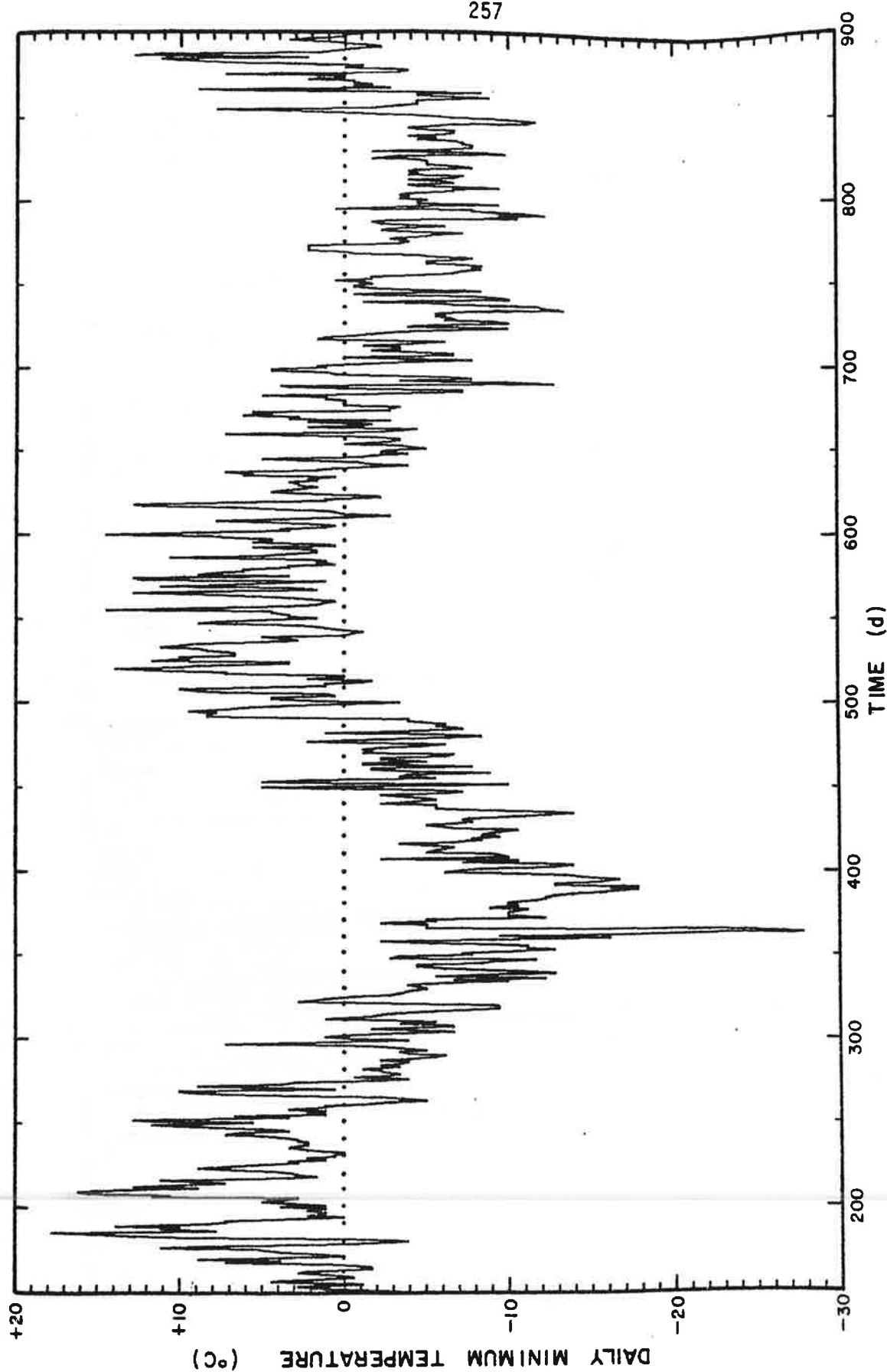


Figure 96. The daily minimum temperature at Paradise, Mount Rainier National Park, as a function of time.

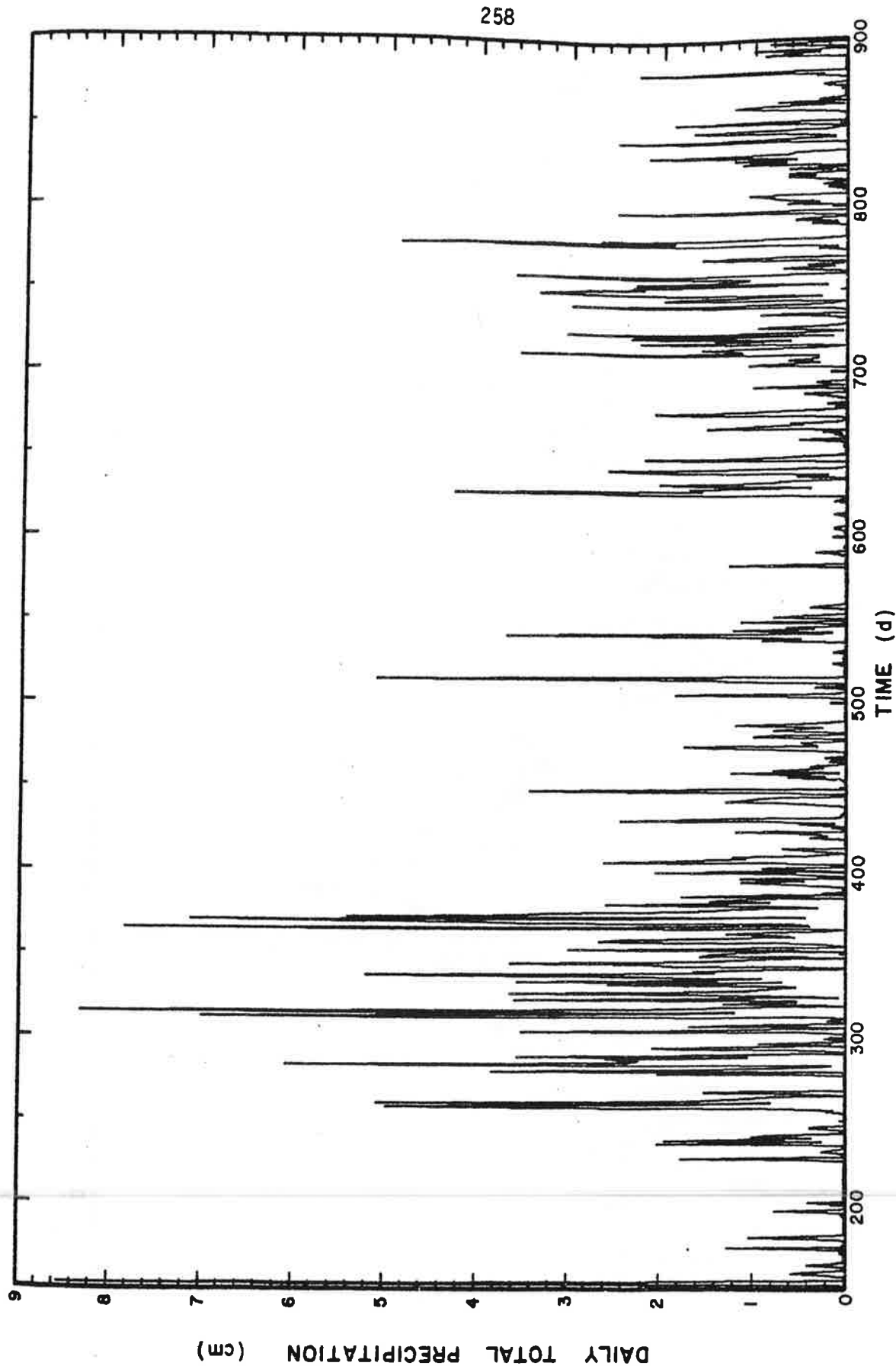


Figure 97. The daily total precipitation at Paradise, Mount Rainier National Park, as a function of time.

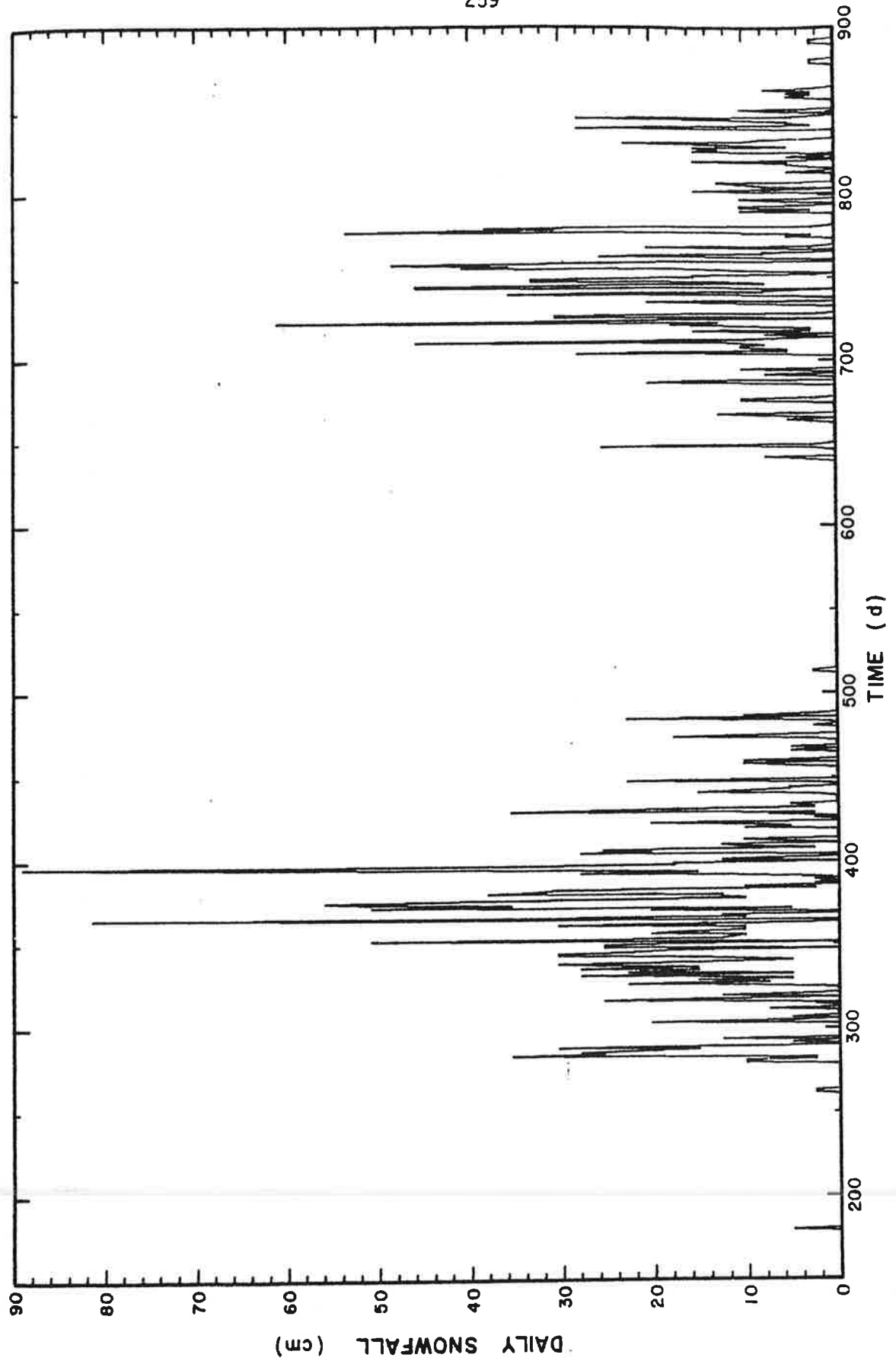


Figure 98. The daily snowfall at Paradise, Mount Rainier National Park, as a function of time.

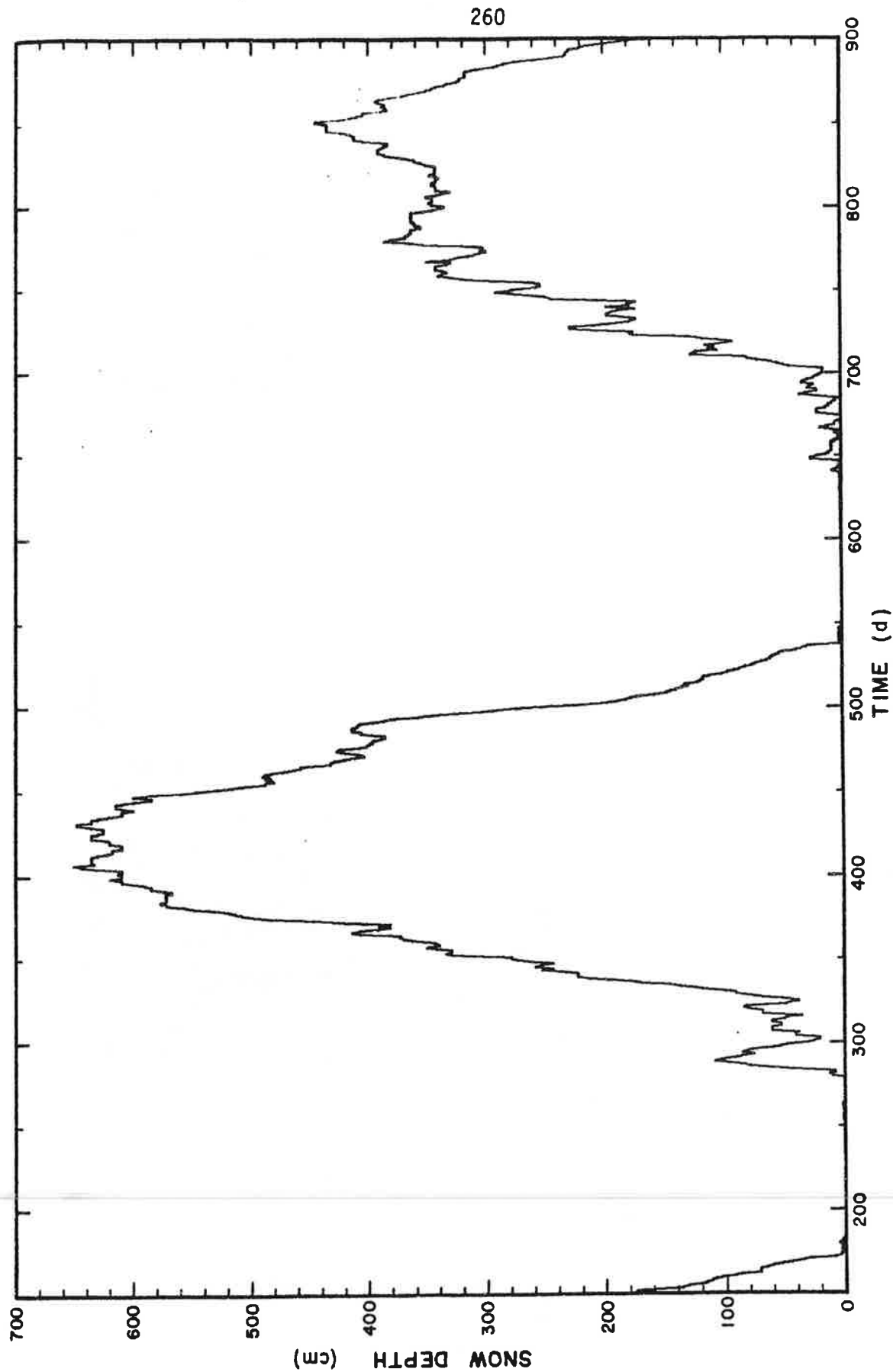


Figure 99. The snow depth at Paradise, Mount Rainier National Park, as a function of time.

Chapter 11

ANALYSIS OF THE DATA

11.1 THEORY

We wish to calculate the sliding velocity by removing from the measured surface velocity the contribution from internal deformation. A theory of glacier flow which relates the driving force, gravity, to the resulting deformation is required. Such theories, largely due to Nye, have been described adequately by Paterson (1969) and Budd (1969) and only an outline will be given here.

The stresses acting on the ice are calculated from the applied force using the equilibrium equations and then these are related to the strain rates using the flow law of ice. Initially the glacier is assumed to be an infinitely wide parallel-sided slab of ice resting on a plane bed, but this will be modified to account for the effect of the valley walls and changes in slope along the glacier.

11.1.1 *Basic Definitions*

The stress tensor is denoted by

$$\tau_{ij} = \begin{Bmatrix} \tau_{xx} & \tau_{xy} & \tau_{xz} \\ \tau_{xy} & \tau_{yy} & \tau_{yz} \\ \tau_{xz} & \tau_{yz} & \tau_{zz} \end{Bmatrix} \quad (1)$$

Because of rotational equilibrium this is a symmetric tensor and has only six independent components. Assuming infinitesimal strain, the definition of strain rate is

$$\dot{\epsilon}_{ij} = \frac{1}{2}(v_{i,j} + v_{j,i}) \quad (2)$$

where $\underline{V} = (v_1, v_2, v_3)$ is the velocity vector*. This is also a symmetric second order tensor:

$$\dot{\epsilon}_{ij} = \begin{pmatrix} \dot{\epsilon}_{xx} & \dot{\epsilon}_{xy} & \dot{\epsilon}_{xz} \\ \dot{\epsilon}_{xy} & \dot{\epsilon}_{yy} & \dot{\epsilon}_{yz} \\ \dot{\epsilon}_{xz} & \dot{\epsilon}_{yz} & \dot{\epsilon}_{zz} \end{pmatrix} \quad (3)$$

Because of this symmetry, the tensors possess principal stresses $(\sigma_1, \sigma_2, \sigma_3)$ and principal strain rates $(\dot{\epsilon}_1, \dot{\epsilon}_2, \dot{\epsilon}_3)$.

The hydrostatic pressure is

$$p = \frac{1}{3} \tau_{ii} = \frac{1}{3}(\sigma_1 + \sigma_2 + \sigma_3) = \frac{1}{3} I_1 \quad (4)$$

where $I_1 = \tau_{ii}$ is the first invariant of the stress tensor. Subtracting p from the stress tensor we get the stress deviator tensor:

$$\tau'_{ij} = \tau_{ij} - \frac{1}{3} \tau_{ii} \delta_{ij} \quad (5)$$

where δ_{ij} is the Kronecker delta. For a discussion of the flow law we will use the "effective shear stress" and "effective shear strain rate" (Nye, 1953):

$$\tau^2 = \frac{1}{2} \tau'_{ij} \tau'_{ij} \quad \text{and} \quad \dot{\epsilon}^2 = \frac{1}{2} \dot{\epsilon}_{ij} \dot{\epsilon}_{ij} \quad (6)$$

* The usual indicial notation will be used where convenient, the indices having the values (1,2,3), corresponding to (x,y,z) respectively. Repeated indices imply summation over that index and differentiation is indicated by a comma: $f_{,j} = \partial f / \partial x_j$.

Since these are related to the second invariants

$$I_2 = \tau'_{ij}\tau'_{ij} \quad \text{and} \quad \dot{E}_2 = \dot{\epsilon}_{ij}\dot{\epsilon}_{ij} \quad (7)$$

of the two tensors, then τ and $\dot{\epsilon}$ are also invariants of the tensors.

In turn, these are related to the octahedral shear stress and strain rate (the values across a plane whose normal makes an equal angle with the three principal directions) by

$$\tau_o = \sqrt{\frac{2}{3}} \tau \quad \text{and} \quad \dot{\epsilon}_o = \sqrt{\frac{2}{3}} \dot{\epsilon} \quad (8)$$

and to the stress and strain rate in uniaxial compression by

$$\sigma = \sqrt{3} \tau \quad \text{and} \quad \dot{\epsilon} = \frac{2}{\sqrt{3}} \dot{\epsilon} \quad (9)$$

11.1.2 Calculation of the Stresses

In glaciers the ice deforms slowly enough that the inertial terms (accelerations) are negligible. Newton's equations of motion then reduce to the equations of static equilibrium:

$$\tau_{ij,j} + F_i = 0 \quad (10)$$

where F is the body force per unit volume.

Consider the glacier to have a plane surface of slope α and to be resting on a plane bed parallel to the surface. Define a coordinate system with x down the glacier, y across the glacier and z upward, normal to the surface (Figure 100). If we assume the thickness h is much less than the length or width of the glacier, and we restrict ourselves to points well in from the

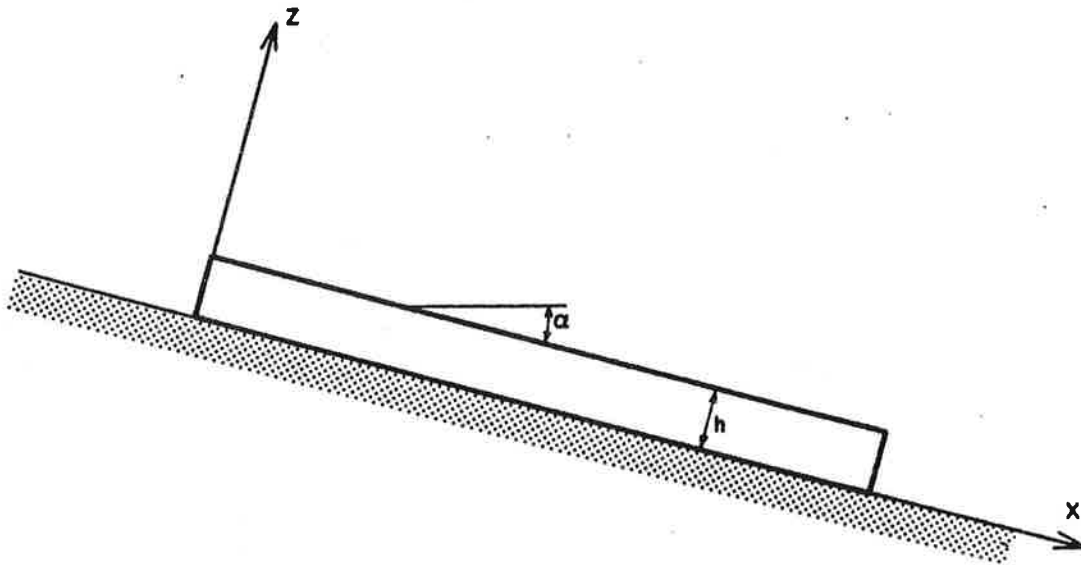


Figure 100. The model of a glacier used in calculating the stresses and the sliding velocity. The thickness h is assumed to be much smaller than the length or width of the glacier. The effect of the valley walls is discussed later.

edges, then all stress gradients in the x or y directions will be negligible and equations 10 will reduce to simply

$$\tau_{i3,3} + F_i = 0 \quad (11)$$

Furthermore, the only non-zero component of the stress deviator tensor will be τ'_{xz} . Thus, substituting (4) and (5) and writing

$$F_i = \rho g_i \quad (12)$$

for the body forces, we are left with the two equations

$$\frac{\partial \tau'_{xz}}{\partial z} - \frac{\partial p}{\partial x} + \rho g \sin \alpha = 0 \quad (13)$$

$$- \frac{\partial p}{\partial z} - \rho g \cos \alpha = 0 \quad (14)$$

Integrating (14) gives

$$p = \rho g z \cos \alpha \quad (15)$$

since the hydrostatic pressure at the surface is zero (neglecting atmospheric pressure). Thus $\partial p / \partial x$ is zero and (13) can be integrated to give

$$\tau'_{xz} = \rho g (h - z) \sin \alpha \quad (16)$$

At $z = 0$, this becomes the basal shear stress:

$$\tau_b = \rho g h \sin \alpha \quad (17)$$

The bar will be used as the unit of stress ($1 \text{ bar} = 10^5 \text{ N m}^{-2}$) since stresses at the bed of a glacier are of the order of 1 bar (roughly one "atmosphere").

11.1.3 The Flow Law of Ice

The experiments of Glen (1955) showed that the strain rate of a specimen of ice subjected to a uniaxial compressive stress followed a power law of the

$$\dot{\epsilon} = A \sigma^n \quad (18)$$

This simple flow law was generalized by Nye (1957) to the more complex stress situation in glaciers by making the following assumptions: (a) the ice is

isotropic, (b) transient effects can be neglected, that is, the stresses have been applied long enough that steady-state creep has been reached, (c) the flow law is unaffected by hydrostatic pressure (this was shown to be valid by Rigsby (1958) provided the temperature is measured with respect to the pressure-melting point), and (d) the ice is incompressible ($\dot{\epsilon}_{ii} = 0$). The resulting "generalized flow law" can be written in the form

$$\dot{\epsilon}_{ij} = \frac{1}{v(\tau)} \tau'_{ij} \quad (19)$$

where $v(\tau)$ is the "effective viscosity" of the ice. In general v is a function of the temperature T as well as the effective shear stress τ . However, the lower Nisqually Glacier can be safely assumed to be "temperate" and that its temperature is at the pressure melting point throughout. Thus we write the viscosity as a function of the stress only.

Comparison with Glen's flow law (equation 18) suggests that

$$v(\tau) = \frac{B^n}{\tau^{n-1}} \quad (20)$$

where B is a constant (in general, temperature dependent). If we use equations 6 we obtain the flow law in terms of the effective stress and strain rate:

$$\dot{\epsilon} = \frac{1}{v(\tau)} \tau = \left(\frac{\tau}{B}\right)^n = A\tau^n \quad (21)$$

where

$$A = B^{-n} \quad (22)$$

So far we have assumed that the exponent n is a constant. However, Meier (1958, 1960) suggested that at low stresses (below 0.5 bar) the stress-strain rate relationship may become essentially linear and that

$$\dot{\epsilon} = A_1 \tau + A_2 \tau^n \quad (23)$$

was a more realistic form for the flow law. The tendency for $n \rightarrow 0$ as $\tau \rightarrow 0$ has also been suggested by the laboratory experiments of Butkovich and Landauer (1960), Mellor and Smith (1966), and Colbeck (unpublished). However, there is other work, for example, Tabor and Walker (1970) or Thomas (1971), which disputes these experiments, or at least suggests that the stress level at which linear behavior dominates is well below 0.5 bar.

Other forms for the flow law have been proposed, such as a power series (Lliboutry, 1969):

$$\dot{\epsilon} = A_1 \tau + A_2 \tau^3 + A_3 \tau^5 \quad (24)$$

or a hyperbolic function (Butkovich and Landauer, 1960):

$$\dot{\epsilon} = A_1 \sinh\left(\frac{\tau}{\tau_0}\right) \quad (25)$$

However, Butkovich and Landauer conclude their data are better represented by a Meier flow law (equation 23).

All these flow laws can be written in the general form

$$\dot{\epsilon} = \sum_{k=1}^K A_k \tau^{n_k} \quad (26)$$

The values of the parameters n_k and A_k are listed in Table 16 for most experiments done to the present time, except for those at temperatures well below 0°C. The experiments involve both laboratory stressing of ice specimens and *in situ* results from the analysis of boreholes or velocity profiles of various glaciers. The values have been adjusted using equations 8 and 9 so that the

effective shear stress and strain rate are used throughout (equation 26).

Each of these flow laws is plotted on a log-log scale in Figure 101. The straight lines are laws with $K = 1$, whereas the curved lines are laws which attempt to account for the decrease of n at low stresses by adding more terms. The range of shear stresses that are likely at the bed of the Nisqually Glacier (0.5 to 1.25 bar^{*}) is shown by the two vertical dotted lines.

It can be seen that, with three exceptions, all flow laws are bounded by the two from the Blue Glacier boreholes. The most viscous flow law (the "hardest ice") is that of Kamb and Shreve (1966), whereas the least viscous (the "softest ice") is that of Shreve and Sharp (1970). The coefficients of Nye (1953) give a line close to the middle of this range.

Two of the exceptions to these limits are laboratory experiments that have not accounted for transient creep. The third (Colbeck, unpublished), distinctly less viscous than all other laws, could also be a transient creep effect. Colbeck applied a correction for crystal size which brought his relation into agreement with others, but the magnitude of this correction is questionable.

The flow law of ice is thus not known very accurately. For a given stress there can be as much as an order of magnitude difference in the strain rate, depending upon the choice of flow law parameters. This scatter may be real (for example, anisotropy, impurities, temperature variations, or differences in density, crystal fabric or grain size) or it may simply reflect the inability to specify the stress system realistically enough. It must be kept in mind that the generalized flow law (equation 19) predicts a coupling of the stresses, since τ is a function of all the individual stress deviator components τ'_{ij} .

In this analysis the flow law parameters will be allowed to vary. To eliminate any possible errors caused by transient creep only those parameters

* Calculated from equation 17 using various limits for the thickness and surface slope. See Figure 112.

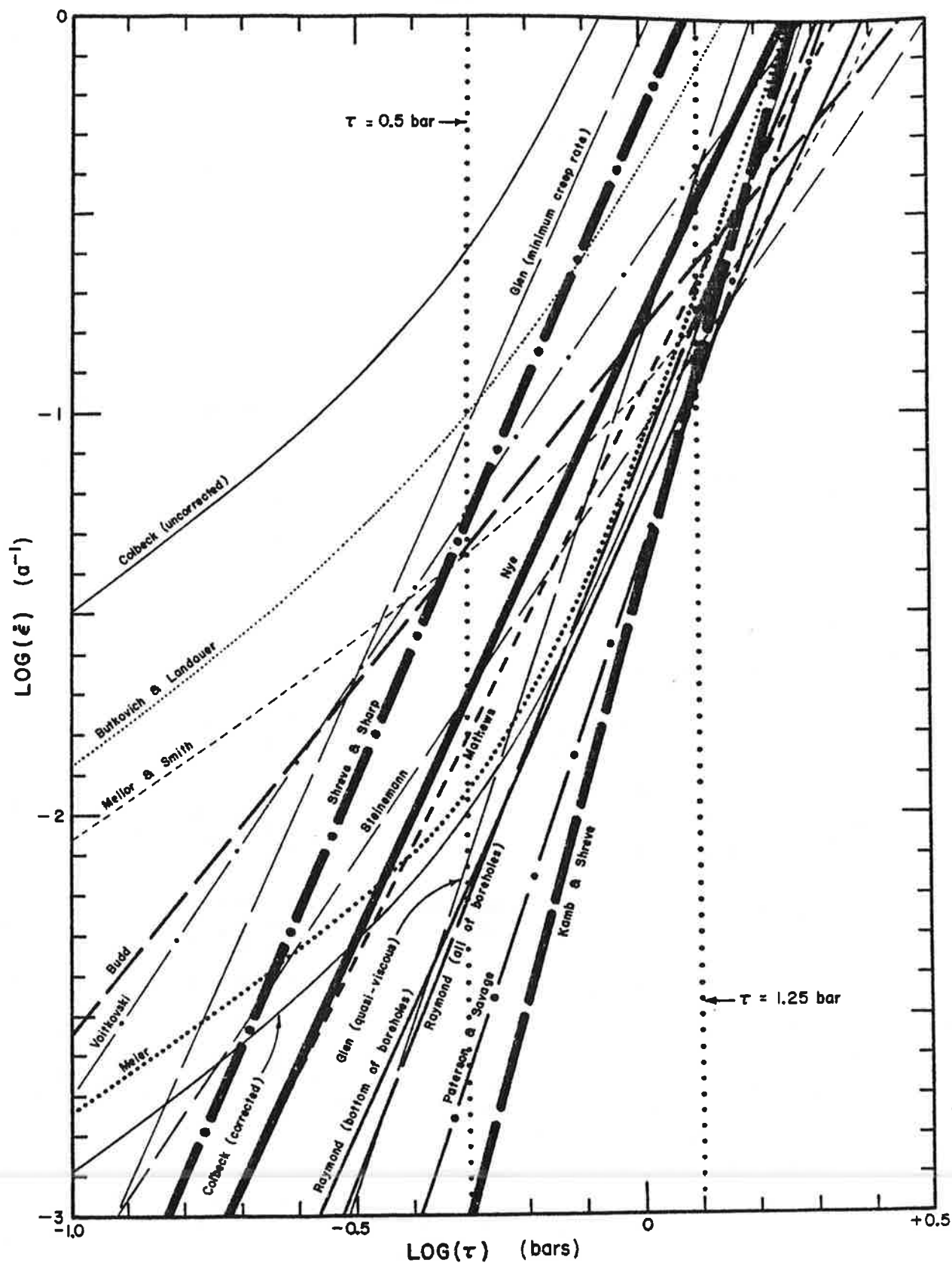


Figure 101. The flow law of ice for the various values of the parameters which have been determined to date (Table 16). Experiments below -5°C have been omitted. The thin lines represent laboratory experiments.

Note	Experiment	K	k	A_k	n_k	T
1	Nye (1953) [contraction of tunnels]	1	1	0.173	3.07	~ 0
2	Glen (1955) [quasi-viscous creep]	1	1	0.148	4.2	-0.02
3	Glen (1955) [minimum creep]	1	1	0.849	3.17	-0.02
4	Steinemann (1958) [from Budd, 1969, p. 21] [lab. exp.]	1	1	0.088	2.1	-1.9
5	Mathews (1959)	1	1	0.111	2.8	~ 0
6	Meier (1960)	2	1	0.018	1	~ 0
			2	0.064	4.5	
7	Butkovich and Landauer (1960) [laboratory experiments]	2	1	0.129	1	-5
			2	0.284	3	
8	Voitkovski (1963) [laboratory experiments]	1	1	0.252	2.1	-1.2
9	Paterson and Savage (1963)	1	1	0.044	4.2	~ 0
10	Mellor and Smith (1966) [laboratory experiments]	2	1	0.085	1	-4
				0.028	3.5	
11	Kamb and Shreve (1966; unpublished data)	1	1	0.040	5.2	~ 0
12	Raymond (unpublished, p. 225) [all of boreholes]	1	1	0.076	3.57	~ 0
13	Raymond (unpublished, p. 225) [bottom of boreholes only]	1	1	0.060	3.13	~ 0
14	Shreve and Sharp (1970)	1	1	0.550	3.3	~ 0
15	Colbeck (unpublished) [lab. exp.] [actual data]	3	1	0.315	1	~ 0
			2	0.63	3	
			3	0.74	5	
16	Colbeck (unpublished) [lab. exp.] [corrected for grain size]	3	1	0.013	1	~ 0
			2	0.025	3	
			3	0.030	5	
17	Budd (unpublished data)	1	1	0.159	1.75	-

Table 16. The parameters for the flow law of ice (equation 26) which have been determined to date. Experiments below -5°C have been omitted. All values have been adjusted so that the effective shear stress and strainⁿ rate are used. The temperature is in $^{\circ}\text{C}$. The units of A_k are $\text{bar}^{-n} \text{a}^{-1}$. Notes are as follows:

- 2, 3 Uniaxial compression tests on laboratory polycrystalline ice. Values are given for two different interpretations of the data. The quasi-viscous interpretation is generally regarded as the more reliable since Andrade's correction for transient creep has been applied.
- 5, 6 Based on deformation of boreholes. The ice is assumed to be at the

pressure-melting point.

- 7,10 No correction for transient creep.
- 9 Based on deformation of boreholes in Athabasca Glacier, Alberta, Canada. The ice was originally assumed to be at the pressure-melting point; however, more recent measurements of Paterson (1972) indicate late summer temperatures of -2°C to 0°C at 10 m below the surface in the ablation area, particularly near the equilibrium line. The accumulation area was found to be at 0°C . The value of n was assumed to be 4.2 because the data appeared to agree with Glen's data.
- 11,14 Based on deformation of boreholes in the lower Blue Glacier, Washington, U.S.A. Temperature measurements of Harrison (1972) ranged from -0.03°C near the surface to -0.13°C at a depth of 105 m in a borehole near the equilibrium line (ice thickness about 125 m). Unpublished data furnished by Raymond (personal communication, 1972).
- 12,13 Based on deformation of boreholes in transverse profiles across Athabasca Glacier, Alberta, Canada. See temperature remarks in note #9.
- 15,16 Uniaxial compression tests on glacier ice from a tunnel in the Blue Glacier, Washington, U.S.A. No correction for transient creep was applied; the experiments were assumed to have continued long enough that steady-state creep had been reached.
- 17 Based on data from as many different glaciers as available, using a plot of $\log(s_d/h)$ versus $\log(\tau_b)$ (equation 36) and assuming no sliding (Raymond, personal communication, 1972).

inferred from *in situ* glacier measurements will be considered. This eliminates the three exceptions noted above. The parameters of Nye (1953) will be used as "average" values and those from the Blue Glacier boreholes as upper and lower limits.

11.1.4 Calculation of the Sliding Velocity

For our glacier model the only non-zero stress deviator component is

τ'_{xz} ; hence $\tau = \tau'_{xz}$ and

$$\dot{\epsilon} = \dot{\epsilon}_{xz} = \frac{1}{2} \frac{\partial v_x(z)}{\partial z} \quad (27)$$

where $v_x(z)$ is the velocity at depth z due to internal deformation. Substituting the flow law (26) and the stress solution (16) into (27), and

integrating, we get

$$s - s_b = 2 \sum_{k=1}^K A_k (\rho g \sin \alpha)^{n_k} \int_0^h (h - z)^{n_k} dz \quad (28)$$

where s is the measured surface velocity and s_b is the sliding velocity.

This yields the solution

$$s_d = s - s_b = 2 \sum_{k=1}^K A_k (\rho g \sin \alpha)^{n_k} \left(\frac{h^{n_k+1}}{n_k + 1} \right) \quad (29)$$

where s_d is the contribution to the measured surface velocity from internal deformation. This was obtained for $K = 1$ by Nye (1952).

11.1.5 *The Effect of the Valley Walls and Longitudinal Stress Gradients*

The glacier model used above must be modified to allow a more realistic channel geometry. The drag exerted by the valley walls and variations in the slope of the bed mean that many, or all, or the other stress components are no longer negligible.

To estimate the effect of the valley walls most workers (for example, Nye, 1952) have used the "classical shape factor":

$$f = \frac{A}{PH} \quad (30)$$

where A is the cross section area, P is the perimeter in contact with the ice, and H is the depth at the centerline (Figure 102). This is determined by balancing the total gravitational force in the downslope direction exerted on a transverse section of unit thickness with the mean shear stress exerted by the bed on the section:

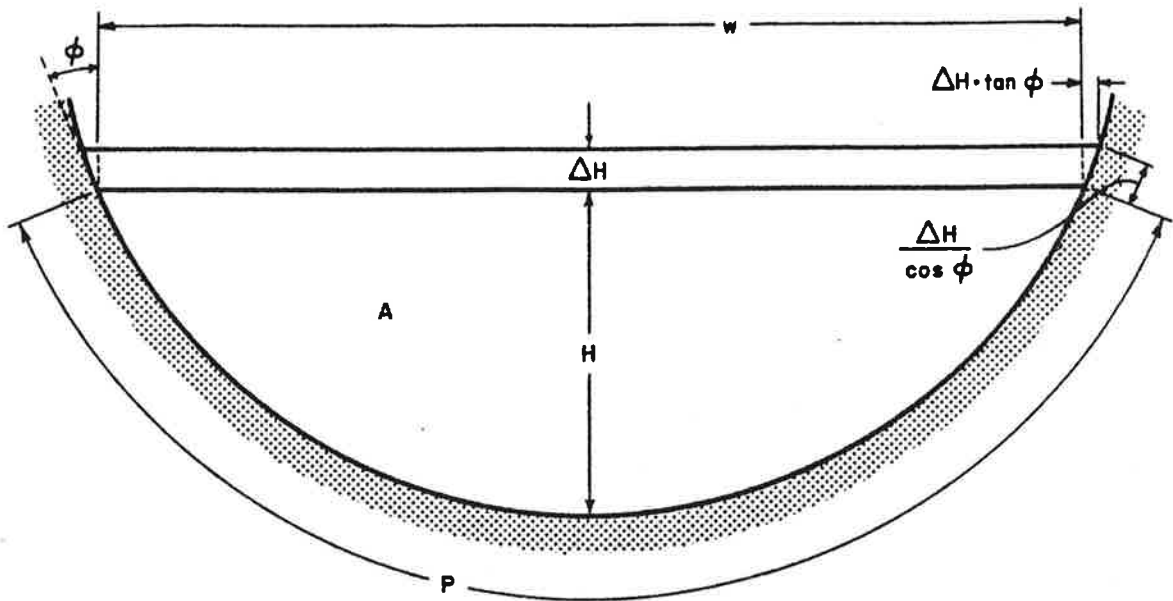


Figure 102. The effect of thickness changes on the classical shape factor. A is the cross section area, P is the perimeter in contact with the ice, w is the width, and H is the depth on the centerline.

$$\rho g(\sin \alpha)A = \langle \tau_b \rangle P \quad (31)$$

$\langle \tau_b \rangle$ is calculated by assuming (a) it is equal to the average shear stress at the bed on the centerline, and (b) the shear stress varies linearly with z :

$$\tau'_{xz} = \left(\frac{H-z}{H} \right) \langle \tau_b \rangle = \frac{A}{PH} \rho g(H-z) \sin \alpha \quad (32)$$

Comparison with equation (16) gives

$$\tau'_{xz} = \rho g f (H-z) \sin \alpha \quad (33)$$

where f is defined by (30). The basal shear stress at the bed of the glacier is reduced by the factor f because now the glacier can be "supported" by the

friction of the valley walls.

The velocity in a transverse section of a glacier was calculated numerically by Nye (1965), assuming there was no longitudinal velocity gradient and no sliding. He found that τ'_{xz} deviated from a linear dependence on z (except in special circumstances), contrary to the above assumption. If, however, equation 33 is integrated up the Z axis and f chosen so that the true velocity at the surface results, Nye was able to calculate an effective shape factor f' . Values of f' and f are listed in Table 17 for various channel cross sections and various half-width to depth ratios W .

W	Rectangle		Ellipse		Parabola	
	f'	f	f'	f	f'	f
0.5	0.31	0.33	0.28	0.33	--	0.29
1	0.56	0.50	0.50	0.50	0.45	0.45
2	0.79	0.67	0.71	0.65	0.65	0.58
3	0.88	0.75	0.80	0.70	0.75	0.62
4	--	0.80	0.85	0.73	0.81	0.64
∞	1.00	1.00	1.00	0.785	1.00	0.67

Table 17. Values of the classical shape factor, f , and the Nye shape factor, f' , for various channel cross sections and various half-width to depth ratios, W . (from Budd, 1969, p. 45)

For $W > 1$, and the particular channel shapes he considered, Nye's shape factors are always greater than the classical shape factors and approach one much faster as $W \rightarrow \infty$. Thus with Nye's assumptions the valley walls are less important than the classical shape factor predicts and the model of an infinitely wide glacier is fairly reasonable, especially for large W .

The effect of the variation of longitudinal stresses along the glacier, caused by variations in the slope of the bed and the surface, is much more difficult to estimate. The results of Collins (1968) show that the basal shear

stress should be given by

$$\tau_b = \rho g h \sin \alpha + \frac{\partial \bar{F}}{\partial x} \quad (34)$$

where

$$\bar{F} = h(\bar{\tau}_{xx} - \bar{\tau}_{zz}) \quad (35)$$

is the mean "longitudinal force" over the glacier thickness. Evaluation of this correction term requires measurements of the longitudinal and transverse strain rates (as well as the use of the flow law and incompressibility). Since the data obtained from the Nisqually Glacier do not allow evaluation of the transverse strain rates, this technique cannot be used.

Budd, however, has studied the effect of longitudinal stresses extensively and he concludes (Budd, 1968; 1969, p. 117; 1970, p. 24) that the term involving longitudinal stress gradients can be neglected on distance scales of the order of 10-20 times the ice thickness. This amounts to smoothing, or averaging, the parameters h , α , and f in the velocity solution (29) over such distances. This is particularly true of the surface slope α since it is the derivative of h and thus is more sensitive to spatial fluctuations.

This result agrees with calculations done on the flow of the Blue Glacier (Meier, Kamb, Allen and Sharp, in press). They found that the ice flux calculated by the theory used here can be made to agree with the ice flux calculated from continuity only if a constant slope, averaged over the entire region studied, was used. The averaging distance was about $10h$. They conclude that the local surface slope influences the local surface velocity field but that the deformation at depth is averaged mechanically by the longitudinal stress gradients.

We shall use this approach. Combining (30) and (33) and denoting the average values of h , α , and f by \bar{h} , $\bar{\alpha}$, and \bar{f} we get the final expression

for the speed due to internal deformation:

$$s_d = 2 \sum_{k=1}^K A_k (\bar{f} \rho g \sin \bar{\alpha})^{n_k} \left(\frac{\bar{h}^{n_k+1}}{n_k + 1} \right) \quad (36)$$

11.2 APPLICATION TO THE NISQUALLY GLACIER

The speed s_d depends on the three variables \bar{h} , $\bar{\alpha}$, and \bar{f} and the choice of the flow law parameters A_k and n_k . The thickness is given by

$$\bar{h} = \bar{h}_0 + \Delta h(x, t) \quad (37)$$

and the surface slope by

$$\bar{\alpha} = \bar{\alpha}_0 + \Delta \alpha(x, y) \quad (38)$$

where $\Delta h(x, t)$ and $\Delta \alpha(x, t)$ are the measured changes in surface elevation and surface slope (chapters 7 and 8 respectively). [From now on we drop all subscripts and primes on x and t , with the understanding that x is the curvilinear value and x and t are specified at the fixed values of the standard grid.] Since Δh and $\Delta \alpha$ are measured with respect to the standard (1966) surface, h_0 and α_0 are the thickness and slope of this surface. By only smoothing h_0 and α_0 , and not Δh and $\Delta \alpha$ as well, we are expressing the fact that the local changes in the velocity field are governed by local variations in depth and slope whereas the overall deformation is governed by long distance averages.

The measured values of thickness are specified in the vertical direction but the theory defined h as normal to the surface. No adjustments were made to the measured data since the corrections (less than 2-3 m) are smaller than

the uncertainty in the depth.

The remaining variable is the shape factor f . The glacier cross sections at each of the standard stake positions are shown in Figures 103 to 105. It is very difficult to decide which approximates each cross section: a parabola, an ellipse or a rectangle. Choosing a Nye shape factor from Table 17 is not easy. Thus it was decided to use the classical shape factor instead. Later, when discussing the effects of uncertainties in h and α we shall also include uncertainties in f .

The Nisqually Glacier undergoes annual thickness changes of approximately 10% of its thickness. To examine the effect of these changes on the shape factor consider a uniform change in surface elevation, ΔH (Figure 102). The corresponding change in the area is approximately

$$\Delta A \approx w\Delta H + \Delta H(\tan \phi)\Delta H \quad (39)$$

and in the "iced perimeter",

$$\Delta P \approx \frac{2\Delta H}{\cos \phi} \quad (40)$$

Differentiating (30),

$$\Delta f \approx \frac{\Delta A}{PH} - \frac{A}{P^2H} \Delta P - \frac{A}{PH^2} \Delta H \quad (41)$$

and substituting (39) and (40) we get

$$\frac{\Delta f}{f} \approx \frac{\Delta H}{H} \left\{ \frac{wH}{A} + \frac{H\Delta H(\tan \phi)}{A} - \frac{2H(\sec \phi)}{P} - 1 \right\} \quad (42)$$

Assume the cross section of the glacier is a triangle. Then

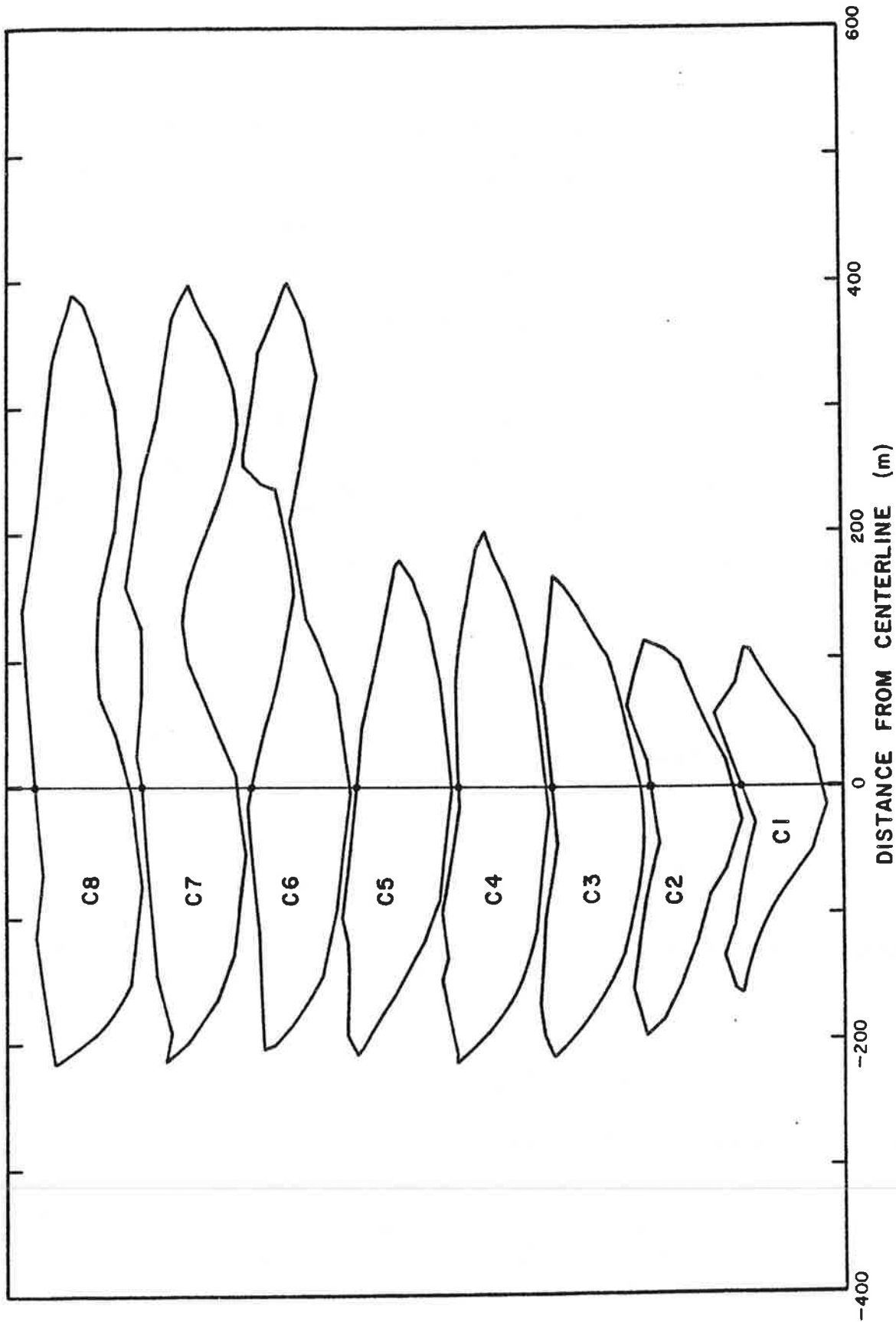


Figure 103. The glacier cross sections at centerline stakes C1 to C8. Each profile is perpendicular to the centerline at the standard stake positions and has an arbitrary Z origin and no vertical exaggeration.

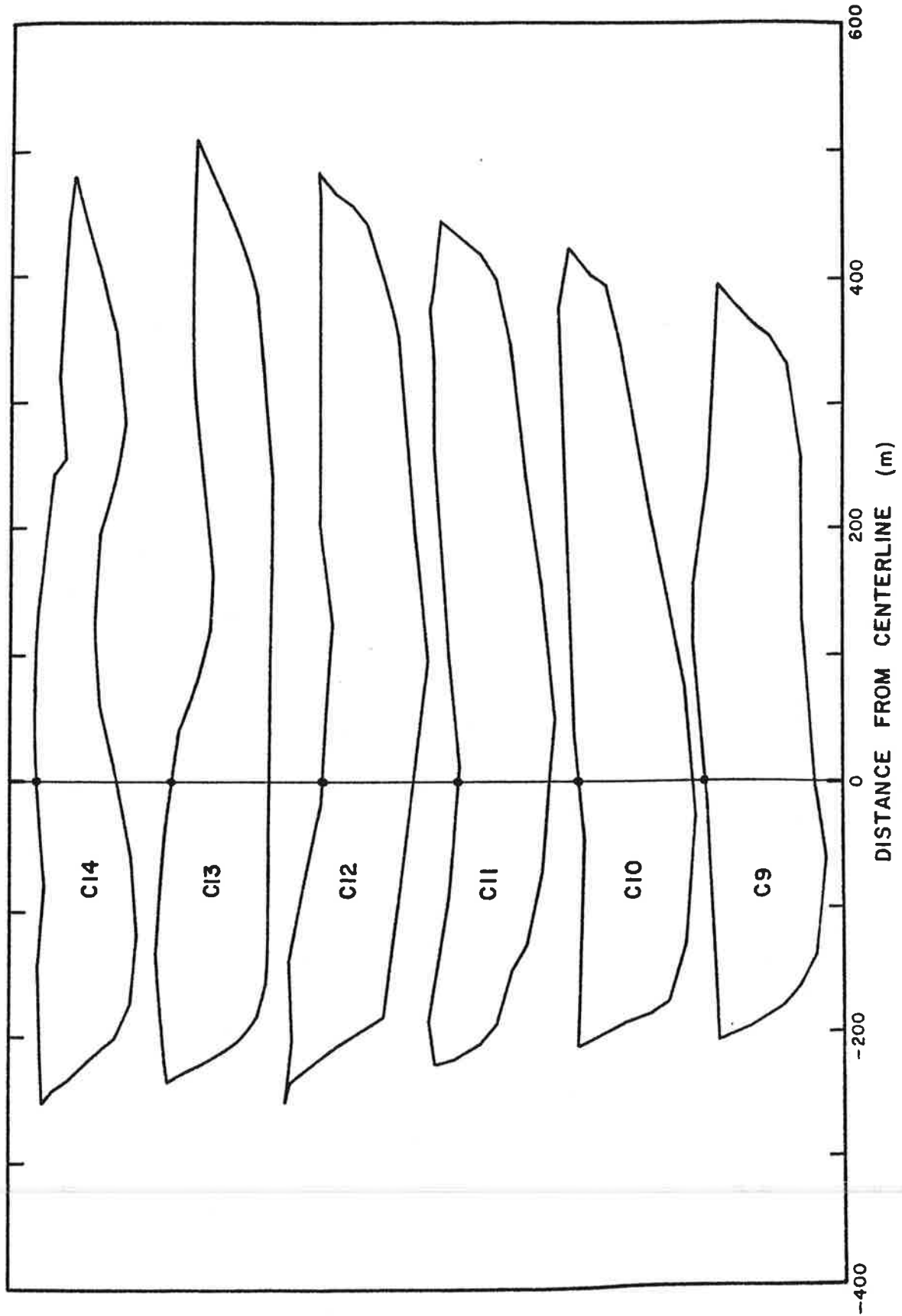


Figure 104. The glacier cross sections at centerline stakes C9 to C14.

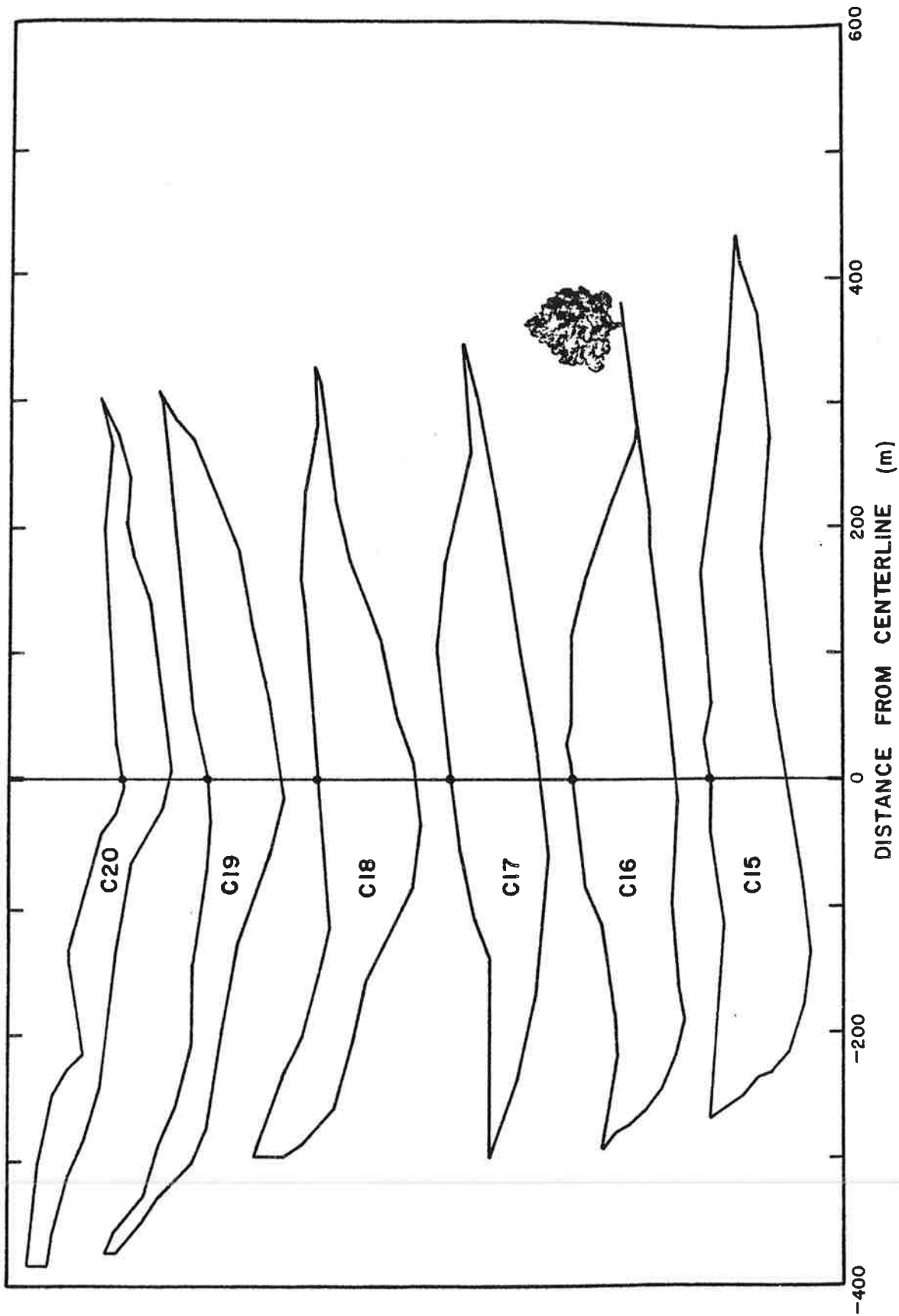


Figure 105. The glacier cross sections at centerline stakes C15 to C20.

$$\Lambda = \frac{wH}{2} \quad \text{and} \quad H \sec \phi \approx \frac{P}{2} \quad (43)$$

Substituting these into (42) gives

$$\frac{\Delta f}{f} \approx \frac{\Delta H}{H} \frac{2\Delta H \tan \phi}{w} \quad (44)$$

In most glaciers, $\tan \phi < 1$. Furthermore, $\frac{\Delta H}{w} \ll 1$ and so $\frac{\Delta f}{f} \ll \frac{\Delta H}{H}$. Since $\frac{\Delta H}{H}$ is small we conclude that $\frac{\Delta f}{f} \ll 1$ and that, to a first approximation, the classical shape factor is unaffected by changes in surface elevation. Therefore we assume f is independent of time.

Figure 106 shows elevation profiles of the bed and the surface along the glacier centerline. These were obtained from Figure 56 using linear interpolation between the 40-foot contours. From this the ice thickness $h_0(x)$ was calculated (Figure 107, dotted line).

A smoothing distance of $D = 600$ m, about eight times the ice thickness, was decided upon. This is reduced as necessary at the ends of the glacier so that unreliable extrapolations are avoided. The value of $D \approx 8h$ is a compromise between Budd's values of $10-20h$ and the desire to keep these regions of reduced interval to a minimum. Later calculations will allow us to examine the effect of choosing a *constant* h , α , or f , equivalent to about $30h$.

For comparison, the calculations were also done using a smoothing distance of $D = 75$ m, approximately the average ice thickness, and Figure 107 shows the smoothed thickness $\bar{h}_0(x)$ for both values of D . All smoothing is done numerically using a simple running average. Three passes are made to eliminate any small wavelength fluctuations.

The surface slopes were calculated from the 1966 surface elevation profile of Figure 106 using the relation

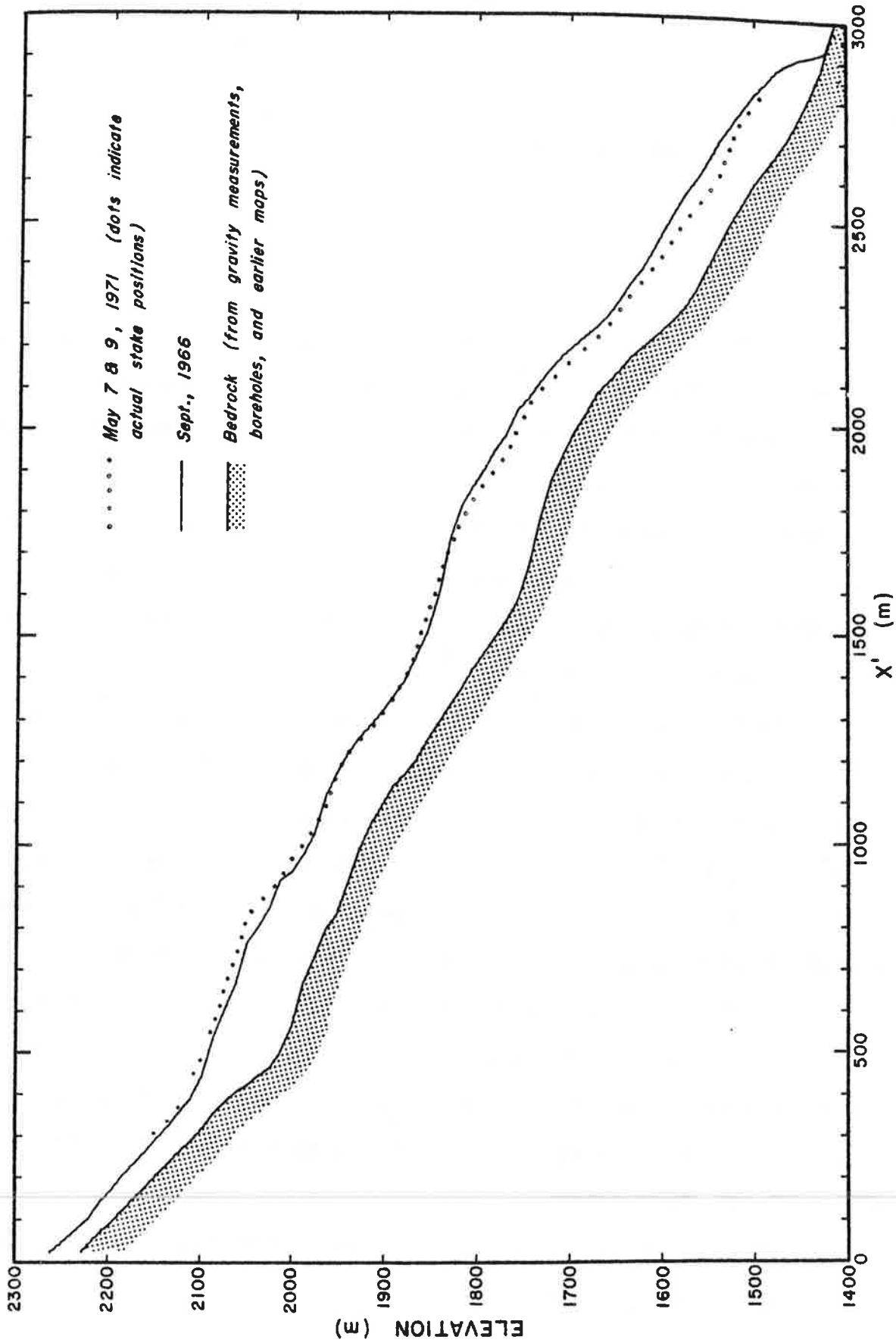


Figure 106. Surface and bed elevation profiles along the centerline of the Nisqually Glacier. The vertical exaggeration is approximately 2.2:1. The dots indicate the surface profile determined in May 1971.

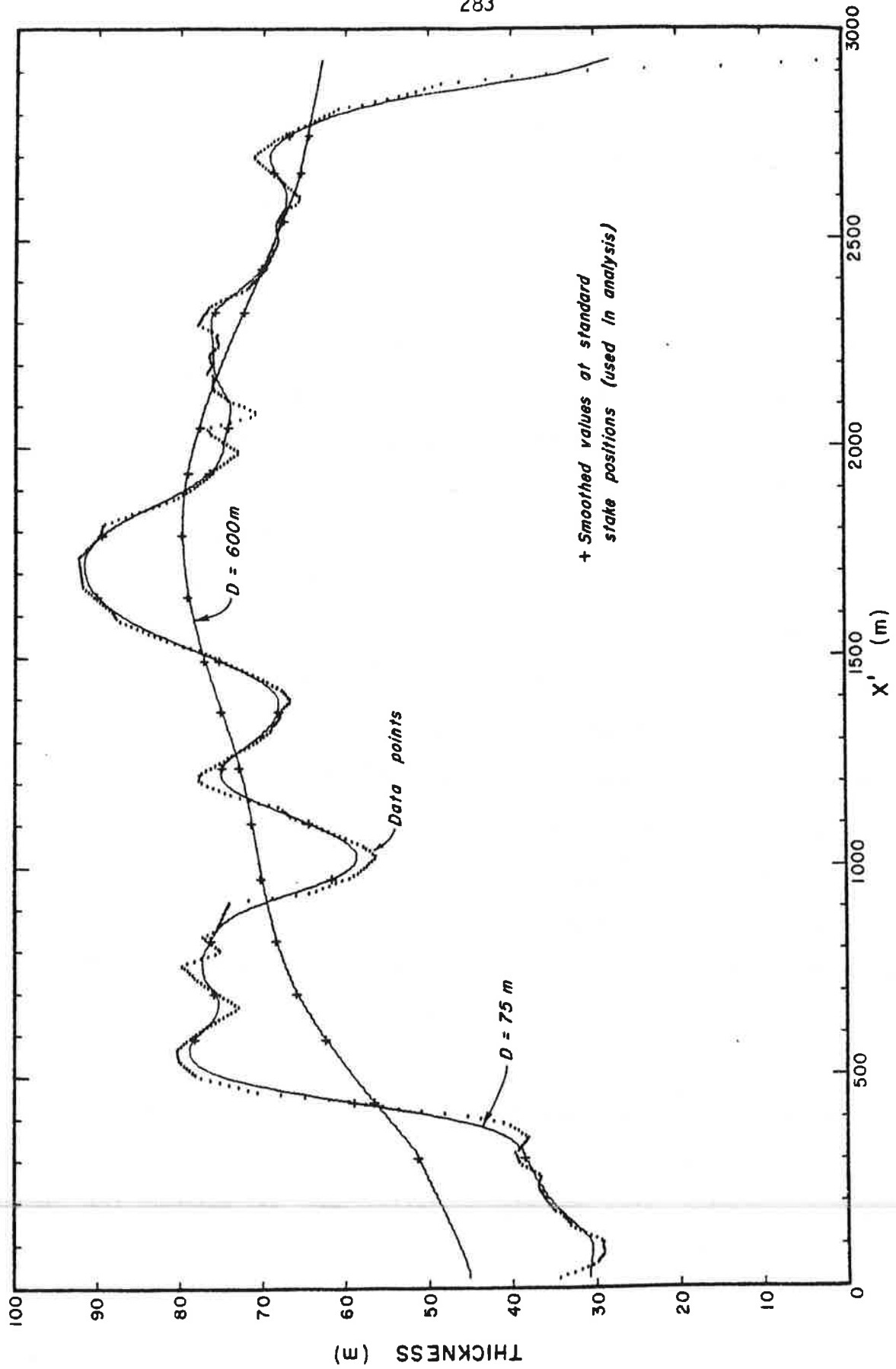


Figure 107. The ice thickness $h_0(x)$. The data points come from Figure 106. The solid lines are averages $\bar{h}_0(x)$ over 75 and 600 m.

$$\alpha = \tan^{-1} \left| \frac{\Delta z}{D} \right| \quad (45)$$

Only two passes were made when smoothing the slopes since use of this equation is itself a smoothing procedure. The $\bar{\alpha}_0(x)$ curves are given in Figure 108 for both $D = 75$ and 600 m.

The classical shape factors were measured from the cross sections of Figures 103 to 105 and are denoted by the square symbols in Figure 109. The smoothed curves $\bar{f}(x)$ are also shown. The portion of the glacier at C6 east of the upper nunatak was omitted from the calculation of the shape factor.

The values of \bar{h} , $\bar{\alpha}$, and \bar{f} that are used in the analysis are indicated by the "+" symbols on each of the smoothed curves in these diagrams.

Figure 110 shows the surface speed due to internal deformation s_d as a function of time and distance. This was calculated with equation 36 using the average flow law parameters and the smoothed* values of \bar{h} , $\bar{\alpha}$, and \bar{f} . The variations of s_d are dominantly in x and not t . It was found that this was almost invariably the case, no matter what parameters were varied; hence the presentation of the results can be simplified by averaging over time. This will be denoted by the symbol $\langle \rangle$. Figure 111 shows $\langle s_d/s \rangle$, expressed in percent, for the average flow law (Nye) and the least viscous flow law (Shreve and Sharp). The "error bars" are the standard deviation in the time average and thus indicate the approximate magnitude of the time variations.

To show the effect of the smoothing, the calculations were repeated for the average flow law using the unsmoothed* variables. For clarity no "error bars" are shown. They are closely equal in size to the corresponding ones for the smoothed variables, since the time variations were not smoothed (see equations 37 and 38).

* The variables averaged over $D = 600$ m will be referred to as "smoothed" and over $D = 75$ m as "unsmoothed".

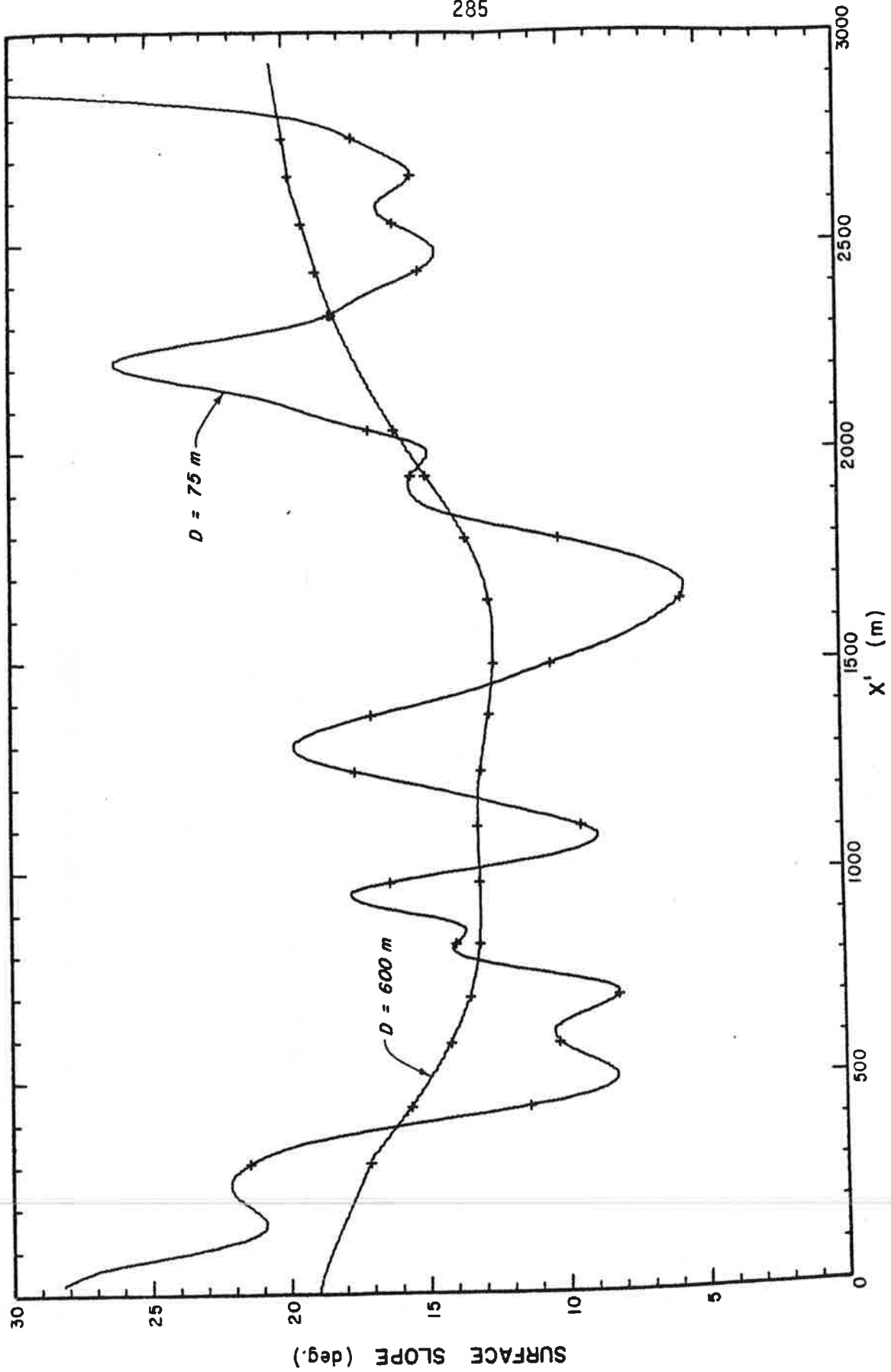


Figure 102. The surface slope $\bar{\alpha}_0(x)$. The values are calculated from the 1966 surface elevation profile of Figure 106, using the two averaging intervals 75 m and 600 m.

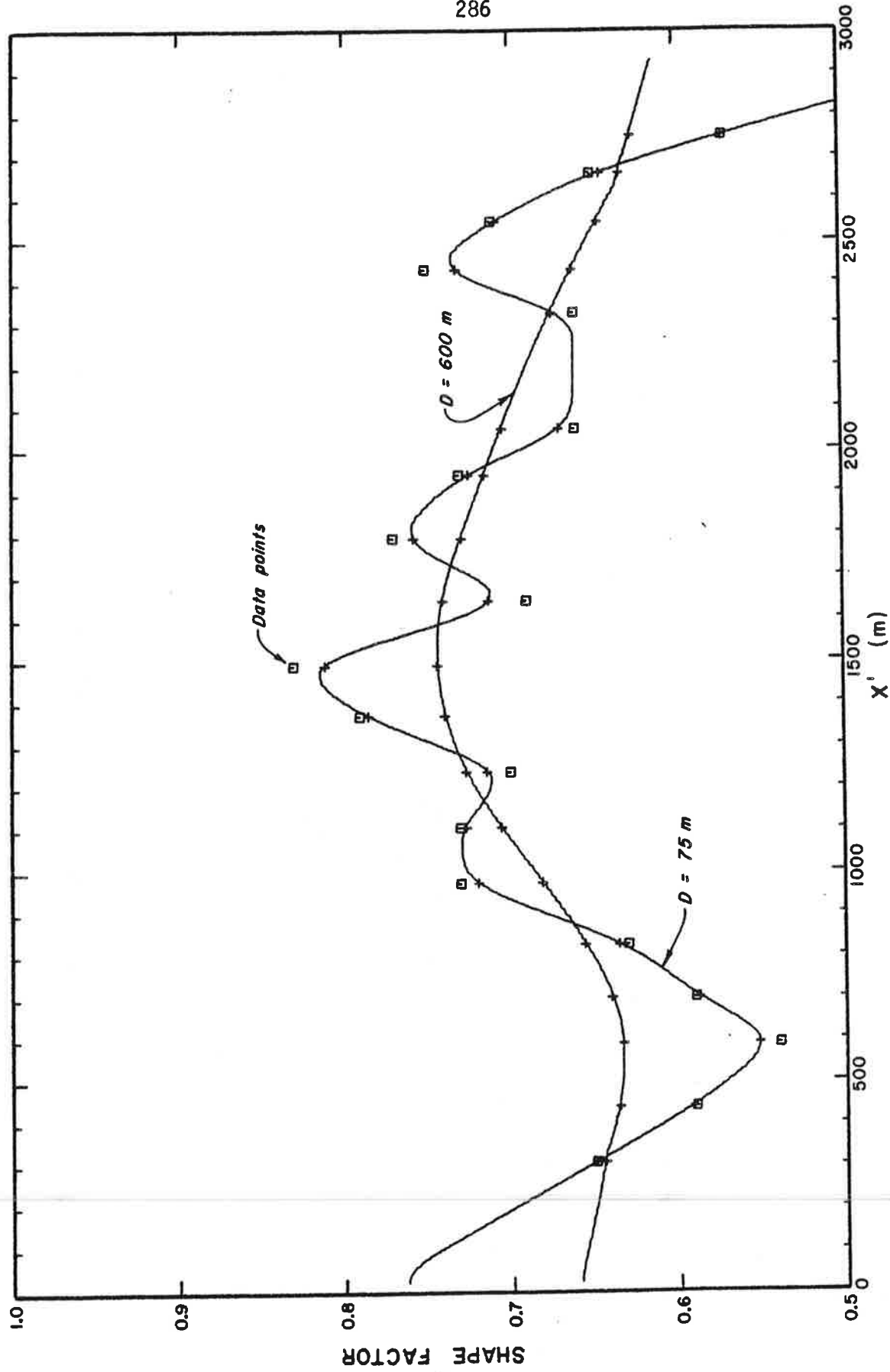


Figure 109. The classical shape factor $f(x)$. The data points (square symbols) are calculated from the cross sections of Figures 103-105. The solid lines are averages $\bar{f}(x)$ over 75 and 600 m.

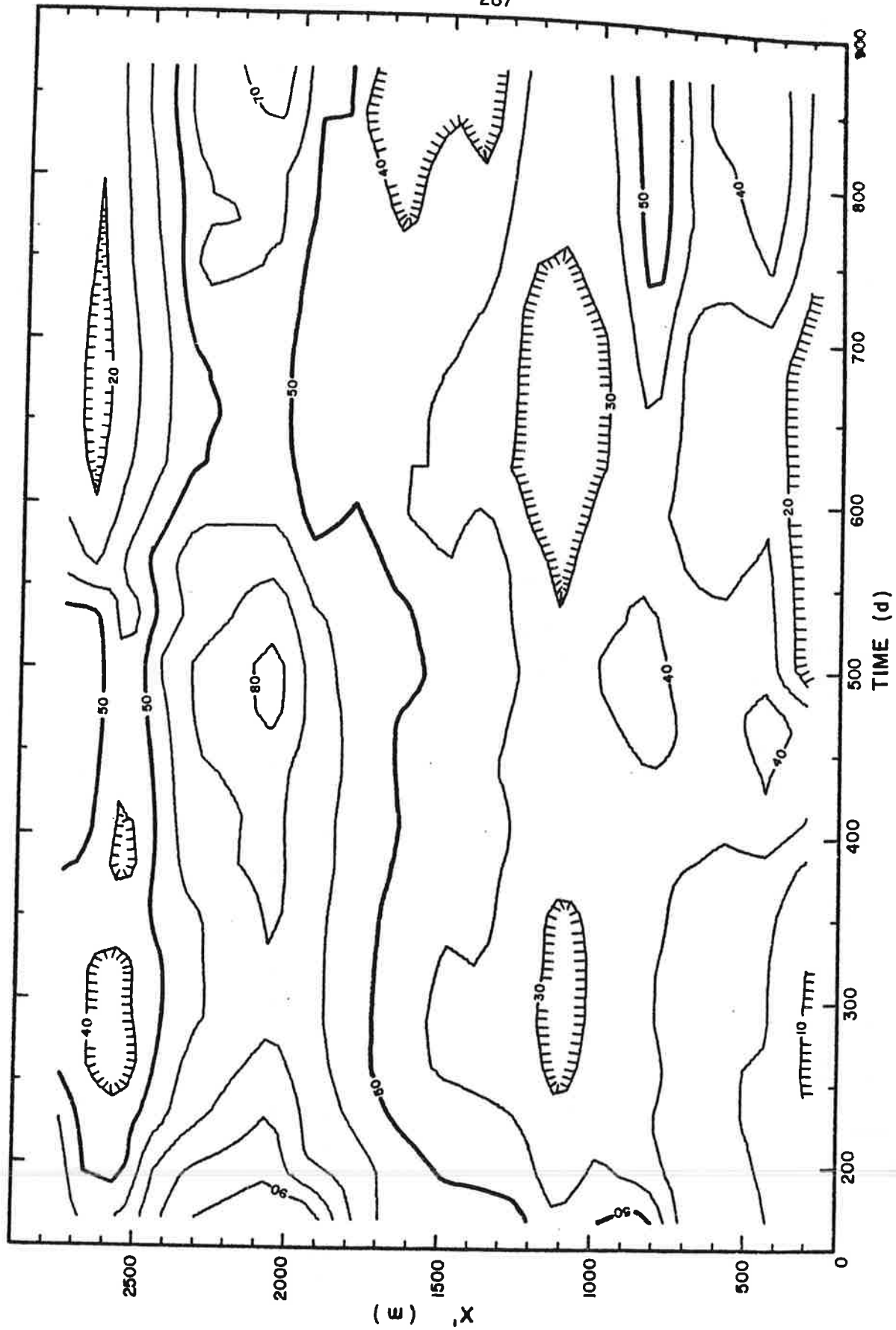


Figure 110. The surface speed due to internal deformation for the average flow law and smooth initial values of h , α , and \bar{f} . The contour interval is 10 mm d^{-1} .

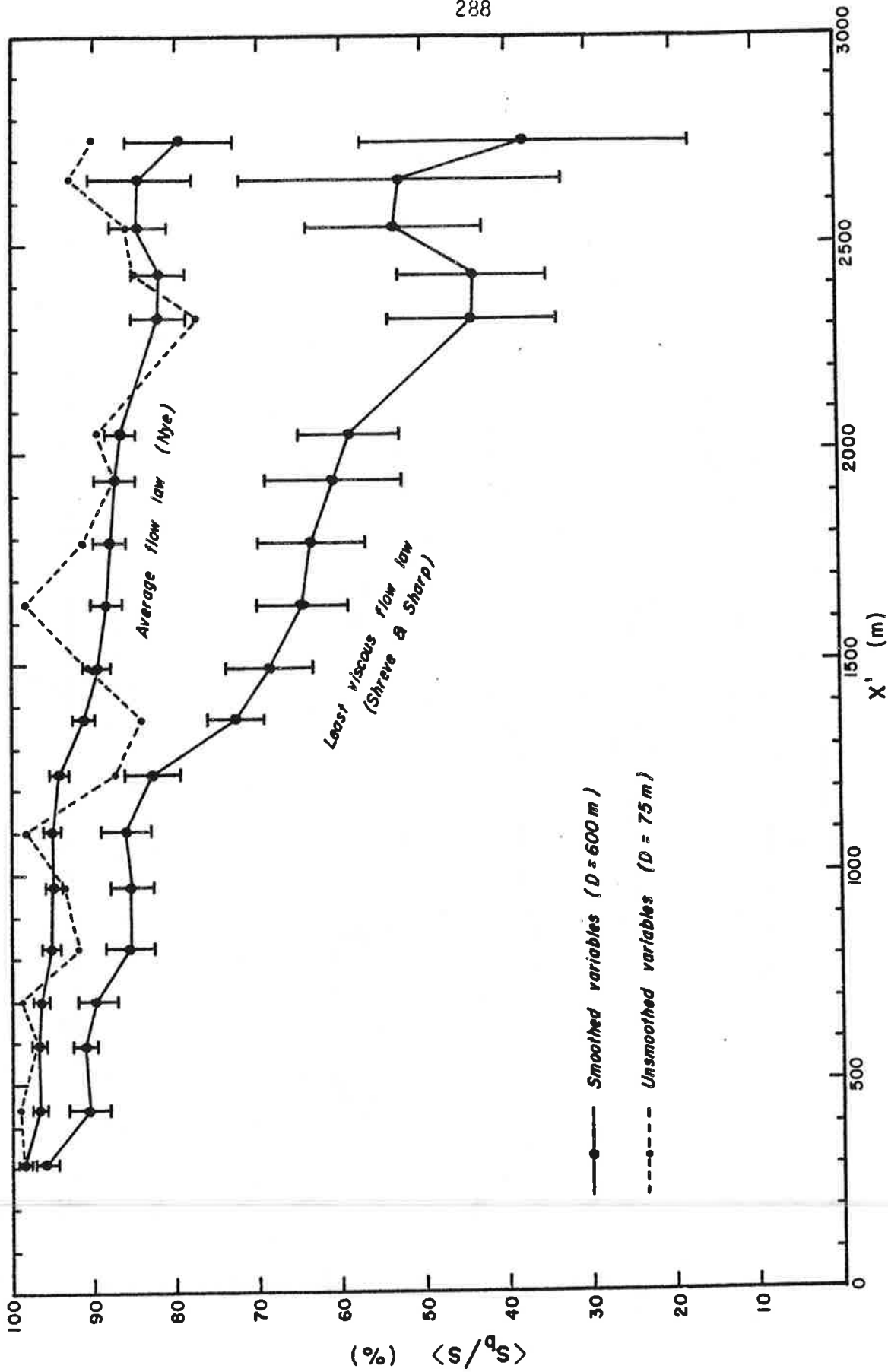


Figure 111. The time average of the ratio of sliding speed to measured surface speed for the average and least viscous flow laws. The "error bars" indicate the approximate magnitude of the time variations.

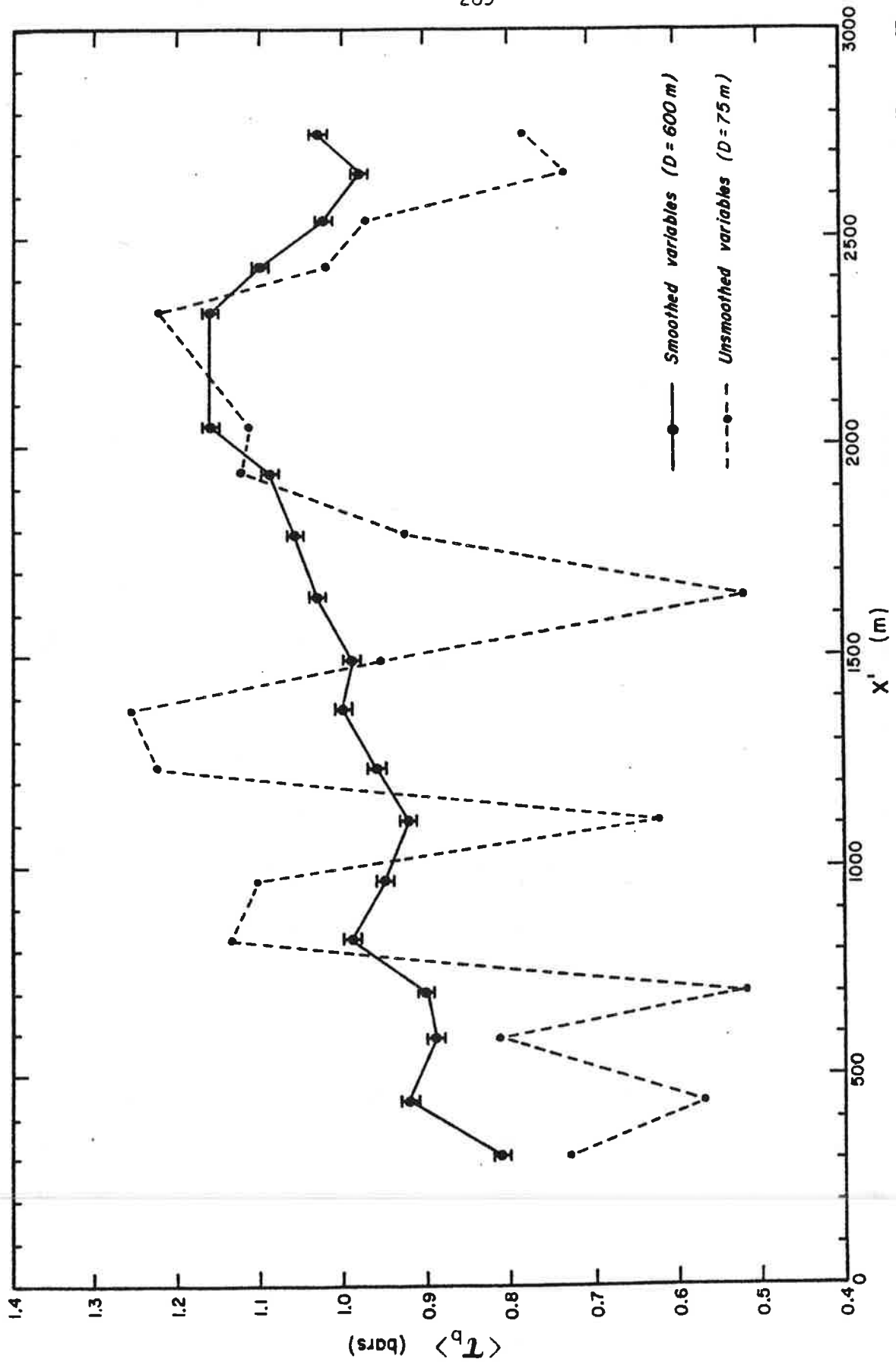


Figure 112. The time average of the basal shear stress for unsmoothed and smoothed values of \bar{h} , \bar{a} , and \bar{f} . The "error bars" indicate the approximate magnitude of the time variations.

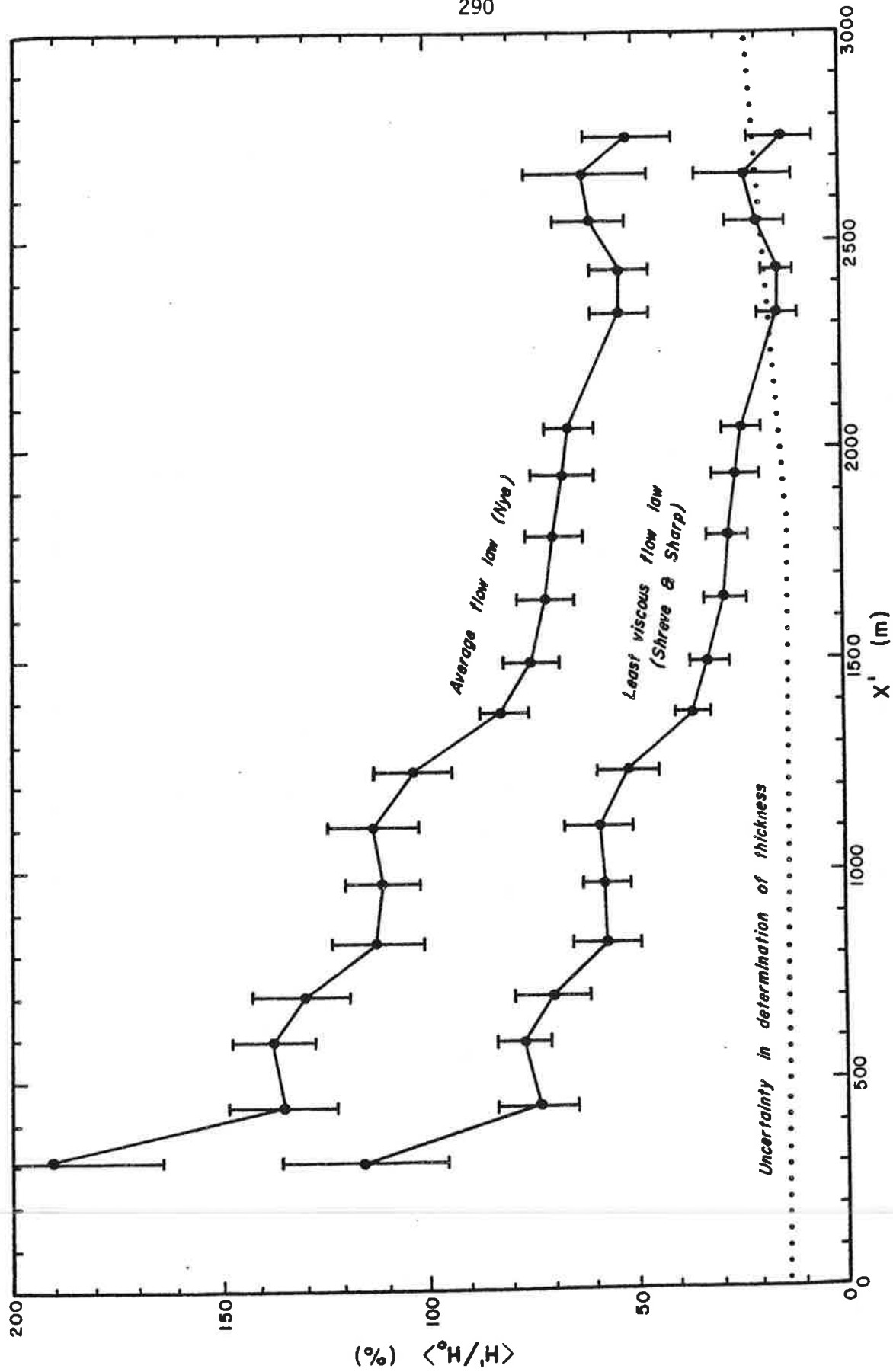


Figure 113. The time average of the ratio of the depth necessary for no sliding to the measured depth, for both the average and least viscous flow laws. The error bars indicate the approximate magnitude of the time variations.

Figure 112 gives a similar plot, this time of the average basal shear stress $\langle \tau_b \rangle$ calculated from equation 33. Only one curve is shown since this is independent of the flow law. The range of basal shear stresses is 0.5 to 1.25 bar ($D = 75$ m) or 0.8 to 1.15 bar ($D = 600$ m). It is interesting to note that the average of the smoothed basal shear stresses is 0.998 bar, in almost perfect agreement with the commonly-quoted "yield stress" of ice, 1 bar.

Since both flow laws we are using have $K = 1$ we can solve (36) for h in terms of s_d :

$$h' = \left\{ \frac{s(n_1 + 1)}{2A_1(\bar{f}\rho g \sin \bar{\alpha})^{n_1}} \right\}^{\frac{1}{n_1+1}} \quad (46)$$

When the measured surface speed is substituted for s_d , h' represents the depth necessary for no sliding. Average values $\langle h'/h_o \rangle$ are shown in Figure 113 for both flow law parameters.

The following points are apparent from these figures: (a) The noise is reduced considerably by using smoothed values of \bar{h} , $\bar{\alpha}$, and \bar{f} . This is to be expected, of course. (b) Internal deformation accounts for very little of the observed surface motion. Only with the least viscous of flow laws can s_d approach 50-60 % of the surface speed. (c) Internal deformation contributes progressively less to the surface motion as the distance from the terminus increases. In the upper third of the glacier, sliding accounts for well over 80 % of the motion. (d) If the ice thickness were the only variable, uncertainties in its determination could permit no sliding only near the terminus and only with the least viscous of flow laws. With average flow law parameters the depth would have to be increased from 50-200 %; it is highly unlikely that the ice depths are known this inaccurately. Furthermore, converting h to the normal component would tend to offset any places where the depths are too shallow.

11.3 THE EFFECT OF UNCERTAINTIES IN THE VARIABLES

The points mentioned at the end of the previous section are very significant results. A thorough examination of the effect of uncertainties in the variables \bar{h} , $\bar{\alpha}$, and \bar{f} , and the flow law parameters A_k and n_k , is essential before proceeding with an interpretation.

Unfortunately we are dealing with a complicated function of five variables and so illustrating the effect of perturbing any one, or combination, of these variables is not a straight-forward matter. The following analysis was developed for this purpose.

Define

$$\zeta = f \rho g \sin \alpha \quad (47)$$

This has dimensions of force per unit volume and can be interpreted as an "effective body force" in the down-slope direction. We choose the symbol ζ to distinguish this from the true body force $\underline{F} = \rho \underline{g}$. ζ is a function of f and α and is independent of the flow law; it is presented graphically in Figure 114. Typical bounds to f and α for the Nisqually Glacier are indicated by the smoothed and unsmoothed data points; the corresponding range in ζ is about 500-2000 N m^{-3} . [$1 \text{ N m}^{-3} = 10^{-5} \text{ bar m}^{-1}$]

Equation 36 now becomes*

$$s_d = 2 \sum_{k=1}^K A_k \zeta^{n_k} \left(\frac{h^{n_k+1}}{n_k + 1} \right) \quad (48)$$

Thus for a given (A_k, n_k) we can plot s_d as a function of ζ and h . This is done on a log scale in Figures 115 and 116 for the two sets of flow law

* We omit the bars over h , α , and f with the understanding that these variables may be smoothed or unsmoothed, as desired.

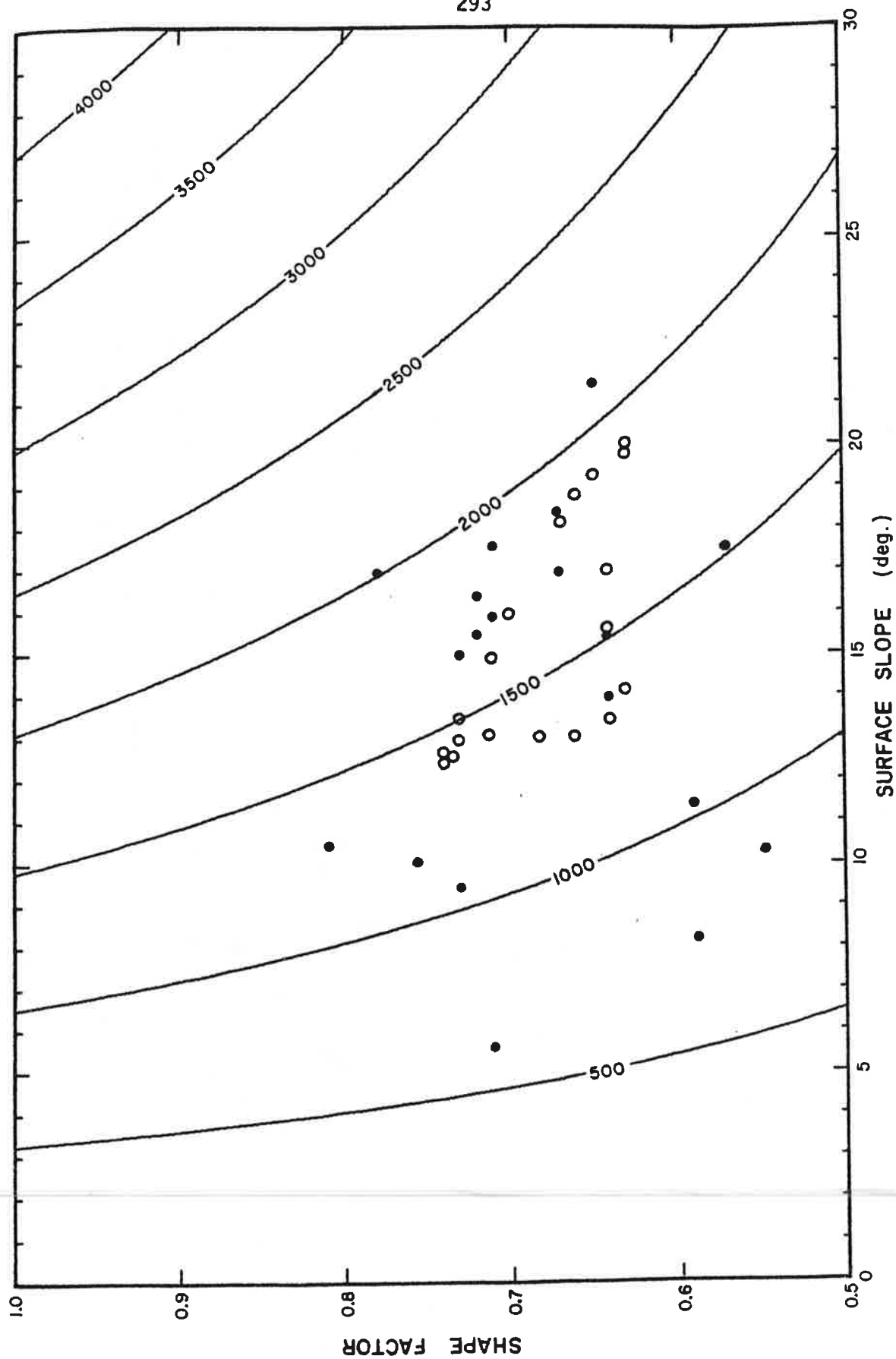


Figure 114. The effective body force τ as a function of surface slope and shape factor. The contour interval is 500 N m^{-3} . Unsmoothed and smoothed data values for the Nisqually Glacier are indicated by solid and open dots respectively.

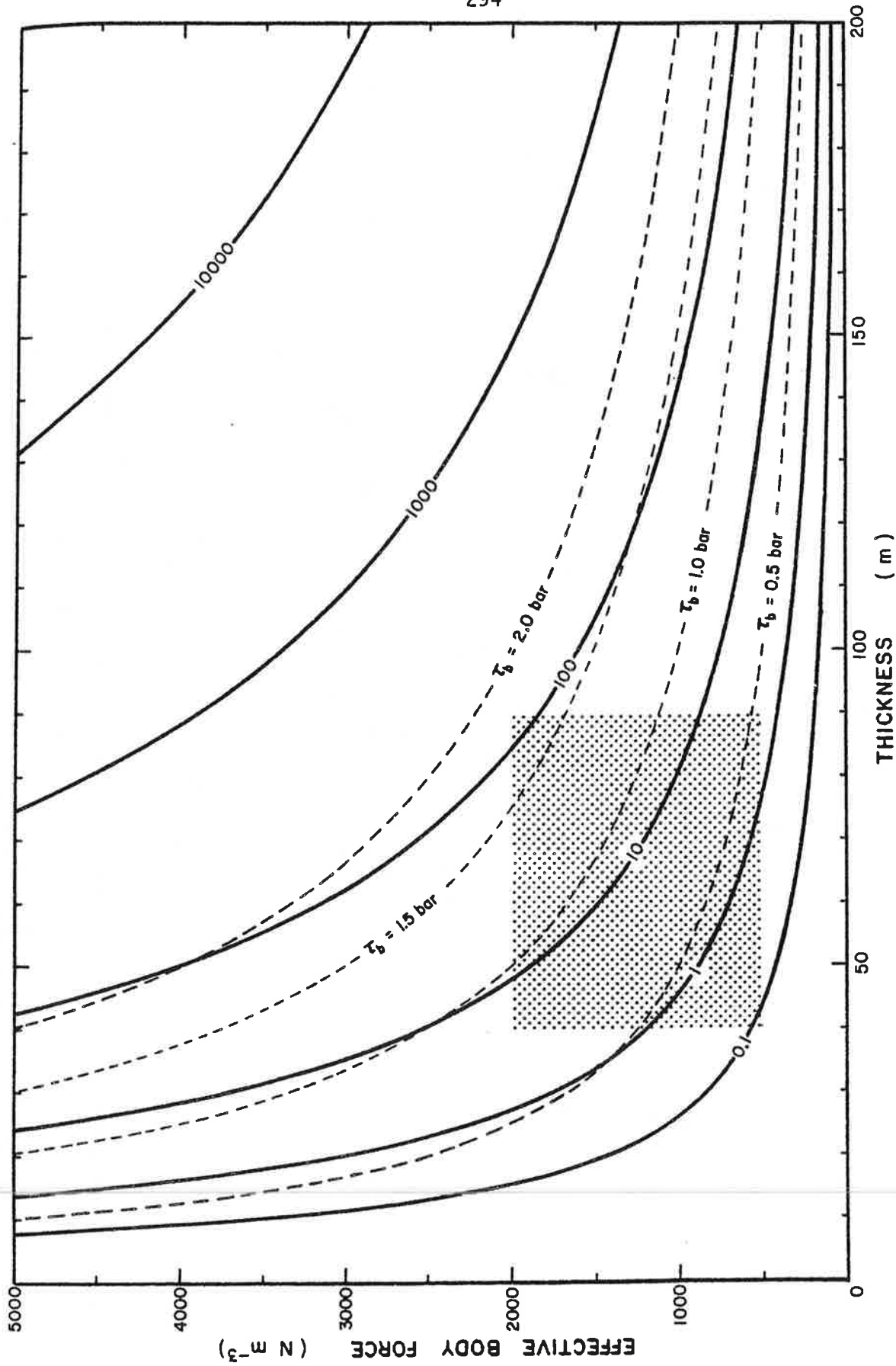


Figure 115. The speed due to internal deformation (solid lines) and the basal shear stress (dashed lines) as a function of thickness and effective body force, for the average flow law. The stippled area is the region pertinent to the Nisqually Glacier. The units of speed are $\text{mm}\ d^{-1}$.

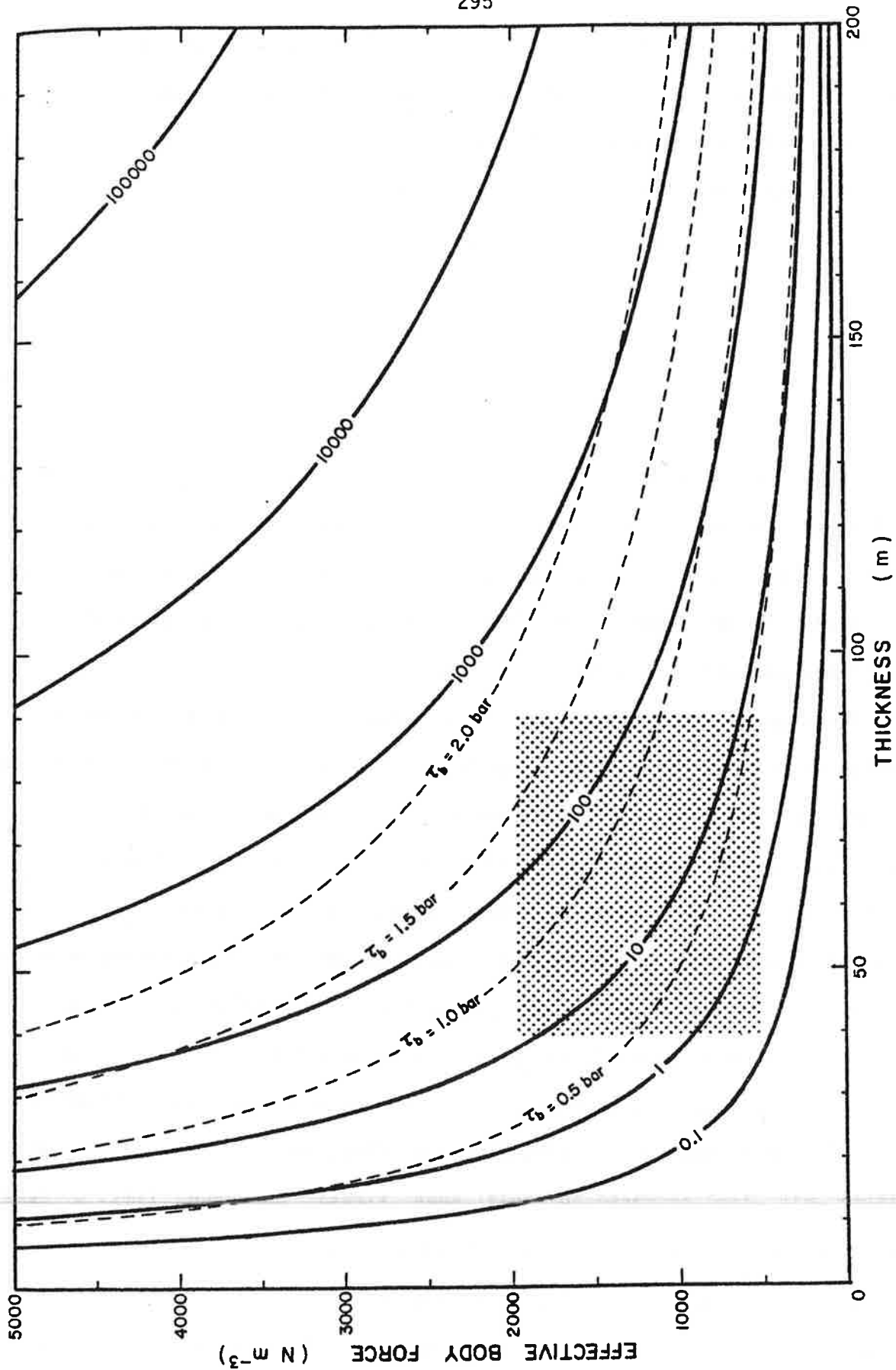


Figure 116. The speed due to internal deformation (solid lines) and the basal shear stress (dashed lines) as a function of thickness and effective body force, for the least viscous flow law. The stippled area is the region pertinent to the Nisqually Glacier. The units of speed are mm d^{-1} .

parameters we are considering. Bounds to h and ζ for the Nisqually Glacier are indicated by the stipled region (neglecting for now any uncertainties). Once a flow law has been decided upon, these $\zeta(\alpha, f)$ and $s_d(h, \zeta)$ plots can be used to determine $s_d(h, \alpha, f)$. The effect of choosing constant values for h , α , and f can now be easily ascertained.

Since

$$\tau_b = \zeta h \quad (49)$$

we can plot ζ as a function of h for various values of τ_b . This is done in Figures 115 and 116 to define the physically realistic region of the diagrams. The range of stresses usually found in ice masses is 0.1 to 1.5 bar and rarely reaches 2 bar (Budd, 1969). The stresses at the bed of the Nisqually Glacier are well within this range (Figure 112).

Now suppose we change f and α by amounts Δf and $\Delta \alpha$ respectively. The corresponding changes in ζ can be obtained from Figure 114, and the two changes $\Delta \zeta$ and Δh can now be used to calculate a new value of s_b/s . In practice, however, we have a grid of values, ζ_{ij} and h_{ij} . Perturbing each of these by $\Delta \zeta$ and Δh gives a corresponding grid of ratios s_b/s . This grid can then be averaged *in both distance and time* to give a single mean ratio $\langle\langle s_b/s \rangle\rangle$. If this procedure is repeated for various values of $\Delta \zeta$ and Δh we can construct a contour plot of $\langle\langle s_b/s \rangle\rangle$ as a function of $\Delta \zeta$ and Δh .

Figures 117 and 118 show such plots for the two flow laws. Given changes in h , α , and f one can now visualize the effect on $\langle\langle s_b/s \rangle\rangle$. These perturbations will also increase the basal shear stress; the upper limit to realistic values of τ_b is indicated by the dashed line.

We must now decide on probable values for $\Delta \alpha$, Δf and Δh . The surface slope is the most reliable of the three and is unlikely to be in error by more

than a degree. From Figure 114 we see that this has a much smaller effect on ζ compared to the uncertainty in the shape factor.

Values of the half-width to depth ratio W for the profiles of Figures 103-105 range from 2.0 to 5.5 (omitting C20, which is an incomplete cross section). The Nye shape factors (Table 17) could then range as high as 0.9, and the effective body force could be as much as 700 N m^{-3} too low.

The uncertainty in the ice thickness is $\pm 10 \text{ m}$ above the upper nunatak. Below here this might increase to $\pm 15 \text{ m}$, but we shall see that the final conclusions are affected little in this region by using the smaller limit. Also, as mentioned earlier, converting h to the normal component would offset some of this uncertainty.

Assuming then, that $\Delta\zeta = 700 \text{ N m}^{-3}$ and $\Delta h = 10 \text{ m}$, we see from Figure 117 that for the average flow law the mean ratio $\langle\langle s_b/s \rangle\rangle$ would drop from 90 % to about 50 %. Even with these uncertainties sliding still dominates the motion. On the other hand, if we use the least viscous flow law (Figure 118) internal deformation can account, on the average, for the magnitude of the surface motion provided h and ζ are increased *everywhere* by appropriate, but acceptable, amounts.

One must bear in mind that $\langle\langle s_b/s \rangle\rangle$ is a mean over the entire glacier, whereas Figure 111 shows that there is a very definite dependence on x . Although internal deformation could be important at the lower elevations, it might still be insignificant higher up the glacier.

To illustrate this effect when h , α , and f are perturbed, the calculation of $\langle s_b/s \rangle$ as a function of x was repeated for various values of Δh , using the average flow law and increasing the shape factors to unity everywhere (Figure 119). Only when h is increased by 10 m does the sliding contribution start to vanish near the terminus.

Figures 120 and 121 show the same plots for the least viscous flow law, the

former with f increased uniformly by 0.1 and the latter with f set to one. For $\Delta f = 0.1$, sliding accounts for over 50 % of the surface motion on the upper half of the glacier, provided Δh is 10 m or less. Even when f is increased to unity sliding is significant for $\Delta h \leq 10$ m.

We conclude, therefore, that *sliding is negligible on the Nisqually Glacier only if (a) the ice obeys the least viscous flow law, (b) the depth is everywhere too shallow by at least 10 m, and (c) the shape factors are close to unity.*

This, of course, is an extreme case and as such we consider it very unlikely. The conclusions reached at the end of the previous section (p. 291) still represent the most probable situation.

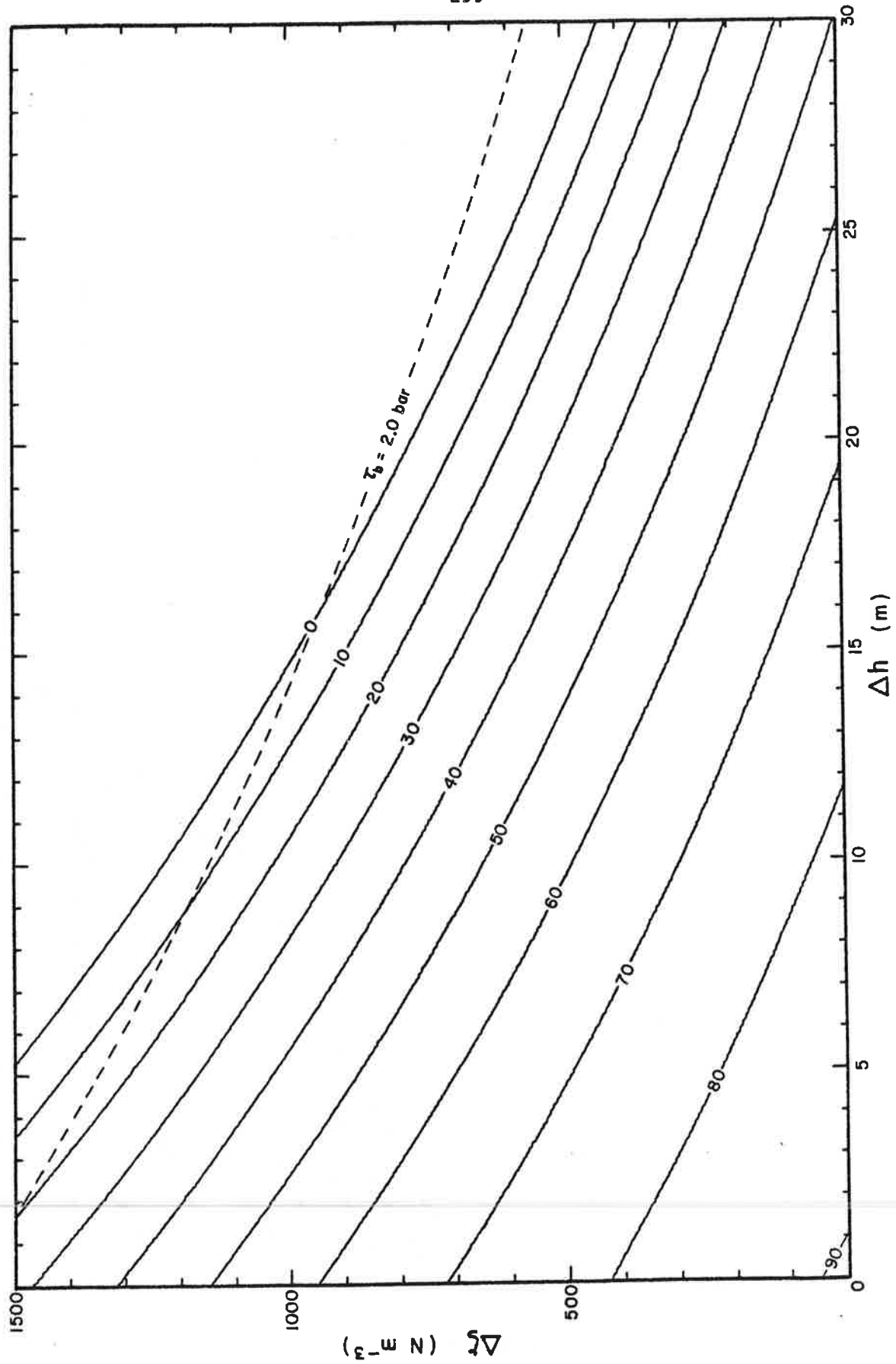


Figure 117. The mean ratio (in percent) of the sliding speed to the measured surface speed as a function of changes in thickness (Δh) and changes in effective body force ($\Delta\xi$), for the average flow law and smoothed values of h , a , and f .

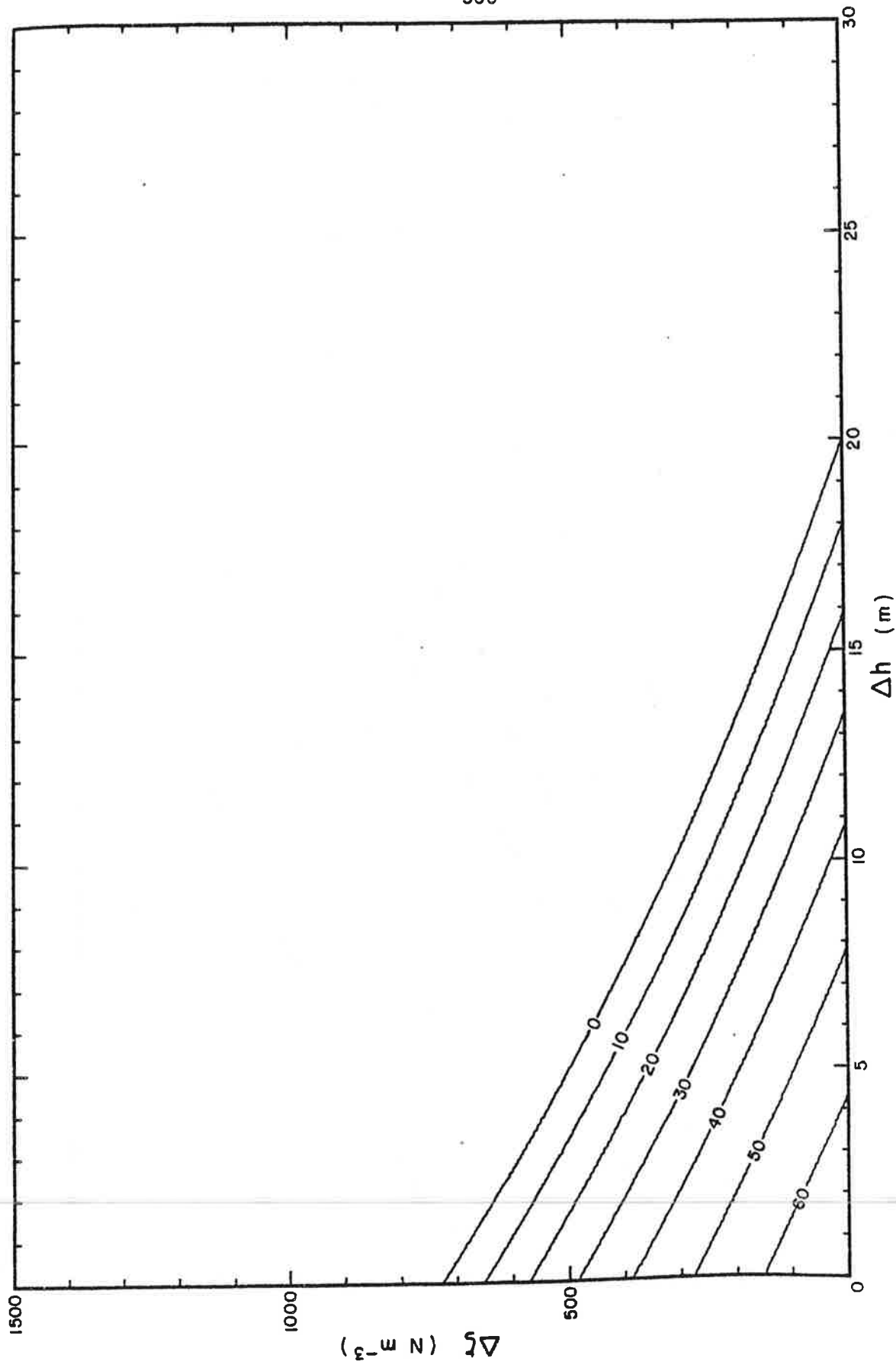


Figure 118. The mean ratio (in percent) of the sliding speed to the measured surface speed as a function of changes in thickness (Δh) and changes in effective body force ($\Delta\tau$), for the least viscous flow law and smoothed values of h , α , and f .

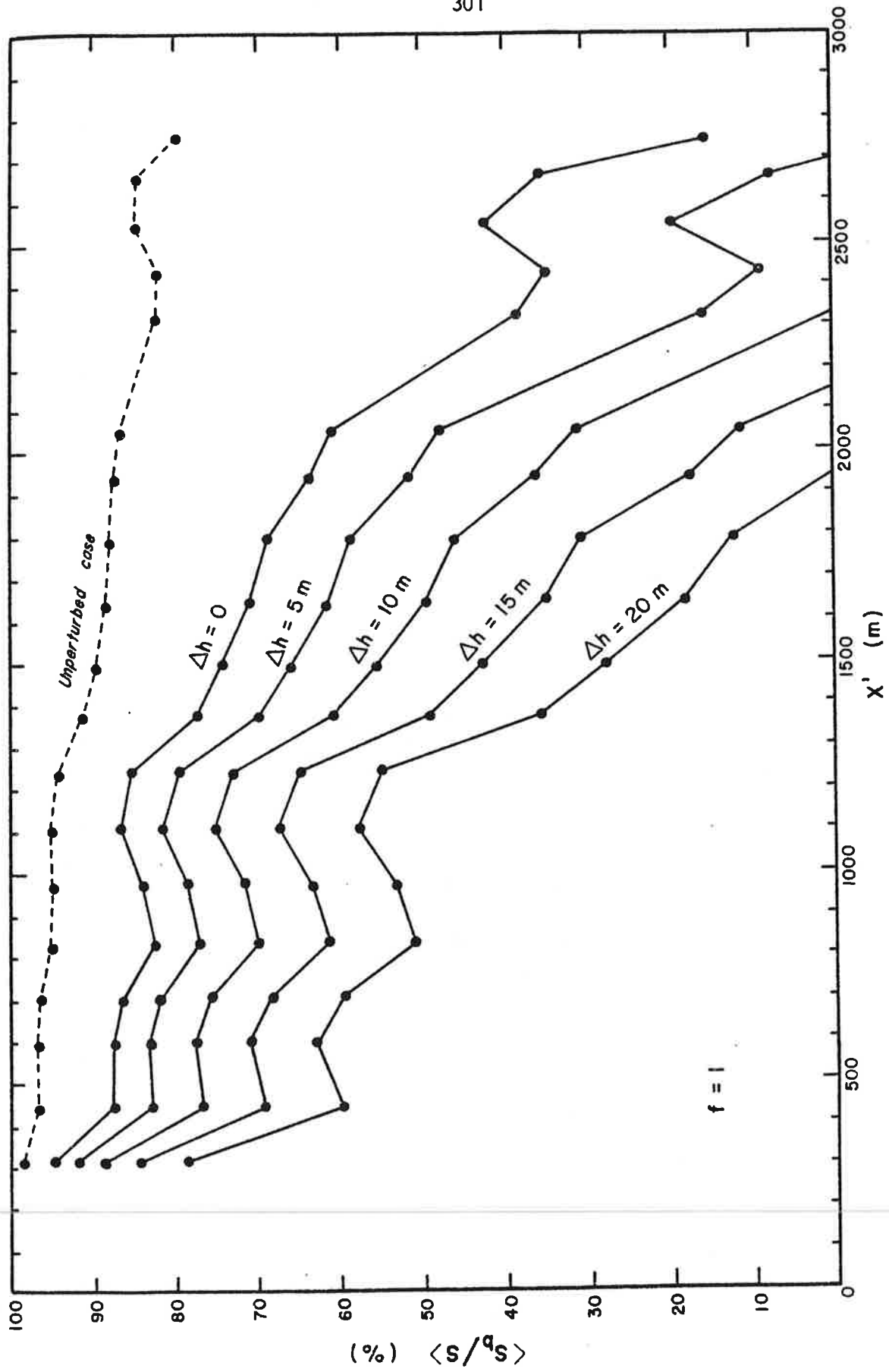


Figure 119. The time average of the ratio s_b/s for various changes in thickness (Δh), using the average flow law and increasing the shape factors to unity everywhere. Smoothed values of h and a were used.

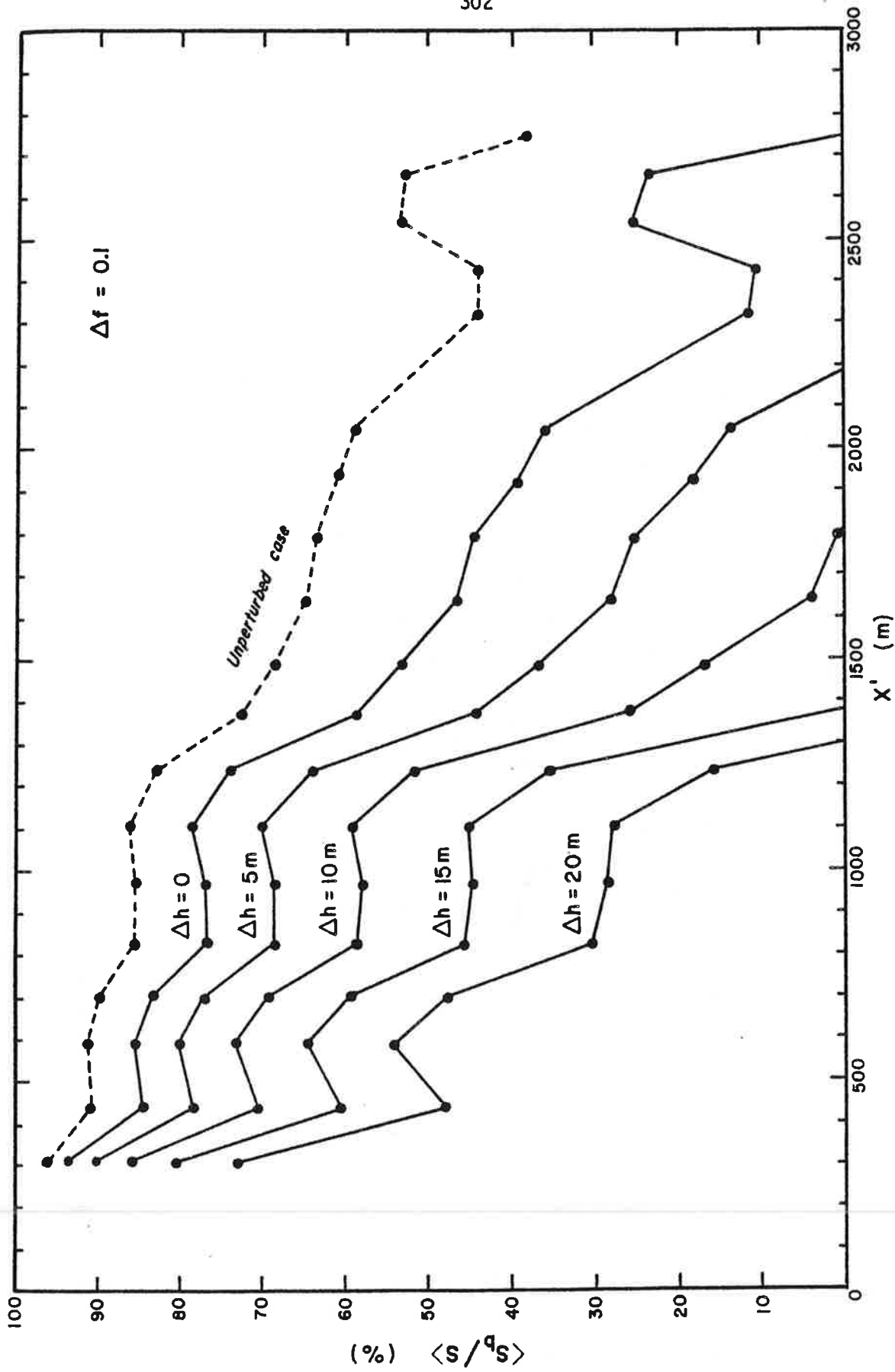


Figure 120. The time average of the ratio s_b/s for various changes in thickness (Δh), using the least viscous flow law and increasing the shape factors by 0.1 everywhere. Smoothed values of h and a were used.

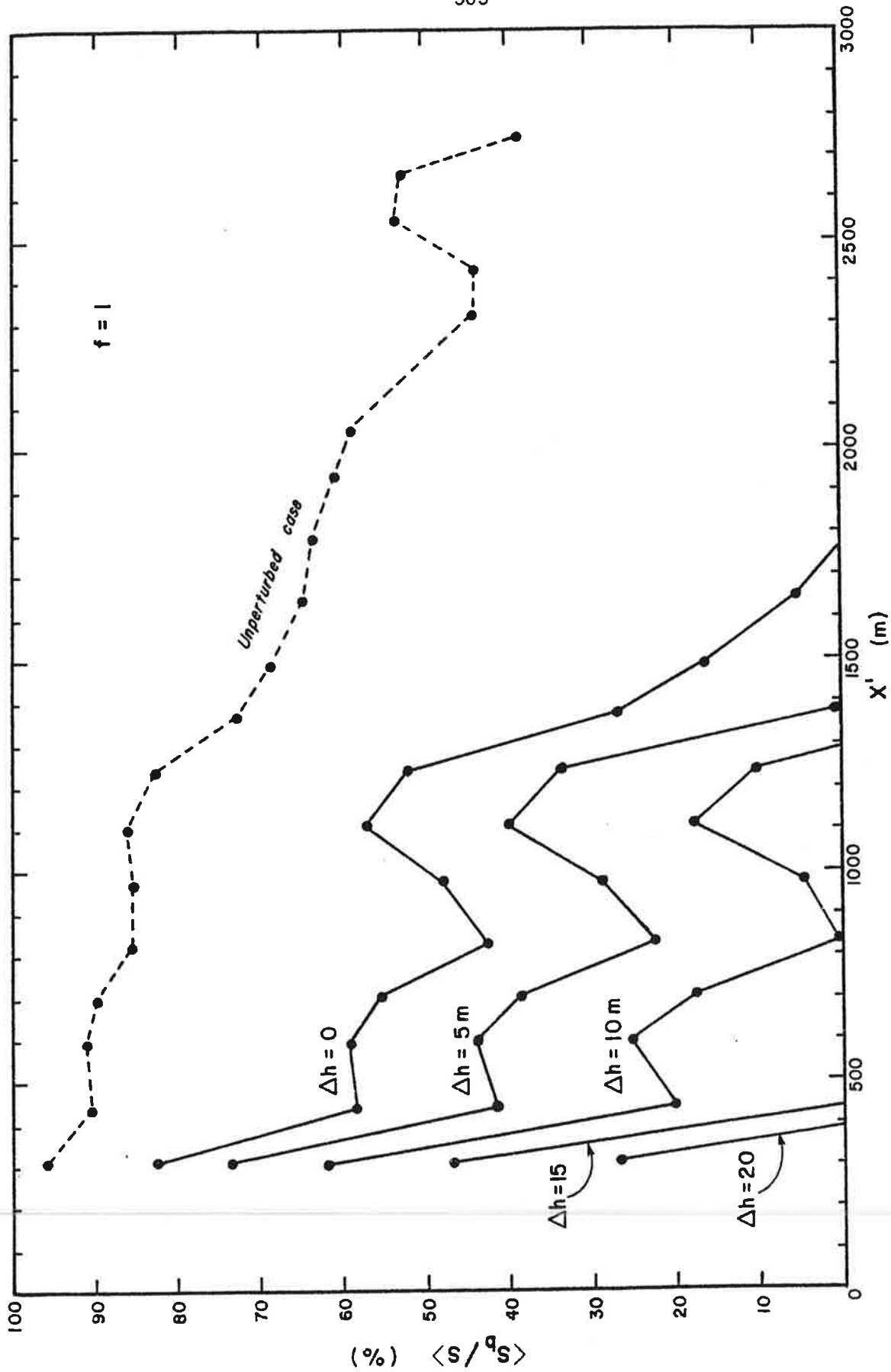


Figure 121. The time average of the ratio s_b/s for various changes in thickness (Δh), using the least viscous flow law and increasing the shape factors to unity everywhere. Smoothed values of h and a were used.

Chapter 12

DISCUSSION AND CONCLUSIONS

12.1 FEATURES OF THE VELOCITY FIELD

The time variations of the surface velocity of the Nisqually Glacier from 1968 to 1970 exhibit two prominent features: a very pronounced seasonal fluctuation superimposed on a longer period trend.

Unfortunately the observations cover too short a time period to define the latter variation satisfactorily. Many of the velocity curves of Appendix C suggest that the yearly motion might be greater in 1968 and 1970 than in 1969. However, this could simply be a subjective bias caused by the fact that three maxima were recorded but only two minima. Instead it was felt safest to assume that the long period trend was linear with time. Figure 122 shows the straight lines fitted by least-squares through the smoothed $\bar{s}'_0(t)$ curves of selected stakes.

In the vicinity of U.S.G.S. Profile II the long period velocity is approximately constant. Below this point it decreases with time, the speed of the lowermost stake dropping by about 50 % over the two year period. Above this point the long period trend reverses direction, the uppermost stake more than doubling its annual speed from 1968 to 1970.

This correlates, at least in the correct sense, with the results of the U.S.G.S. measurements of the mean annual thickness changes at their three profiles. From 1968 to 1970 the lower profile decreased by 5.5 m, the middle one by 4.3 m, but the upper one increased by 4.6 m. Then from 1970 to 1971 the lower profile remained unchanged, the middle one increased by 2.8 m, and the upper profile thickened another 3.4 m (Richardson, written communication, 1971). This implies that during the period of measurements there was a net thinning in

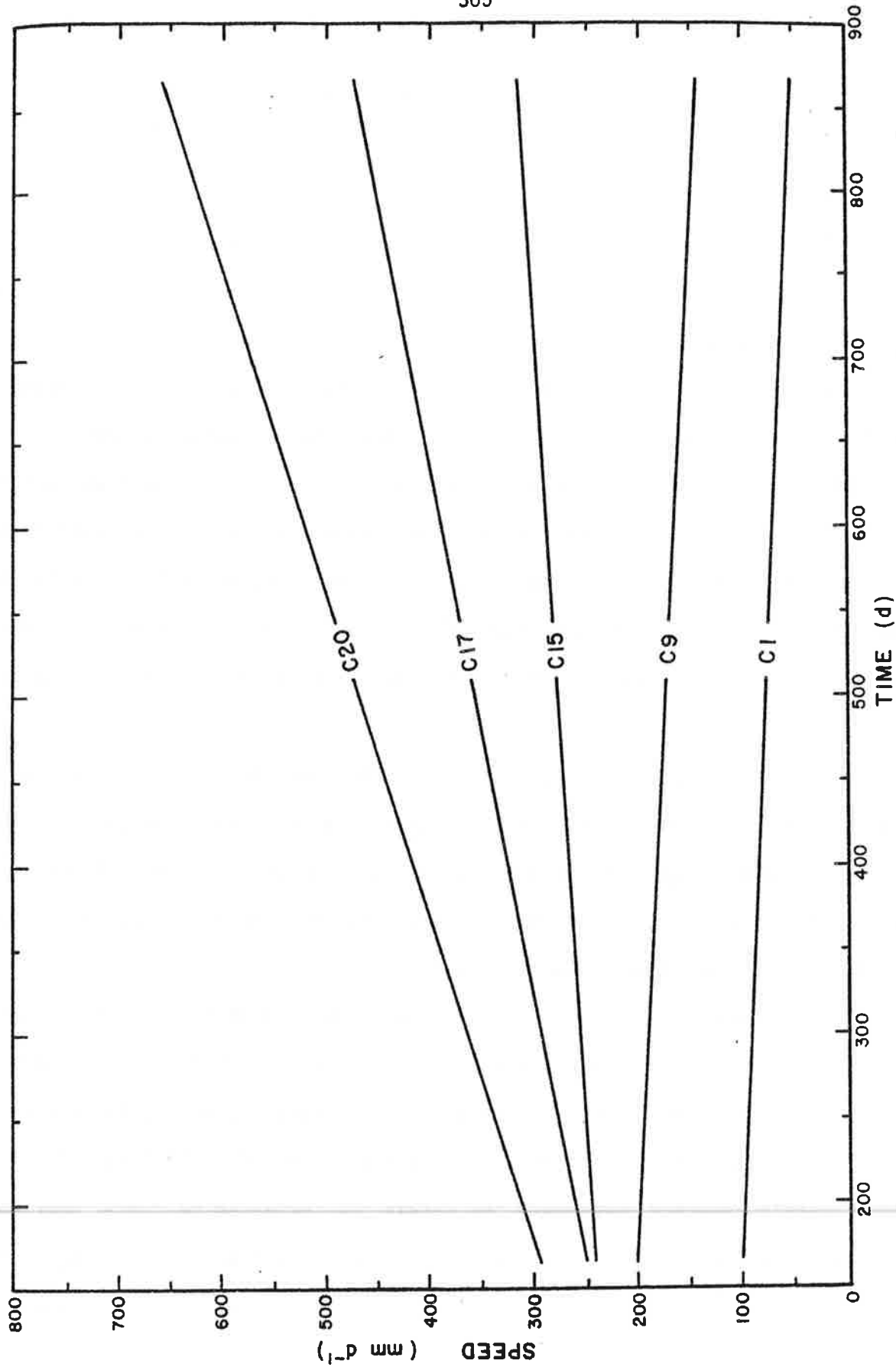


Figure 122. The long period trend of surface velocity over the two years of measurements. This was obtained by fitting straight lines with least-squares to the velocity curves of Appendix C.

the lower part of the glacier and a net thickening in the upper part. This is substantiated by the surface elevation measurements made in May 1971 (Figure 106, p. 282).

Although this could signal the start of another kinematic wave moving down the glacier, the results of the previous chapter show that existing theories of internal deformation can *not* account for the *magnitude* of the velocity change. For $n = 3$, a net thickness increase of 5 m would only increase the velocity by about 30%, or, conversely, the observed velocity increase of 100 % would require a flow law exponent equal to 9.

The interpretation of this will be left to the next section. We now summarize the features of the shorter term, seasonal variations.

In the upper part of the glacier, near the equilibrium line, the maximum velocity occurs in late May or June and the minimum in November (Figure 83). As the terminus is approached both the maximum and minimum occur about one month later, in July and December respectively. This progressive shift of the peaks with distance down-glacier represents a "seasonal wave", as first found by Blümcke and Finsterwalder (1905) on the Hintereisferner. This wave is more apparent with the maxima than the minima as the latter are broader and less well defined, particularly with the lower stakes during the first winter. The longitudinal velocity profiles measured in 1971 (Figure 78) confirm the existence of such a wave. The estimated wave speed is 20 km a^{-1} , in good agreement with Schimpp's results for the Hintereisferner (Schimpp, 1958).

Figure 123 shows the deviation of the maximum and minimum velocities from the long period trend, as a function of distance along the glacier. The dashed lines indicate maxima which were inferred at the beginning and end of the measurement period and consequently should be treated with some reserve. The winter minima are consistently about 25 % below the long period velocity and there is *no* significant variation with distance along the glacier. The 1969

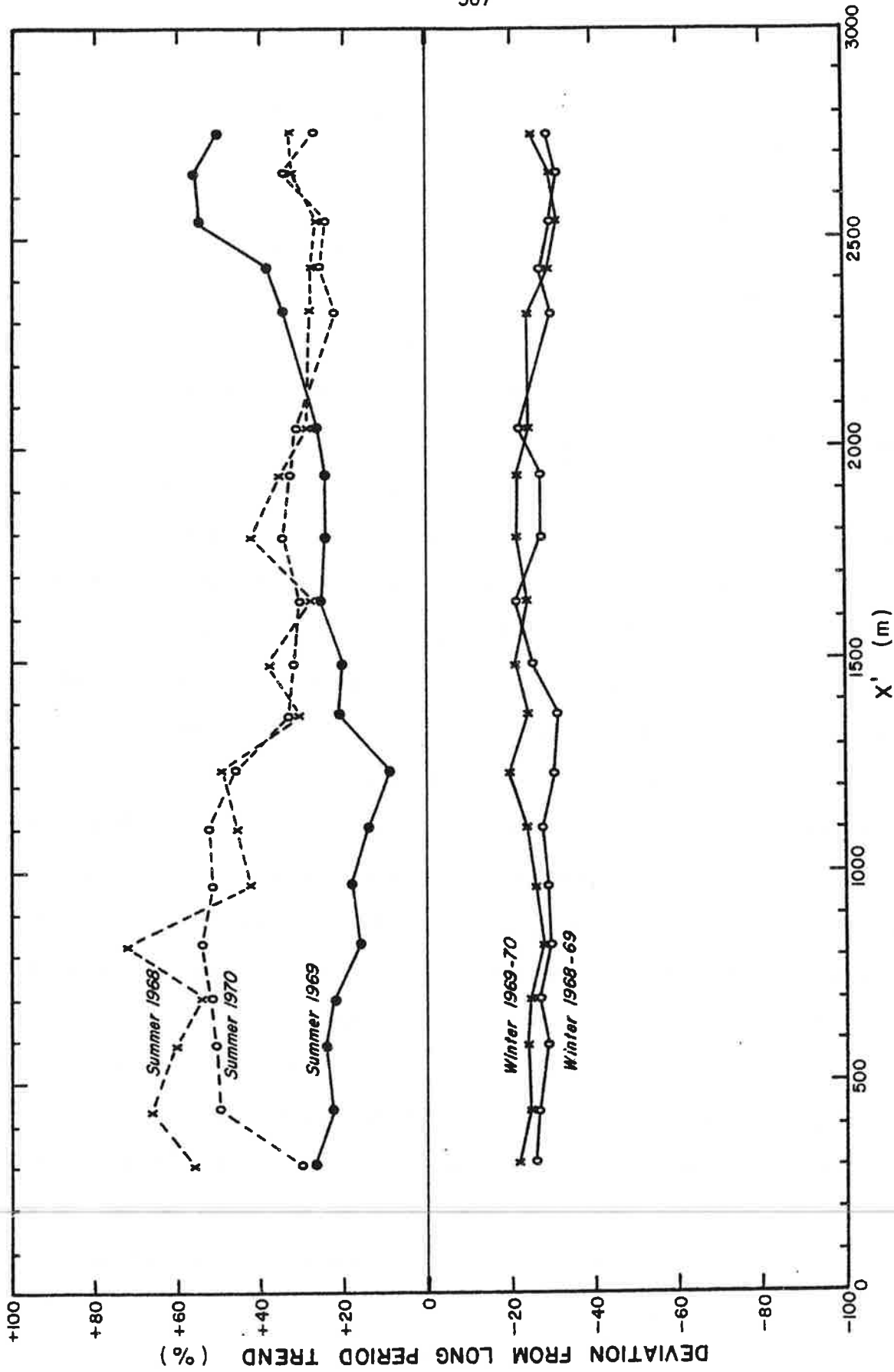


Figure 123. The deviation of the maximum and minimum velocities from the long-period trend. The dashed lines are not as reliable as they were inferred at the beginning and end of the measurement period.

summer maximum is also fairly consistent. Over most of the glacier it averages about 25 % above the long period velocity, but near the terminus it increases to as much as 55 %. This tendency has also been found on other glaciers (Meier, 1960). The dashed lines, on the other hand, indicate a reverse trend, a decrease in the relative deviation as the terminus is approached. This is probably caused by errors in the long period trend. Using parabolas instead of straight lines does in fact reduce the deviations of these maxima to about 20 %. However, since the choice of long period trend is so arbitrary, the simplest case (a straight line) was retained.

Either choice of long period trend still leads to the following observation: there is *no* tendency for the velocity variations to vanish as the equilibrium line is approached, as found on other glaciers (for example, Elliston on the Gornergletscher). Very definite seasonal fluctuations occur on all stakes.

The velocity of the glacier most closely equals the mean annual speed in the months of March-April and August-September. Short term measurements of velocity made at other times of the year do not predict the mean annual speed of a glacier.

12.2 CAUSES OF THE VELOCITY VARIATIONS

The glacier flow model used in the analysis of the motion can only be considered an approximation to the complex Nisqually Glacier. Nevertheless, it is felt that the parameters were varied sufficiently to demonstrate that most of the surface motion is due to sliding of the glacier over its bed. It is very doubtful that more refined flow models would invalidate this result.

The annual thickness changes were found to average about 7 m (± 5 % of the total thickness). For an average flow law ($n = 3$), this would produce variations of ± 22 % in the speed due to internal deformation and ± 10 % in the basal sliding speed, if the latter varies as τ_b^m , where $m = \frac{1}{2}(n + 1)$ (Weertman, 1964).

However, internal deformation almost always accounts for less than 50 % of the surface motion, and is essentially negligible in the upper part of the glacier. Thus, if we assume, as an upper limit, equal contributions from the two mechanisms, then the loading effect can only produce, *at most*, a ± 16 % variation in the surface velocity, which is still not much more than half of the observed variation. Thus the loading effect cannot account for the magnitude of the velocity variations.

Nor can it account for the phase of the velocity variations. In Figure 124 the mean surface speed of all centerline stakes is plotted as a function of time. As expected, the peak velocity occurs in June and the minimum in November-December. However, if the mean speed due to internal deformation^{*} (from Figure 110) is also plotted, we get a maximum in March-April and a minimum in October. Hence there is a phase difference between the surface speed and the loading effect.

Thus we conclude that the seasonal velocity variations are not caused by variations in the internal deformation mechanism or the pressure-melting/enhanced plastic flow mechanism of basal sliding. We are forced to attribute the changes in surface motion to the one unknown in the theories, namely the dependence of the basal sliding mechanism on the "amount of water at the bed of a glacier". This has been proposed before, largely on intuitive grounds, but the data obtained on the Nisqually Glacier allow us to refine this explanation and provide evidence for it.

First, consider the seasonal wave. This was found to have a speed of about 20 km a^{-1} . If this represents a normal kinematic wave (Weertman, 1958; Nye, 1960, 1963) it should have a wave speed given, at least in magnitude, by (Paterson, 1969, p. 199):

* This will also be in phase with any variation in speed due to variations in basal shear stress, assuming, of course, that $s_b \propto \tau_b^m$.

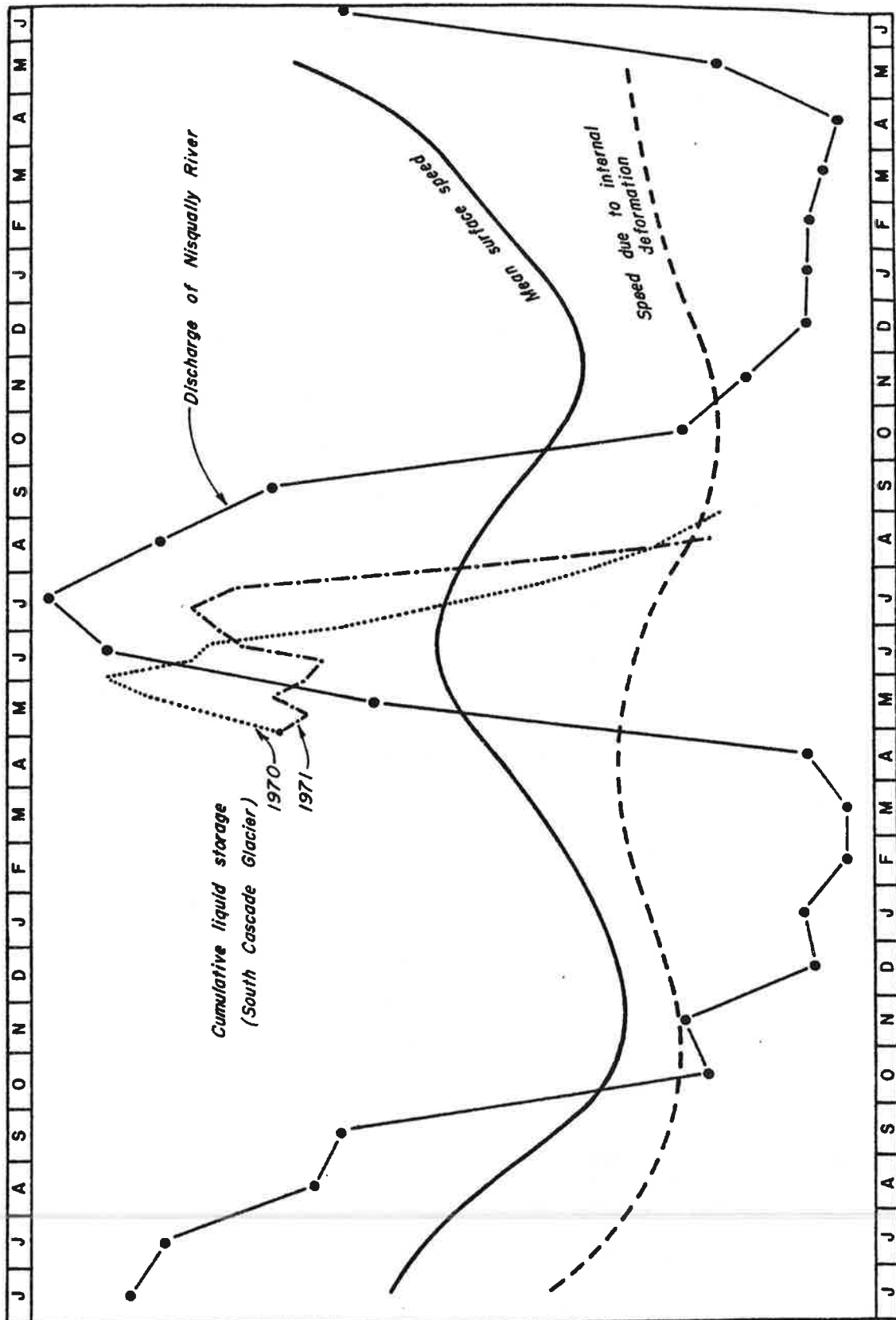


Figure 124. The mean surface speed, the mean speed due to internal deformation, and the monthly discharge of the Nisqually River as a function of time. The cumulative liquid water storage of the South Cascade Glacier is also shown. The ordinates have different scales and origins so that the phase relationships are clear.

$$c = (n + 2)s_a + (m + 1)s_b \quad (1)$$

Since $m < n$, the wave speed is a maximum when all the measured surface speed is due to internal deformation:

$$c \leq (n + 2)d \quad (2)$$

For $n = 4$ and $s = 800 \text{ mm d}^{-1}$ this implies $c = 1.8 \text{ km a}^{-1}$, but for $n = 3$ and $s = 100 \text{ mm d}^{-1}$, $c = 0.18 \text{ km a}^{-1}$. Thus we conclude the seasonal wave travels down the glacier at least one to two orders of magnitude faster than can be accounted for by assuming the ice motion is due to internal deformation or the pressure melting/enhanced plastic flow mechanism of basal sliding.

Second, the basal shear stress was found to increase with distance down-glacier (Figure 112), whereas the measured surface speed does the opposite. Since sliding accounts for most of the surface motion, this means that the sliding speed varies *inversely* with the basal shear stress, contrary to the predictions of basal sliding theory. On the other hand, τ_b was computed for simple "laminar" flow and does not include the effect of longitudinal or transverse normal stresses, which might act to raise the basal shear stress to higher values where the sliding velocity is high. However, the strain rate variations appear to be controlled by local topographic features. There is no obvious correlation between the longitudinal stresses and the sliding velocity and so it is doubtful they can be used to explain this inverse relationship (see Figure 81, p. 218).

If the seasonal velocity variations are due to changes in the amount of water at the bed, they might correlate with the run-off or the surface melting. In Figure 124 the monthly discharge of the Nisqually River 1.8 km below the terminus is plotted against time. The peak in the run-off occurs in July,

about a month, on the average, *after* the peak in the surface speed. Moreover, the minimum occurs in March-April, fully four months *after* the corresponding minimum in the motion. For stakes near the terminus the two maxima are in phase; a similar finding may well have led Elliston to conclude the surface speed was correlated with the stream discharge (to within 1-2 weeks).

The Nisqually data, however, show that this correlation becomes progressively less valid with distance up-glacier and completely breaks down when the minima are examined. During the period November to April, when the run-off is steadily decreasing, the ice is distinctly accelerating.

Furthermore, the surface velocity will not correlate with the surface melting. If it did the peak in the velocity would occur progressively *later* up-glacier rather than the opposite. Surface melting also fails to explain the winter increase in velocity.

This *acceleration of the glacier throughout the winter in the ablation zone*, although evident from some of the earlier work (p. 44), does not appear to have been emphasized in the published literature, possibly because of uncertainties in the existing data. The results obtained here, however, provide conclusive evidence for this acceleration. It is a crucial point since it makes it difficult to correlate the seasonal velocity variations with run-off or surface melting (or, for that matter, temperature).

Instead, the winter acceleration implies that somehow the amount of water at the bed of the glacier increases during the winter, reaches a peak in the late spring and early summer and then decreases through the rest of the summer to a minimum in the fall. The glacier must store water during the winter. Presumably the increased amount of water increases its average hydrostatic pressure and this, in turn, enables a greater area of ice to be liberated from the rock.

This result has already been reached by completely different means by

Tangborn, Krimmel and Meier (in press). In a mass balance study of South Cascade Glacier during 1970 they found that the mass loss calculated from run-off and precipitation measurements (the "hydrologic" method) was 38 % greater than that calculated from surface accumulation-ablation measurements (the "glaciologic" method). Unable to attribute this to measurement errors they conclude the excess run-off is due to the release of water from within the glacier in summer. This extra water must have been stored in the glacier since the end of the previous melt season, that is, during the fall, winter and spring. They term this "liquid water storage".

The South Cascade Glacier is by no means identical to the Nisqually Glacier. However, this excess run-off in the summer has also been reported by Schytt (1970), Stenborg (1970) and Hoinkes (1970) on glaciers in both temperate and sub-polar climates. On the assumption that this is a general phenomenon, the cumulative liquid water storage of the South Cascade Glacier is plotted on Figure 124 for the two years 1970 and 1971. On the average, the storage peaks at the same time that the surface motion does.

We conclude, therefore, that *the seasonal variations in the velocity of a glacier are correlated not with the run-off or surface melting but with the liquid water storage.*

A physical mechanism for this storage and release of meltwater was offered by Tangborn, Krimmel and Meier. It is doubtful a more lucid description could be written and, since further discussion will require such a picture, it is now reproduced in full:

"A glacier differs from a normal porous-medium aquifer in that (1) the fluid is heavier than the solid and pressures in water-filled holes can exceed the pressure in the solid ice nearby, (2) ice is a weak solid and readily deforms by plastic flow resulting in continuous deformation as well as enlargement or reduction of passageways depending on pressure differences between ice and water or air, and (3) heat generated by viscous dissipation (loss of potential energy) or carried from the surface can enlarge passageways by melting. During long periods of little ablation (late fall, winter, early

spring), there is an increased tendency for meltwater passageways to close, causing meltwater and rain to go into storage, likely into small cavities and channels within and at the base of the glacier. Movement of the glacier would tend to further seal off these drainage routes during the fall and winter. After ablation begins in the spring, storage of water continues to take place, but the hydrostatic head of the stored water is increasing rapidly. This causes ice deformation around channels, reopening a three dimensional network of passageways, and water begins to drain from the glacier. Drainage continues at a diminishing rate throughout the summer, and the passageways begin to close up when the production of meltwater tapers off. Thus, much of the water occurring as run-off during the summer actually was produced during the previous spring and fall. Crucial to this argument is the assumption that there is a certain delay between the advent of higher water pressure and the opening of passageways. If the adjustment of passageway size to water pressure were primarily accomplished by plastic flow of the ice, a delay of some months would be expected, because the pressure differences would be relatively small--of the order of 10^{-1} to 10^{-3} bars." (Tangborn, Krimmel and Meier, in press)

We emphasize that the sliding of a glacier is related to the amount of water *stored*, not to the size of the passageways or to the amount of water flowing through them. Thus in the late spring when large quantities of meltwater are descending into the glacier but the channels have not yet had time to open and allow the water to drain, the hydrostatic head of stored water is at a maximum.

12.3 SUPPORTING EVIDENCE

The effect of liquid water storage on the velocity of a glacier is substantiated by other data from the Nisqually Glacier.

Consider the long period trend in velocities. We have shown that this must be due to a large increase in the sliding contribution. This suggests a corresponding increase in the average *annual* liquid water storage, more water being stored in the Nisqually in the spring of 1970 than in the previous two springs. If this is indeed valid it is not surprising that a small outburst flood, or "jökulhlaup", occurred from the glacier on July 4, 1970, about one month after the last seasonal velocity measurements were made.

Figure 125 shows a trace of the recorder chart at the Nisqually Bridge stream gage. The weather had been fair for several days and so rainfall did not cause the high flows on July 4. The two peaks, particularly the second one, occur very abruptly and indicate a "flood wave" hitting the station. The peak discharge is estimated to be about $85 \text{ m}^3 \text{ s}^{-1}$, approximately 20 times greater than the normal summer flow (Richardson, written communication, 1972). This places it in the category of a small glacier outburst flood.

Supplementary to this are the measurements of velocity made in May 1971. Figure 126 shows the longitudinal velocity profiles for approximately the same time of the year for each of four consecutive years. The large increase in speed up to May 1970 is apparent but it did *not* continue through to 1971.

This evidence, admittedly circumstantial, does suggest that the jökulhlaup, by suddenly releasing large amounts of water from within the glacier, was able to arrest the velocity increase. The permanent enlargement of crucial drainage channels could prevent a re-occurrence. Similar releases of stored water from within the Athabasca Glacier have been reported by Mathews (1964a).

This investigation suggests that jökulhlaups are preceded by an abnormal increase in surface motion. Thus an obvious way to predict such floods would be to monitor the surface motion. Probably a measurement of velocity once a year near the equilibrium line would be sufficient to detect major outbursts, but it might be better to make several measurements in the spring so that the acceleration of the glacier can be determined.

If the dependence of sliding on stored water is valid one would expect to find high englacial water pressure values during periods of peak velocity. With this in mind, the water level in the second borehole drilled in the Nisqually Glacier at the end of March 1972 was measured after it was completed. It was found to be within 1 m of the ice surface. Although it is very dubious that this is a representative estimate of the stored water it nevertheless does

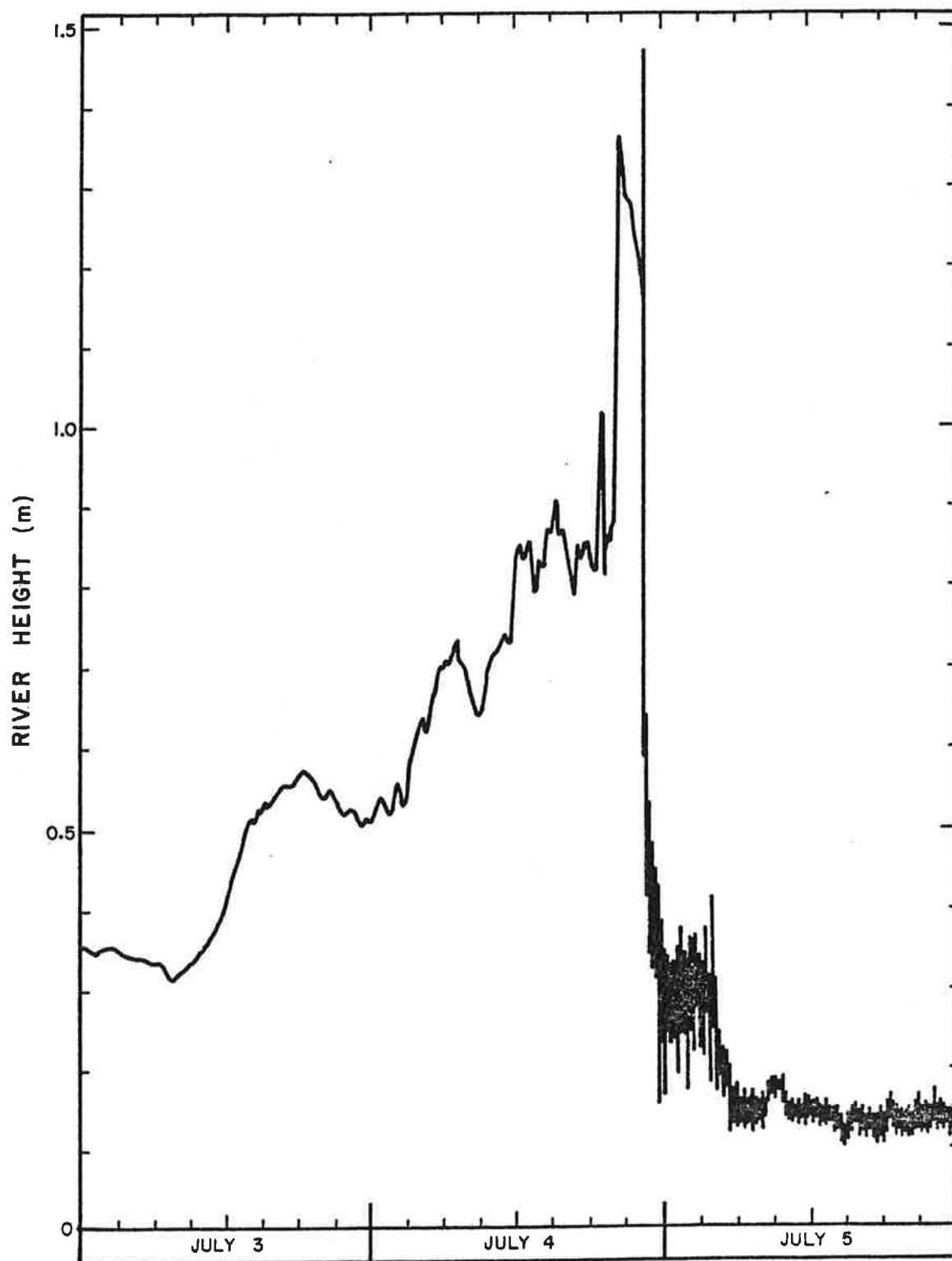


Figure 125. The small jökulhlaup released from the Nisqually Glacier on July 4, 1970. The "noise" is much greater after the flood because the bottom of the stilling well was eroded away, allowing turbulent water to enter. The origin of the ordinate scale is arbitrary.

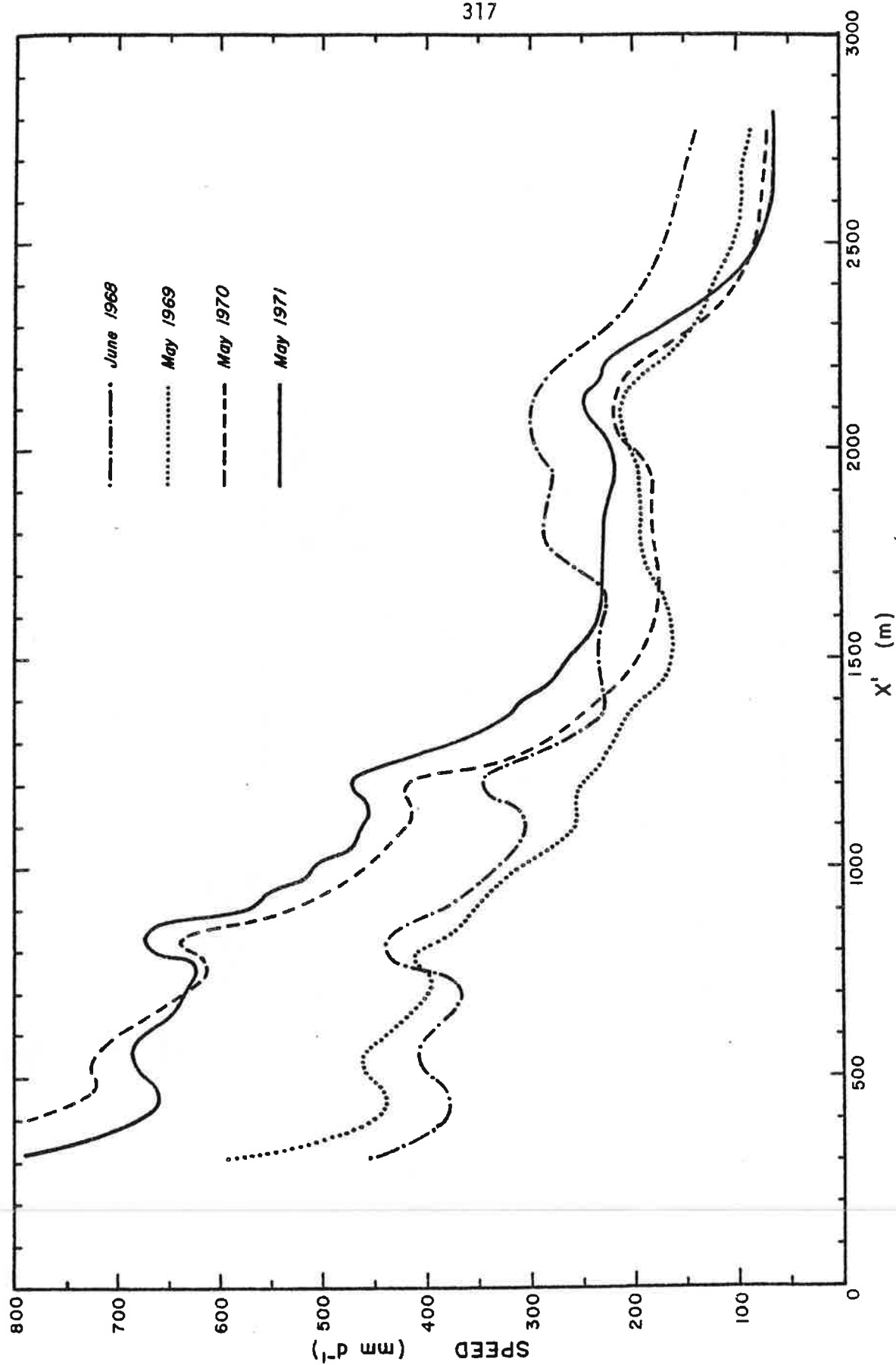


Figure 126. Longitudinal velocity profiles for the four years 1968-71. Each profile refers to approximate by the same time of the year (the time of maximum velocity). The 1971 curve has been used to interpolate missing parts of the other curves.

not refute the above hypothesis.

Other evidence exists in the literature to support this conclusion, however. Haefeli and Brentani (1955) found large reservoirs of water when tunnelling through the ice cap at the Jungfrauoch. Fisher (1963) describes an "enormous reservoir of water" encountered at the end of a tunnel drilled at 4000 m on the Breithorn. Despite the ice being "non-temperate" the water appeared to be in constant supply. Contrary to his expectations the flow of water out of the tunnel "increased materially during the winter".

Mathews (1964b) made observations of the water level in a mine shaft which connected with the bed of the South Leduc Glacier, British Columbia. He found some evidence for a "seasonal cycle in pressure"; "low base levels seemed to occur in late summer and higher base levels in winter".

"Water spouts" have been observed on several glaciers, for example, Wiseman (1963). These can be either intermittent or continuous. Some appear to represent the drainage of isolated cavities whereas others appear to be connected with a more extensive system of drainage channels within the ice. Cavities are often encountered when drilling boreholes in glaciers. Sometimes they contain water under pressure and sometimes they do not. However, after a period of time the water level in the borehole usually returns to its previous level without any obvious filling from the surface (Shreve and Sharp, 1970). This suggests a connection with an overall "englacial water pressure".

In October 1971 a well was placed in the South Cascade Glacier and the water level automatically recorded (Krimmel, written communication, 1972). The level declined steadily to about November 10 and then changed very little until December 12. At this point the recorder stopped but nevertheless the pen trace did show a net increase in water level through the rest of the winter and spring. When recovered in early July 1972 the water level was about 8 m above its minimum of the previous winter.

Finally, another small jökulhlaup may have occurred from the Nisqually Glacier on June 2, 1968 (Figure 94). The recorder at the gaging station was damaged during this flood but it was still possible to estimate the daily discharge. This reached a value three times higher than at any time during the next two years (until the jökulhlaup of July 4, 1970). However, it is not possible to conclude that this was a true glacier outburst flood since it occurred during a period of heavy precipitation. Nonetheless it did occur at the time of maximum liquid water storage and it is not unreasonable to suppose that the heavy rainfall suddenly raised the hydrostatic pressure of the englacial water and thus triggered the opening of channels and the release of stored water. Probably the breaching of some internal "dam" is necessary because of the delay time inherent in the mechanism described on p. 313.

12.4 FURTHER IMPLICATIONS

Additional implications concerning the basal sliding mechanism and the storage of liquid water can be inferred from the Nisqually Glacier data. The first of these concerns the observation that the sliding contribution to the surface motion becomes progressively greater with distance up-glacier. For the uppermost stakes, near the equilibrium line, sliding accounts for over 90 % of the motion. This suggests, but does not prove, that *relatively more water is stored higher up the glacier*. Possibly most of the liquid water storage occurs at the equilibrium line; however, the author hesitates to imply that this is a general feature of glaciers, since the equilibrium line on the Nisqually Glacier is topographically in a unique location, at the boundary between the steep upper half and the flatter lower half where the measurements were made (Plate III).

Nevertheless the storage of large quantities of water at this level on Mount Rainier is confirmed by the South Tahoma Glacier jökulhlaup of August 31,

1967, on the south-west flank of the mountain. Both aerial photographs and an eyewitness account indicate the water was released from the 2300 m level (Richardson, 1968), the same elevation as the equilibrium line of the Nisqually Glacier.

Second, the seasonal wave can be explained with this hypothesis. If there are larger amounts of water stored near the uppermost stakes, the water pressure would be higher here than lower down the glacier. When melting commences in the spring, the critical pressure at which the passageways start to enlarge and connect up rapidly would therefore be reached sooner at the higher elevations. The water which starts to drain down through the glacier would aid the enlargement of channels lower down. On the other hand, the seasonal wave in the minimum is probably a result of the longitudinal velocity gradient. Since the ice is flowing faster higher up the glacier the passageways would be closed off before they would at lower elevations. The winter acceleration would commence sooner and the minimum would be sharper. This was indeed observed.

Could the seasonal wave be due to a kinematic wave in a thin film of water at the bed of the glacier? This was suggested by Weertman (1962) to explain the hourly and daily fluctuations of the surface speed of a glacier, but conceivably it might explain the seasonal wave as well. The wave speed would be about three times the velocity of the water in the film,

$$c \approx \frac{d^2 \rho g \sin \alpha}{4\mu} \quad (3)$$

where d is the thickness of the film and μ is the viscosity of the water. Taking Weertman's values of $d = 0.5$ mm and $\mu = 5.7 \times 10^{-16}$ bar a, and $\alpha = 14^\circ$ for the average slope of the Nisqually Glacier, this gives a wave speed of about 2000 km a^{-1} . Thus either this mechanism is not responsible for the

seasonal wave or the thickness of the water film is an order of magnitude smaller, about 0.05 mm. Making the water film thinner is contrary to the other evidence suggesting large amounts of stored water.

It was also found that the departure of the seasonal component from the long period one was independent of distance along the glacier. Perhaps this is a result of the uniformity, to a first approximation, of the accumulation-ablation pattern over the glacier, since this probably regulates the liquid water storage. Speculation beyond this point, however, is not justified.

Implicit in these conclusions is the assumption that the controlling parameter in the basal sliding mechanism is the englacial water pressure, or, more exactly, the "difference between the average normal stress at the ice interface and the water pressure in the passageways having access to the bed" (Raymond, 1970). Haefeli (1970) and Lliboutry (1968) have also postulated this. The dependence of the basal sliding on the basal shear stress is probably insignificant compared to the effect of water at the bed. Thus it is understandable that Meier (1968) was unable to correlate the sliding velocity to the basal shear stress on the Nisqually Glacier. The similar result of Paterson (1970) on the Athabasca Glacier is also expected. In fact, Paterson's suggestion that the sliding velocity might be correlated with the ice thickness is not unreasonable since thicker glaciers might be able to retain relatively more stored water than thinner ones.

Obviously, simultaneous measurements of the sliding velocity and the liquid water storage, or the englacial water pressure, are needed to confirm or deny the hypotheses proposed here.

In conclusion, the Nisqually Glacier is so thin and moving so rapidly that internal deformation contributes little to the total motion. Seasonal fluctuations in liquid water storage appear to control the seasonal velocity variations by changing the amount of basal sliding. The data support the idea that

the dominant parameter in the basal sliding mechanism is the englacial water pressure and that the dependence on the basal shear stress is probably insignificant.

The liquid water storage thus appears to be crucial to a complete understanding, not only of the hydrology, but also of the dynamics of a glacier.

The large increase in velocity near the equilibrium line in 1970 was probably caused by an increase in liquid water storage over the previous years. Jökulhlaups probably represent the catastrophic release of such water.

Glacier surges, on the other hand, might be caused by a more gradual release, with large amounts of stored water being retained long enough to produce a spectacular advance of the terminus.

EPILOGUE

On July 14, 1972, five days after these conclusions were written, another very high discharge -- possibly a jökulhlaup -- occurred from the Nisqually Glacier. Unfortunately this one destroyed the recorder at the gaging station and so it is not possible to verify that a *sudden* release of water, characteristic of a true jökulhlaup, actually occurred. Richardson (written communication, 1972) estimated that the peak discharge was approximately $140-170 \text{ m}^3 \text{ s}^{-1}$ and that a flow of about $30-60 \text{ m}^3 \text{ s}^{-1}$ was maintained throughout the afternoon of the 14th, when both he and the author were observing the flood. Based on the Paradise weather records, however, a mean discharge of only $8 \text{ m}^3 \text{ s}^{-1}$ can be accounted for by precipitation and snow melt during the preceding six days. Thus it seems certain that some release of stored water must have occurred.

Periods of abnormally high flow in rivers originating from glaciers, usually attributed to high rates of melting, may actually be the release of stored water. As the amount of stored water reaches a maximum in the late spring and early summer, when the rivers are high anyway, many such "outbursts" may go unnoticed.

Abnormal releases of stored water seem to have occurred from the Nisqually Glacier in June or July every two years from 1968 to 1972. It will be interesting to see if another one takes place in June or July of 1974.

BIBLIOGRAPHY

- Agassiz, L. 1838. Upon glaciers, moraines, and erratic blocks: being the address delivered at the opening of the Helvetic Natural History Society, at Neuchâtel, on the 24th of July 1837, by its president. *Edinburgh Philosophical Journal*, Vol. 24, p. 364-383.
- Agassiz, L. 1847. *Nouvelles études et expériences sur les glaciers actuels, leur structure, leur progression et leur action physique sur le sol*. Paris, Victor Masson. 2 vols.
- Agassiz, L. 1967. *Studies on glaciers, preceded by the 'Discourse of Neuchâtel'*. Translated and edited by A. V. Carozzi. New York, Hafner.
- Altmann, J.G. 1751. *Versuch einer historischen und physischen Beschreibung der helvetischen Eisberge*. Zurich.
- Baird, D.C. 1962. *Experimentation: an introduction to measurement theory and experiment design*. Engle Cliffs, Prentice-Hall.
- Battle, W.R.B. 1951. Glacier movement in North-East Greenland, 1949. *Journal of Glaciology*, Vol. 1, No. 10, p. 559-563.
- Bauer, A. 1955. Glaciologie. Groeland. Vol. II: Le Glacier de l'Eque. *Expéditions polaires françaises*. VI. Paris, Hermann and Cie.
- Bender, V.R. and Haines, A.L. 1955. Forty-two years of recession of the Nisqually Glacier on Mount Rainier. *Erdkunde*, Band 9, Heft 4, p. 275-281.
- Blümcke, A. and Finsterwalder, S. 1905. Zeitliche Änderungen in der geschwindigkeit der Gletscherbewegung. *Sitzungsberichte der mathematisch-physikalischen Klasse der K. bayerischen Akademie der Wissenschaften*. München, Band 35, Heft 1, p. 109-131.
- Blümcke, A., and Hess, H. 1899. Untersuchungen am Hintereisferner. *Deutscher und Oesterreichischer Alpenverein, Wissenschaftliche Ergänzungshefte*, Band 1, Heft 2.
- Bordier. 1773. *Picturesque journey to the glaciers of Savoy*.
- Brecher, H.H. 1966. Surface velocity measurements on the Kaskawulsh Glacier, Yukon Territory, Canada. *Ohio State University. Institute of Polar Studies*. Report No. 21, ix, 73p.
- Budd, W.F. 1968. The longitudinal velocity profile of large ice masses. *Union Géodésique et Géophysique Internationale. Association Internationale*

- d'Hydrologie Scientifique. Assemblée générale de Berne, 25 Sept.-7 Oct. 1967. Commission des Neiges et Glaces. Rapports et discussions, p. 58-77.*
- Budd, W.F. 1969. The dynamics of ice masses. *ANARE Scientific Reports. Ser. A(IV). Glaciology. Publication No. 108.*
- Budd, W.F. 1970. The longitudinal stress and strain-rate gradients in ice masses. *Journal of Glaciology*, Vol. 9, No. 55, p. 19-27.
- Butkovich, T.R., and Landauer, J.K. 1960. Creep of ice at low stresses. *U.S. Army Snow, Ice and Permafrost Research Establishment. Research Report 72.*
- Carol, H. 1947. The formation of roches moutonnées. *Journal of Glaciology*, Vol. 1, No. 2, p. 57-59.
- de Charpentier, J.G. 1835. Notice sur les cause probable du transport des blocs erratiques de la Suisse. *Annales des Mines*, Ser. 3, Vol. 8, p. 219-236.
- Colbeck, S.C. Unpublished. The flow law for temperate glacier ice. [Ph.D. thesis, University of Washington, Seattle, Wash., 1970]
- Collins, I.F. 1968. On the use of the equilibrium equations and flow law in relating the surface and bed topography of glaciers and ice-sheets. *Journal of Glaciology*, Vol. 7, No. 50, p. 199-204.
- Corbató, C.E. 1963. Bouguer gravity anomalies of the San Fernando Valley. *University of California. Publications in Geological Sciences*, Vol. 46, No. 1, p. 1-32.
- Corbató, C.E. 1964. Theoretical gravity anomalies of glaciers having parabolic cross-sections. *Journal of Glaciology*, Vol. 5, No. 38, p. 255-257.
- Corbató, C.E. 1965[a]. A least-squares procedure for gravity interpretation. *Geophysics*, Vol. 30. No. 2, p. 228-233.
- Corbató, C.E. 1965[b]. Thickness and basal configuration of lower Blue Glacier, Washington, determined by gravimetry. *Journal of Glaciology*, Vol. 5, No. 41, p. 637-650.
- Crandell, D.R. 1963. Brief description of surficial geology between Seattle and Mount Rainier National National Park. (in Meier, M.F., ed. *The Glaciers of Mount Rainier, I.U.G.G. Glacier Study Tour, September 1963*, p. 2-3.)

- Crossley, D.J., and Clarke, G.K.C. 1970. Gravity measurements on 'Fox Glacier', Yukon Territory, Canada. *Journal of Glaciology*, Vol. 9, No. 57, p. 363-374.
- Deeley, R.M. 1895. The viscous flow of glacier-ice. *Geological Magazine*, Ser. 4, Vol. 2, p. 408-415.
- Deeley, R.M., and Parr, P.H. 1913. The viscosity of glacier ice. *Philosophical Magazine and Journal of Science*, Vol. 26, 6th Series, p. 85-111.
- Deeley, R.M., and Parr, P.H. 1914. The Hintereis Glacier. *Philosophical Magazine and Journal of Science*, Vol. 27, 6th Series, p. 153-176.
- Escher von der Linth, A. 1821. Gegenbernerkungen über die von H.-T. v. Charpentier aufgestellte Erklärung des Vorwaerts Gehens der Gletscher. *Gilbert, Ann. d. Phys.*, Tom. LXIX, p. 113.
- Flotron, A. Unpublished. Jährliche Berichte über die Ergebnisse der Gletschermessungen im Auftrag der Kraftwerke Oberhasli.
- Finsterwalder, S. 1897. Der Vernagtferner, seine Geschichte und seine Vermessung in den Jahren 1888 und 1889. *Deutscher und Oesterreichischer Alpenverein, Graz, Zeitschrift, Wissenschaftliche Ergänzungshefte*, Vol. 1, No. 1.
- Finsterwalder, R. 1961. Review of Schimpp (1960). *Journal of Glaciology*, Vol. 3, No. 30, p. 1159-1160.
- Fisher, J.E. 1963. Two tunnels in cold ice at 4000 m on the Breithorn. *Journal of Glaciology*, Vol. 4, No. 35, p. 513-520.
- Fiske, R.S., Hopson, C.A., and Waters, A.C. 1963. Geology of Mount Rainier National Park, Washington. *U.S. Geological Survey. Professional Paper No. 444*.
- Forbes, J.D. 1843[a]. *Travels through the Alps of Savoy*. Edinburgh, Simpkin.
- Forbes, J.D. 1843[b]. Fourth letter on glaciers. *Edinburgh Philosophical Journal*, Jan. 1843.
- Forbes, J.D. 1846. Illustrations on the viscous theory of glacier motion. *Philosophical Transactions of the Royal Society*, Vol. 136, p. 143-210.
- Friese-Greene, T.W., and Pert, G.J. 1965. Velocity fluctuations of the

- Bersaekerbrae, East Greenland. *Journal of Glaciology*, Vol. 5, No. 41, p. 739-747.
- Galloway, R.W. 1956. Mechanical measurement of glacier motion. *Journal of Glaciology*, Vol. 2, No. 19, p. 642-644.
- Garland, G.D. 1965. *The earth's shape and gravity*. New York, Pergamon.
- Gerrard, J.A.F., Perutz, M.F., and Roch, A. 1952. Measurements of the velocity distribution along a vertical line through a glacier. *Proceedings of the Royal Society, Ser. A*, Vol. 213, No. 1115, p. 546-558.
- Giles, G.E. 1960. Nisqually Glacier, progress report, 1959. *U.S. Geological Survey. Tacoma, Washington*.
- [Glaciological Society.] 1962. *Symposium on problems of mass balance studies, Cambridge, England, 5-7 January 1962. Journal of Glaciology*, Vol. 4, No. 33, p. 289.
- Glen, J.W. 1953. The flow rate of polycrystalline ice. *Nature*, Vol. 172, p. 721.
- Glen, J.W. 1955. The creep of polycrystalline ice. *Proceedings of the Royal Society, Ser. A*, Vol. 228, No. 1175, p. 519-538.
- Glen, J.W. 1958. Measurement of the slip of a glacier past its side wall. *Journal of Glaciology*, Vol. 3, No. 23, p. 188-194.
- Glen, J.W., and Lewis, W.V. 1961. Measurements of side-slip at Austerdalsbreen, 1959. *Journal of Glaciology*, Vol. 3, No. 30, p. 1109-1122.
- Grant, F.S., and West, G.F. 1965. *Interpretation theory in applied geophysics*. New York, McGraw Hill.
- Gruner, G.S. 1760. *Die Eisgebirge des Schweizerlandes*. Bern, A. Wagner.
- Haefeli, R. 1944. *Verh. Schw. Naturf. Ges.*, p. 99-101.
- Haefeli, R. 1970. Changes in the behaviour of the Unteraargletscher in the last 125 years. *Journal of Glaciology*, Vol. 9, No. 56, p. 195-212.
- Haefeli, R., and Brentani, F. 1955. Observations in a cold ice cap. *Journal of Glaciology*, Vol. 2, No. 18, p. 571-581.
- Hall, B. 1841. *Patchwork*, Vol. 3.
- Hammer, S. 1939. Terrain corrections for gravimeter stations. *Geophysics*, Vol. 4, No. 3, p. 184-194.

- Harrison, A.E. 1951. Ice advances during the recession of the Nisqually Glacier. *The Mountaineer*, Vol. 43, Dec. 1951, p. 7-12.
- Harrison, A.E. 1956. Fluctuations of the Nisqually Glacier, Mt. Rainier, Washington, since 1750. *Journal of Glaciology*, Vol. 2, No. 19, p. 675-683.
- Harrison, A.E., and Lee, D. 1971. Electronic measurement of ice velocity. *Journal of Glaciology*, Vol. 10, No. 60, p. 394-399.
- Harrison, W.D. 1972. Temperature of a temperate glacier. *Journal of Glaciology*, Vol. 11, No. 61, p. 15-30.
- Harrison, W.D., and Kamb, W.B. 1970. Direct measurement of sliding velocity at the base of a glacier. *Transactions. American Geophysical Union*. Vol. 51, p. 431.
- Heiskanen, W.A. and Vening-Meinesz, F.A. 1960. *The earth and its gravity field*. New York, McGraw-Hill.
- Hess, H. 1933. Das Eis der Erde. (in Gutenberg, B., ed. *Handbuch der Geophysik*. Berlin, Borntraeger, Band 7, Lief. I, p. 1-121.)
- Hess, H. 1939. Zur Physik des Gletschers. *Petermanns Geographische Mitteilungen*, Vol. 85, No. 7-8, p. 241-244.
- Hodge, S.M. 1971. A new version of a steam-operated ice drill. *Journal of Glaciology*, Vol. 10, No. 60, p. 387-393.
- Hofmann, W. 1955. Kartographie und Gletscherkunde am Nisqually-Gletscher. *Erdkunde*, Band. 9, Heft 4, p. 281-286.
- Hofmann, W. 1958. The advance of the Nisqually Glacier at Mt. Rainier, U.S.A., between 1952 and 1956. *Union Géodésique et Géophysique Internationale. Association Internationale d'Hydrologie Scientifique. Assemblée générale de Toronto*. 3-14 Sept. 1957. Tom. 4, p. 325-330.
- Hoinkes, H. 1970. Methoden und Möglichkeiten von Massenhaushaltsstudien auf Gletschern, Ergebnisse der Messreihe Hintereisferner (Ötztaler Alpen) 1953-1968. *Zeitschrift für Gletscherkunde und Glazialgeologie*, Band 6, Heft 1-2, p. 37-90.
- Hoinkes, H., and Untersteiner, N. 1952. Wärmeumsatz und Ablation auf Alpengletschern. *Geografiska Annaler*, Vol. 34, No. 1-2, p. 99-158.
- Hopkins, W. 1862. On the theory of the motion of glaciers. *Philosophical Transactions*, Vol. 152, Part 2, p. 677-745.

- Hosmer. 1919. *Geodesy*. New York, John Wiley.
- Hubbert, M.K. 1948. A line-integral method of computing the gravimeter effects of two-dimensional masses. *Geophysics*, Vol. 13, No. 2, p. 215-225.
- Hubley, R.C. 1956. Glaciers of the Washington Cascade and Olympic Mountains; their present activity and its relation to local climatic trends. *Journal of Glaciology*, Vol. 2, No. 19, p. 669-674.
- Hugi, F.J. 1830. *Naturhistorische Alpenreise in 8°*. Solothurn, Amiet-Lutiger.
- Ives, J.D., and King, C.A.M. 1955. Glaciological observations on Morsárjökull, S.W. Vatnajökull. Part II: Regime of the glacier, present and past. *Journal of Glaciology*, Vol. 2, No. 17, p. 477-482.
- Johnson, A. 1949. Nisqually Glacier, Washington, progress report 1946, 1947, 1948. *U.S. Geological Survey*. Tacoma, Washington. Report on file, 3p.
- Johnson, A. 1954. Observations on the Nisqually Glacier and other glaciers in the Northwestern United States. *Union Géodésique et Géophysique Internationale. Association Internationale d'Hydrologie Scientifique. Assemblée générale de Rome, 1954*. Tom. 4, p. 511.
- Johnson, A. 1960. Variation in surface elevation of the Nisqually Glacier, Mt. Rainier, Washington. *Union Géodésique et Géophysique Internationale. Association Internationale d'Hydrologie Scientifique. Bulletin No. 19*, p. 54-60.
- Johnson, J.N. 1968. Steady profile of a finite-amplitude kinematic wave on a glacier. *Journal of Glaciology*, Vol. 7, No. 49, p. 117-119.
- Judd, W.R. [ed.] 1964. *State of stress in the earth's crust*. New York, Elsevier.
- Kamalov, B.A. 1969. Movement of the Davydov Glacier. *Soviet Hydrology: Selected Papers*, No. 4. [abstract]
- Kamb, W.B. 1970. Sliding motion of glaciers: theory and observation. *Reviews of Geophysics and Space Physics*, Vol. 8, No. 4, p. 673-728.
- Kamb, W.B., and LaChapelle, E.R. 1964. Direct observation of the mechanism of glacier sliding over bedrock. *Journal of Glaciology*, Vol. 5, No. 38, p. 159-172.

- Kamb, W.B., and LaChapelle, E.R. 1968. Flow dynamics and structure in a fast-moving icefall. *Transactions. American Geophysical Union*. Vol. 49, p. 312.
- Kamb, W.B., and Shreve, R.L. 1966. Results of a new method for measuring internal deformation in glaciers. *Transactions. American Geophysical Union*. Vol. 47, p. 190.
- Kanasewich, E.R. 1963. Gravity measurements on the Athabasca Glacier, Alberta, Canada. *Journal of Glaciology*, Vol. 4, No. 35, p. 617-632.
- Knizhnikov, Yu.F. 1961. Izmenyayetsya li skorost' dvizheniya lednika na protyazhenii sutok. *Vestnik Moskovskogo Universiteta*. Seriya 5. Geografiya. Tom. 16, No. 5, p. 71-72.
- Krimmel, R.M. 1970. Gravimetric ice thickness determination, South Cascade Glacier, Washington. *Northwest Science*, Vol. 44, No. 3, p. 147-153.
- Krimmel, R.M., Tangborn, W.V., and Meier, M.F. In press. Water flow through a temperate glacier. *Symposium on the role of snow and ice in hydrology. Banff, Canada. Sept. 1972. Sponsored by U.N.E.S.C.O. and W.M.O.*
- Kuhn, B.F. 1787. Versuch über den Mechanismus der Gletscher. *A. Höpfner's Magazin für die Naturkunde Helvetiens*. Zurich.
- Lagally, M. 1929. Versuch einer Theorie der paltenbildung in Gletschern. *Zeitschrift für Gletscherkunde*, Band 17, p. 285-301.
- LeConte, J.N. 1906. The motion of the Nisqually Glacier, Mt. Rainier, U.S.A. *Zeitschrift für Gletscherkunde*, Band 1, p. 191-198.
- LeConte, J.N. 1907. The motion of the Nisqually Glacier, Mt. Rainier. *Sierra Club Bulletin*, Vol. 6, No. 2, p. 108-114.
- Lindig, G. 1958. Feinbewegungsmessungen an einigen Ostalpen-Gletschern. *Union Géodésique et Géophysique Internationale. Association Internationale d'Hydrologie Scientifique. Assemblée générale de Toronto, 3-14 Sept. 1957.* Tom. 4, p. 455-474.
- Lliboutry, L. 1958. Contribution à la théorie du frottement du glacier sur son lit. *Comptes Rendus Hebdomadaires des Séances de l'Académie des Sciences (Paris)*, Tom. 247, No. 3, p. 318-320.
- Lliboutry, L. 1959. Une théorie du frottement du glacier sur son lit. *Annales de Géophysique*, Tom. 15, No. 2, p. 250-265.

- Lliboutry, L. 1965. *Traité de glaciologie*. Paris, Masson et Cie. 2 vols. [Vol. 1 published in 1964]
- Lliboutry, L. 1968. General theory of subglacial cavitation and sliding of temperate glaciers. *Journal of Glaciology*, Vol. 7, No. 49, p. 21-58.
- Lliboutry, L. 1969. The dynamics of temperate glaciers from the detailed viewpoint. *Journal of Glaciology*, Vol. 8, No. 53, p. 185-205.
- Lütschg-Lotscher, O. 1944. Surface speed at the terminus of a glacier measured continuously over 7 1/2 years. *Zum Wasseraushalt des Schweizer Hochgebirges, 4 und 5. Kapiteln.* (Beiträge Geol. Schweiz, Hydrologie, n° 4, Band 1, Teil 2, Abt. 2, 101p.)
- Main. 1888. *Proceedings of the Royal Society*, Vol. 42.
- Mathews, W.H. 1959. Vertical distribution of velocity in Salmon Glacier, British Columbia. *Journal of Glaciology*, Vol. 3, No. 26, p. 448-454.
- Mathews, W.H. 1964[a]. Discharge of a glacial stream. *Organisation Météorologique Mondiale et Association Internationale d'Hydrologie Scientifique. Symposium. Eaux de surface, tenu à l'occasion de l'assemblée générale de Berkeley de l'Union Géodésique et Géophysique Internationale, 19 August - 31 August 1963*, p. 290-300.
- Mathews, W.H. 1964[b]. Water pressure under a glacier. *Journal of Glaciology*, Vol. 5, No. 38, p. 235-240.
- McCall, J.G. 1952. The internal structure of a cirque glacier: report on studies of the englacial movements and temperatures. *Journal of Glaciology*, Vol. 2, No. 12, p. 122-131.
- Meany, E.S. 1916. *Mt. Rainier. A record of exploration*. New York, Macmillan.
- Meier, M.F. 1958. Vertical profiles of velocity and the flow law of glacier ice. *Union de Géodésique et Géophysique Internationale. Association Internationale d'Hydrologie Scientifique. Symposium de Chamonix*. Pub. No. 47, p. 1969-1970.
- Meier, M.F. 1960. Mode of flow of Saskatchewan Glacier, Alberta, Canada. *U.S. Geological Survey. Professional Paper 351*.
- Meier, M.F. 1961. Distribution and variations of glaciers in the United States exclusive of Alaska. *Union Géodésique et Géophysique Internationale*.

- Association Internationale d'Hydrologie Scientifique. Symposium de Helsinki. Pub. No. 54, p. 420-429.*
- Meier, M.F. 1963[a]. General setting of Mount Rainier. (in Meier, M.F., ed. *The glaciers of Mount Rainier, I.U.G.G. Glacier Study Tour, September 1963, p. 1-2.*
- Meier, M.F. 1963[b]. General description of the glaciers. (in Meier, M.F., ed. *The glaciers of Mount Rainier, I.U.G.G. Glacier Study Tour, September 1963, p. 5-7.*
- Meier, M.F. 1963[c]. The kinematic wave on Nisqually Glacier. (in Meier, M.F., ed. *The glaciers of Mount Rainier, I.U.G.G. Glacier Study Tour, September 1963, p. 14-17.*
- Meier, M.F. 1965. Comments on Paterson's paper "Variations in velocity of Athabasca Glacier with time". *Journal of glaciology*, Vol. 5, No. 41, p. 761-762. [letter.]
- Meier, M.F. 1968. Calculation of slip of Nisqually Glacier on its bed: no simple relation of sliding velocity to shear stress. *Union Géodésique et Géophysique Internationale. Association Internationale d'Hydrologie Scientifique. Assemblée générale de Berne, 25 Sept. - 7 Oct. 1967. Commission des Neiges et Glaces. Rapports et discussions, p. 49-57.*
- Meier, M.F. 1969. Glaciers and water supply. *Journal of the American Water Works Association*, Vol. 61, No. 1, p. 8-12.
- Meier, M.F., Kamb, W.B., Allen, C.R., and Sharp, R.P. In press. Flow of Blue Glacier, Olympic Mts., Washington. [Submitted to the *Journal of Glaciology*, 1972.]
- Meier, M.F., and Johnson, J.N. 1962. The kinematic wave on Nisqually Glacier, Washington. *Journal of Geophysical Research*, Vol. 67, No. 2, p. 886.
- Meier, M.F., and Post, A. 1962. Recent variations in mass net budgets of glaciers in western North America. *Union Géodésique et Géophysique Internationale. Association Internationale d'Hydrologie Scientifique. Commission des Neiges et Glaces. Colloque d'Obergurgl, 10 Sept. - 18 Sept. 1962. Pub. No. 58, p. 63-77.*
- Mellor, M. and Smith, J.H. 1966. Creep of snow and ice. *U.S. Army CRREL Research Report 220.*

- Mercanton, P.L. 1916. Vermessungen am Rhone Gletscher 1874-1915. *Neue Denkschriften der Schweizerischen Naturforschenden Gesellschaft*, Band 52, p. 37-190.
- Mercanton, P.L. 1950. A propos des changements saisonniers de la vitesse des glaciers. *Zeitschrift für Gletscherkunde und Glazialgeologie*, Band 1, Heft 2, p. 193-194.
- Millecamps, R. 1956[a]. Sur les directions d'écoulement superficiel d'un tronçon de la Mer de Glace. *Comptes Rendus Hebdomadaires des Séances de l'Académie des Sciences* (Paris), Tom. 242, No. 3, p. 397-400.
- Millecamps, R. 1956[b]. Sur la variation des vitesses d'écoulement superficiel de la glace d'un tronçon de glacier. *Comptes Rendus Hebdomadaires des Séances de l'Académie des Sciences* (Paris), Tom. 242, No. 6, p. 803-806.
- Moore, E.A. Unpublished. Configuration of the surface velocity profile of Gulkana Glacier, central Alaska Range, Alaska. [M.S. thesis, University of Alaska, 1962.]
- Müller, F. 1968. Mittelfriertige Schwankungen der Oberflächengeschwindigkeit des Khumbugletschers am Mount Everest. *Schweizerische Bauzeitung*, Jahrg. 86, Heft 31, p. 569-573.
- Müller, F., and Iken, A. In press. Velocity fluctuations and water regime of Arctic valley glaciers. *Union Géodésique et Géophysique Internationale. Association Internationale d'Hydrologie Scientifique. Commission des Neiges et Glaces. Symposium on the hydrology of glaciers, Cambridge, England, Sept. 1969, organized by the Glaciological Society.*
- Mullineaux, D.R., Sigafos, R.S., Hendricks, E.L. 1969. A historic eruption of Mount Rainier, Washington. *U.S. Geological Survey. Professional Paper 650-B*, p. B15-B18.
- Nettleton, L.L. 1940. *Geophysical prospecting for oil*. New York, McGraw-Hill.
- Nye, J.F. 1951. The flow of glaciers and ice sheets as a problem in plasticity. *Proceedings of the Royal Society, Ser. A*, Vol. 207, No. 1091, p. 554-572.
- Nye, J.F. 1952. The mechanics of glacier flow. *Journal of Glaciology*, Vol. 2, No. 12, p. 82-93.

- Nye, J.F. 1953. The flow law of ice from measurements in glacier tunnels, laboratory experiments and the Jungfraufirn borehole experiment. *Proceedings of the Royal Society, Ser. A*, Vol. 219, No. 1139, p. 477-489.
- Nye, J.F. 1957. The distribution of stress and velocity in glaciers and ice-sheets. *Proceedings of the Royal Society, Ser. A*, Vol. 239, No. 1216, p. 113-133.
- Nye, J.F. 1958. A theory of wave formation in glaciers. (Cambridge Austerdalsbre Expedition.) *Union Géodésique et Géophysique Internationale. Association Internationale d'Hydrologie Scientifique. Symposium de Chamonix, 16 Sept. - 24 Sept.*, p. 139-154.
- Nye, J.F. 1960. The response of glaciers and ice-sheets to seasonal and climatic changes. *Proceedings of the Royal Society, Ser. A*, Vol. 256, No. 1287, p. 559-584.
- Nye, J.F. 1963. The response of a glacier to changes in the rate of nourishment and wastage. *Proceedings of the Royal Society, Ser. A*, Vol. 275, No. 1360, p. 87-112.
- Nye, J.F. 1965. The flow of a glacier in a channel of rectangular, elliptic or parabolic cross-section. *Journal of Glaciology*, Vol. 5, No. 41, p. 661-690.
- Nye, J.F. 1969. A calculation of the sliding of an ice mass over a wavy surface using a Newtonian viscous approximation. *Proceedings of the Royal Society, Ser. A*, Vol. 311, No. 1506, p. 445.
- Nye, J.F. 1970. Glacier sliding without cavitation in a linear viscous approximation. *Proceedings of the Royal Society, Ser. A*, Vol. 315, No. 1522, p. 381-403.
- Orowan, E. 1949. [The flow of ice and other solids.] (in Joint Meeting of the British Glaciological Society, the British Rheologists' Club and the Institute of Metals. *Journal of Glaciology*, Vol. 1, No. 5, p. 231-240.)
- Ostenso, N.A., Sellmann, P.V., and Péwé, T.L. 1965. The bottom topography of Gulkana Glacier, Alaska Range, Alaska. *Journal of Glaciology*, Vol. 5, No. 41, p. 651-659.
- Paterson, W.S.B. 1961. Movement of the Sefstrøms Gletscher, N.E. Greenland. *Journal of Glaciology*, Vol. 3, No. 29, p. 845-849.

- Paterson, W.S.B. 1964. Variations in velocity of Athabasca Glacier with time. *Journal of Glaciology*, Vol. 5, No. 39, p. 277-285.
- Paterson, W.S.B. 1969. *The physics of glaciers*. Oxford, Pergamon Press.
- Paterson, W.S.B. 1970. The sliding velocity of Athabasca Glacier, Canada. *Journal of Glaciology*, Vol. 9, No. 55, p. 55-63.
- Paterson, W.S.B. 1972. Temperature distribution in the upper layers of the ablation area of Athabasca Glacier, Alberta, Canada. *Journal of Glaciology*, Vol. 11, No. 61, p. 31-41.
- Paterson, W.S.B., and Savage, J.C. 1963. Measurements on Athabasca Glacier relating to the flow law of ice. *Journal of Geophysical Research*, Vol. 68, No. 15, p. 4537-4543.
- Phillips, E.L. 1960. Mount Rainier National Park, Washington. *U.S. Weather Bureau Climatological Summary*, 4p.
- Pillewizer, W. 1949. Zur Frage jahreszeitlicher Schwankungen in der Geschwindigkeit der Gletscherbewegung. *Zeitschrift für Gletscherkunde und Glazialgeologie*, Band 1, Heft 1, p. 29-38.
- Post, A. 1963. Summary of recent changes in glaciers of Mt. Rainier. (in Meier, M.F., ed. *The glaciers of Mount Rainier, I.U.G.G. Glacier Study Tour, September, 1963*, p. 9-12.)
- Rainsford, H.F. 1958. *Survey adjustments and least-squares*. New York, Ungar.
- Raymond, C.F. Unpublished. Flow in a transverse section of Athabasca Glacier, Alberta, Canada. [Ph.D. thesis, California Institute of Technology, Pasadena, California, 1969]
- Raymond, C.F. 1971. Flow in a section of the Athabasca Glacier. *Journal of Glaciology*, Vol. 10, No. 58, p. 55-84.
- Renaud, A. 1952. Observations on the surface movement and ablation of the Gorner Glacier, Switzerland. *Journal of Glaciology*, Vol. 2, No. 11, p. 54-57.
- Richardson, D. 1968. Glacier outburst floods in the Pacific Northwest. *U.S. Geological Survey. Professional Paper 600-D*, p. D79-D86.
- Rigsby, G.P. 1958. Effect of hydrostatic pressure on velocity of shear

- deformation of single ice crystals. *Journal of Glaciology*, Vol. 3, No. 24, p. 274-275.
- Röthlisberger, H., and Aellen, M. Unpublished. Annual and monthly velocity variations on Aletschgletscher. [Paper presented at the general assembly of the *International Union of Geodesy and Geophysics*, Berne, Switzerland, 1967.]
- Roy, A. 1962. Ambiguity in geophysical interpretation. *Geophysics*, Vol. 27, No. 1, p. 90-99.
- Russell, I.C. 1898. The glaciers of Mt. Rainier. *U.S. Geological Survey 18th Annual Report, 1896-1897*, Part 2, p. 355-409.
- de Saussure, H.B. 1803. *Voyages dans les Alpes, précédés d'un essai sur l'histoire naturelle des environs de Genève*. Neuchâtel, S. Fauche.
- Savage, J.C., and Paterson, W.S.B. 1963. Borehole measurements in the Athabasca Glacier. *Journal of Geophysical Research*, Vol. 68, No. 15, p. 4521-4536.
- Scheuchzer, J.J. 1723. *Helveticus, sive itinera per Helvetiae Alpinae Regiones facta, annis 1702-1711*. Lugduni Batavorum, P. Vander Aa, 4 vols.
- Schimpp, O. 1958. Der Eishaushalt am Hintereisferner in den Jahren 1952-53 und 1953-54. *Union Géodésique et Géophysique Internationale. Association Internationale d'Hydrologie Scientifique. Assemblée générale de Toronto, 3 Sept. - 14 Sept. 1957*, Tom. 4, p. 301-314.
- Schimpp, O. 1960. Der Haushalt des Hintereisferner (Ötztal). *Veröffentlichungen des Museum Ferdinandeum in Innsbruck*, Band 39, Jahrg. 1959, p. 66-138. Innsbruck, Universitätsverlag Wagner.
- Schytt, V. 1970. An attempt at a combined study of the ice and water balance for a partly glacierized drainage basin. *Annual General Meeting of the Glaciological Society, Cambridge, England*. [Oral paper.]
- Selby, S.M. [ed.] 1962. *Handbook of mathematical tables*. Cleveland, Chemical Rubber Publishing Co.
- Seligman, G. 1950. The specific gravity of ice. *Journal of Glaciology*, Vol. 1, No. 8, p. 442.
- de Seue, C. 1876. Undersøgelse af Svartisen og temperaturforhold i enkalte af de Nordlanske fjorde. *Nyt Magazin for Naturvidenskaberne*, 21 de Bd.,

Ht. 3, p. 229-270.

- Shreve, R.L., and Sharp, R.P. 1970. Internal deformation and thermal anomalies in lower Blue Glacier, Mount Olympus, Washington, U.S.A. *Journal of Glaciology*, Vol. 9, No. 55, p. 65-86.
- Shumskii, P.A. 1964. *Principles of structural glaciology*. New York, Dover.
- Sigafoos, R.S., and Hendricks, E.L. 1961. Botanical evidence of the modern history of Nisqually Glacier, Washington. *U.S. Geological Survey. Professional Paper 387-A*.
- Sigafoos, R.S., and Hendricks, E.L. 1963. Modern history of the Nisqually and Emmons Glaciers, Washington. (in Meier, M.F., ed. *The glaciers of Mount Rainier, I.U.G.G. Glacier Study Tour, September 1963*, p. 7-9.)
- Smith, B.M.E., and Evans, S. 1972. Radio echo sounding: absorption and scattering by water inclusion and ice lenses. *Journal of Glaciology*, Vol. 11, No. 61, p. 133-146.
- Somigliana, C. 1925. Sul coefficiente di attrito interno del ghiaccio e la determinazione della profondita dei ghiacciai. *Boll. Com. Glac. Italiano*, Vol. 6, p. 13-25.
- Steinemann, S. 1958. Résultats experimentaux sur la dynamique de la glace et leur corrélation avec le mouvement et la petrographie des glaciers. *Union Géodésique et Géophysique Internationale. Association Internationale d'Hydrologie Scientifique. Symposium de Chamonix. Pub. No. 47*, p. 184-198.
- Stenborg, T. 1970. Delay of run-off from a glacier basin. *Geografiska Annaler*, Vol. 52A, No. 1, p. 1-30.
- Streiff-Becker, R. 1938. Zur Dynamik des Firneises. *Zeitschrift für Gletscherkunde*, Vol. 26, No. 1-2, p. 1-21.
- Tabor, D., and Walker, J.C.F. 1970. Creep and friction of ice. *Nature*, Vol. 228, p. 37-139.
- Talwani, M., and Ewing, M. 1960. Rapid computation of gravitational attraction of three-dimensional bodies of arbitrary shape. *Geophysics*, Vol. 25, No. 1, p. 203-225.
- Talwani, M., Worzel, J.L., and Landisman, M. 1959. Rapid gravity computations for two-dimensional bodies with application to the Mendocino submarine

- fracture zone. *Journal of Geophysical Research*, Vol. 64, No. 1, p. 49-59.
- Tangborn, W.V., Krimmel, R.M., and Meier, M.F. In press. A comparison of glacier mass balance by glaciologic, hydrologic, and mapping methods, South Cascade Glacier, Washington. *Union Géodésique et Géophysique Internationale. Association Internationale d'Hydrologie Scientifique. Assemblée générale de Moscou, 1971.*
- Theakstone, W.H. 1967. Basal sliding and movement near the margin of the glacier Østerdalsisen, Norway. *Journal of Glaciology*, Vol. 6, No. 48, p. 808-816.
- Thomas, R.H. 1971. Flow law for Antarctic ice shelves. *Nature Physical Science*, Vol. 232, No. 30. p. 85-97.
- Tyndall, J. 1876. *Les glaciers et les transformations de l'eau.* Paris, Librairie Germer Baillière et Cie.
- Tyndall, J. 1896. *The forms of water, in clouds and rivers, ice and glaciers.* New York, Appleton.
- [Union Géodésique et Géophysique Internationale.] *Colloque d'Obergurgl (suite). Bulletin de l'Association Internationale d'Hydrologie Scientifique, 8e An., No. 2, p. 50-142.*
- Veatch, F. 1969. Analysis of a 24 year photographic record of Nisqually Glacier, Mount Rainier National Park, Washington. *U.S. Geological Survey. Professional Paper 631.*
- Venetz, I. 1821. Mémoire sur les variations de la température dans les Alpes de la Suisse. *Denkschriften der allg. schweitz. Gesellschaft gesammten Naturwissenschaften*, Vol. 1, Part 2, p. 1-38.
- Vilesov, E.N. 1961. Temperature of ice in the lower parts of the Tuyuksu glaciers. *Union Géodésique et Géophysique Internationale. Association Internationale d'Hydrologie Scientifique. Assemblée générale de Helsinki, 25 July - 6 August 1960. Commission des Neiges et Glaces. Rapports et discussions*, p. 313-324.
- Voitkovskii, K.F. 1960. The mechanical properties of ice. *Moscow Izd. Akademii. Nauk, S.S.S.R.* (Translated from the Russian by the American Meteorological Society, Boston, 100p.)
- Washburn, B., and Goldthwait, R. 1937. Movement of the South Crillon Glacier,

- Crillon Lake, Alaska. *Bulletin of the Geological Society of America*, Vol. 48, p. 1653-1664.
- Weertman, J. 1957. On the sliding of glaciers. *Journal of Glaciology*, Vol. 3, No. 21, p. 33-38.
- Weertman, J. 1958. Travelling waves on glaciers. *Union Géodésique et Géophysique Internationale. Association Internationale d'Hydrology Scientifique. Symposium de Chamonix. Pub. No. 47, p. 162-168.*
- Weertman, J. 1964. The theory of glacier sliding. *Journal of Glaciology*, Vol. 5, No. 39, p. 287-304.
- Weinberg, B. 1906. *Zeitschrift für Gletscherkunde*, Band 1, Heft 5.
- Wiseman, M.L. 1963. Water-spout on the Aletsch Glacier. *Journal of Glaciology*, Vol. 4, No. 35, p. 647-648.

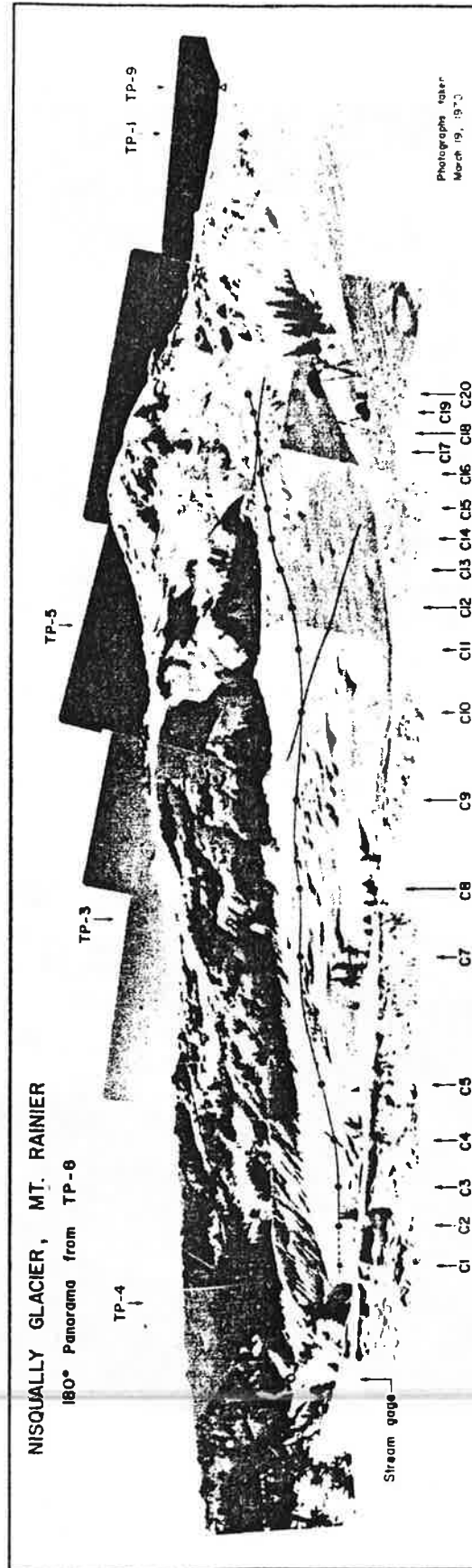


Plate I. Composite 180° panorama of the Nisqually Glacier. The photographs were taken by the author on March 19, 1970, from a triangulation point at 1931 m elevation on the east side of the glacier. The approximate positions of the centerline, the three transverse lines and the centerline stakes are indicated, as well as the other triangulation points which are visible. The stream gage is near the Nisqually River bridge. The terminus is behind the lower nunatak (TP-4). Stake C1 is not visible from TP-8.

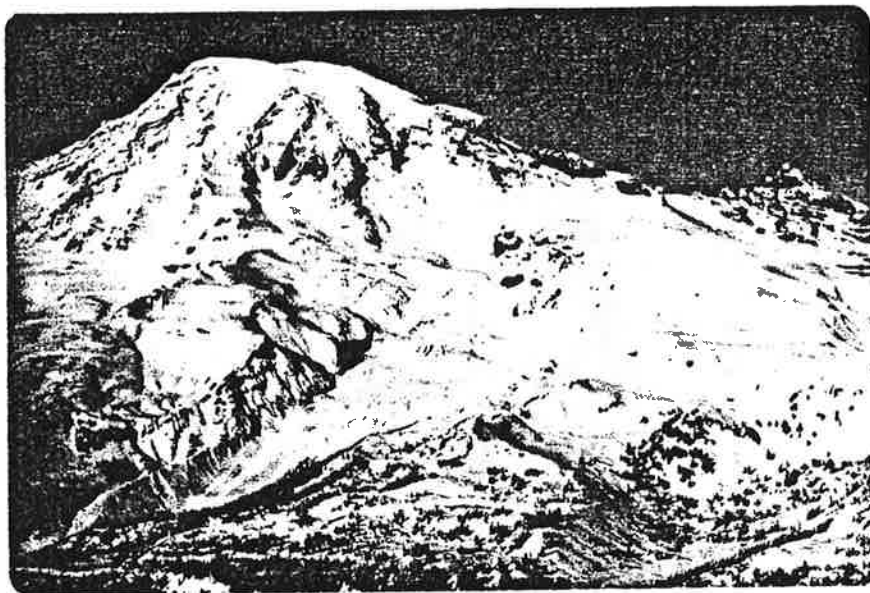


Plate II. The Nisqually Glacier and the south side of Mount Rainier from Pinnacle Peak, January 1972. The portion of the glacier studied extends from the equilibrium line (center of picture) to the terminus (behind the ridge at the lower left). Paradise is in the lower center.

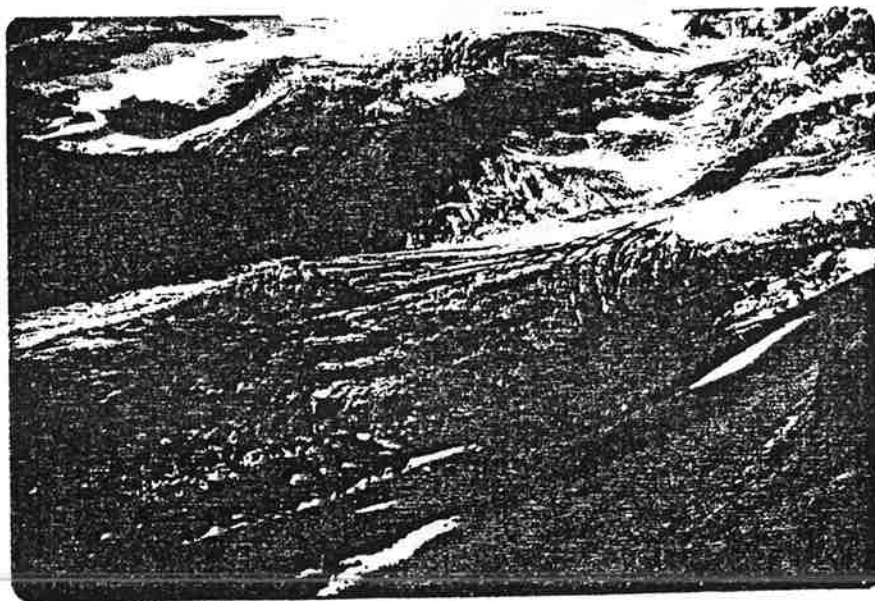








Plate III. The region around the equilibrium line of the Nisqually Glacier from TP-1, September 1968. The band of bare ice along which the center-line stakes were placed is visible behind the rock-covered ice in the foreground. Part of the Wilson Glacier is visible at the top of the picture.

Appendix A

RESULTS OF THE BEDROCK MODELLING

On the following pages are shown the glacier cross sections, in a vertical plane looking up-glacier, at each of the gravity profiles (Figure 30, p. 88). The two dimensional results (dashed lines) are given for the highest value of m (the number of depth variables) which appears to give a physically reasonable solution. Reliable results were not obtained on four profiles (G13, G16, G17 and G18) and so they are omitted from the diagrams. The three dimensional results (solid lines) are taken from Figure 56, p. 148.

Legend:

-  gravity station [the ice surface used in the two dimensional modelling is formed by connecting the stations with straight lines].
-  the digitized surface used in the terrain corrections and the three dimensional modelling [the glacier surface is from the 1966 map and the surrounding terrain is from the 1956 map].
-  the results of the two dimensional modelling
-  the results of the three dimensional modelling
-  the known bedrock [where it extends under the present ice it was obtained from the 1951 map (G5, G6 and G7) or the 1961 map (G1, G2, G3 and G4)].
-  the margins of the glacier [west to the left, east to the right].

Legend (continued):

 a, b

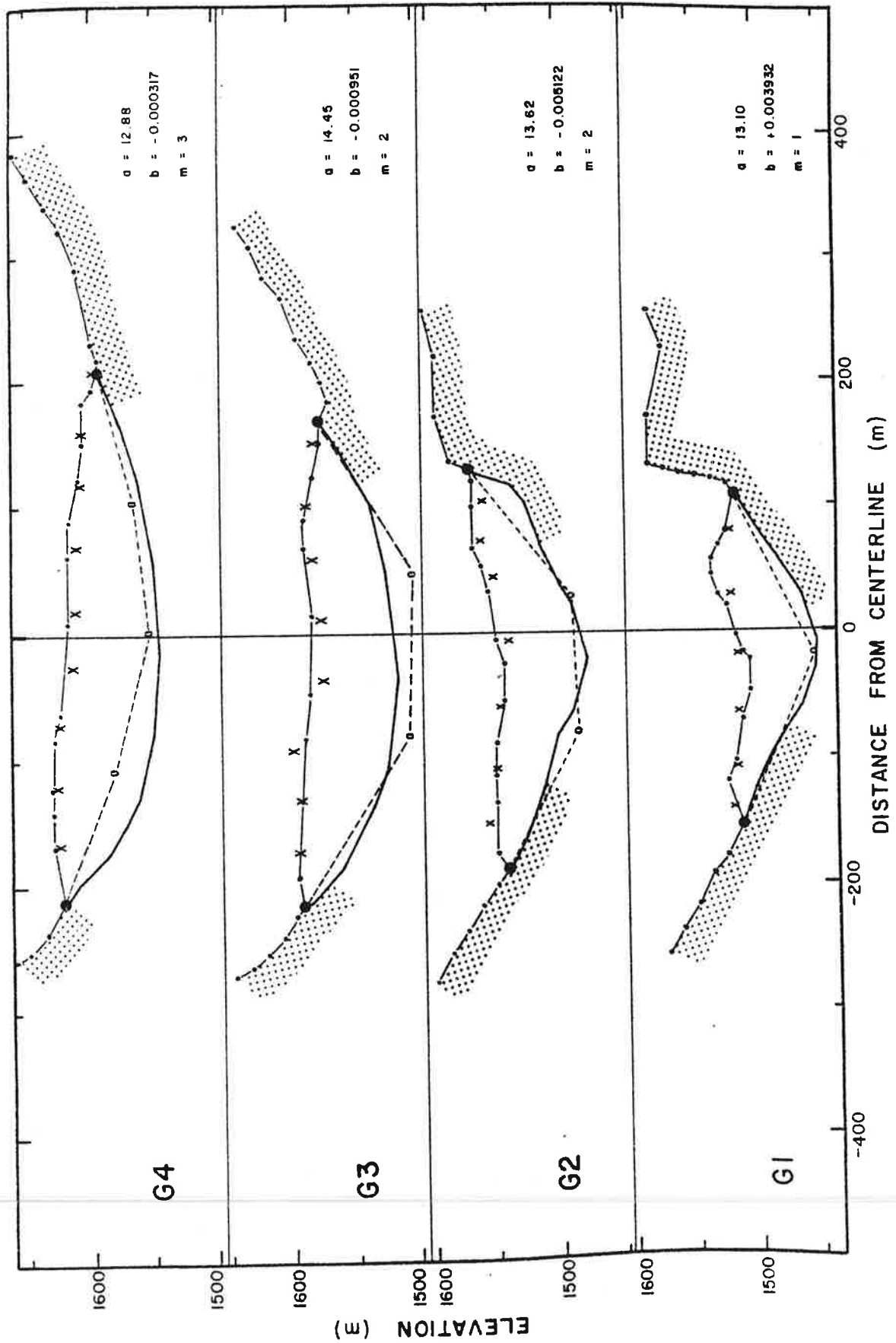
the regional field coefficients determined by the two dimensional modelling:

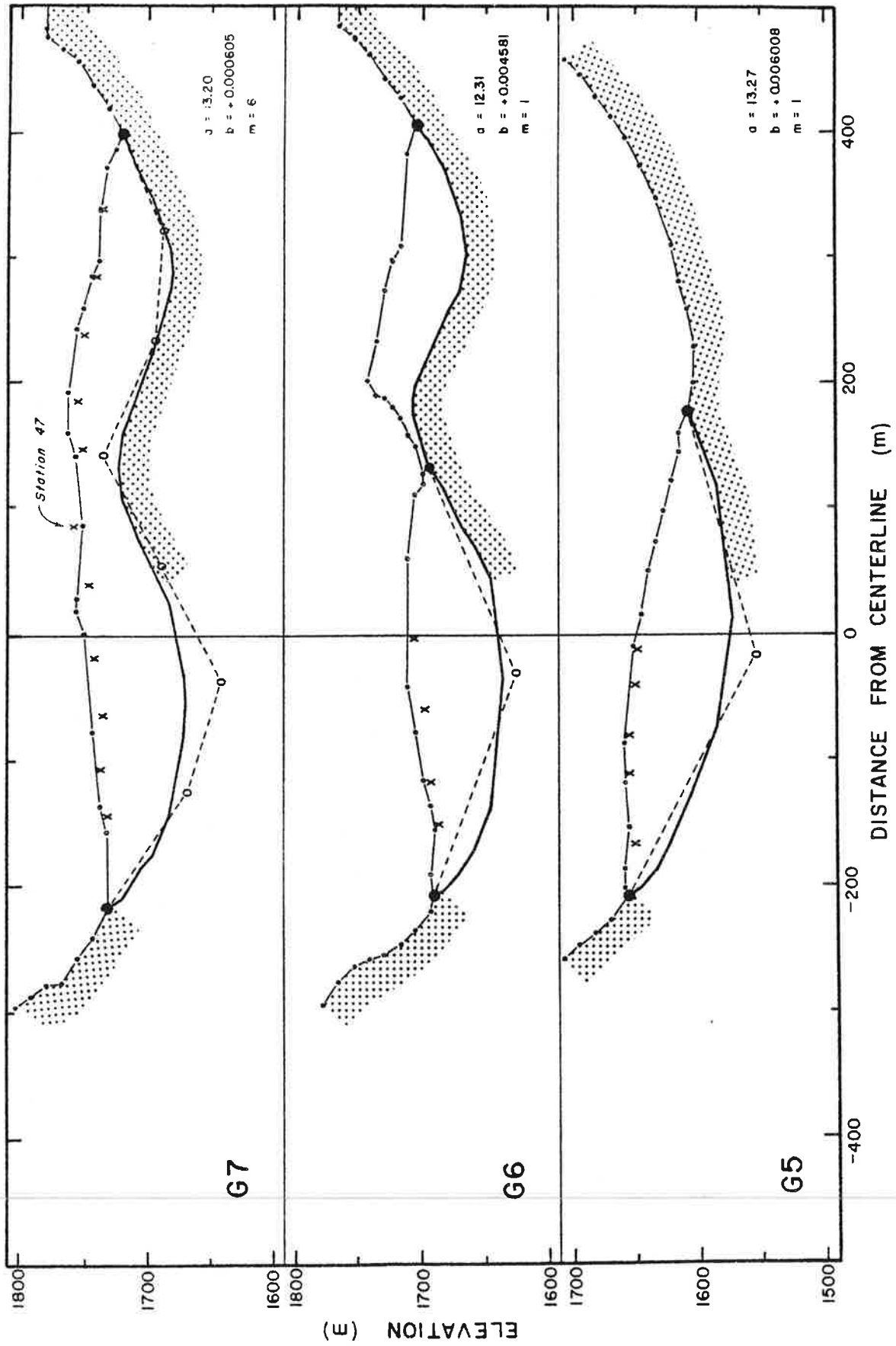
$$g_r = a + bx$$

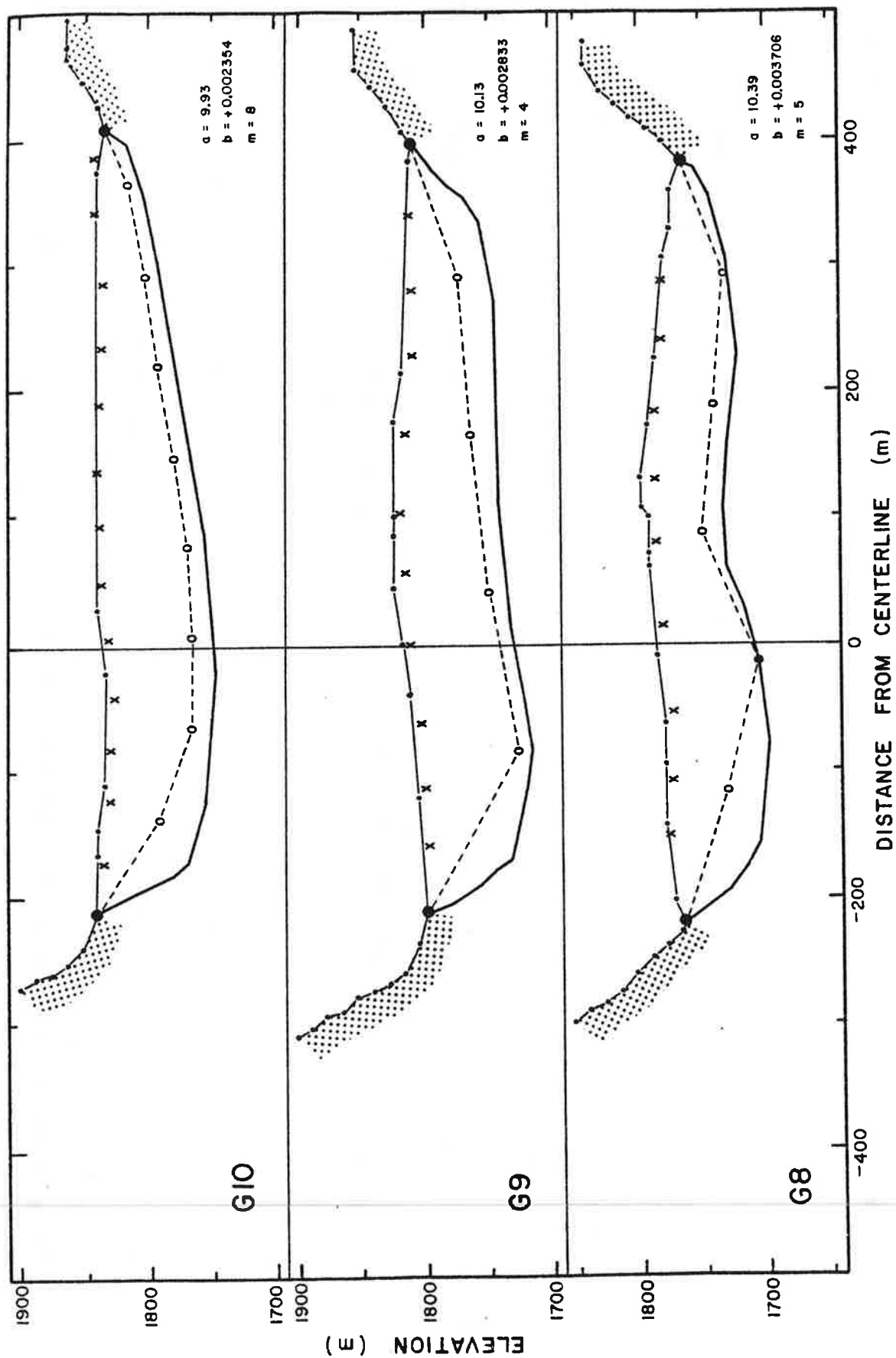
where g_r is the value of the regional gravity (in mgal) and x is the distance across the profile from the *west* margin (not the centerline). [a is given in mgal and b in mgal m^{-1}].

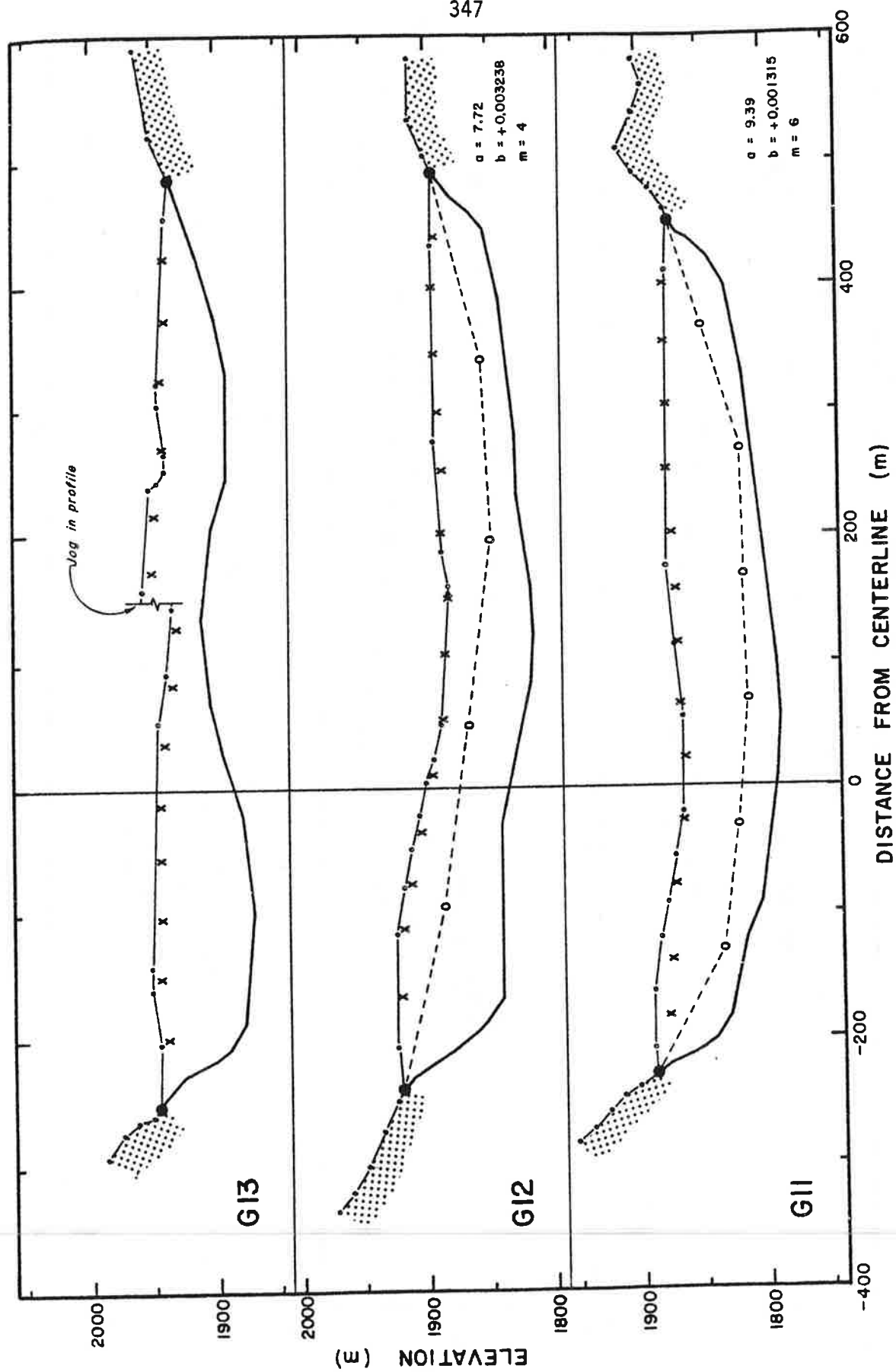
 m

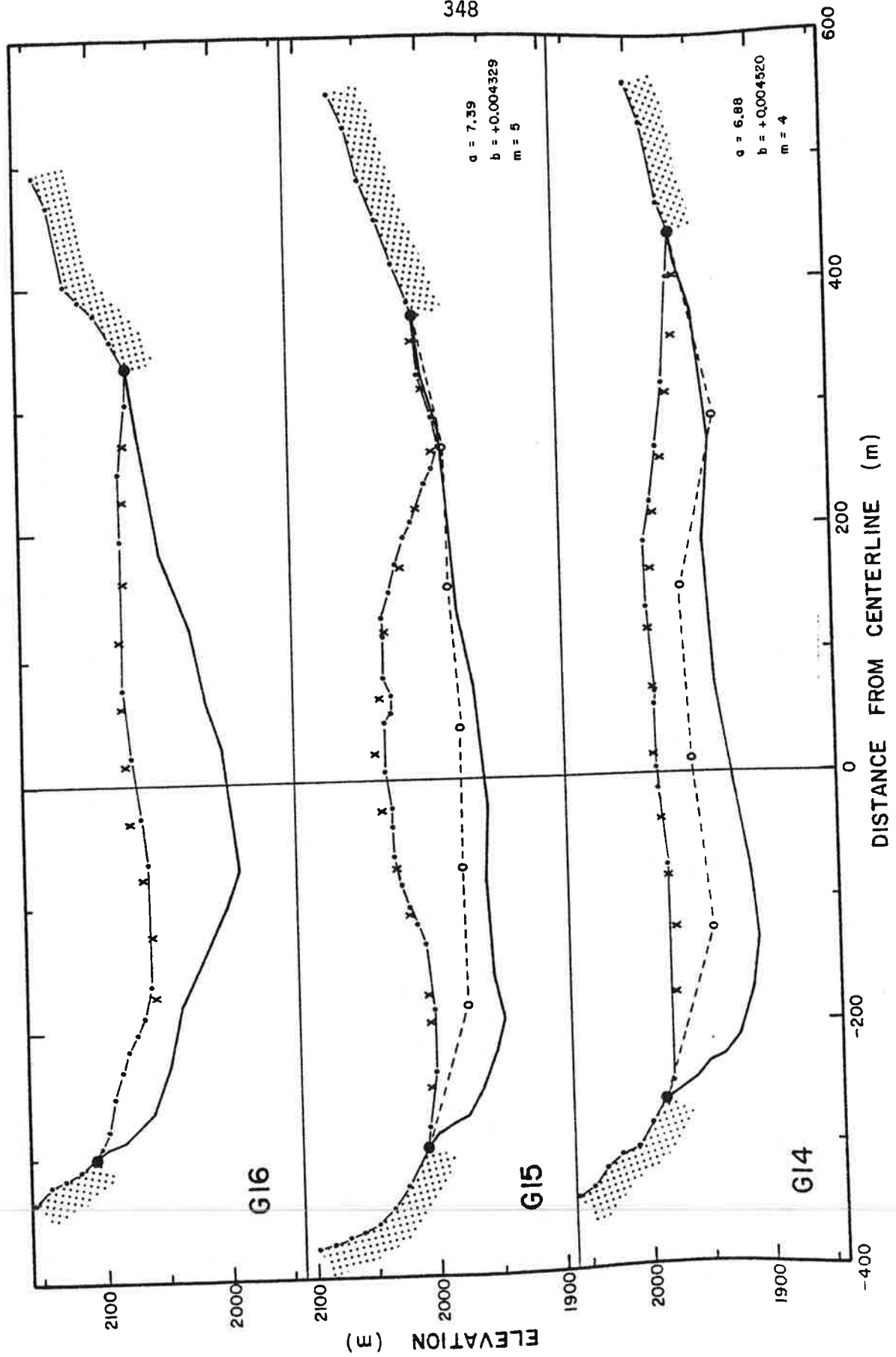
the number of depth variables in the best solution for the two dimensional modelling [equals the number of open circles on the dashed line].

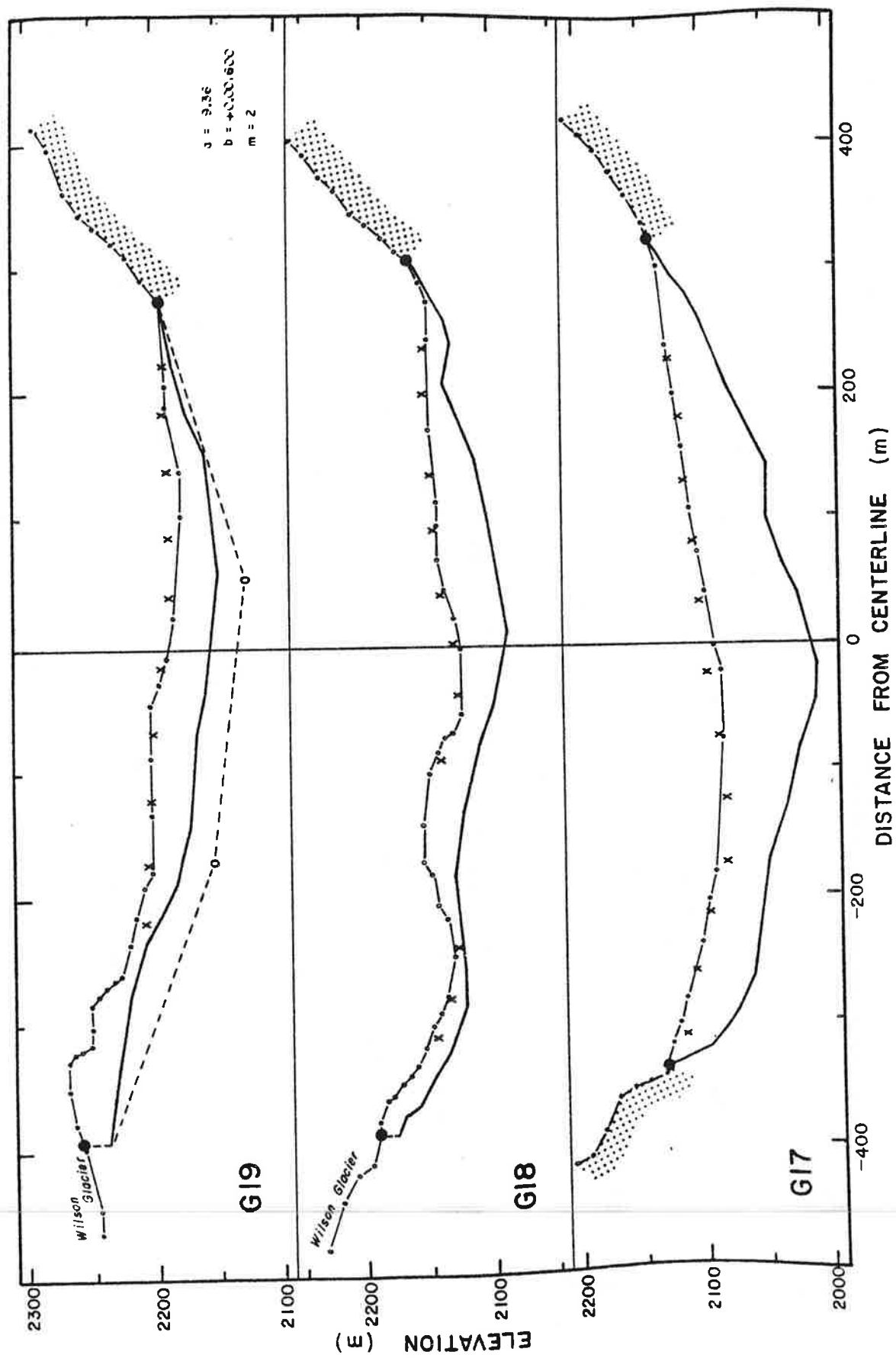












Appendix B

THE TILT OF THE STAKES AND THE MASS BALANCE CURVES

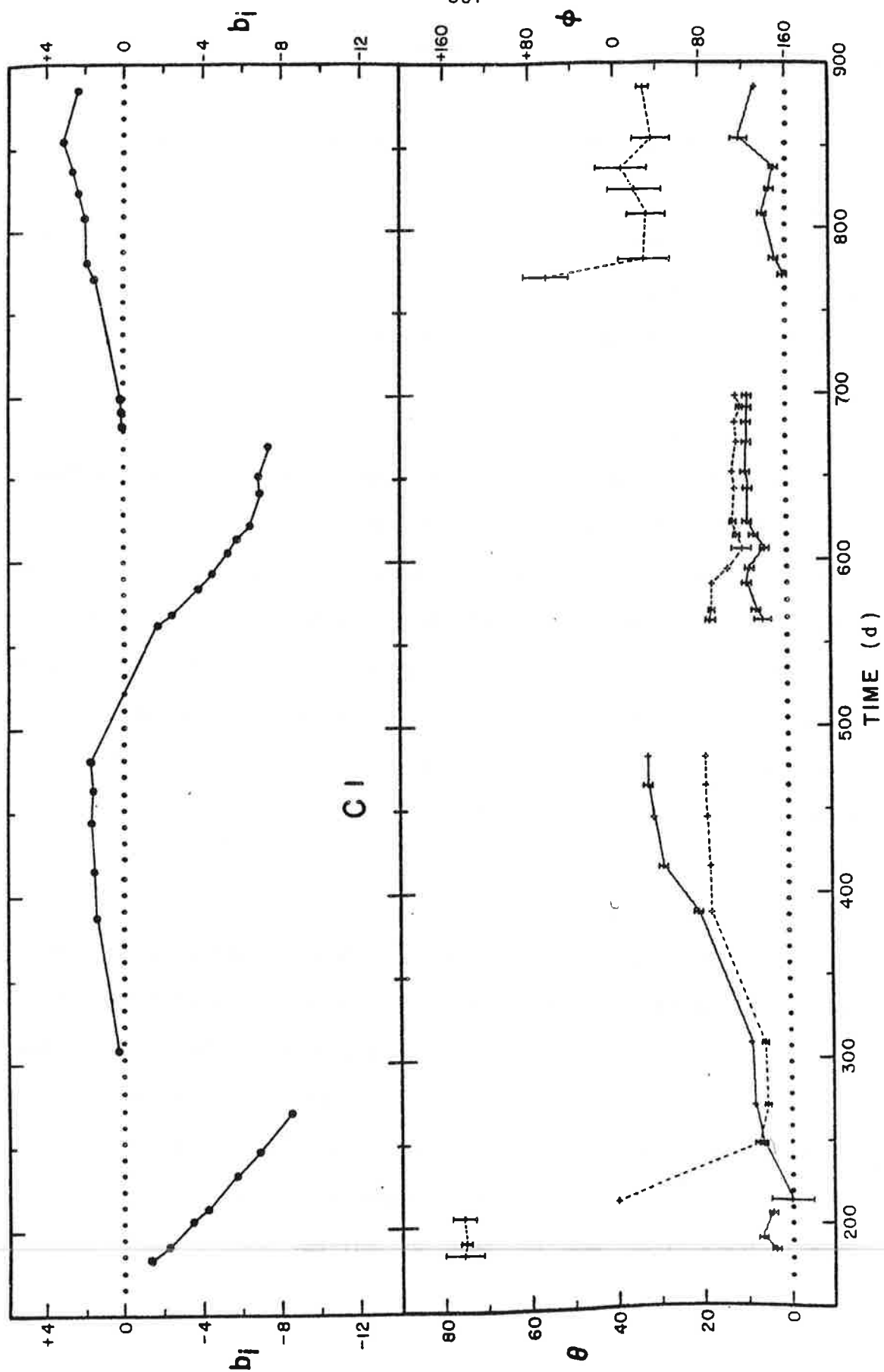
On the following pages are shown the tilt (θ, ϕ) and the mass balance (b_i), as a function of time, for each of the centerline stakes. The overlay in the rear pocket can be used with these diagrams.

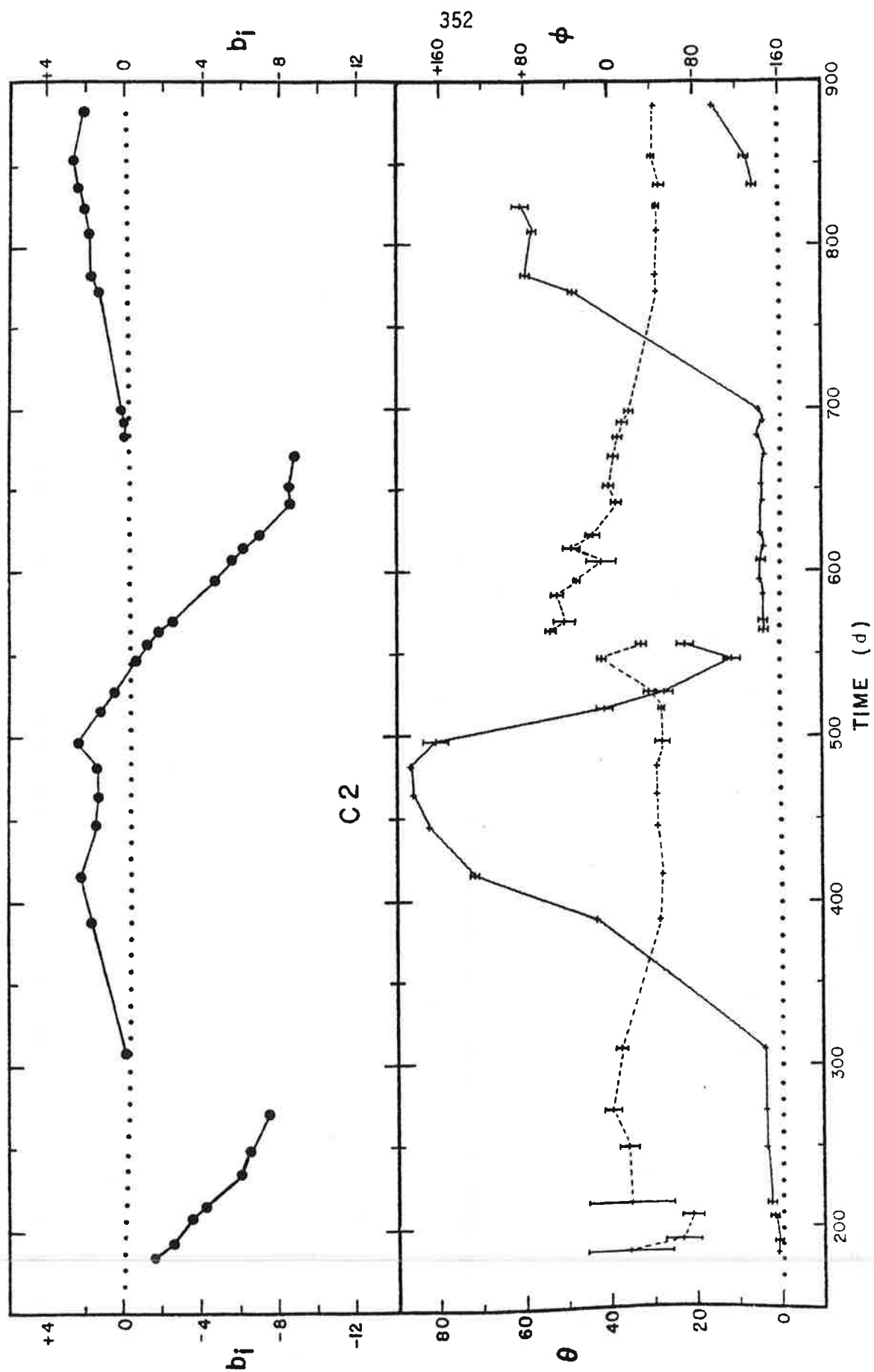
The mass balance

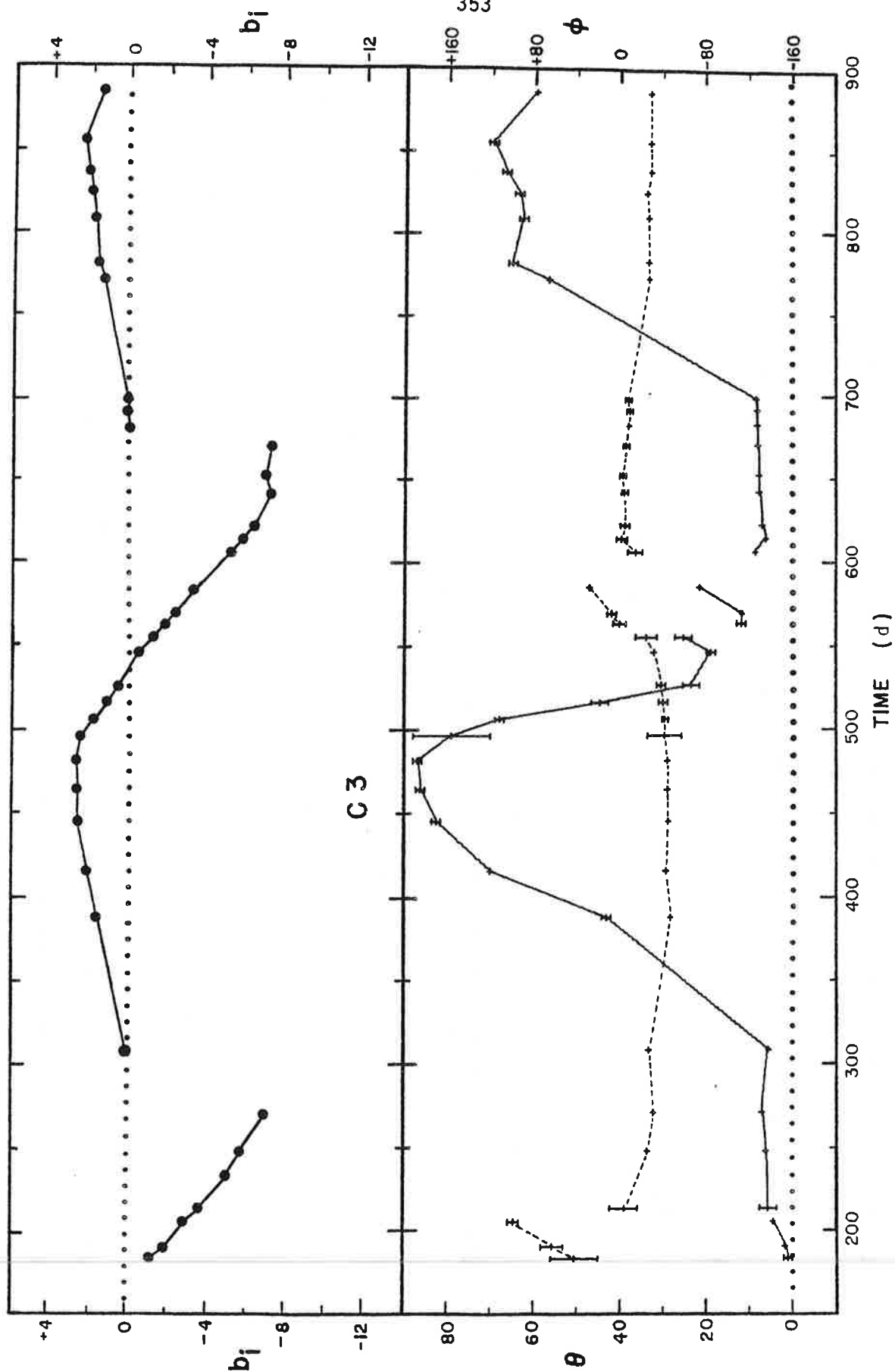
The units are meters of ice equivalent. No error bars are shown since the error of reading the surface level on a stake is less than the size of the plotting symbols. In the winter, however, departures of the stake from the shape assumed in the calculations could produce errors in the bend corrections by as much as ± 0.5 m in the vertical direction. Gaps in the curves indicate times when the origin was reset to the new summer surface, usually in October. Stakes C16 through C20 are assumed to be at the equilibrium line and so the origin does not have to be reset.

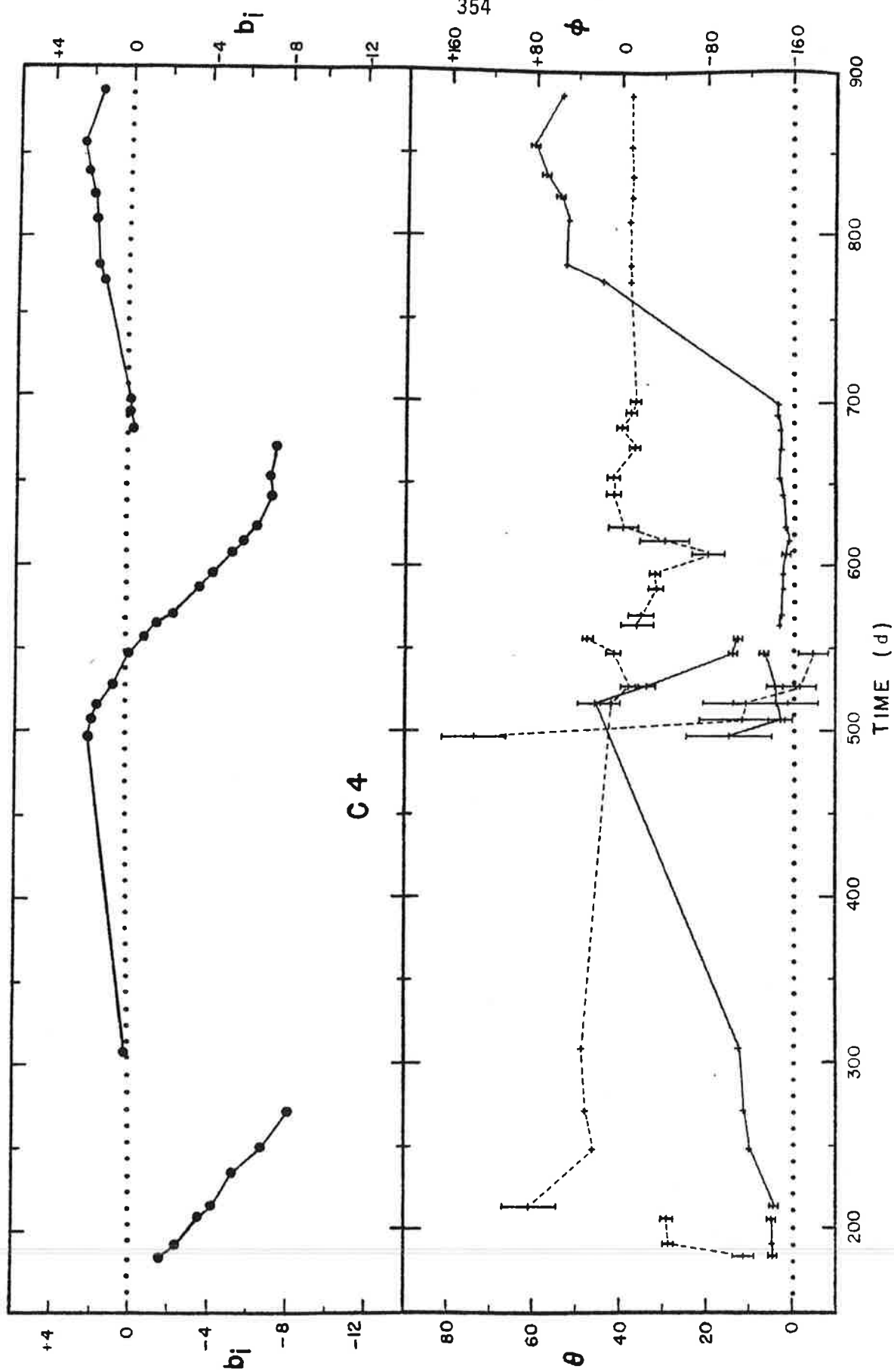
The tilt of the stakes

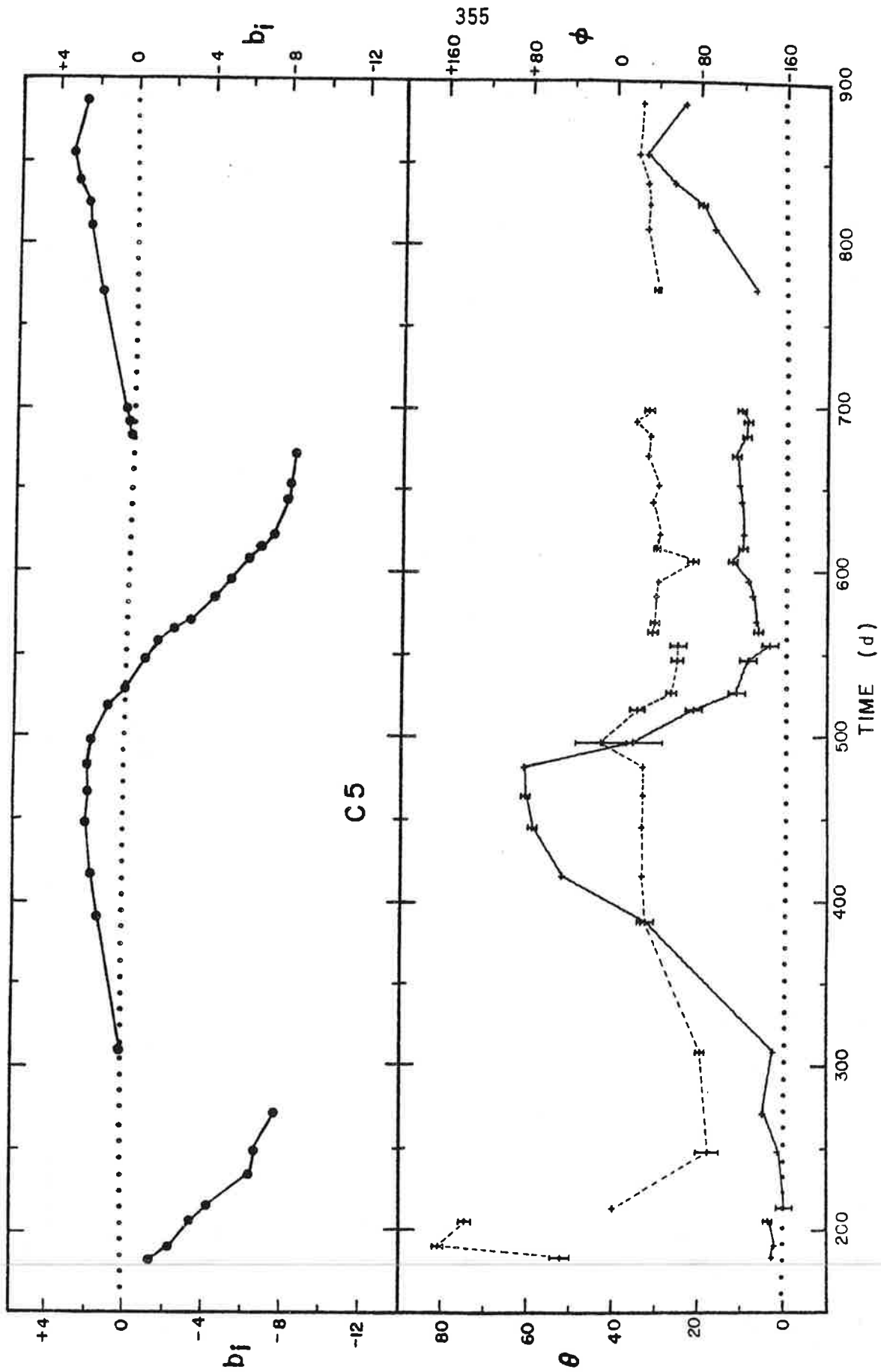
θ is the amount of tilt in degrees from the zenith (solid lines, scale at left). ϕ is the azimuth of the tilt in degrees (dashed lines, scale at right); this is the direction that the top of the stake points, measured from the +X direction (true south), positive to the east and negative to the west. Error bars are the standard deviations in θ and ϕ (calculated from equation 6.57), assuming the errors in the measured angles are $\sigma_h = 3.1''$ and $\sigma_v = 5.3''$. Gaps indicate times when the stake was shifted.

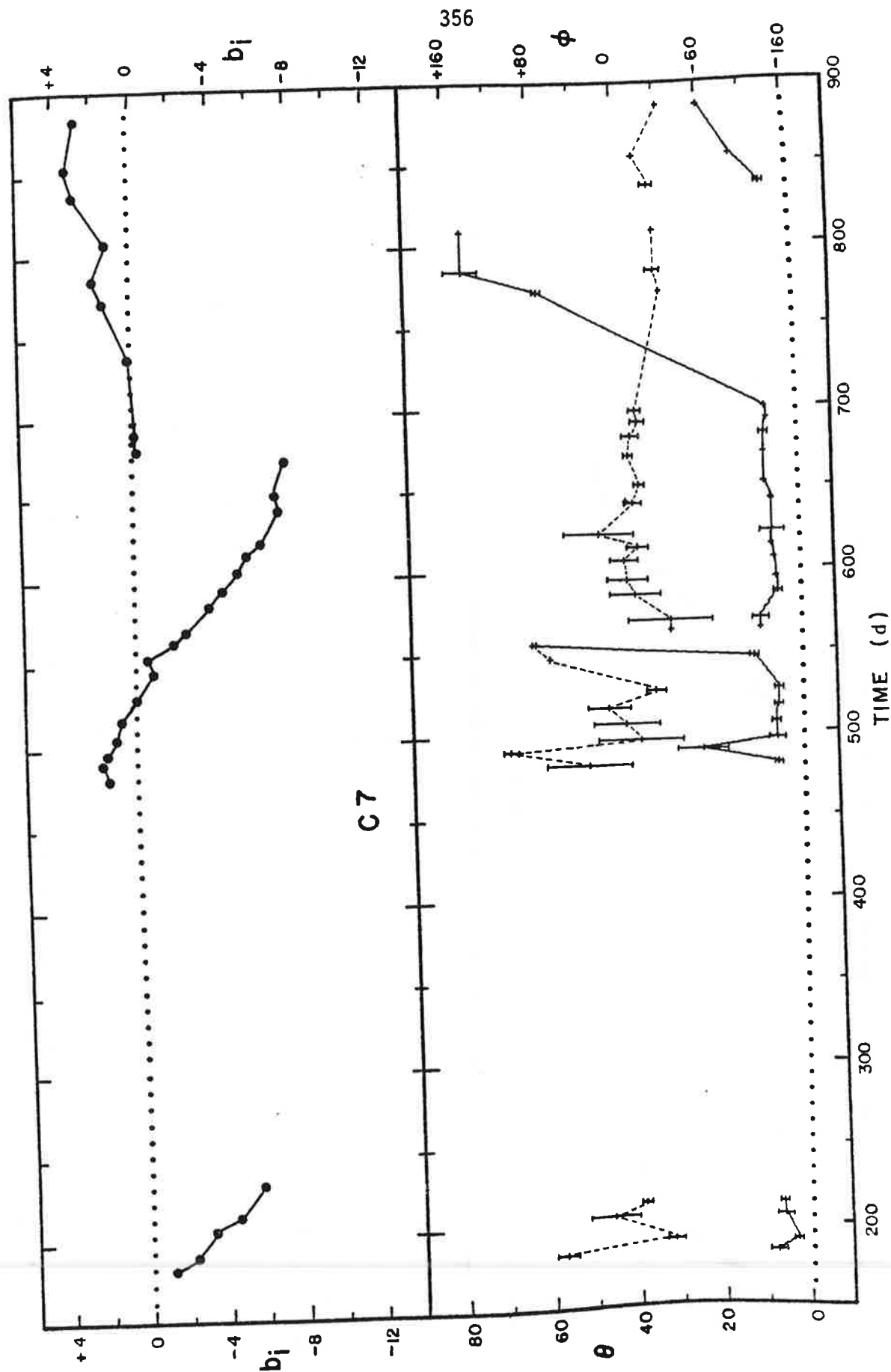


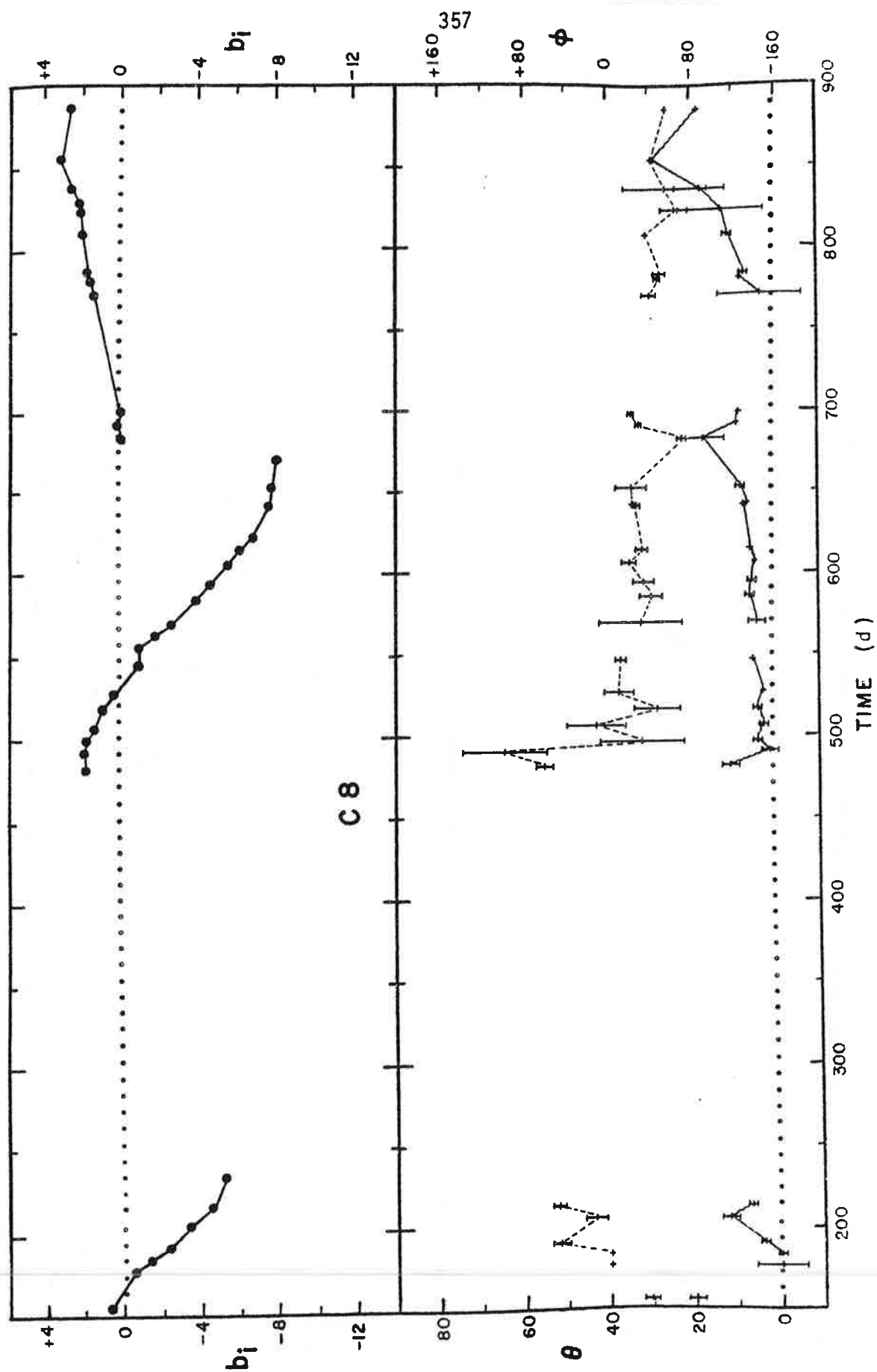


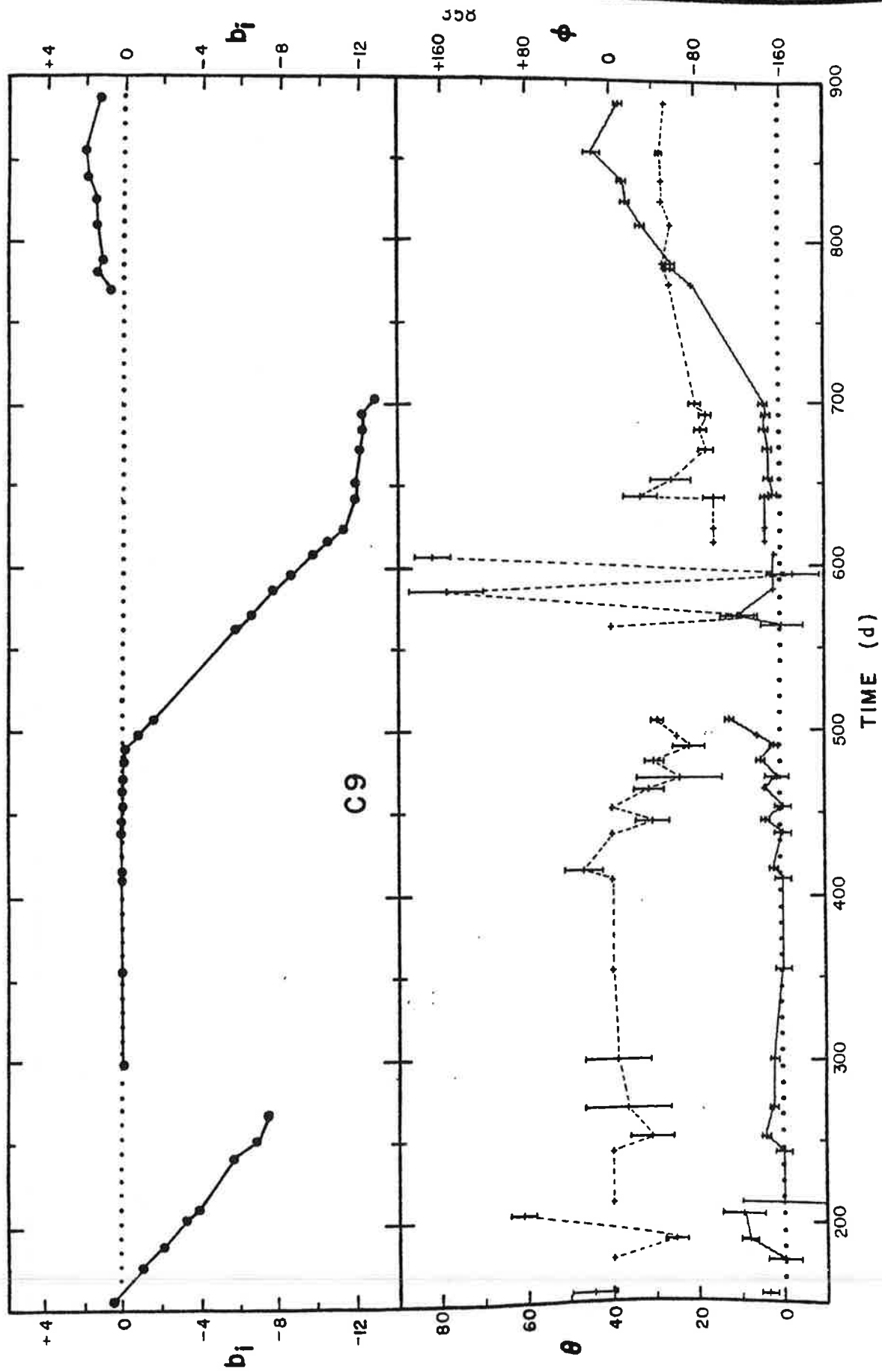


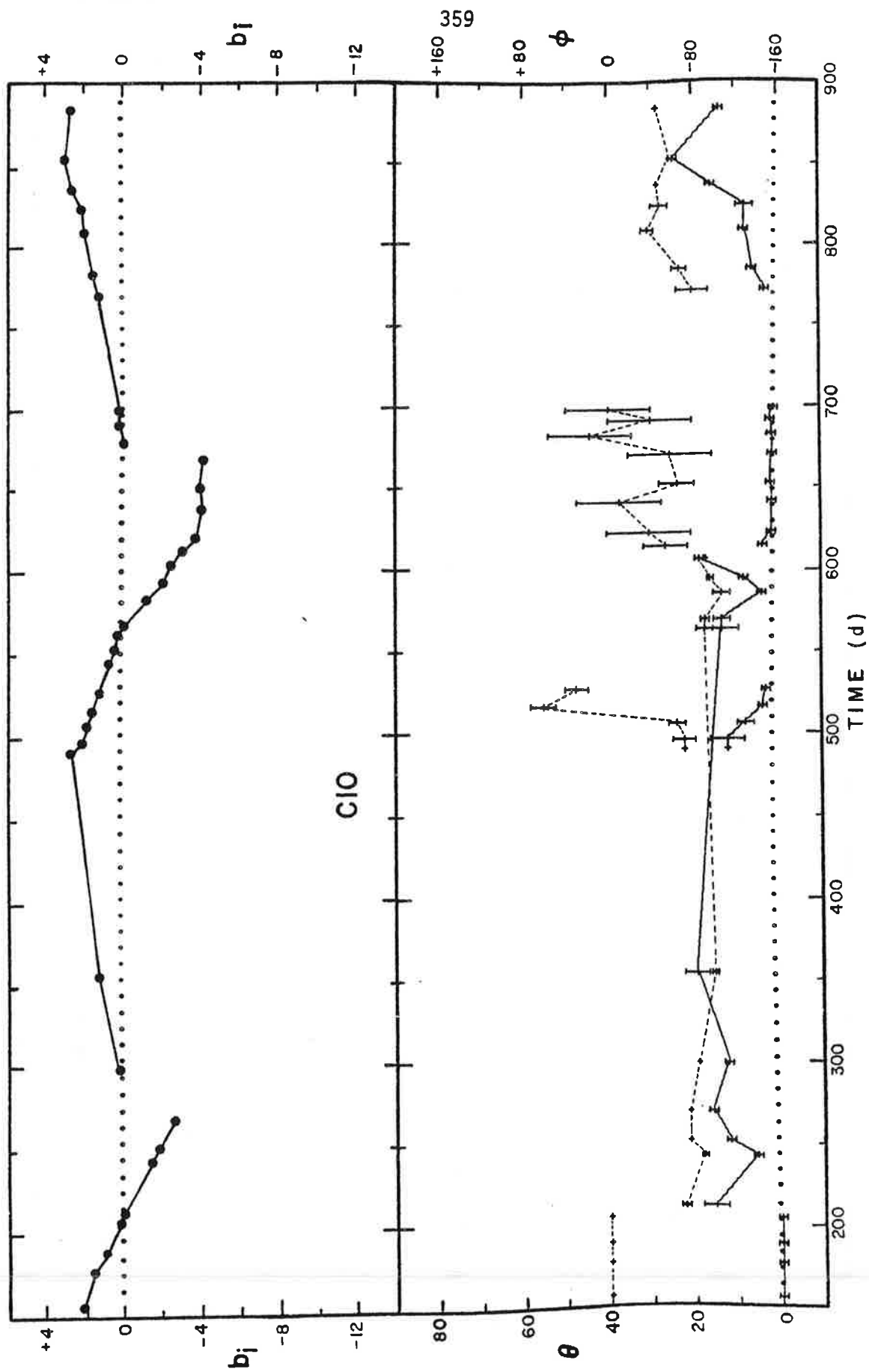


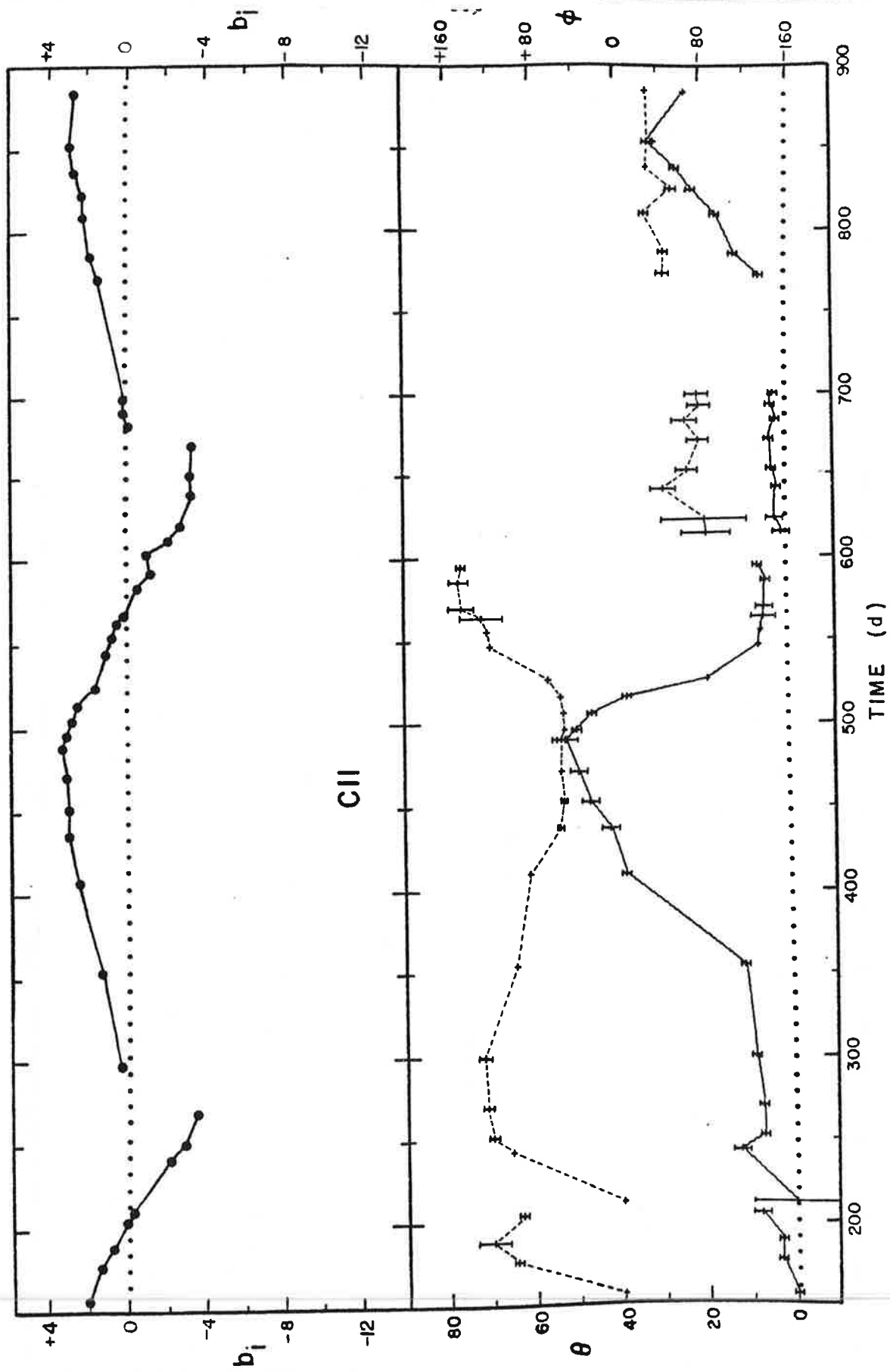


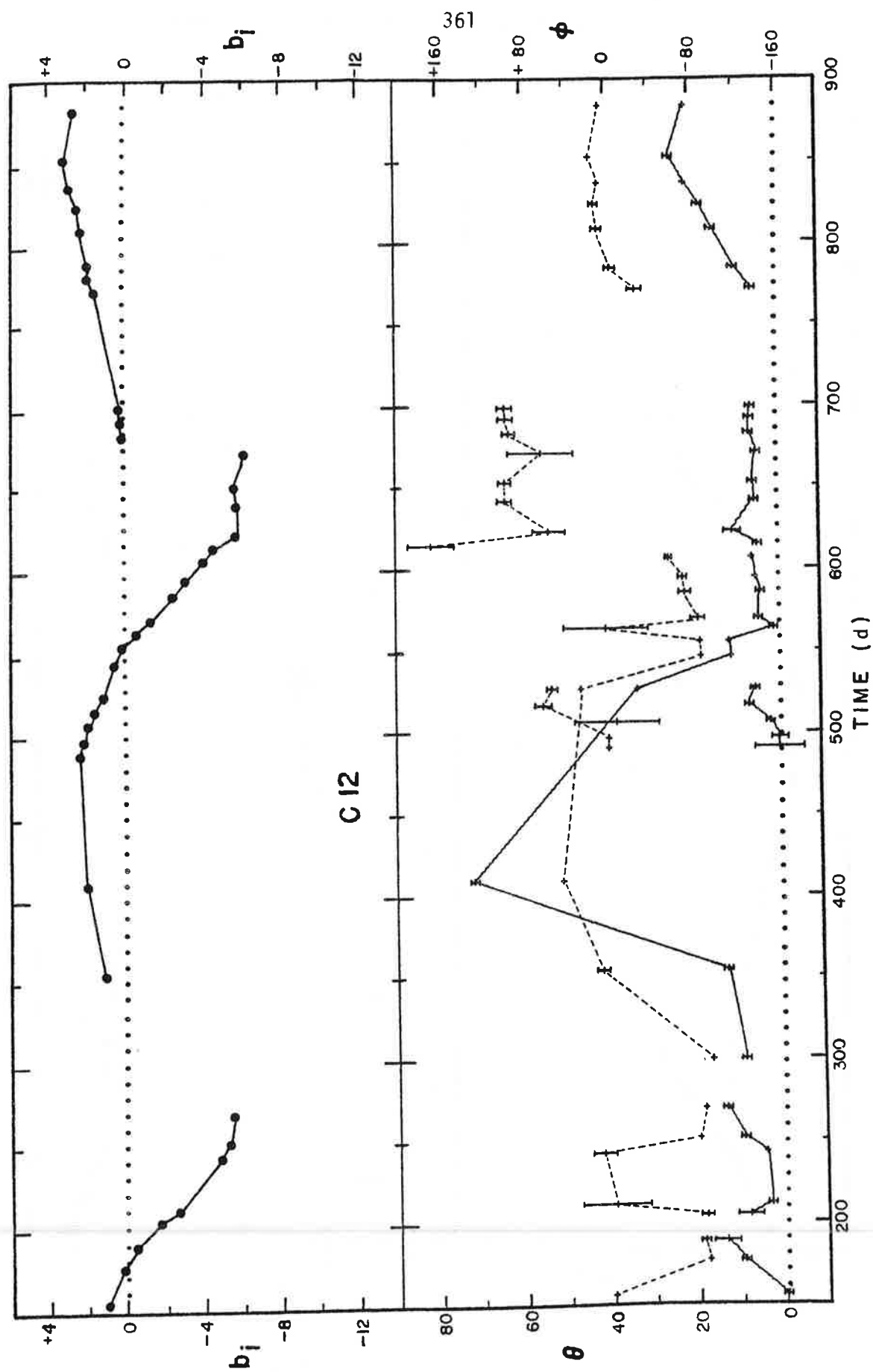


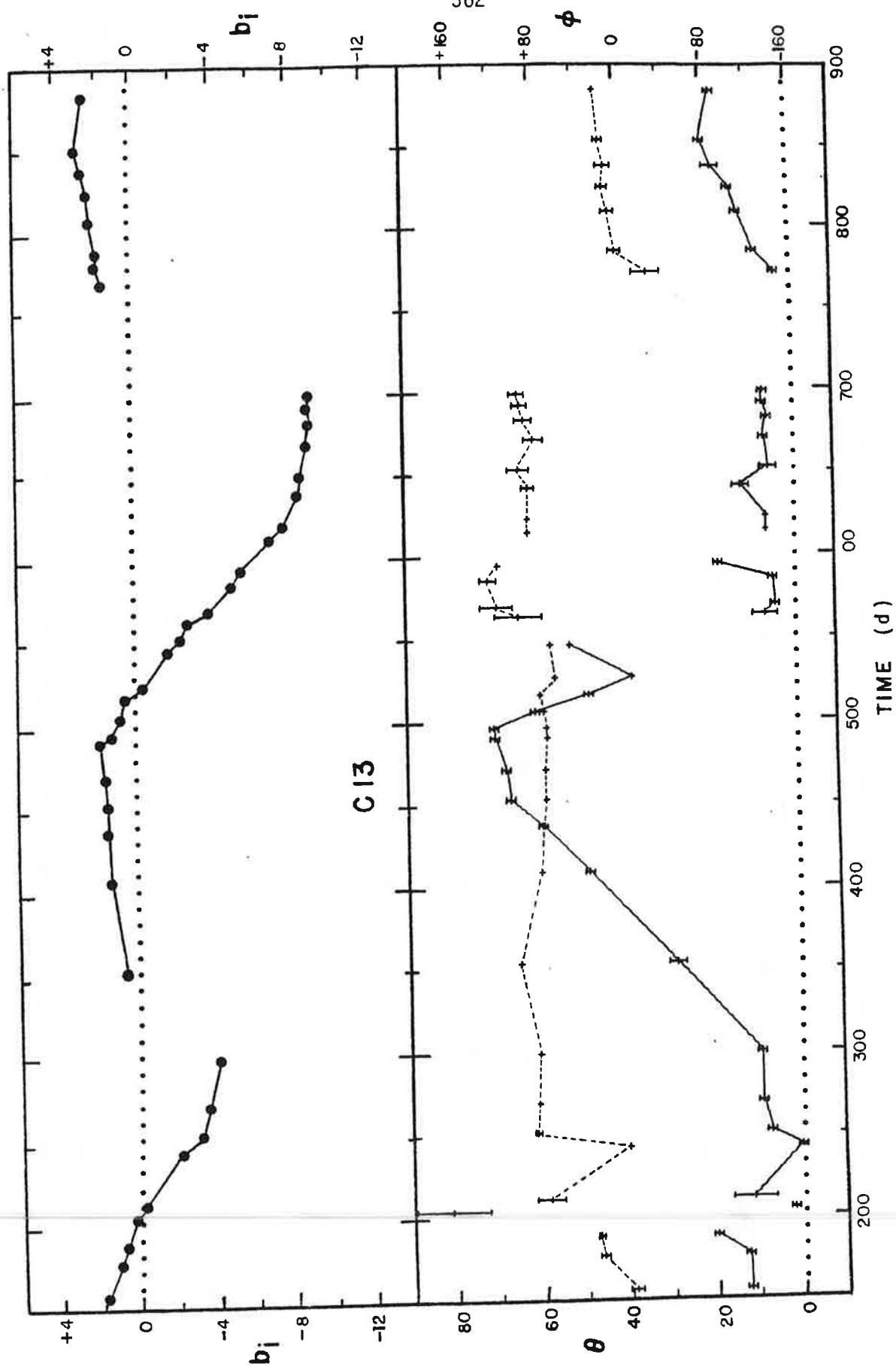


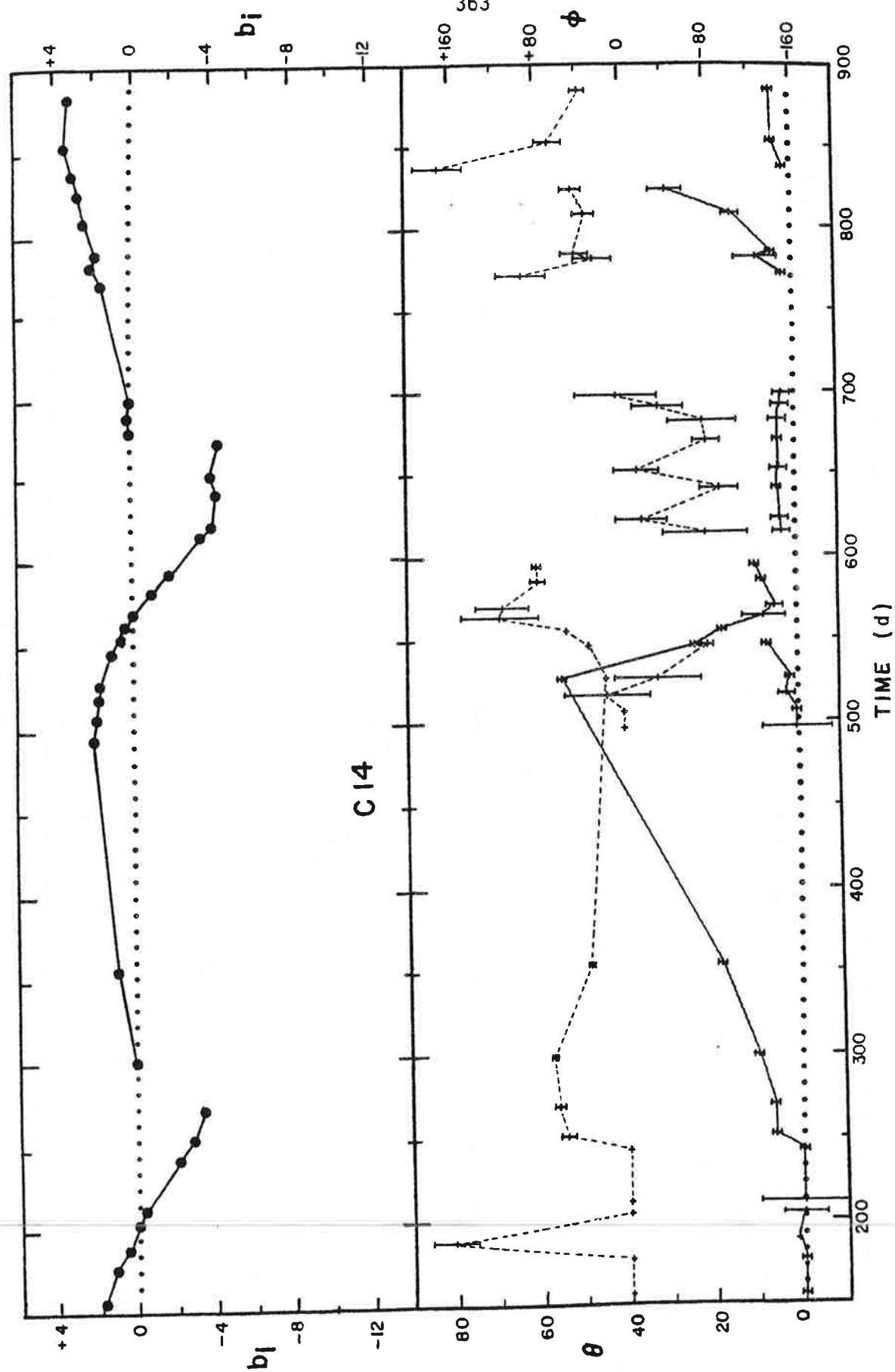


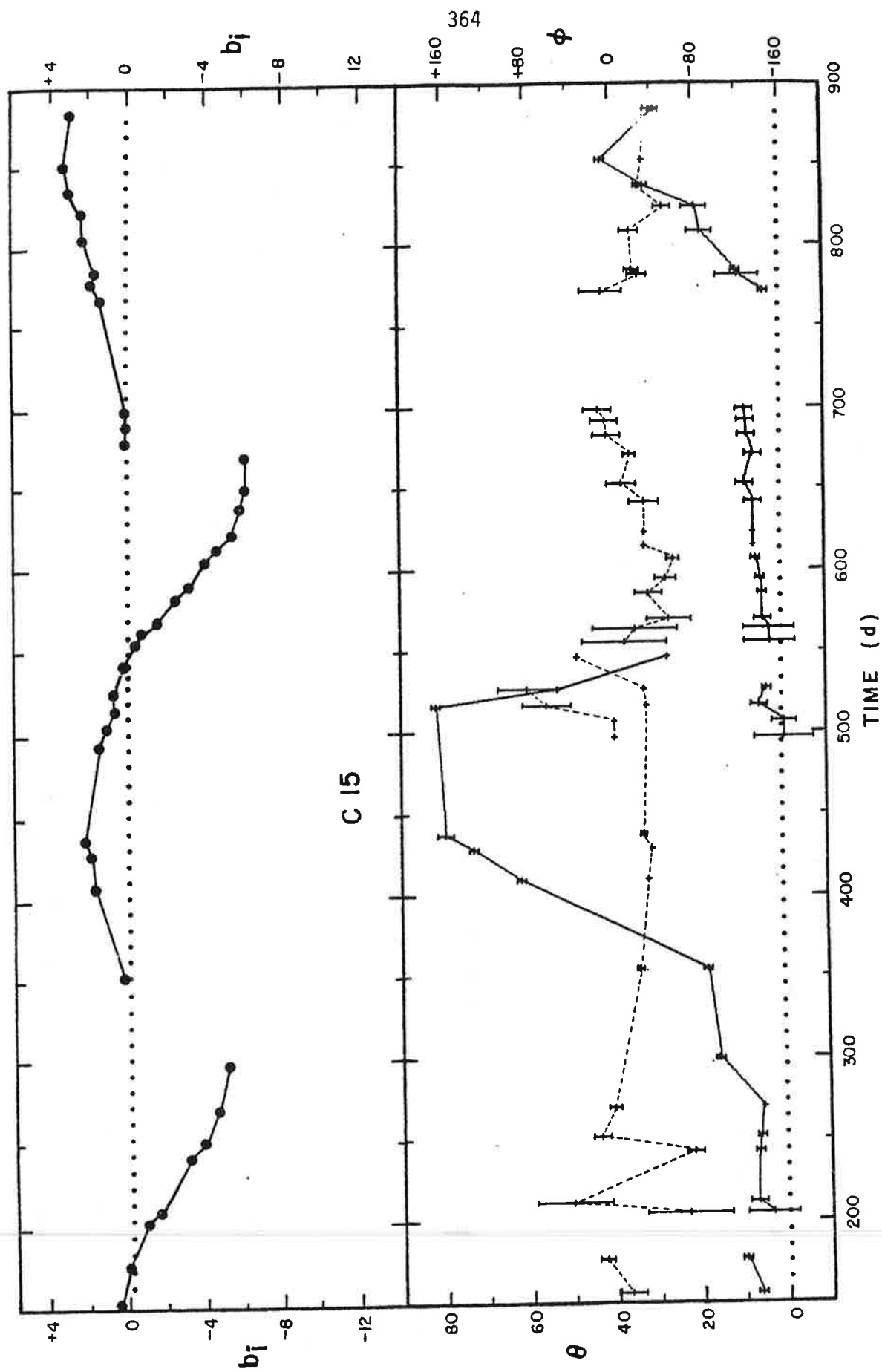


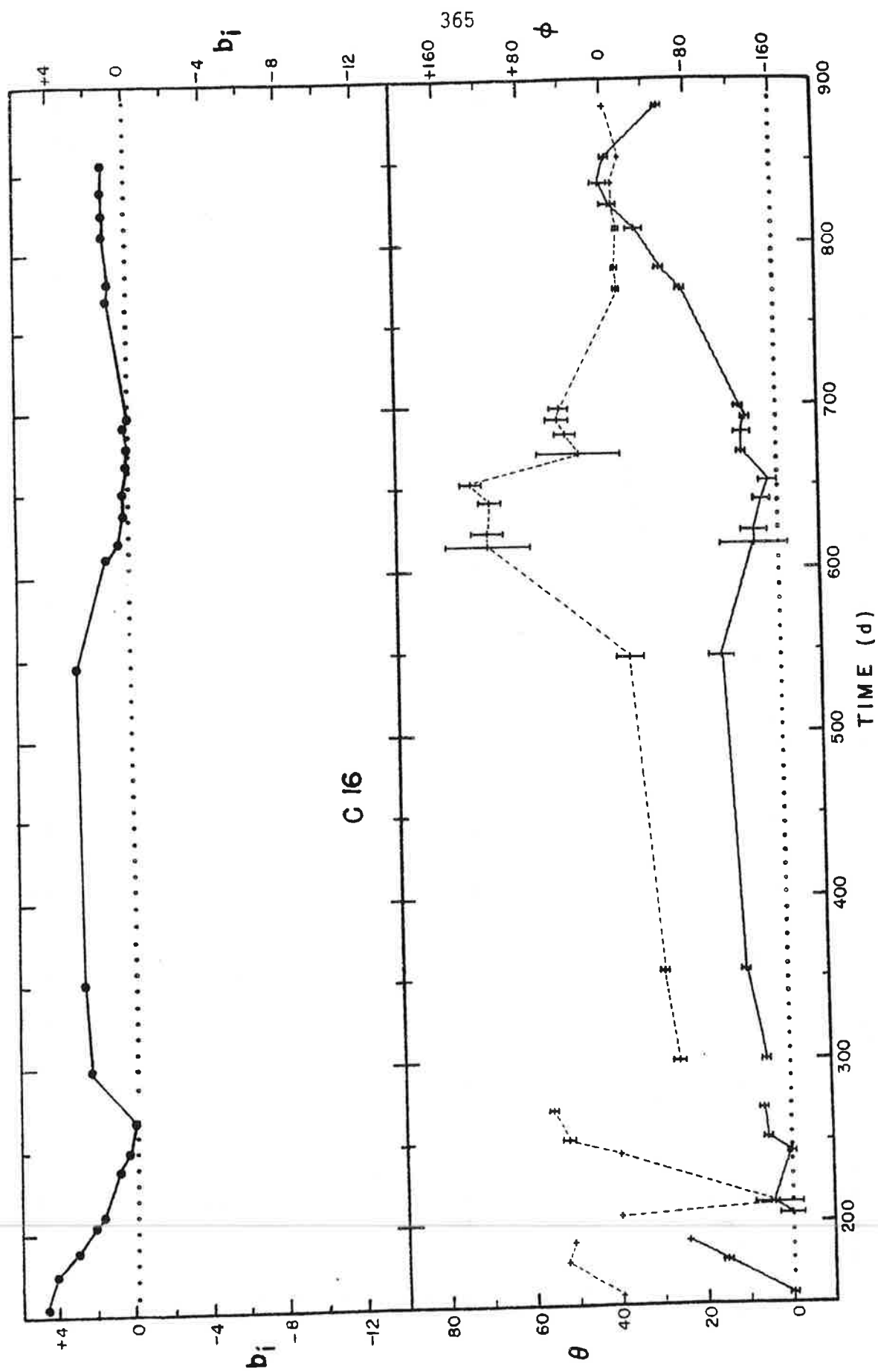


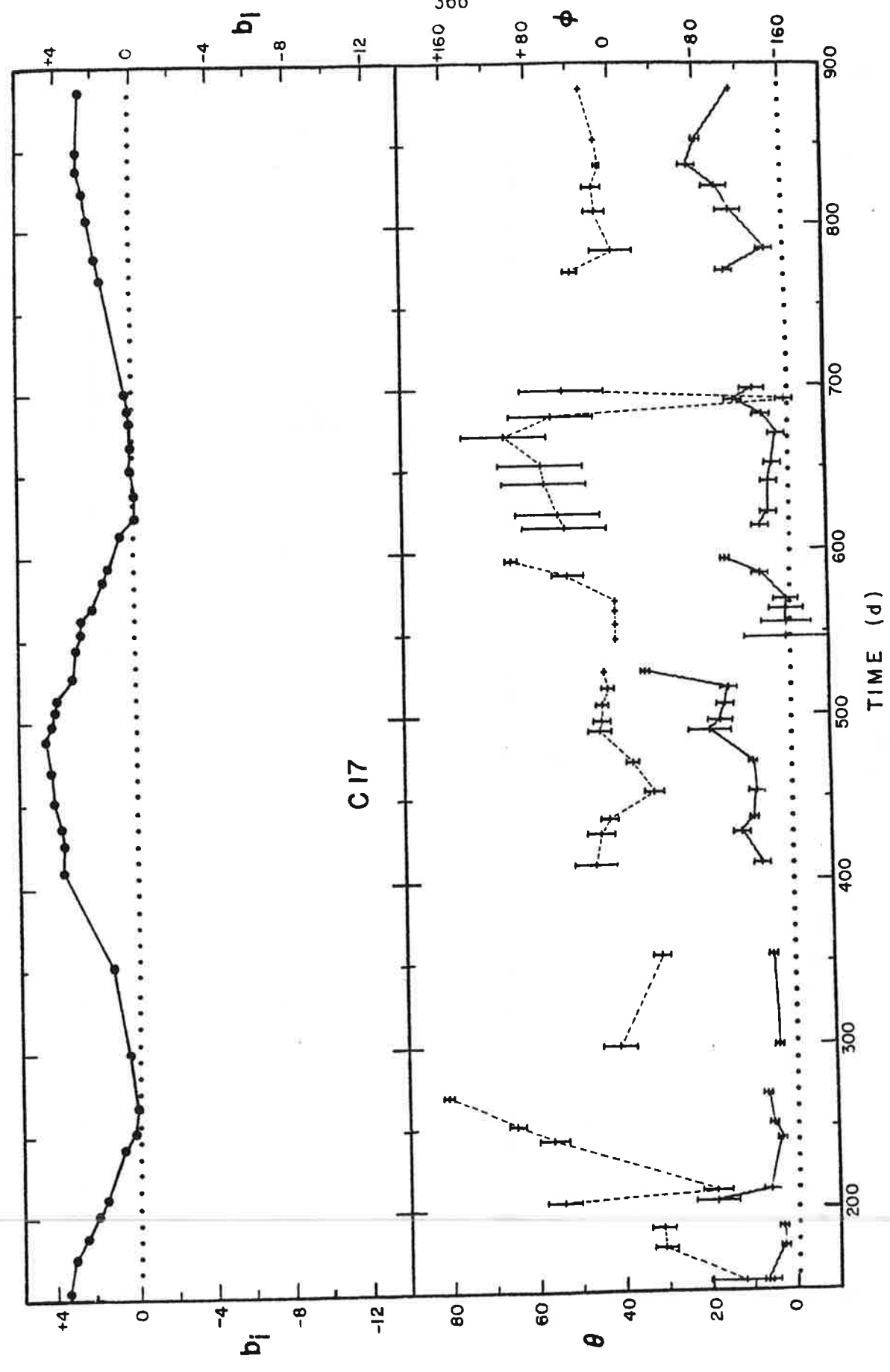


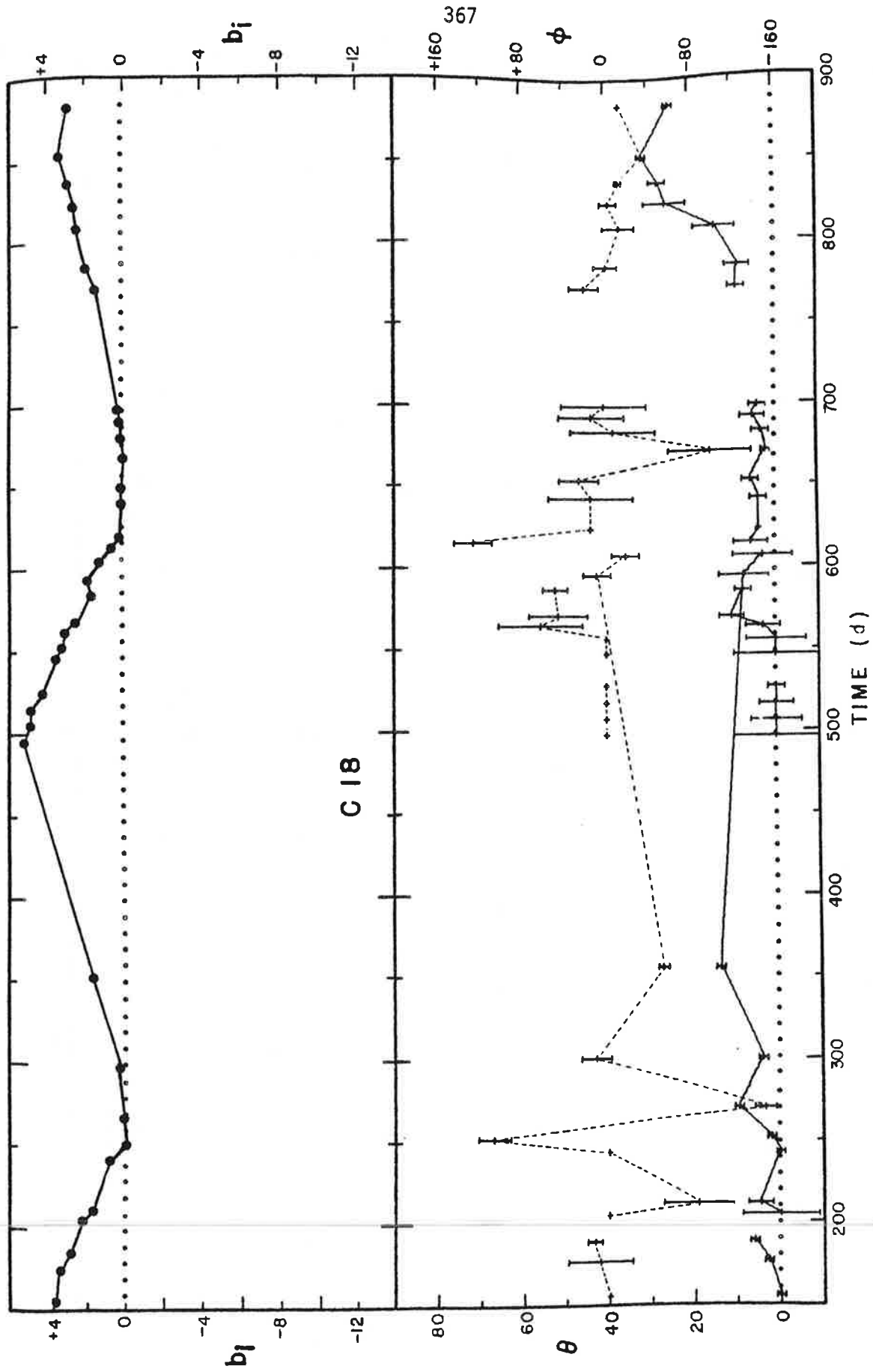


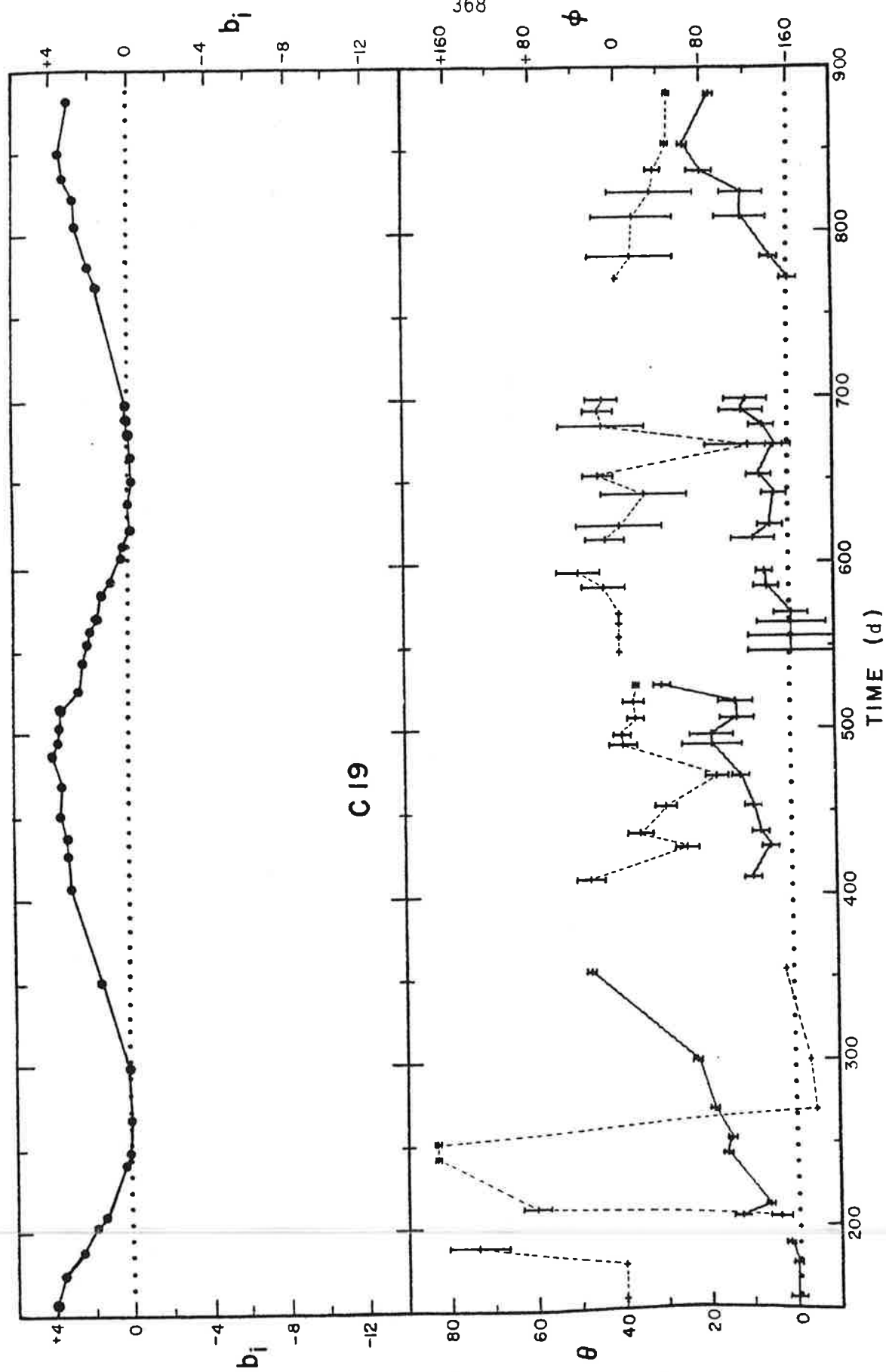


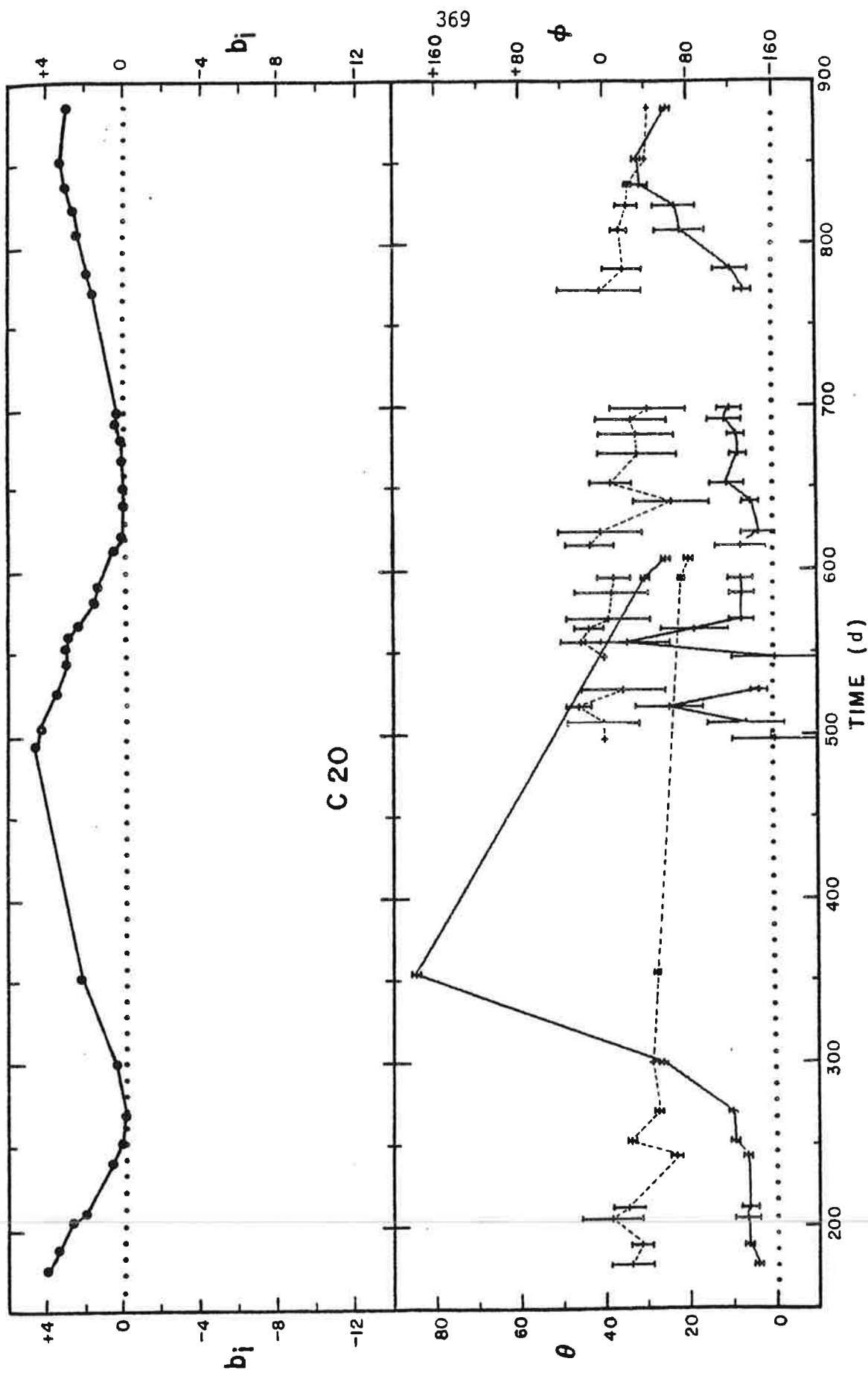












Appendix C

RESULTS OF THE VELOCITY CALCULATIONS

C.1 THE EFFECT OF DIFFERENT REDUCTION METHODS AND CORRECTIONS

On the following pages is shown the effect of the different methods and corrections used to calculate the velocity (see Table 13, p. 209). The effects vary from one stake to the next and so three stakes, C2, C3 and C13, were selected to illustrate the various situations.

The data for each stake consist of four diagrams: the speed versus time for (a) correction method III (changes in tilt and length allowed), (b) correction method IV (changes in shape, tilt and length allowed), (c) the flex method and (d) the flex method plus corrections for transverse velocity gradients and elimination of faulty data points and points whose time interval is less than 15 days.

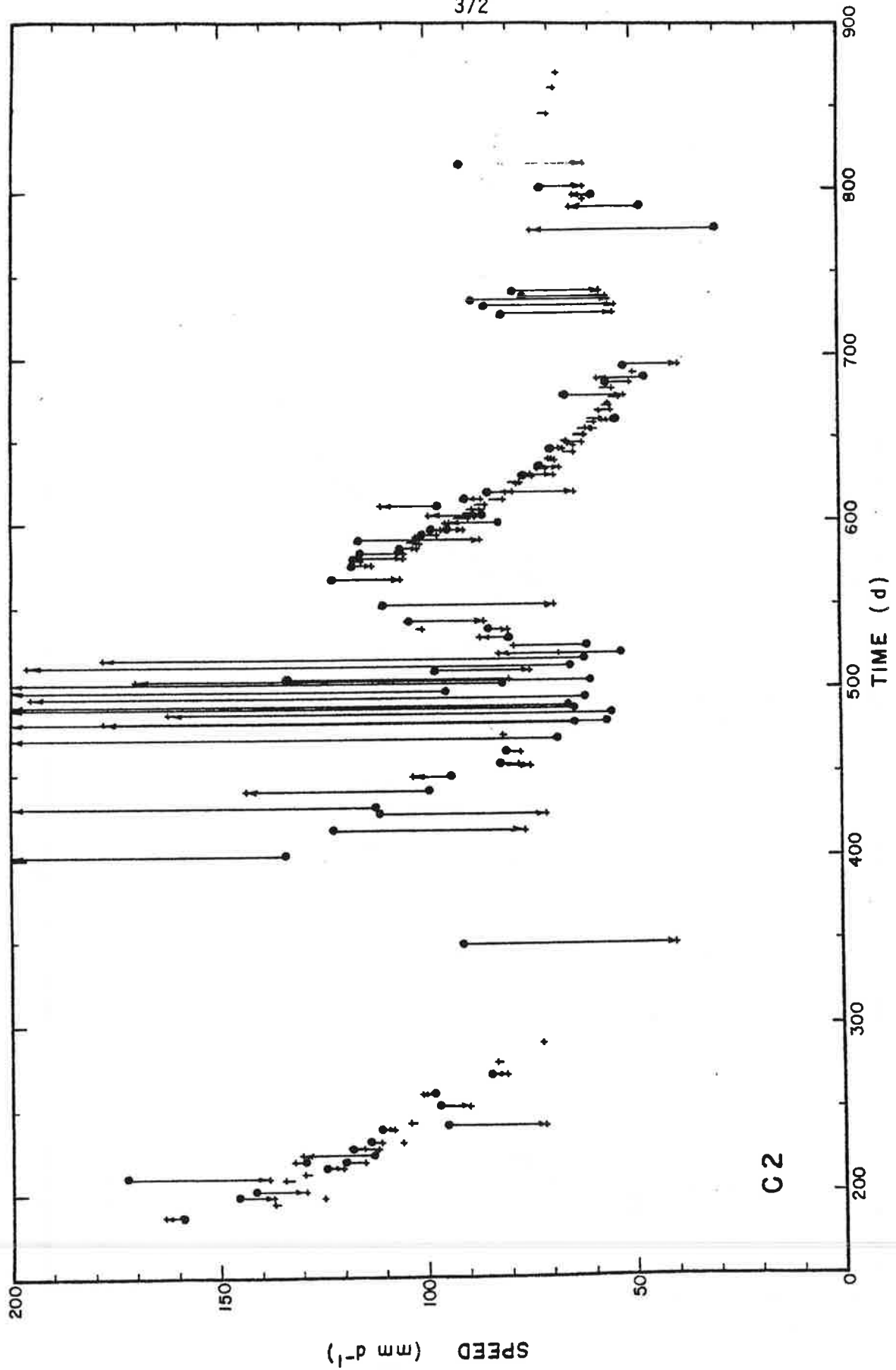
In the first three graphs, the "+" symbols denote the corrected values and the dots the uncorrected values (that is, correction method II, changes in length only). An arrow from the dot to the "+" thus shows the amount and direction of the correction. No dots are indicated if the magnitude of the correction is small (only a short line visible) or if it is negligible (less than the size of the "+" symbol). The scale of the graphs is equal to that used on the final curves (appendix C.2); consequently some points lie outside the border.

In the fourth graph, the "+" symbols denote the values calculated by the flex method. A short line indicates the correction for transverse velocity gradients (p. 222). Square symbols are points eliminated because their time interval was less than 15 days (p. 207) and "X" symbols are faulty data points (p. 224). The final data points $s_o(t_i)$ are therefore at the ends of the short lines on the "+" symbols.

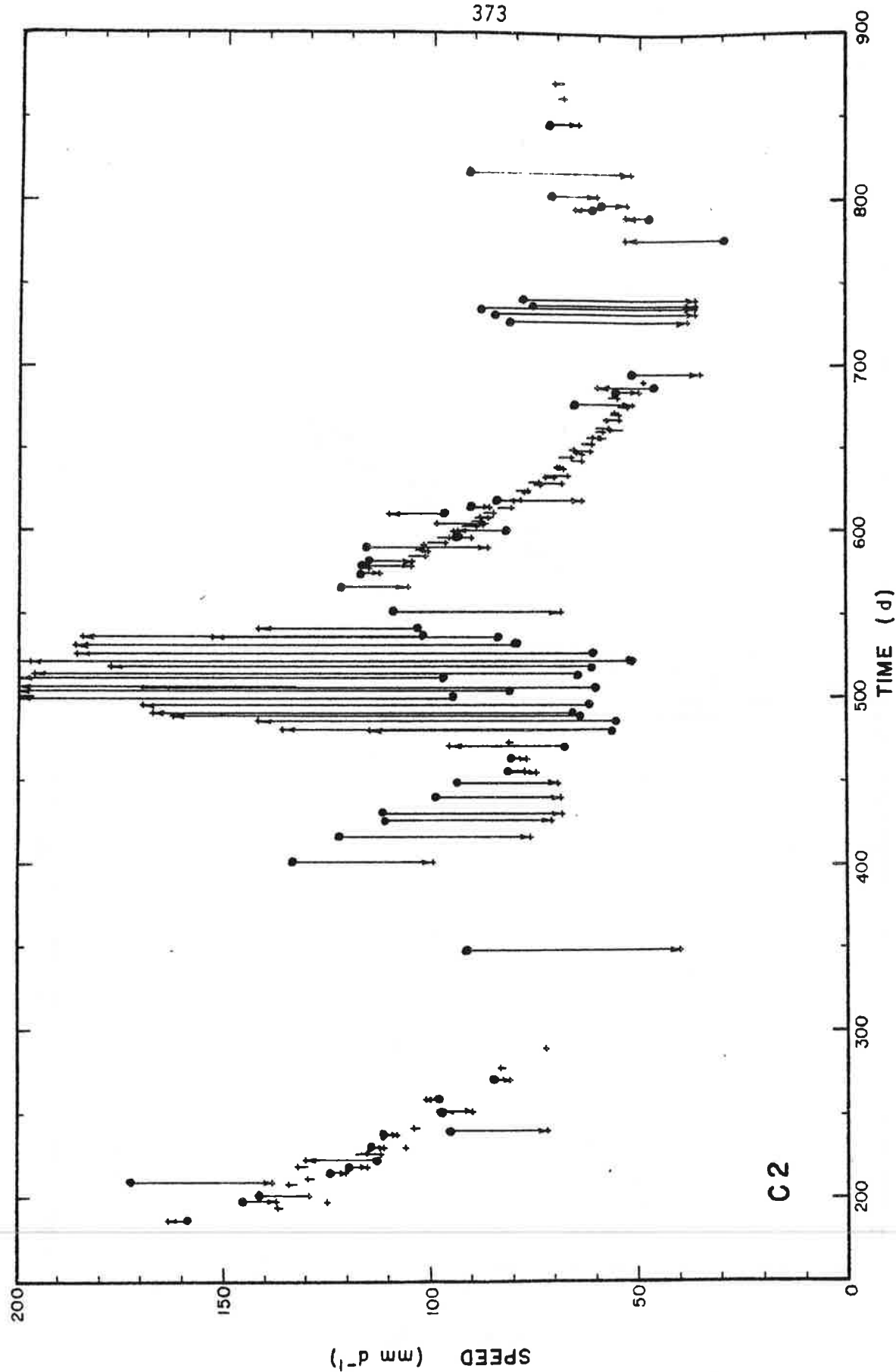
Because the corrections for transverse velocity gradients are small, graph (d) has also been included for stake C7, which has the largest absolute value of the correction. The corrections are essentially constant and do not affect the shape of the curve, except during the spring of 1970, when the stake was shifted closer to the centerline.

The "scatter" mentioned in the captions is defined on p. 208. The "raw data" refers to the values calculated by correction method II (changes in length only).

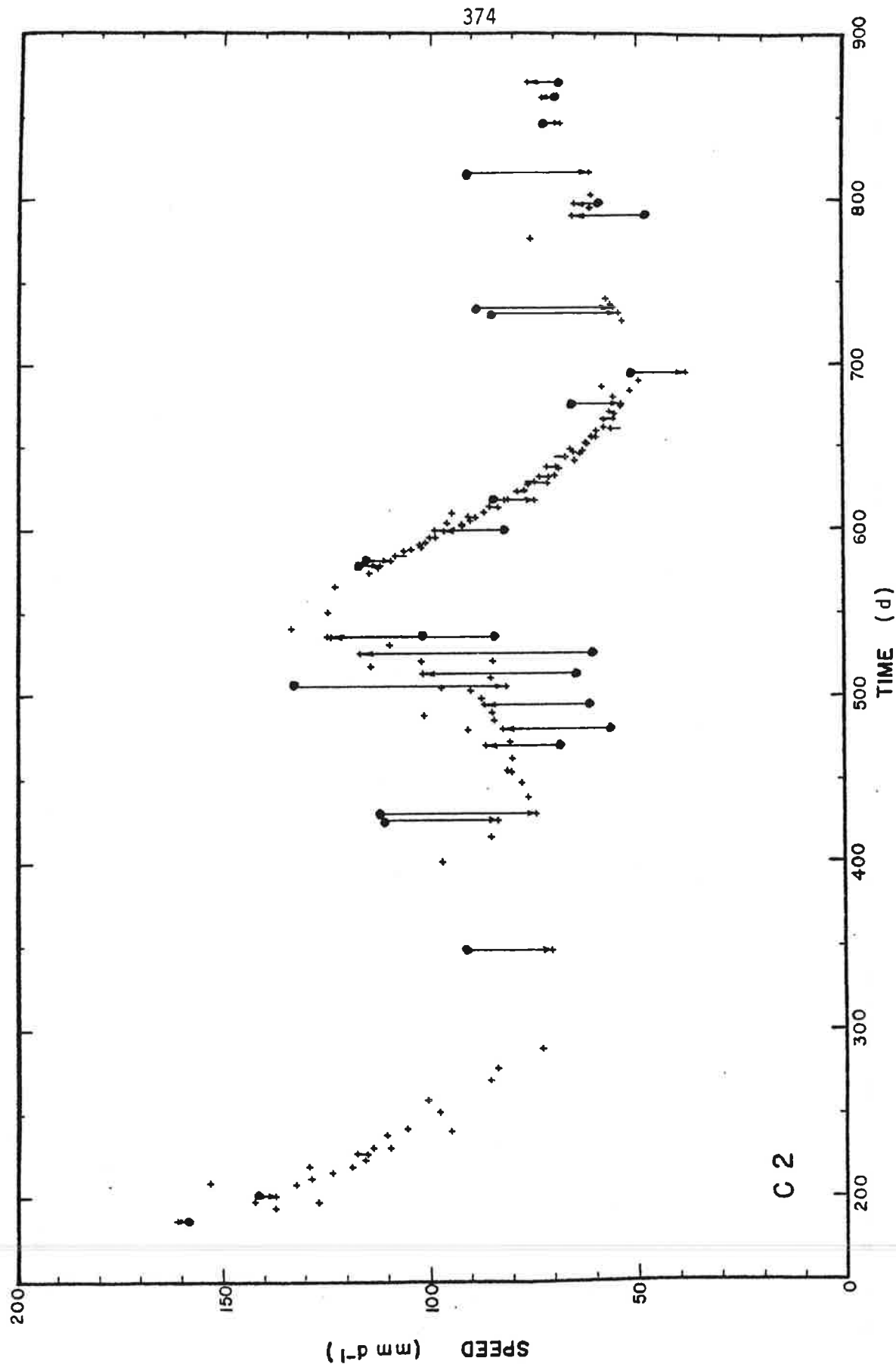
The overlay in the rear pocket can be used with these diagrams.



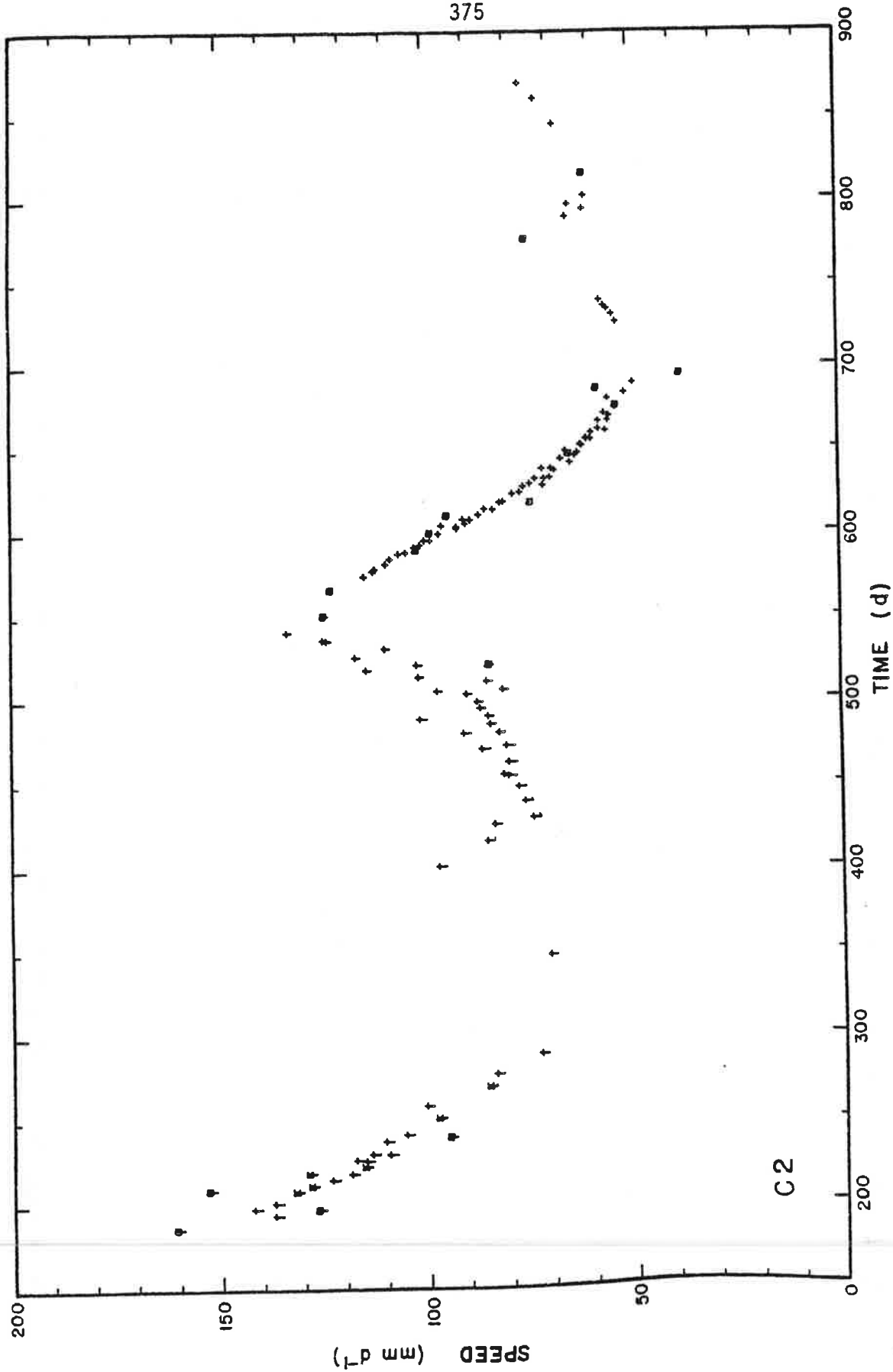
Correction method III. The scatter is increased by 253 % from that for the raw data.



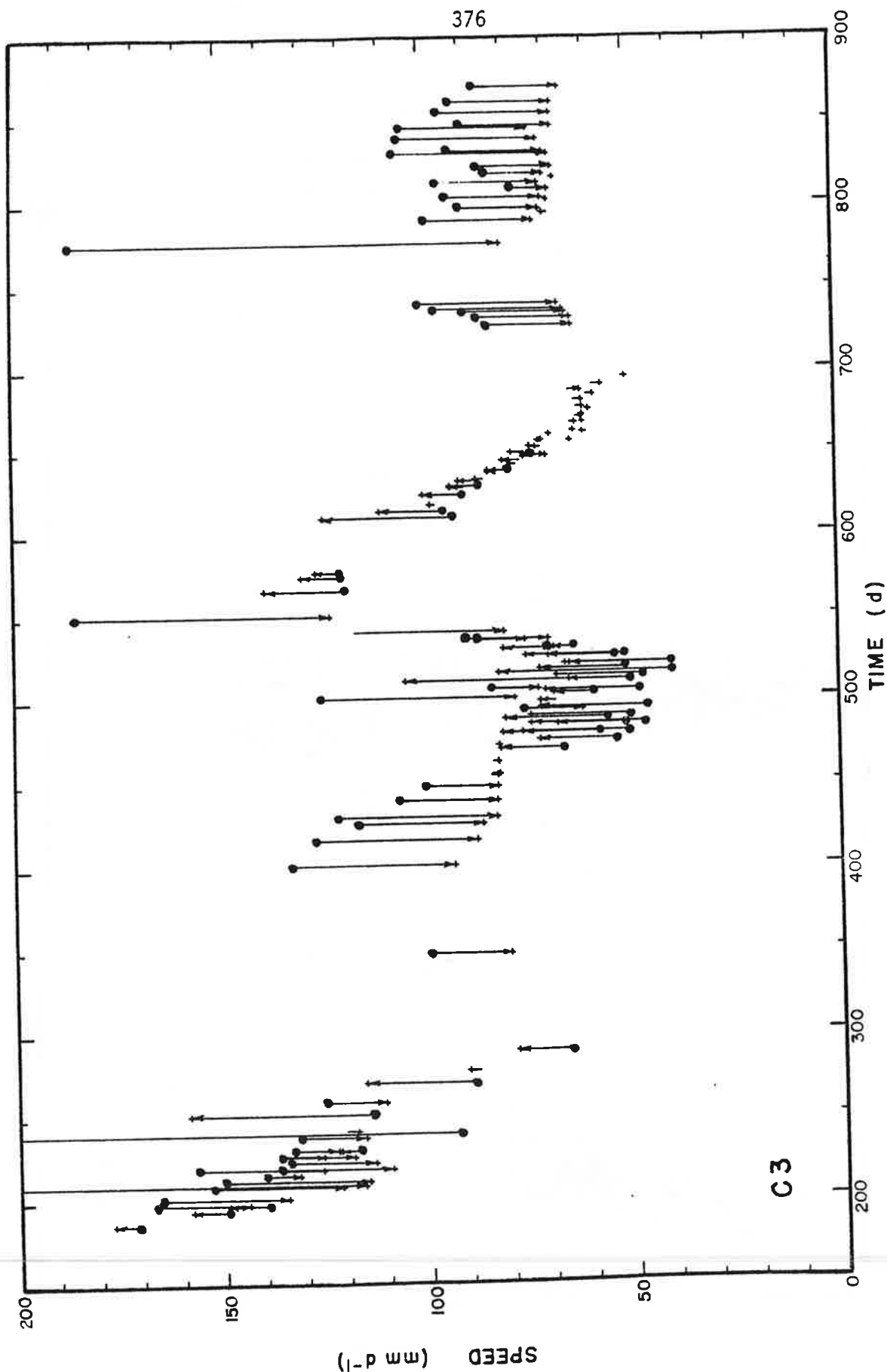
Correction method IV. The scatter is increased by 84 % from that for the raw data. This method is thus an improvement over method III, but not over the raw data.



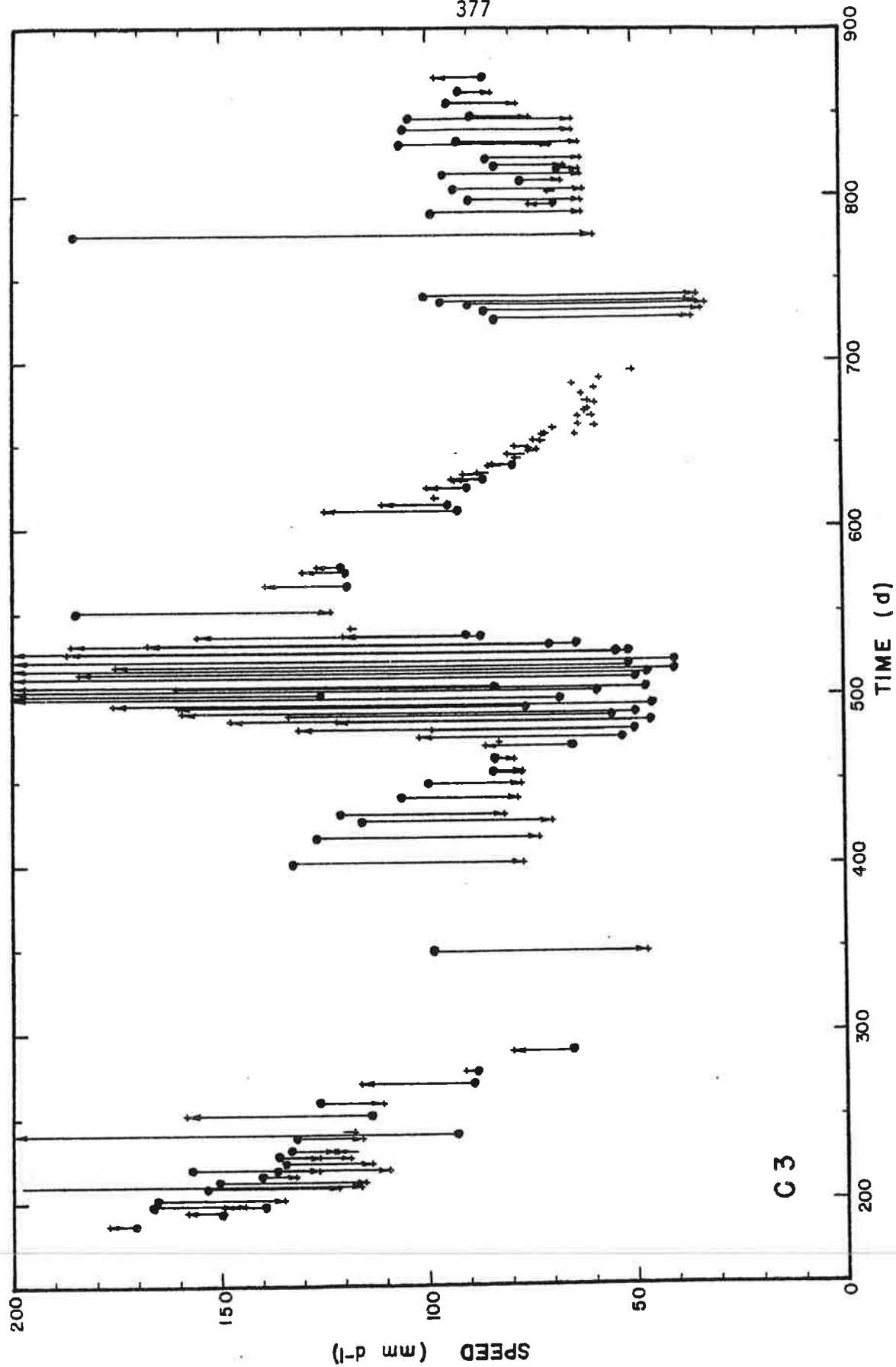
The flex method. The scatter is decreased by 63 % from that for the raw data. This method is thus an improvement over both previous correction methods and over the raw data.



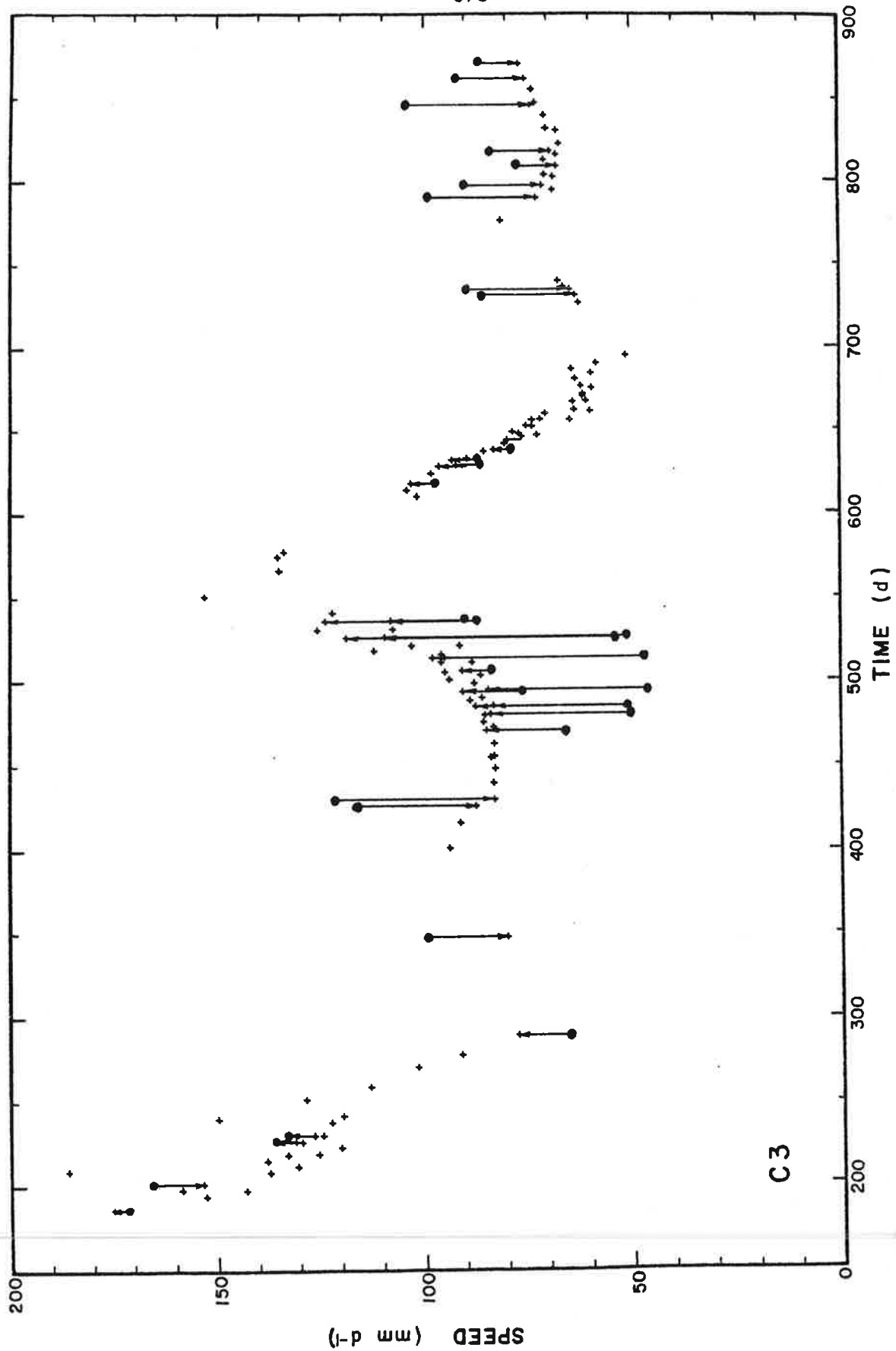
The corrections for transverse velocity gradients, the removal of time intervals less than 15 days and the removal of faulty data points. The scatter of the final data is decreased by 68 % from that for the raw data.



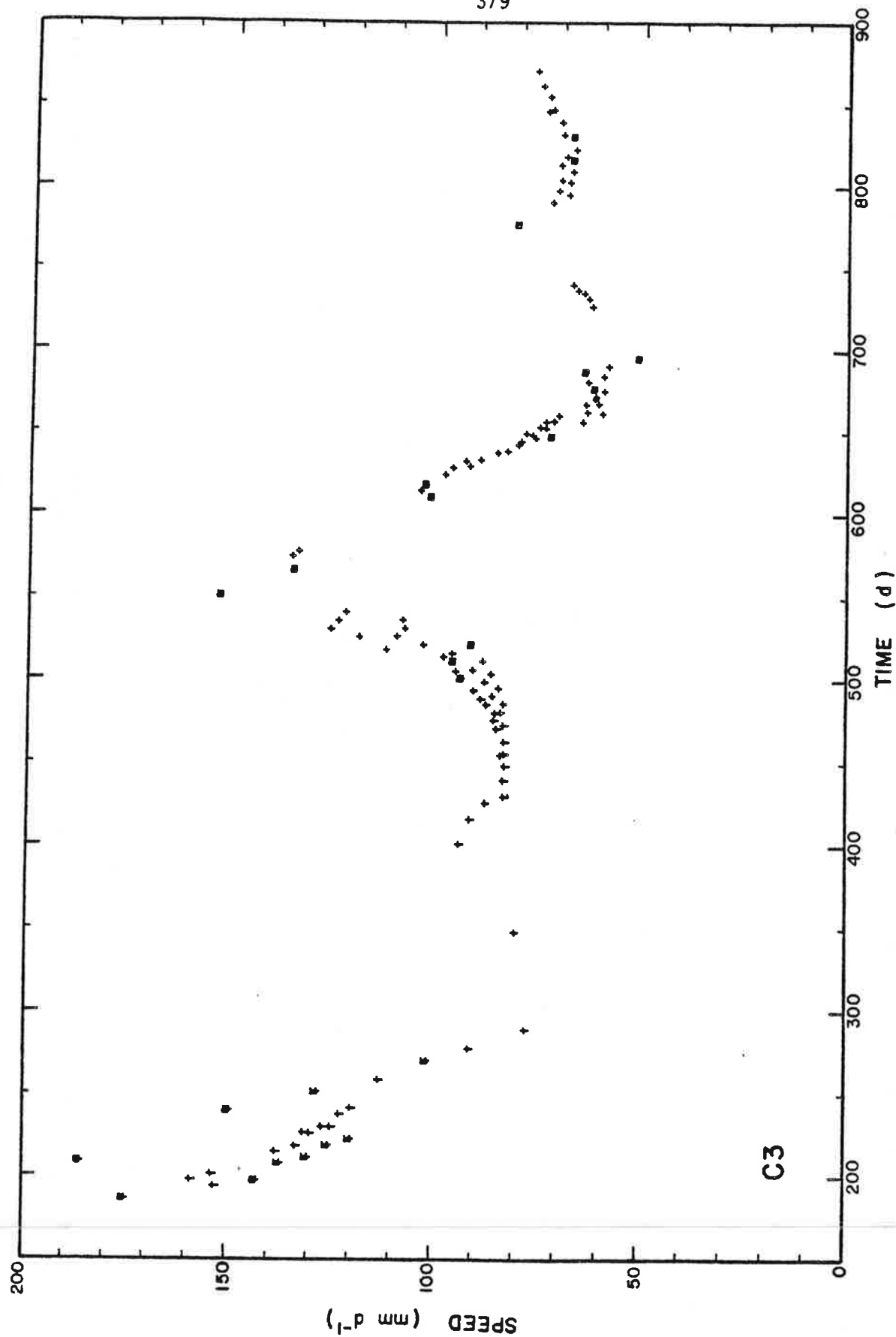
Correction method III. The scatter is decreased by 28 % from that for the raw data.



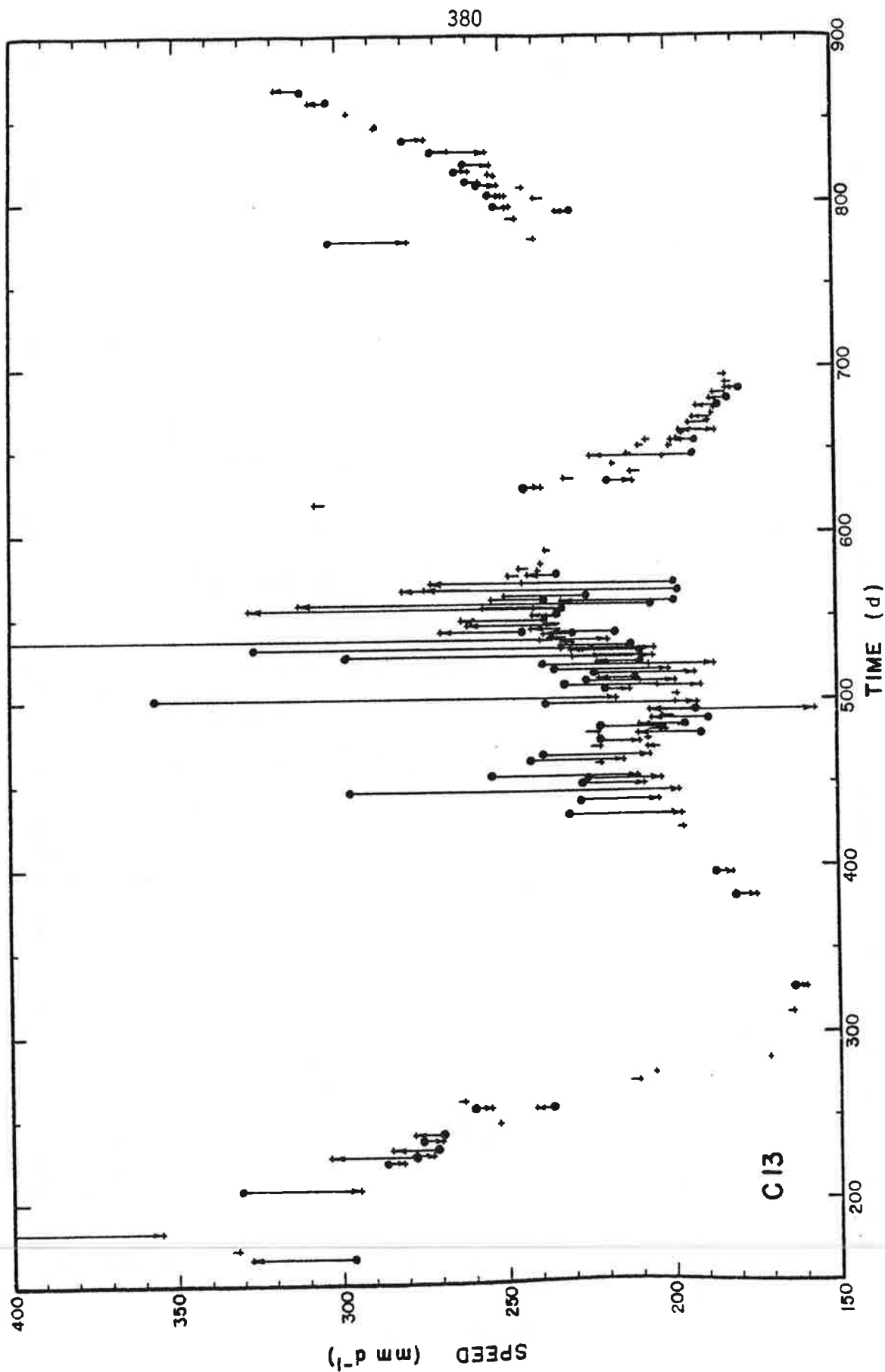
Correction method IV. The scatter is increased by 66 % from that for the raw data. This method is thus not an improvement over the raw data, despite the fact that method III was.



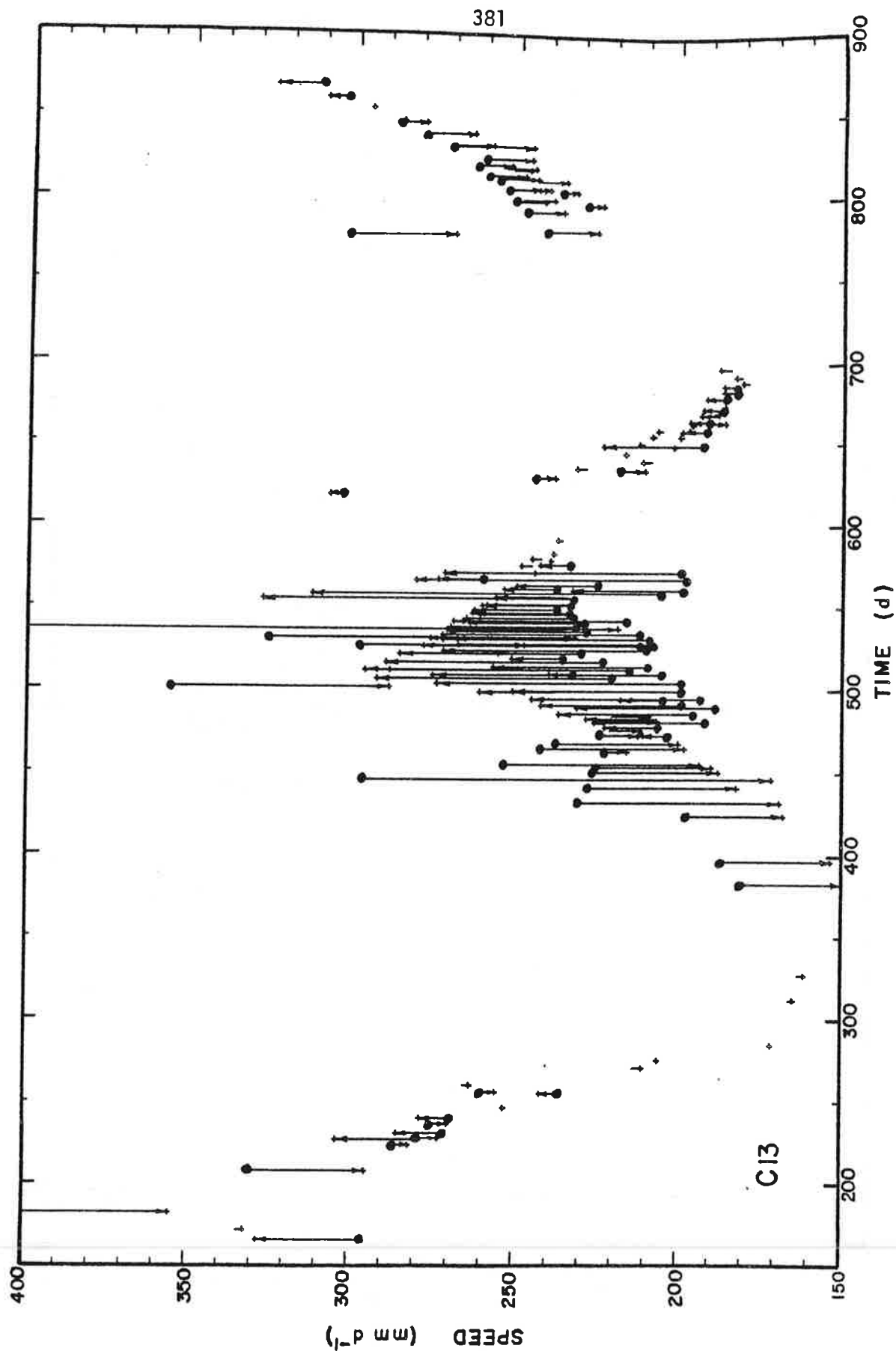
The flex method. The scatter is decreased by 72 % from that for the raw data. This method is thus an improvement over both previous correction methods and over the raw data.



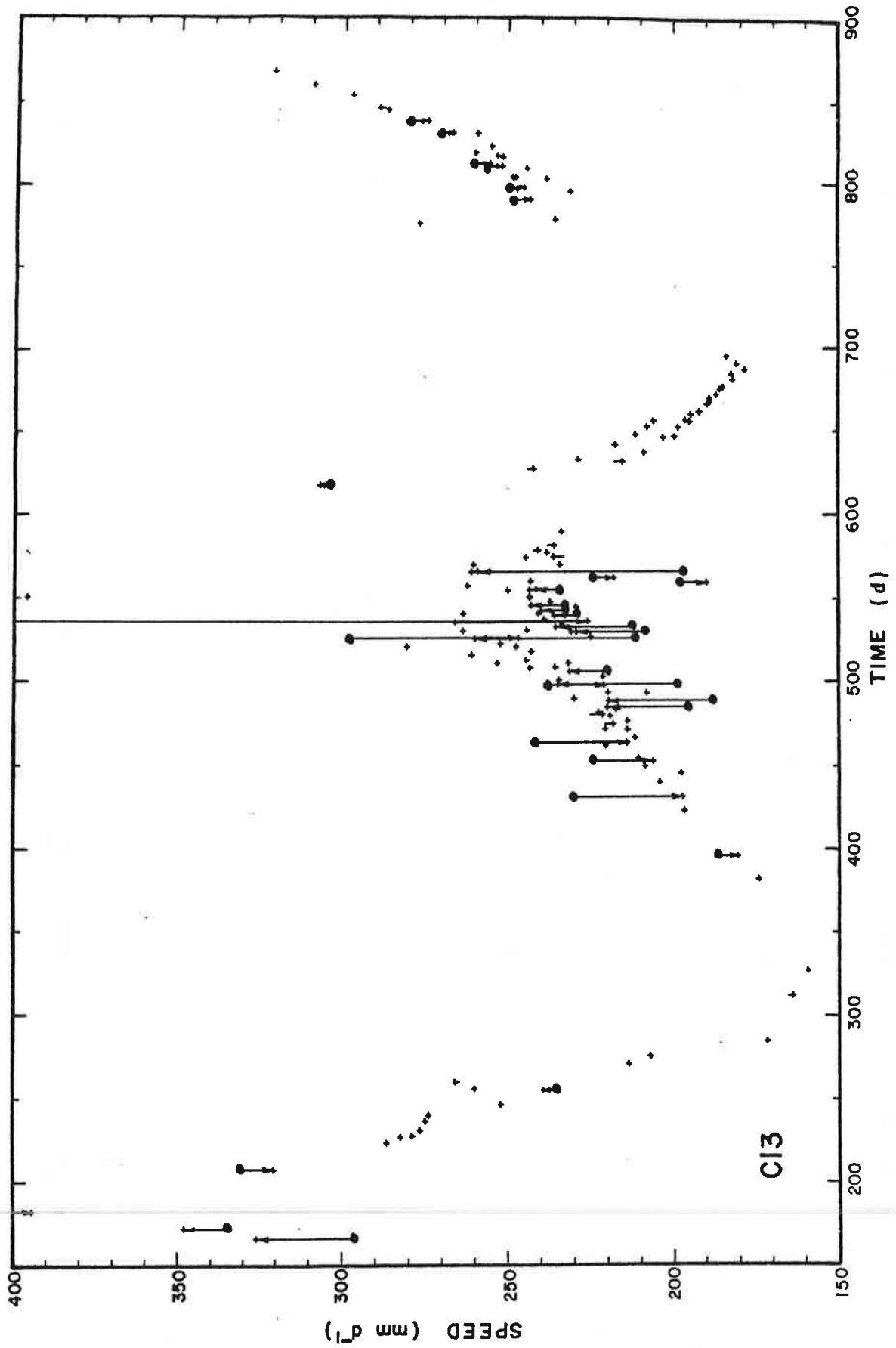
The corrections for transverse velocity gradients, the removal of time intervals less than 15 days and the removal of faulty data points. The scatter of the final data is decreased by 79 % from that for the raw data.



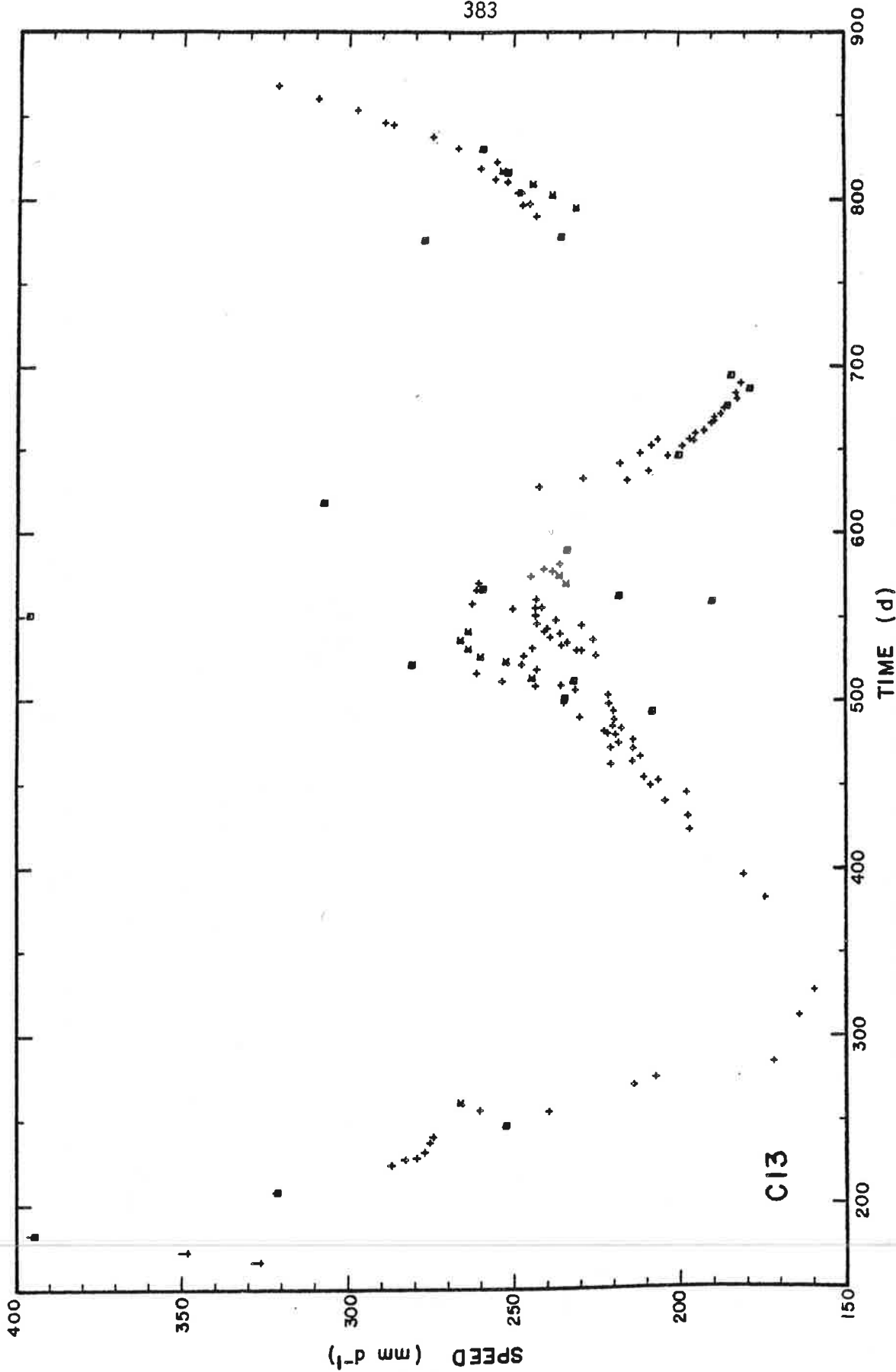
Correction method III. The scatter is decreased by 22 % from that for the raw data.



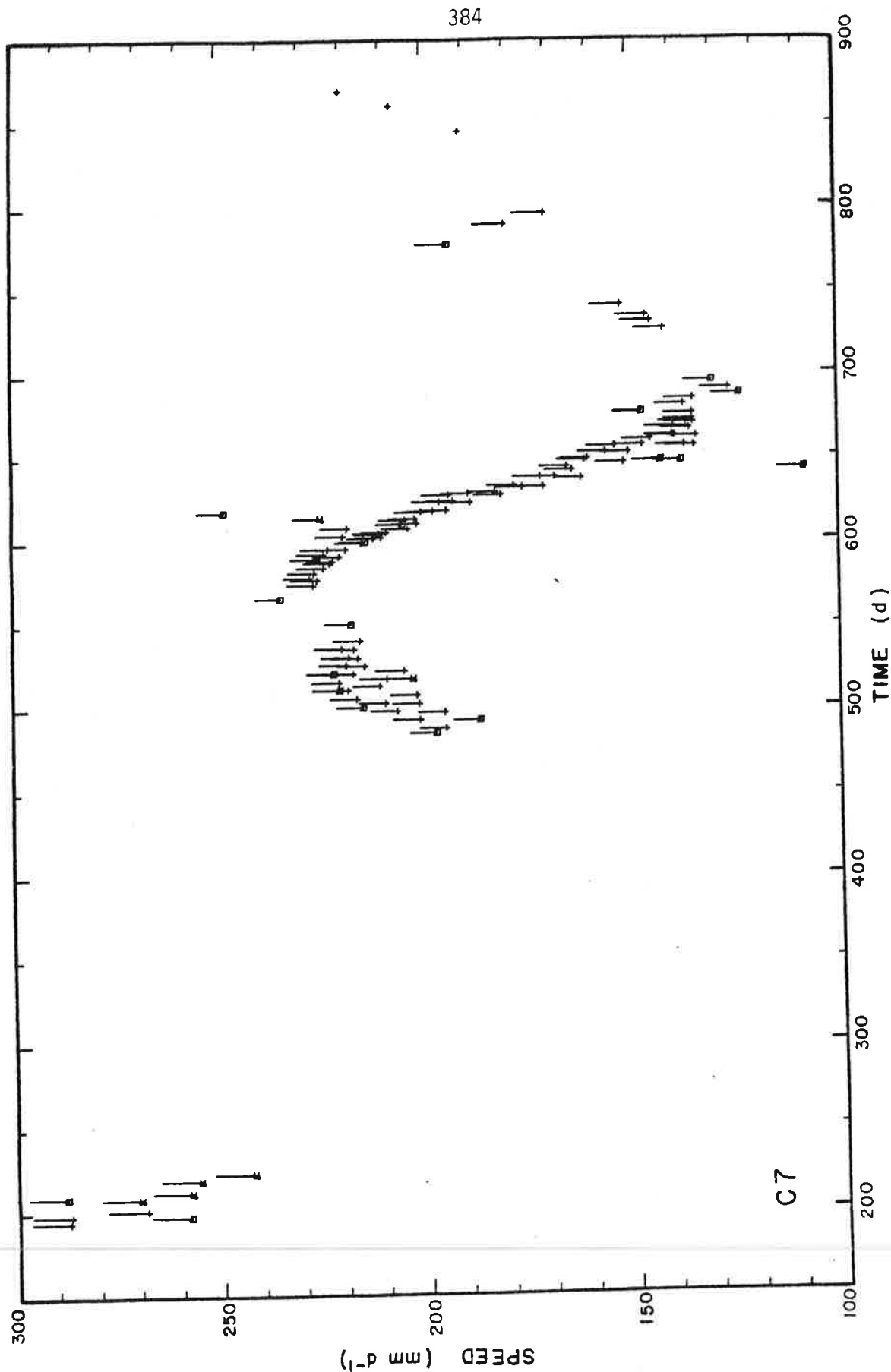
Correction method IV. The scatter is decreased by 22 % from that for the raw data, the same as method III.



The flex method. The scatter is decreased by 39 % from that for the raw data. This method is thus an improvement over both previous correction methods and over the raw data.



The corrections for transverse velocity gradients, the removal of time intervals less than 15 days and the removal of faulty data points. The scatter of the final data is decreased by 72 % from that for the raw data.



The corrections for transverse velocity gradients, the removal of time intervals less than 15 days and the removal of faulty data points. The scatter of the final data is decreased by 71 % from that for the raw data.

C.2 THE SPEED VERSUS TIME CURVES

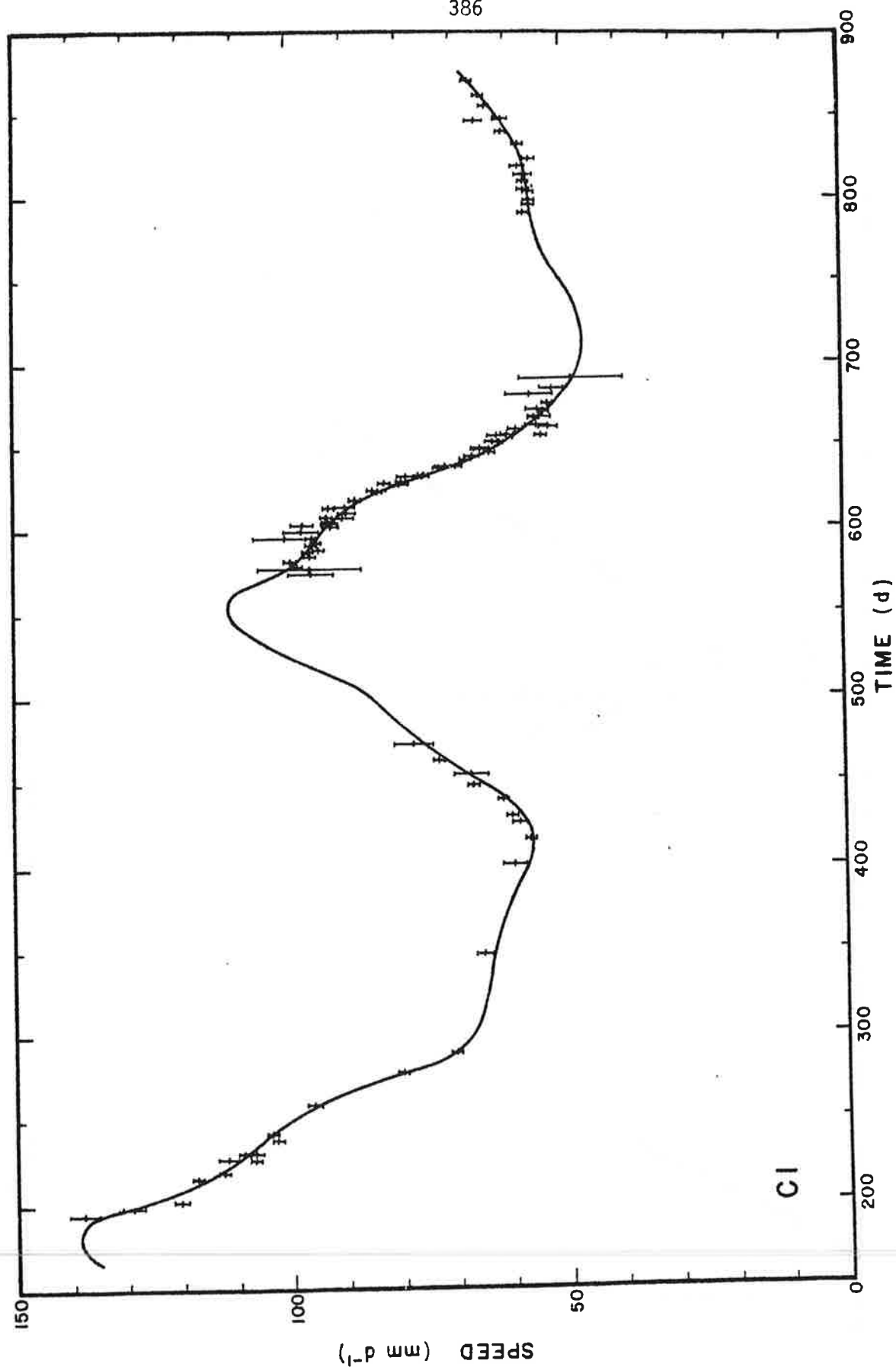
On the following pages is shown the measured surface speed $s'_0(t_1)$ for each centerline stake. The values are corrected for transverse and longitudinal velocity gradients to the standard stake positions ($x' = x'_0$, $y' = 0$). Faulty data points and points whose time interval was less than 15 days have been eliminated. The error bars are calculated from equations 6.79 and 6.80 and are weighted inversely according to the function in Figure 76 (p. 212).

The solid lines are the mean curves $\bar{s}'_0(t)$ used in the analysis of the data (chapter 11). Interpolation in the regions of missing data is done simultaneously in both time *and distance* (p. 223) and so it sometimes appears that the interpolated regions show variations not justified by the data for that particular stake.

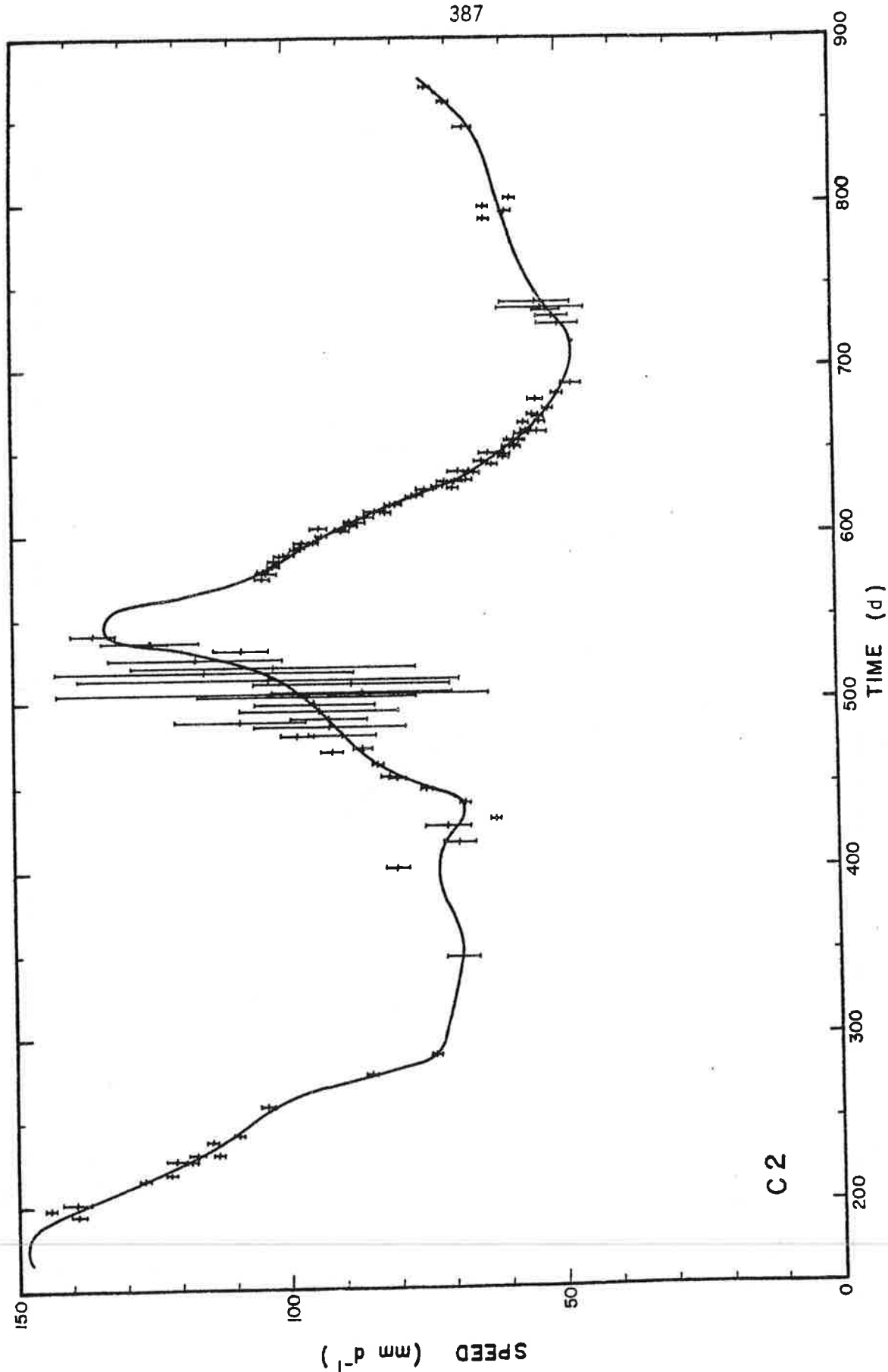
m is the number of measurements of the position of the stake (excluding faulty points) and n is the final number of survey combinations shown on the diagram. x'_0 is the standard position of the stake.

The curves are presented in order of increasing distance up-glacier, from the terminus (C1) to the equilibrium line (C20).

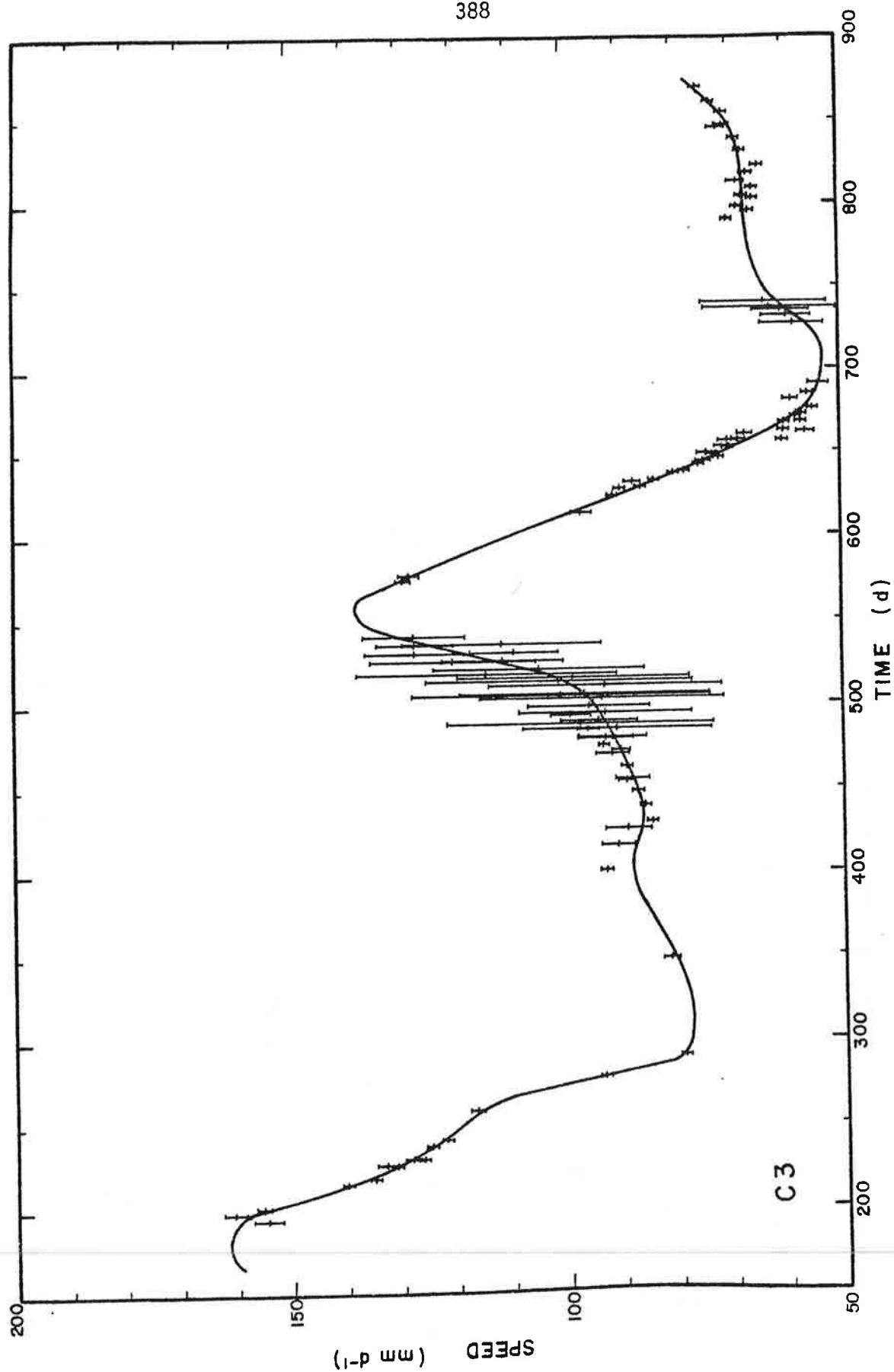
The overlay in the rear pocket can be used with these diagrams.



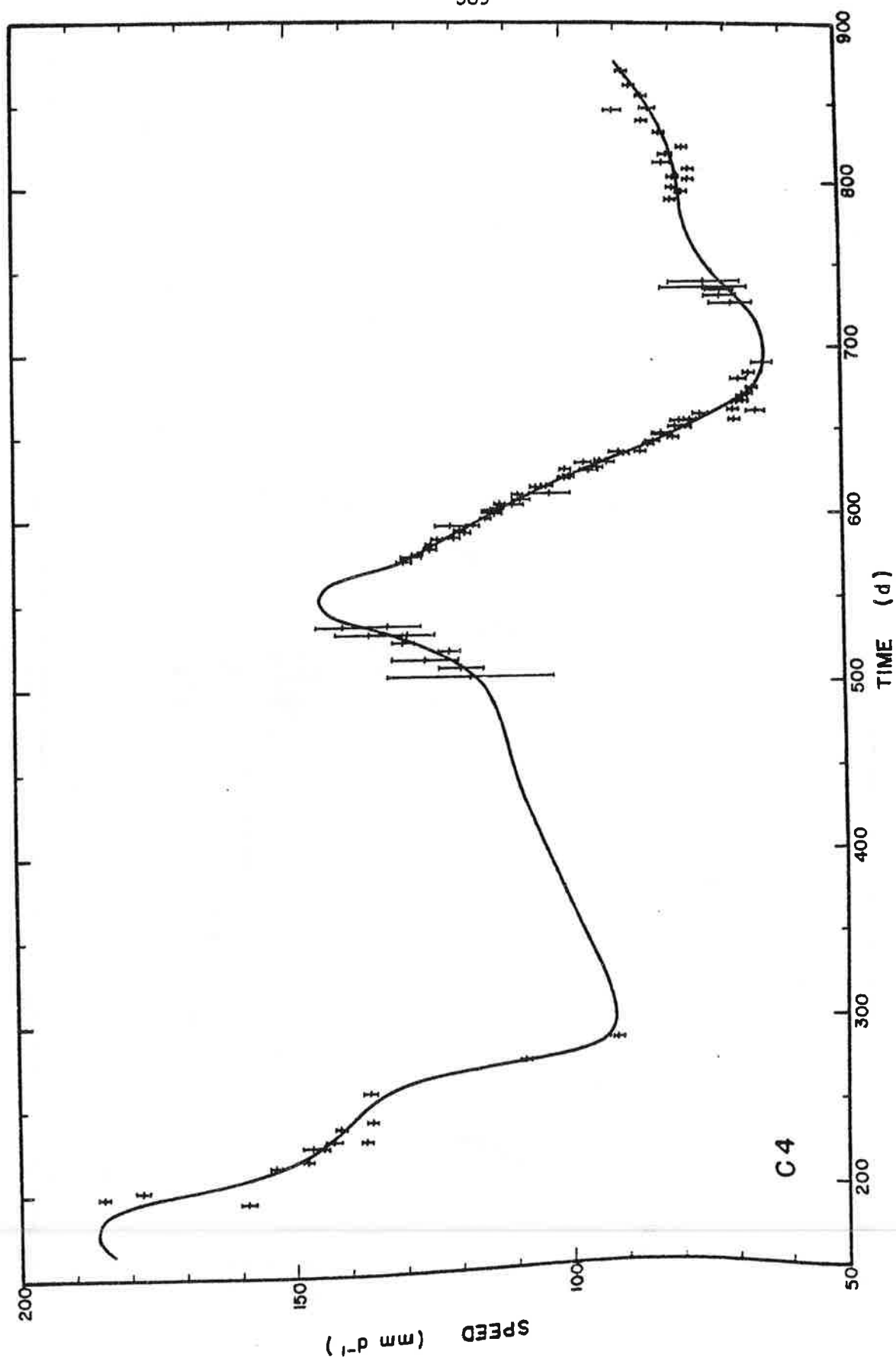
$m = 32, n = 95, x'_0 = 2749 \text{ m.}$



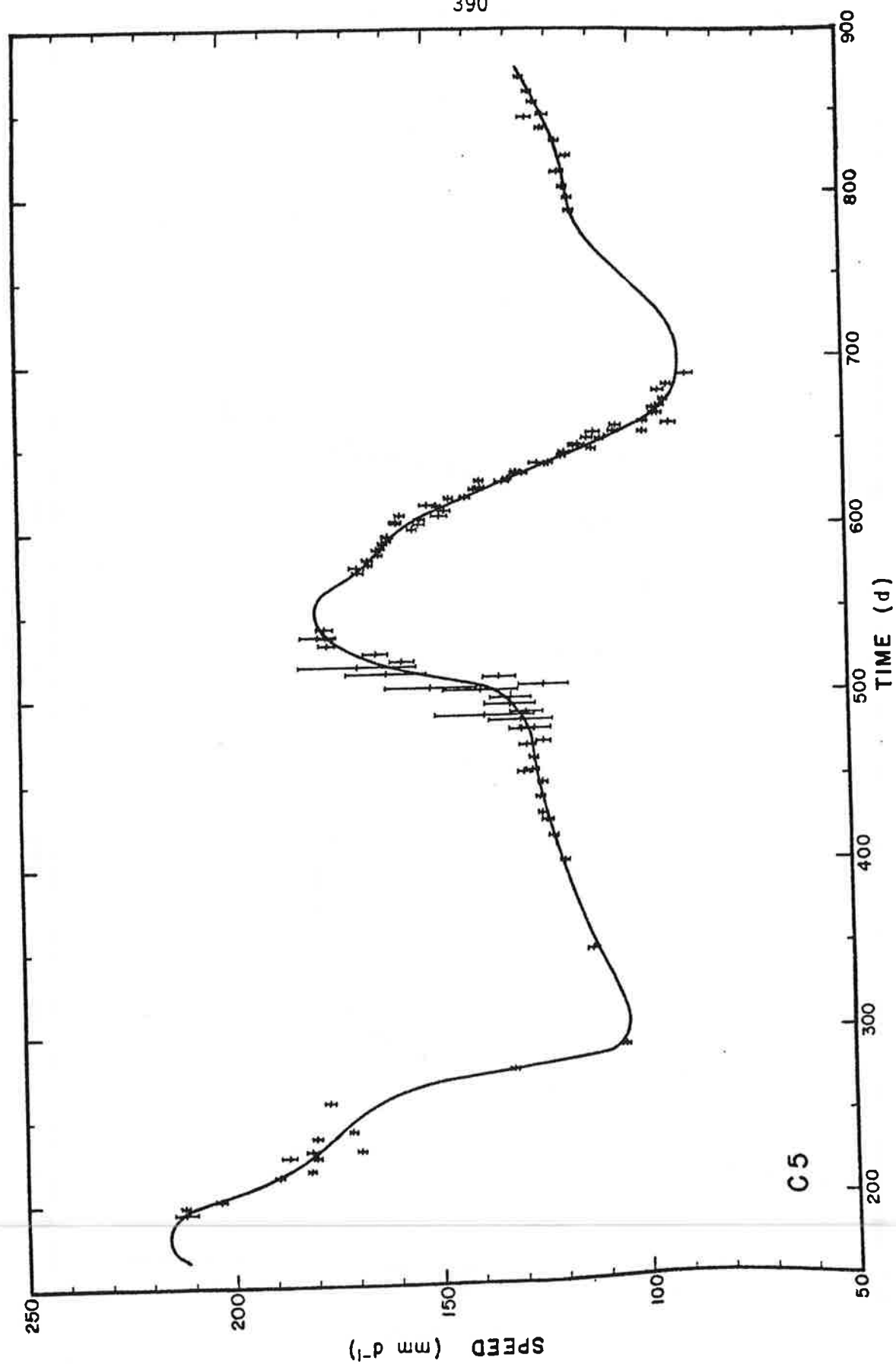
$m = 37, \quad n = 112, \quad x'_0 = 2661 \text{ m.}$



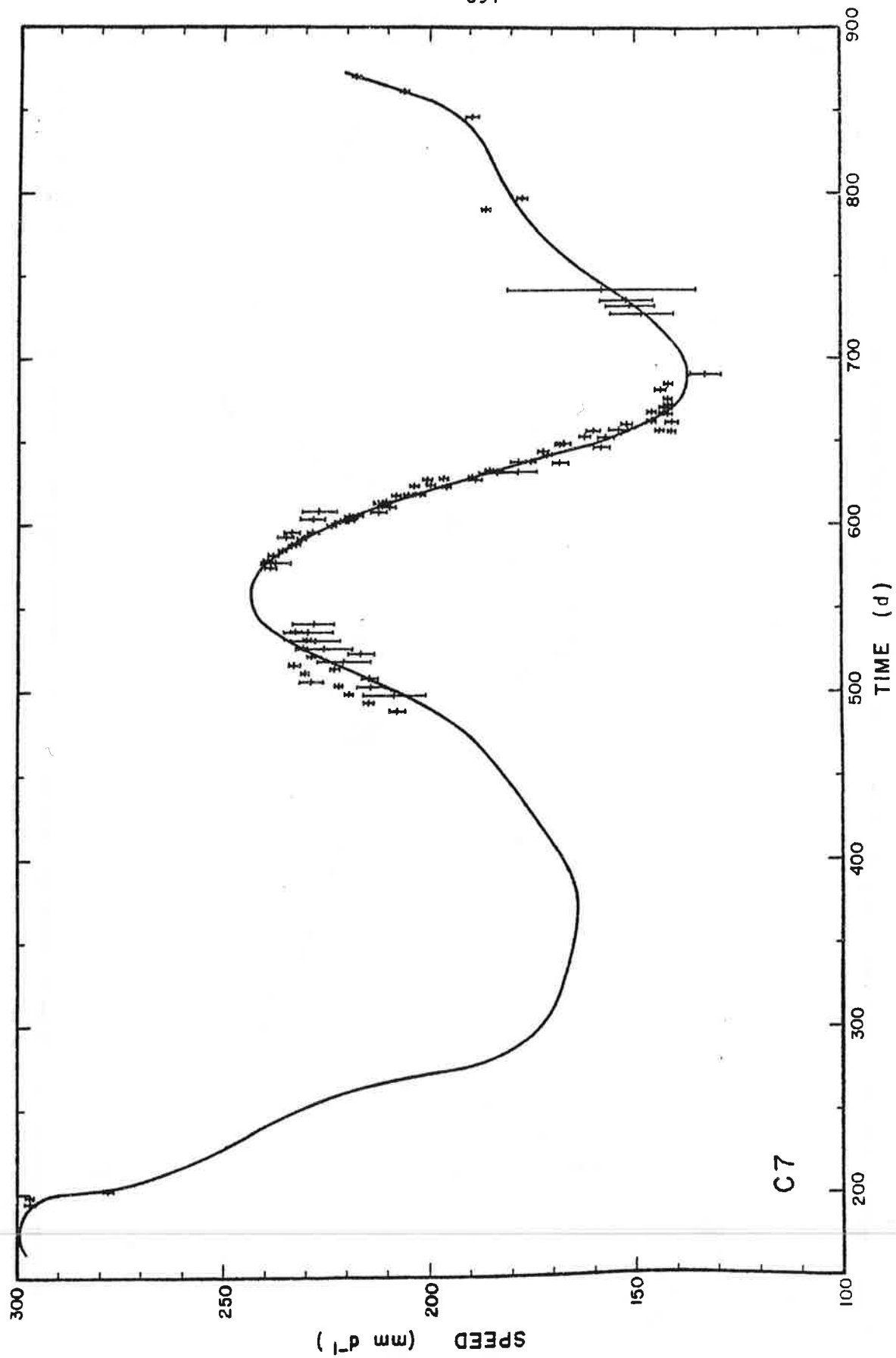
$m = 37, \quad n = 103, \quad x'_0 = 2546 \text{ m.}$



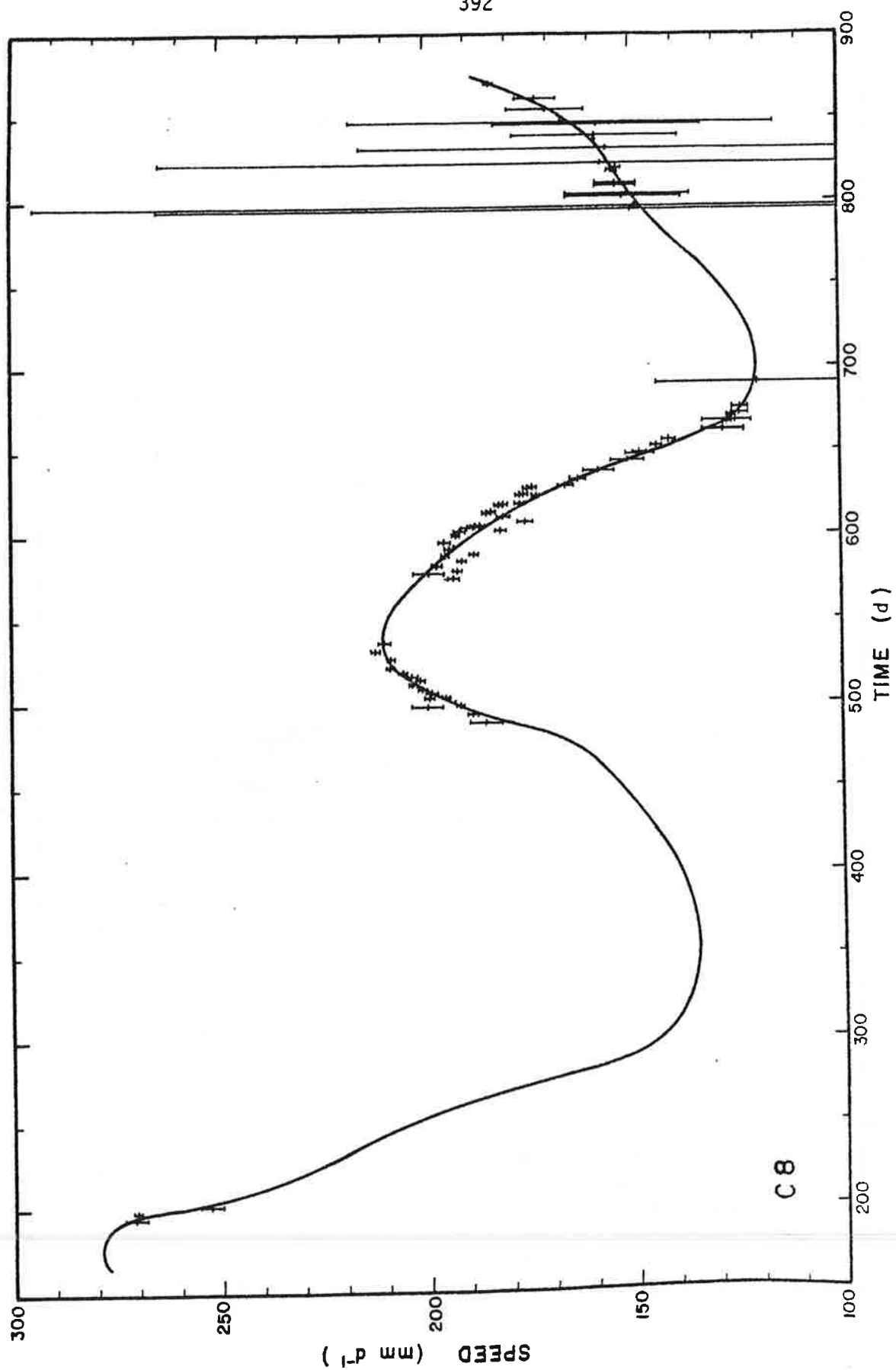
$m = 36, n = 99, x'_0 = 2430 \text{ m.}$



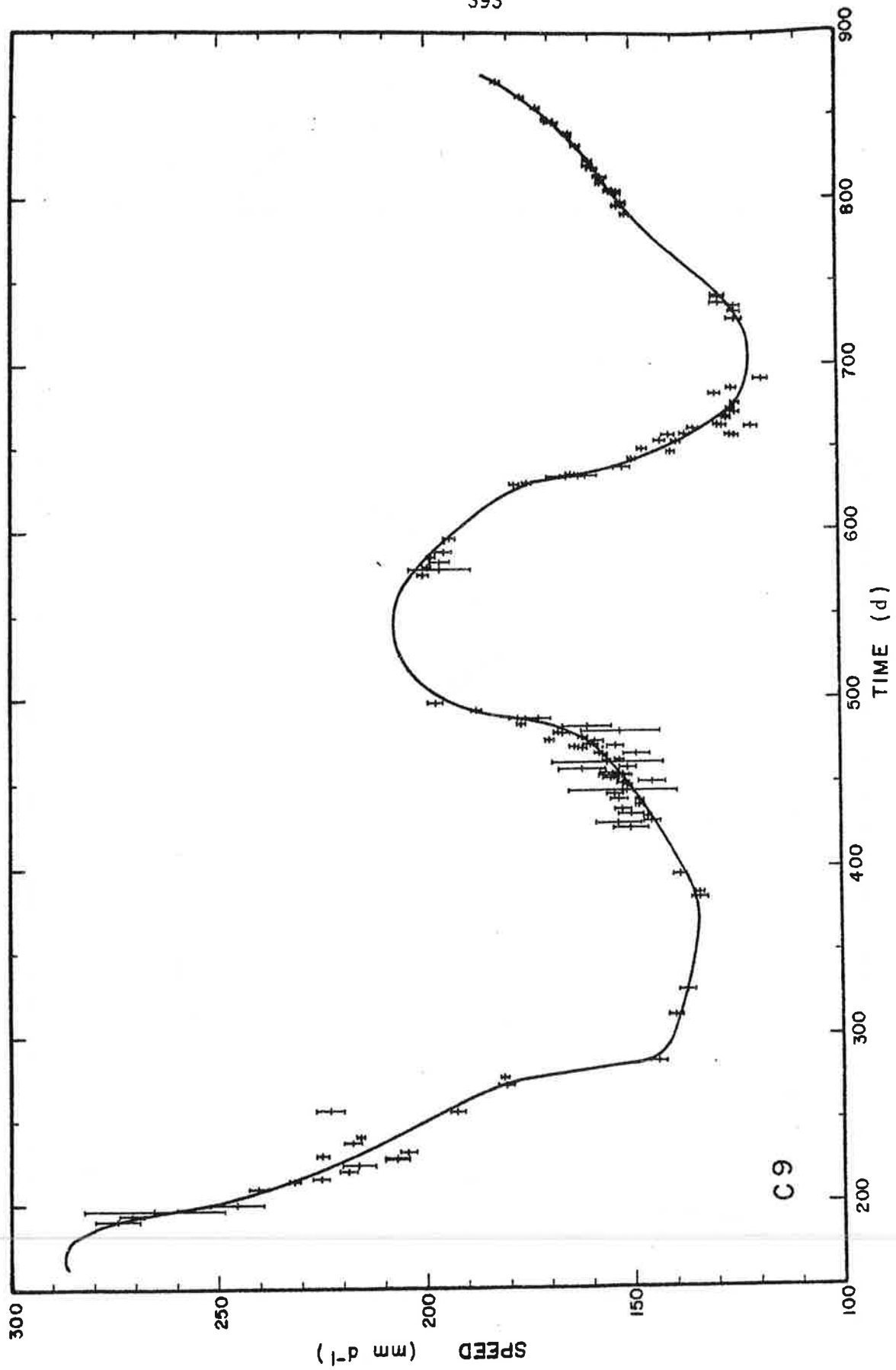
$m = 36, n = 112, x'_0 = 2326 m.$



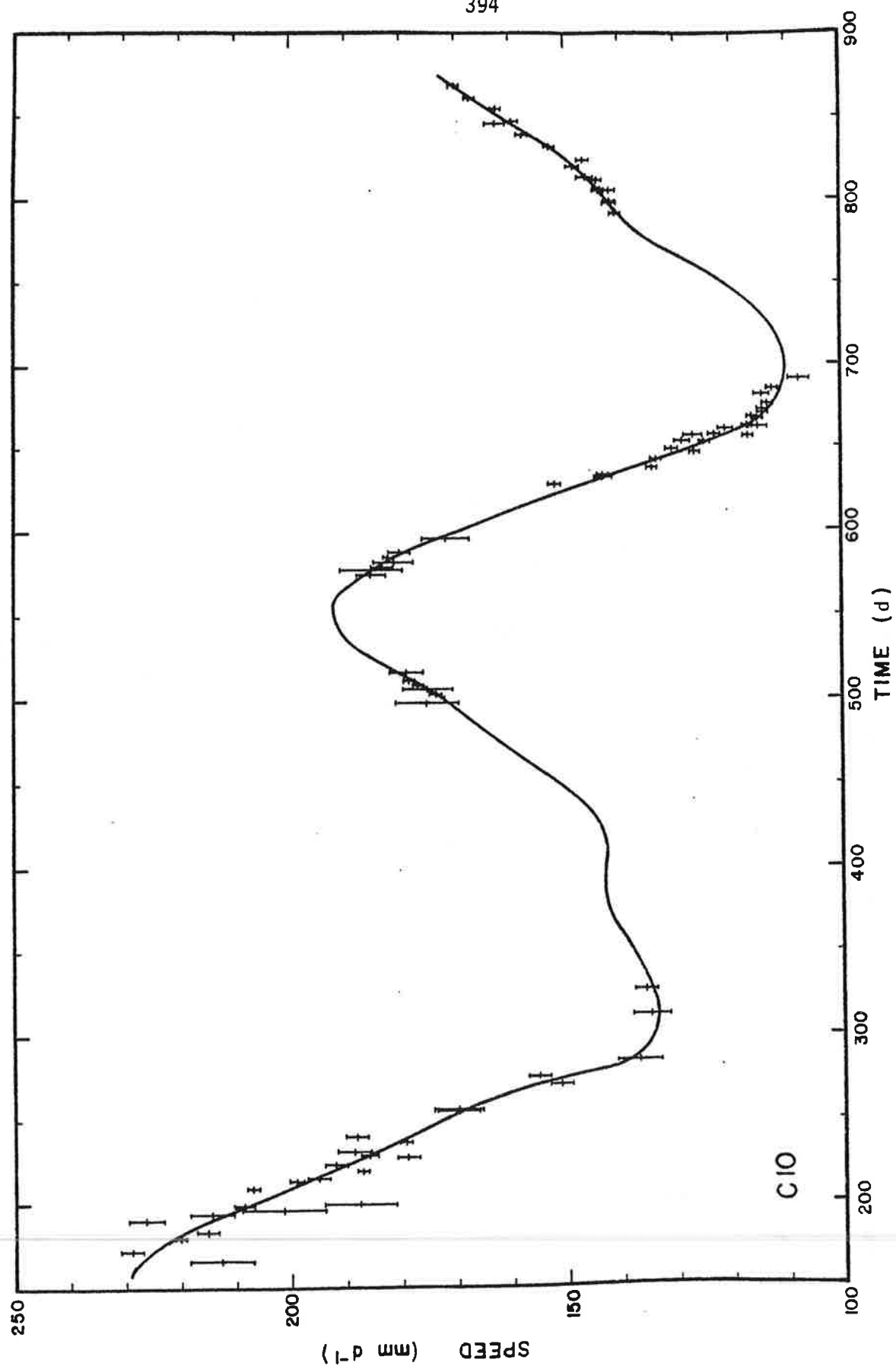
$m = 32, n = 98, x'_0 = 2051 m.$



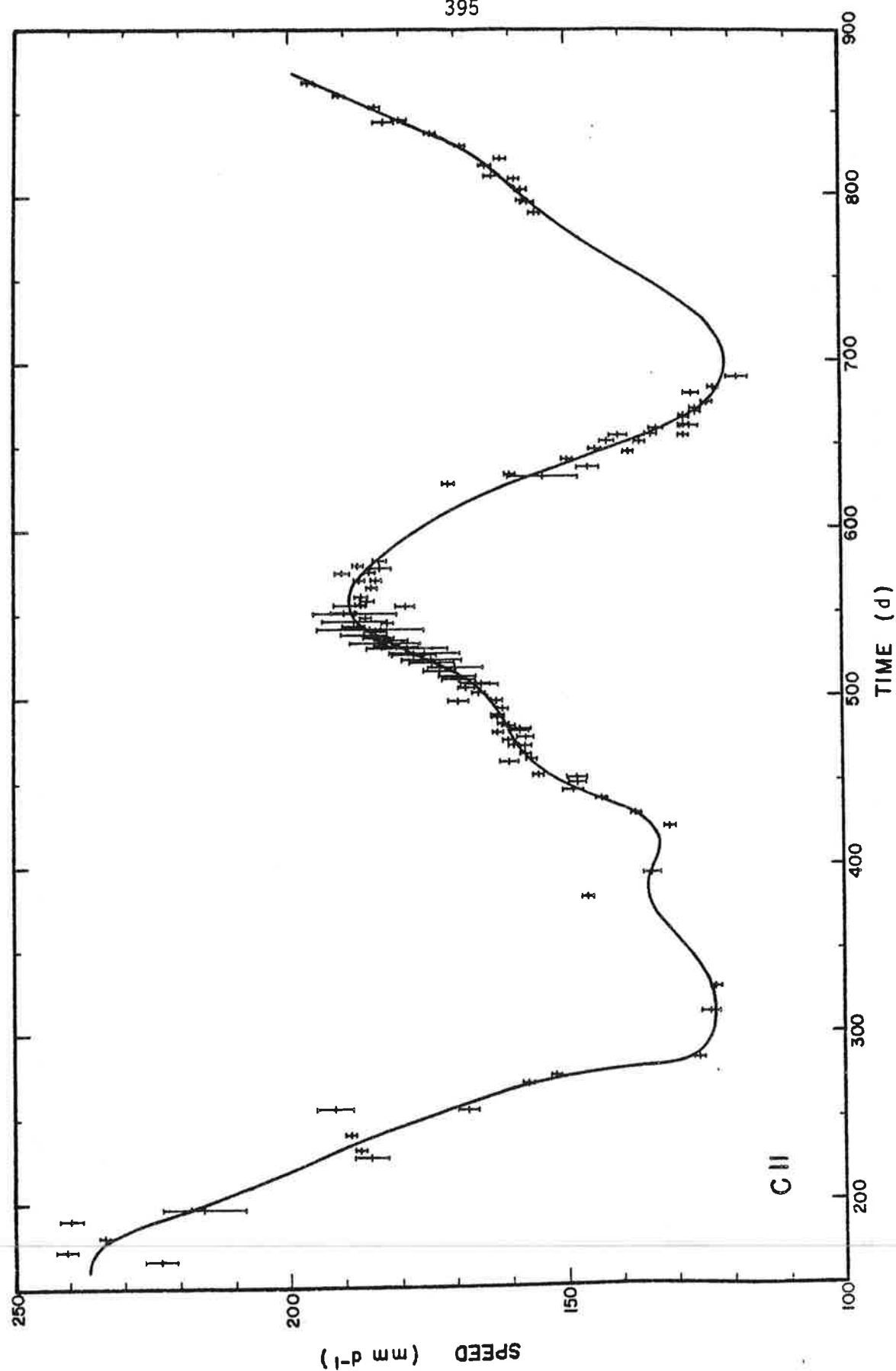
$m = 33, n = 80, x'_0 = 1940 \text{ m.}$



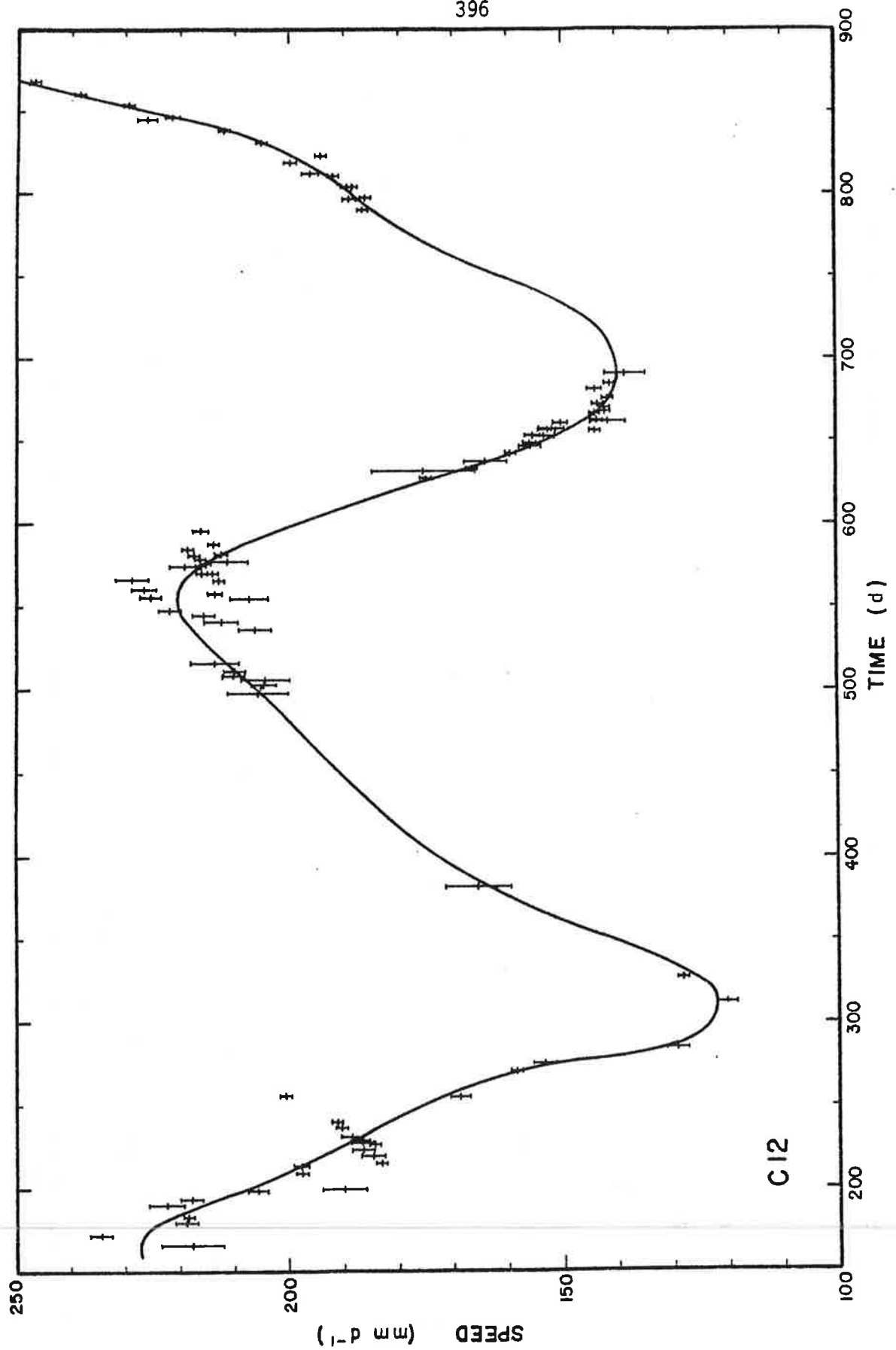
$m = 43$, $n = 131$, $x'_0 = 1791$ m.



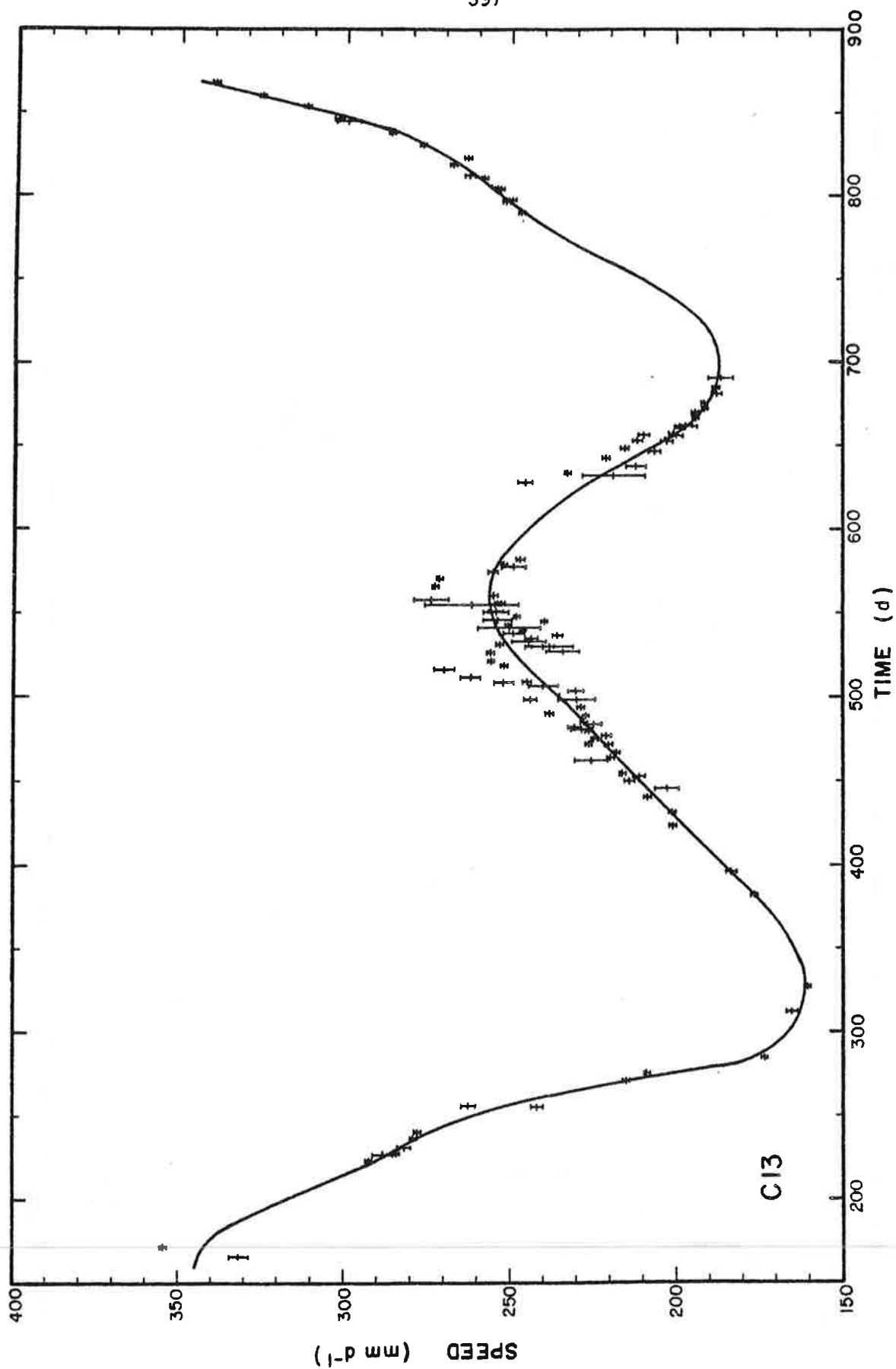
$m = 35, n = 78, x'_0 = 1644 \text{ m.}$



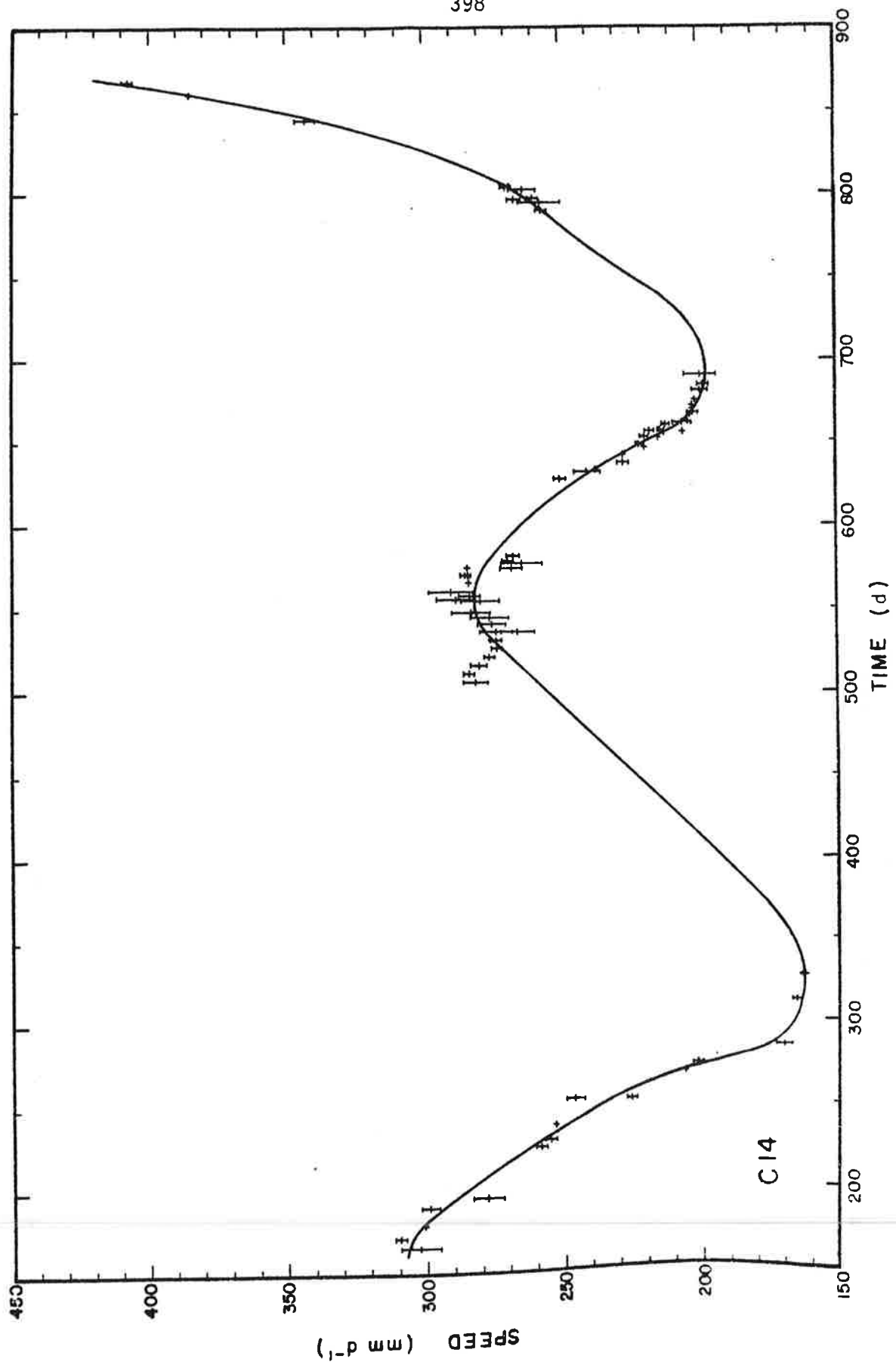
$m = 40, \quad n = 124, \quad x'_0 = 1492 \text{ m.}$



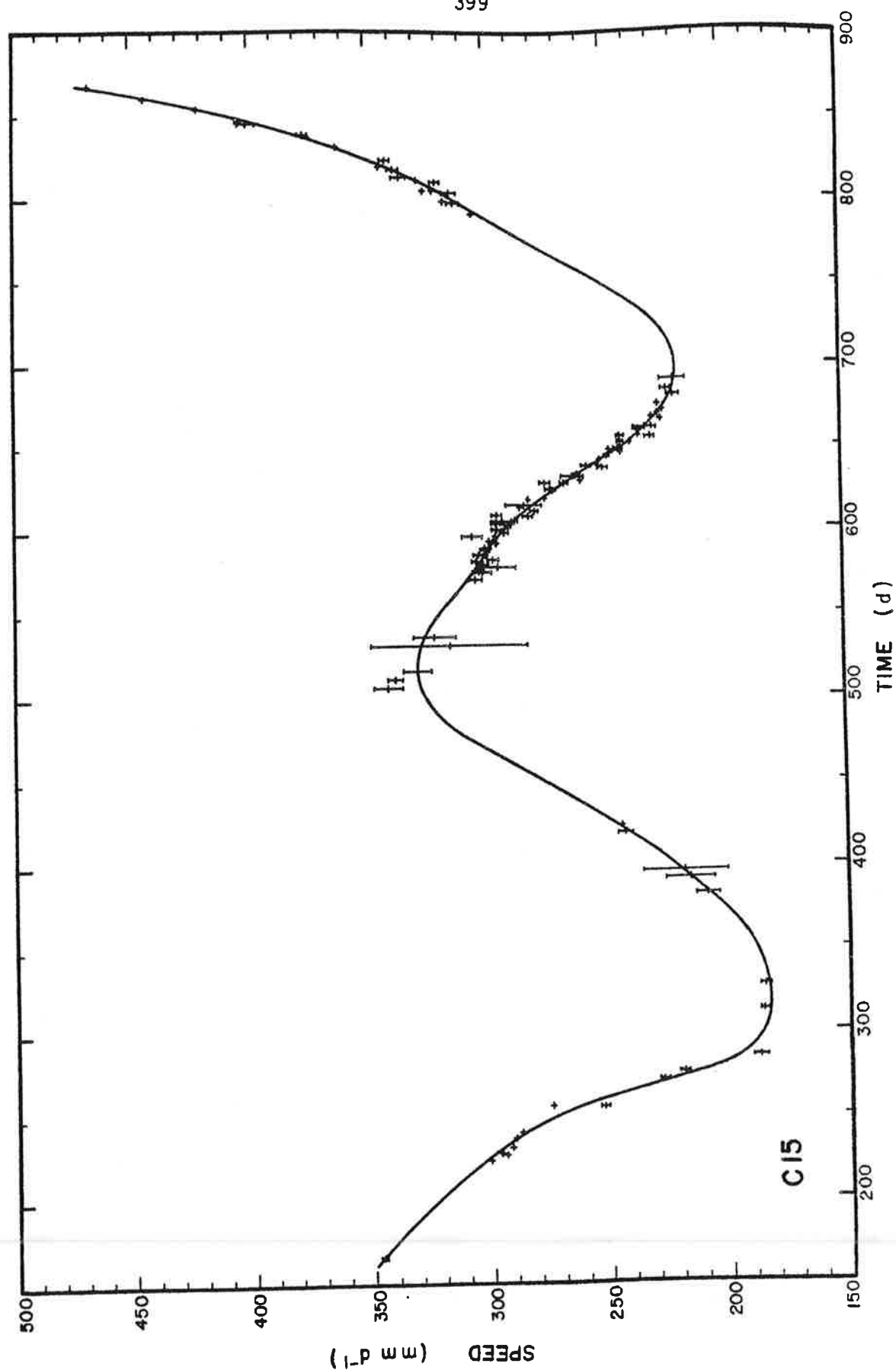
$m = 39, n = 94, x'_0 = 1371 m.$



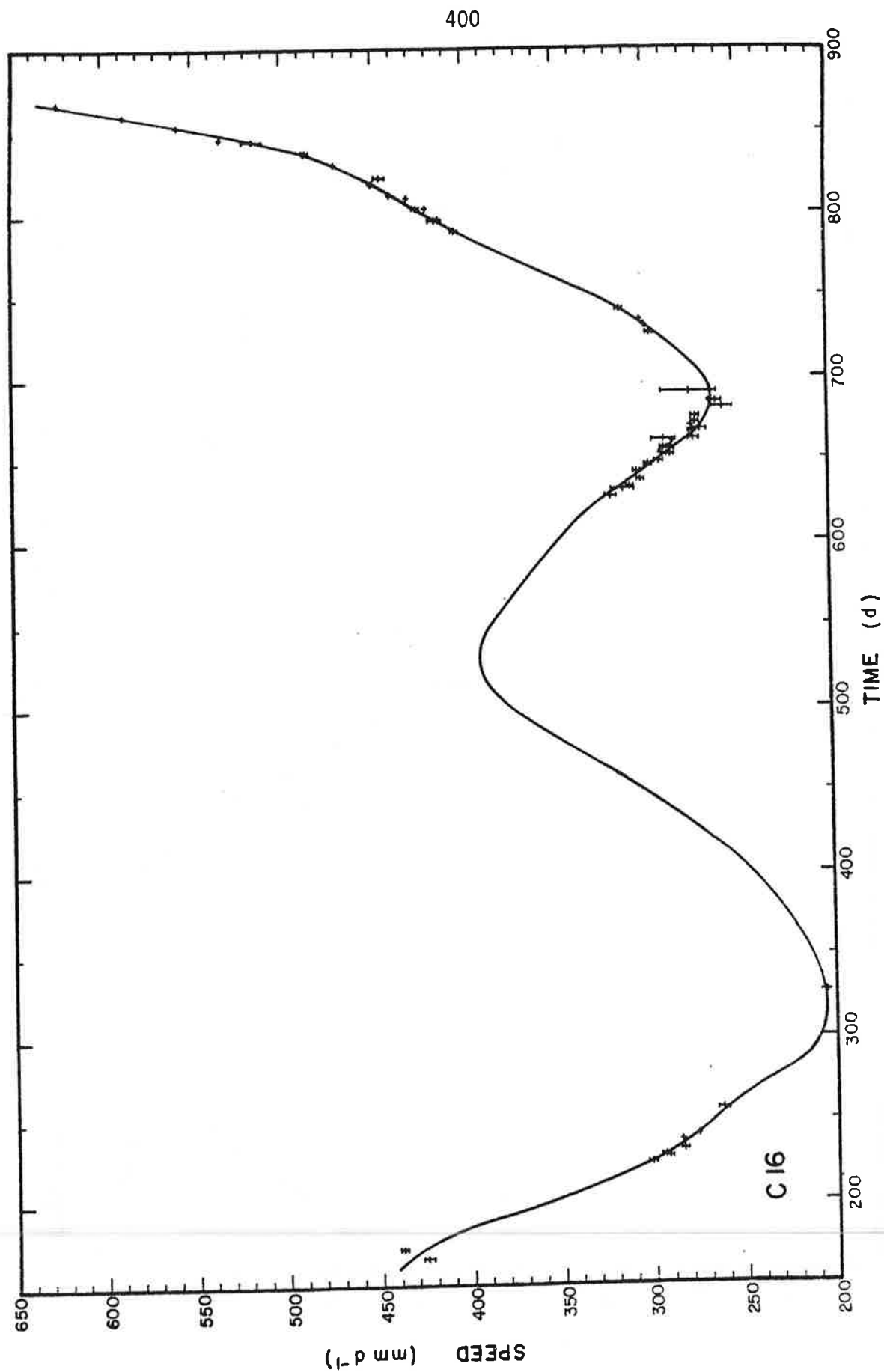
$m = 39, n = 116, x'_0 = 1238 m.$



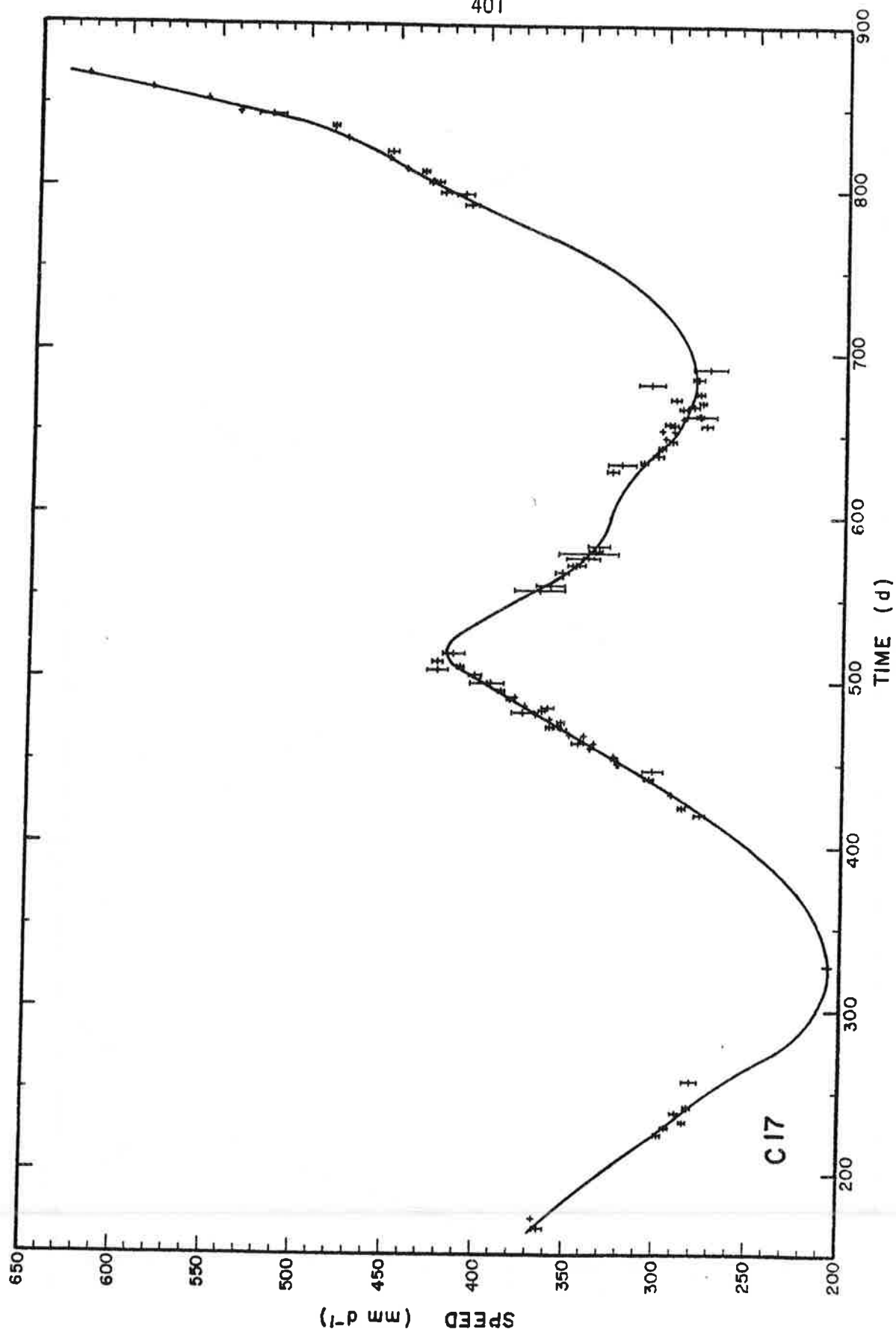
$m = 38, n = 70, x'_0 = 1105 m.$



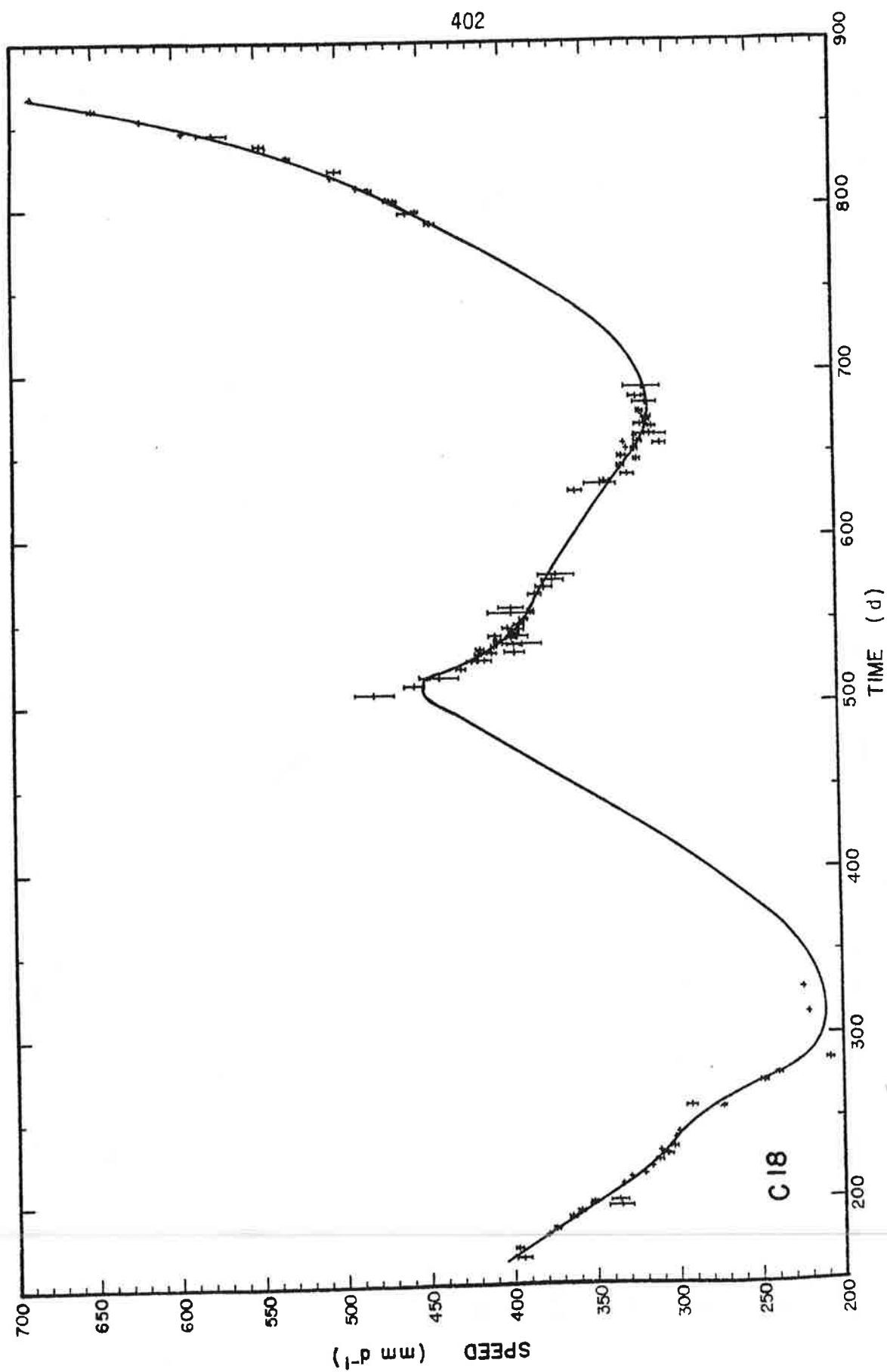
$m = 41, n = 104, x'_0 = 974 m.$



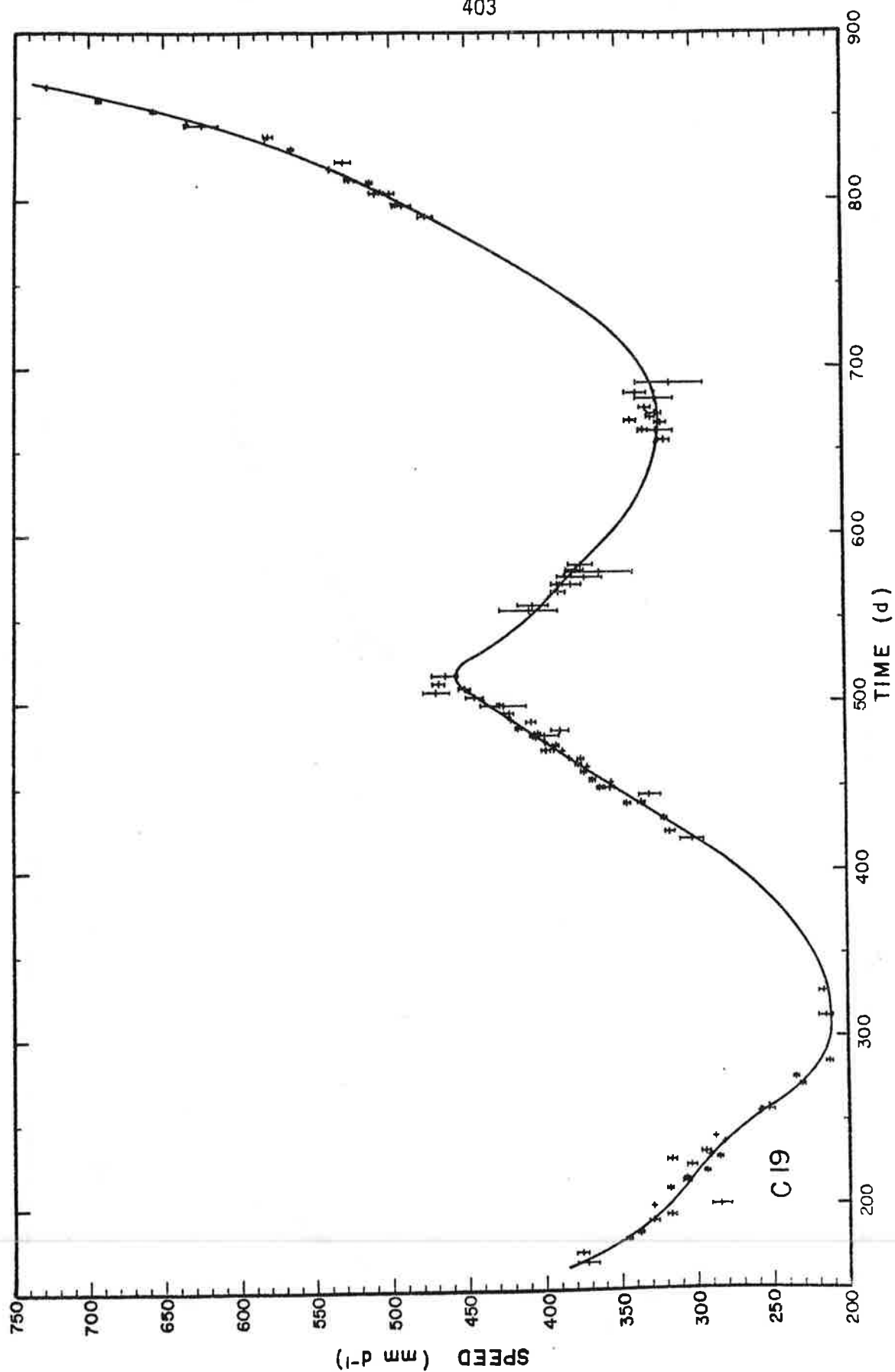
$m = 26, \quad n = 53, \quad x'_0 = 826 \text{ m.}$



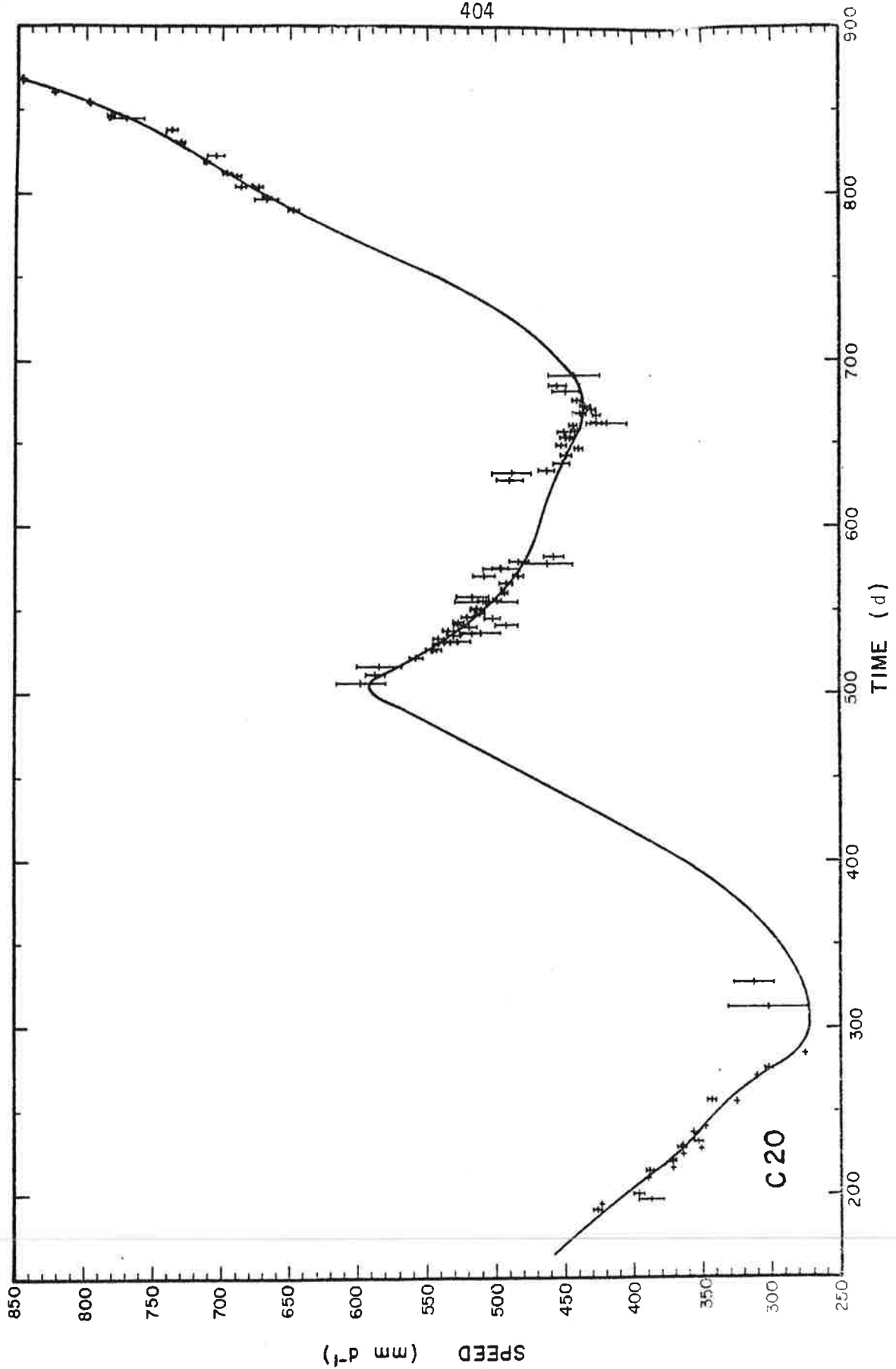
$m = 41, n = 94, x'_0 = 700 m.$



$m = 36, n = 95, x'_0 = 590 \text{ m.}$



$m = 41, n = 98, x'_0 = 439 m.$

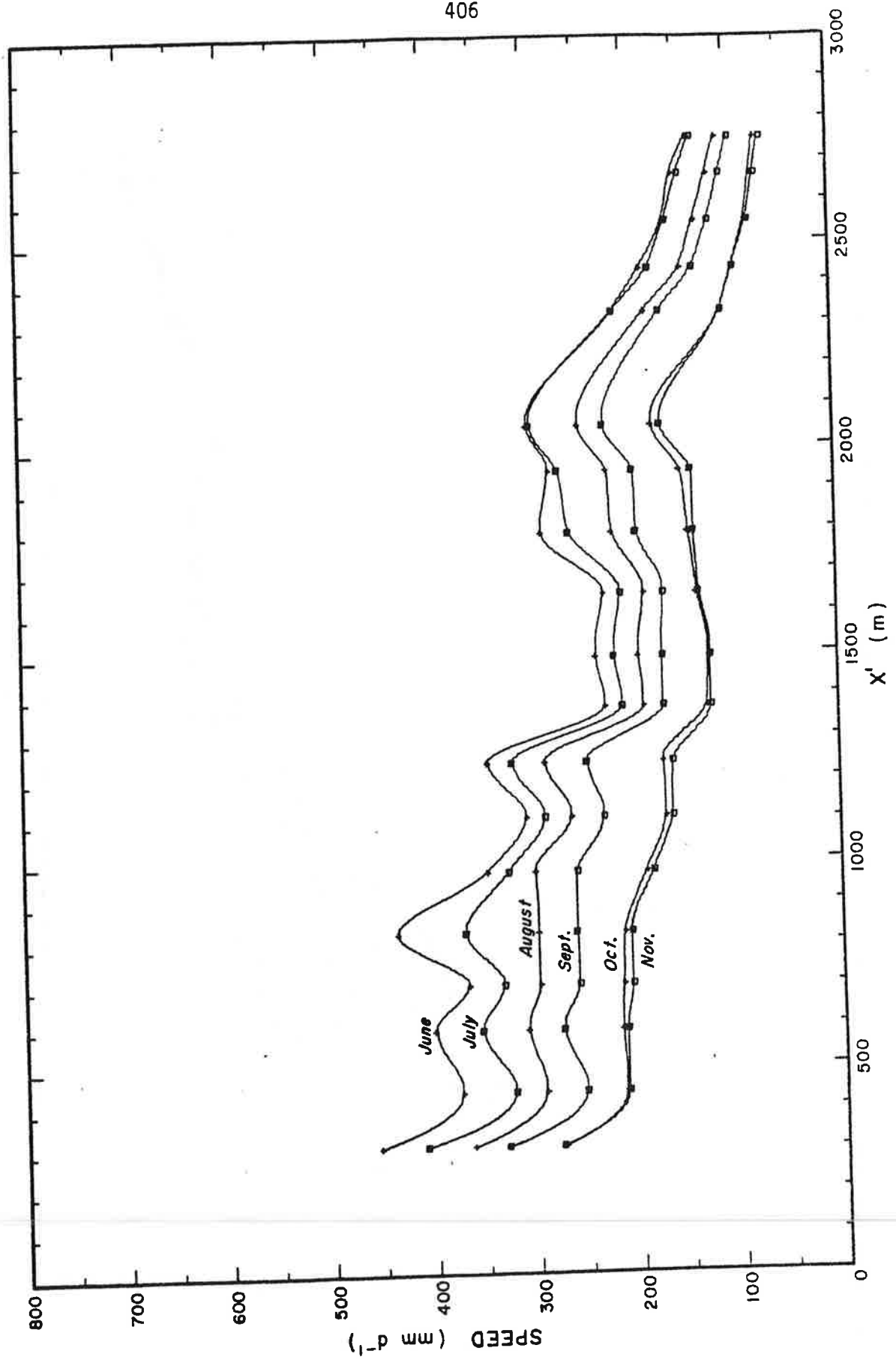


$\mu = 36$, $\nu = 96$, $x' = 306$ m.

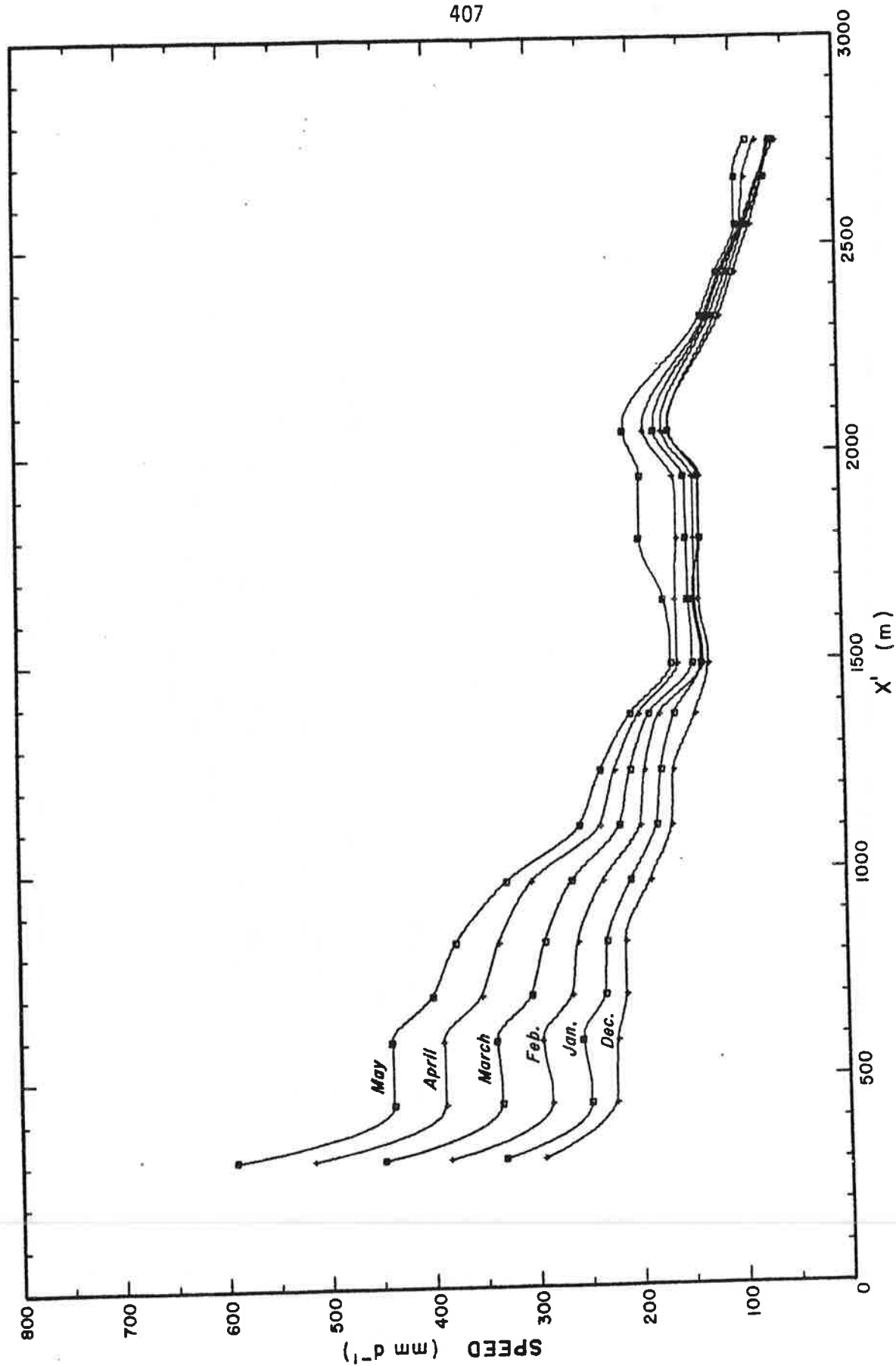
C.3 THE SPEED VERSUS DISTANCE CURVES

On the following pages is shown the measured surface speed $s'_o(x')$ for each month of the two year measurement period, as a function of distance along the centerline. These curves are taken from Figure 83 and thus represent mean, interpolated curves only. Data points are not indicated since they would make the diagrams too confusing; only the values at the standard stake positions are shown (alternating plus and square symbols).

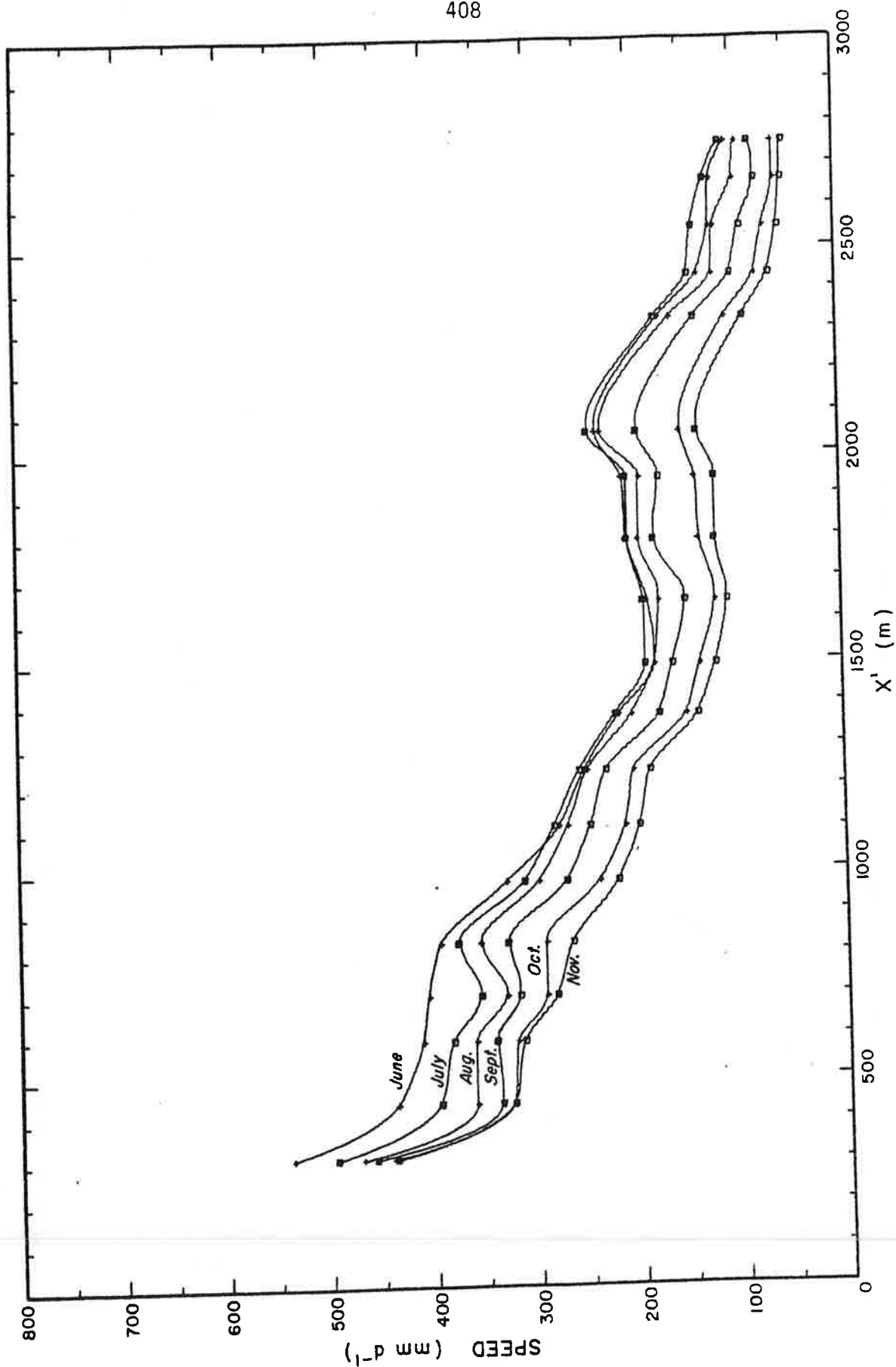
Each curve refers to the mid-point of each month. The curvilinear coordinate x' runs from near the equilibrium line to the terminus.



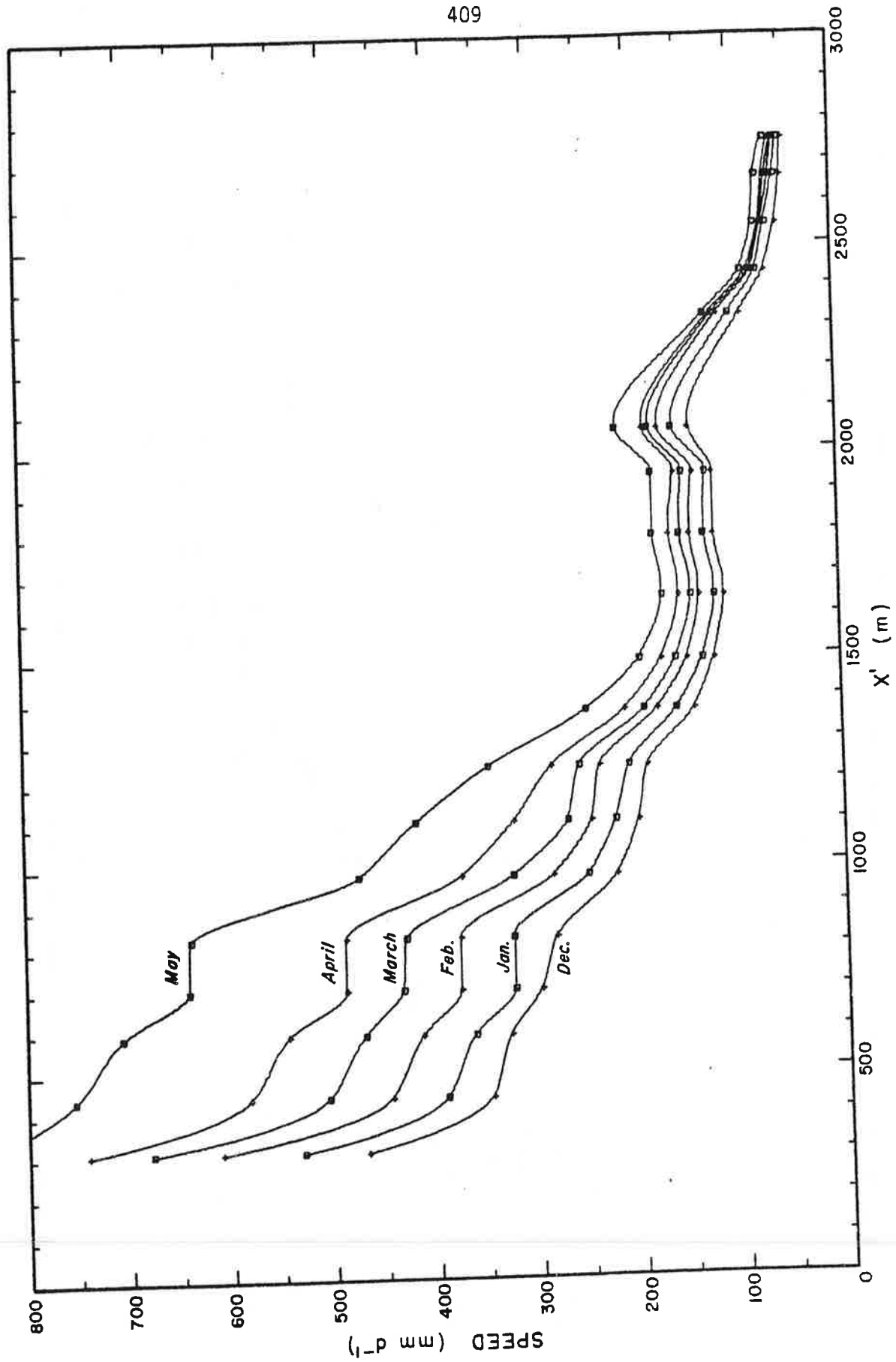
June to November, 1968.



December 1968 to May 1969.



June to November 1969.



December 1969 to May 1970.

BIOGRAPHICAL NOTE

Steven McNiven Hodge was born in London, England on October 15, 1942 to parents George Stevenson Hodge and Kathleen Hodge. He graduated from Victoria High School, Victoria, British Columbia in 1960. He attended the University of British Columbia and received a Bachelor of Science degree in Honors Physics in 1964.



